A TRI-FUNCTIONALIZED ORAL CORE-MELT TABLET (OCMT) FOR ENHANCED DELIVERY OF GASTRO-SENSITIVE PROTEINS AND SYNTHETIC PEPTIDES

BIBI FATIMA CHOONARA

A thesis submitted to the Faculty of Health Sciences, University of the Witwatersrand, in fulfillment of the requirements for the degree of Doctor of Philosophy

Supervisor:
Professor Viness Pillay
Department of Pharmacy and Pharmacology, University of the Witwatersrand, South Africa

Co-Supervisors:
Professor Yahya E. Choonara
Professor Lisa C. du Toit
Mr. Pradeep Kumar
Department of Pharmacy and Pharmacology, University of the Witwatersrand, South Africa

Johannesburg, 2017

DECLARATION

I, Bibi Fatima Choonara, declare that this thesis is my own work. It has being submitted for the degree of Doctor of Philosophy in the Faculty of Health Sciences in the University of the Witwatersrand, Johannesburg. It has not been submitted before for any degree or examination at this or any other University.

……

Signed this …….. day of …….. 2017

PUBLICATIONS

Bibi F. Choonara, Yahya E. Choonara, Pradeep Kumar, Divya Bijukumar, Lisa C. du Toit, Viness Pillay. A Review of Advanced Oral Drug Delivery Technologies Facilitating the Protection and Absorption of Protein and Peptide Molecules. *Biotechnology Advances*, 2014, 32, 1269–1282. *[Review Article]. Accreditation: ISI; IF: 9.599.*

Bibi F. Choonara, Yahya E. Choonara, Pradeep Kumar, Lisa C. du Toit, Lomas K. Tomar, Charu Tyagi, Viness Pillay. A Menthol-Based Solid Dispersion Technique for Enhanced Solubility and Dissolution of Sulfamethoxazole from an Oral Tablet Matrix. *AAPS PharmSciTech*, 2015, 16, 771-786. *[Research Article]*. *Accreditation*: *ISI; IF: 1.641.*

Bibi F. Choonara, Yahya E. Choonara, Pradeep Kumar, Lisa C. du Toit, Viness Pillay. Design of an *In Situ* Cross-Linked Eutectic Tablet for Enhanced Delivery of Gastro-Sensitive Proteins and Peptides. *Journal of Pharmaceutical Sciences*, 2016, 105, 2086-2098. *[Research Article]*. *Accreditation*: *ISI; IF: 2.59.*

Bibi F. Choonara, Yahya E. Choonara, Pradeep Kumar, Lisa C. du Toit, Viness Pillay. *In Vitro* and *In Vivo* Evaluation of a Novel Oral Core-Melt Tablet (OCMT). [To be submitted to *International Journal of Pharmaceutics*].

Bibi F. Choonara, Yahya E. Choonara, Pradeep Kumar, Lisa C. du Toit, Viness Pillay. Design of a Co-inhibitory 'Smart' Polymeric Sheet Surrounding a pH-Modified OCMT for Tri-Functionalization. [To be submitted to the *Journal of Controlled Release*].

Bibi F. Choonara, Yahya E. Choonara, Pradeep Kumar, Lisa C. du Toit, Viness Pillay. Comprehensive *In vitro* and *In vivo* Characterization of the Statistically Optimized Tri-Functionalized Oral Core-Melt Tablet (OCMT) for Enhanced Protein and Synthetic Peptide Delivery. [To be submitted to *Nature Biotechnology*].

RESEARCH PRESENTATIONS

Bibi F. Choonara, Yahya E. Choonara, Lisa C. du Toit, Pradeep Kumar, Viness Pillay. Design of a Novel Oral Core-Melt Tablet (OCMT) for Enhanced Delivery of Gastro-Sensitive Biotech Drug Molecules. ***(Podium Presentation)***. *School of Therapeutic Sciences Research Day, University of the Witwatersrand, Johannesburg, South Africa, September, 2015.*

Bibi F. Choonara, Yahya E. Choonara, Lisa C. du Toit, Pradeep Kumar, Viness Pillay. Design of a Novel *In Situ* Cross-linked Eutectic Tablet for Enhanced Delivery of Gastro-Sensitive Biotech Drug Molecules. ***(Podium Presentation)***. *Boehringer Ingelheim Young Scientist Competition, The 2015 Academy of Pharmaceutical Sciences of the Pharmaceutical Society of South Africa (APSSA) Conference, CedarWoods Conference Centre, Sandton, Johannesburg, South Africa, September 17-19, 2015.*

Bibi F. Choonara, Yahya E. Choonara, Lisa C. du Toit, Pradeep Kumar, Viness Pillay. Design of a Novel Oral Core-Melt Tablet (OCMT) for Enhanced Delivery of Gastro-Sensitive Biotech Drug Molecules. ***(Poster Presentation)***. *The 2015 AAPS Annual Meeting and Exposition, Orange County Convention Centre, Orlando, Florida, United States of America*, *October 25-29, 2015.*

Bibi F. Choonara, Yahya E. Choonara, Lisa C. du Toit, Pradeep Kumar, Viness Pillay. Design of a Novel *In Situ* Crosslinked Oral Core Melt Tablet (OCMT) for Enhanced Delivery of Gastro-sensitive Proteins and Peptides. ***(Podium and Poster Presentation)***. *7th APS International PharmSci Conference, Technology and Innovation Centre, University of Strathclyde, Glasgow, Scotland, United Kingdom, September 5-7, 2016.*

Appendix 10.2

PATENT FILED

An Oral Pharmaceutical Dosage Form for the Delivery of a Peptide and/or Protein. Bibi F. Choonara, Yahya E. Choonara, Lisa C. du Toit, Pradeep Kumar, Viness Pillay. 26 June 2015. PCT filed-PCT/IB2016/053825.

ABSTRACT

The global pharmaceutical biotechnology industry is continually growing and increased amounts of protein and peptide-based therapeutics are entering into the market. Conventionally, these therapeutic proteins and peptides are administered intravenously, subcutaneously or intramuscularly as oral routes of administration may result in their degradation in the gastrointestinal tract (O' Connor, 2009). The parenteral route limits patient acceptability and convenience. Oral dosage forms, particularly tablets, are considered one of the most common and widely used routes of drug administration and accounts for approximately 50% of all dosage forms on the market (Oh *et al*., 2012). Thus, the development of oral technologies for therapeutic proteins and peptides remain a dynamic research field despite its many challenges. Successful oral delivery of proteins and peptides require the accomplishment of three key tasks: protection of the macromolecules from degradation in the gastrointestinal tract (GIT), permeation through the intestinal barrier and the absorption of molecules into the systemic circulation. Currently, no clinically useful oral formulations have been approved but several attempts have been made to overcome the challenges of low oral bioavailability resulting from poor absorption, poor permeation and enzymatic degradation of the proteins and peptides in the GIT. Present strategies attempt to provide structural protection of the proteins and peptides and improved absorption through the use of enzyme inhibitors, absorption enhancers, novel polymeric delivery systems and chemical modification. However, each of these technologies possesses limitations that preclude the successful oral delivery of proteins and peptides.

The design and development of the novel Tri-functionalized OCMT attempts to breakthrough this market by triple targeting the major challenges governing successful oral delivery of proteins and peptides. Essentially, the Tri-functionalized OCMT is made up of three distinct functional components; the core-eutectic region, the outer polymer shell and the 'smart' polymeric sheet. Triple targeting was achieved by incorporating the bioactive into a core-melt archetype within the tablet and facilitating the process of *in situ* crosslinking which significantly affects the way the bioactive is protected within the compressed tablet matrix as well providing desirable bioactive release kinetics. In addition, the incorporation of a co-inhibitory 'smart' polymeric sheet provided added protection and enabled an improved absorption by virtue of its intrinsic properties and co-inhibition of the major determinants, CYP3A4 and Pgp, of poor absorption and low oral bioavailability. Lastly, targeting of enzymatic degradation was achieved by incorporation of a pH modifier that functions to transiently lower the micro-environmental pH and reduce the optimal environment for enzyme activity.

The combination of the distinct formulatory components contained within the Tri-functionalized OCMT was extensively evaluated through in-depth *in vitro* physicochemical and physicomechanical characterization, *ex vivo* analyses and *in vivo* performance. *In vitro* and *ex vivo* characterization enabled the optimization of design variables and promoted the achievement of desirable functionalities for the attainment of optimum *in vivo* performance. *In vivo* analyses of the Tri-functionalized OCMT in the Large White pig model revealed an enhanced oral bioavailability of the incorporated peptides, octreotide and exenatide, following oral administration, as compared to their conventionally administered subcutaneous counterparts. In addition, pharmacokinetic analysis of the Tri-functionalized OCMT confirmed the maintenance of sustained, therapeutic levels of both octreotide and exenatide over the 24 hour period, supporting a convenient once-daily dosing.

The rate at which protein and peptide-based therapeutics are developing is astounding, and this consequently increases the demand and focus towards achieving a simpler and more effective oral delivery of therapeutic proteins and peptides. The Tri-functionalized OCMT has successfully demonstrated its feasibility in enhancing the oral delivery of therapeutic proteins and peptides up to a preclinical stage. It may potentially serve as a viable alternative to the conventional parenteral route of administration for the treatment of various disease conditions by incorporating a multitude of proteins and peptides into its versatile design. The advancement of the Tri-functionalized OCMT to the clinical stage and beyond may ultimately improve patient outcomes and change the face of therapeutic protein and peptide delivery globally.

ACKNOWLEDGEMENTS

Firstly and most importantly, I would like to thank the Almighty, The All-Knowledgeable, The All-Knowing, without Whom none of this would have been possible, for bestowing upon me His countless blessings and accepting my heartfelt prayers.

I would like to thank my parents, Yunoos Choonara and Rahima Vania, for all the sacrifices they have made, for their unwavering support and love and for always keeping me in their sincerest prayers. I owe my every success to you and I hope I continue to make you proud.

To my sisters, Zainib Choonara, Zakkiyya Choonara and Zaahidah Choonara, words are simply not enough to express my eternal gratitude for your constant love, motivation, support and advice. I finally did it! I am certainly blessed to have sisters like you and I only hope that the bond we share continues to strengthen. Thank you for always keeping me in your prayers. A very special thank you to my sister, Zakkiyya Choonara, for assisting me in every possible way, for listening to my endless complaints and for making this journey so much more easier.

To my adorable nieces and nephews, Ammaarah, Zahraa, Abdur Rahman, Zaynah and Eesa, thank you for being a constant source of joy and a much needed distraction from my work. You are all growing up to be such unique and delightful children. I hope I may inspire you to seek your own path of knowledge and success.

To my supervisor, Professor Viness Pillay, thank you for giving me the opportunity to undertake this research. I have flourished under your excellent mentorship, guidance and invaluable advice. Thank you for always being available to assist in every aspect of my research. Your passion and dedication to the field shines through and you inspire me to achieve greatness.

To my co-supervisor, Professor Yahya Essop Choonara, thank you for pushing me beyond my limits and always expecting me to strive for nothing less than the best. You have enabled me to build great strength of character that will certainly carry me through any challenge that I may face in the future.

To my co-supervisor, Professor Lisa Claire du Toit, thank you for always assisting me with a smile on your face, for always being confident in my abilities and for providing me with much needed motivation and advice. Your quiet strength and shining personality reflects in everything that you do. I am astounded at all your amazing achievements and successes and you certainly encourage me to believe that anything is possible.

To my co-supervisor, Mr. Pradeep Kumar, thank you for dedicating so much of your hard work and time towards assisting me in carrying out my research. Your immense knowledge and unique outlook is second to none. I have learnt so much invaluable knowledge and skills from you and I am thankful that I had your constant support. I wish you continued success in all your future endeavors.

To my closest and dearest friends, Poornima Ramburrun and Karmani Murugan, thank you for all the laughter, motivation, advice, supportive chats and invaluable assistance. Together, the “three musketeers”, we make a formidable team. We embarked on this tremendous journey together, seen it through to its completion and came out stronger on the other side. You certainly made the journey a more memorable one and I will miss you both dearly as we path ways in search of new successes.

I would also like to thank my dear friends Famida Ghulam-Hoosain, Naeema Mayet and Margaret Siyawamwaya for all their support, motivation and assistance.

To my colleagues, Fatema Mia, Mukasa Eliphaz, Az-Zamakshariy Zardad, Derusha Frank, Zikhona Hayiyana, Pakama Mahlamba, Simphiwe Mavuso, Mduduzi Sithole, Gretta Mbitsi-ibouily, Lusanda Mapela, Jonathan Pantshwa, Felix Mashingaidze, Angus Hibbins, Latavia Singh, Thiresen Govender, Khadija Rhoda, Olufemi Akilo, Khuphukile Madida, Sunaina Indermun, Mershen Govender, Nonhlanhla Masina, Mpho Ngoepe, Samson Adeyemi and Pierre Kondiah for all their assistance and support.

To Mr. Sello Ramarumo, Mr. Kleinbooi Mohlabi, Mr. Bafana Temba, Ms. Pride Mothobi and Ms. Phumzile Madondo for their valuable technical assistance and effective running of the laboratories.

To the staff of the Central Animal Services (CAS) at the University of the Witwatersrand, thank you for being an instrumental part of my *in vivo* studies. I am grateful for all your assistance, hard work and dedication towards caring for the animals and facilitating the smooth running of my studies.

To the staff of the Department of Pharmacy and Pharmacology, Mr. David Bayever, Dr. Thashree Marimuthu, Professor Paul Danckwerts and Ms. Nompumelelo Damane, thank you for all your support, motivation and assistance.

A special thank you to Dr. Marketa Toman for your valuable time and unconditional assistance. You thought me the value of perseverance in order to achieve the best possible results.

This research would not have been possible without the financial assistance of the National Research Foundation (NRF) of South Africa, their support is greatly appreciated.

DEDICATION

I dedicate this thesis to the immeasurable hard work undertaken by every scientist in their quest to achieve research success

Science knows no country, because knowledge belongs to humanity,
and is the torch which illuminates the world.
Science is the highest personification of the nation
because that nation will remain the first which carries
the furthest the works of thought and intelligence.

-Louis Pasteur-

TABLE OF CONTENTS

CHAPTER 1

INTRODUCTION AND MOTIVATION FOR STUDY

CHAPTER 2

A REVIEW OF ADVANCED ORAL DRUG DELIVERY TECHNOLOGIES FACILITATING THE PROTECTION AND ABSORPTION OF PROTEIN AND PEPTIDE MOLECULES

CHAPTER 3

A PROOF OF CONCEPT STUDY DEPICTING A MENTHOL-BASED SOLID DISPERSION TECHNIQUE FOR ENHANCED SOLUBILITY AND DISSOLUTION OF SULFAMETHOXAZOLE FROM AN ORAL TABLET MATRIX

CHAPTER 4

PRELIMINARY DESIGN OF AN *IN SITU* CROSS-LINKED EUTECTIC TABLET FOR ENHANCED ORAL PROTEIN AND PEPTIDE DELIVERY

CHAPTER 5

PHYSICOCHEMICAL AND PHYSICOMECHANICAL EVALUATION OF THE STATISTICALLY OPTIMIZED ORAL CORE-MELT TABLET (OCMT)

CHAPTER 6

DESIGN OF THE CO-INHIBITORY 'SMART' POLYMERIC SHEET SURROUNDING A pH-MODIFIED OCMT FOR TRI-FUNCTIONALIZATION

CHAPTER 7

COMPREHENSIVE CHARACTERIZATION OF THE STATISTICALLY OPTIMIZED TRI-FUNCTIONALIZED ORAL CORE-MELT TABLET (OCMT) FOR ENHANCED PROTEIN AND SYNTHETIC PEPTIDE DELIVERY

CHAPTER 8

IN VIVO EVALUATION OF OCTREOTIDE AND EXENATIDE RELEASE FROM THE TRI-FUNCTIONALIZED OCMT IN THE LARGE WHITE PIG MODEL

CHAPTER 9

CONCLUSIONS, RECOMMENDATIONS AND FUTURE OUTLOOK

LIST OF ABBREVIATIONS

OCMT - Oral Core-Melt Tablet

GIT – Gastro-intestinal Tract

CYP3A4 – Cytochrome P450 3A4

Pgp – P-glycoprotein

BCS - Biopharmaceutics Classification System

FCCCD – Face-Centered Central Composite Design

IVIVC – *In vitro-In vivo* Correlation

SMX – Sulfamethoxazole

DSC – Differential Scanning Calorimetry

FTIR – Fourier Transform Infrared Spectroscopy

BHN – Brinell Hardness Number

MDT – Mean Dissolution Time

SHIF – Simulated Human Intestinal Fluid

IV – Intravenous

SC – Subcutaneous

IM – Intramuscular

BSA – Bovine Serum Albumin

MH – Matrix Hardness

MR – Matrix Resilience

DE – Deformation Energy

AUC – Area under the curve

EPB – Eutectic Powder Blend

SEM – Scanning Electron Microscopy

MRI - Magnetic Resonance Imaging

PEO – Polyethylene oxide

BET - Brunauer-Emmett-Teller

BJH – Barrett-Joyner-Halenda

pH_M – pH-modified

MDR – Multi-drug resistant

RFU – Relative Fluorescence Unit

ANOVA – Analysis of Variance

SGF – Simulated Gastric Fluid

ELISA – Enzyme-linked Immunosorbent Assay

MTT – 3-(4, 5-Dimethylthiazol-2-yl)-2, 5-diphenyltetrazolium bromide

MRT – Mean Residence Time

SS – Sum of squares

SE – Standard error

AIC - Akaike's information criterion

SC - Schwarz criterion

LIST OF EQUATIONS

LIST OF FIGURES

LIST OF TABLES

CHAPTER 1

INTRODUCTION AND MOTIVATION FOR STUDY

1.1. Background to the Study

The oral delivery of drugs, particularly tablets, is considered one of the most common and widely used routes of drug administration and accounts for approximately 50% of all dosage forms on the market (Oh *et al*., 2013). Tablets are a safe and cost-effective drug delivery system that provides good physical and chemical stability, high level of patient acceptability and ease of accurate dosing (Al-Hilal *et al.*, 2012). However, oral drug delivery can be particularly challenging when considering the variations that occur in the absorption of a drug due to interactions with food and gastric contents/secretions as well as the varying rates of intestinal transit, gastric emptying and tablet dissolution, particularly with respect to delivery of gastro-sensitive biotech drug molecules (Marques *et al*., 2011). Biotech drug molecules are unlike conventional medicines, in that they are biopharmaceutical agents such as proteins and peptides that are produced using biotechnology (Schellack, 2010). Biotech drugs are primarily administered intravenously, subcutaneously or intramuscularly as oral routes of administration may result in its degradation in the gastrointestinal tract (O' Connor, 2009).

Therapeutic proteins and peptides have gained increased popularity, owing to advances in biotechnology that enables them to be the molecules of choice for multiple disease conditions (Park *et al*., 2011; Chin *et al*., 2012). The industry is continually growing and a multitude of protein and peptide-based medicines are entering into the market, significantly increasing the demand and focus towards achieving simpler and more effective delivery routes. Although significant progress has been made towards the development of oral delivery systems for proteins and peptides, the field is limited by the low membrane permeability of these high molecular mass compounds, as well as their hydrophilicity, instability and rapid enzymatic degradation in the GIT (Donovan *et al*., 1990; Camenich *et al*., 1998; Park *et al*., 2011). Present strategies attempt to provide structural protection of the proteins and peptides and improved absorption through the use of enzyme inhibitors, absorption enhancers, novel polymeric delivery systems and chemical modification (Park *et al*., 2011). However, each of these technologies possesses limitations that prevent their successful delivery. No clinically useful oral formulations have been approved and thus advancements towards successful oral delivery of proteins and peptides through protection and increased absorption remains an active area of research.

The subject of eutectics in polymeric protein delivery systems has not been researched and the microstructure, that is typical of polymer eutectics, has not yet been fully explored as a means of increasing absorption and improving bioavailability of protein and peptide therapeutics (Tuntarawongsa and Phaechamud, 2012). A eutectic mixture is a physical mixture of two crystalline components which are completely miscible in the liquid state but to a very limited extent in the solid state. Eutectics have a melting point that is lower than that of any of the components contained in the mixture (Arnikar *et al.*, 1992; Sharma *et al.,* 2012). A recent study investigated the effects of a borneol/menthol eutectic mixture for enhanced bioavailability in the delivery of a polypeptide (daidzein) used in the treatment of breast and colon cancer (Shen *et al*., 2011). The results from this study depicted the potential use of eutectic mixtures for enhancing the absorption of peptide-based therapeutics.

This research attempts to bridge the gap between the indispensable protein and peptide-based therapies that are available and their safe and effective administration through the pragmatic design of an effective oral delivery system. The proposed Tri-functionalized OCMT may enhance the oral delivery of therapeutic proteins and peptides and possibly provide a viable alternative to the parenteral route of administration by virtue of its characteristic functional components which include; a core eutectic region, an outer polymer shell and a 'smart' polymeric sheet. The premise of the design is based on the achievement of a core eutectic region within a tablet that contains the incorporated protein or peptide and suitable crosslinking agents which provides structural protection and ensures controlled release of the biotech drug molecule due to *in situ* crosslinking within the tablet core, facilitated by the proposed melting of the core eutectic region at body temperature (37°C). Furthermore, the outer polymer shell of the tablet with incorporated pH modifier is expected to facilitate the controlled release of protein and peptide molecules, in addition to influencing the micro-environmental pH. The design of an additional prolamine-based 'smart' polymeric sheet with incorporated cytochrome P450 and P-gp efflux pump intestinal inhibitor may further protect the incorporated protein and peptide and enhance its oral bioavailability. The proposed configuration of the Tri-functionalized OCMT is such that it will enable the site-specific, improved oral delivery of proteins and peptides.

Moreover, the design of the Tri-functionalized OCMT is expected to provide an intrinsic versatility that will enable the incorporation of a multitude of protein and peptide molecules. This could prove to be efficacious in the delivery of biopharmaceuticals such as; enfuvirtide (a synthetic peptide that inhibits the process of HIV-1 entry into the cell), octreotide (used for the

treatment of acromegaly and the symptoms of gastro-intestinal tumours) , cyclosporine (a cyclic peptide that functions as a potent immunosuppressive agent), insulin and exenatide (used in diabetes) and peptide antibiotics such as polymixin and colistin (used for *Pseudomonas aeruginosa* infections) (Edwards *et al*., 1999). In addition, this technology could provide a useful intervention for overcoming some of the challenges of Biopharmaceutics Classification System (BCS) Class drugs including those with low oral bioavailability (<30%), such as the calcium channel blockers (e.g. felodipine and nimodipine) used in the treatment of hypertension and angina (Cadario and Leathem, 2003).

1.2. Rationale and Motivation for this Study

The GIT epithelium acts as a physical and chemical barrier towards the absorption of proteins and peptides (Lee, 2002; Antunes *et al*., 2013). Typically, proteins and peptides possess a high susceptibility to proteolytic enzymes which are present at various regions along the GIT (Zhou, 1994). The acidic nature of the gastric media results in denaturation and degradation of protein molecules through acquisition of similar charges causing internal repulsion or loss of attractive forces that previously held the protein molecule together (Cantor, 1994). Moreover, enzyme activity assists in the hydrolytic, irreversible cleavage of proteins and peptides into amino acids and small, absorbable oligopeptides (Fei *et al*., 1994; Zhou, 1994). Chemical digestion of proteins in the stomach is also triggered by pepsin with minimal absorption due to the small surface area and non-absorptive nature of the epithelium (Lee, 2002). Majority of the absorption occurs within the small intestine, however, pancreatic and brush-border enzymes such as trypsin, chymotrypsin, exopeptidases and endopeptidases contribute to the breakdown of proteins and peptides into non-essential amino acids (Zhou, 1994; Lee, 2002). In addition, cytochrome P450 facilitated metabolism of drug substances and P-glycoprotein mediated efflux of drug molecules from inside the cell back into the intestinal lumen account for the reduced absorption and low oral bioavailability of proteins and peptides (Liu *et al*., 2009).

In addition, the mucosal surface of the GIT is a large interface that is protected by a monolayer of epithelial cells, connected by tight junctions that provide an effective barrier against the absorption of proteins and peptides. Essentially, it represents a physical gatekeeper that selectively restricts the entry of large molecules into the systemic circulation (Neutra and Kraehenbuhl, 1993; Antunes *et al*., 2013). The combination of all these factors lead to the identification of three major challenges governing the successful oral delivery of proteins and peptides which include; 1) the exposure of proteins and peptides to unfavorable conditions

within the GIT 2) poor absorption through the GIT membrane and 3) enzymatic degradation within the GIT (Antunes *et al*., 2013). Thus, the proposed triple targeting by the Tri-functionalized OCMT may prove to be invaluable in overcoming the major challenges governing the successful oral delivery of proteins and peptides.

Figure 1.1a represents a schematic of the OCMT concept depicting the tablet during the formulation stages with the outer shell of the core-melt containing a porous polymer that allows the ingress of fluid, while still maintaining its characteristic shape and enabling *in situ* crosslinking. The outer polymer shell will undergo surface erosion, facilitating the controlled release of drug molecules as depicted in the insert. The characteristic feature of the eutectic component within the core-melt region of the tablet enables it to remain solid at room temperature and melt upon entering the body at temperatures of 37°C. This proposed melting in combination with the ingress of fluid through the outer polymer shell facilitates the process of *in situ* crosslinking within the tablet core. The *in situ* crosslinking will facilitate prolonged drug delivery due to formation of bonds between the salt and polymer chains resulting in a slower chain relaxation within polymer networks due to crosslinks, thereby initiating a delayed bioactive release profile (Hennink and van Nostrum, 2002). Furthermore, the components of the eutectic region are expected to enhance the permeation of drug across the intestinal tissue. Figure 1.1b depicts the tablet during compression where the bottom layer of the shell surrounding the core-melt matrix will be compressed under low pressure and the top layer under high pressure to form a single tablet with an inner core-melt matrix as shown in Figure 1.1c.

Moreover, the incorporation of a pH modifier facilitates indirect inhibition of enzyme activity at the brush border by transiently lowering the micro-environmental pH and subsequently reducing the optimal environment for enzyme activity. Further encapsulation of the OCMT with a co-inhibitory prolamine-based ‘smart’ polymeric sheet possessing hydrophobic, mucoadhesive, lipid-binding characteristics and interacting well with hydrophilic molecules (i.e. proteins and peptides) will function to enable passage of the proteins and peptides through the GIT membrane. The sheet provides a protective function within the stomach and has sustained release capabilities in direct tablet compression. Cytochrome P450 enzymes are responsible for metabolism of drug substances with the most potent enzyme being CYP3A4 which are at levels in the small intestine of generally 10-15% of those found in the liver. Additionally, the Pgp (P-glycoprotein) efflux pump is an ATP dependent transmembrane pump that actively transports molecules out of the cell. Both CYP3A4 and Pgp account for the reduced absorption and low

oral bioavailability of proteins and peptides. Thus, co-inhibition of CYP3A4 and Pgp will enable increased absorption by reducing the metabolism and inhibiting transmembrane efflux.

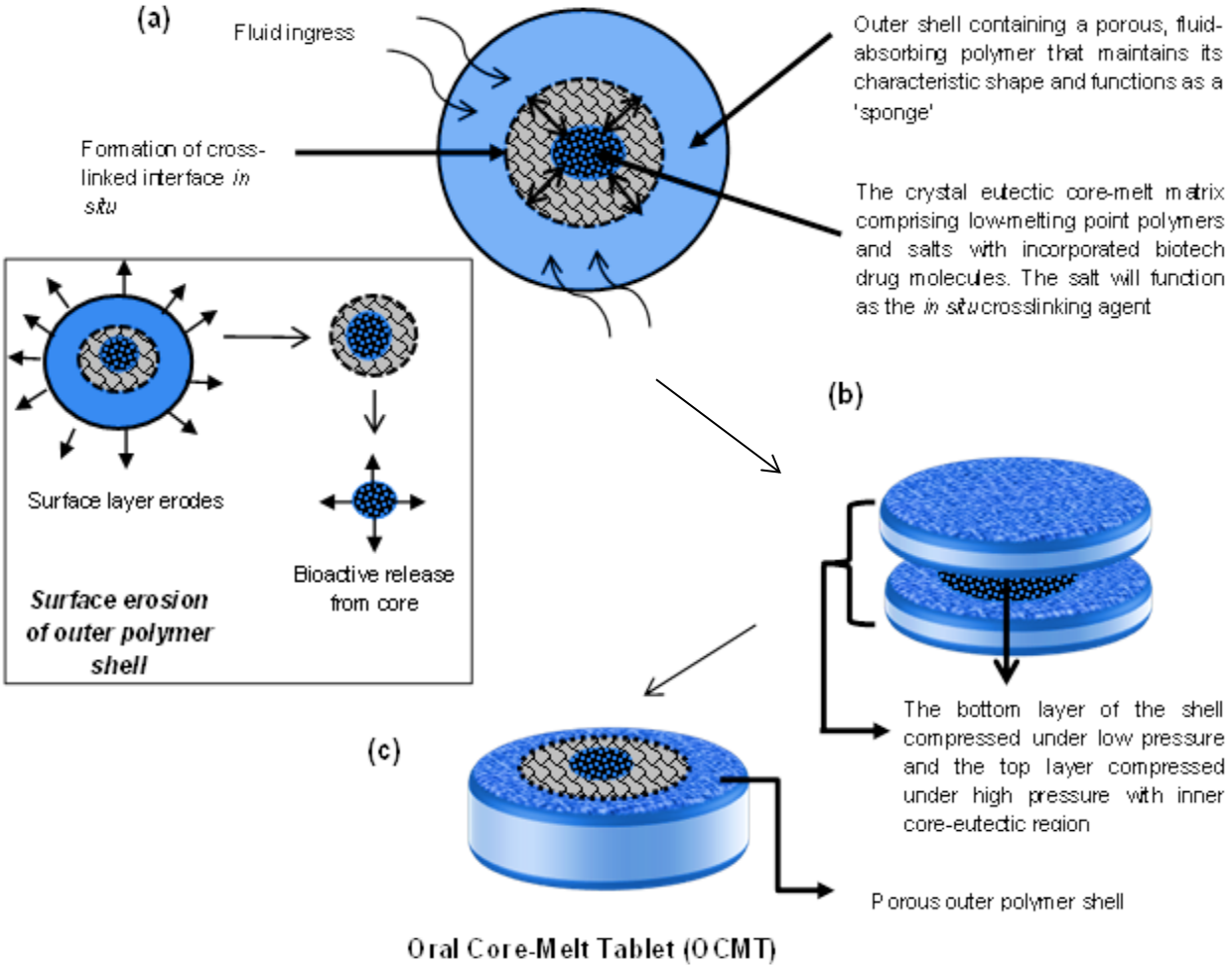

Figure 1.1: Schematic representation of the OCMT that is shown in **a)** in the formulation stages **b)** during compression and **c)** after compression, *in situ.*

While the OCMT provides critical structural protection, the incorporation of a pH modifier and a co-inhibitory 'smart' polymeric sheet may overcome the enzymatic degradation at the brush border and the poor absorption through the GIT membrane. This results in the formation of a Tri-Functionalized 'Smart' Polymer Modulated Co-inhibitory (Cytochrome P450 and P-glycoprotein) pH Modified Oral Core-Melt Tablet (OCMT), as shown in Figure 1.2, that aims to collectively and optimally target the three major challenges governing successful oral protein and peptide delivery. This device ultimately creates a platform for the structural protection of the incorporated protein and peptide, control of enzymatic degradation and improvement in the absorption of the incorporated protein or peptide by up to 70-90%.

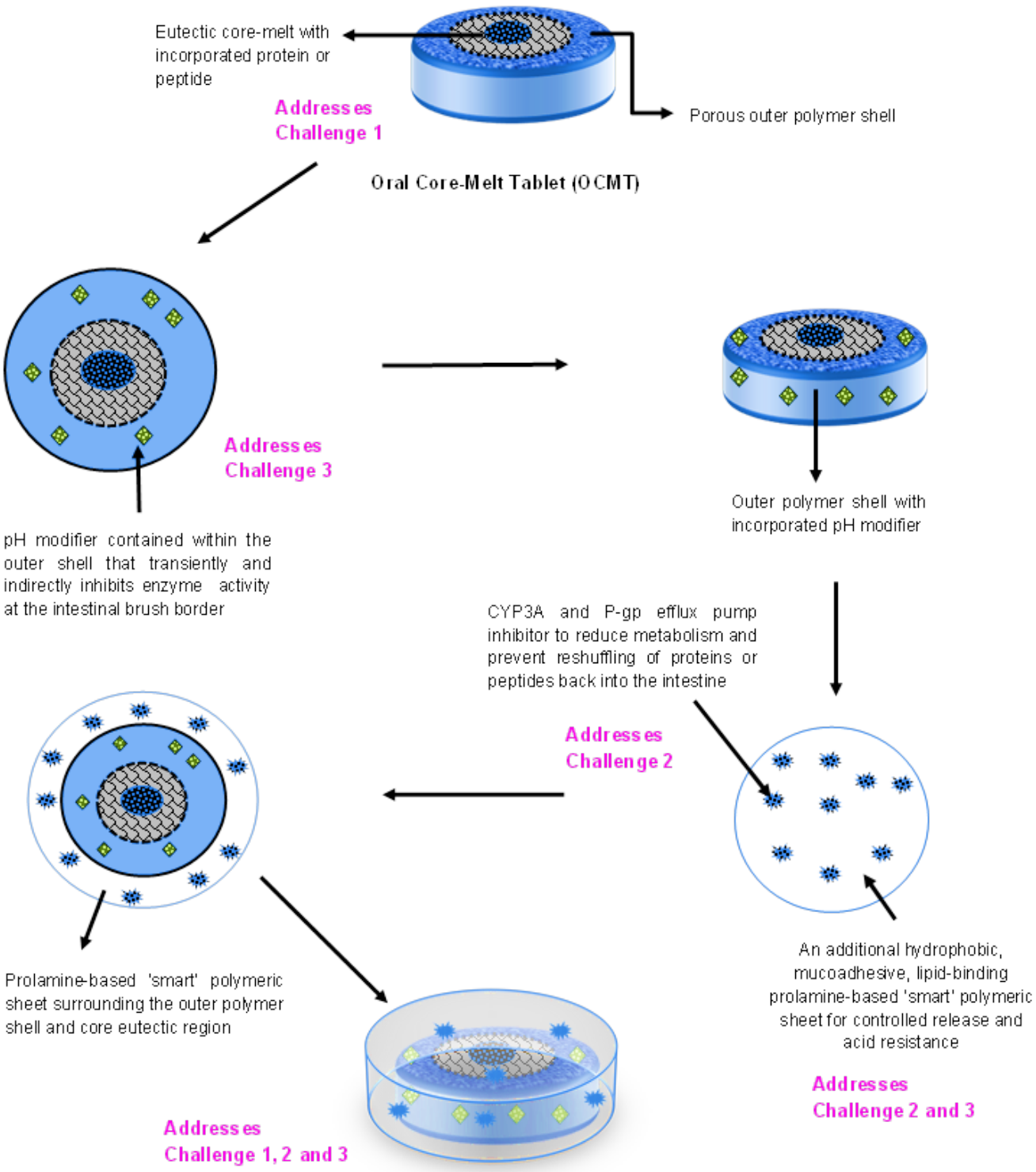

Figure 1.2: Schematic representation of the Tri-functionalized OCMT, highlighting the different components and the challenges they address.

1.3. Mechanism by which the Tri-functionalized OCMT will Achieve Enhanced Delivery of Gastro-sensitive Proteins and Synthetic Peptides

The mechanism of action of the Tri-functionalized OCMT is critical towards understanding the impact of different components and their functional effects. The proposed mechanism of action of the entire system from ingestion of the tablet right through to its passage along the GIT and ultimate absorption is illustrated in Figure 1.3.

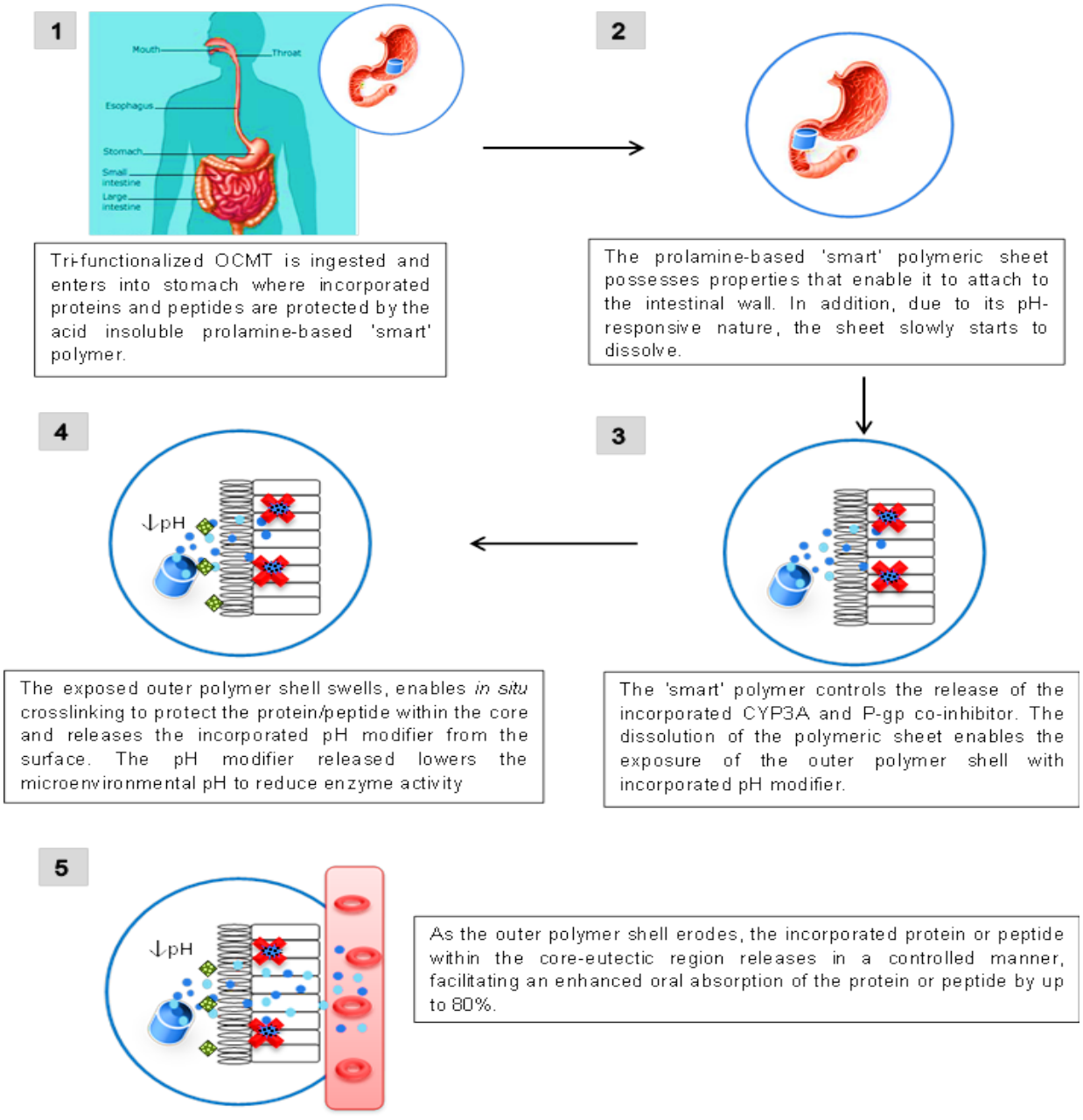

Figure 1.3: Diagrammatic representation of the proposed *modus operandi* of the Tri-Functionalized OCMT.

1.4. Novelty of the Study

The novelty of the study lies in its characteristic ability to enhance the oral delivery of protein and peptides by the achievement of a Tri-functionalized component system. It provides a unique core-eutectic region in the tablet that enables the incorporation of proteins and peptides. In addition, it provides a platform for controlled release and enhanced protein and peptide protection by facilitating *in situ* crosslinking between the outer polymer shell and the core-eutectic region. The initiation of *in situ* crosslinking by a combination of the melting of the crosslinker-containing core eutectic region at 37°C, as well as fluid ingress into the outer polymer shell further supports its innovativeness. The novelty of the system is further extended by the incorporation of a micro-environmental pH modifier and a co-inhibitory 'smart' polymeric sheet. Ultimately, the conceptualized design characteristics will innovatively associate to provide an orally bioavailable, sustained release of the incorporated protein and peptide that will potentially serve as a unique alternative to the conventional parenteral route of administration for the treatment of multiple disease conditions.

1.5. Possible Therapeutic Applications of the Delivery System

A recent report by the Pharmaceutical Research and Manufacturers of America (PhRMA) on "Biologic Medicines in Development" identified over 900 protein and peptide-based medicines in development, targeting more than 100 diseases, of which 353 for cancer and related conditions, 187 for infectious diseases, 69 for autoimmune diseases and 59 for cardiovascular diseases. Thus, this expands on the potential of the Tri-functionalized OCMT to possibly target a multitude of disease conditions that require treatment with protein and peptide-based therapeutics. In addition, due to its proposed ability to enhance oral absorption, it can possibly improve the clinical outcomes of BCS Class drugs and those with oral bioavailabilities of <30%. Furthermore, the versatility of the device enables easy adaptability for the incorporation of drugs requiring controlled release over extended periods of time.

1.6. Aim and Objectives

The aim of this study is the design of a Tri-Functionalized 'Smart' Polymer Modulated Co-inhibitory (Cytochrome P450 and P-glycoprotein) pH Modified Oral Core-Melt Tablet (OCMT) for enhanced oral delivery of gastro-sensitive proteins and peptides through the mechanistic action of characteristic functional components, serving to expand the limited number of available administration methods for these sensitive molecules. Accomplishment of the following objectives was critical towards the fulfilment of the aim:

1. To design and formulate the OCMT through the process of eutectic formation, *in situ* crosslinking initiator selection and component assemblage.
2. To characterize the OCMT via physicochemical and physicomechanical tests, including advanced bench-top Magnetic Resonance Imaging, porositometric analysis, textural profiling, thermal analysis and rheological characterization to determine matrix durability and tensile strength.
3. To design a co-inhibitory 'smart' polymeric sheet surrounding a pH-modified OCMT to achieve Tri-functionalization, ultimately producing the Tri-functionalized OCMT, for enhanced oral delivery of gastro-sensitive proteins and peptides via structural protection, enhanced absorption and prevention of enzymatic degradation.
4. To comprehensively analyze the *in vitro* capabilities of the Tri-functionalized OCMT through extensive physicochemical and physicomechanical profiling, *in vitro* bioactive release analysis, extensive cellular characterization and cytotoxicity determinations.
5. Following the successful design and testing of the prototype Tri-functionalized OCMT and its ability to meet design criteria *in vitro*, its clinical potential was assessed in the Large White Pig to determine the *in vivo* release mechanisms, pharmacokinetics and the establishment of an *in vitro-in vivo* correlation.

1.7. Synopsis of the Thesis

The thesis was deconstructed as follows to provide a logical and rational overview of the processes involved in the design and development of the Tri-functionalized OCMT.

Chapter 1 provides an introduction and background to this study, highlighting the rationalization and novelty of the research undertaken, as well as the aim and objectives and potential benefit of this study.

Chapter 2 critically reviews the advanced oral drug delivery technologies facilitating the protection and absorption of protein and peptide molecules. It discusses current approaches to overcome GIT absorption barriers and assimilates the non-parenteral routes of protein and peptide delivery. Furthermore, the chapter critically elaborates on the advanced oral macromolecular technologies developed and in clinical trials, as well as providing an analysis of their inherent pharmacokinetic profiles. Lastly it outlines future challenges and opportunities for ideal oral protein and peptide delivery.

Chapter 3 presents the results obtained from a proof-of-concept study depicting a menthol-based solid dispersion technique for enhanced solubility and dissolution of drug from an oral tablet matrix. The chapter characteristically demonstrates the ability of menthol to improve the solubility of a poorly soluble drug and control the release rate from an oral tablet matrix. In addition, it conclusively highlights the possibility of a menthol-based eutectic transformation.

Chapter 4 takes it cue from the previous chapter and leads to the synthesis of a menthol-based eutectic powder blend for the preliminary design of an *in situ* cross-linked eutectic tablet for enhanced oral protein and peptide delivery. The chapter investigates the attributes of the *in situ* cross-linked eutectic tablet through establishment of a Box-Behnken experimental design. Extensive physicochemical and physicomechanical characterization, as well as the *in vitro* release of a model protein from the eutectic tablet is presented. Furthermore, statistical optimization via response surface analysis was undertaken.

Chapter 5 alludes to the characterization of the optimized OCMT, following statistical optimization of the eutectic tablet in Chapter 3 and the subsequent incorporation of a therapeutic peptide. The chapter highlights the *in vitro* physicochemical and physicomechanical characterization of the optimized OCMT and its pertinent characteristics in achieving an ideal *in vitro* profile for optimum *in vivo* performance.

Chapter 6 describes the preparation of the co-inhibitory 'smart' polymeric sheet surrounding the pH-modified OCMT for Tri-functionalization. The applicability of the components were assessed through the establishment of a Face-Centered Central Composite Design (FCCCD). Physicochemical and physicomechanical characterization was undertaken to explicate the delivery of the advanced components. In addition, the chapter determines the optimum concentration required for co-inhibition of CYP3A4 and Pgp. A response surface analysis, embodied by the FCCCD design, was undertaken to optimize the system.

Chapter 7 follows from the intensive device optimization by providing a comprehensive characterization of the statistically optimized Tri-functionalized OCMT for ultimate enhancement of oral protein and peptide delivery. The chapter elucidates on the *modus operandi* by in-depth analysis of the pertinent physicochemical and physicomechanical properties. Furthermore, cytotoxicity studies were undertaken to determine the safety of the synthesized device

components. Ultimately, this chapter provides a summative assessment of the prototype device prior to evaluating its performance *in vivo.*

Chapter 8 details the *in vivo* evaluation of peptide release from the Tri-functionalized OCMT in the Large White Pig model. The chapter includes a comparative analysis of the Tri-functionalized OCMT with the conventional, marketed formulations. Moreover, comprehensive pharmacokinetic analysis was undertaken and an *in vitro-in vivo* correlation (IVIVC) was established.

Chapter 9 presents the conclusions drawn regarding the success of the investigation, followed by the recommendations for scale-up and manufacture and further investigations required to bring to fruition the commercial potential of the Tri-functionalized OCMT.

1.8. Concluding Remarks

This chapter highlighted the need for overcoming the limitations associated with the oral delivery of proteins and peptides, owing to widespread use of these biotech drug molecules for the treatment of multiple disease conditions. The overall design strategy and rationalization for development of a prototype oral system was presented. In summary, this investigation is centered on the design of a Tri-functionalized OCMT that would collectively and optimally target the three major challenges governing successful oral protein and peptide delivery.

Reviewing oral protein and peptide technologies before ensuing with experimental device synthesis is important as it provides crucial insight into the possibility for modification and improved functionalization. Ultimately, it creates a platform for the fabrication of a device with unique characteristics. Thus, the following chapter attempts to identify, unravel and critically analyze these technologies.

1.9. References

Al-hilal, T.A., Alam, F., Byun, Y. (2012). Oral drug delivery systems using chemical conjugates or physical complexes. *Advanced Drug Delivery Reviews.* In Press (DOI: 10.1016/j.addr.2012.11.002).

Antunes, F., Andrade, F., Ferreira, D., Nielson, H.M., Sarmento, B. (2013). Models to Predict Intestinal Absorption of Therapeutic Peptides and Proteins. *Current Drug Metabolism*, 14, 4-20.

Arnikar, A.J., Kadam, S.S., Gujar, K.N. (1992). *Essentials of Physical Chemistry and Pharmacy*. Bombay: Orient Longman Limited. pp. 1-6.

Cadario, B.J., Leathem, A.M. (2003). *Drug Information Reference*, Vancouver: BC Drug and Poison Information Centre.

Camenich, G., Alsenz, J., van de Waterbeemd, H., Folkers, G. (1998). Estimation of permeability by passive diffusion through Caco-2 cell monolayers using the drugs' lipophilicity and molecular weight. *European Journal of Pharmaceutical Sciences*, 6, 317-24.

Cantor, C.R. (1994). *Protein Purification: Principles and Practice*. New York: Springer Science. pp. 95-100.

Chin, J., Mahmud, K.A.F., Kim, S.E., Park, K., Byun, Y. (2012). Insight of current technologies for oral delivery of proteins and peptides. *Drug Discovery Today Technologies*, 9, 105-12.

Donovan, M.D., Flynn, G.L., Amidon, G.L. (1990). Absorption of polyethylene glycols 600 through 2000: the molecular weight dependence of gastrointestinal and nasal absorption. *Journal of Pharmaceutical Research*, 7, 863-68.

Edwards, C.M.B., Cohen, M.A., Bloom, S.R. (1999). Peptides as drugs. *International Journal of Medicine,* 92, 1–4*.*

Fei, Y.J., Kanai, Y., Nussberger, S., Ganapathy, V., Leibach, F.H., Romero, M.F., et al. (1994). Expression cloning of a mammalian proton-coupled oligopeptide transporter. *Nature*, 368, 563-66.

Hennink, W.E., van Nostrum, C.F. (2002). Novel crosslinking methods to design Hydrogels, *Advanced Drug Delivery Reviews*, 54, 13–36.

Lee, J.H. (2002). Protein Drug Oral Delivery: The Recent Progress. *Archives of Pharmaceutical Research*, 25, 572-84.

Liu, Z., Wang, S., Hui, M. (2009). *Oral Absorption Basics: Pathways, physico-chemical and biological factors affecting absorption*. Oxford: Elsevier Science and Technology. pp. 265-88.

Marques, M.R.C., Loebenberg, R., Almukainzi, M. (2011). Simulated Biological Fluids with Possible Application in Dissolution Testing. *Dissolution technologies,* 60, 15-28.

Neutra, M.R., Kraehenbuhl, J.P. (1993). *Transepithelial Transport of Proteins by Intestinal Epithelial Cells.* New York: Plenum Press, pp. 107-22.

O' Connor, A. (2009). *Introduction to biotech drugs*, North Carolina: Regulatory Rapporteur.

Oh, T., Kim, J., Ha, J., Chi, S., Rheeb, Y., Park, C., Park, E. (2013). Preparation of highly porous gastroretentive metformin tablets using a sublimation method. *European Journal of Pharmaceutics and Biopharmaceutics,* 83*,* 460-467.

Park, K., Kwan, I.C., Park, K. (2011). Oral protein delivery: Current status and future prospect. *Reactive and Functional Polymers*, 71, 280-87.

Schellack, G. (2010). *Pharmacology in clinical practice: application made easy for nurses and allied health professionals*, 2nd edition, Claremont: Juta and Company. pp. 23-34.

Sharma, J.P.K., Bansal, S., Banik, A. (2012). Noninvasive Routes of Proteins and Peptides Drug Delivery. *International Journal of Pharmaceutical Sciences*, 4, 367-75.

Shen, Q., Li, X., Li, W., Zhao, X. (2011). Enhanced intestinal absorption of Daidzein by borneol/menthol eutectic mixture and microemulsion. *AAPSPharmSciTech*, 12, 1044-1049.

Tuntarawongsa, S., Phaechamud, T. (2012). Polymeric Eutectic Drug Delivery System. *Journal of Medicine*, 22, 27-32.

Zhou, X.H. (1994). Overcoming enzymatic and absorption barriers to non-parenterally administered protein and peptide drugs. *Journal of Controlled Release*, 29, 239-52.

CHAPTER 2

A REVIEW OF ADVANCED ORAL DRUG DELIVERY TECHNOLOGIES FACILITATING THE PROTECTION AND ABSORPTION OF PROTEIN AND PEPTIDE MOLECULES

Published in Biotechnology Advances

Bibi F. Choonara, Yahya E. Choonara, Pradeep Kumar, Divya Bijukumar, Lisa C. du Toit, Viness Pillay. A Review of Advanced Oral Drug Delivery Technologies Facilitating the Protection and Absorption of Protein and Peptide Molecules. Biotechnology Advances, 2014, 32, 1269–1282.

Abstract

The oral delivery of proteins and peptides is a dynamic research field despite the numerous challenges limiting their effective delivery. Successful oral delivery of proteins and peptides requires the accomplishment of three key tasks: protection of the macromolecules from degradation in the gastrointestinal tract (GIT), permeation through the intestinal barrier and absorption of molecules into the systemic circulation. Currently, no clinically useful oral formulations have been developed but several attempts have been made to overcome the challenges of low oral bioavailability resulting from poor absorption, poor permeation and enzymatic degradation of the proteins and peptides in the GIT. Present strategies attempt to provide structural protection of the proteins and peptides and improved absorption through the use of enzyme inhibitors, absorption enhancers, novel polymeric delivery systems and chemical modification. However, each of these technologies has their limitations despite showing positive results. This review attempts to discuss the physical and chemical barriers of the GIT with particular emphasis on the current approaches employed to overcome these barriers, including the evaluation of other non-parenteral routes of protein and peptide delivery. In addition, this review assimilates oral formulation strategies under development and within the clinical trial stage in relation to their benefits and drawbacks with regards to facilitating optimal protection and absorption of proteins and peptides, as well as pertinent future challenges and opportunities governing oral drug delivery.

Keywords: oral drug delivery; therapeutic proteins and peptides; bioavailability; gastrointestinal barrier; advanced oral biotechnology

2.1. Introduction

The oral delivery of proteins and peptides, although a highly attractive approach, remains a significant challenge in drug delivery technology, as a result of their unfavorable physicochemical properties (Catnach *et al.,* 1994; Hamman *et al.,* 2005; Park *et al.*, 2011). Administering drugs by the oral route is preferred due to its improved convenience and patient compliance (Brayden and O'Mahony, 1998; Park *et al.*, 2011). However, oral drug delivery can be particularly challenging when considering the variations that occur in the absorption of a molecule due to interactions with gastric contents/secretions, membrane permeability, intestinal transit and gastric emptying. This is particularly with respect to the delivery of sensitive proteins and peptides (Marques *et al.*, 2011).

Therapeutic proteins and peptides are gaining increased popularity, owing to advances in biotechnology that enables them to be the molecules of choice for an assortment of diseases (Park *et al.*, 2011; Chin *et al.*, 2012). The high specificity and activity of proteins and peptides makes them applicable for targeted delivery in clinical practice (Brayden and O'Mahony, 1998; Park *et al.*, 2011; Chin *et al.*, 2012). The new 2013 Pharmaceutical Research and Manufacturers of America (PhRMA) report on "Biologic Medicines in Development" identified over 900 protein and peptide-based medicines in development, targeting more than 100 diseases, of which 353 for cancer and related conditions, 187 for infectious diseases, 69 for autoimmune diseases and 59 for cardiovascular diseases. This significantly increases the demand and focus towards achieving effective and simple routes of delivering proteins and peptides via the oral route.

Conventionally, therapeutic proteins and peptides are administered intravenously, subcutaneously or intramuscularly since the oral route of administration may result in degradation in the gastrointestinal tract (GIT) (O' Connor, 2009; Schiffter, 2011). Although significant progress has been made towards the development of oral delivery systems for proteins and peptides, the field is limited by the low membrane permeability of these high molecular mass compounds, as well as their hydrophilicity, instability and rapid enzymatic degradation in the GIT (Donovan *et al*., 1990; Camenich *et al.*, 1998; Park *et al*., 2011). Proposed technologies and approaches targeting the complications in the oral delivery of proteins and peptides although useful in some instances, nevertheless hold limitations that enable successful delivery (Park *et al*., 2011).

Therapeutic proteins and peptides have gained a significant market interest owing to their increased development and applicability to multiple disease conditions (Park *et al.*, 2011; Chin *et al.*, 2012). Consequently, advancements towards successful oral delivery of proteins and peptides through protection and increased absorption remains an active area of research and researchers have intensified their research towards achieving this goal (Chiasma Inc.; Cosmo Pharmaceuticals, Inc.; Diabetology Ltd.; Emisphere Technology, Inc.; Enteris BioPharma, Inc; Merrion Pharmaceuticals, Ltd.; Oramed Pharmaceuticals, Inc.; Proxima Concepts, Ltd; Tarsa Therapeutics, Inc). This review article summarizes the major challenges facing oral protein and peptide delivery as well as the various attempts at overcoming these challenges. Current and new technologies within this dynamic field of research will be discussed, including the potential benefits of each technology and possible limitations that exist. Potential for improvement is a key focus in the development of new formulation strategies and technologies.

2.2. The Gastrointestinal Barrier: A Physical and Chemical Impediment to Oral Protein and Peptide Delivery

The GIT epithelium acts as a physical and chemical barrier towards the absorption of proteins and peptides (Lee, 2002; Antunes *et al.*, 2013). The mucosal surface of the GIT is a large interface that is protected by a monolayer of epithelial cells, connected by tight junctions that provides an effective barrier against the absorption of proteins and peptides and thus, represents a physical gatekeeper that selectively restricts the entry of large molecules into the systemic circulation (Neutra and Kraehenbuhl, 1993; Antunes *et al*., 2013). Owing to the large molecular mass and hydrophilic properties of proteins and peptides, transport across the intestinal epithelium becomes extremely challenging (Lee, 2002). Nevertheless, studies have suggested that the transport of macromolecules across the intestinal epithelium is possible provided that there is minimal degradation of the protein or peptide molecule in the GIT through the use of permeation enhancers, physicochemical modification strategies and stimuli-responsive and mucoadhesive polymeric systems. (Lundin and Vilhardt, 1986; Takaori *et al.,* 1986; Walker *et al.,* 1990).

2.2.1. The GIT as a physical barrier for protein and peptide absorption

The possible mechanisms by which proteins and peptides are absorbed from the GIT include passive transport, active transport and endocytosis (Potocky *et al.,* 2003; Artursson *et al.*, 2007). The passive transport of molecules across the intestinal membrane occurs through simple or facilitated diffusion, along a concentration gradient, independent of chemical energy

and principally dependent on the intrinsic physicochemical properties of the transported molecule, including its ability to diffuse across cellular barriers (Stein, 1986). The low lipophilicity and large molecular mass of proteins and peptides limits its absorption by this mechanism. However, it proves beneficial for the absorption of di/tripeptides (Catnach *et al.,* 1994). In contrast, active transport of molecules is a process involving chemical expenditure, occurring against a concentration gradient for the transport of molecules across the GIT epithelium (Stein, 1986). Lastly, molecules may be transported through endocytosis which is an energy-consuming process involving the engulfment of molecules for absorption (Potocky *et al.,* 2003; Artursson *et al.*, 2007).

The pathways available for the potential transport of proteins and peptides through these mechanisms include the transcellular pathway and paracellular route as shown in Figure 2.1 (Ménard *et al.,* 2012). The transcellular pathway involves the transport of molecules across cells which can take place by either passive diffusion, a specific carrier or through trancystosis and receptor-mediated endocytosis (Ménard *et al.,* 2012). Transcellular passive diffusion is dependent on the physico-chemical properties of the molecule such as size, charge and lipophilicity in order to facilitate the passive flux of molecules through the lipophilic, apical and basolateral membranes of the intestinal epithelium (Liu *et al.,* 2009). Molecules may also be absorbed transcellularly using specific carriers such as peptide and amino acid transporters that transport molecules such from the intestinal lumen into the cell (Liu *et al.,* 2009; Antunes *et al.,* 2013).

Intact di- and tripeptides can be actively transported for absorption in the small intestine by specific carrier systems, distinctive from the typical amino acid transporters (Catnach *et al.*, 1994). The intestinal peptide carrier has an extensive substrate specificity that is energized by an internal proton gradient resulting in the transfer of a positive charge across the intestinal epithelium (Ganapathy *et al.,* 1985; Takuwa *et al.,* 1985). Studies undertaken on peptide mimetic drugs such as cyclosporine, β-lactams and angiotensin-converting enzyme inhibitors also displayed positive evidence for their transport by di- and tripeptide carriers (Nakashima *et al.,* 1984; Sinko and Amidon, 1988; Friedman and Amidon, 1989; Kramer *et al.,* 1990). The intestinal peptide system has an unrecognized potential for the transport of peptide and peptide-like drugs across the intestinal membrane and a greater understanding of its molecular specificity could prove to be favorable for the synthesis of orally active peptides (Bai and Amidon, 1992). However, compounds that are absorbed through the transcellular pathway are

substrates for p-glycoprotein-mediated efflux which transports the molecules from inside the cell back into the intestinal lumen (Liu *et al.,* 2009). The lipophilicity of a molecule is one of the main factors that governs transport via the transcellular route as molecules need to pass through the lipid bilayer of the intestinal membrane and thus, the transport of proteins and peptides through this pathway poses a significant challenge.

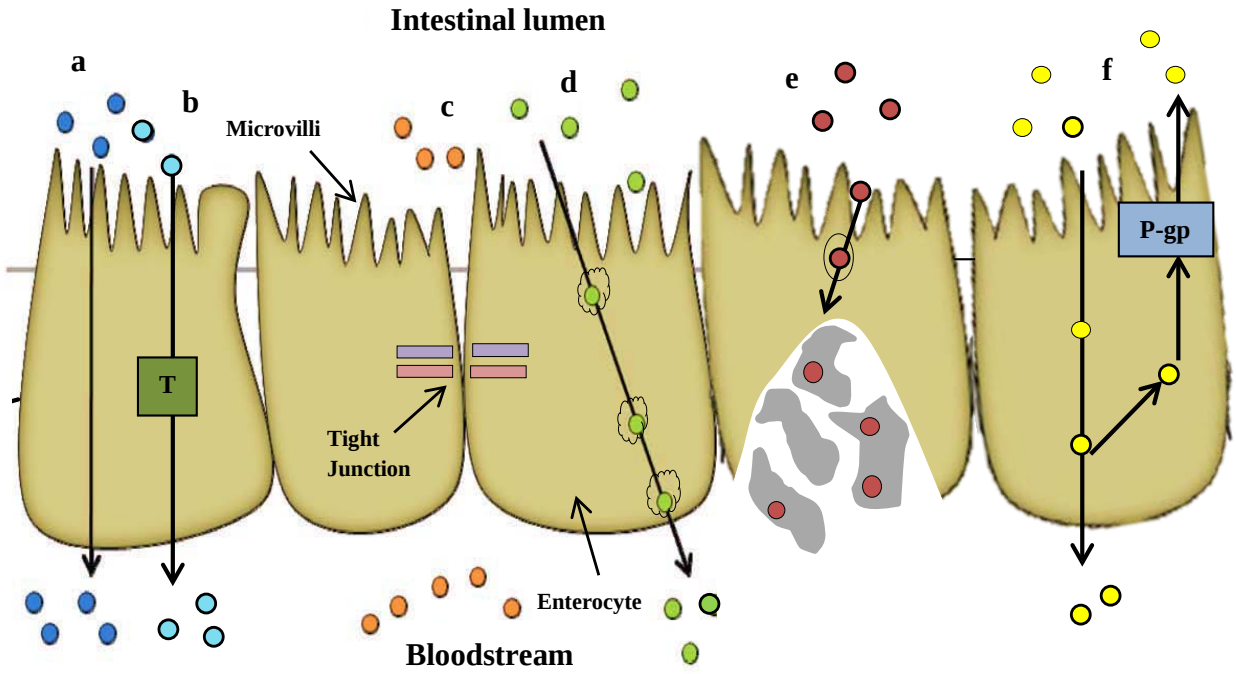

Figure 2.1: Schematic of the multiple transport mechanisms through the intestinal epithelium and pathways available for protein and peptide absorption, **a)** transcellular transport via passive cellular diffusion, **b)** carrier-mediated transport, **c)** paracellular transport via cell-cell junctions, **d)** transcytosis and receptor-mediated endocytosis, **e)** absorption into lymphatic circulation via M-cells of Peyer's patches and **f)** p-glycoprotein efflux of drug into the intestinal lumen [Adapted from Goldberg and Gomez-Orellana, 2003 with permission from Macmillan Publishers Ltd. © 2003 and from Li, 2001 with permission from Elsevier Science Ltd. © 2001].

The transepithelial transport of macromolecules by intestinal epithelial cells occurs to a limited extent through absorption into the lymphatic circulation via M-cells of Peyer's patches (Neutra and Kraehenbuhl, 1993). The surface of the M-cells are densely populated with microvilli and contain limited lysosomes, making it readily accessible to proteins and peptides and enabling the intact transport of macromolecules with minimal degradation during transit through the cells (Ho *et al.*, 1990; Takeuchi and Gonda, 2004). Furthermore, the close proximity of the lymphocytes to the M-cells, as well as, to the apical surface of the intestinal membrane reduces the resident pathway for absorption of macromolecules (Ho *et al.*, 1990). Absorption through

Peyer's patches appears to be a promising mechanism, however, limited information is available regarding the quantities of proteins and peptides that are absorbed through this route (Shakweh *et al.,* 2005).

Absorption via the paracellular route is typically restricted by the narrow space between adjacent enterocytes and the presence of tight junctions that are implicated in the adherence mechanism between adjacent cells (Stevenson and Keon, 1998; Baum and Georgiou, 2011; Oda and Takeichi, 2011). The paracellular pathway does not rely as much on the lipophilicity and hydrogen bonding capacity of molecules compared with the transcellular pathway as it inherently involves the transport of peptides across the aqueous channels in cell junctions (Oda and Takeichi, 2011). However, the paracellular route is not an ideal option for the absorption of macromolecules as it is restricted to relatively small hydrophilic molecules of <100-200 daltons (Rubas *et al.,* 1996; Antunes *et al.,* 2013). The addition of a novel functionality to the protein and peptide molecules or the use of novel delivery systems may be necessary to enable optimal absorption (Catnach *et al.,* 1994; Wang and Zhang, 2004).

2.2.2. The GIT as a chemical barrier for protein and peptide absorption

The fluid contents of the GIT, the functioning environment and the secretion of degradative enzymes are major factors that make oral delivery of proteins and peptides tremendously challenging (Lee, 2002). Proteins possess a high susceptibility to proteolytic enzymes which are present at various regions along the GIT (Zhou, 1994). The acidic nature of the gastric media results in denaturation and degradation of protein molecules through acquisition of similar charges causing internal repulsion or loss of attractive forces that previously held the protein molecule together (Cantor, 1994). Moreover, enzyme activity assists in the hydrolytic, irreversible cleavage of proteins and peptides into amino acids and small, absorbable oligopeptides (Fei *et al.,* 1994; Zhou, 1994). Chemical digestion of proteins in the stomach is also triggered by pepsin with minimal absorption due to the small surface area and nonabsorptive nature of the epithelium (Lee, 2002). Majority of the absorption occurs within the small intestine, however, pancreatic and brush-border enzymes such as trypsin, chymotrypsin, exopeptidases and endopeptidases contribute to the breakdown of proteins and peptides into non-essential amino acids (Zhou, 1994; Lee, 2002).

2.3. Potential Sites for Non-Parenteral Delivery of Proteins and Peptides

Possible non-parenteral administration routes for the delivery of protein and peptides include the nasal, buccal, vaginal, rectal, transdermal, pulmonary, ocular and oral routes of delivery (Zhou and Li Wan Po, 1991; Antosova *et al.,* 2009). The parenteral administration of proteins and peptides is necessary for achieving a therapeutic outcome. However, low patient acceptability and tolerance towards continuous intramuscular, intravenous or subcutaneous injections has led to poor patient compliance an increased interest in alternative extra-parenteral protein and peptide delivery systems (Zhou, 1994).

Permeation enhancers, enzyme inhibitors and appropriate formulation vehicles are essential in the application of non-invasive routes as the absence thereof makes them much less effective as compared to the parenteral route of administration (Banga and Chien, 1988; Sharma *et al.,* 2011). Therapeutic proteins and peptides are conventionally designed for parenteral administration, primarily relying on bypassing first pass metabolism (Fogueri and Singh, 2009). Thus, non-parenteral routes for the delivery of proteins and peptides need to be evaluated for their ease of development, impact on the physicochemical properties of the molecules and bioavailability and toxicity of their individual routes. Table 2.1 summarizes the various non-parenteral routes for protein and peptide delivery, their bioavailability, proteolytic barriers and the various challenges in delivery through each route.

Non-parenteral routes of delivery possess low bioavailability and display various challenges in the successful delivery of proteins and peptides. Regardless of these challenges, the oral route of delivery still holds preference over other non-parenteral routes for systemic administration of active compounds as it is the most acceptable and convenient for the patient (Brown, 2005). The non-parenteral oral delivery of therapeutic proteins and peptides is by far the most popular route of delivery, making it an active area of research for many researchers and academic laboratories and is therefore the focus of this review (Zhou and Li Wan Po, 1991).

Table 2.1: Summary of the various challenges facing the delivery of proteins and peptides through non-parenteral routes.

Routes of delivery	Bioavailability	Proteolytic barrier	Challenges in delivery	References
Nasal	Variable bioavailability (<1%; >30%)	Enzyme leucine aminopeptidase ↓ bioavailability of protein/peptide drugs	Requires the use of permeation enhancers, enzyme degradation, variable absorption, nasal mucosal irritation following prolonged use	Zhou and Li Wan Po, 1991; Valensi *et al.,* 1996; Taylor, 1997; Brown, 2005; Fogueri and Singh, 2009
Ocular	<10%	Proteinases such as neutral protease and aminopeptidase	↑ Tear turnover, drug-binding to tear proteins, ↓ residence time, possible corneal irritation, low patient acceptability, protease degradation	Zhou and Li Wan Po, 1991; Fogueri and Singh, 2009; El Sanhawari *et al.,* 2010
Pulmonary	~10%	Proteases, peroxidases, inflammatory and immunomodulatory mediators secreted by alveoli macrophages	Restrictive alveolar epithelium, mucociliary clearance, protease degradation, removal by alveolar macrophages, limited dosing, permeability challenges in diseased and smoking patients	Banga and Chien,1988; Adjei and Gupta, 1994; Zhou, 1994; Brown, 2005; Antosova *et al.,* 2009; Fogueri and Singh, 2009
Rectal	~10-20% with substantial increases following administration of absorption enhancers	Proteolytic enzymes such as enkephalinase, protease, cathepsin B and H, urokinase and collagen and protease-like peptidases	Low patient acceptability, limited surface area for absorption, possible first-pass metabolism, expulsion of formulation during bowel movements	Zhou and Li Wan Po, 1991; Muranishi *et al.*, 1993; Brown, 2005; Fogueri and Singh, 2009
Transdermal	Variable to very low bioavailability, iontophoresis and microneedle technologies ↑ the bioavailability up to 30%	Low proteolytic activity, minimal amounts of leucine aminopeptidase	Poor permeability (stratum corneum barrier), limitations in surface area and rate of administration, local irritation at administration site	Chien *et al.,* 1990; Zhou and Li Wan Po, 1991; Cormier *et al.,* 2004; Fogueri and Singh, 2009; Chiranjib *et al.,* 2010
Buccal	<1%, improved by use of permeation enhancers	Mucosal and proteolytic enzymes, oxidases, reductase, cyclooxygenases, peptidases;	Uncertain reproducibility, enzymatic degradation, penetrability, ↓ dosage form retention	Zhou and Li Wan Po, 1991; Brown, 2005; Antosova *et al.,* 2009; Fogueri and Singh, 2009; Sharma *et al.,* 2011
Oral	<2%	Pepsin and brush-border peptidases	Acid-catalyzed degradation in stomach, intestinal epithelial cell barrier, proteolytic breakdown, poor permeability	Zhou and Li Wan Po, 1991; Brown, 2005; Antosova *et al.,* 2009; Fogueri and Singh, 2009; Sharma *et al.,* 2011

2.4. Current Approaches Employed for the Oral Delivery of Proteins and Peptides for Enhanced GIT Absorption

Numerous strategies have been investigated in an effort to effectively deliver proteins and peptides via the oral route (Fogueri and Singh, 2009). Most of these systems target the GIT barrier in an attempt to overcome its restrictive nature and subsequently increase the oral bioavailability (Brown, 2005; Fogueri and Singh, 2009). Enteric coating has also been used to enable protection of the protein or peptide from pepsin digestion in the stomach, however, the reliability and efficiency of enteric coating is variable due to the presence of a wide range of pH values and enzymes present in the GIT (Hussan *et al.,* 2012). In addition, polymers used for enteric coating may undergo uncontrolled polymerization, during handling and storage, resulting in failure to release the molecule at the target site (Fawzi *et al.,* 1991). Therefore, protection from proteolytic enzymes and improved absorption of these molecules through the intestinal epithelium requires the use of more advanced pharmaceutical technologies (Brown, 2005).

Several key approaches that are available for maximizing oral protein and peptide absorption include: (1) the co-administration of protease inhibitors and absorption enhancers to inhibit enzymatic degradation and improve permeability, respectively; (2) modification of the physicochemical nature of the macromolecules to improve membrane permeability and proteolytic stability; (3) design of particulate drug delivery systems such as nanoparticles, microparticles and liposomes that protects the fragile molecules from enzymatic degradation and the harsh environment of the GIT; (4) mucoadhesive polymeric drug delivery systems to prolong the residence time at the target site and ; (5) site-specific delivery to the colon, where proteolytic activity is low (Chien, 1992; Ichikawa and Peppas, 2003; Malik *et al.,* 2007; Kumar and Mishra, 2008; Aungst, 2011). These technologies may be used singly or in combination to achieve an optimal oral delivery system for proteins and peptides. The following is a detailed discussion of each of the key approaches with examples in each case.

2.4.1. The use of permeation enhancers

It is known that absorption of a protein or peptide is improved by the co-administration of amphiphilic, low molecular mass permeation enhancers (Lee, 1990; Sinko *et al.,* 1999; Del Curto *et al.,* 2011). These are functional adjuvants that are included to function as membrane permeating enhancers (Aungst, 2011). Generally, permeation enhancers improve protein and peptide absorption by a combination of several mechanisms, including (1) the disruption and opening of tight junctions to increase paracellular permeability, (2) decrease in mucus viscosity

and (3) increase in membrane fluidity specific to their class (Anilkumar *et al.,* 2011; Aungst, 2011; Antunes *et al.,* 2013). Table 2.2 lists the different classes of intestinal permeation enhancers, including examples of agents in each class.

Table 2.2: Classification of intestinal permeation enhancers

Type	Examples	References
Surfactants	*Ionic*: Sodium lauryl sulphate *Nonionic*: Polysorbitate, Tween 80	Xia and Onyuksel, 2000; Anilkumar *et al*., 2011
Bile Salts	Sodium glycholate, sodium deoxycholate	Sakai *et al.,* 1997; Maher and Brayden, 2012
Fatty Acids	Sodium caprate, acyl carnites, oleic acid, lauric acid	Anilkumar *et al*., 2011; Park *et al*., 2011
Chitosan and derivatives	N-trimethyl chitosan chloride	Dodane and Vilivalam, 1998; Maher and Brayden, 2012
Chelating agents	EDTA, salicylates, citric acid	Thanou *et al.,* 2001; Park *et al*., 2011
Other enhancers	Zonula occludens toxin, PCP-cysteine	Anilkumar *et al*., 2011; Maher and Brayden, 2012

Surfactants disrupt the intestinal membrane, leading to increased permeability of proteins and peptides crossing the cell epithelium through the transcellular pathway (Xia and Onyuksel, 2000). Bile salts increases drug permeability through the decrease in mucus viscosity and peptidase activity, phospholipid acyl chain disruption and formation of mixed micelles (Sakai *et al.,* 1997). Similarly, fatty acids result in the formation of mixed micelles and contribute towards modulating paracellular permeability by increasing intracellular calcium levels that cause contraction of junction-associated microfilaments (Anilkumar *et al.,* 2011).

Chelating agents interfere with the calcium ions present between intestinal epithelial cells and its ability to maintain the structural feature of the intercellular space, subsequently opening tight junctions (Thanou *et al.,* 2001). Chitosan and its derivatives improve permeability of macromolecules by bioadhesion and reduction of tight junction integrity (Dodane and Vilivalam, 1998). Other enhancers which include zonula occludens toxin and polycarbophyl cysteine conjugate (PCP-cys) enable the reversible opening of tight junctions by interacting with specific receptors on the surface of epithelial cells that activate a cascade of events leading to tight junction permeability and increased phosphorylated occludin via glutathione to increase tight junction opening, respectively (Anilkumar *et al.,* 2011). Several studies have shown an increase in the permeability of proteins such as human growth hormone, insulin, interferon and calcitonin following co-administration with permeation enhancers (Bernkop-Schnürch, 2000; Stoll *et al.,* 2000; Lee, 2002; Kidron *et al.,* 2004; Lee *et al.,* 2005).

The three main factors that influence the efficacy of permeation enhancers includes: (1) the type of protein or peptide and its ability to cross the intestinal membrane, (2) the intrinsic nature of the permeation enhancer and its capability to increase permeation and, (3) the delivery system which can possibly affect the rate of release of the enhancer in relation to the physicochemically different protein or peptide (Okada *et al.,* 1982; Nishihata *et al.,* 1984). In addition to these three factors, due consideration needs to be given to the potential toxicities of permeation enhancers as well as the direct toxic effects to the intestinal epithelial cells (Antunes *et al.,* 2013). A few permeation enhancers transiently disrupt tight junctions and result in the unwanted permeation of luminal contents and potentially toxic molecules (Tscheik *et al.,* 2013). Major toxicity issues include the ulceration of the intestinal epithelium with 'pin-point' membrane erosions, immunological concerns and the rapid accessibility of a pathway for bacteria and viruses to gain entry into the systemic circulation (Anilkumar *et al.,* 2011). Although permeation enhancers are an attractive approach for increasing the oral bioavailability of proteins and peptides, the safety of these adjuvants needs to be addressed and more safer alternatives of permeation enhancers are readily required to be applicable for chronic therapy (Zhou, 1994).

2.4.2. The use of protease/enzyme inhibitors

The co-administration of enzyme inhibitors assists in targeting the enzymatic barrier hindering the successful oral absorption of proteins and peptides (Lee, 1990). Enzyme inhibitors exert their effects by binding reversibly/irreversibly to the target enzyme, inactivating it and thereby decreasing its activity (Copeland, 2013). Various enzyme inhibitors are available for intestinal enzyme inhibition with the appropriate selection being dependent on the target enzyme that is required to be inactivated (Lee, 1990). Examples of intestinal protease inhibitors include; aprotinin (inhibitor of trypsin and chymotrypsin), soybean trypsin inhibitor (inhibitor of pancreatic endopeptidases), FK448 (chymotrypsin inhibitor) and chicken ovamucoid (trypsin inhibitor) (Hussain *et al.,* 1989; Zhou, 1994; Bai, 1995). Furthermore, indirect enzyme inhibition can occur through the use of pH modifiers that subsequently reduces the optimal environment for enzyme activity (Bai *et al.,* 1995).

Studies have shown the positive effects of delivering of insulin orally, *in vivo* and *in vitro*, following co-administration of specific enzyme inhibitors (Fujii *et al.*, 1985; Morishita *et al.*, 1992; Langguth *et al.*, 1994; Yamamoto et al., 1994). Nevertheless, its individual administration with proteins or peptides may prove inadequate in improving the absorption due to the high enzyme activity at the intestinal membrane site (Lee, 2002). A combination of protease inhibitors with

permeation enhancers may prove to be more feasible in improving bioavailability since the protease inhibitors will inhibit the enzymes causing degradation of the protein while the permeation enhancer facilitates absorption through the intestinal membrane (Araújo *et al.,* 2012). Figure 2.2 depicts the use of permeation enhancers and protease inhibitors as formulation strategies for enhancing protein and peptide delivery. Similarly, as with permeation enhancers, cognizance of the safety of these agents is critical as it may lead to non-specific interaction with dietary proteins, intestinal mucosal damage and feedback-regulated protease secretion following chronic therapy (Lee, 1990; Yamamoto *et al.*, 1994). Therefore, safer alternatives need to be considered to enable the safe use of protease inhibitors for chronic therapy.

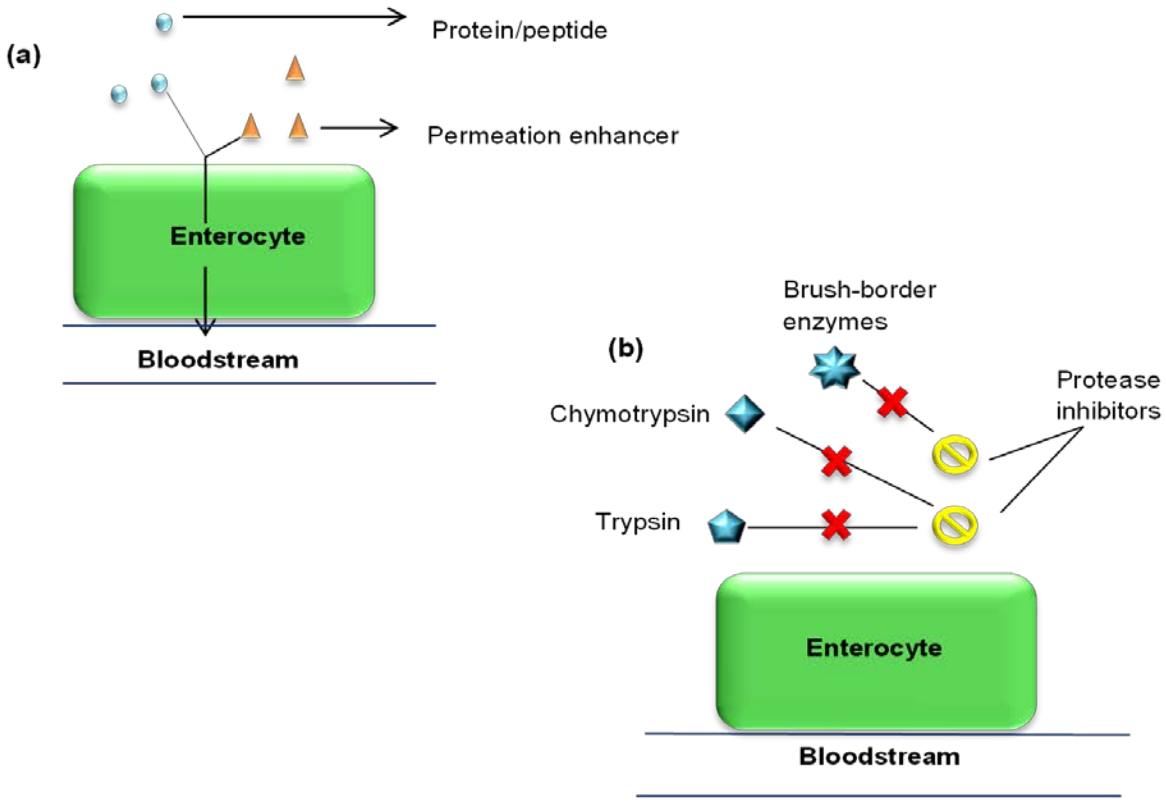

Figure 2.2: Formulation strategies for enhancing protein and peptide delivery, **a)** permeation enhancers and **b)** protease inhibitors.

2.4.3. Modification of the physicochemical properties of proteins and peptides to improve oral absorption

Physicochemical modification of proteins and peptides can be achieved by the addition of functional groups or by conjugation to polymers for improving the proteolytic stability and/or

membrane permeability (Herman *et al.,* 1995). Chemical modification can also serve as a strategy for reducing the ability of proteins and peptides to induce an immune response (Herman *et al.,* 1995). PEGylation, hydrophibization and amino acid alterations are some of the key approaches that can result in protein modifications (Brown, 2005). The general requirements for polymers used in protein-polymer conjugation are that they be water-soluble, non-immunogenic, biocompatible and devoid of any biological activity (Grover and Maynard, 2010). Ideally, the polymer selected should enhance the intrinsic properties of the macromolecules and not increase its toxicity or minimize its biological activity (Grover and Maynard, 2010). *N-(*-2-hydroxypropyl) methylacrylamide and poly(ethylene glycol) are polymers that display the ideal properties with the latter being the polymer of choice for protein conjugation (Grover and Maynard, 2010).

PEGylation, or covalent attachment of poly(ethylene glycol) (PEG) to proteins is widely used in parenteral formulations for enhancing their therapeutic potential (Lewis *et al.,* 2004; Alconcel *et al.,* 2011). However, its applicability in the oral delivery of proteins and peptides has been reported (Jensen-Pippo *et al.,* 1996; Rekha and Sharma, 2013). PEGylation results in the formation of a steric shield that protects the macromolecule from recognition by the body's immune system as well as increasing their enzymatic stability (Werle and Berknop-Schńurch, 2006; Alconcel *et al.,* 2011). In addition, the increase in molecular size results in a reduction in renal clearance of the protein or peptide (Werle and Berknop-Schńurch, 2006). Results from a study conducted on PEGylation of recombinant human granulocyte colony stimulating factor (PEG-G-CSF) indicated that oral delivery of PEG-G-CSF may be feasible and possibly favored to the unmodified form of the protein (Jensen-Pippo *et al.,* 1996).

A replacement of one or more L-amino acids with D-amino acids which are known to be inclined to enzymatic cleavage is another strategy to delay degradation and increase enzymatic stability of proteins/peptides (Werle and Berknop-Schńurch, 2006; Yang, 2013). An example of chemical modification of a peptide utilizing this strategy is the various analogues of the endogenous opioid pentapeptide methionine (Met)-enkephalin (Bohner *et al.,* 1994). Metabolism of the Met-enkephalin analogues by brush-border membrane vesicles displayed significant differences in degradation rates as well as effective permeability across Caco-2 cells (Bohner *et al.,* 1994). An alternative approach is the surface modification of proteins by hydrophobization which can occur either by including more hydrophobic amino acids within the peptide backbone or by covalent conjugation with lipophilic moieties that can enhance the transcellular uptake (des Rieux *et al.,*

2006; Yuan *et al.,* 2011). For example, significant increase in intestinal membrane permeability was observed by covalent conjugation of fatty acids such as lauric, palmitic and butyric acid with insulin and desmopressin (Muranishi, 1991; Hashizume *et al.,* 1992; Kahns *et al.,* 1993; Michael *et al.,* 2000). Although valuable to increasing transport of macromolecules, these methodologies possess a major risk of weakening the biological activity of the protein/peptide as a result of the chemical modification (Grover and Maynard, 2010).

2.4.4. The use of specialized particulate formulation vehicles

Several specialized strategies have been proposed to overcome the GIT barrier by the use of microemulsions, liposomes, nanoparticles and microspheres to successfully deliver proteins and peptides via the oral route (Zhou, 1994; Lasic, 1998; Yin *et al.,* 2009). Thermodynamically stable microemulsions protect proteins and peptides from chemical and enzymatic degradation due to solid-oil-in-water (S/O/W) emulsions which enhance GIT penetration and absorption (Toorisaka *et al.,* 2003). Studies undertaken on the oral delivery of S/O/W emulsions showed an increase in hypoglycemic activity following administration of insulin to diabetic rats with decreased enzymatic degradation and enhanced permeability (Toorisaka *et al.,* 2003; Park *et al.,* 2011). However, in order to enable optimal design and development of microemulsions for the delivery of proteins and peptides, several challenges need to be overcome such as its reduced loading capacity and low physicochemical stability during long term storage (Park *et al.,* 2011).

An alternate particulate delivery system used is liposomes as protein and peptide carriers (Torchilin, 2005). Such lipid-based delivery systems have been extensively studied for improving the absorption of proteins and peptides (Constantinides *et al.,* 1994; 1995; Del Curto *et al.,* 2003; Martins *et al.,* 2007). Although promising results have shown an increased plasma half-life and decreased blood glucose levels in diabetic mice after intravenous administration, the use of conventional liposomes in oral protein and peptide delivery is still limited (Lasic, 1998). Alternatively, archeosomes which is a specialized lipid-based oral delivery system characteristically composed of archaeobacterial membrane lipids containing diether and/or tetraether lipids may prove valuable for oral protein or peptide delivery (Li *et al.,* 2010). These archeosomes display increased stability against low pH and the action of bile salts and pancreatic lipases, thereby increasing the hypoglycemic effect in diabetic mice following insulin administration (Lasic, 1998; Li *et al.,* 2010; Park et al., 2011).

Another approach for improving liposomes is the use of nanotechnology systems at the surface of liposomes as is for silica nanoparticle coated liposomes (Mohanraj *et al.,* 2010). This system increases protein encapsulation and provides protection against enzymatic degradation (Mohanraj *et al.,* 2010). Amongst the different particulate-based delivery strategies employed, nanoparticles (10-1000nm) have captured the majority of interest as a promising approach for protein and peptide delivery (Lee, 2002; Lewis *et al.,* 2004). The size, surface charge and nature of the encapsulated nanoparticles influences the absorption of proteins through the intestinal epithelium, especially through Peyer's patches as shown by Lee, 2002. Various natural and synthetic polymers such as poly(lactic-coglycolic acid) (PLGA), poly(methyl methacrylate) (PMMA), poly(lactic acid) (PLA), alginate, cyclodextrins, chitosan and its derivatives have been utilized for the production of nanoparticles that encapsulate proteins and peptides (Tobio *et al.,* 2000; Li *et al.,* 2001; Reis *et al.,* 2007; Sarmento *et al.,* 2007). Inorganic nanoparticles are also receiving increased interest owing to their desirable properties and their ability to incorporate proteins and peptides (Xu *et al.,* 2006). Although nanotechnology appears to be seemingly flawless, it does have some challenges with regard to the low protein and peptide incorporation efficiency, uncontrolled molecule release, susceptibility to particle aggregation and possible accumulation of non-biodegradable polymers in tissues (Park *et al.,* 2011).

Microspheres (1-1000μm) can be employed as another strategy for enhancing oral protein or peptide delivery (Park *et al.,* 2011; Prasanth *et al.,* 2011). The major advantage of microspheres is their provision of stability for labile compounds that are easily degraded in the intestinal epithelium (Degim and Celebi, 2007). Many possible mechanisms may be considered for the release of proteins or peptides from microparticles, namely; surface or bulk erosion, diffusion though pores and pulsed delivery (Couvreur and Puisieux, 1993). Figure 2.3 illustrates the biphasic release of luteinizing hormone releasing hormone (LHRH) from polylactic co-glycolic acid (PLGA) microspheres depicting an initial burst release, lag phase and subsequent bulk erosion leading to a second phase of release (Sanders *et al.,* 1985).

Microparticles and nanoparticles have shown potential for protein and peptide delivery, however their differences should be noted when deciding on the appropriate selection of a particulate system. The physicochemical properties of proteins and peptides is a major challenge in the formulation process of micro- and nanoparticle encapsulation (Couvreur and Puisieux, 1993). Most work that has been undertaken on microencapsulation has shown its compatibility with the

handling of numerous peptides (Couvreur and Puisieux, 1993). In contrast, limited examples exist for the incorporation of peptides into nanoparticles owing to the complexity and incompatibility of the formulation process with the physicochemical conditions required for peptide stability (Couvreur and Puisieux, 1993). Additionally, different mechanisms may be considered for the release of proteins and peptides from micro- and nanoparticles (Couvreur and Puisieux, 1993). Nanoparticles may be more suitable for controlled delivery of proteins and peptides whereas microparticles may be employed for immediate and pulsed release. (Sanders *et al.,* 1985; Couvreur and Puisieux, 1993). A clear understanding of the *in vitro* release mechanism is required for appropriate selection of micro- or nanoparticle systems.

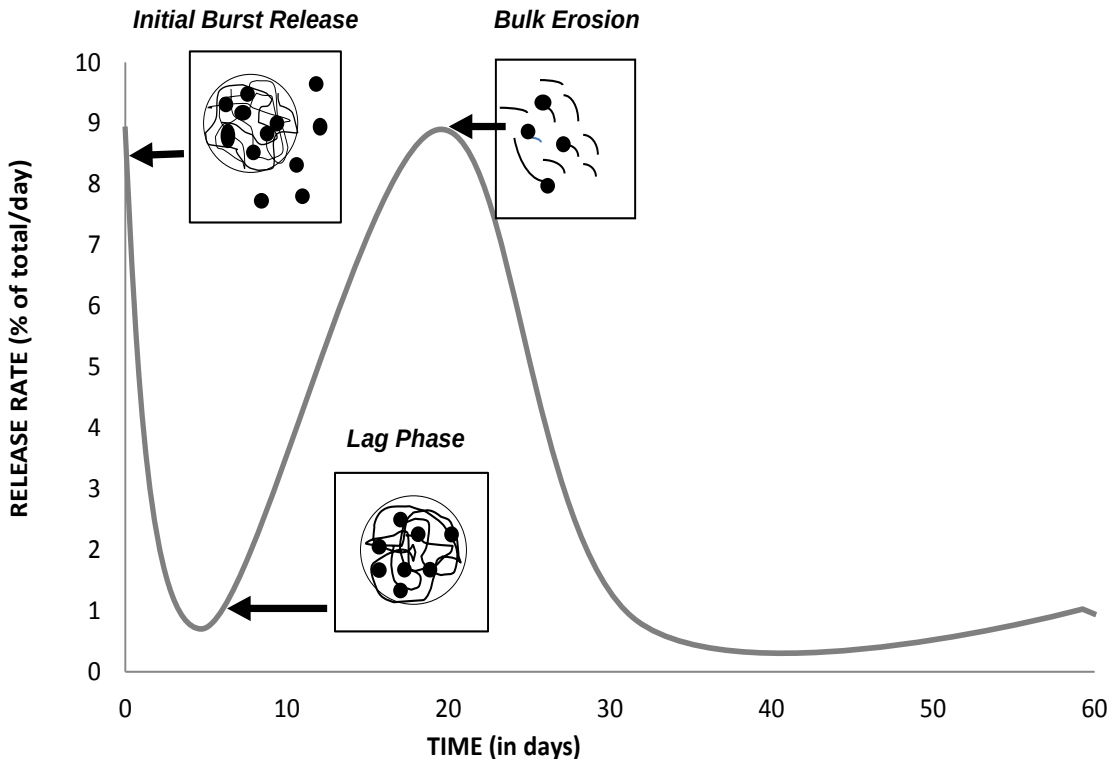

Figure 2.3: Illustration of the biphasic release of LHRH from PLGA microspheres. Black dots represent the drug-LHRH and curved lines represent the polymer-PLGA [Adapted from Couvreur and Puisieux, 1993, with permission from Elsevier Science Ltd. © 1993].

2.4.5. Stimuli-responsive hydrogels and mucoadhesive polymeric systems for enhanced oral absorption of proteins and peptides

Stimuli-responsive hydrogels represent suitable formulation vehicles for the protection of proteins and peptides (Malik *et al.,* 2007). Hydrogels are highly absorbent polymers that can respond to changes in pH by remaining unswollen at gastric pH and releasing their incorporated

protein or peptide only in the small intestine, thereby protecting the protein or peptide from the harsh gastric environment (Malik *et al.*, 2007). In addition, mucoadhesive polymeric systems are of great interest in the delivery of proteins and peptides as they retain their contact with the mucus membrane, enabling prolonged residence time at the absorption site (Peppas, 2004). Thiolated polymers are a representative example of mucoadhesive systems that provides a sharp drug concentration gradient at the absorption site and display additional permeation enhancing effects (Peppas, 2004). Various stimuli-responsive polymers (sometimes referred to as 'smart polymers') which are sensitive to temperature, phase, pH, electric charge, light, and biochemicals are available for controlling the release of incorporated proteins and peptides to achieve improved plasma levels (Fogueri and Singh, 2009). Table 2.3 lists the different stimuli-responsive polymers applied to the oral delivery of proteins and peptides with a brief description of each type.

Table 2.3: 'Smart' polymers for controlled oral delivery of proteins and peptides.

'Smart' Polymers	**Description**
Temperature sensitive polymer	Sol-to-gel transition responding to changes in pH from ambient to physiological temperatures; possess low critical solution temperature (LCST) or high critical solution temperature (HCST) (Sophie *et al.,* 2008; Fogueri and Singh, 2009).
pH sensitive polymer	Contains acidic or basic groups that either accept or donate protons in response to environmental pH (Bawa *et al.,* 2009; Fogueri and Singh, 2009).
Biochemical sensitive polymers	Highly sensitive to signals generated by a disease and releases drug in accordance with the magnitude of the signal (Chourasia and Jain, 2004; Fogueri and Singh, 2009).

2.4.6. Site-specific delivery of proteins and peptides to the colon

The common belief that absorption is uniform throughout the GIT is frequently challenged as increasing confirmatory evidence shows site-specific absorption (Neutra and Forstner, 1987). Colonic delivery appears to be advantageous for the absorption of proteins and peptides owing to their prolonged transit time, decreased enzyme activity and higher receptiveness towards permeation enhancers (Brayden and O'Mahony, 1998; Hamman *et al.,* 2007). In addition, the alkaline pH of the colon makes it an attractive target for absorption as it may lead to reduced degradation of the protein or peptide compared with the luminal digestion/degradation within the acidic gastric environment (Gazzaniga *et al.,* 2006). Examples of oral colon delivery systems for insulin release are based on microflora, pH and time-dependent strategies to enable enhanced protein absorption (Saffran *et al.,* 1986; Touitou and Rubinstein, 1986; Maroni *et al.,* 2009). Similarly, as with other approaches for enhancing protein or peptide delivery, oral colonic delivery has several challenges (Lee, 2002). Amongst these are the adherence of bacteria to

solid surfaces resulting in the formation of biofilm barriers that can affect release as well as variable transit times ranging from a few hours to several days (Lee, 2002).

2.4.7. Alternative approaches for enhancing the absorption of proteins and peptides

Other less common, but nevertheless significant approaches towards achieving optimum oral delivery of proteins and peptides include the use of eutectic mixtures and cell penetrating peptides which assist in increasing the solubility and permeation of proteins and peptides as well as enabling transport across cellular membranes, respectively (Mäe and Langel, 2006; Shen *et al.*, 2011). The subject of eutectics in polymeric delivery systems has hardly been researched and the microstructure that is typical of polymer eutectics, has not yet been fully explored (Tuntarawongsa and Phaechamud, 2012). A more recent study investigated the effects of a borneol/menthol eutectic mixture for enhanced bioavailability in the delivery of a polypeptide (daidzein) used for the treatment of breast and colon cancer (Shen *et al*., 2011). The results from this study showed the potential use of eutectic mixtures for enhancing the absorption of protein and peptide drugs. However, since the borneol/menthol eutectic mixture is a permeation-enhancing system it may disrupt tight junctions and result in the unwanted permeation of luminal contents and potentially toxic molecules (Tscheik *et al.,* 2013).

Cell-penetrating peptides (CPPs) also represent a possibility for the oral delivery of protein and peptides by enhancing the permeability through the intestinal epithelial cells (Foged and Nielson, 2008). CPPs work by improving the delivery of macromolecules into the cells when conjugated to a specific protein or peptide (Massodi *et al.,* 2005). A study undertaken by Morishita and co-workers, (2007) to determine the ability of the CPPs to increase intestinal absorption of insulin revealed positive results. Insulin absorption showed a marked increase in intestinal permeability when co-administered with the CPP oligoarginine (Morishita *et al.,* 2007). However, relatively high doses of the CPP are required which may pose a safety risk following multiple administrations (Morishita *et al.,* 2007; Kamei *et al.,* 2008). Thus, there is a need for more safer and effective CPPs for the oral delivery of proteins and peptides (Kamei *et al.,* 2008).

2.5. Advanced Oral Protein and Peptide Technology Platforms for Clinical Application

There are several oral protein and peptide technologies produced by pharmaceutical companies for application in various clinical situations (Park *et al.,* 2011). Although most of the formulations based on these technologies are in the development phase, many have progressed to the

clinical trial stage (Park *et al.,* 2011). The technologies are summarized below, highlighting their favorable characteristics that would improve their absorption and oral bioavailability as well as their potential limitations.

2.5.1. Oramed POD™ (Protein Oral Delivery) technology for oral delivery of insulin

Oramed Pharmaceuticals, Inc. (Jerusalem, Israel) have developed a POD™ technology to significantly enhance the absorption of proteins and peptides across the GIT epithelium by exploiting the action of protease inhibitors and absorption enhancers. ORMD-0801 is an oral insulin formulation based on POD™ technology that is currently undergoing U.S. Phase 2a clinical trials (Oramed Pharmaceuticals, 2014). The orally ingestible insulin capsule (ORMD-0801) produced positive results upon assessment of its glucose-lowering effect (Eldor *et al.,* 2013; Oramed Pharmaceuticals, 2014). The formulation composition is not precisely known but it is thought to be composed of an enteric coated oral capsule comprising a protease inhibitor, absorption enhancer and emulsifier (Eldor *et al.,* 2013; Oramed Pharmaceuticals, 2014). According to Kidron, (2011), the emulsifier, protease inhibitor and absorption enhancer could be omega 3 fatty acids, soybean as a trypsin inhibitor and EDTA, respectively (Kidron, 2011). This approach although promising, has several disadvantages such as the increased paracellular permeability of possible toxic molecules and the safety considerations associated with EDTA salts used orally (Kidron, 2011; Tscheik *et al.,* 2013).

2.5.2. Transient Permeability Enhancer (TPE™) system for oral delivery of octreotide

TPE™ is an absorption-enhancing system produced by Chiasma, Inc. (Jerusalem, Israel), consisting of an oily suspension of a medium-chain fatty acid salt, embodied by sodium caprylate and a matrix-forming polymer in a hydrophobic glyceryl triglyceride medium (Salama *et al.,* 2010; Chiasma, 2014). TPE™ system not only functions to protect the proteins and peptides from the GIT environment, but also acts on the GIT wall to enhance permeation (Salama *et al.,* 2010). TPE™ functions by a paracellular mechanism through transient opening of tight junctions between adjacent epithelial cells (Salama *et al.,* 2010; Chiasma, 2014). It was able to improve the bioavailability of the peptide octreotide in a study by Tuvia and co-workers, (2012). Octreolin® is an oral octreotide capsule produced by Chiasma for the treatment of acromegaly that is based on their proprietary TPE™ system (Chiasma, 2014). Octreolin® is currently in Phase 3 trials for acromegaly and if successful is expected to be launched in 2015 (Chiasma, 2014). A comparative disadvantage of this technology is the use of various excipients

in an emulsion format to form the TPE™ as compared to simple admixed formulations (Salama *et al.,* 2010).

2.5.3. Eligen® Technology for oral delivery of vitamin B12, calcitonin, heparin and insulin

Emisphere Technologies, Inc. (Roseland, New Jersey, United States) have produced a proprietary oral drug delivery platform knows as the Eligen® Technology which enhances the transcellular permeation across intestinal cell membranes (Aungst, 2011; Emisphere Technologies, 2014). This technology is based on sodium N-[8-(2-hydroxybenzoyl) aminocaprylate] (SNAC) which is proposed to interact with the drug molecule by forming weak, non-covalent complexes that enables transcellular absorption, without altering the tight junctions as depicted in Figure 2.4a (Ding *et al.*, 2004; Aungst, 2011; Park *et al.,* 2011). This approach has been shown to reversibly and safely deliver macromolecules without altering the drug, damaging epithelial membranes or creating new toxicities (Goldberg and Gomez-Orellana, 2003). Emisphere Technologies, Inc. has developed an oral formulation of Eligen® B12 for vitamin B12 deficient individuals and is currently in the process of evaluating results from clinical trials and market research (Emisphere Technologies, 2014). Eligen® technology has served as a hydrophobic carrier for the delivery of various macromolecules such as heparin, insulin and calcitonin, thereby increasing their lipophilicity (Goldberg and Gomez-Orellana, 2003). Novo Nordisk® (Bagsvaerd, Denmark) has partnered with Emisphere Technologies, Inc. to develop and commercialize Novo Nordisk's insulin and GLP-1 agonists (Emisphere Technologies, 2014). In 2013, Novo Nordisk® announced that it had commenced its first Phase 2 clinical trial with a long-acting oral GLP-1 analog (Emisphere Technologies, 2014). However, although this technology has shown promising results in oral protein and peptide delivery, its clinical application is difficult since it causes nausea in patients. In addition the technology requires co-administration of higher amounts of delivery agent as compared to the protein or peptide which ultimately decreases patient compliance (Hoffman and Qadri, 2008).

2.5.4. Chronotropic™: a "two-pulse" colonic device for oral delivery of insulin

A "two-pulse" delivery system comprising a tablet core surrounded by an inner swellable/erodible hydroxypropyl methylcellulose (HPMC) layer that is enclosed by an intermediate adjuvant layer and an additional HPMC outer coating was designed by Dexcel Pharma Technologies, Ltd. (Jerusalem, Israel) (Gazzaniga *et al.,* 1994; Maroni *et al.,* 2009; Del Curto *et al.,* 2011). This technology may prove useful for the oral delivery of insulin (Del Curto

et al., 2011). Studies undertaken have shown that the “two-pulse” colonic release of insulin, the protease inhibitor (camostat mesilate) and absorption enhancer (sodium glycocholate) was able to produce acceptable lag phases between the release of the adjuvant and the protein. The adjuvant is released prior to the protein, creating a more stable environment in advance (Gazzaniga *et al.,* 1994; Maroni *et al.,* 2009; Del Curto *et al.,* 2011). The Chronotopic™ device consists of inner and outer HPMC coatings that are meant to delay the release of adjuvants and the protein (Del Curto *et al.,* 2011). The major drawback of this multilayered system is that it is complex, requiring numerous polymer coating steps and adjuvants making formulation extremely cumbersome. In addition this system would require an enteric coating to enable time-dependent colon delivery which is a challenge when considering that the reliability and efficiency of enteric coating is variable due to the presence of a wide range of pH values and enzymes present in the GIT (Del Curto *et al.,* 2011; Hussan *et al.,* 2012).

2.5.5. CODES™ (Colon Specific Delivery System) technology for oral delivery of insulin

CODES™ Technology was produced for colonic specific delivery by Yamanouchi Pharmaceutical Co., Ltd. (Tokyo, Japan) and consists of lactulose-containing tablet that is coated with two acrylic films that display pH-dependent solubility (Katsuma *et al.,* 2002). The acrylic films comprise an inner acid-soluble polymer (Eudragit® E) and an outer enteric soluble polymer (Eudragit® L), that are separated by an HPMC layer (Yang *et al.,* 2003). The principle underpinning this technology is based on the knowledge that the enteric soluble polymer protects the tablet form the harsh gastric conditions within the stomach but rapidly dissolves within the intestine (Kotla and Shivapooja, 2014). The Eudragit® E coating subsequently protects the tablet through its passage within the alkaline environment of the small intestine (Yang *et al.,* 2003). On arrival within the colon, the bacteria present enzymatically degrades the lactulose into an organic acid (Katsuma et al., 2004). As a result, the pH surrounding the tablet is lowered sufficiently to enable the dissolution of the acid soluble polymer and initiate drug release (Yang *et al.,* 2003). Figure 2.4b depicts the different layers of the CODES™ technology and its response in various GIT media. This technology may prove significant for oral insulin delivery as studies undertaken showed decreased blood glucose levels with supplementary use of absorption enhancers and sustained delivery (Katsuma *et al.,* 2004).

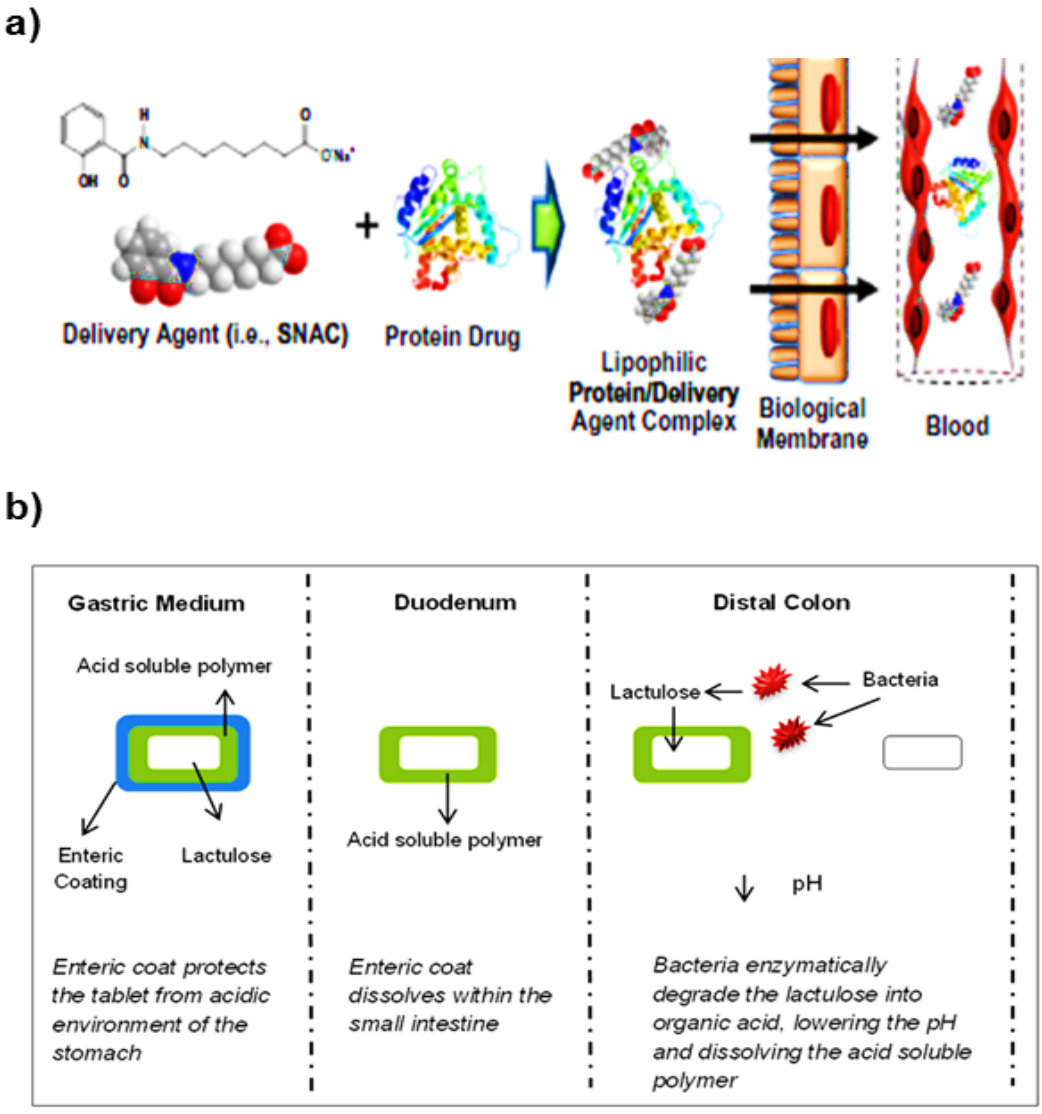

Figure 2.4: **a)** Emisphere Eligen™ Technology [Adapted from Park *et al.,* 2011, with permission from Elsevier Science Ltd. © 2011]. **b)** Illustration of the CODES™ technology depicting the different layers of the tablet and their response within each GIT media [Adapted from Katsuma *et al.,* 2004, with permission from John Wiley and Sons © 2004].

2.5.6. GIPET™ (Gastrointestinal Permeation Enhancement Technology) for oral delivery of acyline, heparin, insulin and GLP-1 agonists

Merrion Pharmaceuticals, Ltd. (Dublin, Ireland) GIPET™ technology utilizes medium chain fatty acids, salts and their derivatives to enhance the protein and peptide absorption from the small intestine (Leonard *et al.,* 2006). A few of the products in the pipeline by Merrion Pharmaceuticals, Ltd. that utilizes GIPET™ technology include acyline and ultra-low molecular weight heparin (uLMWH) (Leonard *et al.,* 2006; Merrion Pharmaceuticals, 2014). Acyline (MER-104), an oral GnRH antagonist used for oncology and other indications as well as MER-102 which is a unique tablet of uLMWH used in the treatment of deep vein thrombosis is currently

under development (Merrion Pharmaceuticals, 2014). This technology is preferably delivered using an enteric-coated formulation containing the main adjuvant, sodium caprate which has shown to enhance the bioavailability of heparin as compared to conventional delivery systems (Leonard *et al.,* 2006). In addition, Merrion Pharmaceuticals, Ltd. has partnered with Novo Nordisk® (Bagsvaerd, Denmark) to develop and commercialize Novo Nordisk's insulin and GLP-1 agonists using GIPET™ (Merrion Pharmaceuticals, 2014). However, this technology, as is the case with many permeation-enhancement technologies, result in an enhancement in absorption of toxic molecules causing damage to the intestinal epithelium which presents a significant disadvantage (Tshceik *et al.,* 2013).

2.5.7. Axcess™ oral delivery system for insulin

Proxima Concepts, Ltd. (London, United Kingdom) have developed an Axcess™ delivery system to enhance the oral absorption of proteins, peptides and other macromolecules across the GIT epithelium without chemical modification (Diabetology, 2014). The system is based on an oral capsule that contains the protein or peptide as well as registered pharmacopoeial excipients such as permeation enhancers and solubilizers to enhance transcellular absorption (Proxima Concepts, 2014). Capsulin™ IR (Insulin Replacement) is an enteric-coated insulin capsule that is produced by Diabetology, Ltd. (London, United Kingdom) in partnership with Proxima Concepts, Ltd (Luzio *et al.,* 2010). The capsule is based on Proxima's proprietary Axcess™ delivery system and has completed Phase 2a clinical trials (Luzio *et al.,* 2010). Despite the simplicity of this technology, the use of permeation enhancers could prove to be a challenge as it may disrupt tight junctions between epithelial cells causing the permeation of potentially toxic molecules (Tshceik *et al.,* 2013).

2.5.8. Peptelligence™ technology for oral delivery of salmon calcitonin

Enteris BioPharma, Inc. (Boonton, New Jersey, United States) has developed the clinically proven Peptelligence™ Technology that enables the oral delivery of peptides (Carl *et al.,* 2013). Peptelligence™ Technology comprises an enteric-coated tablet with two key components; a permeation enhancer and the main excipient citric acid (Enteris BioPharma, 2014). The enteric coating prevents the tablet from disintegration within the stomach and enables dissolution within the intestinal pH (Carl *et al.,* 2013). The two key components are released within the small intestine (Carl *et al.,* 2013). The permeation enhancer loosens tight junctions between intestinal epithelial cells and promotes paracellular transport while the citric acid functions to transiently

decrease intestinal pH to prevent degradation of the peptide by intestinal proteases and peptidases, which generally function optimally at neutral to alkaline pH (Carl *et al.,* 2013; Enteris BioPharma, 2014; Steinbach, 2014). This mechanism of release from Peptelligence™ Technology functions to facilitate oral peptide delivery. Tarsa Therapeutics, Inc. (Philadelphia, United States) has developed and oral salmon calcitonin formulation (Oracal®) used for the treatment of osteoporosis (Binkley *et al.,* 2012). The preferred formulation composition is a tablet containing salmon calcitonin, granular citric acid and an enteric coating of Eudragit® (Stern and Gilligan*,* 1999; Tarsa Therapeutics, 2014). Phase III clinical trials of Oracal® showed enhanced safety and efficacy results in women with postmenopausal osteoporosis, depicting better outcomes as compared to placebo and nasal calcitonin spray in enhancing bone mineral density in the lumbar spine after 48 weeks (Binkley *et al.,* 2012). Despite these positive results, the loosening of tight junctions caused by permeation enhancers presents a significant disadvantage as it may enable passage of potentially toxic molecules. In addition, polymers used for enteric coating may undergo uncontrolled polymerization, during handling and storage, resulting in failure to release the molecule at the target site (Fawzi *et al.,* 1991).

2.5.9. Multi Matrix MMX® technology for oral delivery of low molecular weight heparin

The MMX® Technology was designed by Cosmo Pharmaceuticals, Inc. (Lainate, Italy) for the oral delivery of active pharmaceutical agents into the lumen of the colon through tablets which delay and control release (Cosmo Pharmaceuticals, 2014). The tablets are enteric coated with pH-resistant acrylic copolymers which delay the release until the tablet reaches the target site (Pastorelli *et al.,* 2008). The coating allows for the protection of the molecule from adverse pH conditions and enzymes within the GIT (Cosmo Pharmaceuticals, 2014). In addition, the technology enables the controlled release of molecules over the length of the colon (Pastorelli *et al.,* 2008; Fiorino *et al.,* 2010). Low molecular weight (LMW) heparin MMX® is a novel oral colon release formulation produced by Cosmo Pharmaceuticals, Inc. for the treatment of mild to moderate ulcerative colitis (Pastorelli *et al.,* 2008). A study undertaken by Pastorelli and co-workers, (2008) showed positive results for the delivery of the LMWH Parnaprin with the MMX® Technology by avoiding the systemic action of the drug while allowing its local therapeutic action. LMW heparin MMX® Technology also has potential in the treatment of inflammatory bowel disease as a phase 2b clinical trial demonstrated that LMW heparin MMX® when associated with 5-ASA is more effective than 5-ASAs alone (Cosmo Pharmaceuticals, 2014). Although this technology enables the oral delivery of proteins and peptides, it does not contain

any pharmacopoeial excipients which may promote absorption or protection of the incorporated protein or peptide. The only protection it offers is the enteric coating which may pose a challenge when considering that the reliability and efficiency of enteric coating is variable due to the presence of a wide range of pH values and enzymes present in the GIT (Hussan *et al.,* 2012).

2.6. Advancement in Pharmacokinetic Profiles of Peptide Therapeutics through Specialized Platforms for Clinical Applications

Pharmacokinetics is an essential scientific discipline that governs applied therapeutics (Tripathi, 2013). The study of the Absorption, Distribution, Metabolism and Excretion (ADME) of proteins and peptides from drug delivery platforms are key pharmacokinetic parameters that determine the response of the body towards the incorporated macromolecules (Tripathi, 2013). Fundamental pharmacokinetic information is required to improve the pharmacodynamic response (Tripathi, 2013). Thus, a critical analysis of the pharmacokinetic profiles of the advanced technology platforms mentioned above is necessary in determining their efficacy in various clinical situations. The pharmacokinetic advancement contributed by different technologies is briefly discussed below, highlighting the key findings.

An open-label pilot study was used to assess the safety, tolerability and pharmacokinetic profile of Oramed POD™ technology for the oral delivery of insulin (Eldor *et al*., 2010). The study revealed lower values of post administration mean AUC ($AUC_{60\text{-}300}$) of 6.1-14% for c-peptide and 3.3-5% for glucose as compared to the $AUC_{0\text{-}60}$ (Eldor *et al*., 2010). In addition, insulin peaks characterized by a 1.5-2.4 fold increase from basal readings were observed 120 minutes after drug administration (Eldor *et al*., 2010). The technology offered better antiproteolytic and absorption enhancement by means of inert and safe adjuvants in comparison to the response obtained from other chemical adjuvants. This increase may be attributed to the action of protease inhibitors and absorption enhancers present within the formulation. However, despite the presence of absorption enhancers, hepatic uptake of insulin is highly variable and can exceed 80% of the portal delivered insulin reflecting poorly on oral insulin absorption (Eldor *et al*., 2010).

The pharmacokinetic profile of the oral formulation Octreolin® was investigated by Tuvia and co-workers, (2012) in comparison to the subcutaneous injection of octreotide. Oral octreotide (20mg) and subcutaneous octreotide injection (0.1mg) depicted comparable pharmacokinetic

parameters (mean C_{max}= 3.77±0.25 *vs*. 3.97±0.19 ng/ml; mean AUC= 16.2±1.25 *vs*. 12.1±0.45 h x ng/ml; and median time of ≥0.5 ng/ml, 7.67 *vs.* 5.88 h, respectively) (Tuvia *et al*., 2012). In addition, the orally administered octreotide resulted in effective growth hormone suppression in basal and GHRH-stimulated patients by 49 and 80%, respectively (Tuvia *et al*., 2012). In general Octreolin® has similar pharmacokinetic characteristics in comparison to subcutaneous octreotide which could be attributed to the its characteristic TPE™ system which protects the incorporated peptide in addition to enhancing permeation through the GIT wall (Tuvia *et al*., 2012).

A comparative study of pharmacokinetic evaluation of salmon calcitonin was carried out using oral formulation (Eligen® technology) and conventional nasal spray. An investigation into the effect of water intake and timing of dose on the pharmacokinetic parameters of an oral formulation of salmon calcitonin (sCT) based on Eligen® technology was conducted by Karsdal and co-workers (2008). The oral formulation was compared to a conventional nasal spray. The study indicated a two-fold increase in C_{max} and AUC_{0-4}, when administered with 50mL of water ranging from 46.0-86.5pg/ml x hrs depending on dosing time pre-meal as compared to 200mL (25.3-38.1pg/ml x hrs). In addition, the AUC_{0-4} of oral sCT with 50mL of water was 4-fold higher than the conventional nasal spray. However, the time to reach peak plasma concentrations (T_{max}) was equivalent for all formulations, including the nasal sCT. Hence, in addition to the enhanced transcellular permeation across intestinal cell membrane the Eligen® based oral sCT formulation (administered with 50mL of water and 60 minutes pre-meal) showed greater sCT bioavailability (Karsdal *et al*., 2008).

CODES™ was orally administered to fasting and fed dogs to determine and evaluate the pharmacokinetic profile of lactulose. The values for C_{max} and AUC were comparable in fasting and fed conditions, however, the T_{max} was delayed by 9 hours in fed dogs when compared to fasting dogs. The peak plasma concentration in fasting and fed dogs was 3.1±0.2µg/ml and 2.1±0.2µg/ml, respectively. The AUC in fasting conditions was 16.6±5.4µg/ml x h while in the fed conditions it was slightly lower with a value of 14.4±1.54µg/ml x h. However, in comparison to the pharmacokinetic profile of Timed-controlled release capsules, CODES™ technology, utilizing the action of enterobacteria, has a higher potential for colon-specific drug delivery (Katsuma *et al*., 2002).

A phase 1 study on a GIPET™ formulation of low molecular weight heparin (LMWH) was conducted to determine the increase in oral bioavailability as compared to the standard subcutaneous dose of 3200IU (Leonard *et al.,* 2006). Results displayed an oral bioavailability of 3.9% and 7.6% with respect to subcutaneous administration for LMWH-GIPET™ 45000IU and LMWH-GIPET™ 90000IU, respectively. The relatively low oral bioavailability may be attributed to the transient effects of the absorption enhancer, suggesting for the further improvement in design by enabling the co-release of the absorption enhancer and active protein or peptide to further increase oral bioavailability (Leonard *et al.,* 2006).

A randomized open study was conducted by Luzio and co-workers (2010) to determine the pharmacokinetic and pharmacodynamic properties of subcutaneous human insulin and Capsulin™ (oral insulin capsule) (Luzio *et al*., 2010). Results depicted lower insulin AUC_{0-6} for Capsulin™ as compared to the subcutaneous injection (910 ± 270 *vs*. 472 ± 245 pmol h/L for subcutaneous injection *vs.* Capsulin™ 150IU; 950±446 *vs*. 433±218 pmol.h/L for subcutaneous injection *vs.* Capsulin™ 300IU). In addition, the peak plasma concentrations of Capsulin™ were lower than subcutaneous insulin injections. However, comparable AUC and peak plasma concentrations were noted for Capsulin™ 150IU and Capsulin™ 300IU (Luzio *et al*., 2010). Despite the significant hypoglycemic effect of Capsulin™, the low insulin plasma concentrations recorded may be attributed to the increased enzyme activity at the intestinal epithelium which can result in degradation of the protein. Capsulin™ does not target enzymes within the intestine and thus this creates a significant window for improvement.

The efficacy of Peptelligence™ technology in delivering oral sCT was investigated by Carl and co-workers (2013). Even though absolute pharmacokinetic measurements were lacking in their study, the efficacy was demonstrated by an increase in baseline lumbar spine bone mineral density by 1.53% in women that were given oral sCT as compared to nasal spray (0.78%) or placebo (0.47%) administration (Carl *et al.,* 2013). In addition, the oral sCT displayed greater improvements in trochanteric and total proximal femur bone mineral density as compared to nasal sCT (Carl *et al.,* 2013). These positive results may be attributed to the action of the permeation enhancer and indirect enzyme inhibitor contained within the formulation. Similarly, studies conducted on the efficacy of MMX® technology in the oral delivery of LMWH yielded results that were not direct pharmacokinetic measurements (Pastorelli *et al.,* 2008). However, Clinical activity index (CAI) and Disease activity index (DAI) measurements revealed a significant improvement from the baseline (Pastorelli *et al.,* 2008). Despite these positive

results, extensive pharmacokinetic data is required to reliably determine the capability of the system to improve the bioavailability.

2.7. Concluding Remarks

Proteins and peptides display an increasingly important role as therapeutic agents for the treatment of various diseases (Zhou, 1994). Thus, improved non-parenteral delivery technologies are essential in ensuring optimal patient compliance and acceptance. The three major challenges with the delivery of proteins and peptides through non-parenteral routes (particularly the oral route) as assimilated in this review is their low bioavailability, susceptibility to enzymatic degradation and low membrane permeability (Maher and Brayden, 2012). Several oral delivery strategies have been proposed to enhance the permeation of protein and peptide molecules through the GIT. The aim of these strategies is to improve the oral bioavailability by either protecting the molecules from enzymatic degradation within the GIT or by improving their transport across intestinal cell barriers. Several technologies have been proposed which specifically target these barriers to successfully deliver oral proteins and peptides. Results from clinical trials conducted on the various technologies show positive results for its formulation into effective oral protein and peptide delivery systems. However, challenges still exist with each of the technologies proposed and these need to be addressed to enable optimal oral delivery. In general, the research and development of protein and peptide-based therapeutics is a dynamic field of research, with increasing numbers of candidates entering clinical studies in a wide variety of therapeutic categories. There is no doubt that pharmaceutical and biotechnology industries will continue to focus on these versatile molecules in association with the development of new oral formulations and delivery technologies.

2.8. References

Adjei, A., Gupta, P. (1994). Pulmonary delivery of therapeutic peptides and proteins. *Journal of Controlled Release,* 29, 361-373.

Alconcel, S.N.S., Baas, A.S., Maynard, H.D. (2011). FDA-approved poly (ethylene glycol)–protein conjugate drugs. *Journal of Polymer Chemistry,* 2, 1444-1448.

Anilkumar, P., Badarinath, A.V., Naveen, N., Prasad, K., Ravi Shankar Reddy, B., Hyndhavi, M., *et al*., (2011). Rationalized description on study of intestinal barrier, drug permeability and permeation enhancers. *Journal of Global Trends in Pharmaceutical Sciences,* 2, 431-449.

Antosova, Z., Mackova, M., Kral, V., Macek, T. (2009). Therapeutic application of peptides and proteins: parenteral forever? *Trends Biotechnology*, 27, 628-635.

Antunes, F., Andrade, F., Ferreira, D., Nielson, H.M., Sarmento, B. (2013). Models to Predict Intestinal Absorption of Therapeutic Peptides and Proteins. *Current Drug Metabolism*, 14, 4-20.

Araújo, F., Fonte, P., Sarmento, B. (2012). Oral Delivery of Glucagon-Like Peptide-1 and Analogs: Alternatives for Diabetes Control. *Journal of Diabetes Science and Technology*, 6, 1486-1497.

Artursson, P., Neuhoff, S., Matsson, P. (2007). Passive Permeability and Active Transport Models for the Prediction of Oral Absorption. In: Taylor, J.B., Triggle, J., editors. *Comprehensive Medicinal Chemistry II*. Oxford: Elsevier Science and Technology. pp. 259-278.

Aungst, B.J. (2011). Absorption Enhancers: Applications and Advances. *AAPS Journal,* 14, 10-18.

Bai, J.B.F., Amidon, G.L. (1992). Structural specificity of mucosal-cell transport and metabolism of peptide drugs: Implication for oral peptide drug delivery. *Pharmaceutical Research*, 9: 969-978.

Bai, J.P.F. (1995) Colonic delivery of peptide and protein drugs: consideration of intracellular proteolytic enzymes. *STP Pharmaceutical Sciences*, 5, 30–35

Bai, J.P.F., Chang, L.L., Guo, J.H. (1995). Effects of polyacrylic polymers on the luminal proteolysis of peptide drugs in the colon. *Journal of Pharmaceutical Sciences*, 84, 1291–1294.

Banga, A.K., Chien, Y.W. (1988). Systemic delivery of therapeutic peptides and proteins. *International Journal of Pharmaceutics*, 48, 15-50.

Baum, B., Georgiou, M. (2011). Dynamics of adherens junctions in epithelial establishment, maintenance, and remodeling. *Journal of Cell Biology*, 192, 907–917.

Bawa, P., Pillay, V., Choonara, Y.E., du Toit L.C. (2009). Stimuli-responsive polymers and their applications in drug delivery. *Journal of Biomedical Materials*, 4, 1-15.

Bernkop-Schnürch, A. (2000). Chitosan and its derivatives: potential excipients for peroral peptide delivery systems. *International Journal of Pharmaceutics*, 194, 1-13.

Binkley, N., Bolognese, M., Sidorowicz-Bialynicka, A., Vally, T., Trout, R., Miller, C., *et al*., (2012). A Phase 3 Trial of the Efficacy and Safety of Oral Recombinant Calcitonin: The Oral Calcitonin in Postmenopausal Osteoporosis (ORACAL) Trial. *Journal of Bone and Mineral and Research*, 27, 1821-1829.

Bohner, V., Langguth, P., Biber, J., Morkel, H.P. (1994). *Intestinal mucosal transport and metabolism of pentapeptides*. Deerfield: Controlled Released Society Inc. pp. 895-896.

Brayden, D.J., O'Mahony, D.J. (1998). Novel oral drug delivery gateways for biotechnology products: polypeptides and vaccines. *Pharmaceutical Science and Technology Today*, 1,291-299.

Brayden, D.J., Mrsny, R.J. (2011). Oral peptide delivery: prioritizing the leading technologies. *Therapeutic Delivery,* 2, 1567-1572.

Brown, L.R. (2005). Commercial challenges of protein drug delivery. *Expert Opinion Drug Delivery*, 2, 29-42.

Camenich, G., Alsenz, J., van de Waterbeemd, H., Folkers, G. (1998). Estimation of permeability by passive diffusion through Caco-2 cell monolayers using the drugs' lipophilicity and molecular weight. *European Journal of Pharmaceutical Sciences*, 6, 317-324.

Cantor, C.R. (1994). Separation by Precipitation. In: Scopes RK, editor. *Protein Purification: Principles and Practice*. New York: Springer Science. pp. 95-100.

Carl, S.M., Mehta, N., Stern, W. (2013). Oral Delivery of Peptides by Peptelligence™ Technology. *Drug Development and Delivery,* 27, 12-5.

Catnach, S.M., Fairclough, P.D., Hammond, S.M. (1994). Intestinal absorption of peptide drugs: advances in our understanding and clinical implications. *Gut*, 35, 441-444.

Chiasma, Inc. 2014, *Octreolin®,* Available from: <http://www.chiasmapharma.com/page.asp?id=20>. [14 April 2014].

Chien, Y. (1992). Oral drug delivery and delivery systems. In: Chien YW, editor. *Novel Drug Delivery Systems*. New York: Marcel Dekker Inc. pp. 139–196.

Chien, Y.W., Lelawongs, P., Siddiqui, O., Sun, Y., Shi, W.M. (1990). Facilitated transdermal delivery of therapeutic peptides and proteins by iontophoretic delivery devices. *Journal of Controlled Release*, 13, 263-278.

Chin, J., Mahmud, K.A.F., Kim, S.E., Park, K., Byun, Y. (2012). Insight of current technologies for oral delivery of proteins and peptides. *Drug Discovery Today Technologies*, 9, 105-112.

Chiranjib, D.B., Chandira, M., Jayakar, B., Sampath, K.P. (2010). Recent Advances in Transdermal Drug Delivery System. *International Journal of PharmTech Research,* 2, 68-77.

Chourasia, M.K., Jain, S.K. (2004). Polysaccharides for colon targeted drug delivery. *Drug Delivery,* 111, 29-48.

Constantinides, P.P., Lancaster, C.M., Marcello, J., Chiosone, D., Orner, D., Hidalgo, I., et al. (1995). Enhanced intestinal absorption of an RGD peptide form water-in-oil microemulsions of different composition and particle size. *Journal of Controlled Release,* 34, 109-116.

Constantinides, P.P., Scalart, J.P., Lancaster, C., Marcello, J., Marks, G., Ellens, H., Smith, P.L. (1994). Formulation and intestinal absorption enhancement evaluation of water-in-oil microemulsions incorporating medium-chain glycerides. *Pharmaceutical Research*, 11, 1385-1390.

Copeland, R.A. (2013). *Evaluation of Enzyme Inhibitors in Drug Discovery: A Guide for Medicinal Chemist and Pharmacologists*. New Jersey: John Wiley and Sons. pp. 57-59.

Cormier, M., Johnson, B., Ameri, M., Nyam, K., Libiran, L., Zhang, D.D., et al. (2004). Transdermal delivery of desmopressin using a coated microneedle array patch system. *Journal of Controlled Release*, 97, 503-511.

Cosmo Pharmaceuticals, Inc. 2014, Multi Matrix MMX® Technology, Available from: <http://www.cosmopharmaceuticals.com/activities/technology.aspx>. [16 April 2014].

Couvreur, P., Puisieux, F. (1993). Nano- and microparticles for the delivery of polypeptides and proteins. *Advanced Drug Delivery Reviews*, 10, 141-62.

Degim, I.T., Celebi, N. (2007). Controlled Delivery of Peptides and Proteins. *Journal of Current Pharmaceutical Research*, 13, 99-117.

Del Curto, M.D., Chicco, D., D'Antonio, M., Ciolli, V., Dannan, H., D'Urso, S., *et al*., (2003). Lipid microparticles as sustained release system for a GnRH antagonist (Antide). *Journal of Controlled Release*, 89, 297-310.

Del Curto, M.D., Maroni, A., Palugan, L., Zema, L., Gazzaniga, A., Sangalli, M.E. (2011). Oral Delivery System for Two-pulse Colonic Release of Protein Drugs and Protease Inhibitor/Absorption Enhancer Compounds. *Journal of Pharmaceutical Sciences,* 100, 3251-3259.

des Rieux, A., Fievez, V., Garinot, M., Schneider, Y.J., Préat, V. (2006). Nanoparticles as potential oral delivery systems of proteins and vaccines: a mechanistic approach. *Journal of Controlled Release,* 116, 1-27.

Diabetology, Ltd. 2014, Capsulin™, Available from: <http://www.diabetology.co.uk/platforms.htm >. [15 April 2014].

Ding, X., Rath, P., Angelo, R., Stringfellow, T., Flanders, E., Dinh, S., *et al*., (2004). Oral absorption enhancement of cromolyn through noncovalent complexation. *Journal of Pharmaceutical Research,* 21, 2196-2206.

Dodane, V., Vilivalam, V.D. (1998). Pharmaceutical applications of chitosan. *Pharmaceutical Science and Technology,* 1, 246-253.

Donovan, M.D., Flynn, G.L., Amidon, G.L. (1990). Absorption of polyethylene glycols 600 through 2000: the molecular weight dependence of gastrointestinal and nasal absorption. *Journal of Pharmaceutical Research,* 7, 863-868.

El Sanhawari, M., Kowalczuk, L., Touchard, E., Omri, S., de Kozak, Y., Behar-Cohen, F. (2010). Protein delivery for retinal diseases: from basic considerations to clinical applications. *Progress in Retinal and Eye Research*, 29, 443-465.

Eldor, R., Kidron, M., Arbit, E. (2010). Open-label study to assess the safety and pharmacodynamics of five oral insulin formulations in healthy subjects. *Diabetes, Obesity and Metabolism*, 12, 219-223.

Eldor, R., Arbit, E., Corcos, A., Kidron, M. (2013). Glucose-Reducing Effect of the ORMD-0801 Oral Insulin Preparation in Patients with Uncontrolled Type 1 Diabetes: A Pilot Study. *PLoS ONE*, doi: 10.1371/journal.pone.

Emisphere Technology, Inc. 2014, Eligen® Technology, Available from: <http://www.emisphere.com/eligen.html>. [14 April 2014].

Enteris BioPharma, Inc. 2014, Peptelligence™ Technology, Available from: <http://enterisbiopharma.com/technology-services/>. [15 April 2014].

Fawzi, M.B., Kubert, D.A., Murthy, K.S., (1991), inventors; Warner-Lambert Company, assignee. Stabilization of enteric coated dosage form. *United States Patent* US 5068110 A. Nov 26.

Fei, Y.J., Kanai, Y., Nussberger, S., Ganapathy, V., Leibach, F.H., Romero, M.F., *et al*., (1994). Expression cloning of a mammalian proton-coupled oligopeptide transporter. *Nature*, 368, 563-566.

Fiorino, G., Fries, W., De La Rue, S.A., Malesci, A.C., Repici, A., Danese, S. (2010). New drug delivery systems in inflammatory bowel disease: MMX and tailored delivery to the gut. *Current Medicinal Chemistry,* 17, 1851-1857.

Foged, C., Nielsen, H.M. (2008). Cell-penetrating peptides for drug delivery across membrane barriers. *Expert Opinion Drug Delivery*, 5, 105–117.

Fogueri, L.R., Singh, S. (2009). Smart Polymers for Controlled Delivery of Proteins and Peptides: A Review of Patents. *Recent Patents on Drug Delivery and Formulation*, 3, 40-48.

Friedman, D.I., Amidon, G.L. (1989). Intestinal absorption mechanism of dipeptide angiotensin converting enzyme inhibitors of the lysyl-proline type: lisinopril and SQ 29, 852. *Journal of Pharmaceutical Science*, 78, 995-998.

Friedman, D.I., Amidon, G.L. (1989). Passive and carrier-mediated intestinal absorption components of two angiotensin converting enzyme (ACE) inhibitor prodrugs in rats: enalapril and fosinopril. *Journal of Pharmaceutical Research*, 6, 1043-1047.

Fujii, S., Yokohama, T., Ikegaya, K., Salo, F., Yakoo, N. (1985). Promoting effect of the new chymotrypsin inhibitor FK-448 on the intestinal absorption of insulin in rats and dogs. *Journal of Pharmacy and Pharmacology*, 37, 545–549.

Futaki, S., Suzuki, T., Ohashi, W., Yagami, T., Tanaka, S., Ueda, K., *et al*., (2001). Arginine rich peptides. An abundant source of membrane-permeable peptides having potential as carriers for intracellular protein delivery. *Journal of Biological Chemistry*, 276, 5836–5840.

Ganapathy, V., Burckhardt, G., Leibach, F.H. (1985). Peptide transport in rabbit intestinal brush-border membrane vesicles studied with a potential-sensitive dye. *Biochimica et Biophysica Acta*, 816, 234-240.

Ganapathy, V., Leibach, F.H. (1985). Is intestinal peptide transport energized by a proton gradient. *American Journal of Physiology*, 249, 153-160.

Gazzaniga, A., Maroni, A., Sangalli, M.E., Zema, L. (2006). Time-controlled oral delivery systems for colon targeting. *Expert Opinion Drug Delivery*, 3, 583–597.

Gazzaniga, A., Sangalli, M.E., Giordano, F. (1994). Oral Chronotopic® drug delivery systems: Achievement of time and/or site specificity. *European Journal of Pharmaceutics and Biopharmaceutics*, 40, 246-350.

Goldberg, M., Gomez-Orellana, I. (2003). Challenges for the oral delivery of macromolecules. *Nature Review Drug Discovery*, 2, 289-295.

Grover, G.N., Maynard, H.D. (2010). Protein-Polymer Conjugates: Synthetic Approaches by Controlled Radical Polymerizations & Interesting Applications. *Current Opinion in Chemistry and Biology*, 14, 818-827.

Hamman, J.H., Demana, P.H., Olivier, E. (2007). Targeting Receptors, Transporters and Site of Absorption to Improve Oral Drug Delivery. *Drug Target Insights*, 2, 71-81.

Hamman, J.H., Enslin, G.M., Kotzé, A.F. (2005). Oral delivery of peptide drugs. *BioDrugs*, 19, 165-177.

Hashizume, M., Douen, T., Murakami, M., Yamamoto, A., Takada, K., Muranishi, S. (1992). Improvement of Large Intestinal Absorption of Insulin by Chemical Modification with Palmitic Acid in Rats. *Journal of Pharmacy and Pharmacology,* 44: 555-559.

Herman, S., Hooftman, G., Schacht, E. (1995). Poly (ethylene glycol) with reactive endgroups: I. Modification of proteins. *Journal of Bioactive and Compatible Polymers*, 10, 145 -87.

Ho, N.F.H., Day, J.S., Barsuhn, C.L., Burton, P.S., Raub, T.J. (1990). Biophysical model approaches to mechanistic transepithelial studies of peptides. *Journal of Controlled Release*, 11, 3-24.

Hoffman, A., Qadri, B. (2008). Eligen insulin--a system for the oral delivery of insulin for diabetes. *Investigative Drugs Journal*, 11, 433-441.

Hussain, M.A., Shenvi, A.B., Rowe, S.M., Shefter, E. (1989). The use of alpha-aminoboronic acid derivatives to stabilize peptide drugs during their intranasal absorption. *Journal of Pharmaceutical Research*, 6, 186-189.

Hussan, S.D., Santanu, R., Verma, P., Bhandari, V. (2012). A review on recent advances of enteric coating. *IOSR Journal of Pharmacy,* 2, 5-11.

Ichikawa, H., Peppas, N.A. (2003). Novel complexation hydrogels for oral peptide delivery: in vitro evaluation of their cytocompatibility and insulin-transport enhancing effects using Caco-2 cell monolayers. *Journal of Biomedical Material Research*, 67, 609–617.

Jensen-Pippo, K.E., Whitcomb, K.L., DePrince, R.B., Ralph, L., Habberfield, A.D. (1996). Enteral Bioavailability of Human Granulocyte Colony Stimulating Factor Conjugated with Poly(ethylene glycol). *Pharmaceutical Research,* 13, 102-107.

Kahns, A.H., Buur, A., Bundgaard, H. (1993). Prodrugs of peptides. Synthesis and evaluation of various esters of desmopressin (dDAVP). *Journal of Pharmaceutical Research*, 10, 68–74.

Kamei. N., Morishita, M., Eda, Y., Ida, N., Nishio, R., Takayama, R. (2008). Usefulness of cell-penetrating peptides to improve intestinal insulin absorption. *Journal of Controlled Release,* 132, 21-25.

Karsdal, M.A., Byrjalsen, I., Riss, B.J., Christiansen, C. (2008). Optimizing bioavailability of oral administration of small peptides through pharmacokinetic and pharmacodynamic parameters: The effect of water and timing of meal intake on oral delivery of Salmon Calcitonin. *BMC Clinical Pharmacology,* 8, 5-10.

Katsuma, M., Watanabe, S., Kawai, H., Takemura, S., Masuda, Y., Fukui, M. (2002). Studies on lactulose formulations for colon-specific drug delivery. *International Journal of Pharmaceutics*, 249, 33–43.

Katsuma, M., Watanabe, S., Takemura, S., Sako, K., Sawada, T., Masuda, Y., et al. (2004). Scintigraphic evaluation of a novel Colon-Targeted Delivery System (CODES™) in healthy volunteers. *Journal of Pharmaceutical Sciences*, 93, 1287–1299.

Khedkar, A., Iyer, H., Anand, A., Verma, M., Krishnamurthy, S., Savale, S., et al. (2010). A dose range finding study of novel oral insulin (IN-105) under fed conditions in type 2 diabetes mellitus subjects. *Diabetes, Obesity Metabolism*, 12, 659-664.

Kidron, M. (2011), inventor. Methods and compositions for oral administration of proteins. *United States Patent* US 0014247 A1, Jan 1.

Kidron, M., Dinh, S., Menachem, Y., Abbas, R., Variano, B., Goldberg, M., et al. (2004). A novel per-oral insulin formulation: proof of concept study in non-diabetic subjects. *Diabetes Medicine*, 21, 354-357.

Kotla, N.J., Shivapooja, A. (2014). Recent Developments in Colon Specific Drug Delivery Systems Approaches Promising in Targeting Colon. *International Journal of Pharmaceutical and Clinical Research*, 6, 101-106.

Kramer, W., Girbig, F., Gutjahr, U., Kleemann, H.W., Leipe, I., Urbach, H., et al. (1990). Interaction of renin inhibitors with the intestinal uptake system for oligopeptides and beta-lactam antibiotics. *Biochimica Biophysica Acta,* 1027, 25-30.

Kumar, P., Mishra, B. (2008). Colon targeted drug delivery systems-an overview*. Current Drug Delivery*, 5, 186-198.

Langguth, P., Merkle, H.P., Amidon, G. (1994). Oral absorption of peptides-the effect of absorption side and enzyme inhibition on the systemic availability of metkephamid. *Journal of Pharmaceutical Research*, 11, 528–535.

Lasic, D.D. (1998). Novel applications of liposomes. *Trends Biotechnology*, 16, 307–321.

Lee, J.H. (2002). Protein Drug Oral Delivery: The Recent Progress. *Archives of Pharmaceutical Research*, 25, 572-584.

Lee, S., Lee, J., Lee, D.Y., Kim, S.K., Lee, Y., Byun, Y. (2005). A new drug carrier, Nα -deoxycholyl-l-lysyl-methylester, for enhancing insulin absorption in the intestine. *Diabetologia*, 48, 405-411.

Lee, V.H.L. (1990). Protease inhibitors and penetration enhancers as approaches to modify peptide absorption. *Journal of Controlled Release*, 13, 213-223.

Lee, V.H.L., Yamamoto, A. (1990). Penetration and enzymatic barriers to peptide and protein absorption. *Advanced Drug Delivery Reviews*, 4, 171-207.

Lee, Y.H., Sinko, P.J. (2000). Oral delivery of salmon calcitonin. *Advanced Drug Delivery Review*, 42, 225–238.

Leonard, T.W., Lynch, J., McKenna, M.J., Brayden, D.J. (2006). Promoting absorption of drugs in humans using medium-chain fatty acid-based solid dosage forms: GIPET. *Expert Opinion Drug Delivery*, 3, 685-692.

Lewis, D., Schmidt, P., Hinds, K. (2004), inventors; Pr Pharmaceuticals, Inc., assignee. Methods and Compositions for Enhanced Delivery of Bioactive Molecules. *United States Patent* US 09/999,820. Mar 16.

Li, A.P. (2001). Screening for human ADME/Tox drug properties in drug discovery. *Drug Discovery Today*, 6, 357-366.

Li, Y., Pei, Y., Zhang, X., Gu, Z., Zhou, Z., Yuan, W., et al. (2001). PEGylated PLGA nanoparticles as protein carriers: synthesis, preparation and biodistribution in rats. *Journal of Controlled Release*, 71, 203-211.

Li, Z., Chen, J., Sun, W., Xu, Y. (2010). Investigation of archaeosomes as carriers for oral delivery of peptides. *Journal of Biochemical Biophysical Research Communications*, 394: 412–417.

Liu, Z., Wang, S., Hui, M. (2009). Oral Absorption Basics: Pathways, physico-chemical and biological factors affecting absorption. In: Qui Y, Chen Y, Zhang GGZ, editors. *Developing Oral Solid Dosage Form*. Oxford: Elsevier Science and Technology. pp. 265-288.

Lundin, S., Vilhardt, H. (1986). Absorption of intragastrically administered DDAVP on conscious dogs. *Life Sciences*, 38, 703-709.

Luzio, S.D., Dunseath, G., Lockett, A., Broke-Smith, T.P., New, R.R., Owens, D.R. (2010). The glucose lowering effect of an oral insulin (Capsulin) during an isoglycaemic clamp study in persons with type 2 diabetes. *Diabetes, Obesity Metabolism*, 12, 82-87.

Mäe, M., Langel, U. (2006). Cell-penetrating peptides as vectors for peptide, protein and oligonucleotide delivery. *Current Opinion in Pharmacology,* 6, 509-514.

Maher, S., Brayden, D.J. (2012). Overcoming poor permeability: translating permeation enhancers for oral peptide delivery. *Drug Discovery Today: Technologies*, 9, 113-119.

Malik, K.M., Baboota, S., Ahuja, A., Hasan, S., Ali, J. (2007). Recent Advances in Protein and Peptide Drug Delivery Systems. *Current Drug Delivery*, 4, 141-151.

Maroni, A., Del Curto, M.D., Serratoni, M., Zema, L., Foppoli, A., Gazzaniga, A., *et al*., (2009). Feasibility, stability and release performance of a time-dependent insulin delivery system intended for oral colon release. *European Journal of Pharmaceutics and Biopharmaceutics*, 72, 246–251.

Marques, M.R.C., Loebenberg, R., Almukainzi, M. (2011). Simulated Biological Fluids with Possible Application in Dissolution Testing. *Dissolution Technologies*, 60, 15-28.

Martins, S., Sarmento, B., Souto, E.B. (2007). Lipid-based colloidal carriers for peptide and protein delivery – liposomes versus lipid nanoparticles. *International Journal of Nanomedicine*, 2, 595-607.

Massodi, I., Bidwell, G.L., Raucher, D. (2005). Evaluation of cell penetrating peptides fused to elastin-like polypeptide for drug delivery. *Journal of Controlled Release*, 108, 396–408.

Ménard, S., Lebreton, C., Schumann, M., Matysiak-Budnik, T., Dugave, C., Bouhnik, Y., et al. (2012). Paracellular versus transcellular intestinal permeability to gliadin peptides in active celiac disease. *American Journal of Pathology*, 180, 608-615.

Merrion Pharmaceuticals, Ltd. 2014, GIPET™, Available from: <http://www.merrionpharma.com/content/about/profile.asp.>[15 April 2014].

Michael, S., Thöle, M., Dillmann, R., Fahr, A., Drewe, J., Fricker, G. (2000). Improvement of intestinal peptide absorption by a synthetic bile acid derivative, cholylsarcosine. *European Journal of Pharmaceutical Sciences*, 10, 133-140.

Mohanraj, V.J., Barnes, T.J., Prestridge, C.A. (2010). Silica nanoparticle coated liposomes: A new type of hybrid nanocapsule for proteins. *International Journal of Pharmaceutics*, 392, 285-93.

Morishita, I., Morishita, M., Takayama, K., Machida, Y., Nagai, T. (1992). Hypoglycemic effect of novel oral microspheres of insulin with protease inhibitor in normal and diabetic rats. *International Journal of Pharmaceutics*, 78, 9–16.

Morishita, M., Kamei, N., Ehara, J., Isowa, K., Takayama, K. (2007). Novel approach using functional peptides for efficient intestinal absorption of insulin. *Journal of Controlled Release,* 118, 177-184.

Muranishi, S. (1991). *Improvement of intestinal absorption of peptides by chemical modification of peptides.* Greenwood: Capsugel Symposia Series. pp. 73-77.

Muranishi, S., Yamamoto, A., Okada, H. (1993). Rectal and Vaginal Absorption of Peptide and Proteins. In: Kenneth L, Audus JR, Thomas JR, editors. *Biological Barriers to Protein Delivery*. New York: Plenum Press. pp. 199-200.

Nakashima, E., Tsuji, A., Kagatani, S., Yamana, T. (1984). Intestinal absorption mechanism of amino-beta-lactam antibiotics. III. Kinetics of carrier-mediated transport across the rat small intestine in situ. *Journal of Pharmacobiodynamics*, 7, 452-464.

Neutra, M.R., Forstner, J.F. (1987). Gastrointestinal mucus: synthesis, secretion and function. In: Johnson LR, Christensen J, Jackson MJ, Jacobson ED, Walsh JH, editors. *Physiology of the Gastrointestinal Tract*. New York: Raven Press. pp. 975-1009.

Neutra, M.R., Kraehenbuhl, J.P. (1993). Transepithelial Transport of Proteins by Intestinal Epithelial Cells. In: Kenneth L, Audus JR, Thomas JR, editors. *Biological Barriers to Protein Delivery*. New York: Plenum Press. pp. 107-122.

Nishihata, T., Higuchi, T., Kamada, A. (1984). Salicylate-promoted permeation of cefoxitin, insulin and phenylalanine across red cell membrane. *Life Sciences*, 34, 437-445.

O' Connor, A. (2009). Introduction to biotech drugs. North Carolina: *Regulatory Rapporteur*.

Oda, H., Takeichi, M. (2011). Evolution: structural and functional diversity of cadherin at the adherens junction. *Journal of Cell Biology*, 193, 1137–1146.

Okada, H., Yamazaki, I., Ogawa, Y., Hirai, S., Yashiki, T., Mima, H. (1982). Vaginal absorption of a potent luteinizing hormone-releasing hormone analog (leuprolide) in rats I: absorption by various routes and absorption enhancement. *Journal of Pharmaceutical Sciences*, 71, 1367-1371.

Oramed Pharmaceuticals Inc. 2014, *ORMD-0801-Oral Insulin Capsule.* Available from: <http://oramed.com/index.php?page=14>. [14 April 2014].

Palermo, A., Napoli, N., Manfrini, S., Lauria, A., Strollo, R., Pozzilli, P. (2011). Buccal spray insulin in subjects with impaired glucose tolerance: the prevoral study. *Diabetes, Obesity and Metabolism*, 13, 42-46.

Pastorelli, L., Saibeni, S., Spina, L., Signorelli, C., Celasco, G., Franchis, R.D., et al. (2008). Oral, colonic-release low-molecular-weight heparin: an initial open study of Parnaparin-MMX for the treatment of mild-to-moderate left-sided ulcerative colitis. *Alimentary Pharmacology and Therapeutics*, 28, 581–588.

Park, K., Kwan, I.C., Park, K. (2011). Oral protein delivery: Current status and future prospect. *Reactive and Functional Polymers*, 71, 280-287.

Pennings, A.J., Smith, P. (1960). Eutectic Crystallisation in Polymer Solutions. *Progress in Material Science,* 12, 460-465.

Peppas, N.A. (2004). Devices based on intelligent biopolymers for oral protein delivery. *International Journal of Pharmaceutics*, 277,11–17.

Petrus, A.K., Fairchild, T.J., Doyle, R.P. (2009). Traveling the Vitamin B12 Pathway: Oral Delivery of Protein and Peptide Drugs. *Angewandte Chemie International Edition*, 48, 1022-1028.

Pharmaceutical Research and Manufacturers of America (PhRMA). (2014), "Biologic Medicines in Development", Available from: <http://www.phrma.org. [23 November 2013].

Pillai, O., Panchagnula, R. (2001). Insulin therapies – past, present and future. *Drug Delivery Technologies*, 6, 1056-1061.

Potocky, T.B., Menon, A.K., Gellman, S.H. (2003). Cytoplasmic and Nuclear delivery of a TAT-derived peptide and a β-peptide after endocytic uptake into HeLa cells. *Journal of Biological Chemistry*, 278, 50188-50194.

Prasanth VV, Moy AC, Matthew ST, Mathapan R. (2011). Microspheres - An Overview. *International Journal of Research in Pharmaceutical and Biomedical Sciences*, 2, 332-328.

Proxima Concepts, Ltd. 2014, Axcess™ Oral Delivery System, Available from: <http://www.proximaconcepts.com/axcess.htm>. [15 April 2014].

Raoof, A.A., Chiu, P., Ramtoola, Z., Cumming, I.K., Teng, C., Weinbach, S.P., et al. (2004). Oral bioavailability and multiple dose tolerability of an antisense oligonucleotide tablet formulated with sodium caprate. *Journal of Pharmaceutical Sciences*, 93, 1431-1439.

Reis, C.P., Ribeiro, A.J., Houng, S., Veiga, F., Neufeld, R.J. (2007). Nanoparticulate delivery system for insulin: design, characterization and *in vitro/in vivo* bioactivity. *European Journal of Pharmaceutical Sciences*, 30, 392-397.

Rekha, M.R., Sharma, C.P. (2013). Oral delivery of therapeutic protein/peptide for diabetes – Future perspectives. *International Journal of Pharmaceutics,* 440, 48-62.

Rubas, W., Cromwell, M.E.M., Shahrokh, Z., Villagran, J., Nguyen, T.N., Wellton, M., et al. (1996). Flux measurements across Caco-2 monolayers may predict transport in human large intestinal tissue. *Journal of Pharmaceutical Sciences*, 85, 165–169.

Sakai, M., Imai, T., Ohtake, H., Azuma, H., Otagiri, M. (1997). Effects of absorption enhancers on the transport of model compounds in Caco-2 cell monolayers: assessment by confocal laser scanning microscopy. *Journal of Pharmaceutical Sciences*, 86, 779–785.

Saffran, M., Kumar, G.S., Savariarm, C. (1986). A new approach to the oral administration of insulin and other peptide drugs. *Science*, 233, 1081–1084.

Salama, P., Mamluk, R., Marom, K., Weinstein, I., Tzabari, M. (2010), inventors; Chiasma Inc., assignee. Pharmaceutical compositions and related methods of delivery. *United States Patent* US 0105627 A1. Sep 17.

Sanders, L.M., McRae, G.I., Vitale, K.M., Kell, B.A. (1985). Controlled delivery of an LHRH analogue from biodegradable injectable microspheres. *Journal of Controlled Release*, 2, 187-195.

Sarmento, B., Ribeiro, A., Veiga, F., Sampaio, P., Neufeld, R., Ferreira, D. (2007). Alginate/chitosan nanoparticles are effective for oral insulin delivery. *Pharmaceutical Research*, 24, 2198–2206.

Schiffter, H.A. (2011). The Delivery of Drugs-Peptides and Proteins. *Comprehensive Biotechnology,* 5, 587-604.

Senel, S., Rathbone, M.J., Canzis, M., Pather, I. (2012). Recent developments in buccal and sublingual delivery systems. *Expert Opinion Drug Delivery*, 9, 615-628.

Shakweh, M., Besnard, M., Nicolas, V., Fattalm, E. (2005). Poly (lactide-co-glycolide) particles of different physicochemical properties and their uptake by peyer's patches in mice. *European Journal of Pharmaceutics and Biopharmaceutics*, 61, 1-13.

Sharma, J.P.K., Bansal, S., Banik, A. (2011). Noninvasive Routes of Proteins and Peptides Drug Delivery. *International Journal of Pharmaceutical Sciences*, 4, 367-375.

Shen, Q., Li, X., Li, W., Zhao, X. (2011). Enhanced intestinal absorption of Daidzein by borneol/menthol eutectic mixture and microemulsion. *AAPSPharmSciTech*, 12, 1044-1049.

Sinko, P.J., Amidon, G.L. (1988). Characterization of the oral absorption of beta-lactam antibiotics. I. Cephalosporins: determination of intrinsic membrane absorption parameters in the rat intestine in situ. *Journal of Pharmaceutical Research*, 5, 645-650.

Sinko, P.J., Lee, V.H., Makhey, V., Leesman, G.D., Sutyak, J.P., Yu, H., et al. (1999). Biopharmaceutical approaches for developing and assessing oral peptide delivery strategies and systems: in vitro permeability and in vivo oral absorption of salmon calcitonin. *Journal of Pharmaceutical Research*, 4, 527-533.

Sophie, R., Tomme, V., Storm, G., Hennink, W.E. (2008). *In situ* Gelling hydrogels for pharmaceutical and biomedical applications. *International Journal of Pharmaceutics*, 355, 1-18.

Starr, C., Ever, C.A., Starr, L. (2011). *Biology: Concepts and Applications: Concepts and Applications*. United States of America: Cengage Learning. pp. 601-602.

Stein, D.W. (1986). *Transport and diffusion across cell membrane*. London: Academic Press. pp. 69-337.

Steinbach, O.C. (2014). The latest developments in therapeutic delivery. *Therapeutic Delivery,* 5, 15-19.

Stern, W., Gilligan, J.P. (1999), inventors; Unigene Laboratories Inc., assignee. Oral Salmon Calcitonin Pharmaceutical Products. *United States Patent* US 5.912.014. Jun 15.

Stevenson, B.R., Keon, B.H. (1998). The tight junction: morphology to molecules. *Annual Review of Cell and Developmental Biology*, 14, 89-109.

Stoll, B.R., Leipold, H.R., Milstein, S., Edwards, D.A. (2000). A mechanistic analysis of carrier-mediated oral delivery of protein therapeutics. *Journal of Controlled Release*, 64: 217-228.

Takaori, K., Burton, J., Donowitz, M. (1986). The transport of an intact oligopeptide across adult mammalian jejunum. *Biochemica Biophysica Research Communication*, 137, 682-687.

Takeuchi, T., Gonda, T. (2004). Cellular kinetics of villous epithelial cells and M cells in rabbit small intestine. *Journal of Veterinary Medical Science*, 66, 689–693.

Takuwa, N., Shimada, T., Matsumoto, H., Himukai, M., Hoshi, T. (1985). Effect of hydrogen ion-gradient on carrier-mediated transport of glycylglycine across brush border membrane vesicles from rabbit intestine. *Japanese Journal of Physiology*, 35, 629-642.

Tarsa Therapeutics, Inc. 2014, Oracal®, Available from: <http://www.tarsatherapeutics.com/Products/calcitonin.html>. [15 April 2014].

Taylor, K.M.G. (1997). Inhalation Delivery of Therapeutic Peptides and Proteins. In: Adjei AL, Gupta PK, editors. *Lung Biology in Health and Disease*. New York: Marcel Dekker. pp. 159-259.

Thanou, M., Verhoef, J.C., Junginger, H.E. (2001). Chitosan and its derivatives as intestinal absorption enhancers. *Advanced Drug Delivery Review*, 50, 91-101.

Tobio, M., Sánchez, A., Vila. A., Soriano, I., Evora, J.L., Vila-Jato, J.L., et al. (2000). The role of PEG on the stability in digestive fluids and in vivo fate of PEG–PLA nanoparticles following oral administration. *Colloid Surface B Biointerfaces*, 18, 315-322.

Toorisaka, E., Ono, H., Arimori, K., Kamiya, N., Goto, M. (2003). Hypoglycemic effect of surfactant-coated insulin solubilized in a novel solid-in-oil-in-water (S/O/W) emulsion. *International Journal of Pharmaceutics*, 252, 271–274.

Touitou, E., Rubinstein, A. (1986). Targeted enteral delivery of insulin to rats. *International Journal of Pharmaceutics*, 30, 95–99.

Tripathi, K.D. (2013). *Essential of medical pharmacology*. Bangladesh: Jaypee Brothers Medical Publishers Ltd. pp. 10-22.

Tscheik, C., Blasig, I.E., Winkler, L. (2013). Trends in drug delivery through tissue barriers containing tight junctions. *Tissue Barriers*. Forthcoming 2013. doi: 10.4161/tisb. 2013.04.04.

Tuntarawongsa, S., Phaechamud, T. (2012). Polymeric Eutectic Drug Delivery System. *Journal of Medicine,* 22, 27-32.

Tuvia, S., Atsmon, J., Teichman, S.L., Katz, S., Salama, P., Pelled, P.D., et al. (2012). Oral Octreotide Absorption in Human Subjects: Comparable Pharmacokinetics to Parenteral Octreotide and Effective Growth Hormone Suppression. *Journal of Clinical Endocrinology Metabolism*, 97, 1-8.

Valensi, P., Zirinis, P., Nicolas, P., Perret, G., Sandr-Banon, D., Attali, J.R. (1996). Effect of insulin concentration on bioavailability during nasal spray administration. *Pathologie Biologie (Paris)*, 44, 235-240.

Walker, R.F., Codd, E.E., Barone, F.C., Nelson, A.H., Goodwin, T., Campbell, S.A. (1990). Oral activity of the growth hormone releasing peptide His-D-Trp-Ala-Trp-D-Phe-Lys-NH2 in rats, dogs and monkeys. *Life Science*, 47, 26-36.

Wang, Z., Zhang, Q. (2004). Transport of proteins and peptides across human cultured alveolar A549 cell monolayer. *International Journal of Pharmaceutics*, 269, 451-456.

Werle, M., Berknop-Schńurch, A. (2006). Strategies to improve plasma half life time of peptide and protein drugs. *Journal of Amino Acids*, 30, 351-367.

Xia, W.J., Onyuksel, H. (2000). Mechanistic studies on surfactant-induced membrane permeability enhancement. *Pharmaceutical Research*, 17, 612-618.

Xu, Z., Zeng, Q.H., Lu, G.Q., Yu, A.B. (2006). Inorganic nanoparticles as carriers for efficient cellular delivery. *Chemical Engineering Science*, 61, 1027-1040.

Yamamoto, A., Taniguchi, T., Rikyun, K., Tsuji, T., Fujita, T., Murakami, M., et al. (1994). Effects of various protease inhibitors on the intestinal absorption and degradation of insulin in rats. *Journal of Pharmaceutical Research*, 11, 1496–1500.

Yang, L., Watanabe, S., Li, J., Chu, J.S., Katsuma, M., Yokohama, S., et al. (2003). Effect of colonic lactulose availability on the timing of drug release onset in vivo from a unique colon-specific drug delivery system (CODES™). *Pharmaceutical Research*, 20, 429–434.

Yang, T. (2013). PEGylation – Successful Approach for Therapeutic Protein Conjugation. *Modern Chemistry and Application*. Forthcoming 2013. doi: 10.4172/mca.

Yin, L., Ding, J., He, C., Cui, L., Tang, C., Yin, C. (2009). Drug permeability and mucoadhesion properties of thiolated trimethyl chitosan nanoparticles in oral insulin delivery. *Biomaterials*, 30, 5691–5700.

Yuan, L., Yu, Q., Li, D., Chen, H. (2011). Surface Modification to Control Protein/Surface Interactions. *Macromolecular Bioscience*, 11, 1031-1040.

Zhou, X.H. (1994). Overcoming enzymatic and absorption barriers to non-parenterally administered protein and peptide drugs. *Journal of Controlled Release*, 29, 239-252.

Zhou, X.H., Li Wan Po, A. (1991). Peptide and protein drugs: II. Non-parenteral routes of delivery. *International Journal of Pharmaceutics*, 75, 117-130.

CHAPTER 3

A PROOF OF CONCEPT STUDY DEPICTING A MENTHOL-BASED SOLID DISPERSION TECHNIQUE FOR ENHANCED SOLUBILITY AND DISSOLUTION OF SULFAMETHOXAZOLE FROM AN ORAL TABLET MATRIX

Published in AAPS PharmSciTech

Bibi F. Choonara, Yahya E. Choonara, Pradeep Kumar, Lisa C. du Toit, Lomas K. Tomar, Charu Tyagi, Viness Pillay. A Menthol-Based Solid Dispersion Technique for Enhanced Solubility and Dissolution of Sulfamethoxazole from an Oral Tablet Matrix. AAPS PharmSciTech, 2015, 16, 771-786.

Abstract

A menthol-based solid dispersion was designed to improve the intrinsic solubility of the poorly soluble sulfamethoxazole - a class II drug molecule of Biopharmaceutics Classification System (BCS) displaying widespread antibacterial activity. Solid dispersions of menthol and sulfamethoxazole were compressed with hydroxypropylmethylcellulose (HPMC) into suitable sulfamethoxazole-loaded matrix tablets for oral drug delivery. The sulfamethoxazole-loaded solid dispersions and compressed tablets were characterized for their physicochemical and physicomechanical properties such as changes in crystallinity, melting point, molecular transitions and textural analysis for critical analysis of their effects on the solubility and dissolution of sulfamethoxazole. The formulations were further evaluated for swelling, degradation, solubility and *in vitro* drug release behavior. *In vitro* drug release from the sulfamethoxazole-loaded matrix tablets displayed a minimum and maximum fractional release of 0.714 and 0.970, respectively. The tablets further displayed different release rate profiles over the study periods of 12, 16, 48 and 56 hours which was attributed to the varying concentrations of menthol within each formulation. Menthol was determined as a suitable hydrophilic carrier for sulfamethoxazole since it functioned as a solubilizing and release-retarding agent for improving the solubility and dissolution of sulfamethoxazole as well as controlling the rate at which it was released.

Keywords: crystallinity; menthol; oral solubility and dissolution; solid dispersion; sulfamethoxazole

3.1. Introduction

The aqueous solubility of a drug molecule is a major pharmaceutical formulation challenge as it is critical for achieving optimal oral bioavailability (Savjani *et al*., 2012). Various approaches have been explored for improving the solubility of poorly soluble drug molecules such as sulfamethoxazole (SMX). SMX was selected for this study as it is a bacteriostatic antibiotic within the sulfonamide class of drugs with activity against a wide range of organisms including susceptible strains of *Staphylococcus aureus, Streptococcus, Haemophilus influenza, Escherichia coli* and *Enterobacter* (Petri, 2011). SMX is commonly used in combination with trimethoprim for urinary tract infections (UTIs) (Petri, 2011). Due to its limited aqueous solubility (610mg/L at 37°C), SMX is used at high doses which facilitates the development of resistance and as a result poses a significant drawback (Petri, 2011).

The modification of the physicochemical property of the molecule, the use of supercritical fluid processes, surfactants, solubilizers and novel excipients are some of the approaches used to improve solubility of poorly soluble drug molecules (Sareen *et al*., 2004; Dohrn *et al*., 2007; Seedhar and Agarwal, 2009; Savjani *et al*., 2012). Modification of the physicochemical property of a molecule includes the reduction of the particle size to increase the surface area through micronization and nanosuspensions as well as crystal engineering to decrease the crystallinity through the formation of solid dispersions (Liu *et al*., 2006; Savjani *et al*., 2012). Chemical modification of a molecule comprises techniques such as change in pH, complexation and salt formation (Savjani *et al*., 2012). Although the reduction in particle size is most commonly used it often imparts an inordinate amount of physical stress on the drug molecule that results in degradation especially for thermosensitive and unstable molecules (Savjani *et al*., 2012). Solid dispersions have been considered as one of the most promising approaches to enhance the solubility, dissolution and subsequent oral bioavailability of poorly soluble drugs through various techniques (Liu *et al*., 2006; Savjani *et al*., 2012).

Typically, solid dispersions refer to a group of solid products consisting of two different components (Chiou and Riegelman, 1971; Luener and Dressman, 2000). The two components are generally a hydrophobic drug, molecularly dispersed within a hydrophilic polymer which may be crystalline or amorphous in nature (Vasconceles *et al.*, 2007). Solid dispersions can be classified into five main categories namely; simple eutectic mixtures, amorphous precipitations in a crystalline matrix, solid solutions, glass suspensions and glass solutions (Chiou and Riegelman, 1971). Sekiguchi and Obi, (1961) first demonstrated the use of solid dispersions by

creating a eutectic mixture for the delivery of the sulfonamide drug, sulfathiazole (aqueous solubility=373mg/L at 25°C). Subsequently, Levy (1963) established a basic and precise method for the preparation of solid dispersions and solid solutions. Conclusive results from both studies displayed the improvement of solubility and dissolution by the use of solid dispersions (Sekiguchi and Obi, 1961; Levy, 1963). Since its innovation in 1961, solid dispersions have become the cornerstone for improvement in the oral delivery of poorly water soluble drugs today (Bhatnagar *et al*., 2014).

Solid dispersions for the improvement of poorly soluble SMX have not been investigated and thus the aim of this study was to improve the solubility and dissolution rate of SMX through the formation of a menthol-based solid dispersion. According to the BCS classification system, SMX is classified as a Class II molecule with poor solubility and high permeability (Lindenburg *et al*., 2004; Safoon *et al*., 2011). SMX has limited solubility in water but is optimally soluble in alcohol, acetone and alkali hydroxides (Reynolds, 1993). Thus, this system demonstrates the solubility improvement of SMX through the use of hydrophilic menthol. SMX-loaded matrix tablets of the solid dispersions of menthol and SMX were formulated to significantly improve the oral delivery of SMX. This system may potentially decrease the dose required to achieve a therapeutic effect and improve resistance rates. The physicochemical and physicomechanical characteristics of the system as well as the solubility and *in vitro* evaluation of the solid dispersions have been investigated and presented in this chapter.

3.2. Materials and Methods

3.2.1. Materials

Menthol(2-isopropyl-5-methylcyclohexanol,99% purity, M_W=156.27g/mol), (hydroxypropyl)methyl cellulose (Methocel, viscosity grade=2%), sulfamethoxazole (SMX) (M_W=253.28g/mol) and excipients such as sodium carboxymethylcellulose (CMC) and magnesium stearate were purchased from Sigma-Aldrich Corp. (St. Louis, MO, USA). All other materials were of analytical grade and were employed as received.

3.2.2. Preparation of the SMX-loaded solid dispersions

Solid dispersions were prepared according to a co-melt method, involving the combination of menthol and SMX by a heating and mixing process as proposed by Arnikar and co-workers, (1992). The upper (10g) and lower (1g) limits of menthol for achievement of a solid dispersion

were determined based on preformulation studies. Various concentrations were selected within these limits as shown in Table 3.1. In addition, since SMX had an experimental aqueous solubility of 610mg/L at 37°C, an excess of ±10mg/mL was utilized to determine the improvement in solubility of SMX when formulated as a solid dispersion. Based on the upper and lower limits determined from preformulation studies, various concentrations of menthol were heated using a heated magnetic stirrer to a temperature of 37±0.5°C until a liquid melt was obtained. SMX (50mg) was subsequently added to the liquid melt (±5mL) and heated to a temperature of 160±0.5°C to enable the melting of SMX. The physical mixtures underwent constant magnetic stirring at a speed of 300rpm for ±30 minutes (maintained at a temperature of 160±0.5°C) until homogenous solid dispersions were formed. Thereafter, a 5%$^{w}/_{w}$ concentration of a cryoprotectant (sucrose) was added in equal volume to the solid dispersion. The resultant solid dispersions were placed in a freezer at -80°C for 24 hours. Thereafter, the frozen SMX-loaded solid dispersions were lyophilized (Labconco Freeze-Dry Systems, Labconco Corp., Kansas City, MO, USA) for 48 hours to form freeze-dried SMX-loaded solid dispersion powders for physicochemical and physicomechanical characterization. Typically, lyophilization is used as a method for the sublimation of menthol from a formulation, however, the high percentage of cryoprotectant that was added to the solid dispersion was used to protect the menthol from freezing and desiccation stresses during the lyophilization process (Thakur and Gupta, 2006; Lee *et al*., 2009; Williams *et al*., 2012). As a result, excess menthol was absorbed onto the cryoprotectant thereby minimizing processing losses. The lyophilized solid dispersions were then combined with 100mg of HPMC, 12mg of CMC and 1mg of magnesium stearate before compression at 5 tons to form SMX-loaded matrix tablets with dimensions of ~10mm x 4.5mm (diameter x thickness) using a Carver Tableting Press (Wabash, Indiana, USA).

Table 3.1: Solid dispersions synthesized using the co-melt method

Formulation no.	Menthol (g)	Sulfamethoxazole (mg)
1	1	50
2	4	50
3	4.5	50
4	5	50
5	5.5	50
6	6	50
7	10	50

3.2.3. In-process validation of the SMX-loaded solid dispersions and the SMX-loaded matrix tablets

The solid dispersions were analyzed with respect to their physical appearance, particle size and powder flow properties whilst the matrix tablets were evaluated for their uniformity in mass, thickness and friability. The physical appearance was assessed based on colour and texture and the average particle size was determined by ZetaSizer Nano ZS (Malvern Instruments Ltd., UK). The samples were thoroughly dispersed in 10mL of distilled water prior to filtering 2mL of the sample through a 0.22µm pore filter into a cuvette for analysis by Zetasizer. Measurement of the angle of repose and Carr's compressibility index was used to classify the flow properties of the lyophilized SMX-loaded solid dispersions. The weight of each matrix tablet was determined using an analytical digital balance (Mettler, Model AE 240, Griefensee, Switzerland) while the thickness of the matrix tablets were determined using a digital caliper (25 × 0.01mm capacity) (Taizhou hangyu tools gauge and blades Co., Ltd., Wenqiao, Zhejiang, China). The friability was determined on a Friabilator (Erweka D-63150, Heusenstamm, Germany) at 25 rpm for 4 minutes with 1% set as the upper limit of acceptability.

3.2.4. Thermal analysis of the SMX-loaded solid dispersions

Thermal analysis was performed on each of the SMX-loaded solid dispersions using Temperature Modulated Differential Scanning Calorimetry (TMDSC) (Mettler Toledo, DSC1, STAR^{e}System, Schwerzenback, Switzerland) to determine a change in the melting point of SMX when formulated as a solid dispersion. Accurately weighed samples (10±0.25mg) were placed in perforated 40µl aluminum crucibles which were hermetically sealed and ramped between a temperature range of 25-240°C at a constant rate of 10°C/min with a constant purge of N_2 atmosphere. The glass transition temperature (T_g), onset of melting (T_o), melting peak temperature (T_p), heat of fusion (ΔH_m) and temperature of crystallization (T_c) were determined for each of the native molecules and the SMX-loaded solid dispersions. Thermogravimetric analysis (TGA) was used to determine the thermal degradation of the SMX-loaded solid dispersions upon heating. A Thermogravimetric Analyzer (TGA) (PerkinElmer TGA 4000, Llantrisant, Wales, UK) was used and samples were prepared by weighing 5mg of lyophilized powders within ceramic crucibles. The weights were tarred prior to running the samples and were heated from 25-900°C at a rate of 10°C/min with a constant purge of N_2 atmosphere.

3.2.5. Determination of molecular and vibrational transitions of the SMX-loaded solid dispersions

ATR-FTIR spectra were obtained for the native molecules, menthol and SMX, as well as the different concentrations of SMX-loaded solid dispersions to determine the presence of menthol and SMX within the solid dispersion. PerkinElmer Spectrum 2000 FTIR spectrophotometer with a single-reflection diamond MIRTGS detector (PerkinElmer Spectrum 100, Llantrisant, Wales, UK) was used. Samples were prepared and placed on the diamond crystal and processed by universal ATR polarization accessory for the FTIR spectrum series at a resolution of $4cm^{-1}$. Samples were analyzed between a scanning range of $4000\text{-}650cm^{-1}$ at a constant pressure of 120psi with 32 accumulations.

3.2.6. Determination of Matrix Hardness, Matrix Resilience and Deformation Energy of the SMX-loaded matrix tablets

The SMX-loaded matrix tablets were analyzed with respect to Matrix Resilience (MR), Matrix Hardness (MH) and Deformation Energy (DE) to determine their structural integrity. A calibrated Texture Analyzer (TA.XT *plus*, Stable Microsystems, Surrey, UK) fitted with a flat-tipped steel probe (2mm diameter) was used for the determination of MR, MH and DE values. Data was captured at a rate of 200 points per second using Texture Exponent Software (V3.2). MR was computed as a percentage of the ratio between the Area under the Curve (AUC) of the peak to baseline (AUC_{2-3}) and the baseline to peak (AUC_{1-2}) from a Force-Time profile as displayed in Figure 3.1. The MH and DE values were both obtained from the gradient and AUC of the Force-Distance profiles, respectively.

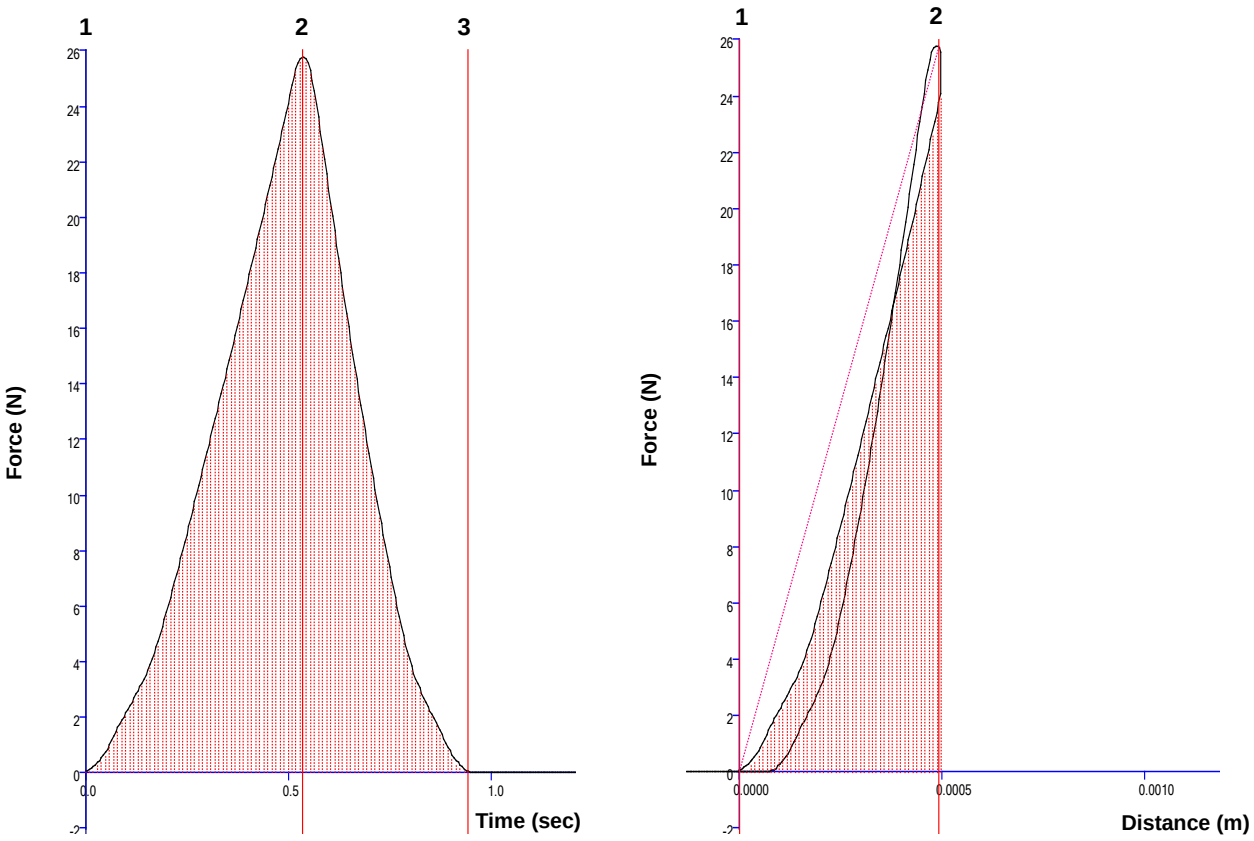

Figure 3.1: Typical Force-Time and Force-Distance profiles for determination of MR (Force-Time profile; AUC_{2-3}/AUC_{1-2}), MH (gradient of a Force-Distance profile) and DE (AUC of a Force-Distance profile).

The MH was calculated using the Brinell Hardness Number (BHN) (Equation 3.1). Textural analysis on all the SMX-loaded matrix tablets was performed in triplicate. The parameters employed for the analysis are listed in Table 3.2.

$$\mathrm{BHN} = \frac{2\mathrm{F}}{\pi \mathrm{D}\left(\mathrm{D}-\sqrt{\mathrm{D}^2-\mathrm{d}^2}\right)} \qquad \textbf{(3.1)}$$

Where, BHN is Brinell Hardness Number; D is diameter of indenter (mm); F is elucidated from the gradient of the initial force and the final force obtained and d is diameter of indentation (mm).

Table 3.2: Textural profiling parameters used for determining the Matrix Hardness, Matrix Resilience and Deformation Energy of the SMX-loaded matrix tablets

Parameters	Matrix Hardness	Matrix Resilience	Deformation Energy
Pre-test speed	1 mm/s	1 mm/s	1 mm/s
Test speed	0.5 mm/s	0.5mm/s	0.5mm/s
Post-test speed	1 mm/s	10mm/s	10mm/s
Trigger type	Auto	Auto	Auto
Trigger force	0.05 N	0.05 N	0.05 N
Compression strain	N/A	40%	N/A

3.2.7. Qualitative and quantitative analysis of the crystallinity of the SMX-loaded solid dispersions

The change in the percentage crystallinity of the SMX-loaded solid dispersions compared to the native molecules, menthol and SMX, were determined using an X-ray Diffractometer (XRD) fitted with a high speed silicon strip detector and operating at 600W X-ray source for high resolution scanning (Rigaku Miniflex Guidance 600W, Tokyo, Japan). This characterization test was used to determine the change in crystallinity of the native molecules as compared to the SMX-loaded solid dispersions. Samples were prepared by weighing ±10mg of lyophilized powders and placing them in aluminium sample holders. Each sample ran between an operating range of 0-80° 2-theta. Data was captured and analyzed using the Rigaku Powder Diffraction Analysis Software (PDXL2). Similarity of diffraction patterns, peak positions and percentage crystallinity were determined from the various profiles obtained.

3.2.8. Morphological characterization of the SMX-loaded solid dispersions

The surface morphology of the SMX-loaded solid dispersions were observed using a Scanning Electron Microscope (SEM) (FEI Company, Hillsboro, Oregon, USA) to determine characteristic changes in their crystalline and amorphous structures. Samples were fixated on aluminum stubs and sputter coated with gold for 60 seconds using a SPI-Module™ Sputter Coater (SPI Supplies, Structure Probe, West Chester, PA). Samples were then placed in the FEI Phenom™ Scanning Electron Microscope operated at 10kV in the electron imaging mode and observed at varying degrees of magnification.

3.2.9. Degree of swelling and erosion of the SMX-loaded matrix tablets

The degree of swelling of the SMX-loaded matrix tablets was determined using the weight gain method (Efentakis and Vlachou, 2000). Tablets were weighed initially and placed in 50mL of buffer at pH 6.8 over a period of 24 hours. At predetermined time intervals (0, 1, 2, 3, 6, 8, 12, 16, 24 hours), samples were removed and reweighed to determine changes in swelling. The

degree of swelling at each time interval was determined using Equation 3.2. Erosion studies were conducted on the same samples after 24 hours by drying to a constant weight. The percentage erosion was calculated using Equation 3.3.

$$\% \ \Delta Swelling = \frac{W_f - W_i}{W_i} \times 100 \quad \textbf{(3.2)}$$

Where, W_f is the weight of the swollen tablet at time *t* and W_i is the initial weight of the tablet. (N=3).

$$\% \, Erosion = \frac{W_i - W_f}{W_i} \times 100 \quad \textbf{(3.3)}$$

Where, W_i is the initial weight of the tablet and W_f is the final dried weight of the tablets after 24 hours. (N=3).

3.2.10. Determination of the comparative solubility of SMX and SMX-loaded solid dispersions

The solubility of SMX was determined by separately dissolving 50mg of SMX in 20mL of menthol and simulated human intestinal fluid (SHIF) at pH 6.8 maintained at 37±0.5°C with constant magnetic stirring (300rpm) for 48 hours. SMX-loaded solid dispersions as listed in Table I were similarly dissolved in SHIF (pH 6.8) to determine the change in solubility of the solid dispersions as compared to the pure SMX dissolved in simulated intestinal medium. Sampling of 3mL was undertaken after 48 hours and the SMX content was determined using a UV spectrophotometer, at a wavelength of 271nm (Implen Nanophotometer™, Implen GmbH, München, Germany). All samples were filtered using a 0.45µm membrane filter prior to UV analysis.

3.2.11. *In vitro* drug release from SMX-loaded matrix tablets

In vitro drug release studies were performed using a USP35 dissolution apparatus II (Caleva, Model 7ST, UK). The SMX-loaded matrix tablets were placed in 900mL SHIF at pH 6.8. Each tablet was placed beneath a ring mesh assembly within the dissolution vessel to prevent floatation. Dissolution was performed at a speed of 50rpm (37±0.5°C). Sampling of 3mL was undertaken at predetermined time intervals (0, 1, 2, 3, 6, 8, 10, 12, 16, 24, 48, 56 hours) and replaced with an equal quantity (3mL) of drug-free dissolution medium to maintain sink

conditions. The quantity of SMX released was determined using a UV spectrophotometer at a wavelength of 271nm (Implen Nanophotometer™, Implen GmbH, München, Germany). All samples removed were filtered using a 0.45µm membrane filter prior to UV analysis. Drug release was calculated as a mean of three determinations as all studies were conducted in triplicate. In addition, the mean dissolution time (MDT) (Equation 3.4) was calculated from dissolution data to determine the drug release rate (Sathish and Syed, 2013).

$$\mathrm{MDT} = \frac{\sum_{i=1}^{i=n} t_{mid} \times \Delta M}{\sum_{i=1}^{i=n} \Delta M} \quad \textbf{(3.4)}$$

Where, MDT is Mean Dissolution Time; i is the dissolution sample number; n is the number of dissolution sample time; t_{mid} is time at mid-point between i and i=1; ΔM is the additional amount of drug dissolved between i and i=1.

In addition, the drug release data was fitted into various mathematical modelling equations in order to elucidate the mechanism of drug release.

3.3. Results and Discussion

3.3.1. In-process validation analysis of the SMX-loaded solid dispersions and matrix tablets

SMX-loaded solid dispersions were prepared in accordance with the varying concentrations listed in Table 3.1. The lyophilized SMX-loaded solid dispersions were successfully formulated and produced white, crystalline powders with an average particle size of 110nm with a minimum and maximum particle size of 90nm and 200nm, respectively. The powder flow properties of the SMX-loaded solid dispersions were determined using the angle of repose and Carr's compressibility index (McGlinchey, 2005). The average Carr's compressibility index and angle of repose of the SMX-loaded solid dispersions were 9.17% and 19.29°, respectively. The minimum and maximum values of the solid dispersions for Carr's compressibility index were 8.93% and 9.21%, whereas the angle of repose was 18.99° and 19.54°. According to McGlinchey (2005), the values obtained indicated excellent powder flow properties as they fall within the range of 5-15% for Carr's compressibility index and <20° for angle of repose. The SMX-loaded matrix tablets were evaluated for uniformity of mass, thickness and friability. All the SMX-loaded matrix tablets were uniform in mass, each having an average weight of

550±0.5mg. The thickness ranged from 4.5±0.05mm to 5.1±0.03mm while the friability was at an average of 0.7% (i.e. within the set limit 1%), demonstrating desirable compressibility and resistance to chipping.

3.3.2. Thermal analysis of the SMX-loaded solid dispersions

SMX and menthol are pure, low molecular weight molecules (<500 g/mol) and thus the onset of melting (T_o) was considered as the melting temperature (T_m) (Gabott, 2008). In addition, between the T_o and T_p (melting peak) the sample continues to melt (Gabott, 2008). The TMDSC thermograms of SMX and menthol are depicted in Figure 3.2a. SMX displayed a single, narrow, defined peak with an onset of melting (T_o) at 169.02°C which corresponded to the melting temperature (T_m). The quantity of heat per unit mass that was required to change the SMX from a solid to liquid at its melting point was 120.92Jg^{-1}. In contrast, menthol displayed a heat of fusion (ΔH_m) of 79.62Jg^{-1} with a melting onset at 37.19°C and a T_p at 40.44°C. The first endothermic shift that was noticed for menthol was indicative of the glass transition temperature (T_g) at approximately 28.36°C and corresponded to the softening of the menthol (Widmann, 2000). In addition, another endothermic event was observed in the TMDSC thermogram for menthol at a temperature of 205.97°C confirming a phase change (sublimation) since menthol has a boiling point of 212°C (Neubert *et al*., 1997).

On comparison of the TMDSC thermograms of the individual molecules with the SMX-loaded solid dispersions, a predictable melting peak was noticeable between 37-40°C for all formulations. The first endothermic events for F1-7 (Figure 3.2b) were identical to the peak observed for the individual menthol, thus indicating the melting of menthol within these formulations. Consequently, the endothermic event between 195.89-216.77°C in F1-7 was characteristic of the sublimation of menthol. The reduction in intensity and the shifting of the sharp melting peak of SMX in the solid dispersions were noticeable for F1-7. F1-3 (Figure 3.2b) displayed melting endotherms similar to the endothermic peak of SMX with a melting temperature of 149.24°C, 145.32°C and 150.48, respectively. Analysis of the SMX melting peak in F1-7 showed the successive decrease in intensity. This corresponded to the decreased ΔH_m observed for each of the formulations with F1 showing the highest value (22.68Jg^{-1}), F6 displaying the lowest value (1.12Jg^{-1}) and F7 showing a complete absence of the drug peak. It was speculated that the decrease in intensity of the SMX peak is attributed to the dissolving of SMX within the melted menthol during DSC measurements and as a result distinct endothermic peaks corresponding to the melting of menthol was observed (Yamashita *et al*., 2003; Sinha *et*

al., 2010, Sharma *et al*., 2013). In addition, the results may indicate that the degree of crystallinity was substantially reduced and the SMX was present in an amorphous form within the solid dispersion, thus accounting for the reduced intensity and shifting peaks (Yamashita *et al*., 2003; Sinha *et al*., 2010).

The results obtained for DSC were analogous to existing data that depicted the absence of drug peaks in the thermograms of solid dispersions of the poorly water soluble drugs, tacrolimus and piroxicam (Tantishaiyakul *et al.,* 1999; Yamashita *et al*., 2003). This was attributed to its dissolution within the melted carrier during DSC measurements and only displayed the appearance of an endothermic peak corresponding to the melting of the carrier (Tantishaiyakul *et al.,* 1999; Yamashita *et al*., 2003).

The TGA profiles of SMX and menthol displayed the change in mass of the native molecules as a function of temperature (Figure 3.3a). Upon heating the samples, SMX displayed a stepped decrease in percentage weight with an initial loss of 21.827% at a temperature of 301.92°C. Subsequently, as the temperature increased to 400°C a 50% decrease in sample weight was noticed and at the end of the temperature range (894.87°C) only 27% of the sample had remained. In contrast, menthol displayed a complete decrease in mass of 99.092% at 194.27°C which was attributed to the vaporization of the menthol (Widmann, 2000). The TGA profiles of the native molecules were compared to the SMX-loaded solid dispersions and the differences were noted (Figure 3.3b). F1 depicted a similar stepped, but significantly larger decrease (97.869%) in the mass as compared to SMX. All the other curves were representative of F2-7 (Figure 3.3b). The curves displayed were characteristically similar to menthol, displaying a significant mass loss (± 90%) within the temperature range of 188.30°C-203.85°C. These results corresponded to the decreased intensity of the SMX peaks and the prominent menthol peaks observed in the TMDSC thermograms. In summary, the concentration of menthol contained within each formulation directed the thermal degradation and melting behavior of F1-7. TMDSC and TGA data confirmed the formation of a solid dispersion.

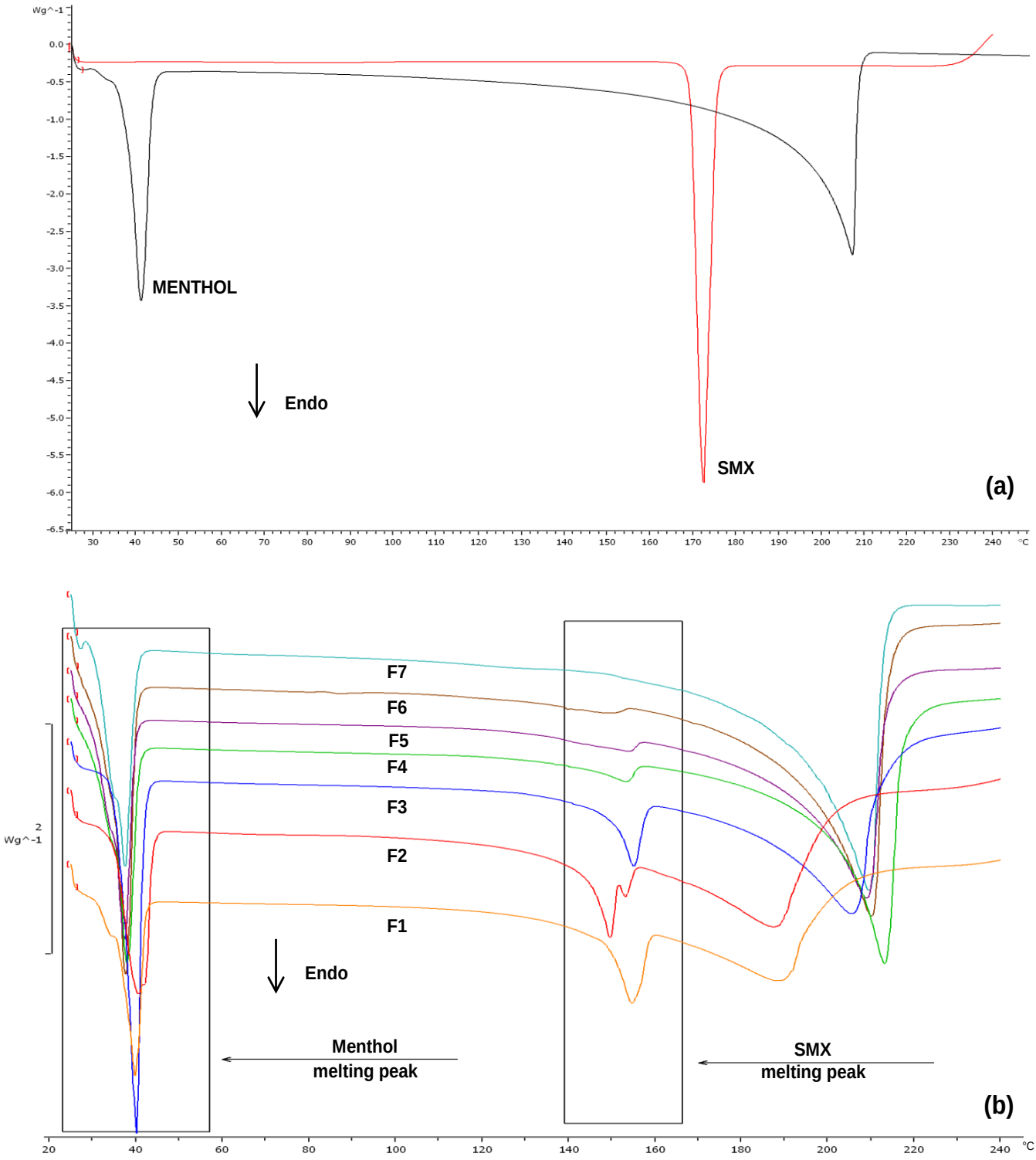

Figure 3.2: TMDSC thermal profiles for **a)** native SMX and menthol and **b)** SMX-loaded solid dispersions F1-7.

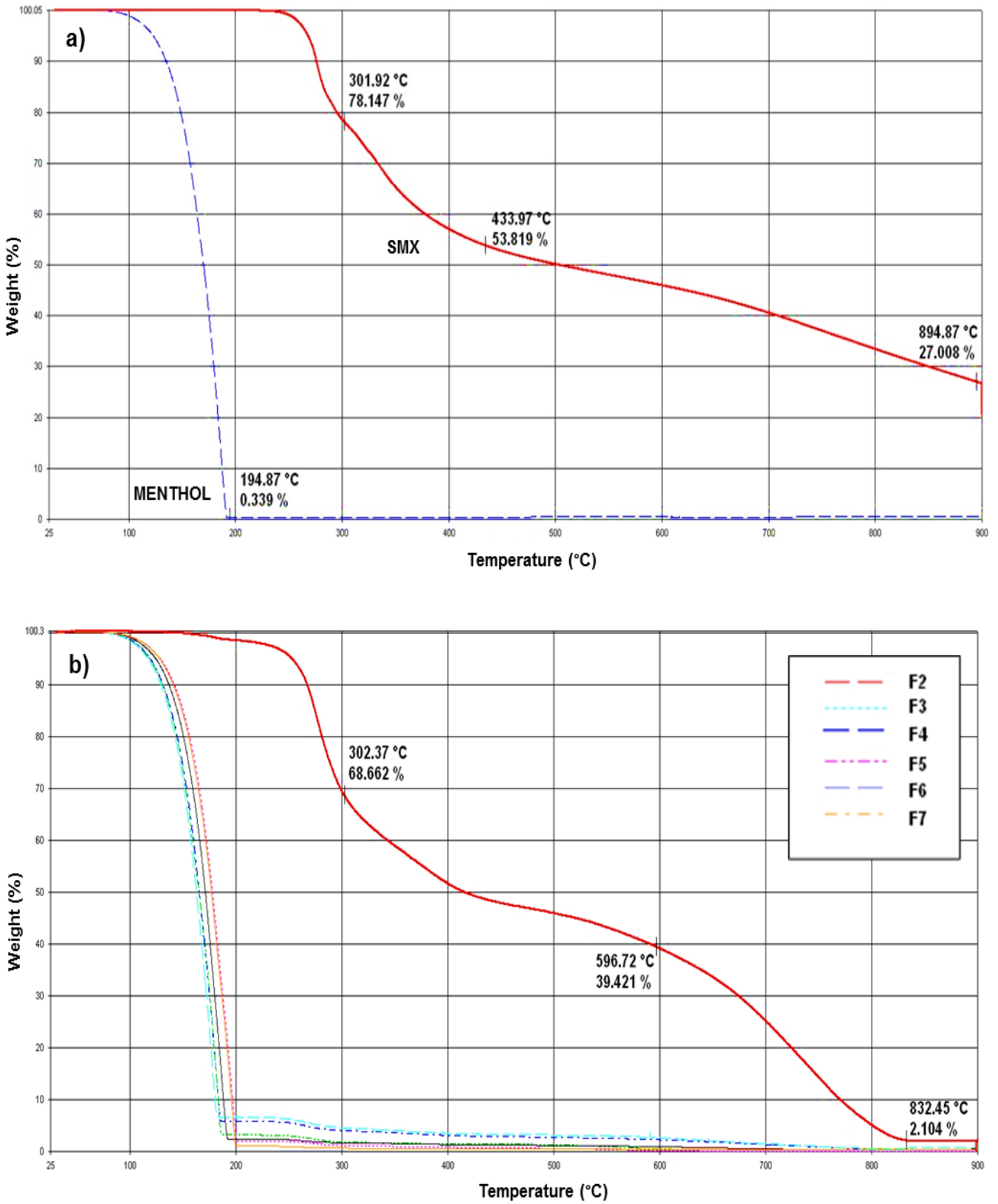

Figure 3.3: TGA profiles of **a)** native SMX and menthol and **b)** SMX-loaded solid dispersions F1-7.

3.3.3. Analysis of the ATR-FTIR spectra of the SMX-loaded solid dispersions

Complete ATR-FTIR split transmittance spectra of menthol and SMX as well as the varying concentrations of SMX-loaded solid dispersions listed in Table 3.1 are shown in Figure 3.4 with characteristic peaks identified. Sucrose was used as the background spectrum for FTIR measurements and was subtracted from the sample spectrum so as to gain information about the solid dispersion only. Since menthol is a terpene alcohol it displayed a strong, broad peak at 3270cm^{-1} which was indicative of -O-H stretching (Coates, 2000). In addition, absorption due to carbon-hydrogen stretching was observed between 2800cm^{-1} and 2900cm^{-1}. At lower frequencies (1375cm^{-1} to 1470cm^{-1}) menthol displayed carbon-hydrogen bending typical of methyl groups present within menthol. The defining peaks of SMX were observed between a wavelength of 3000cm^{-1} to 3500cm^{-1} and 1200cm^{-1} to 1500cm^{-1} which corresponded to –N-H and SO_2 stretching vibrations, respectively (Coates, 2000).

The distinct bands spanning from 3000cm^{-1} to 3500cm^{-1} in solid dispersions F1-3 were characteristic of –N-H stretching, identical to those found in SMX. The bands were narrower and less intense than –O-H bands of alcohols and phenols and thus diagnostic of primary amide groups present (Coates, 2000). A decrease in peak intensity within the wavelength range of 3100cm^{-1} to 3200cm^{-1} was noticeable as the concentration of menthol increased from F1-3, with F3 showing the largest decrease in intensity as evidenced by the increased transmittance shown in Figure 3.4a). Smaller and more variable peaks appearing within the regions of 2800cm^{-1} to 2960cm^{-1} in the split spectra of F1-3 indicated absorption due to –C-H stretching which occurred at the high-frequency end of the spectrum, typically indicating hybridization of the carbon (Coates, 2000). The bands were similar to those observed for the native molecule menthol, showing absorption peaks at 2918cm^{-1}, 2951cm^{-1}, 2867cm^{-1} and 2845cm^{-1}. Strong absorption peaks at 1090cm^{-1} and 1032cm^{-1} on the F1 spectrum, 1092cm^{-1} and 1030cm^{-1} on the F2 spectrum, and 1091cm^{-1} and 1025cm^{-1} on the F3 spectrum were characteristic of an overlap of primary alcohol –C-O stretching vibrations and primary amine –C-N stretching vibrations (Coates, 2000). Both the absorption bands were characteristically observed in the spectra for menthol and SMX, indicating the presence of both molecules within the solid dispersion.

A pair of split absorption bands centered around 1500cm^{-1} and 1600cm^{-1} were present in all three spectra (F1-3) and corresponded to –C=C aromatic ring stretching vibrations, indicative of the presence of an aromatic ring which is a defining feature of SMX. The distinctive band observed at a wavelength of 1594cm^{-1} for all three spectra F1-3 indicated δ–N-H (amide II band)

stretching vibrations (Coates, 2000). Hetero-oxy stretching frequencies were observed within the main fingerprint spectral region of 1200cm^{-1}-1470cm^{-1} in spectra F1-3 with peaks observed between the ranges of 1200-1250cm^{-1} and 1350-1470cm^{-1} indicating symmetrical and asymmetrical SO_2 stretching vibrations (Coates, 2000). This confirmed the presence of a sulphur group within the three formulations which is a determining feature of SMX.

FTIR absorption spectra of F4-7 had characteristic absorption bands identified which included, a broad band spanning from 3200cm^{-1} to 3600cm^{-1} which was as a result of the decrease in intensity and subsequent disappearance of the –N-H stretching vibrations (characteristic of the primary amide of SMX) corresponding to the increased concentrations of menthol from F4-7. Consequently, the appearance of the broad band indicated a hydrogen-bonded –OH stretching vibration comparable to that of menthol. In addition, the absorption peaks that were smaller and more variable within the region 2800cm^{-1} to 2960cm^{-1} for F1-3 appeared as strong, distinct peaks in the split spectra for F4-7 indicating definite –C-H stretching vibrations (Coates, 2000).

The appearance of a new peak, uncharacteristic from either menthol or SMX, at 1735cm^{-1} on the F4 spectrum, 1745cm^{-1} on the F5 spectrum, 1745cm^{-1} on the F6 spectrum, and 1740cm^{-1} on the F7 spectrum indicated –C=O stretching vibrations (Coates, 2000). This strong band represented a carboxylic acid derivative and signified intense hydrogen-bonding between the –OH group of menthol and –C-O group of SMX (Coates, 2000; Stoker, 2013). Although solid dispersions F1-3 depicted a peak within this region, the peak was slight and inconspicuous and thus its effect was considered unremarkable. Aromatic –C=C ring stretching and –N-H bending vibrations in the regions of 1500-1600cm^{-1} and 1500-1650cm^{-1}, respectively, were present for F4-7 showing decreasing intensities as the concentration of menthol increased. Other typical peaks occurred in the range of 1000-1090cm^{-1} due to –C-O/-C-N overlapping stretch vibrations and medium to weak δ–N-H loop bands within the region of 630-800cm^{-1} for F4-7 (Coates, 2000).

Comparison of the split transmittance spectra of F1-7 clearly depicted the altered molecular and vibrational transitions as the concentration of menthol increased in relation to the constant concentration of SMX. F1-3 depicted peaks significantly alike to that of SMX, whereas F4-7 showed absorption spectrums similar to that of menthol confirming the increased concentrations contained within these formulations (Coates, 2000; Stoker, 2013). However, formation of a new

band and appearance of peaks characteristic to both menthol and SMX indicated successful combination of the two components in the formation of a solid dispersion (Coates, 2000).

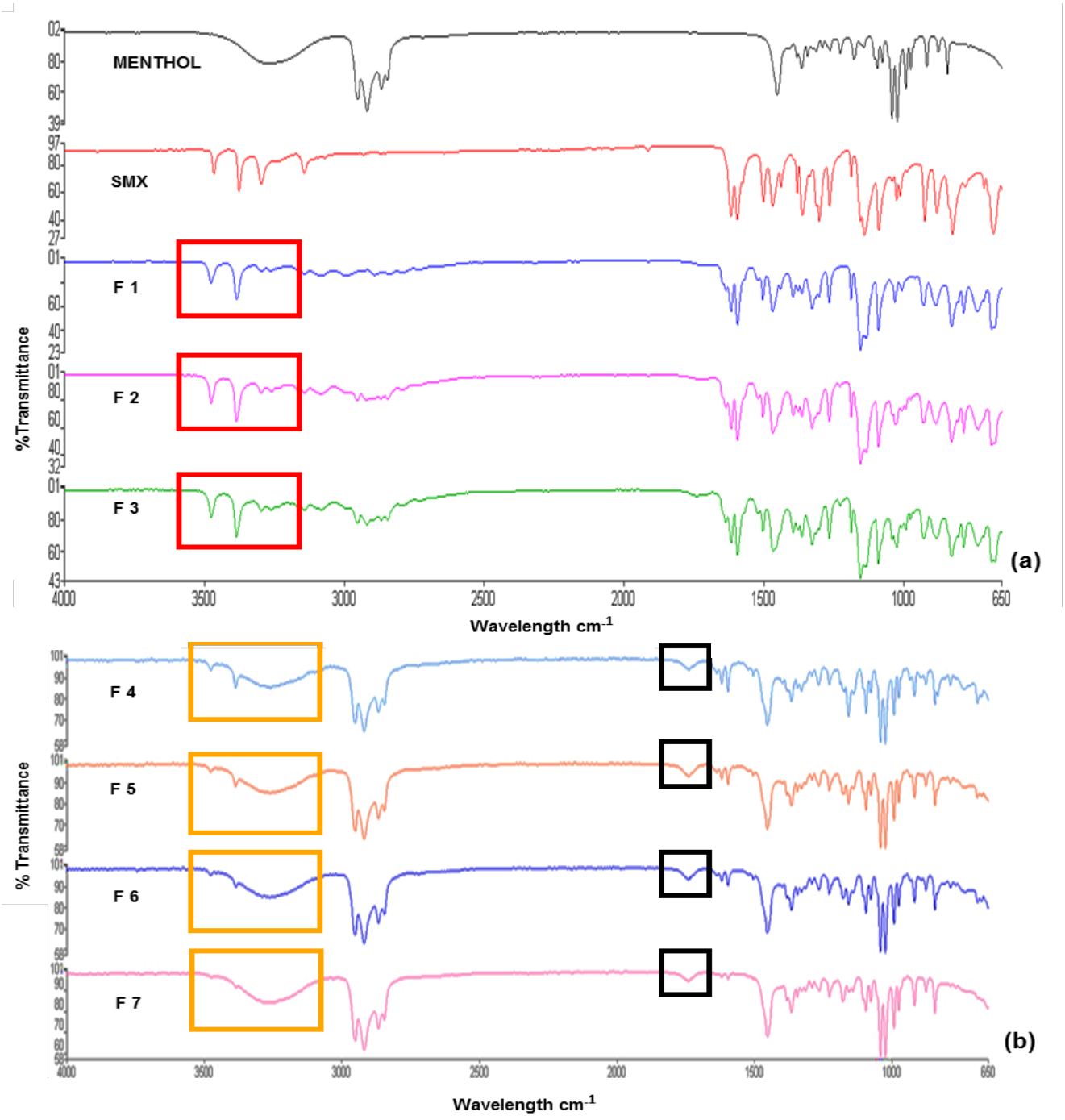

Figure 3.4: ATR-FTIR transmittance spectra: **a)** split spectra of menthol, SMX and SMX-loaded solid dispersions F1-3 and **b)** split spectra of SMX-loaded solid dispersions F4-7. Red blocks highlight the –N-H stretching vibrations (primary amide), orange blocks highlight the disappearance of the primary amide bond and appearance of an –O-H stretching vibration, black blocks indicate –C=O stretching and formation of the strong hydrogen bonding between menthol and SMX.

3.3.4. Textural profiling of the SMX-loaded matrix tablets

Textural profiling of the SMX-loaded matrix tablets was performed to determine the MH, MR and DE using Force-Time and Force-Distance profiles. MR was calculated in order to determine the ability of the matrices to return to their original dimensions after being subjected to a compression strain by the textural probe (Pillay and Fassihi, 1999). The MR decreased from F1 to F3, corresponding to the decreased hardness and increased concentrations of menthol within the SMX-loaded solid dispersions. It was determined that at a consistent strain of 40%, F1 proved to be the most resilient at 55.42%, compared to the slightly lower resilience percentages for F2 (50.04%) and F3 (44.80%) (Figure 3.5a). Results indicated that with higher concentrations of menthol, the flexibility of the formulations and its ability to return to its original state decreased. Accordingly, this would warrant that F4-7 would have correspondingly lower resilience values as compared to F1-3. However, this was not the case as results proved that F4 (52.80%) and F7 (57.70%) showed higher resilience values with the latter being the most resilient. This deviation was attributed to the formation of a strong hydrogen bond in F4-7 which imparted a structural flexibility typical of esters (Johnson, 1999).

MH is a pertinent physicomechanical property essential towards controlling drug release, swelling, erosion and matrix stability. In this study, MH was represented as an index of the ability of the matrices to resist and overcome adhesive and cohesive forces (deformation). F1 displayed the greatest hardness with a value of 240.40N.mm^2 and correspondingly high deformation energy (0.011J), whereas F7 showed a hardness value of 55.67N.mm^2 and a correspondingly low deformation energy (0.007J). MH decreased accordingly from F1-7 with increasing concentrations of menthol, creating relatively softer matrices that were more susceptible to matrix deformation.

In addition, matrix rigidity (Figure 3.5b) was elucidated from the Force-Distance profiles of F1-7. Analysis of results depicted a predictably high matrix rigidity for F1 (95.08N.mm^2) with F2-7 displaying lower matrix rigidities. The decrease in rigidity was attributed to the distinct formation of an ester bond (Figure 3.4b) within subsequent formulations leading to a less rigid structure and lower melting point as compared to the corresponding amide band (Figure 3.4a) that was characteristic of SMX. In other words, as the concentration of menthol increased from F1-7 it resulted in the dampening of the characteristic structural features of SMX, thereby creating softer and less rigid structural matrices.

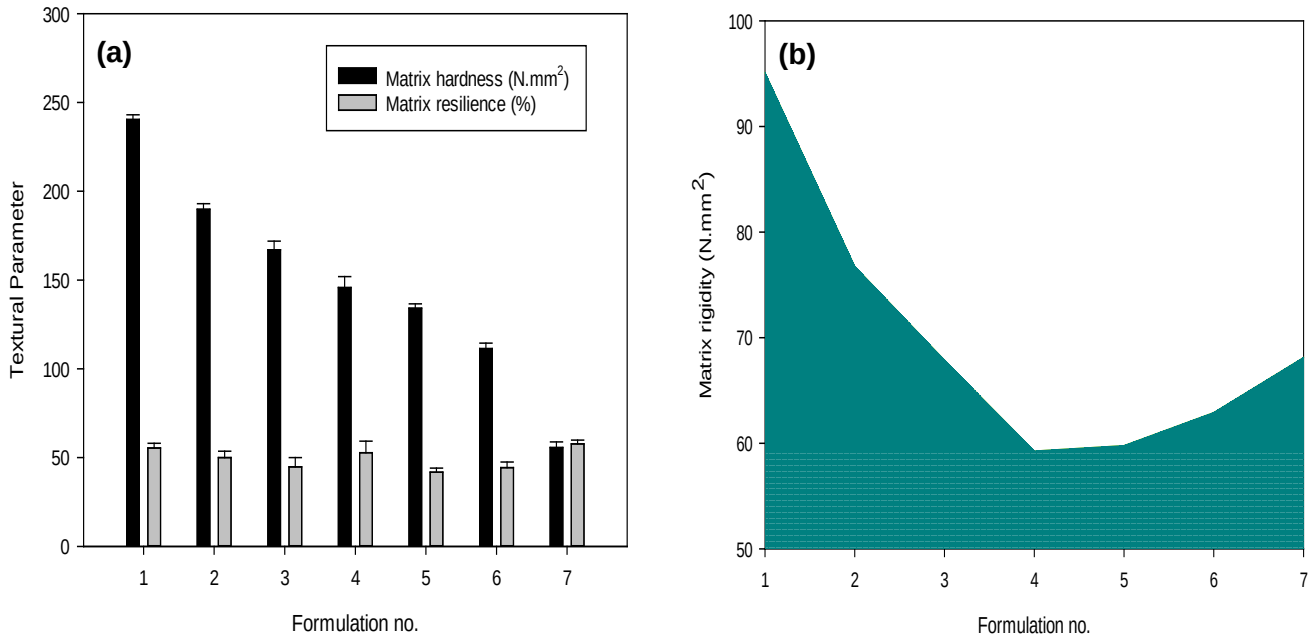

Figure 3.5: Graphical representation of the **a)** MH, MR and **b)** rigidity of SMX-loaded matrix tablet formulations F1-7. Significant differences noticed were F1 which achieved the highest matrix hardness (240.40N.mm^2) with the lowest concentration of menthol (1g) and F7 achieved the lowest matrix hardness (55.67N.mm^2) with the highest concentration of menthol (10g).

3.3.5. Analysis of the crystal nature of the SMX-loaded solid dispersions

The crystallinity of the SMX-loaded solid dispersions were assessed using XRD. All spectrums that were obtained displayed to varying degrees, diffraction peaks which were sharp and narrow indicating the crystallinity of the test sample with wider and flatter peaks indicating the amorphous component. The hydrophilic carrier menthol displayed a crystallinity percentage of 30% with seven major crystalline diffraction peaks identified (Figure 3.6a). Conversely, the drug molecule SMX showed 12% crystallinity with four major crystalline diffraction peaks identified on the diffraction spectra (Figure 3.6b). The SMX-loaded solid dispersions were assessed according to their percentage crystallinity in relation to the native molecules, menthol and SMX.

F1 (Figure 3.6c) depicted fewer diffraction peaks than menthol and SMX, displaying a high intensity Bragg diffraction peak at ±40°2-theta which was uncharacteristic of either menthol or SMX. F2 and F3 (Figure 3.6d-e) displayed characteristic Bragg peaks at ±20°2-theta, similar to that of SMX, with F2 showing an additional low intensity narrow peak at ±10°2-theta comparable to that of menthol. Bragg diffraction peaks were discernable for F4-7 (Figure 3.6f-j) at ±20°2-theta and ±10°2-theta which was typical of the reference powder diffraction spectrums obtained for menthol and SMX. Furthermore, it was apparent that the intensities of the diffraction peaks varied with the different concentrations of menthol within each formulation.

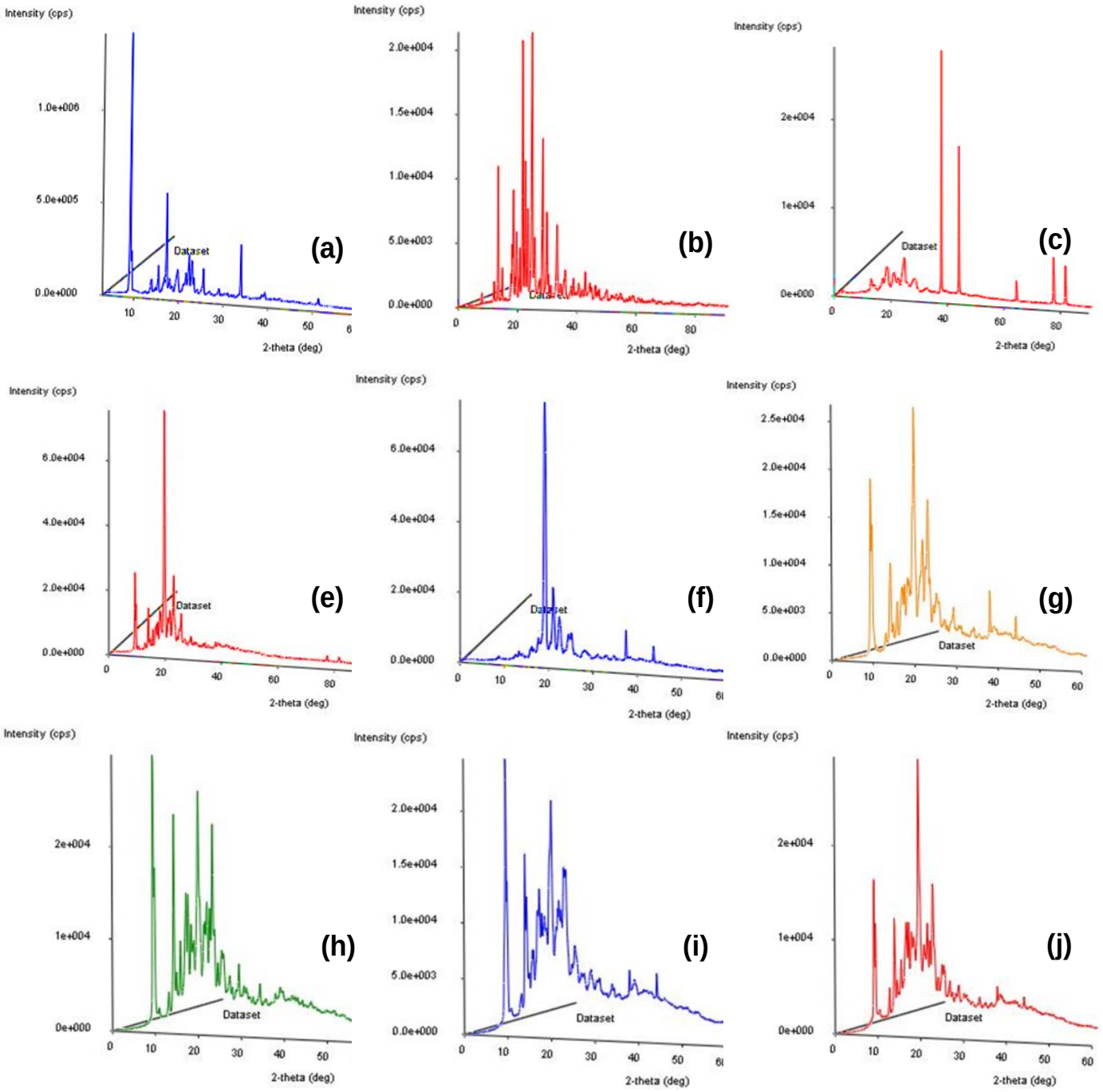

Figure 3.6: XRD spectra of **a)** menthol, **b)** SMX and **c-j)** SMX-loaded solid dispersions F1-7. The diffraction spectrums are represented as a plot of the reflected intensities (cps) as a function of the diffraction angle 2-theta (deg).

All the SMX-loaded solid dispersions displayed decreased percentage crystallinities within the range of 11-21%. The decrease in the crystallinity observed supports the idea that modification of the physical nature of the drug through the formation of solid dispersions decreases the crystallinity and thus results in the presence of more amorphous material which has a much

higher water affinity and solubility as compared to the crystalline counterpart (Council of Europe, 2001; Liu *et al*., 2006; Savjani *et al*., 2012). The results obtained confirmed the analysis of the TMDSC thermograms (Figure 3.2b) and was consistent with the existence of a solid dispersion system. Critical analysis of XRD data on solid dispersions of carbamazepine and felodipine provided conclusive results on the potential decrease in crystallinity and presence of the amorphous state within the solid dispersion (Sethia and Squillante, 2004; Won *et al*., 2005).

In addition, multivariate experimental techniques were applied to the analysis of the data obtained from DSC and XRD in order to comprehensively link the crystallinity data for the solid dispersions. Table 3.3 summarizes the crystallinity data obtained for DSC and XRD. The melting point decreases in the menthol and SMX peak noted in the solid dispersion thermograms in Figure 3.2 were represented in Table 3.3. The decrease in the melting temperature for the characteristic menthol and SMX peak indicated the increase in the amorphous constituent within the solid dispersions as compared to the crystalline counterpart and thus resulted in the easy melting of the formulation at lower temperatures (Yamashita *et al*., 2003).

Furthermore, the comparison of the XRD diffraction peaks of the native molecules with the solid dispersions depicted a decrease in intensity at the diffraction angles characterized in Table 3.3. These broad, low intensity peaks observed in the XRD spectrums of the solid dispersions indicated that the formulations were in the amorphous form (Sethia and Squillante, 2004). These summarized results further highlighted the expected decrease in crystallinity that is typical of solid dispersions (Tantishaiyakul *et al.,* 1999; Sethia and Squillante, 2004). In correlating the results obtained for DSC and XRD, it was noted that the solid dispersions of SMX and menthol showed a significant decrease in the endothermic peak of SMX with a similar broadening and decreased intensity of the peaks derived from SMX in the XRD data (Yamashita *et al*., 2003). This indicated the presence of the amorphous state in all the solid dispersion formulations (Yamashita *et al*., 2003).

Table 3.3: Comparative analysis of the crystallinity obtained for DSC and XRD

Formulation no.	DSC melting points (°C)*	XRD diffraction peaks 2-theta (deg)
F1	35.43/149.24	10-20
F2	35.82/145.32	25-40
F3	34.74/150.48	9-17
F4	33.86/145.19	23-34
F5	33.05/absent peak	30-35
F6	33.59/absent peak	20-40
F7	32.60/absent peak	23-43

* The DSC melting points are indicative of the menthol/SMX melting peak

3.3.6. Surface morphological characterization of the SMX-loaded solid dispersions

The SMX-loaded solid dispersions were analyzed using SEM and the images obtained are depicted in Figure 3.7. F1 displayed largely ordered, regular and distinct crystal forms in the SEM images (Figure 3.7a and b). In contrast, F4 (Figure 3.7c and d) depicted particles that were more spherical in shape with a less rugged surface structure. Furthermore, F7 (Figure 3.7e and f) which contained the highest mass ratio of menthol (10g) depicted large, irregular smooth surfaces with minimal crystalline regions indicating homogeneity of the formulation. Noticeable changes were observed in the surface morphology on comparison of the various SMX-loaded solid dispersions. Most distinguishing features noted were the changes from a more rigid crystalline structure in F1 to a distinctly amorphous and smooth structure in F7. The results obtained corresponded to the decrease in crystallinity in subsequent formulations as confirmed by XRD spectra (Figure 3.6). It was deduced that as the concentration of menthol increased, the surface morphology displayed characteristically amorphous regions. The appearance of amorphous regions within the SEM images confirmed the decrease in crystallinity, characteristic to solid dispersions as highlighted in the SEM micrographs obtained for the solid dispersions of carvedilol and tacrolimus (Yamashita *et al*., 2003; Sharma *et al*., 2013).

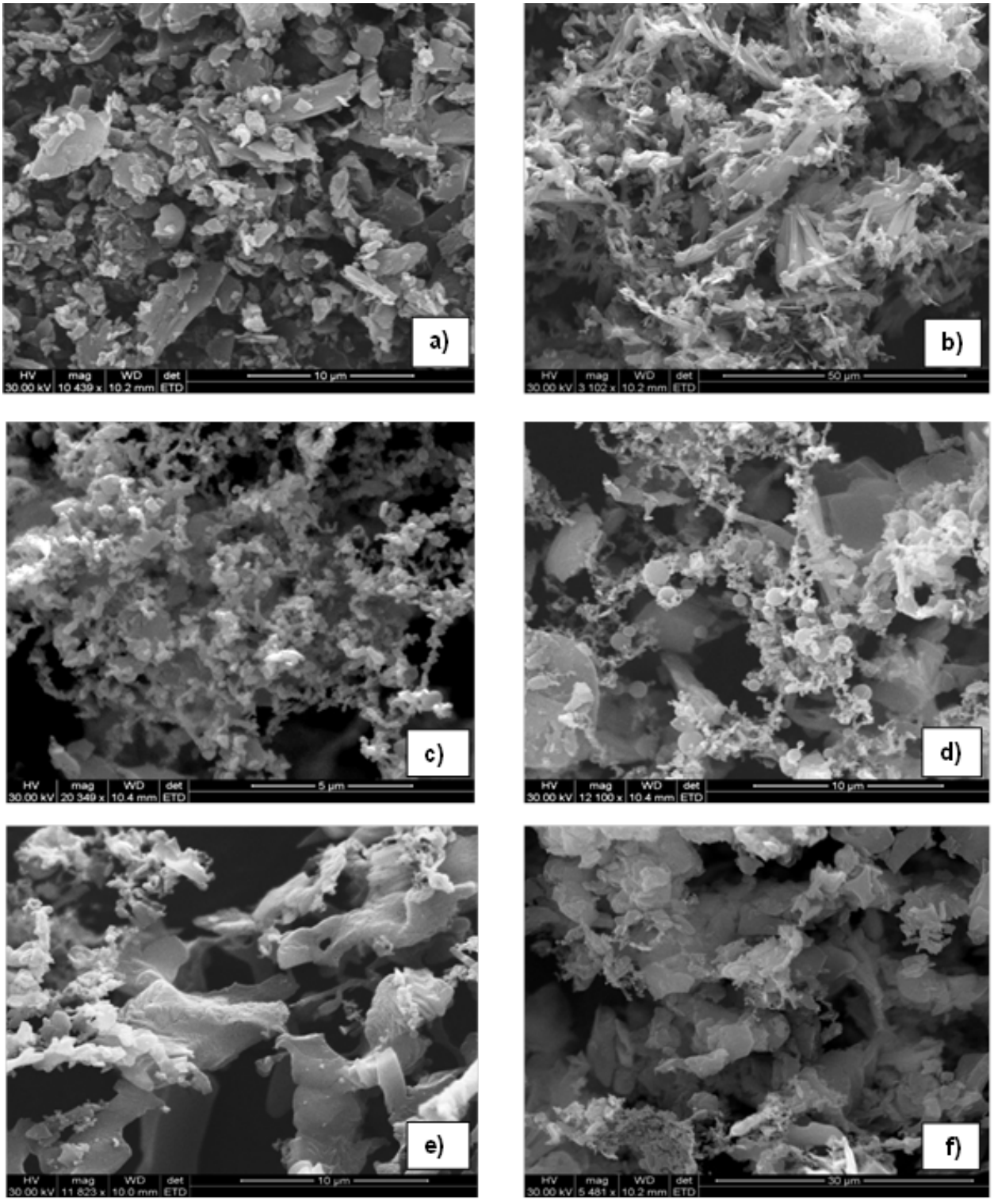

Figure 3.7: SEM images at high (left) and low magnifications (right) for **(a-b)** F1, **(c-d)** F4 and **(e-f)** F7.

3.3.7. Swelling and erosion studies on the SMX-loaded matrix tablets

Swelling and erosion studies were performed on F1-7 of the SMX-loaded matrix tablets to obtain supplementary evidence for the observed drug release kinetics (Figure 3.8). F1 swelled to ±140% of its original size in the first hour with a steady increase over the following two hours to approximately 170% of the original mass. F2 swelled to approximately 119% of its original size in the first 3 hours with both F1 and F2 showing a sharp decrease in swelling after 4 hours (Figure 3.8a). The swelling profile obtained for F1 and F2 accounted for the 90% erosion obtained after 24 hours. F3 and F4 swelled to approximately 100% and 95% of its original size, respectively (Figure 3.8a). Likewise as for F1-2, F3-4 displayed increased erosion percentages after 24 hours (Figure 3.8c). The swelling profiles of F1-4 decreased steadily after approximately 4 hours while F5-7 steadily increased after 4 hours (Figure 3.8a-b). In addition, the erosion percentages for F5-7 was <50% (Figure 3.8c). All formulations displayed different swelling profiles regardless of their constant concentration of HPMC. Thus the changes were attributed to the varying concentrations of menthol contained in each formulation.

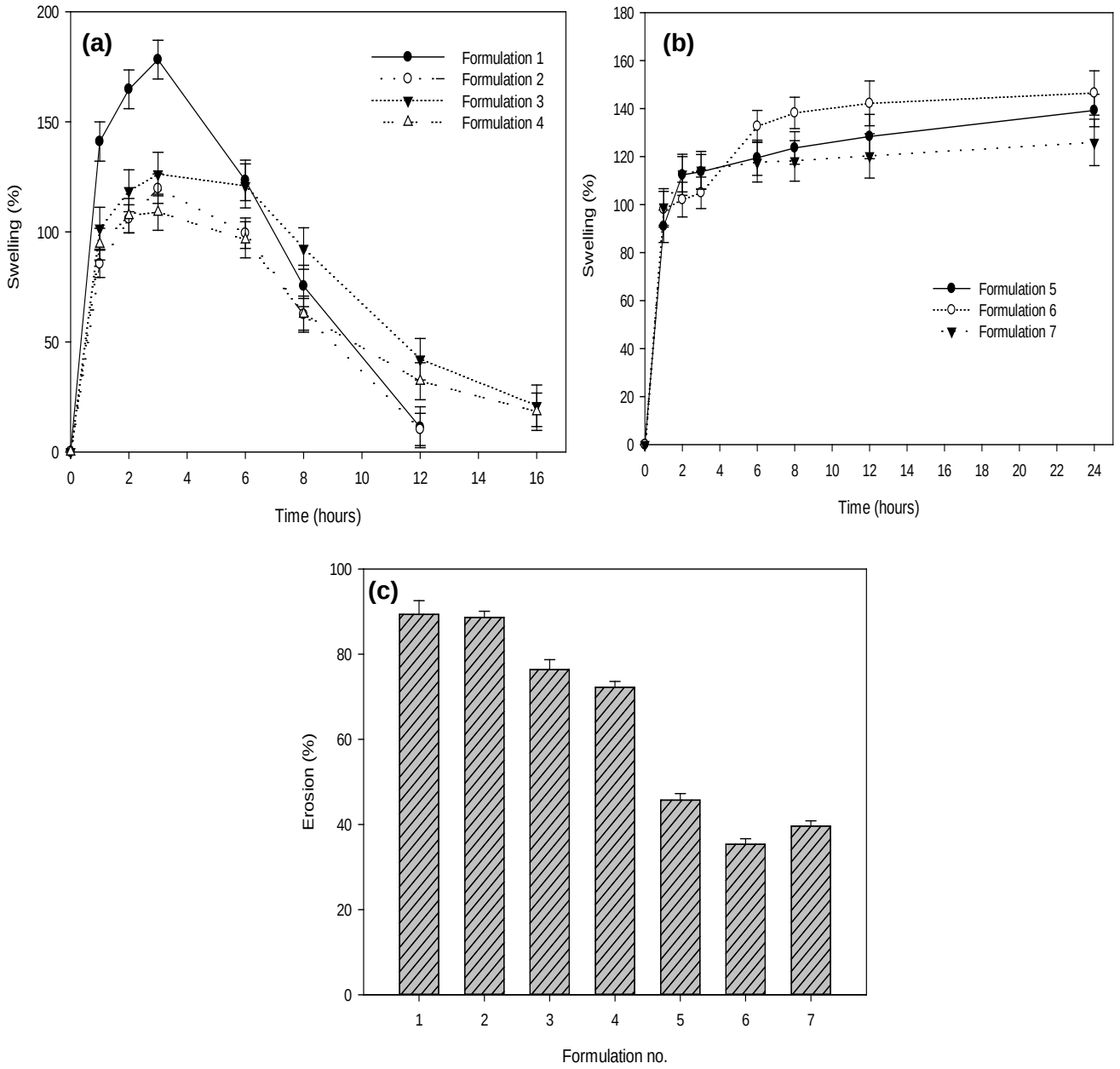

Figure 3.8: Profiles depicting **(a-b)** percentage swelling over a period of 24 hours for F1-7 and **c)** Percentage erosion for F1-F7 as a function of the dried weight of the tablets after 24 hours.

3.3.8. Solubility analysis of SMX and SMX-loaded solid dispersions in SHIF

The solubility of SMX in menthol as well as SHIF at pH 6.8 was determined and compared to the solubility of each of the SMX-loaded solid dispersions in SHIF at pH 6.8. Results indicated that the solubility of SMX in menthol at 37°C was 990µg/mL and the solubility of SMX in SHIF at pH 6.8 (37°C) was 790µg/mL. These results were compared to the solubility of the SMX-loaded solid dispersions (F1-7) which showed a marked increase in solubility as compared to pure SMX dissolved in SHIF at pH 6.8. Results depicted only slight differences in the solubility of pure

SMX in menthol as compared to the SMX-loaded solid dispersions in SHIF at pH 6.8. F1 displayed the lowest solubility in SHIF whereas F7 depicted the highest solubility of 998.75µg/mL and 1241.2µg/mL, respectively (Figure 3.9). F2 showed an approximate 9% increase in solubility as compared to F1. The solubility increased steadily from F3-6 with F7 showing a ±6% increase in solubility as compared to F6. The results displayed in Figure 3.9 suggested that a proportional increase in solubility was noted with increasing concentrations of menthol. F1 and F7 depicted the lowest and highest solubility from all the formulations as they contained the lowest (1g) and highest concentrations (10g) of menthol, respectively. The increase in solubility of a drug molecule when formulated as a solid dispersion is highlighted extensively in literature and is founding characteristic of solid dispersions (Tantishaiyakul *et al.,* 1999; Yamashita *et al*., 2003; Sinha *et al*., 2010; Sharma *et al*., 2013).

According to Vasconcelos *et al.,* (2007), solid dispersion directed decrease in particle size and change to an amorphous state increases the solubility of a drug molecule and thus enhances the bioavailability. The association between drug solubility, dissolution and its subsequent increase in bioavailability is theoretically described by the Noyes-Whitney Equation 3.5 (Martin, 1993; Hattori *et al*., 2013):

$$\frac{dM}{dt} = \frac{DS}{h}(C_s - C) \qquad \textbf{(3.5)}$$

Where, *M* is the mass of solute dissolved in time *t;* $\frac{dM}{dt}$ is the mass rate of dissolution (mass/time); *D* is the diffusion coefficient of the solute in solution; *S* is the surface area of the exposed solid; *h* is the thickness of the diffusion layer; C_s is the solubility of the solid; *C* is the concentration of solute in the bulk solution at time *t.*

Therefore, according to Noyes-Whitney, an increase in the solubility of a drug molecule would correspond to an increased dissolution with subsequent increase in bioavailability (Martin, 1993). The experimental measurements obtained showed a substantial increase in the solubility of the solid dispersions and comparative interpretations were made in relation to the solubility of the native molecule in the same dissolution medium.

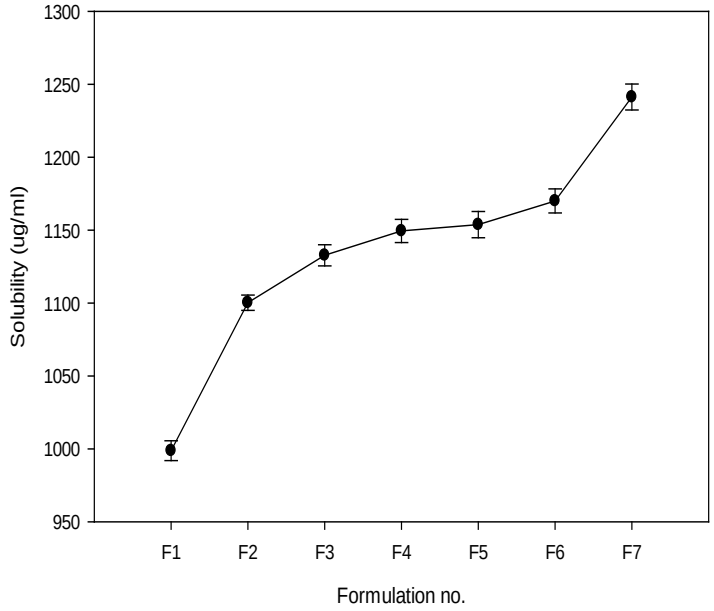

Figure 3.9: Graphical representation of the solubility of SMX-loaded solid dispersions F1-7 in SHIF at pH 6.8 (37°C).

3.3.9. *In vitro* drug release analysis

In vitro SMX release was performed in SHIF (pH 6.8) and the fractional drug release profiles of the SMX-loaded matrix tablets is presented in Figure 3.10. Each formulation demonstrated diverse drug release behavior based on their varying solubility. In addition, the formulations displayed different time-release profiles. F1 and F2 released drug over a period of 12 hours with the maximum release being >50% (Figure 3.10a). F3 and F4 displayed prolonged release over 16 hours, followed by F5 and F6 which released drug over a period of 48 hours (Figure 3.10b and c). F7 displayed the most prolonged drug release over a period of 56 hours (Figure 3.10d).

Noticeable in all the drug release profiles was the burst release which was attributed to the initial swelling within the first 3 hours. Despite the decrease in swelling after 4 hours for F1-4 (Figure 3.8a), the drug release increased accordingly (Figure 3.10a and b). This indicated that the drug release in the later phase was erosion-controlled. F5-7 (Figure 3.8b) displayed a more constant swelling profile following the initial burst swelling. The swelling profile of F5-7 corresponded to the increase in drug release displayed in Figure 3.10c and d. These results suggested that the release of SMX from F5-7 was swelling-controlled in contrast to F1-4. Typically, amorphous materials display increased erosion as compared to their crystalline counterparts, however, the atypical behavior observed was attributed to the distinct ester bond formation within F5-7 (Figure 3.4) causing a decreased susceptibility of the solid dispersion to hydrolytic cleavage and thus slower erosion as compared to F1-4 (Ratner *et al*., 2012).

Formulations having a higher concentration of menthol, such as F7 (10g), depicted the highest fractional release (0.97). This paralleled the increased solubility of F7 which enabled the increased dissolution of SMX. On the other extreme, the lowest fractional release (0.71) was noticed for formulations that had lower concentrations of menthol such as F1 (1g). Similarly, F1 had the lowest solubility in SHIF at pH 6.8 (Figure 3.9). Consequently, it was concluded that the concentration of menthol used in each formulation impacted significantly on the drug release profiles obtained for the SMX-loaded solid dispersions F1-7. The solubility results (Figure 3.9) correlated with the drug release profiles (Figure 3.10a, b, c and d) showing that increases in solubility from F1-7 displayed correspondingly higher cumulative drug release percentages. The improved solubility and dissolution of the solid dispersions was attributed to the amorphization of the drug and the reduction in the particle size to the nanometer range. The particle size is inherently associated with the solubility of a drug molecule, therefore a reduction in particle size leads to an increase in the surface area with a consequently enhanced dissolution profile (Sareen *et al*., 2004).

Since the quantity of HPMC remained constant within each formulation, it was determined that menthol served to control the release rate of SMX from each of the SMX-loaded matrix tablets by prolonging its release as was evidenced by the mean dissolution time (MDT) obtained for F1-7. The MDT was used to depict the drug release rate from the SMX-loaded matrix tablets as well as the release-retarding ability of menthol (Roni *et al*., 2009; Wadher *et al*., 2011). Overall, the MDT gave an indication of the rate of the dissolution process (Sathish and Syed, 2013). The mean dissolution time at which 80% of drug was released (MDT_{80}) for F7 was 15.044±1.5. This was the highest MDT_{80} from all formulations and it indicated that F7 had a higher drug release retarding ability and thus slower release of drug as compared to other formulations. Typically, F1 and F2 had the lowest MDT_{80} of 4.592±0.5 and 5.076±0.5, respectively and as a result the fastest release over 12 hours (Figure 3.10a). Thus, it was apparent that the increasing concentrations of menthol impacted on the release rate profile and served as a controlling agent that retarded drug release from the SMX-loaded matrix tablets.

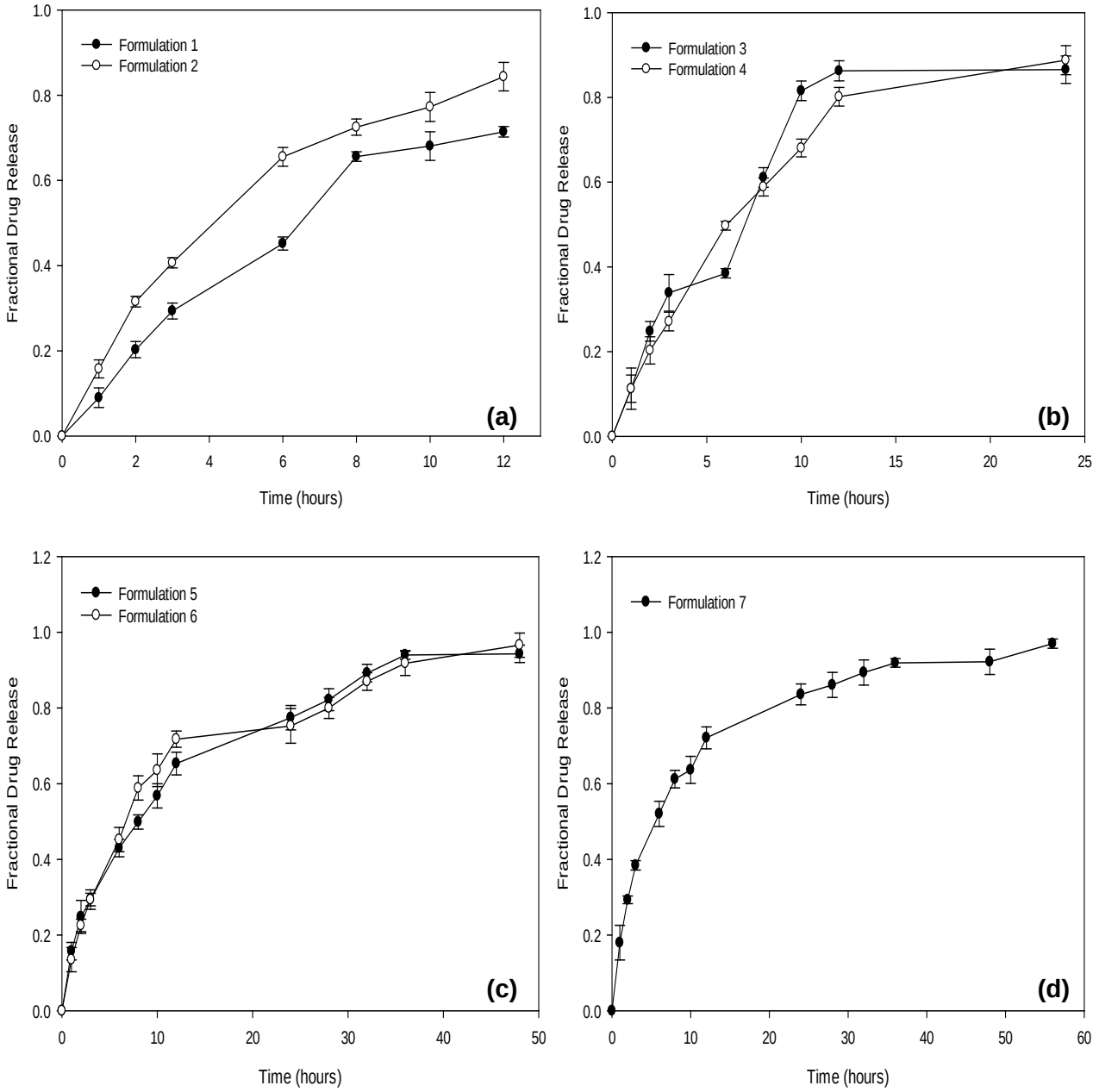

Figure 3.10: Graphical representation of the fractional drug release of SMX from compressed matrix tablets F1-7. **a)** F1-2 releases over a period of 12 hours, **b)** F3-4 releases over a period of 16 hours, **c)** F5-6 releases over a period of 48 hours and **d)** F7 releases over a period of 56 hours.

3.3.10. Mathematical modeling of drug release profiles

The drug release profiles of the solid dispersions F1-F7 were fitted into various mathematical modeling equations to identify the release mechanism of the drug. The regression coefficients of F1-F7 for each of the algorithms are summarized in Table 3.4. The best-fit model for the formulations is based on the closeness of the regression coefficient to a value of 1. A model depicting a value closest to 1 amongst the formulations would demonstrate the appropriateness

of that model in explaining the drug release mechanism. The zero-order and first-order models are based on systems where the drug release is independent and dependent on drug concentrations, respectively (Singh and Singh, 2011). The zero-order and first-order models used are shown in Equation 3.6 and 3.7 (Siepmann and Siepmann, 2008).

$$Q = K_0\ t \quad \textbf{(3.6)}$$

Where, Q is the cumulative amount of drug released; K_0 is the zero-order constant; *t* is the time. The regression coefficients were elucidated for the zero-order model by plotting a graph of cumulative drug release (%) *versus* time based on *in vitro* drug release data.

$$\ln Q_t = \ln Q_0\, K_0 t \quad \textbf{(3.7)}$$

Where, Q_t is the cumulative amount of drug released; Q_0 is the initial amount of drug in the dissolution medium (usually zero); K_0 is the first-order constant; *t* is the time. The regression coefficients for the first order model was determined by plotting a graph of the log of cumulative release *versus* time based on data obtained from *in vitro* drug release.

Since the release of SMX was not concentration dependent it did not fit into the first-order release kinetic model as displayed in Table 3.4. Regardless of the nearness to linearity of the zero-order model, the results were not ideal and thus was not considered the best-fit model. In addition, the drug release data was fitted into the Higuchi model since it has been developed to describe the drug release from HPMC-based pharmaceutical delivery systems (Siepmann and Peppas, 2012). The Higuchi model is the most commonly used method to describe the release rate of drug from a matrix system and is represented by Equation 3.8 (Merchant *et al.*, 2006).

$$Q = K_H t^{1/2} \quad \textbf{(3.8)}$$

Where, Q is the cumulative amount of drug released; K_H is the Higuchi dissolution constant; *t* is the time. A plot of the cumulative percentage released *versus* the square root of time of the drug release data, generated regression coefficients for the Higuchi model.

Based on the regression coefficients, the Higuchi model displayed the best linearity for majority of the formulations with an R^2 value of between 0.8497 and 0.9824 indicating that the drug

release mechanism was based on a square root of a time dependent process based on Fickian diffusion (Yadhav *et al*., 2013). Despite the Higuchi equation being the best-fit model, further mathematical analysis is required to obtain definite mechanistic deductions (Siepmann and Peppas, 2012).

Table 3.4: Mathematical modelling of SMX release from the solid dispersions

	Zero-order	**First order**	**Higuchi**	
Formulation No.	Regression Coefficient (R^2)	Regression Coefficient (R^2)	Regression Coefficient (R^2)	Best-fit Model
F1	0.9473	0.8255	0.9795	Higuchi
F2	0.9295	0.8031	0.9824	Higuchi
F3	0.7107	0.6008	0.8497	Higuchi
F4	0.8063	0.6475	0.9372	Higuchi
F5	0.8693	0.7113	0.9669	Higuchi
F6	0.8042	0.6201	0.9226	Higuchi
F7	0.7641	0.5986	0.9079	Higuchi

3.4. Concluding Remarks

The menthol-based solid dispersions for improvement of the solubility and dissolution of SMX were successfully formulated as evidenced by the results obtained from physicochemical and physicomechanical characterization. SMX is used to treat various urinary tract pathogens and in combination with trimethoprim is considered the “gold standard” in the treatment of urinary tract infections (UTIs) (Petri, 2011). Thus, improvement in its solubility and dissolution is critical towards achieving optimal therapeutic effects. Characterization results confirmed successful formulation of the solid dispersions and its subsequent enhancement of the solubility and dissolution of SMX. A reduction in the particle size to the nanometer range for the solid dispersions resulted in an increased surface area and thus improved solubility and dissolution. Thermal analysis depicted a characteristic decrease in melting point for all the SMX-loaded solid dispersions. In addition, a decrease in the crystallinity and corresponding increase in the amorphous nature was apparent within the formulations as the concentration of menthol increased thus allowing for the increase in the water affinity and solubility of SMX. Results from erosion, swelling and solubility studies determined that the varying concentrations of menthol present within each formulation controlled the quantity of SMX released over time**.** The physicomechanical properties of MH and MR correlated with changes in crystallinity observed in the different formulations of SMX-loaded matrix tablets. Analysis of the molecular and vibrational transitions of the SMX-loaded solid dispersions determined the formation of new bonds resulting from the interaction between SMX and menthol. Solubility studies indicated the

significant intrinsic increase in solubility of SMX as a component of the solid dispersions (998.75µg/mL-1241.2µg/mL) as compared to native SMX in SHIF pH 6.8 (790µg/mL). In addition, *in vitro* drug release analysis displayed atypical, controlled drug release profiles for the various solid dispersions. This may be extremely useful within an oral drug delivery system where the properties of the system can be synchronously enhanced using a customizable solid dispersion. Selection of the best solid dispersion may be ascertained based on physicochemical, physicomechanical, drug release and release-rate profiles desired to meet the needs of the particular drug delivery system. In addition, eutectic, monotectic and peritectic transformation may be associated with a matrix solid dispersion system such as the menthol-SMX combination. However, achievement of these transformations would require further investigation and evaluation that would commence with basic phase studies to determine the composition at which the menthol-SMX combination would exist as a eutectic mixture.

Ultimately, this study led to the further investigation of menthol as a component in eutectic mixtures, evidenced by the design of the eutectic powder blend in Chapter 4.

3.5. References

Arnikar, A.J., Kadam, S.S., Gujar, K.N. (1992). *Essentials of Physical Chemistry and Pharmacy*. Bombay: Orient Longman Limited. pp. 1-8.

Bhatnagar, P., Dhote, V., Mahajan, S.C., Mishra, P.K., Mishra, D.K. (2014). Solid dispersion in pharmaceutical drug development: from basics to clinical applications. *Current Drug Delivery,* 11, 155-171.

Chiou, W.L., Riegelman, S. (1971). Pharmaceutical Applications of Solid Dispersion Systems. *Journal of Pharmaceutical Sciences,* 60, 1281-1302.

Coates, J. (2000). *Interpretation of Infrared Spectra, A Practical Approach*. Chichester: John Wiley and Sons Ltd. pp. 10815-10837.

Council of Europe. (2001). *The European Pharmacopoeia*. France: Maisonneuve S.A. pp. 723-727.

Dohrn, R., Bertakis, E., Behrend, O., Voutsas, E., Tassios, D. (2007). Melting point depression by using supercritical CO_2 for a novel melt dispersion micronization process. *Journal of Molecular Liquids,* 131, 53-59.

Efentakis, M., Vlachou, M. (2000). Evaluation of high molecular weight poly(oxyethylene) (Polyox)polymer: studies of flow properties and release rates of furosemide and captopril from controlled-release hard gelatin capsules. *Pharmaceutical Development and Technology*, 5, 339-346.

Gabbott, P. (2008) *Principles and Applications of Thermal Analysis.* Oxford: Blackwell Publishing Ltd. pp. 17-40.

Hattori, Y., Haruna, Y., Otsuka, M. (2013). Dissolution process analysis using model-free Noyes-Whitney integral equation. *Colloids Surfaces B Biointerfaces,* 102, 227-231.

Johnson, A.W. (1999). *Invitation to Organic Chemistry.* Canada: Jones and Bartlett Publishing. pp. 543-546.

Lee, M.Y., Kim, M.Y., Kim, S., Lee, J. (2009). Cryoprotectants for Freeze Drying of Drug Nano-Suspensions: Effect of Freezing Rate. *Journal of Pharmaceutical Sciences,* 98, 4808-4817.

Levy, G. (1963). Effect of particle size on dissolution and gastrointestinal absorption rates of pharmaceuticals. *American Journal of Pharmaceutical Sciences,* 135, 78-92.

Lindenburg, M., Kopp, S., Dressman, J.B. (2004). Classification of orally administered drugs on the World Health Organization Model list of Essential Medicines according to the biopharmaceutics classification system. *European Journal of Pharmaceutics and Biopharmaceutics*, 58, 265–278.

Liu, D., Fei, X., Wang, S., Jiang, T., Su, D. (2006). Increasing solubility and dissolution rate of drugs via solid dispersions: itraconazole–poloxamer188 system. *Asian Journal of Pharmaceutical Sciences,* 1, 213-221.

Luener, C., Dressman, J. (2000). Improving drug solubility for oral delivery using solid dispersions. *European Journal of Pharmaceutics and Biopharmaceutics,* 50, 47-60.

Martin, A. (1993). *Physical Pharmacy: Physical Chemical Principles in the Pharmaceutical Sciences.* Philadelphia: Lea and Febiger. pp. 41-42.

McGlinchey, D. (2005). *Characterisation of Bulk Solids.* Oxford*:* Blackwell Publishing Ltd. pp. 50-52.

Merchant, H., Shoaib, H., Tazeen, J., Yousuf, R. (2006). Once-daily tablet formulation and in vitro release evaluation of cefpodoxime using hydroxypropyl methylcellulose: a technical note. *AAPS PharmSciTech*, 7, 178–183.

Neubert, R., Rettig, W., Wartewig, S., Wegener, M., Wienhold, A. (1997). Structure of stratum corneum lipids characterized by FT-Raman spectroscopy and DSC. II. Mixtures of ceramides and saturated fatty acids. *Chemistry and Physics of Lipids,* 89: 3-14.

Petri, W.A. (2011). 'Sulfonamides, Trimethoprim-Sulfamethoxazole, Quinolones, and Agents for Urinary Tract Infections'. In: Chabner BA, Knollmann BC, editors. *Goodman and Gilman's: The Pharmacological Basis of Therapeutics*. New York: McGraw-Hill. pp. 252-288.

Pillay, V., Fassihi, R. (1999). In vitro release modulation from crosslinked pellets for site-specific drug delivery to the gastrointestinal tract: II. Physicochemical characterization of calcium–alginate, calcium–pectinate and calcium–alginate–pectinate pellets. *Journal of Controlled Release*, 59, 243–256.

Ratner, B.R., Hoffman, A.S., Schoen, F.J., Lemons, J.E. (2012). *Biomaterials Science: An Introduction to Materials in Medicine*. Oxford: Elsevier. pp. 187-194.

Reynolds, J.E.F. (1993). *Martindale: The Extra Pharmacopoeia.* London*:* Pharmaceutical Press. pp. 154, 209.

Roni, M.A., Kibria, G., Jalil, R. (2009). Formulation and *in vitro* Evaluation of Alfusozin Extended Release Tablets Using Directly Compressible Eudragit. *Indian Journal of Pharmaceutical Sciences*, 71, 252-258.

Saffoon, N., Uddin, R., Huda, N.H., Sutradhar, K.B. (2011). Enhancement of Oral Bioavailability and Solid Dispersion: A Review. *Journal of Applied Pharmaceutical Science*, 1, 13-20.

Sareen, S., Mathew, G., Lincy, J. (2012). Improvement in solubility of poor water-soluble drugs by solid dispersion*. International Journal of Pharmaceutical Investigation*, 2, 12-17.

Sathish, U., Syed, I.A. (2013). Formulation and characterization of matrix and triple layer matrix tablets for controlled delivery of tramadol hydrochloride*. International Journal of Pharmaceutical Sciences*, 5, 458-464.

Savjani, K.T., Gajjar, A.K., Savjani, J.K. (2012). Drug Solubility: Importance and Enhancement Techniques. *ISRN Pharmacy.* doi: 10.5402/2012/195727.

Seedhar, N., Agarwal, P. (2009). Various solvent systems for solubility enhancement of enorfloxacin. *Indian Journal of Pharmaceutical Sciences,* 71, 82-87.

Sekiguchi, K., Obi, N. (1961). Studies on absorption of solid dispersions. I. A Comparison of the behaviour of solid dispersions of sulphathiazole and that of ordinary sulphathiazole in man. *Chemical and Pharmaceutical Bulletin*, 9, 866–872.

Sethia, S., Squillante, E. (2004). Solid dispersion of carbamazepine in PVP K30 by conventional solvent evaporation and supercritical methods. *International Journal of Pharmaceutics,* 272: 1-10.

Sharma, A., Jain, C.P., Tanwar, Y.S. (2013). Preparation and characterization of solid dispersions of carvedilol with poloxamer 188. *Journal of the Chilean Chemical Society,* 58, 1553-1557.

Siepmann, J., Peppas, N.A. (2012). Modeling of drug release from delivery systems based on hydroxypropyl methylcellulose (HPMC). *Advanced Drug Delivery Reviews,* 64, 163-174.

Siepmann, J., Siepmann, F. (2008). Mathematical modeling of drug delivery. *International Journal of Pharmaceutics*, 364, 328‑343.

Singh, V., Singh, M. (2011). Review: *In-Vitro* Drug Release Characterization Models. *International Journal of Pharmaceutical Studies Research,* 2, 77-84.

Sinha, S., Ali, M., Baboota, S., Ahuja, A., Kumar, A., Ali, J. (2010). Solid Dispersion as an Approach for Bioavailability Enhancement of Poorly Water-Soluble Drug Ritonavir. *AAPS PharmSciTech,* 11, 518-527.

Stoker, H.S. (2013). *Organic and Biological Chemistry.* Belmont*:* Brooks/Cole Cengage Learning. pp. 83-128.

Tantishaiyakul, V., Kaewnopparat, N., Ingkatawornwong, S. (1999). Properties of solid dispersions of piroxicam in polyvinylpyrrolidone. *International Journal of Pharmaceutics,* 181, 143-151.

Thakur, R., Gupta, R.B. (2006). Rapid expansion of supercritical solution with solid cosolvent (RESS-SC) process: Formation of 2-aminobenzoic acid nanoparticle. *Journal of Supercritical Fluids,* 37, 307-315.

Vasconcelos, T., Sarmento, B., Costa, P. (2007). Solid dispersions as strategy to improve oral bioavailability of poor water soluble drugs. *Drug Discovery Today,* 12, 1068-1075.

Wadher, K.J., Kakde, R.B., Umekhar, M.J. (2011). Study on sustained-release metformin hydrochloride from matrix tablet: Influence of hydrophilic polymers and *in vitro* evaluation. *International Journal of Pharmaceutical Investigation*, 1, 157-163.

Widmann, J., Schubnell, M., Riesen. R., Schawe, J., Darribére, C., Jörimann, U. (2000). Interpreting DSC curves: Part 2: Isothermal measurements. *UserCom*, 2, 1-10.

Widmann, J., Schubnell, M., Riesen, R., Schawe, J., Darribére, C., Jörimann, U. (2001). Interpreting TGA curves. *UserCom*, 1, 1-20.

Williams, R.O., Watts, A.B., Miller, D.A. (2012). *Formulating Poorly Water Soluble Drugs*. New York: Springer. pp. 526-529.

Won, D., Kim, M., Lee, S., Park, J., Hwang, S. (2005). Improved physicochemical characteristics of felodipine solid dispersion particles by supercritical anti-solvent precipitation process. *International Journal of Pharmaceutics*, 301, 199-208.

Yadav, G., Bansal, M., Thakur, N., Khare, S., Khare, P. (2013). Multilayer Tablets and Their Drug Release Kinetic Models for Oral Controlled Drug Delivery System. *Journal of Scientific Research*, 16, 782-795.

Yamashita, K., Nakate, T., Okimoto, K., Ohike, A., Tokunagu, Y., Ibuki, R., Higaki, K., Kimura, T. (2003). Establishment of new preparation method for solid dispersion formulation of tacrolimus. *International Journal of Pharmaceutics,* 267, 79-91.

CHAPTER 4

PRELIMINARY DESIGN OF AN *IN SITU* CROSS-LINKED EUTECTIC TABLET FOR ENHANCED ORAL PROTEIN AND PEPTIDE DELIVERY

Published in Journal of Pharmaceutical Sciences

Bibi F. Choonara, Yahya E. Choonara, Pradeep Kumar, Lisa C. du Toit, Viness Pillay. Design of an In Situ Cross-Linked Eutectic Tablet for Enhanced Delivery of Gastro-Sensitive Proteins and Peptides. Journal of Pharmaceutical Sciences, 2016, 105, 2086-2098.

Abstract

In the present chapter, a eutectic platform was designed as an *In Situ* Crosslinked Eutectic Tablet for structural protection, enhanced intestinal permeation and controlled release of proteins after oral administration. Physicochemical and physicomechanical analysis of the Eutectic Tablets were undertaken to elucidate the *in situ* crosslinking mechanism, thermal transitions, crystallinity, *ex vivo* permeation and *in vitro* release of the protein. Following thermal characterization, results revealed successful eutectic formation with a melting point to 37°C. Protein release from the formulation was controlled over 24 hours with a maximum fractional release of ±0.8 for all formulations. The release pattern alternated between phases of burst and slow release which was attributed to the combined effects of swelling, surface erosion and *in situ* crosslinking. Mathematical modelling of the protein release kinetics corresponded best with the Higuchi model with near zero-order (R^2≈0.9787) release. The permeation enhancing effect of menthol contained within the eutectic powder blend was investigated and results showed an enhanced protein flux (0.0576-0.0720mg.cm^{-2}h^{-1}) across the intestinal tissue model compared with a control formulation. Extensive *in vitro* characterization highlighted the successful design of the Eutectic Tablets as a potential oral delivery system for proteins with structural protection, enhanced intestinal permeation and controlled release.

Keywords: oral protein delivery; bovine serum albumin; controlled release; solid dispersion; intestinal absorption; eutectic mixture

4.1. Introduction

Oral drug delivery, particularly tablets, is considered one of the most common and widely used routes of drug administration, accounting for approximately 50% of all dosage forms on the market (Oh *et al*., 2013). Tablets are considered safe and cost-effective with desirable physical and chemical stability, high levels of patient acceptability and ease of accurate dosing (Al-hilal *et al*., 2013). Despite its many advantages, oral drug delivery can be particularly challenging when considering enzymatic degradation of drug molecules within the gastrointestinal tract (GIT), low membrane permeability and limited absorption of drugs into the systemic circulation, especially for gastro-sensitive biotech drug molecules (Marques *et al*., 2011). Biotech drug molecules are unlike conventional drugs, in that they are biopharmaceutical agents such as proteins and peptides that are produced using biotechnology (Schellack, 2010). Owing to their complexity and inherent instability, biotech drug molecules are primarily administered parenterally (IV, SC or IM) as oral routes of administration may result in its degradation in the GIT (O' Connor, 2009).

Therapeutic proteins and peptides have gained increased popularity as molecules of choice for multiple disease conditions (Park *et al*., 2011; Chin *et al*., 2012). Although significant progress has been made in the development of oral delivery systems for proteins and peptides, the field is limited by the GIT barrier which acts as a physical and chemical impediment in achieving successful oral drug delivery (Donovan *et al*., 1990; Camenich *et al*., 1998; Park *et al*., 2011). Pharmaceutical strategies and technologies targeting these limitations are faced with continuous challenges, preventing optimal delivery (Park *et al*., 2011). To date, this remains an active area of research.

The subject of eutectics in polymer-based protein delivery systems has not been fully explored. The microstructure that is typical of polymer eutectics still has to be explored as a strategy to increase absorption and improve the bioavailability of protein and peptide molecules (Tuntarawongsa and Phaechamud, 2012). A eutectic mixture is a physical blend of two crystalline components that are completely miscible in the liquid state but to a very limited extent in the solid state (Arnikar *et al*., 1992). Eutectics have a melting point that is lower than that of any of the individual components contained in the mixture (Arnikar *et al*., 1992; Sharma *et al*., 2011). A recent study by Shen *et al*, (2011) investigated the effects of a borneol/menthol eutectic mixture for enhancing the bioavailability in the delivery of a polypeptide (daidzein) used for the treatment of breast and colon cancer (Shen *et al*., 2011). The results from this study

depicted the potential use of a eutectic mixture for enhancing the absorption of peptide molecules. However, the mechanism of absorption still remains unclear, reflecting no significant effect on the efflux of daidzein with the addition of a P-gp inhibitor (Shen *et al*., 2011).

Therefore, this study focused on the development of an *in situ* crosslinked eutectic tablet that provides an alternative to the parenteral route of administration for sensitive protein and peptide molecules. The premise is the design of a core eutectic region within the tablet using eutectic reagents and suitable crosslinking agents which structurally protects and ensures controlled release of the incorporated protein or peptide molecule. The structural protection is achieved by *in situ* crosslinking within the tablet core, arising from the proposed melting of the core eutectic region at body temperature (37°C) and the ingress of fluid into the tablet. In addition, the eutectic reagents within the core region of the tablet will enhance the permeation across the intestinal tissue. The outer shell of the tablet comprises a porous, fluid-absorbing polymer that maintains its characteristic shape and functions as a 'sponge' that controls the release of protein or peptide molecules from the core. Using a Box–Behnken experimental design approach, a series of formulations were synthesized and analyzed using bovine serum albumin as a prototype peptide for release and permeation studies. Bovine serum albumin has been widely used as a model protein in numerous studies and thus it was selected as a model for this study (Kim *et al.*, 2005; Almeida and Suoto, 2007; Muller *et al*., 2012; Azimi *et al.*, 2013; Zheng *et al*., 2014).

4.2. Materials and Methods

4.2.1. Materials

Menthol(2-isopropyl-5-methylcyclohexanol, 99% purity, M_w=156,27g/mol), cetomacrogol 1000, poly(ethylene oxide) (PEO) (Polyox™, WSR-303), bovine serum albumin (BSA) (≥96%, agarose gel electrophoresis) and excipients, sodium carboxymethylcellulose (CMC), magnesium stearate and sucrose were purchased from Sigma-Aldrich Corp. (St. Louis, MO, USA). The crosslinker sodium carbonate ($NaCO_3$) was purchased from Associated Chemical Enterprises (ACE) (Pty) Ltd. (Johannesburg, Gauteng, South Africa). Pectin citrous (poly-D-galacturonic acid methyl ester) and the crosslinker di-potassium hydrogen orthophosphate anhydrous (K_2HPO_4; M_w=174.18g/mol) were procured from Merck Chemicals (Pty) Ltd. (Modderfontein, Gauteng, South Africa). All other reagents were of analytical grade and were employed as received.

4.2.2. Synthesis of the lyophilized eutectic powder blend for the core region to the tablet

The lyophilized eutectic powder melt was synthesized using a co-melt method adapted from Arnikar and co-workers, (1992). Menthol and cetomacrogol 1000 were used as the eutectic reagents for formation of the eutectic melt in a 3:1 mass ratio. Menthol was initially melted at a temperature of 40±0.5°C by a calibrated magnetic stirrer with hotplate MSH 300 (Boeckel and Co., Hamburg, Germany). As soon as the liquid melt was obtained, cetomacrogol 1000 was added. Once the solid mass of cetomacrogol 1000 was also melted and homogenously distributed within the molten menthol, a $5\%^{w}/_{w}$ concentration of sucrose (as a cryoprotectant) was added in equal volume to the eutectic melt. After uniform distribution, the eutectic melt was then removed from the heated magnetic stirrer and allowed to cool under constant agitation at 300rpm for ±30 minutes. The resultant eutectic blend was placed in a freezer at -80°C for 24 hours before lyophilization (Labconco Freeze-Dry Systems, Labconco Corp., Kansas City, MO, USA) for 48 hours to produce a lyophilized eutectic powder melt. Typically, lyophilization ensures the sublimation of menthol from the formulation. However, the high concentration of cryoprotectant that was added to the eutectic blend was used to protect the menthol from freezing and the associated desiccation stresses during the lyophilization process (Thakur and Gupta, 2006; Lee *et al*., 2009; Williams *et al*., 2012). As a result, excess menthol was absorbed onto the cryoprotectant thereby minimizing the processing losses of menthol from the eutectic blend.

4.2.3. Formulation of the core eutectic region for the *In Situ* Cross-linked Eutectic Tablet

The lyophilized eutectic powder blend together with the crosslinking agents ($NaCO_3$ and K_2HPO_4) were weighed in accordance with a 3-factor Box–Behnken experimental design template (Minitab®V15 statistical software, Minitab®Inc., PA, USA) as shown in Table 4.1 (Aslan and Cebeci, 2007). The processing parameters included the concentration of crosslinking agent, concentration of the eutectic powder blend as well as the quantity of pectin. Functional components were weighed and blended with 20mg of BSA before compression at 5 tons using a Carver Tableting Press (Wabash, Indiana, USA) to produce a core eutectic tablet (5 x 2.5mm) as illustrated in Figure 4.1a.

4.2.4. Formulation of the outer polymer shell of the *In Situ* Cross-linked Eutectic Tablet

The bottom and top layers of the outer polymer shell were prepared by measuring and blending two separate sets of polymeric powder blends containing 100mg each of PEO, 12mg of CMC, 1mg of magnesium stearate and specific quantities of pectin as shown in Table 4.1.

Table 4.1: Formulation concentrations generated by the Box-Behnken design.

Formulation No.	Eutectic Powder Blend ($\%^{w}/_{w}$)	Crosslinkers* ($\%^{w}/_{w}$)	Pectin (mg)
1	12	20	80
2	12	20	65
3	18	25	65
4	18	15	65
5	18	20	72.5
6	18	20	72.5
7	12	15	72.5
8	18	25	80
9	12	25	72.5
10	24	15	72.5
11	18	20	72.5
12	24	20	80
13	24	20	65
14	24	25	72.5
15	18	15	80

*Crosslinker concentrations shown represent the total concentration of crosslinkers (sodium carbonate and di-potassium hydrogen orthophosphate anhydrous) added in equal parts (1:1).

4.2.5. Assembly of the *In Situ* Cross-linked Eutectic Tablet

A schematic of the Eutectic Tablet is shown in Figure 4.1b-c. The figure expands on the previously highlighted schematic represented in Chapter 1. The polymeric powder blend for the bottom layer of the outer polymer shell was directly compressed at 2 tons of pressure using a Carver Tableting Press (Wabash, Indiana, USA) loaded with punch and dies with a diameter of 10mm to produce a loosely compressed layer. Subsequently, the core eutectic tablet was placed above this layer and centered using the tip of a needle. The polymeric powder blend for the top layer of the tablet was added above the core eutectic tablet and levelled out. The punch was then inserted and the tablet was compressed at 5 tons of pressure using a Carver Tableting Press (Wabash, Indiana, USA) fitted with a flat-faced punch and die (diameter of 10mm) to produce the Eutectic Tablet. To minimize processing variables, all tablets were produced under identical conditions.

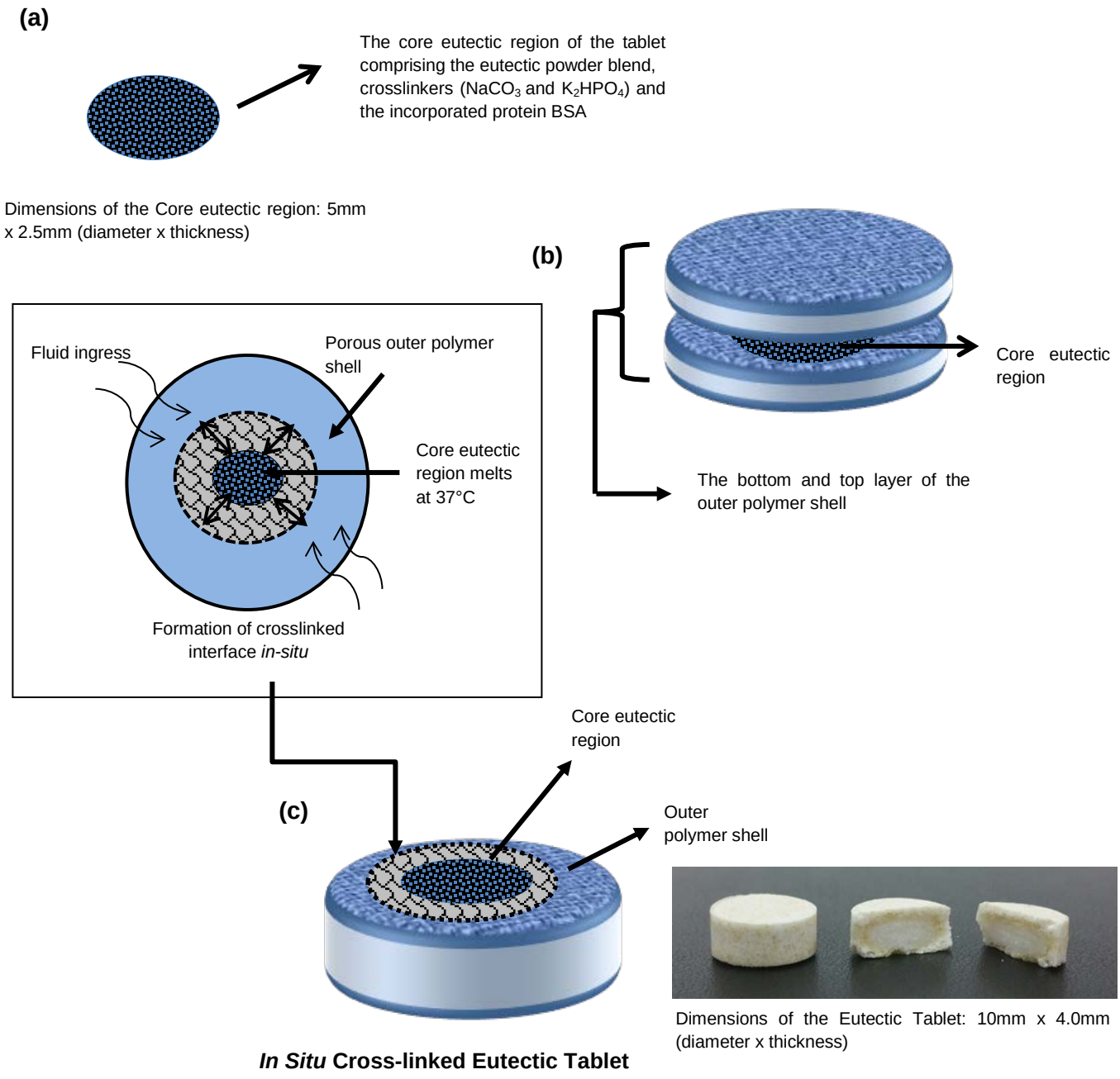

Figure 4.1: Schematic representation of the Eutectic Tablet: **(a)** core eutectic region **(b)** top and bottom layer of the outer polymer shell surrounding the core eutectic region and **(c)** after compression forming a single tablet with proposed *in situ* crosslinking mechanism (insert).

4.2.6. In-process validation tests on the *In Situ* Cross-linked Eutectic Tablet and the eutectic powder blend

Uniformity in mass, friability and thickness analyses were undertaken on the eutectic tablets while the eutectic powder blend was evaluated for particle size, powder flow properties and

physical appearance. A sample of 5 units of each eutectic tablet was analyzed to determine the standardization of the tablet-assembly process. The weight of each eutectic tablet was determined using an analytical digital balance (Mettler, Model AE 240, Griefensee, Switzerland) and the thickness of the eutectic tablets were determined using a digital caliper (25 × 0.01mm capacity) (Taizhou hangyu tools gauge and blades Co., Ltd., Wenqiao, Zhejiang, China). The friability was determined using a Friabilator (Erweka D-63150, Heusenstamm, Germany) set at 25 rpm for 4 minutes with 1% set as the upper limit of acceptability. Comparative evaluations of flow properties for the eutectic powder melt were determined by measuring the angle of repose and the Carr's compressibility index (McGlinchey, 2005). The average particle size was determined by ZetaSizer Nano ZS (Malvern Instruments Ltd., UK). The samples were dispersed in 10mL of distilled water prior to filtering (2mL) of the sample through a 0.22μm pore filter into a cuvette for Zetasize analysis.

4.2.7. Thermal characterization of the eutectic powder blend and construction of a eutectic phase diagram

Assessment of the thermal transitions was performed on each of the eutectic reagents (menthol and cetomacrogol) and the eutectic powder blend to determine characteristic changes in the melting temperature by using a Temperature Modulated Differential Scanning Calorimetry (TMDSC) (Mettler Toledo, DSC1, STAR^{e}System, Schwerzenback, Switzerland). Accurately weighed samples (10±0.25mg) were placed in perforated 40μl aluminium crucibles which were hermetically sealed and ramped between a temperature range of 0-240°C at a constant rate of 10°C/min with a constant purge of N_2. Thermal events of significance included the glass transition temperature (T_g), onset of melting (T_o), melting peak temperature (T_p), heat of fusion (ΔH_m) and temperature of crystallization (T_c) which was determined for each of the eutectic reagents and the eutectic powder blend. Thermogravimetric analysis was used to determine the thermal degradation of the eutectic powder blend upon heating. A Thermogravimetric Analyzer (TGA) (PerkinElmer TGA 4000, Llantrisant, Wales, UK) was used and 5mg samples were weighed and placed in ceramic crucibles. The weights were tarred prior to running the samples and were evaluated between a temperature range of 25-900°C at a rate of 10°C/min with a constant purge of N_2. Furthermore, a phase diagram was constructed by employing the melting points of the eutectic reagents and the eutectic powder blend from the TMDSC results generated.

4.2.8. Characterization of molecular and vibrational transitions of the *In Situ* Cross-linked Eutectic Tablet

Attenuated Total Reflectance-Fourier Transform Infrared Spectroscopy (ATR-FTIR) was used to determine the vibrational molecular transitions of the *in situ* cross-linked outer shell of the tablet with the inner core eutectic region. The eutectic tablets were compared with the native crosslinkers and polymers as well as an *in vitro* cross-linked formulation (PEO 1%; 50mg sodium carbonate; 50mg di-potassium hydrogen orthophosphate) to acquire important microstructural information via comprehensive analysis of the transmittance spectra. Results were recorded on a PerkinElmer Spectrum 2000 FTIR spectrophotometer with a single-reflection diamond MIRTGS detector (PerkinElmer Spectrum 100, Llantrisant, Wales, UK) fitted with a universal ATR polarization accessory for the FTIR spectrum series at a resolution of $4cm^{-1}$. Samples were prepared by immersing the prepared eutectic tablets (containing no pectin) in 50mL of simulated human intestinal fluid (SHIF) pH 6.8 for ±5 hours to allow the process of *in situ* crosslinking. Thereafter, the eutectic tablets were removed from the SHIF and lyophilized (Labconco Freeze-Dry Systems, Labconco Corp., Kansas City, MO, USA) for 48 hours. The resultant lyophilized eutectic tablets were powdered, placed on a diamond crystal and analyzed between a scanning range of $4000\text{-}600cm^{-1}$ at a constant pressure of 120psi with 32 accumulations.

4.2.9. Physicomechanical characterization of the *In Situ* Cross-linked Eutectic Tablet

The eutectic tablets were analyzed with respect to Matrix Hardness (MH), Matrix Resilience (MR) and Deformation Energy (DE) to determine the structural integrity of the eutectic tablets formulated. A calibrated Texture Analyzer (TA.XT *plus*, Stable Microsystems, Surrey, UK) fitted with a flat-tipped steel probe (2mm diameter) was used for surface determination of MH and MR values of the Eutectic Tablets. Further textural analyses of the eutectic tablets were undertaken using a needle-tipped steel probe (2mm diameter) for determination of the MH and DE through penetration of the complete thickness of the eutectic tablets. The samples were prepared and placed in a Temperature Controlled Peltier Cabinet (XT/PC) coupled to a Peltier Control Unit (PCU) (Stable Microsystems, Surrey, UK) for analysis by Texture Analyzer to mimic the internal body temperature environment. The Thermal Cabinet was equilibrated to 37°C (body temperature) to enable the melting of the core region of the eutectic tablet before testing was performed within the cabinet. Data was captured at a rate of 200 points per second using Texture Exponent Software (V3.2). MR was computed as a percentage of the ratio between the Area under the Curve (AUC) of the peak to baseline (AUC_{2-3}) and the baseline to peak (AUC_{1-2})

from a Force-Time profile. The MH and DE values were both obtained from the gradient and AUC of the Force-Distance profiles, respectively. The MH was calculated using the Brinell Hardness Number (BHN) (Equation 4.1). Textural analyses on all the eutectic tablets were performed in triplicate. The parameters employed for the analysis are listed in Table 4.2.

$$\mathrm{BHN} = \frac{2\mathrm{F}}{\pi\mathrm{D}\left(\mathrm{D}-\sqrt{\mathrm{D}^2-\mathrm{d}^2}\right)} \quad \textbf{(4.1)}$$

Where, BHN is Brinell Hardness Number; D is diameter of indenter (mm); F is elucidated from the gradient of the initial force and the final force obtained and d is diameter of indentation (mm).

Table 4.2: Textural profiling parameters used for determining the Matrix Hardness, Matrix Resilience and Deformation Energy of the eutectic tablets

Parameters	Matrix Hardness	Matrix Resilience	Deformation Energy
Pre-test speed	1 mm/s	1 mm/s	1 mm/s
Test speed	0.5 mm/s	0.5mm/s	0.5mm/s
Post-test speed	1 mm/s	10mm/s	10mm/s
Trigger type	Auto	Auto	Auto
Trigger force	0.05 N	0.05 N	0.05 N
Compression strain	N/A	40%	N/A

*The distance for probe penetration into the tablet was set at 4mm for the needle-tipped steel probe

4.2.10. Crystallinity characterization of the eutectic powder blend

The diffraction spectra of the eutectic powder blend was compared to the individual eutectic reagents, menthol and cetomacrogol, for determination of the change in the crystallinity. An X-ray Diffractometer (XRD) fitted with a high-speed silicon strip detector and operating at 600W X-ray source for high resolution scanning (Rigaku Miniflex Guidance 600W, Tokyo, Japan) was used for qualitative and quantitative crystallinity analysis. Samples were prepared by weighing ±10mg of the eutectic reagents and eutectic powder blend and placing them in aluminium sample holders. Each sample ran between an operating range of 0-40° 2-theta. Data was captured and analyzed using the Rigaku Powder Diffraction Analysis Software (PDXL2). Similarity of diffraction patterns, peak positions and crystallinity were determined from the various profiles obtained.

4.2.11. Swelling and erosion studies on the *In Situ* Cross-linked Eutectic Tablets

The degree of swelling of the eutectic tablets was determined using the equilibrium weight gain method (Efentakis and Vlachou, 2000). The eutectic tablets were weighed initially and placed in 50mL of simulated human intestinal fluid (SHIF) at pH 6.8 over a period of 24 hours. At

predetermined time intervals (0, 1, 2, 3, 6, 8, 12, 24 hours), the eutectic tablets were removed and reweighed to determine changes in swelling. The degree of swelling at each time interval was determined using Equation 4.2. Erosion studies were conducted on the same samples after 24 hours by drying to a constant weight. The percentage erosion was calculated using Equation 4.3.

$$\% \ \Delta Swelling = \frac{W_f - W_i}{W_i} \times 100 \quad \textbf{(4.2)}$$

Where, W_f is the weight of the swollen tablet at time *t* and W_i is the initial weight of the tablet. (N=3).

$$\% \, Erosion = \frac{W_i - W_f}{W_i} \times 100 \quad \textbf{(4.3)}$$

Where, W_i is the initial weight of the tablet and W_f is the final dried weight of the tablets after 24 hours. (N=3).

4.2.12. Morphological characterization of the eutectic powder blend

The surface morphology of the eutectic powder blend was analyzed using a Scanning Electron Microscope (SEM) (FEI Company, Hillsboro, OR, USA) to determine characteristic changes in its crystalline and amorphous microstructures in relation to the blend of eutectic reagents employed. Samples were fixated on aluminum stubs and loose particles were removed by spraying with compressed air. Thereafter, the samples were sputter coated with gold for 60 seconds using a SPI-Module™ Sputter Coater (SPI Supplies, Structure Probe, West Chester, PA). After coating, the samples were re-sprayed with compressed air and placed in the FEI Phenom™ Scanning Electron Microscope operated at 10kV in the electron imaging mode for subsequent viewing at varying degrees of magnification.

4.2.13. *In vitro* protein release studies

Intrinsic to the functioning of the eutectic tablets was its *in vitro* protein release performance. *In vitro* protein release studies were performed using a USP35 dissolution apparatus II (Caleva, Model 7ST, UK). The eutectic tablets were placed in 900mL SHIF at pH 6.8. Each eutectic tablet was placed beneath a ring mesh assembly within the dissolution vessel to prevent floatation. Dissolution was performed at a speed of 50rpm (37±0.5°C). Sampling of 3mL was

undertaken at predetermined time intervals (0, 1, 2, 3, 6, 8, 10, 12, 24) and replaced with an equal quantity (3mL) of drug-free dissolution medium to maintain sink conditions. The quantity of intact BSA released was determined using a UV spectrophotometer at a wavelength of 285nm (Analytik Jena^{TM}, Specord 40, United Scientific Pty., Ltd., South Africa, Natal) (Kim *et al*., 2005; Muller *et al*., 2012; Azimi *et al*., 2013). All samples removed were filtered using a 0.45µm membrane filter prior to UV analysis. Protein release was calculated as a mean of three determinations as all studies were conducted in triplicate. In addition, the mean dissolution time (MDT) (Equation 4.4) was calculated from dissolution data to determine the protein release rate (Sathish and Syed, 2013).

$$MDT = \frac{\sum_{i=1}^{i=n} t_{mid} \times \Delta M}{\sum_{i=1}^{i=n} \Delta M} \quad \textbf{(4.4)}$$

Where, *MDT* is Mean Dissolution Time; *i* is the dissolution sample number; *n* is the number of dissolution sample time; t_{mid} is time at mid-point between *i* and *i=1*; *ΔM* is the additional amount of protein dissolved between *i* and *i=1*.

In addition, the *in vitro* protein release data obtained were fitted into various mathematical modelling equations to determine the mechanism of protein release from the eutectic tablets.

4.2.14. *Ex vivo* permeation studies through the Large White Pig intestinal tissue model

Intermediary *ex vivo* permeation studies were undertaken using intestinal tissue excised from a Large White Pig to determine the permeation-enhancing effects of menthol. The pig was euthanized according to standard operating procedures and the intestinal tissue was carefully removed. Following removal, the tissue was thoroughly cleaned and appropriately preserved until further use. Prior to experimental procedures, the adipose tissue and muscular layers were carefully incised to isolate the intestinal epithelium with attached blood vessels. To ensure the integrity of the tissue sections throughout the study, the potential difference across the intestinal tissue was measured before and after permeation studies. This was performed by passing a fixed current across the intestinal tissue sections using a Mettler Toledo Seven Multi GmbH Meter (Analytical CH-8603, Schwerzenbach, Switzerland) connected to an electrode that was adjusted to isotonic environments by placing the probe into isotonic PBS solution. Thereafter, the potential difference was recorded while the tissue was dispersed in distilled water.

A Franz Diffusion Cell apparatus (United Scientific Pty., Ltd., South Africa, KwaZuluNatal) containing a receptor compartment, donor compartment and membrane platform was the apparatus used for determination of the diffusion across the intestinal membrane. The tissue samples were incised to fit receptor compartments with a surface area of approximately 1.8cm^2. The samples for the donor compartment were prepared by immersing the eutectic tablets (containing three different concentrations of eutectic powder blend as depicted in Table 4.1) in SHIF pH 6.8 over 24 hours until the tablet was completely dissolved. In addition, a tablet was prepared without the eutectic powder blend (control) and immersed in SHIF pH 6.8 over 24 hours until the tablet was completely dissolved. This was done for comparison purposes in determining the permeation-enhancing effects of menthol. The resultant solutions with the completely dissolved tablets were stirred thoroughly and 2mL samples were removed for the donor compartment. Each receptor compartment was filled with 12mL of phosphate buffer solution (pH 7.4) to simulate the pH of blood which was further thermoregulated at 37°C by a water jacket throughout the study. Receptor compartments were constantly stirred using a magnetic stirrer.

The prepared tissues were placed on the membrane platform between the receptor and donor compartments of the Franz Diffusion Cell apparatus. At predetermined intervals (0, 1, 2, 3, 6, 8, 10, 12, 24), 0.1mL of sample was removed from the receptor compartment and replaced with an equal amount of fresh phosphate buffer solution. Samples were then evaluated using a UV spectrophotometer at a wavelength of 285nm (Analytik Jena^{TM}, Specord 40, United Scientific Pty., Ltd., South Africa, Kwa Zulu Natal). Protein-free formulations were used as a reference/blank for UV analysis. The values obtained were computed as protein flux across the intestinal membrane. The flux (mg.cm^{-2} h^{-1}) of BSA across the intestinal membrane was calculated per unit area by linear regression analysis of permeation data using Equation 4.5.

$$Js = \frac{Qr}{A \times t} \quad \textbf{(4.5)}$$

Where, *Js* is the flux of BSA; *Qr* (mg) is the quantity of drug which permeated across the intestinal membrane into the receptor compartment; *A* (cm^2) is the effective cross-sectional area that is available for permeation; *t* (h) is the time of protein exposure to the intestinal tissue membrane.

4.3. Results and Discussion

4.3.1. Formulation validation of the eutectic powder blend and Eutectic Tablets

Synthesis of the eutectic powder blend yielded a soft, white, deliquesced powder with an average uniform particle size of 142.1nm and a Polydispersitiy Index (PDI) of 0.303. The flow properties of the eutectic powder blend was determined using the angle of repose and Carr's compressibility index. The results obtained were atypical for the eutectic powder blend which displayed an angle of repose value and Carr's compressibility index of 70.23° and 4.22%, respectively. These results indicated an easily consolidated powder with excellent compressibility characteristics18, thus displaying ideal characteristics for this system as it allowed for simple moulding and compression of the inner core eutectic region of the tablet. A uniformity of mass among the 5 units of each formulated eutectic tablet was displayed. Across formulations 1-15, the weight of the eutectic tablets was 500±0.6mg. The thickness was 4.0±0.5mm while the friability was at an average of 0.6% which was within the set limit of 1%, indicating desirable compressibility and resistance to fracture.

4.3.2. Assessment of the thermodynamic behavior of the eutectic powder blend

Thermal analysis was used to characterize and compare pertinent transitions such as melting, glass transitions, phase changes and heat of fusion of the native eutectic reagents and the eutectic powder blend in order to determine the change in the melting point that is characteristic of eutectic mixtures. The TMDSC thermograms of the eutectic reagents, menthol and cetomacrogol, are depicted in Figure 4.2 (a-b). Menthol displayed a distinct melting peak (T_p) at 40.44°C which indicated the melting temperature (T_m) of the eutectic reagent. The heat per unit mass that was required to change the menthol from a solid to a liquid at its T_m was quantified as 73.55Jg^{-1}. The first endothermic shift from the baseline noticeable in the menthol thermogram was indicative of the glass transition temperature (T_g) at 28.45°C, representing the softening of the material and melting of the amorphous regions within the menthol (Widmann *et al*., 2000) Continued heating of the menthol resulted in a transition with a distinct loss of weight, confirmed by the endothermic boiling point (T_b) peak at 205.97°C (Widmann *et al*., 2000; Gabbott, 2008). The melting temperature of the eutectic reagent cetomacrogol was defined by a T_p at 51.67°C and a heat of fusion (ΔH_m) of 154.50Jg^{-1}. In addition, cetomacrogrol displayed an onset of melting (T_o) at 46.07°C and an endothermic peak comparable to that of menthol at 36.45° which was indicative of the T_g.

Assessment of the TMDSC thermograms of the native eutectic reagents in comparison with the eutectic powder blend, yielded similar endothermic peaks with a measured decrease in the melting point (Figure 4.2c). The eutectic powder blend displayed a T_g at 33°C which incidentally corresponded to the onset of melting at 33.62°C. This indicated the change in the amorphous region of the eutectic powder blend to a more viscous and liquid-like condition (Widmann *et al*., 2000). The eutectic powder blend displayed a shift in the T_p to a lower temperature 37.30°C (physiological) and a ΔH_m of 9.56Jg^{-1} which was considerably lower than the T_p and ΔH_m for either menthol or cetomacrogol. This indicated that less energy was required to convert the solid eutectic powder blend to a liquid at its melting temperature (Gabbott, 2008). The T_b for the eutectic powder blend was typically lower than that of menthol at 188.01°C, consistent with the lower melting temperature. The negligible peaks noticed between 210°C-230°C were artefacts resulting from the closing/opening of the crucible pan hole during the sublimation process (Gabbott, 2008).

Furthermore, the change in mass of the eutectic reagents and the eutectic powder blend as a function of temperature was analyzed from thermogravimetric data obtained (Figure 4.3). TGA results displayed clear weight loss of menthol at 199.39°C with only 1.505% of sample remaining, following the rapid decrease in the sample weight upon heating at 121.28°C. These results obtained for menthol were synonymous with TMDSC data which indicated the boiling of menthol at 205.97°C with subsequent evaporation, resulting in sample weight loss. Menthol displayed typical thermal decomposition with the formation of gaseous reaction products (Widmann, 2001).

Cetomacrogol displayed a similar one-stepped thermal decomposition at 235.73°C and an almost complete weight loss at 398.01°C. In contrast, the eutectic powder blend displayed multi-step decomposition at notable temperatures characteristic of menthol and cetomacrogol. Each stepped increase in temperature displayed a 20-25% weight loss with the last step displaying a significant 35% weight loss with only 9.651% of sample remaining.

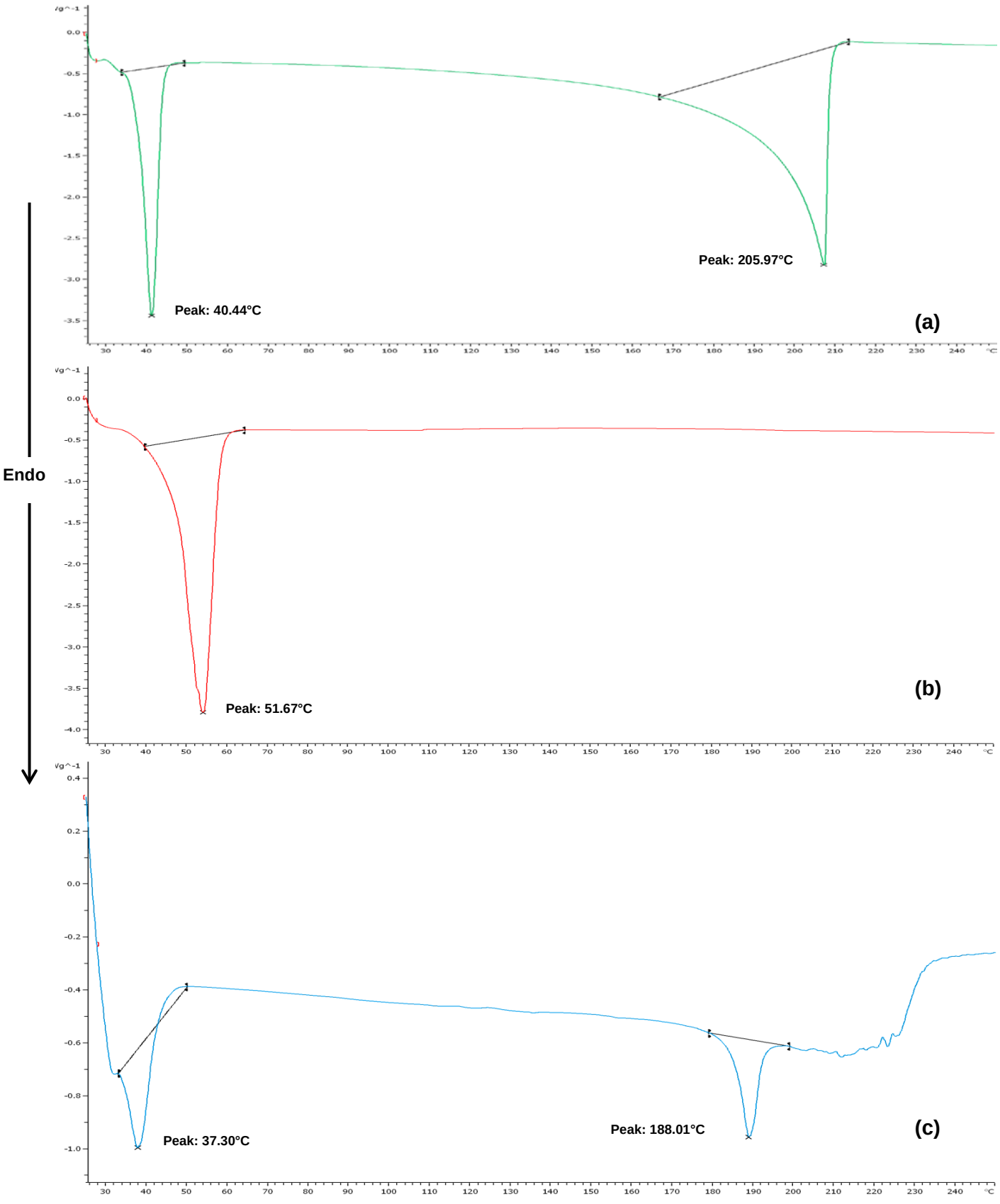

Figure 4.2: TMDSC thermograms for **a)** native eutectic reagent menthol, **b)** native eutectic reagent cetomacrogol and **c)** eutectic powder blend (menthol: cetomacrogol (3:1)).

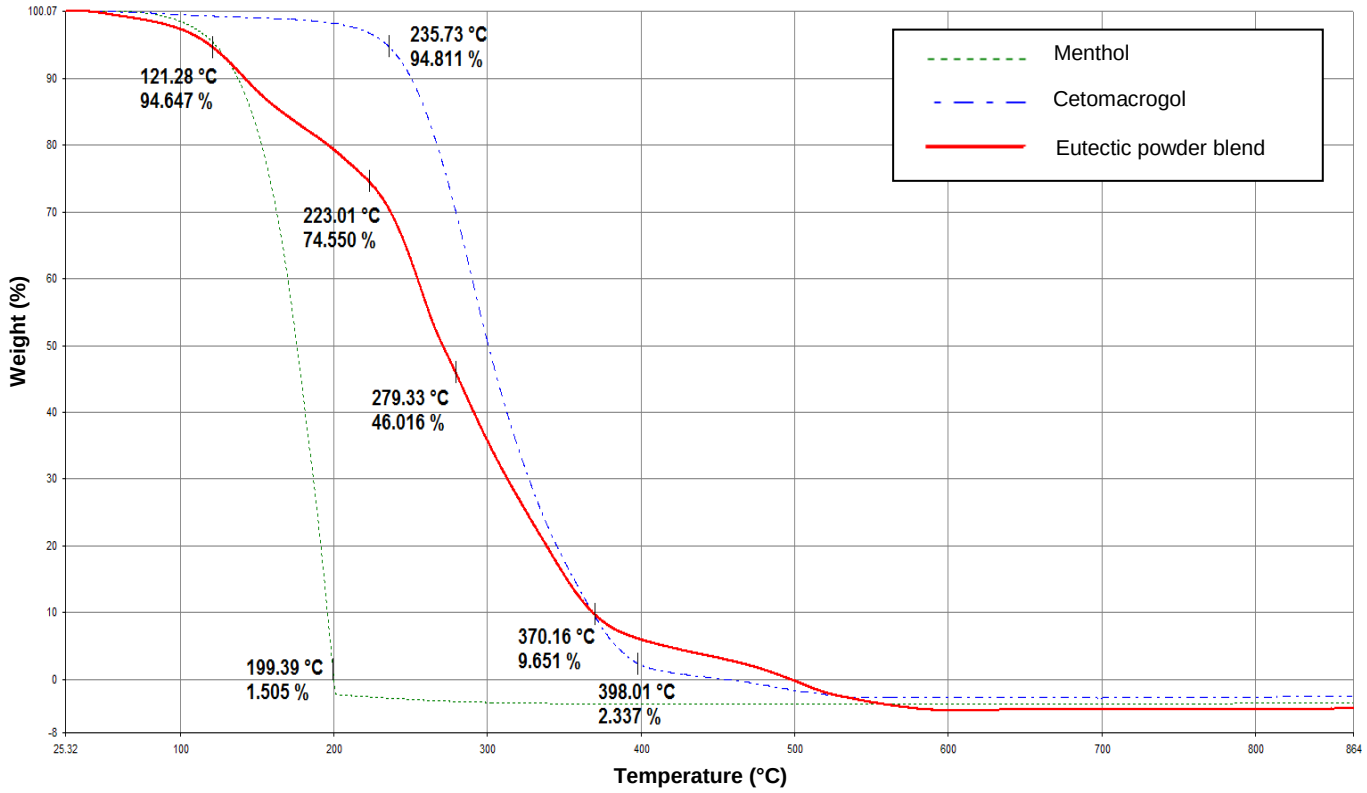

Figure 4.3: TGA profiles displaying the main thermal degradation events of the eutectic reagents: menthol, cetomacrogol and the eutectic powder melt (menthol: cetomacrogol (3:1)).

Complete thermal analysis was essential in determining pertinent information that supports the successful formulation of the eutectic powder blend. The results unmistakably displayed the decrease in the melting point of the eutectic powder blend which is a typical feature of eutectic mixtures (Widmann *et al*., 2000). The thermogravimetric analysis provided valuable degradation data in support of the TMDSC results generated. The results were further emphasized by the formation of a binary phase diagram (Figure 4.4).

4.3.3. Binary phase diagram

A binary phase diagram (Figure 4.4) was constructed based on the melting points of the eutectic reagents and the eutectic powder blend obtained from TMDSC thermograms (Figure 4.2). Typically within a eutectic system, the eutectic temperature (T_e) is lower than the T_m^A and T_m^B, the melting point of the pure components A and B (Koningsveld *et al*., 2001). The lowest temperature at which the liquid phase existed in the menthol-cetomacrogol eutectic powder melt system was 37.30°C (lower T_m than either component), occurring in a mixture with a eutectic composition of 70% menthol and 30% cetomacrogol. This point on the phase diagram was marked as the eutectic point in which the three phases (liquid, solid menthol and solid cetomacrogol) coexisted (Martin, 1993). Additional markers that were of importance were the

liquidus curve which seperated the entire liquid phase from the liquid-solid phase, the solidus curve which separated the complete solid phase from the liquid-solid phase and the liquid and solid markers which indicated the complete melt and crystals of A and B, respectively. In addition, the effect of the cryoprotectant on the phase behavior of the eutectic powder blend was considered to be neglible as it displayed no significant effect on the binary phase diagram constructed.

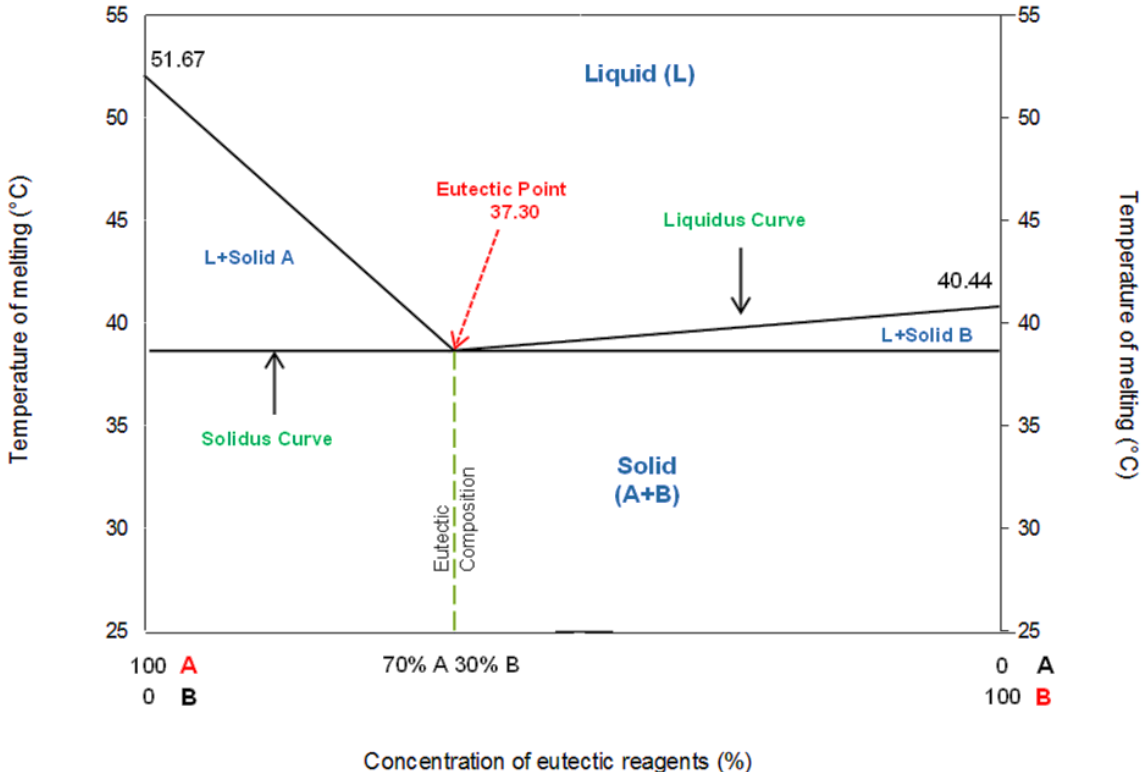

Figure 4.4: Binary phase diagram of the eutectic powder blend displaying the eutectic point of the melt containing eutectic reagents A (menthol) and B (cetomacrogol) at a 70%:30% composition.

4.3.4. Chemical Structure Integrity Analysis of the *In Situ* Cross-linked Eutectic Tablets

The transitions in the chemical structure of the native compound PEO, crosslinkers ($NaCO_3$ and K_2HPO_4) and the eutectic powder blend in comparison to an in vitro crosslinked formulation (PEO 1%; 50mg sodium carbonate; 50mg di-potassium hydrogen orthophosphate) as well as the eutectic tablets containing varying crosslinker concentrations are displayed in the ATR-FTIR split spectra as a function of % transmittance against wavelength (Figure 4.5a-b). The spectra for the eutectic tablets are represented as crosslinker concentrations ($15\%^{w}/_{w}$, $20\%^{w}/_{w}$ and $25\%^{w}/_{w}$) as all formulations displaying these varying concentrations of crosslinker displayed the

same transmittance spectra. The eutectic tablets displayed bands characteristic to all its components with a reduction as well as an increase in intensity of certain bands and the appearance of new bands, attributed to the in situ crosslinking initiated by the presence of the chemical crosslinkers ($NaCO_3$ and K_2HPO_4).

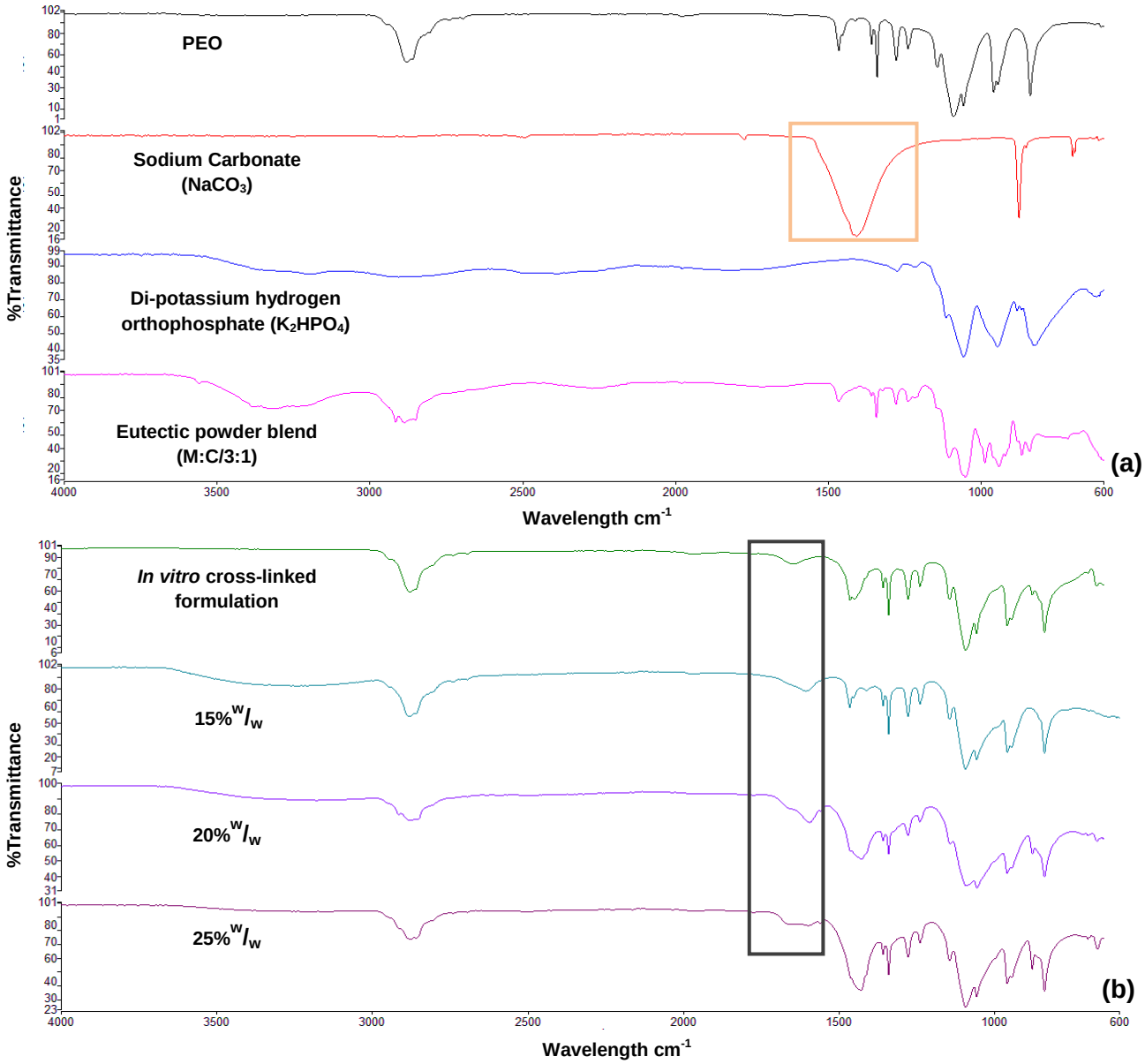

Figure 4.5: ATR-FTIR transmittance spectra: **a)** split spectra of the native compound PEO, crosslinkers ($NaCO_3$ and K_2HPO_4) and the eutectic powder blend and **b)** split spectra of the *In Vitro* Cross-linked (IVC) formulation (PEO 1%; 50mg $NaCO_3$; 50mg K_2HPO_4) and the eutectic tablets containing 15%$^{w}/_{w}$, 20%$^{w}/_{w}$ and 25%$^{w}/_{w}$ crosslinker concentrations. In **a)** highlighted block indicates the characteristic sodium carbonate peaks that were observed in the IVC formulation and the 20%$^{w}/_{w}$ and 25%$^{w}/_{w}$ formulation concentrations of eutectic tablets. In **b)** highlighted block indicates the formation of a new band.

Summative bond designations of the *in vitro* cross-linked formulation and eutectic tablets are displayed in Table 4.3 with distinctive peaks identified in Figure 4.5b. The *in vitro* cross-linked formulation displayed similar peaks to that of the eutectic tablets, indicating successful intra- and intermolecular crosslink formation of PEO *in situ*. In addition, the eutectic tablets displayed a broad, low intensity peak at 3248cm^{-1}, indicating the presence of menthol within the formulations (Sharma *et al*., 2013)

Table 4.3: Bond designations for the *In Vitro* Cross-linked (IVC) formulation and the eutectic tablets (15%$^{w}/_{w}$, 20%$^{w}/_{w}$ and 25%$^{w}/_{w}$) (Coates, 2000; Sharma *et al*., 2013).

Bond origin	Group Frequency	Assignment	Appearance
$>CH_2$	2877-2880cm^{-1}	Aliphatic group, Methylene asym/sym stretch	Medium to strong ↓intensity (20%$^{w}/_{w}$, 25%$^{w}/_{w}$)
C=O	1595-1643cm^{-1}	Carbonyl group, hydrogen-bonded carboxylic acid stretching	Medium, new band
CO_3^{2-}	1453-1465cm^{-1} (IVC) 1466cm^{-1} (15%$^{w}/_{w}$) 1428cm^{-1} (20%$^{w}/_{w}$) 1430cm^{-1} (25%$^{w}/_{w}$)	Carbonate ion, in-plane and out-of-plane bending	Broad, intense peak characteristic of sodium carbonate, ↑intensity (IVC, 20%$^{w}/_{w}$ and 25%$^{w}/_{w}$)
>CH-	1341/1359cm^{-1}	Aliphatic group, methyl bending vibrations	Sharp, narrow peak, ↓intensity (15% $^{w}/_{w}$, 20%$^{w}/_{w}$ and 25% $^{w}/_{w}$) at 1341cm^{-1}/ ↑intensity (IVC, 15%$^{w}/_{w}$, 20%$^{w}/_{w}$ and 25%$^{w}/_{w}$) at 1359cm^{-1}
C-O /P=O	1278-1279cm^{-1}	Ethers, stretching vibrations/ phosphorous-oxy compounds, organic phosphate stretch	Two peaks often overlapped
C-H/ P-O-C	940-1058cm^{-1}	Alkene, out-of-plane bending/ phosphorus-oxy compounds, aliphatic phosphate stretch	Multiple overlapping bands with varying intensities, ↓intensity (IVC, 20%$^{w}/_{w}$ and 25%$^{w}/_{w}$) at 945 cm^{-1}
CO_3^{2-}	879-880cm^{-1} 670-701cm^{-1}	Carbonate ion, in-plane and out-of-plane bending	Narrow, weak to medium intensity peaks

Several bond origins (>CH2, >CH-, C-O, C-H) characteristic to PEO were noticeable in the split transmittance spectra for the *in vitro* crosslinked formulation and the eutectic tablets as designated in Table 4.3. A new peak, uncharacteristic from the polymer or crosslinker entities was observed in the formulation spectrums. The peak represented a C=O stretching vibration, characteristic of hydrogen-bonded carboxylic acids indicating crosslinks formed between PEO, $NaCO_3$ and K_2HPO_4. Formulations containing a 20%$^w/_w$ crosslinker concentration displayed the lowest transmittance (75.05%) for the new peak, suggesting an increased intensity and stronger bond formation. A characteristic sodium carbonate peak was observed between a frequency range of 1428-1466cm^{-1} for all formulations which resulted in the dwarfing of the narrow, low intensity peak of PEO for the *in vitro* crosslinked formulation and the eutectic tablets (20%$^w/_w$ and 25%$^w/_w$). Disappearance of the native peak for PEO at 1413cm^{-1} for the *in vitro* cross-linked formulation and eutectic tablets (20%$^w/_w$ and 25%$^w/_w$) was attributed to macromolecular interactions and substantiated the formation of the distinguishing sodium carbonate peak.

Furthermore, carbonate ion bending was characterized by new bands at the lower end of the spectrum between 879-880cm^{-1} and 670-701cm^{-1} for the *in vitro* cross-linked formulation and eutectic tablets (20%$^w/_w$ and 25%$^w/_w$) (Coates, 2000; Sharma *et al*., 2013). Typically, the first absorption for carbonate ions is broad and intense and the second absorption is narrow with a weak to medium intensity as was evidenced by the results obtained (Coates, 2000). The influence of K_2HPO_4 in the crosslinking process was evidenced by the overlapping organic (P=O conjugation) and aliphatic (P-O-C conjugation) phosphate stretching vibrations characterized in Table 4.3. The crosslinking process is expected to create an interpenetrating cross-linked interface *in situ* between the core region of the eutectic tablet and the outer shell, facilitating a controlled release rate and protection of the incorporated protein or peptide.

Evidentiary results from ATR-FTIR molecular and vibrational transitions confirmed the *in situ* crosslinking within the eutectic tablets which was further supported by its comparativeness to the *in vitro* cross-linked formulation. The *in vitro* crosslinked formulation containing 20%$^w/_v$ of crosslinker displayed transmittance peaks identical to the eutectic tablets containing 20%$^w/_w$ of crosslinker. Formulation concentrations of 15%$^w/_w$ were the lowest concentrations and displayed lower crosslinking ability as was demonstrated by the lower intensity of some peaks and absence of other peaks which were present in eutectic tablets containing 20%$^w/_w$ and 25%$^w/_w$. In contrast, a 25%$^w/_w$ crosslinker concentration displayed higher intensities for some peaks, however medium intensities were observed for the new bands as compared to a 20%$^w/_w$.

Consequently, a 20%$^{w}/_{w}$ concentration of crosslinker was considered the optimal crosslinking concentration as it displayed higher intensities for the new bands indicating improved conjugation and superior crosslinking ability.

4.3.5. Quantification of the physicomechanical behaviour of the *In Situ* Cross-linked Eutectic Tablets

The physicomechanical behavior of the eutectic tablets was characterized with respect to MH, MR and DE in response to compressive and penetrative forces applied. The MH, MR and DE were quantified from Force-Time and Force-Distance profiles obtained for surface and core tablet textural profiling. Typical Force-Time and Force-Distance profiles for surface and core tablet textural profiling is displayed in Figure 4.6a-b. The force for the calculation of MH was determined from the steepness of the upward gradient of the Force-Distance profile up to the primary fracture point (between anchors 1 and 2). The initial gradient represented by the slight increase in force indicates a low resistance to adhesive and cohesive forces and thus a reduced strength matrix (Pillay and Danckwerts, 2002). Consequently, the steeper secondary gradient indicates an increased resistance to deformation and thus harder matrix.

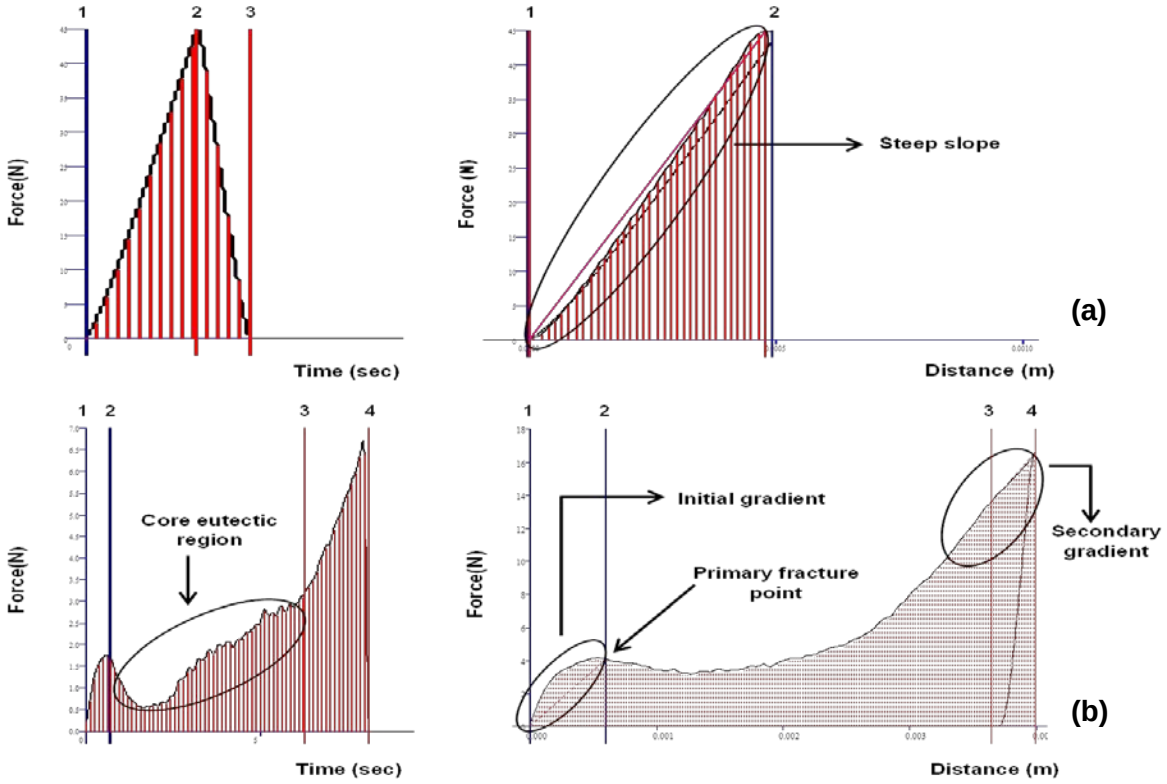

Figure 4.6: Typical Force-Time and Force-Distance profiles generated from: **a)** compressive force and **b)** penetrative force.

The MH is a critical textural parameter that influences the drug release, swelling, erosion and stability of the tablet matrices. The surface hardness of the eutectic tablets was calculated and the results are presented in Figure 4.7. F9 displayed the greatest hardness value of 227.76N.mm^2 which corresponded to the lowest concentration of eutectic powder blend and highest crosslinker and pectin concentration (Table 4.1) within the eutectic tablet. The lower concentrations of eutectic powder melt with higher crosslinking concentrations create core eutectic tablets that are somewhat harder. In addition, the pectin contained within the outer shell of the tablet provides a degree of structural hardness due to its good compressibility and flowability and thus accounts for the greater hardness values obtained. Formulations containing higher concentrations of eutectic powder blend (F10, F12, F13 and F14) displayed lower hardness values, representative of relatively softer matrices with low resistance to deformation. The core matrix hardness was determined using a needle-probe which penetrated the full thickness of the tablet. Since the measurements for the core matrix hardness was determined in a temperature-controlled cabinet set at 37°C to mimic physiological temperature, the predictable melting of the core eutectic powder blend was inevitable as emphasized by TMDSC results in Figure 4.2. The melting of the core eutectic region created softer core matrices for the eutectic tablets (Figure 4.7a). F1-F15 displayed significantly lower hardness values for the core matrix as compared to the surface matrix of the eutectic tablets.

The ability of the eutectic tablets to return to their original state after being subjected to a compression force was computed as the MR (Figure 4.7b) (Pillay and Fassihi, 1999). The corresponding MR in response to a compression strain of 40% was measured for F1-F15. F7 demonstrated the highest resilience value (60.54%) while F10 displayed the lowest resilience (39.27%). These values corresponded to lower and higher and concentrations of eutectic powder blend, respectively. This indicated that with higher concentrations of eutectic powder blend, the flexibility of the formulation decreased due to the softer matrices. However, this was not the case for all formulations and results indicated comparatively good resilience values around the median of 50%.

Typically, in the characterization of tablets, high values for matrix hardness and resilience are considered optimal. Nevertheless, the results obtained for the eutectic tablets reflect the proposed aim of the formulation and as such is considered ideal. The softer matrices of the core eutectic region at 37°C was the ultimate goal for facilitating *in situ* crosslinking. The surface matrix hardness and resilience was acceptable in providing suitable structural integrity.

Nonetheless, the results obtained does not reflect the process of *in situ* crosslinking which will provide a structural flexibility, improved hardness and higher fracture energy with improved resistance to cohesive and adhesive forces.

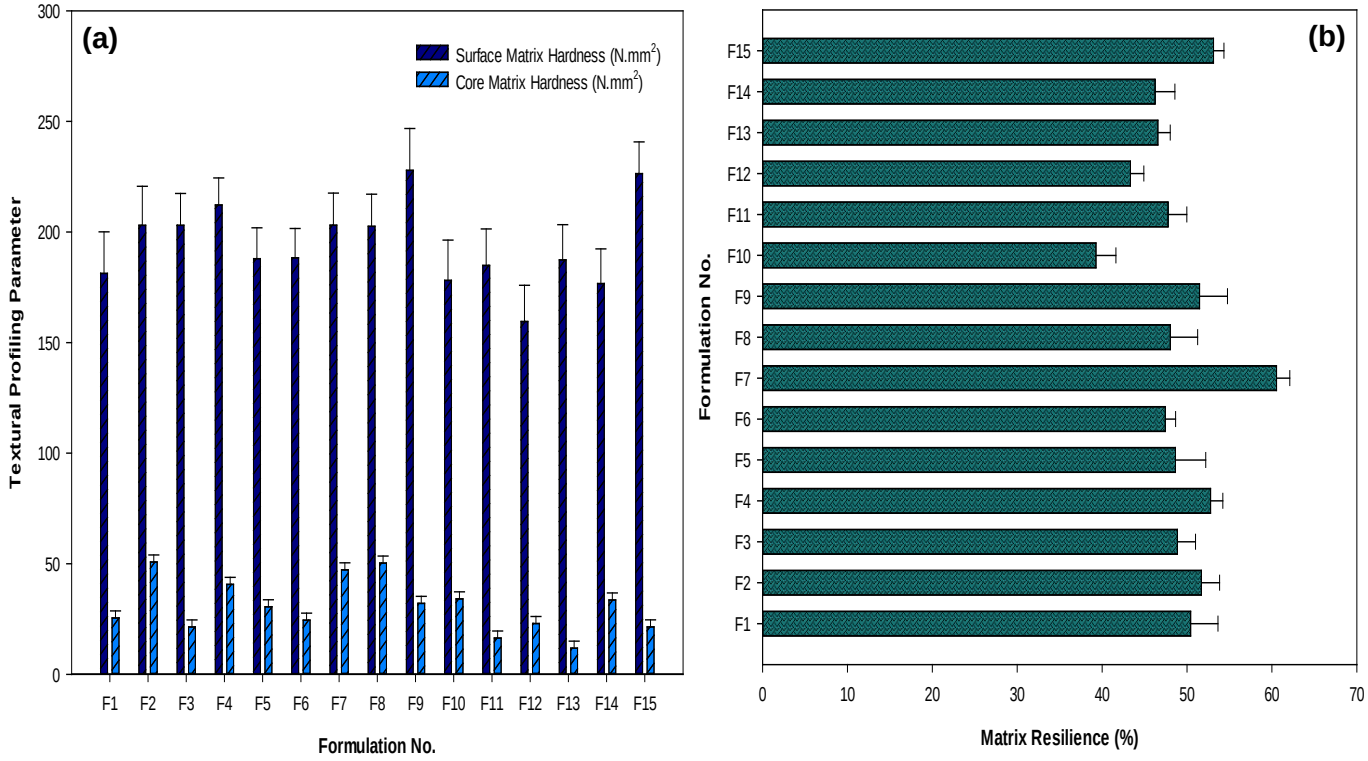

Figure 4.7: Graphical representation of textural analysis results of the eutectic tablets depicting: **a)** surface and core matrix hardness (N.mm^2) and **b)** matrix resilience (%).

4.3.6. Crystallinity analysis of the eutectic powder blend through qualitative and quantitative assessment

The spectrum for the eutectic powder blend was compared to the XRD spectra for eutectic reagents menthol and cetomacrogol (Figure 4.8). Typically, crystalline components appear as sharp and narrow peaks on the XRD spectrum stemming from the ordered and regular arrangement of the atoms. In contrast, the amorphous parts appear as flat and broad peaks reflecting the random and disordered arrangement of atoms. Following this, the eutectic reagents (menthol and cetomacrogol) were considered to be crystalline as they displayed sharp, narrow peaks with high intensities. In contrast, the eutectic powder blend displayed broad, low intensity peaks indicative of the presence of amorphous material. These differences in the eutectic powder blend were attributed to the increased concentration of menthol within the formulation which imparted an amorphous element. The formation of eutectic mixtures typically results in a decrease in crystallinity and the presence of more amorphous material with a higher

water affinity and improved solubility at all temperatures below the melting point of the mixture (Liu *et al*., 2006; Qui *et al*., 2009). Thermal analysis results further supports the XRD data obtained for the eutectic powder melt as the decrease in the melting point corresponded to the increase in the amorphous content within the eutectic powder blend which subsequently decreased the crystallinity and confirmed the presence of a eutectic system.

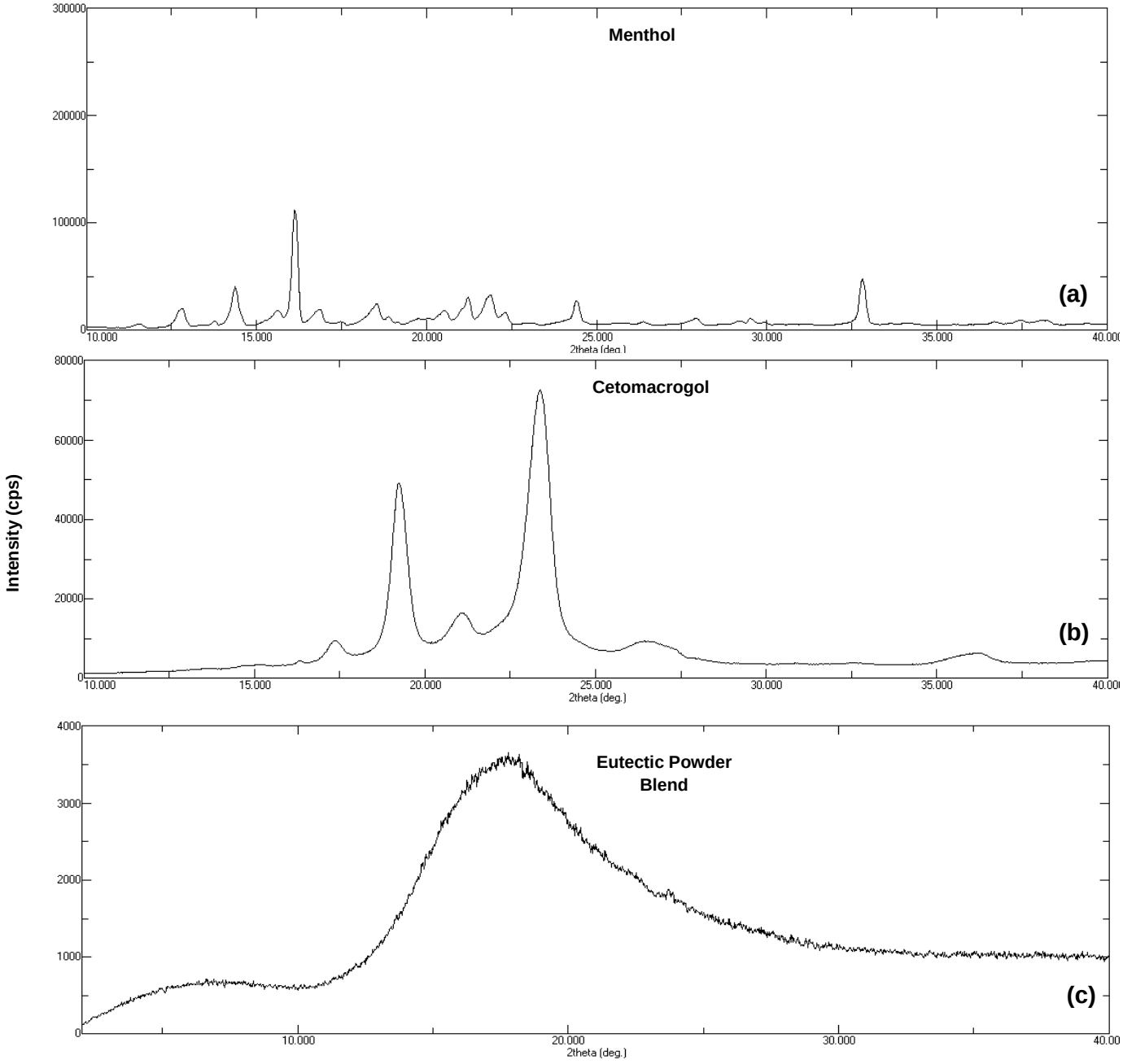

Figure 4.8: XRD spectra: **a)** eutectic reagent menthol, **b)** eutectic reagent cetomacrogol and **c)** eutectic powder blend (menthol: cetomacrogol/3:1) as a function of the reflected intensities (cps) versus the diffraction angle 2-theta (deg).

4.3.7. Assessment of the swelling and erosion behavior of the *In Situ* Cross-linked Eutectic Tablets

The swelling and erosion of the eutectic tablets were analyzed by monitoring the change in weight over a predetermined period of time. All formulations displayed increased swelling over 24 hours as was evidenced by the swelling profiles obtained in Figure 4.9 (a-c). The porous nature of the polymeric material PEO contained within the outer polymer shell was a major contributing factor towards the high water uptake observed for F1-F15. The PEO created pores within the eutectic tablets which facilitated increased water uptake when the tablet came into contact with the dissolution medium and thus ultimately affected the rate and extent of swelling observed (Vlachou *et al*., 2001; Ahuja and Pathak, 2009). F1-F15 swelled to ±1000% of its original mass over 24 hours with initial high water uptakes producing swelling behavior ranging between 150-250%

Another major determinant of the swelling behavior is the degree of crosslinking that occurs (Pillay and Danckwerts, 2002). A higher degree of crosslinking decreases the overall swelling capacity as was evidenced by the results obtained. F7 displayed the highest swelling percentage (1354%) and correspondingly contained a lower concentration of crosslinker ($15\%^{w}/_{w}$). Likewise, F8 depicted the lowest swelling percentage (1053.93) with a higher concentration of crosslinker ($25\%^{w}/_{w}$). These results indicated that the swelling behavior was directly proportional the concentration of crosslinker contained within the formulations. All other formulations displayed similar results depending on the concentration of crosslinker contained within the eutectic tablet.

The erosional behavior of the tablets was influenced by the different concentration of pectin present within each eutectic tablet. This was demonstrated by the results obtained in Figure 4.9d which showed F1 as having an understandably higher erosion percentage (53.97%) as it contained 80mg of pectin as compared to the 65mg of pectin contained within F13 which showed a 20% lower erosion percentage of 33.96%. Overall, the results calculated for erosion of the tablets after 24 hours for all formulations were centered around a median value of 50% which indicated relatively controlled, surface erosion. The tablets maintained its characteristic shape after 24 hours and as a result achieved the proposed objective. The swelling and erosion behavior was influenced by the porosity and crosslinking capabilities which in turn influenced the dissolution and rate of drug release in controlled release systems (Vlachou *et al*., 2001)

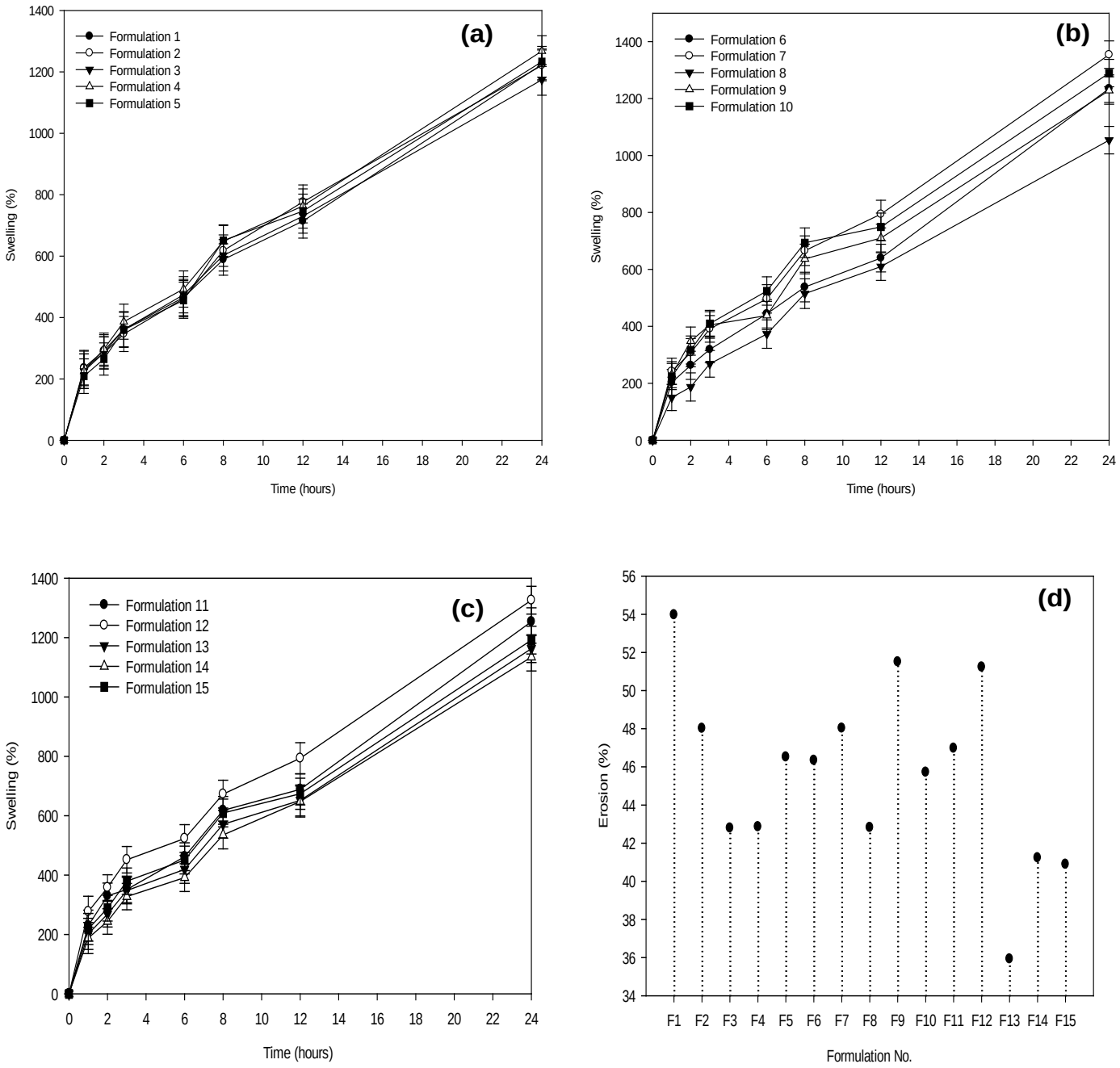

Figure 4.9: Profiles depicting: **(a-c)** percentage swelling over a period of 24 hours for F1-F15 and **d)** percentage erosion of the eutectic tablets F1-F15 as a function of the dried weight of the tablets after 24 hours.

4.3.8. Analysis of the surface morphologies of the eutectic powder blend

The morphological characteristics of the eutectic powder blend and the native eutectic reagents, menthol and cetomacrogol, were analyzed using SEM. The images obtained before and after eutectic formation are shown in Figure 4.10 (a-c). The SEM images for the eutectic reagents before eutectic formation displayed large, irregular and sharp crystal forms as illustrated in

Figure 4.10 (a-b). However, upon analysis of the eutectic powder blend after formation at eutectic composition, distinct changes in the morphological structure were noted. The particles appeared to be more consistent in shape with almost spherical, smooth surface edges as compared to the rugged surface structure of the eutectic reagents (Figure 4.10c). The homogeneity of the eutectic powder blend was reflected in the images difficulty to isolate single drug crystals. The change in morphological structure from crystalline (before eutectic formation) to amorphous (after eutectic formation) was demonstrated in the SEM images obtained. The images obtained are characteristic to the formation of eutectic mixtures and incidentally mirror the results obtained for XRD (Figure 4.8) which displayed a phase change from crystalline to amorphous.

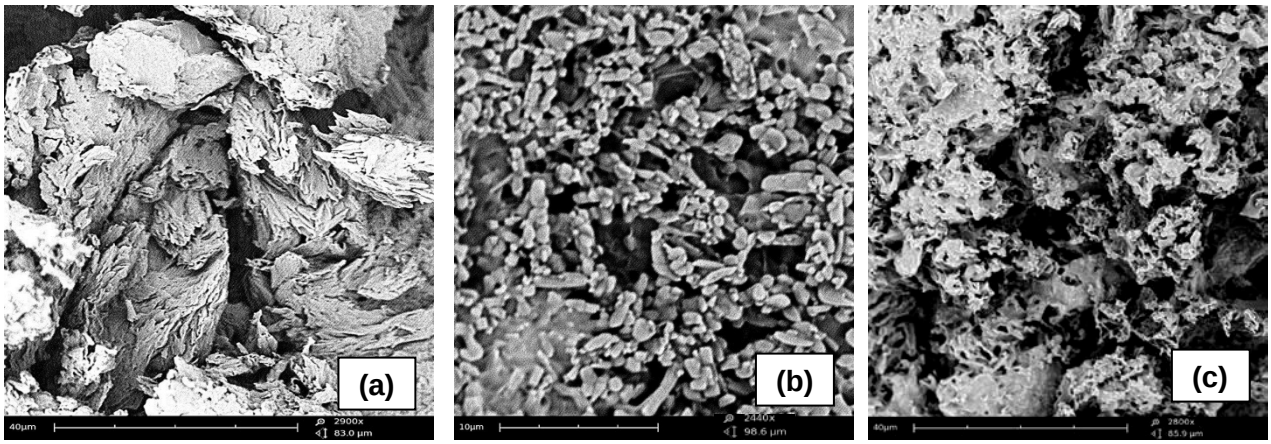

Figure 4.10: Scanning electron micrographs at ±2700x magnification showing the eutectic reagents before eutectic formation: **a)** cetomacrogol **b)** menthol and after eutectic formation **c)** eutectic powder blend at eutectic composition (menthol: cetomacrogol/3:1).

4.3.9. *In vitro* protein release analysis

In vitro release experiments were conducted in SHIF (pH 6.8) in order to obtain the protein release patterns of BSA from the eutectic tablets F1-F15. Since the active is assembled within the eutectic powder blend, the eutectic reagents would be expected to display release profiles corroborating with that of the active and thus was not investigated separately. All formulations displayed similar release patterns over the 24 hour period with variations in the crosslinkers, eutectic powder blend and pectin concentrations influencing the drug release patterns that were observed (Figure 4.11a-c). All formulations displayed controlled release over the 24 hour period. The protein release profiles displayed an initial burst release after 1 hour (0.128). This reflected the initial high swelling capacity of all the formulations after 1 hour as displayed in the swelling profiles shown in Figure 4.9. The following two hours displayed a slower release of BSA which

corresponded to only slight changes in the swelling capacity. This was attributed to the formation of the crosslinked interface *in situ* which decreased the water uptake and swelling capacity and subsequently controlled the release of protein. The protein release pattern after 3 hours displayed phases of slow release and burst release up to 24 hours. This was attributed to the combined effects of swelling, surface erosion and *in situ* crosslinking. The amorphous nature of the eutectic powder blend resulted in the diffusion of the protein out of the matrix network producing an enhanced dissolution and fractional release up to ±0.8. The eutectic powder blend and its decrease in particle size to the nanometer range (142.1nm) facilitated the enhanced dissolution due to the increase in surface area. In addition, the mean dissolution time (MDT) was used to represent the protein release rate from the eutectic tablets and provided supplementary evidence of the ability of *in situ* crosslinking in controlling the release rate (Roni *et al*., 2009; Wadher *et al*., 2011). Formulations containing 20%$^{w}/_{w}$ of crosslinker displayed an MDT_{50} ranging from 5.2-6.5 which was higher than the MDT_{50} obtained for formulations that contained 15%$^{w}/_{w}$ of crosslinker. This indicated that the higher crosslinking ability imparted by the increased concentration of crosslinker served to control the protein release and thus displayed a slower release rate. Ultimately, the MDT gave an indication of the rate of the dissolution process (Sathish and Syed, 2013). In addition, the porosity of the outer polymer shell may have influenced the protein release rate from the eutectic tablets and this was noticeably apparent in the initial burst release observed with an increase in swelling after 1 hour. Based on the results obtained, it was evident that the protein release was influenced by the swelling and erosional behavior, crosslinking concentrations and amorphous nature of the eutectic powder blend.

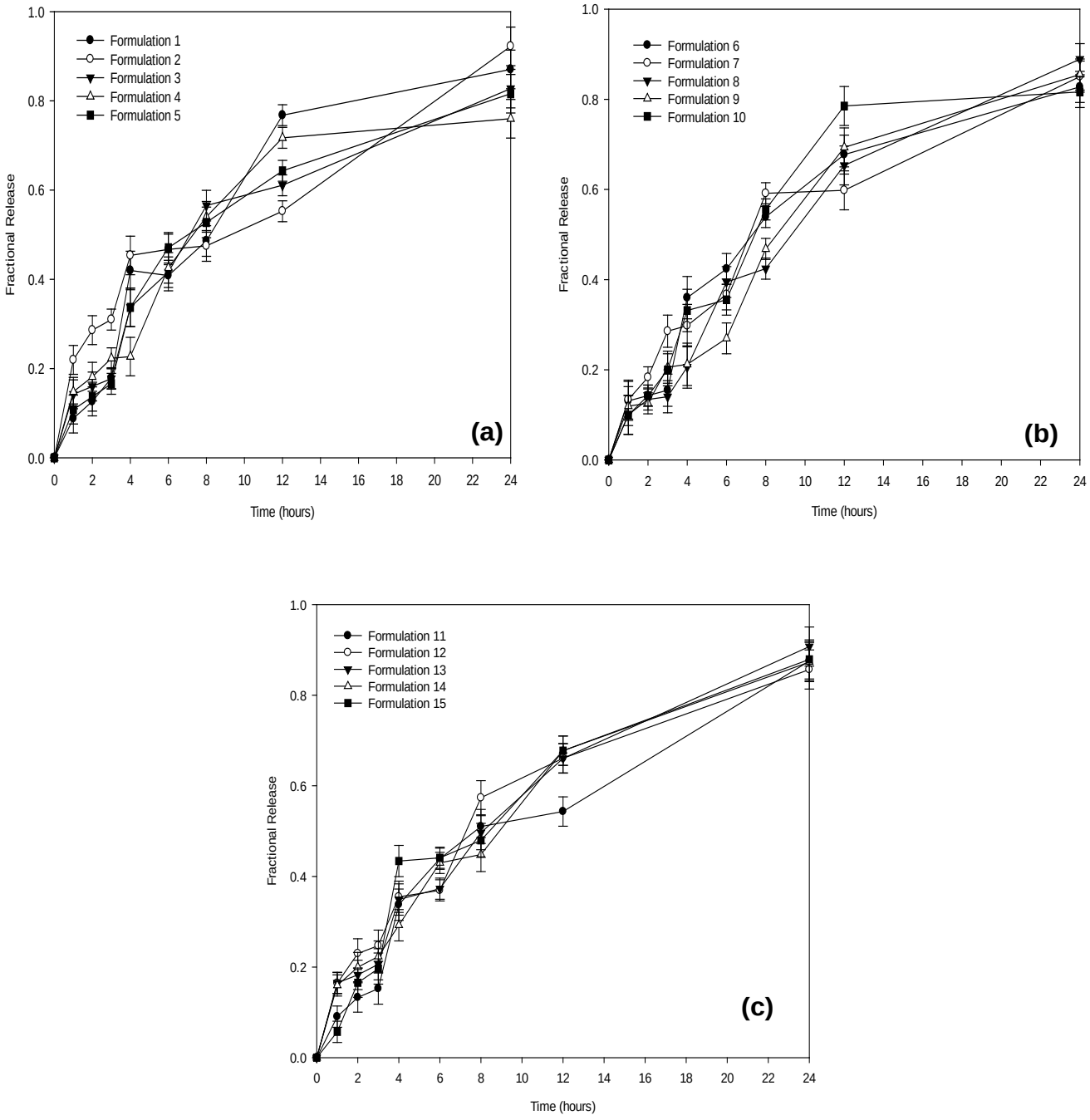

Figure 4.11: Fractional release of BSA from eutectic tablets: **a)** formulations 1-5, **b)** formulations 6-10 and **c)** formulations 11-15.

4.3.10. Mathematical modelling of protein release profiles

The protein release profiles were fitted into various kinetic algorithms and the data obtained is shown in Table 4.4. The best-fit model for the protein release data observed was based on the kinetic modelling of the regression coefficients and its proximity to the numeral 1. A model depicting a value closest to 1 amongst the formulations would demonstrate the appropriateness

of that model in explaining the protein release mechanism. The zero-order and first-order models are based on systems where the protein release is independent and dependent on protein concentrations, respectively (Singhvi and Singh, 2011). The zero-order and first-order models used are shown in Equation 4.6 and 4.7 (Siepmann and Siepmann, 2008).

$$Q = K_0\ t \quad \textbf{(4.6)}$$

Where, Q is the cumulative amount of protein released; K_0 is the zero-order constant; *t* is the time. The regression coefficients were elucidated for the zero-order model by plotting a graph of cumulative protein release (%) *versus* time based on *in vitro* protein release data.

$$\ln Q_t = \ln Q_0\, K_0 t \quad \textbf{(4.7)}$$

Where, Q_t is the cumulative amount of protein released; Q_0 is the initial amount of protein in the dissolution medium (usually zero); K_0 is the first-order constant; *t* is the time. The regression coefficients for the first order model was determined by plotting a graph of the log of cumulative release *versus* time based on data obtained from *in vitro* protein release.

The protein release profiles obtained for the eutectic tablets F1-F15 did not fit into the first-order release kinetic model as displayed in Table 4.4 and thus indicated that the release was not concentration dependent. Controlled release, multilayered tablet systems typically display zero-order or near zero-order release with a constant release of protein over time (Yadhav *et al.,* 2013). Since the eutectic tablets displayed almost phased release with alternating slow and burst release of protein (Figure 4.11a-c), the regression coefficients depicted a near zero-order release of between 0.8041 and 0.9356. In addition, the protein release data was fitted into the Higuchi and Korsmeyer–Peppas kinetic modeling equations to obtain the overall best-fit model for all the eutectic tablets F1-F15 (Yadhav *et al.,* 2013).

Table 4.4: Mathematical modelling of BSA release from the eutectic tablets

Formulation No.	Zero-order	First order	Higuchi	Korsmeyer–Peppas	
	Regression Coefficient (R^2)	Regression Coefficient (R^2)	Regression Coefficient (R^2)	Regression Coefficient (R^2)	Best-fit Model
F1	0.8388	0.6362	0.9264	0.924	Higuchi
F2	0.8744	0.8364	0.9502	0.9512	Korsmeyer–Peppas
F3	0.8627	0.7082	0.9519	0.9245	Higuchi
F4	0.8041	0.7109	0.9007	0.9229	Korsmeyer–Peppas
F5	0.8431	0.6549	0.9427	0.9263	Higuchi
F6	0.8471	0.6729	0.948	0.9296	Higuchi
F7	0.8768	0.7366	0.9614	0.9695	Korsmeyer–Peppas
F8	0.9356	0.7781	0.97	0.9496	Higuchi
F9	0.9107	0.7976	0.9422	0.9356	Higuchi
F10	0.8141	0.6677	0.9061	0.949	Korsmeyer–Peppas
F11	0.8410	0.6767	0.956	0.9378	Higuchi
F12	0.8732	0.7719	0.9655	0.967	Korsmeyer–Peppas
F13	0.9238	0.8049	0.9782	0.9489	Higuchi
F14	0.9117	0.8111	0.9757	0.9686	Higuchi
F15	0.8579	0.5709	0.9487	0.907	Higuchi

The Higuchi model describes the release of protein from a matrix as a function of the square-root of a time-dependent process based on Fickian diffusion and the equation is represented by Equation 4.8 (Merchant *et al*., 2006).

$$Q = K_H t^{1/2} \quad \textbf{(4.8)}$$

Where, Q is the cumulative amount of protein released; K_H is the Higuchi dissolution constant; *t* is the time. A plot of the cumulative percentage released *versus* the square root of time of the protein release data, generated regression coefficients for the Higuchi model. The Korsmeyer–Peppas modeling equation (Equation 4.9) was used to describe the protein release mechanism from a polymeric system.

$$\frac{Q_t}{Q_\infty} = K_t{}^n \quad \textbf{(4.9)}$$

Where, $\frac{Q_t}{Q_\infty}$ is the cumulative amount of protein released per time *t*; K is the rate constant; *n* is the release exponent. The regression coefficient was obtained by plotting a graph of the log of

cumulative release (first 60% of protein release data) *versus* the log of time of the protein release data.

Based on the regression coefficients, the Higuchi model displayed the best linearity for majority of the formulations with an R^2 value of between 0.9007 and 0.975 indicating that the protein release mechanism was based on Fickian diffusion. Although, the Korsmeyer–Peppas model displayed the best-fit for some formulations, limitations exist as the power law gives limited insight into the exact protein release mechanism (Siepmann and Peppas, 2012). Thus, the protein release kinetics corresponded best with the Higuchi model with near zero-order protein release obtained.

4.3.11. Analysis of the *ex vivo* permeation through the Large White Pig intestinal tissue model

Menthol is widely used as a flavouring and fragrance enhancer in oral and topical dosage forms with the major benefit of its use being its safety profile (FDA, 1973; Williams and Barry, 1991; Kommuru *et al*., 1998; Shojaei *et al*., 1999; Shen *et al*., 2011). However, its applicability as a permeation enhancer for transdermal and transbuccal drug delivery has been widely reported (FDA, 1973; Kommuru *et al*., 1998; Shojaei *et al*., 1999; Shen *et al*., 2011). Thus, its effect on intestinal permeation as part of the Eutectic Powder Blend (EPB) was investigated. Results of protein flux obtained from permeation studies are displayed in Figure 4.12. Eutectic tablet formulations containing 12%$^{w}/_{w}$, 18%$^{w}/_{w}$ and 24%$^{w}/_{w}$ of EPB were compared to a tablet that was EPB-free. The results demonstrated the increased permeation of the formulations containing the EPB as compared to the EPB-free formulation which displayed a maximum protein flux of 0.0289mg.cm^{-2} h^{-1} as compared to the EPM-containing formulations which displayed a protein flux between 0.0576-0.0720mg.cm^{-2}h^{-1}. In addition, it was noted that the permeation-enhancing effect of menthol was independent of the concentration of EPB contained within the eutectic tablets as they displayed similar protein flux results. Overall, the results proved that the menthol contained within the eutectic tablets as part of the EPB facilitated the permeation of BSA across the intestinal tissue model. To ensure that the tissue maintained its integrity throughout the study, the transepithelial potential difference across the intestinal tissue was measured before and after permeation studies. The results (before permeation: 118.1mV; after permeation: 116.1mV) displayed only slight differences in potential difference which indicated that the viability of the tissue was maintained (Söderholm *et al*., 1998; Ehrhardt and Kim, 2007; Antunes *et al*., 2013; Sarmento, 2015).

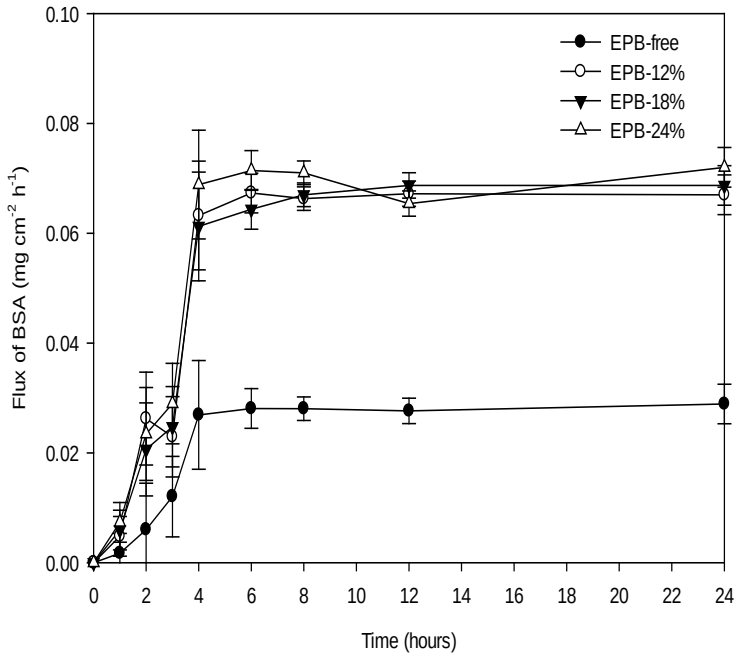

Figure 4.12: *Ex vivo* permeation profiles of the BSA-loaded tablets comprising; a Eutectic Powder Blend (EPB)—free tablet, EPB-12%$^{w}/_{w}$, EPB-18%$^{w}/_{w}$ and EPB-24%$^{w}/_{w}$.

4.3.12. Constraint optimization and response surface analysis of the eutectic tablets

Statistical optimization using a Box-Behnken design model was used to optimize the eutectic tablets. The design program generated responses from the results of each formulation to ascertain the ideal combination of eutectic powder blend, crosslinkers ($NaCO_3$ and K_2HPO_4) and pectin required capable of attaining desirable MDT, swelling and erosion efficiencies. Minitab® V15 statistical software was used for the generation of the optimal responses as depicted by the plots in Figure 4.13. According to the predictions of the statistical design, the optimal tablet that would permit a desirable MDT, swelling and erosion would comprise concentrations of 23.093%$^{w}/_{w}$ (115.47mg) of crosslinkers ($NaCO_3$ and K_2HPO_4), 12%$^{w}/_{w}$ (60mg) of eutectic powder blend and 65.313mg of pectin. Response surface analysis plots were obtained using Minitab® V15 statistical software. The plots represented the functional relationship between the experimental design variables and the responses achieved. A maximal swelling, erosion and MDT value is favoured at the optimal concentrations of the design variables as shown in Figure 4.13a. Notable interaction effects from the swelling response surface plots (Figure 4.13b) indicated that higher concentrations of crosslinker and EPB produced a lower swelling capacity. Alternatively, the erosion response surface plots (Figure 4.13c) revealed that higher concentrations of the surface-eroding agent (pectin) and correspondingly higher concentrations

of the crosslinking agents ($NaCO_3$ and K_2HPO_4) produced a predictably greater erosion percentage. In addition, MDT was best promoted at higher concentrations of pectin and crosslinking agents as shown in Figure 4.13d.

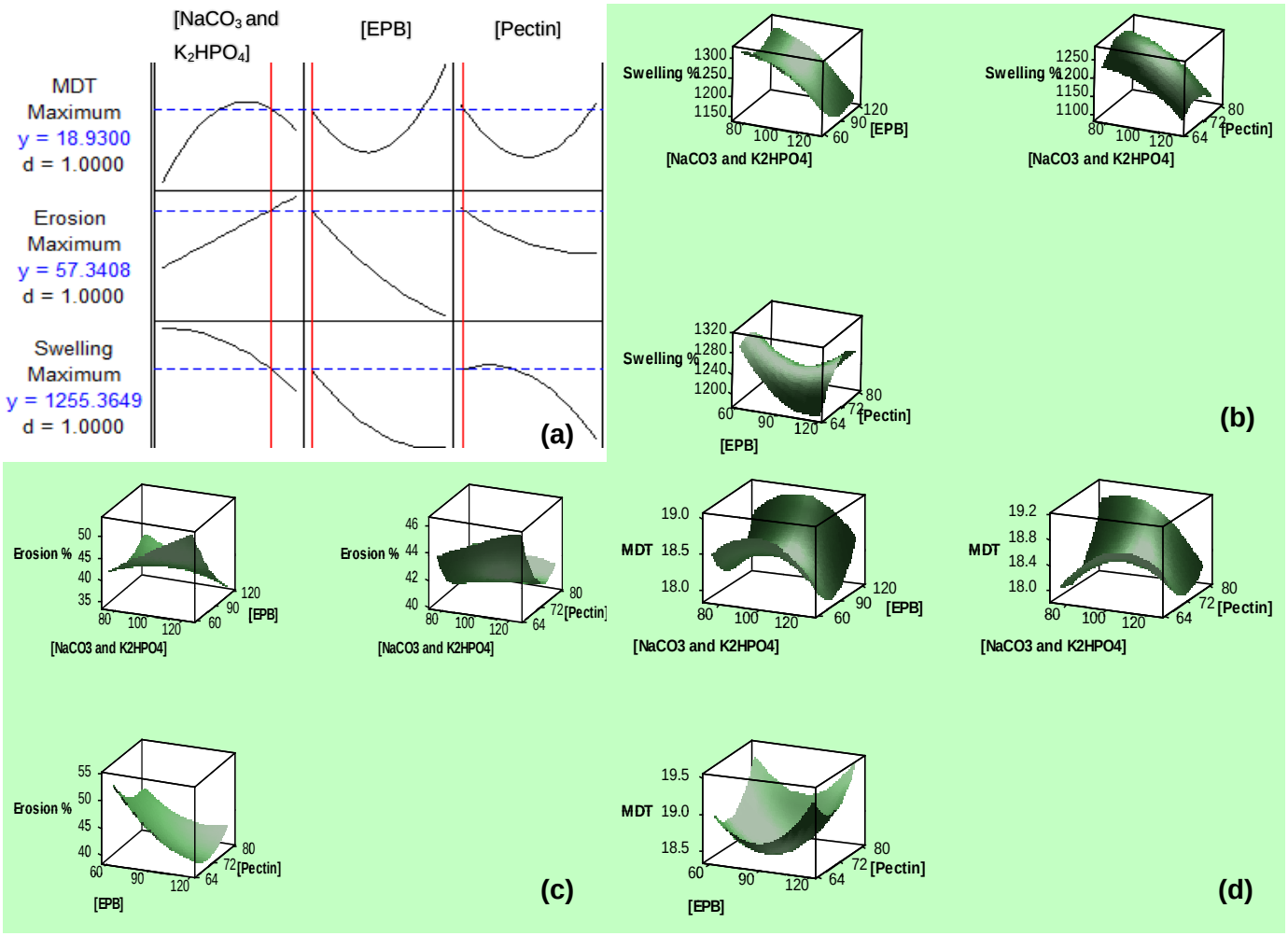

Figure 4.13: Statistical optimization of the eutectic tablets: (**a)** desirability plots depicting the variables for producing a eutectic tablet with the desired targeted responses and response surface plots depicting the effects of variables on **(b)** percentage of swelling, **(c)** percentage of erosion and **(d)** mean dissolution time**.**

4.4. Concluding Remarks

The *in situ* cross-linked eutectic was designed for the purpose of creating an advanced oral delivery system for therapeutic proteins and peptides. Thus, it was essential that the design of the tablet overcame the barriers that enabled successful oral protein/peptide delivery. Physicochemical and physicomechanical characterization tests confirmed eutectic formation as was evidenced by the lowering of the melting point, the decreased crystallinity and the shift in

the SEM images to an amorphous structure. FTIR results highlighted the presence of *in situ* crosslinking within the core eutectic region (facilitated by the proposed melting of the core at 37°C). Physicomechanical profiling displayed a decrease in the tablet hardness upon penetration into the core of the tablet due to the melting of the core eutectic region. The *in vitro* protein release behavior was influenced by the combined effects of swelling, surface erosion, *in situ* crosslinking and the amorphous nature of the eutectic powder blend. The amorphous transformation of the eutectic powder blend is an important tool in influencing the ADME profile of protein and peptide molecules. Due to the phased release of protein from the system, the protein release mechanism was based on Fickian diffusion and displayed near zero-order release. The permeation-enhancing effects of menthol was evident by the enhanced protein flux (0.0576-0.0720mg.cm^{-2}h^{-1}) obtained as compared to the control formulation (0.0289mg.cm^{-2} h^{-1}). Thus, it can be concluded that physicochemical and physicomechanical characterization that was undertaken was essential for delineating the *in vitro* attributes, optimizing the formulation variables, predicting the *in vivo* performance of the device and demonstrating the applicability of the design in improving the oral delivery of a multitude of proteins and peptides.

The preliminary design of the *In Situ* Cross-linked Eutectic Tablet, discussed in this chapter, and its subsequent optimization led to the formation of the optimized Oral Core-Melt Tablet (OCMT) which will be extensively characterized in Chapter 5.

4.5. References

Ahuja, G., Pathak, K. (2009). Porous carriers for controlled/modulated drug delivery. *Indian Journal of Pharmaceutical Sciences*, 71, 599–607.

Al-hilal, T.A., Alam, F., Byun, Y. (2013). Oral drug delivery systems using chemical conjugates or physical complexes. *Advanced Drug Delivery Reviews*, 6, 845-864.

Almeida, A.J., Souto, E. (2007). Solid lipid nanoparticles as a drug delivery system for peptides and proteins. *Advanced Drug Delivery Reviews*, 59, 478-490.

Antunes, F., Andrade, F., Ferreira, D., Nielsen, H.M., Sarmento, B. (2013). Models to Predict Intestinal Absorption of Therapeutic Peptides and Proteins. *Current Drug Metabolism*, 14, 4-20.

Arnikar, A.J., Kadam, S.S., Gujar, K.N. (1992). *Essentials of Physical Chemistry and Pharmacy*. Bombay: Orient Longman Limited. pp 245-247.

Aslan, N., Cebeci, Y. (2007). Application of Box‐Behnken design and response surface methodology for modeling of some Turkish coals. *Fuel*, 86, 90-97.

Azimi, B., Nourpanah, P., Rabiee, M., Arbab, S. (2013). Producing Gelatin Nanoparticles as Delivery System for Bovine Serum Albumin. *Iranian Biomedical Journal*, 18, 34-40.

Camenich, G., Alsenz, J., van de Waterbeemd, H., Folkers, G. (1998). Estimation of permeability by passive diffusion through Caco-2 cell monolayers using the drugs' lipophilicity and molecular weight. *European Journal of Pharmaceutical Science*, 6, 317-324.

Chin, J., Mahmud, K.A.F., Kim, S.E., Park, K., Byun, Y. (2012). Insight of current technologies for oral delivery of proteins and peptides. *Drug Discovery Today Technologies*, 9, 105-112.

Coates, J. (2000). *Interpretation of Infrared Spectra, A Practical Approach*. Chichester: John Wiley and Sons Ltd. pp. 10815-10837.

Donovan, M.D., Flynn, G.L., Amidon, G.L. (1990). Absorption of polyethylene glycols 600 through 2000: the molecular weight dependence of gastrointestinal and nasal absorption. *Journal of Pharmaceutical Research*, 7, 863-868.

Efentakis, M., Vlachou, M. (2000). Evaluation of high molecular weight poly(oxyethylene) (Polyox)polymer: studies of flow properties and release rates of furosemide and captopril from controlled-release hard gelatin capsules. *Pharmaceutical Development and Technology*, 5, 339-346.

Ehrhardt, C., Kim, K. (2007). *Drug Absorption Studies: In Situ, In Vitro and In Silico Models*. New York: Springer Science and Business Media. pp. 201-203.

FDA. (1973). Teratologic evaluation of FDA-71-57 (Menthol, natural, Brazilian). Food Drug Research Laboratories.

Gabbott, P. (2008). *Principles and Applications of Thermal Analysis.* Oxford: Blackwell Publishing Ltd. pp. 17-40.

Kim, J., Taluja, A., Knutson, K., Bae, Y.H. (2005). Stability of bovine serum albumin complexed with PEG-poly (l-histidine) diblock copolymer in PLGA microspheres. *Journal of Controlled Release*, 109, 86-100.

Kommuru, T.R., Khan, M.A., Reddy, I.K. (1998). Racemate and enantiomers of ketoprofen: phase diagram, thermodynamic studies, skin permeability, and use of chiral permeation enhancers. *Journal of Pharmaceutical Sciences*, 87, 833–840.

Koningsveld, R., Stockmayer, W.H., Nies, E. (2001). *Polymer Phase Diagrams.* New York: Oxford University Press Inc. pp. 21-24.

Lee, M.Y., Kim, M.Y., Kim, S., Lee, J. (2009). Cryoprotectants for Freeze Drying of Drug Nano-Suspensions: Effect of Freezing Rate. *Journal of Pharmaceutical Sciences,* 98, 4808-4817.

Liu, D., Fei, X., Wang, S., Jiang, T., Su, D. (2006). Increasing solubility and dissolution rate of drugs via solid dispersions: itraconazole–poloxamer188 system. *Asian Journal of Pharmaceutical Sciences,* 1, 213-221.

Marques, M.R.C., Loebenberg, R., Almukainzi M. (2011). Simulated Biological Fluids with Possible Application in Dissolution Testing. *Dissolution Technology,* 60, 15-28.

Martin, A. (1993). *Physical Pharmacy: Physical Chemical Principles in the Pharmaceutical Sciences.* Philadelphia: Lea and Febiger. pp. 41-42.

McGlinchey, D. (2005). *Characterisation of Bulk Solids.* Oxford*:* Blackwell Publishing Ltd. pp. 50-52.

Merchant, H., Shoaib, H., Tazeen, J., Yousuf, R. (2006). Once-daily tablet formulation and in vitro release evaluation of cefpodoxime using hydroxypropyl methylcellulose: a technical note. *AAPS PharmSciTech*, 7, 178–183.

Muller, A., Ni, Z., Hessler, N., Wesarg, F., Muller, F.A., Kralisch, D., Fischer, D. (2012). The Biopolymer Bacterial Nanocellulose as Drug Delivery System: Investigation of Drug Loading and Release using the Model Protein Albumin. *Journal of Pharmaceutical Sciences,* 102, 579-592.

O' Connor, A. (2009). Introduction to biotech drugs, North Carolina: Regulatory Rapporteur.

Oh, T., Kim, J., Ha, J., Chi, S., Rheeb, Y., Park, C., Park, E. (2013). Preparation of highly porous gastroretentive metformin tablets using a sublimation method. *European Journal of Pharmaceutics and Biopharmaceutics,* 83, 460-467.

Park, K., Kwan, I.C., Park, K. (2011). Oral protein delivery: Current status and future prospect. *Reactive and Functional Polymers*, 71, 280-287.

Pillay, V., Danckwerts, M.P. (2002). Textural Profiling and Statistical Optimization of Crosslinked Calcium-Alginate-Pectinate-Cellulose Acetophthalate Gelisphere Matrices. *Journal of Pharmaceutical Sciences,* 91, 2559-2570.

Pillay, V., Fassihi, R. (1999). In vitro release modulation from crosslinked pellets for site-specific drug delivery to the gastrointestinal tract: II. Physicochemical characterization of calcium-

alginate, calcium‐pectinate and calcium‐alginate‐pectinate pellets. *Journal of Controlled Release*, 59, 243‐256.

Qui, Y., Chen, Y., Zhang, G.G.Z. (2009). *Developing Solid Oral Dosage Forms: Pharmaceutical Theory and Practice*. Burlington: Elsevier. pp. 37-39.

Roni, M.A., Kibria, G., Jalil, R. (2009). Formulation and *in vitro* Evaluation of Alfusozin Extended Release Tablets Using Directly Compressible Eudragit. *Indian Journal of Pharmaceutical Sciences*, 71, 252-258.

Sarmento, B. (2015). *Concepts and Models for Drug Permeability Studies: Cell and Tissue based In Vitro Culture Models*. Sawston: Woodhead Publishing. pp. 216.

Sathish, U., Syed, I.A. (2013). Formulation and characterization of matrix and triple layer matrix tablets for controlled delivery of tramadol hydrochloride*. International Journal of Pharmaceutical Sciences*, 5, 458-464.

Schellack, G. (2010). *Pharmacology in clinical practice: application made easy for nurses and allied health professionals*. 2nd ed. Claremont: Juta and Company. pp. 185-187.

Sharma, A., Jain, C.P., Tanwar, Y.S. (2013). Preparation and characterization of solid dispersions of carvedilol with poloxamer 188*. Journal of Chilean Chemical Society,* 58, 1553-1557.

Sharma, J.P.K., Bansal, S., Banik, A. (2011). Noninvasive Routes of Proteins and Peptides Drug Delivery. *International Journal of Pharmaceutical Sciences*, 4, 367-375.

Shen, Q., Li, X., Li, W., Zhao, X. (2011). Enhanced intestinal absorption of Daidzein by borneol/menthol eutectic mixture and microemulsion. *AAPSPharmSciTech*, 12, 1044-1049.

Shojaei, A.H., Khan, M., Lim, G., Khosravan, R. (1999). Transbuccal permeation of a nucleoside analog, dideoxycytidine: effects of menthol as a permeation enhancer. *International Journal of Pharmaceutics*, 192, 139–146.

Siepmann, J., Peppas, N.A. (2012). Modeling of drug release from delivery systems based on hydroxypropyl methylcellulose (HPMC). *Advanced Drug Delivery Reviews*, 64, 163-174.

Siepmann, J., Siepmann, F. (2008). Mathematical modeling of drug delivery. *International Journal of Pharmaceutics*, 364, 328‐343.

Singhvi, V., Singh, M. (2011). Review: *In-Vitro* Drug Release Characterization Models. *International Journal of Pharmaceutical Studies and Research,* 2, 77-84.

Söderholm, J.D., Hedman, L., Artursson, P., Franzén, L., Larsson, J., Pantzar, N., Permert, J., Olaison, G. (1998). Integrity and metabolism of human ileal mucosa in vitro in the Ussing chamber. *Acta Physiology Scandinavia*, 162, 47-56.

Thakur, R., Gupta, R.B. (2006). Rapid expansion of supercritical solution with solid cosolvent (RESS-SC) process: Formation of 2-aminobenzoic acid nanoparticle. *Journal of Supercritical Fluids,* 37, 307-315.

Tuntarawongsa, S., Phaechamud, T. (2012). Polymeric Eutectic Drug Delivery System. *Journal of Medicine*, 22, 27-32.

Vlachou, M., Naseef, H., Efentakis, M., Tarantili, A., Andreopoulos, G. (2001). Swelling Properties of Various Polymers Used in Controlled Release Systems. *Journal of Biomaterial Applications*, 16, 125-138.

Wadher, K.J., Kakde, R.B., Umekhar, M.J. (2011). Study on sustained-release metformin hydrochloride from matrix tablet: Influence of hydrophilic polymers and *in vitro* evaluation. *International Journal of Pharmaceutical Investigation*, 1, 157-163.

Widmann, J., Schubnell, M., Riesen, R., Schawe, J., Darribére, C., Jörimann, U. (2000). Interpreting DSC curves: Part 2: Isothermal measurements. *UserCom*, 2, 1-10.

Widmann, J., Schubnell, M., Riesen, R., Schawe, J., Darribére, C., Jörimann, U. (2001). Interpreting TGA curves. *UserCom*, 1, 1-20.

Williams, A.C., Barry, B.W. (1991). Terpenes and the lipid–protein-partitioning theory of skin penetration enhancement. *Pharmaceutical Research*, 8, 17–24.

Williams, R.O., Watts, A.B., Miller, D.A. (2012). *Formulating Poorly Water Soluble Drugs*. New York: Springer. pp. 526-529.

Yadav, G., Bansal, M., Thakur, N., Khare, S., Khare, P. (2013). Multilayer Tablets and Their Drug Release Kinetic Models for Oral Controlled Drug Delivery System. *Middle-East Journal of Scientific Research*, 16, 782-795.

Zheng, X., Lian, Q., Yang, H., Zhu, H. (2015). Alkyl Pectin: Hydrophobic Matrices for Controlled Drug Release. *Journal of Applied Polymer Science*, doi :10.1002/app.41302.

CHAPTER 5

PHYSICOCHEMICAL AND PHYSICOMECHANICAL EVALUATION OF THE STATISTICALLY OPTIMIZED ORAL CORE-MELT TABLET (OCMT)

To be submitted to International Journal of Pharmaceutics

Bibi F. Choonara, Yahya E. Choonara, Pradeep Kumar, Lisa C. du Toit, Viness Pillay. In Vitro and In Vivo Evaluation of a Novel Oral Core-Melt Tablet (OCMT).

Abstract

A complex polymer-eutectic platform was optimized as an Oral Core-Melt Tablet (OCMT), producing a novel oral controlled release system for the delivery of gastro-sensitive therapeutic proteins and synthetic peptides. Physicochemical and physicomechanical characterization techniques were undertaken to determine the rheological properties, *in situ* crosslinking mechanisms, porositometric evaluations, imagery and *in vitro* peptide release from the OCMT. The inherent transitions observed in the Fourier Transform Infrared Spectroscopy spectrums confirmed the presence of *in situ* crosslinking, facilitated by the porous structure promoting the ingress of fluid into the OCMT. This was corroborated with MRI which highlighted the device hydration over 24 hours as a significant predictor of the *in vitro* peptide release profile. The *in vitro* release of the peptide was influenced by the combined effects of swelling, surface erosion and *in situ* crosslinking, displaying a fractional release up to ±0.8. Owing to the complexity of the system, the mechanism of release was attributable to both the zero-order (R^2=0.95) and Higuchi models (R^2=0.98). Conclusive results from extensive *in vitro* characterization emphasized the applicability of the optimized OCMT in providing a controlled release alternative system capable of delivering peptides orally.

Keywords: oral peptide delivery; octreotide; controlled release; eutectic powder blend; physicochemical properties; physicomechanical properties

5.1. Introduction

Therapeutic proteins and peptides have become the front-runner in the treatment of multiple diseases conditions, significantly dominating research studies in the pharmaceutical industry (Park *et al*., 2011; Chin *et al*., 2012). This widespread interest has catapulted into the design of sophisticated pharmaceutical technologies primarily focused on achieving successful oral delivery of proteins and peptides (Park *et al*., 2011). The oral route of delivery, despite its numerous challenges, still remains the preferred route of delivery as compared to its conventional injectable counterpart (Park *et al*., 2011).

The pragmatic design of the OCMT which has been previously highlighted, proposed the incorporation of an *in situ* crosslinked core eutectic region that structurally protects the incorporated protein or peptide and ensures controlled release (Choonara *et al*., 2016). The statistical design of the OCMT formulations and their corresponding responses was a critical factor in determining the ideal combinations of variables to produce an optimized OCMT (Choonara *et al*., 2016). The functional ability of the OCMT to deliver on its proposed characteristics was demonstrated using Octreotide as the incorporated therapeutic active.

Octreotide is a synthetic octapeptide, similar to the naturally occurring somatostatin, responsible for inhibiting Growth Hormone (GH), insulin, glucagon and various other pituitary and gastroenteropancreatic hormones (Chen *et al*., 2000; Jabarian *et al*., 2012). Somatostatin's clinical effectiveness is impeded by its short plasma half-life (1-3 min) and as a result its analogue, octreotide, has been found to be the most effective option thus far for the treatment of acromegaly and neuroendocrine tumors (Tuvia *et al*., 2012). However, octreotide has a major shortcoming with regards to its therapeutic use as it requires frequent and daily subcutaneous or intravenous injections resulting from rapid enzymatic degradation in plasma (Chen *et al*., 2000).

Several approaches have been investigated to eliminate the inconvenience and discomfort associated with frequent subcutaneous dosing with the most successful formulation being the intramuscular depot injection system (Jabarian *et al*., 2012). No clinically useful oral octreotide formulation has been approved despite the numerous approaches that have been explored. Thus, the need to create a therapeutically active oral octreotide formulation still remains an active area of research for the pharmaceutical industry.

Evaluation of the distinct properties of the optimized OCMT is essential in determining its ability to produce the desired therapeutic response both *in vitro* and *in vivo.* Prior to commencing with *in vivo* studies, it is of paramount importance that extensive *in vitro* analysis is undertaken to determine the effects of the physicochemical and physicomechanical properties on the peptide-release behavior and overall performance of the device. Thus, this study primarily focused on the overall pertinent characteristics of the optimized OCMT by undertaking various studies such as; swelling and erosion to determine the swelling capabilities and peptide-release mechanism, Fourier Transform Infrared Spectroscopy studies to determine the chemical structure composition, Textural Analysis to determine the tablet's mechanical properties, Porosity and Magnetic Resonance Imaging to determine the morphology and physical structure of the OCMT and, *in vitro* pharmacokinetic analysis to determine the peptide-release profile.

5.2. Materials and Methods

5.2.1. Materials

Menthol (2-isopropyl-5-methylcyclohexanol, 99% purity, M_w=156,27g/mol), cetomacrogol 1000, poly(ethylene oxide) (PEO) (Polyox™, WSR-303) and excipients, sodium carboxymethylcellulose (CMC), magnesium stearate and sucrose were purchased from Sigma-Aldrich Corp. (St. Louis, MO, USA). The crosslinker sodium carbonate ($NaCO_3$) was purchased from Associated Chemical Enterprises (ACE) (Pty) Ltd. (Johannesburg, Gauteng, South Africa). Pectin citrous (poly-D-galacturonic acid methyl ester) and the crosslinker di-potassium hydrogen orthophosphate anhydrous (K_2HPO_4; M_w=174.18g/mol) were procured from Merck Chemicals (Pty) Ltd. (Modderfontein, Gauteng, South Africa). Octreotide acetate ($C_{49}H_{66}N_{10}O_{10}S_2$; M_w=1019.247g/mol) was purchased from Bolon Pharmachem Co., Ltd. (Taizhou, Zheijang, China). All other reagents were of analytical grade and were employed as received.

5.2.2. Fabrication of the optimized OCMT

The responses from a 3-factor Box–Behnken experimental design of the eutectic tablets generated an ideal combination of components that would produce the desired responses shown in Figure 5.1. The optimized OCMT comprised an outer polymer shell surrounding a core eutectic region. The core eutectic region of the tablet consisted of a compressed combination of; a Eutectic Powder Blend (EPB) that was prepared by a co-melt method in a 3:1 mass ratio of menthol: cetomacrogol, crosslinking agents ($NaCO_3$ and K_2HPO_4) and 20mg Octreotide. The outer polymer shell consisted of a top and bottom layer each containing a polymeric blend of

100mg each of PEO, 12mg of CMC, 1mg of magnesium stearate and the optimum concentration of pectin as shown in Figure 5.1. Detailed methods on the synthesis of the EPB and formulation of the core eutectic region and outer polymer shell have been previously described in Choonara *et al,* (2016).

The OCMT was assembled by directly compressing the polymeric powder blend of the bottom layer at 2 tons of pressure using a Carver Tableting Press (Wabash, Indiana, USA) loaded with punch and dies with a diameter of 10mm to produce a loosely compressed layer. Subsequently, the core eutectic tablet was placed above this layer and centered using the tip of a needle. The polymeric powder blend for the top layer of the tablet was added above the core eutectic tablet and levelled out. The punch was then inserted and the tablet was compressed at 5 tons of pressure using a Carver Tableting Press (Wabash, Indiana, USA) fitted with a flat-faced punch and die (diameter of 10mm) to produce the optimized OCMT. To minimize processing variables, all tablets were produced under identical conditions.

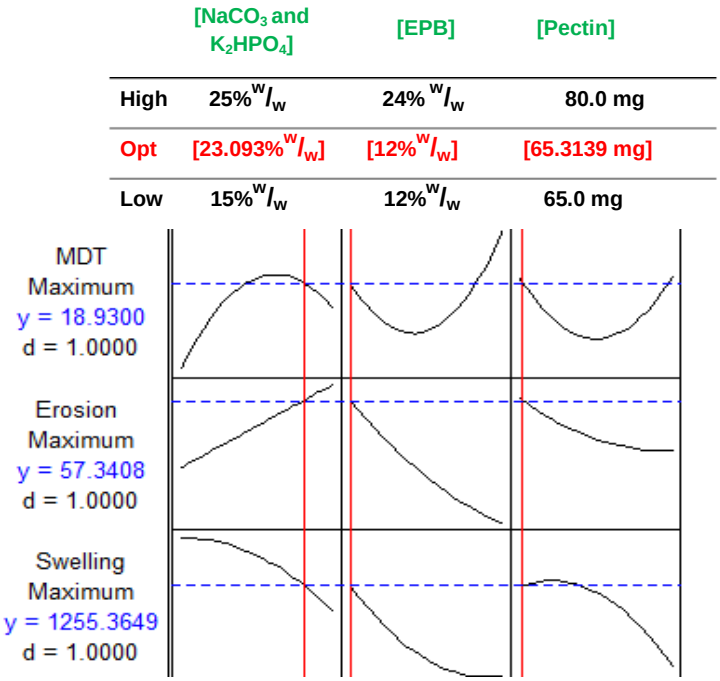

Figure 5.1: Optimized formulation ID for the OCMT displaying desired targeted responses.

5.2.3. In-process validation of the optimized OCMT

Weight uniformity, thickness and friability analyses were performed on the optimized OCMT. A sample of 5 units of the OCMT was analyzed to determine the standardization of the tablet-

assembly process. The weight of the OCMT was determined using an analytical digital balance (Mettler, Model AE 240, Griefensee, Switzerland) with readings recorded to 2 decimal places. The thickness of the OCMTs were determined using a digital caliper (25 × 0.01mm capacity) (Taizhou hangyu tools gauge and blades Co., Ltd., Wenqiao, Zhejiang, China). The friability was determined using a Friabilator (Erweka D-63150, Heusenstamm, Germany) set at 25 rpm for 4 minutes with 1% set as the upper limit of acceptability. The friability was calculated as percentage loss using Equation 5.1.

$$WL_t = \frac{(W_0 - W_t)}{W_0} \times 100 \quad \textbf{(5.1)}$$

Where, WL_t is the total weight loss; W_0 is the initial weight of the tablet and W_t is the final weight of the tablet.

5.2.4. Rheological characterization of the eutectic powder blend

Pertinent rheological properties such as the viscosity (η), storage (elastic) modulus (*G'*) and loss (viscous) modulus (*G"*) of the eutectic powder blend was determined using a Haake Modular Advanced Rheometer System (MARS) (ThermoFisher Scientific, Karlsruhe, Germany). Samples were placed on a sample plate fitted with a C35/1° titanium rotor sensor. Measurements were performed employing the rheological parameters shown in Table 5.1. Dynamic oscillatory temperature ramp measurements were performed from 25 to 45°C, at ramp rates of 1°C/min at an optimal frequency of 1 Hz.

Table 5.1: Rheological parameters employed for the analysis of the EPB

Parameter	Value
Cone and plate gap	0.050mm
Driver version	1.29
Inertia	1.721 x 10^{-6} kg.m^2
A-factor	89051.00 Pa/Nm
M-factor	57.010 (1/s)/((rad/s)
Temperature	25°C-45°C
Damping	30.00

5.2.5. Chemical structure analysis of the optimized OCMT

Attenuated Total Reflectance-Fourier Transform Infrared Spectroscopy (ATR-FTIR) was used to determine the vibrational molecular transitions between the outer polymer shell of the OCMT with the inner core eutectic region following simulated *in situ* crosslinking. FTIR analysis was

conducted on the OCMT, the native crosslinkers and polymers as well as an *in vitro* crosslinked formulation (PEO 1%; 50mg sodium carbonate; 50mg di-potassium hydrogen orthophosphate) to acquire important microstructural information and provide validation of successful *in situ* crosslinking processes. Results were recorded on a PerkinElmer Spectrum 2000 FTIR spectrophotometer with a single-reflection diamond MIRTGS detector (PerkinElmer Spectrum 100, Llantrisant, Wales, UK) fitted with a universal ATR polarization accessory for the FTIR spectrum series at a resolution of 4cm^{-1}. Samples were prepared by hydrating the optimized OCMTs (containing no pectin) in simulated human intestinal fluid (SHIF) pH 6.8 for ±5 hours to simulate *in situ* crosslinking. Following the removal and lyophilization (Labconco Freeze-Dry Systems, Labconco Corp., Kansas City, MO, USA) of the OCMTs, the tablets were powdered and placed on a diamond crystal for analysis between a scanning range of 4000-600cm^{-1} at a constant pressure of 120psi with 32 accumulations.

5.2.6. Evaluation of the swelling and erosion of the optimized OCMT

The mean percentage swelling and erosion of the OCMT was determined by gravimetric analysis of the degree of swelling and erosion over a 24-hour period. The initial weight of the optimized OCMT was recorded prior to being placed in 50mL of SHIF pH 6.8 for 24 hours. At predetermined time intervals (0, 1, 2, 3, 6, 8, 12, 24 hours) the OCMTs were removed and blotted dry to remove surface water before being weighed on a calibrated electronic scale. The percentage increase in tablet weight, attributed to fluid uptake at each time point was determined using Equation 5.2. The erosion of the matrix, following its drying to a constant weight at each time interval was calculated using Equation 5.3.

$$\%\,\Delta\, Swelling = \frac{W_f - W_i}{W_i} \times 100 \qquad \textbf{(5.2)}$$

Where, W_f is the weight of the swollen tablet at time *t* and W_i is the initial weight of the tablet. (N=3).

$$\%\, Erosion = \frac{W_i - W_f}{W_i} \times 100 \qquad \textbf{(5.3)}$$

Where, W_i is the initial weight of the tablet and W_f is the final dried weight of the tablets after 24 hours. (N=3).

5.2.7. Water content determination of the optimized OCMT employing Karl-Fischer analysis (KF)

The optimized OCMT was analyzed using a Karl Fischer volumetric titrator (Mettler Toledo V30 Volumetric KF Titrator, Mettler Toledo Instruments Inc., Greifensee, Switzerland) with a DN143-SC electrode sensor attachment. The control parameters that were used in the volumetric KF titration are shown in Table 5.2.

Table 5.2: Control parameters used for KF volumetric analysis

Parameters	1-Comp titrant
Sensor Ipol [µA]	24
Stirrer speed [%]	35
End point [mV]	100
Control band [mV]	400
Dosing rate (min) [µL/min]	80
Dosing rate (max) [mL/min]	5
Start	Normal
Driftstop relative [µg/min]	15

Methanol was used as the moisture standard and water was quantified using electrical conductivity. Weighed samples were placed in the solvent holder and analysis was performed until the titration endpoint was reached. The water content determination was based on the Karl Fischer chemical reaction proposed by Scholz, E. (1982) as shown in Equation 5.4.

$$ROH + SO_2 + 3RN + I_2 + H_2O \rightarrow (RNH) \cdot SO_4R + 2(RNH)I \quad \textbf{(5.4)}$$

5.2.8. Correlative *in vitro* and *ex vivo* mucoadhesive strength determination of the optimized OCMT

Mucoadhesive studies were performed for the optimized OCMT to determine the influence of the outer polymer shell on the amount of mucoadhesion provided by the OCMT. The *in vitro* mucoadhesive strength determination study involved the preparation of 0.1%$^{w}/_{v}$ solution of mucin in SHIF pH 6.8. The optimized OCMT was incubated in this solution in an orbital shaker maintained at 37˚C and 50 rpm. The concentration of free mucin in the solution, after 6h duration, was determined by a UV spectrophotometer, at 201nm (IMPLEN NanophotometerTM, Implen GmbH, München Germany), using a 10 times dilution factor of path-length 0.1 mm. The difference in the concentration of the mucin solution before and after incubation was the indication of the amount crosslinked with the outer polymer shell as seen in Equation 5.5 (He *et al.,* 1998).

$$\text{Mucoadhesion}\% = \frac{[\text{Mucin before}]-[\text{Mucin after}]}{[\text{Mucin before}]} \times 100 \quad \textbf{(5.5)}$$

Where, [Mucin before] is the concentration of the mucin solution before incubation and [Mucin after] is the concentration of the mucin solution after incubation.

In addition, a Texture Analyzer (TA.XT *plus*, Stable Microsystems, Surrey, UK) was used to determine the *ex vivo* bioadhesivity of the OCMT. A mucoadhesion rig provided a vessel of a temperature-controlled (37°C) intestinal fluid and mucin environment for the pig intestinal tissue set-up. The OCMT was slightly hydrated in SHIF and attached to a cylindrical probe of the mucoadhesion rig using double-sided bioadhesive tape. The probe with attached OCMT was lowered at a constant speed of 0.1mm/s and bonded with the mucin-coated tissue at a predetermined compression force (0.08N) for a period of 120s. After the contact time, the probe withdrew at a constant speed (0.1mm/s) from the intestinal tissue and the adhesive properties were measured. A Force-time and Force-Distance profile was obtained and the tensile stress and work of adhesion were calculated using Equation 5.6 and 5.7 (Cevher *et al*., 2008).

$$\text{Tensile stress } (\text{N.cm}^2) = \frac{\text{F}}{\pi \text{r}^2} \quad \textbf{(5.6)}$$

Where, F is the detachment force and πr^2 is the surface area of the OCMT.

$$\text{Work of adhesion } (\text{mJ.cm}^2) = \frac{\text{AUC}_{\text{F-D}}}{\pi \text{r}^2} \quad \textbf{(5.7)}$$

Where, AUC is the area under the curve of a Force-Distance profile and πr^2 is the surface area of the OCMT.

5.2.9. Determination of the surface and core matrix hardness, matrix resilience and deformation energy of the optimized OCMT

The physicomechanical properties of the optimized OCMT was assessed through textural profiling using a calibrated Texture Analyzer (TA.XT *plus*, Stable Microsystems, Surrey, UK) fitted with a 5kg load cell, for determination of Matrix Hardness (MH), Matrix Resilience (MR), Deformation Energy (DE) and rigidity. A flat-tipped steel probe (2mm diameter) was used for surface determination of MH and MR values of the OCMT. Further textural analyses of the OCMT were undertaken using a needle-tipped steel probe (2mm diameter) for determination of

the MH and DE through penetration of the complete thickness of the OCMT. The samples were prepared and placed in a Temperature Controlled Peltier Cabinet (XT/PC) coupled to a Peltier Control Unit (PCU) (Stable Microsystems, Surrey, UK) for analysis by Texture Analyzer to mimic the internal body temperature environment. The Thermal Cabinet was equilibrated to 37°C (body temperature) to enable the melting of the core region of the OCMT before testing was performed within the cabinet. Data was captured at a rate of 200 points per second using Texture Exponent Software (V3.2). MR was computed as a percentage of the ratio between the Area under the Curve (AUC) of the peak to baseline (AUC_{2-3}) and the baseline to peak (AUC_{1-2}) from a Force-Time profile as shown in Equation 5.8.

$$\text{Resilience } \% = \left(\frac{\text{Area 2:3}}{\text{Area 1:2}}\right) \times 100 \quad \textbf{(5.8)}$$

The DE and matrix rigidity were both obtained from the AUC and gradient of the Force-Distance profiles, respectively. The MH was calculated using the Brinell Hardness Number (BHN) (Equation 5.9). Textural analysis on the OCMT was performed in triplicate. The parameters employed for the analysis are listed in Table 5.3.

$$\text{BHN} = \frac{2\text{F}}{\pi\text{D}\left(\text{D}-\sqrt{\text{D}^2-\text{d}^2}\right)} \quad \textbf{(5.9)}$$

Where, BHN is Brinell Hardness Number; D is diameter of indenter (mm); F is elucidated from the gradient of the initial force and the final force obtained and d is diameter of indentation (mm).

Table 5.3: Textural profiling parameters used for determining the Matrix Hardness, Matrix Resilience and Deformation Energy of the OCMT

Parameters	**Matrix Hardness, Deformation Energy & matrix rigidity**	**Matrix Resilience**
Pre-test speed	1 mm/s	1 mm/s
Test speed	0.5 mm/s	1mm/s
Post-test speed	1 mm/s	1mm/s
Trigger type	Auto	Auto
Trigger force	0.05 N	0.05 N
Compression strain	N/A	40%

*The distance for probe penetration into the tablet was set at 4mm for the needle-tipped steel probe

5.2.10. Porositometric analysis of the OCMT

The surface porositometric analysis of the optimized OCMT was performed using a Porositometric Analyzer (Micrometritics ASAP 2020, Norcross, GA, USA). Quantifiable aspects of the OCMTs surface area, pore diameter, total pore volume and bulk and absolute densities were determined. Samples were prepared by placing the optimized OCMT in SHIF pH 6.8 for 4 hours to allow the outer polymer shell to interact with the simulated fluid. Thereafter, the samples were removed and lyophilized (Labconco Freeze-Dry Systems, Labconco Corp., Kansas City, MO, USA) to expel excess fluid. The lyophilized samples were treated with a heat gradient and were evacuated with Nitrogen gas (N_2) for the removal of surface moisture and gas particles. Samples were then weighed and inserted into sample tubes for degassing. The degassing parameters were set up and included evacuation and heating phases as shown in Table 5.4.

Table 5.4: Evacuation and heating phase parameters employed for porositometric analysis

Parameter	Rate/Target
Evacuation Phase	
Temperature ramp rate	10°C/min
Target temperature	40°C
Evacuation rate	50.0mmHg/s
Unrestricted evacuation from	30mmHg
Vacuum set point	500µmHg
Evacuation time	60 min
Heating Phase	
Temperature ramp rate	10°C/min
Hold temperature	30°C
Hold time	1320min

Following complete degassing (21 hours), the sample tube was transferred to the analysis port where the Barrett, Joyner and Halenda (BJH) and Brunauer-Emmett-Teller (BET) adsorption and desorption relationships were subsequently generated. The determination of the surface area was based on the BET gas adsorption theory which is a widely used standard for porous materials (Singh *et al*., 1985). The BET equation was used in the linear form as shown in Equation 5.10.

$$\frac{p}{n^a \cdot (p^o - p)} = \frac{1}{n_m^a \cdot C} + \frac{(C-1)p}{n_m^a \cdot C\, p^o} \qquad \textbf{(5.10)}$$

Where, n^a refers to the quantity of N_2, $\frac{p}{p^o}$ refers to the relative pressure, n_m^a was the monolayer capacity and *C* was exponentially related to the enthalpy of adsorption in the first adsorption layer.

The total and specific surface area was determined from the monolayer capacity using Equation 5.11 and 5.12, respectively.

$$A_s\,(BET) = n_m^a \cdot L \cdot a_m \quad \textbf{(5.11)}$$

$$a_s(BET) = A_s\ (BET)/m \quad \textbf{(5.12)}$$

Where, $A_s\,(BET)$ and $a_s(BET)$ are the total and specific areas, respectively, of the adsorbent of mass (m) and L is the Avogadro constant.

5.2.11. Surface structure morphology of the outer polymer shell of the optimized OCMT

The surface morphology of the outer polymer shell was analyzed using a Scanning Electron Microscope (SEM) (FEI Company, Hillsboro, OR, USA). Samples were prepared by placing the optimized OCMT in SHIF pH 6.8 for 4 hours to allow the outer polymer shell to interact with the simulated fluid. Thereafter, the samples were removed and lyophilized (Labconco Freeze-Dry Systems, Labconco Corp., Kansas City, MO, USA) to expel excess fluid. The lyophilized samples were fixated on aluminum stubs and loose particles were removed by spraying with compressed air. Thereafter, the samples were sputter coated with gold for 60 seconds using a SPI-Module™ Sputter Coater (SPI Supplies, Structure Probe, West Chester, PA). After coating, the samples were re-sprayed with compressed air and placed in the FEI Phenom™ Scanning Electron Microscope operated at 10kV in the electron imaging mode for subsequent viewing at varying degrees of magnification to determine the surface architectures and qualitatively determine the shape and size of the porous outer polymer shell.

5.2.12. Magnetic Resonance Imaging (MRI) of the optimized OCMT

Magnetic Resonance Imaging (MRI) was undertaken in SHIF (pH 6.8) to monitor the fate of the dosage form *in vivo* and correlate it with the *in vitro* behavior**.** Live-acquisition of the pH-responsive transitions of the OCMT was determined using a digital MARAN-i System configured with a DRX2 HF Spectrometer console (Oxford Instruments Magnetic Resonance, Oxon, UK) equipped with a compact 0.5 Tesla permanent magnet and stabilized at 37°C. The dynamics of

fluid ingress into a drug delivery system is a contributing factor towards controlling drug release (Tajiri *et al*., 2010). The hydrational morphological transitions of the OCMT were captured every 5 min with MARAN-i version 1.0 software. MARAN-i software comprises image acquisition software and image analysis software. The image acquisition parameters are depicted in Table 5.5.

Table 5.5: MARAN-i image acquisition parameters employed for magnetic resonance imaging

S.No.	Parameter	Value
1.	Imaging protocol	FSHEF
2.	Requested gain (%)	4.17
3.	Signal strength	68.92
4.	Average	2
5.	Matrix size	128
6.	Repetition time (ms)	1000.00
7.	Spin Echo Tau (ms)	6.80
8.	Image acquired after	60min
9.	Total scans	64

T_1 weighted images were produced in the spin echo method and the signal intensity of the MRI images were defined according to Equation 5.13.

$$S = \mathrm{M_O} + \exp\frac{-\mathrm{TE}}{\mathrm{T_2}} \times \left(1 - \exp\frac{-\mathrm{TR}}{\mathrm{T_1}}\right) \quad \textbf{(5.13)}$$

Where, $\mathrm{M_O}$ is magnetization, T_1 and T_2 are relaxation times, TR is repetition time and TE is echo time.

5.2.13. *In vitro* peptide release

Intrinsic to the functioning of the OCMT was its *in vitro* peptide release performance. *In vitro* peptide release studies were performed using a USP35 dissolution apparatus II (Caleva, Model 7ST, UK). The OCMT was placed in 900mL SHIF at pH 6.8, beneath a ring mesh assembly within the dissolution vessel to prevent floatation. Dissolution was performed at a speed of 50rpm (37±0.5°C). Sampling of 3mL was undertaken at predetermined time intervals (0, 1, 2, 3, 6, 8, 10, 12, 24) and replaced with an equal quantity (3mL) of peptide-free dissolution medium to maintain sink conditions. Samples were analyzed using a Peptide Enzyme Immunoassay (Peninsula Laboratories International, Inc. San Carlos, CA, USA) which is a high sensitivity absorbance assay specific for the detection of Octreotide. Prior to sample analysis a standard curve was obtained by preparing the standards shown in Table 5.6.

Table 5.6: Standards prepared for construction of a calibration curve

Standard	Concentration (ng/ml)
S1	10.00
S2	2.50
S3	0.63
S4	0.16
S5	0.04

Peptide release was calculated as a mean of three determinations as all studies were conducted in triplicate. In addition, the mean dissolution time (MDT) (Equation 5.14) was calculated from dissolution data to determine the peptide release rate (Sathish and Syed, 2013).

$$MDT = \frac{\sum_{i=1}^{i=n} t_{mid} \times \Delta M}{\sum_{i=1}^{i=n} \Delta M} \quad \textbf{(5.14)}$$

Where, *MDT* is Mean Dissolution Time; *i* is the dissolution sample number; *n* is the number of dissolution sample time; t_{mid} is time at mid-point between *i* and *i=1*; *ΔM* is the additional amount of protein dissolved between *i* and *i=1*.

In addition, the *in vitro* peptide release data obtained were fitted into various mathematical modelling equations to determine the mechanism of peptide release from the optimized OCMT.

5.3. Results and Discussion

5.3.1. Analysis of weight uniformity, thickness and friability of the optimized OCMT

The optimized OCMTs (*N=5*) displayed a uniformity in mass, each having an average weight of 514.34±0.75mg. Measurement of the thickness of the tablets displayed average readings of 4.1±0.45mg, whilst evaluation of the friability of the OCMT revealed results of 0.68±0.02%. The friability value was within the 1% limit of acceptability as defined in the USP and as a result reflected positively on the ability of the OCMT to withstand external stresses during storage. The overall results obtained for weight uniformity, thickness and friability served as a reliable indicator of the reproducibility of the formulation methods and the tablet assembly process. Figure 5.2 displays the dimensions of the optimized OCMT with in-process validation results and a digital image of the optimized OCMT.

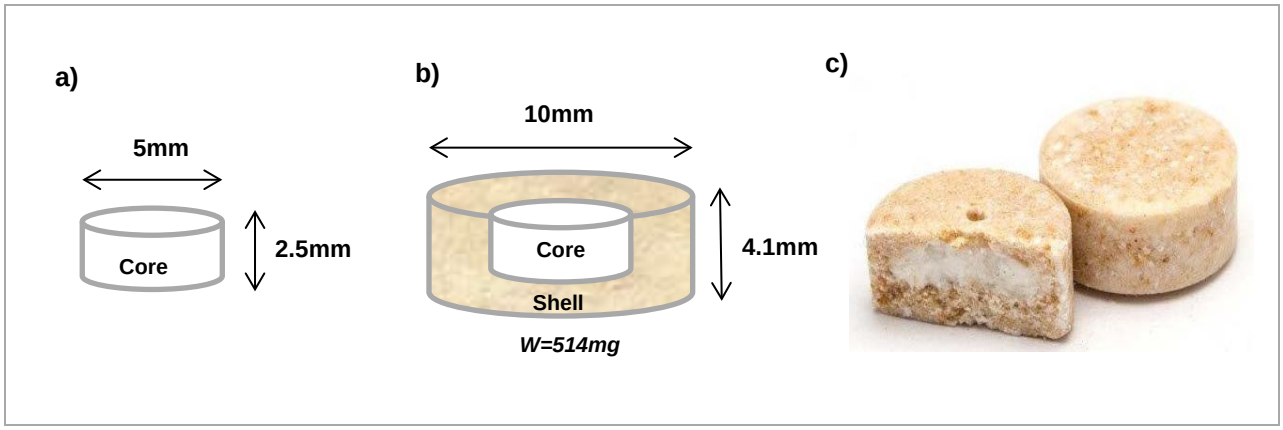

Figure 5.2: Schematic representation of the dimensions of **a)** the core eutectic region, **b)** the optimized OCMT and **c)** a digital image of the OCMT with the outer polymer shell surrounding the inner core eutectic region.

5.3.2. Analysis of the pertinent rheological properties of the EPB

Due to the unique features of the EPB; its characteristic melting at body temperature (37°C), change in crystallinity and surface morphological structure as detailed previously by Choonara and co-workers (2016), further investigations into its intrinsic properties became a necessity. Thus, the EPBs flow and deformation behavior in response to applied stresses was determined. The EPB was found to have both viscous and elastic properties as it transitions from a solid at room temperature (25°C) to a melt at body temperature (37°C). Consequently, particular attention was focused on the viscoelastic and thermo-mechanical characterization of the EPB.

Dynamic oscillatory tests were performed to determine the rigidity and integrity of the EPBs internal structure resulting from macro- and micro-structural transitions over a temperature range (White, 1990). Figure 5.3 displays the basic principle of the oscillatory rheological measurements with its back and forth movement and sinusoidal signal applied to the sample. Typically measured parameters included; the complex viscosity [η*], the elastic (storage) modulus (G') and the viscous (loss) modulus (G") which respectively gives an indication of the solid-like and liquid-like properties of the substance in response to temperature (T) changes (Lippacher *et al.,* 2002).

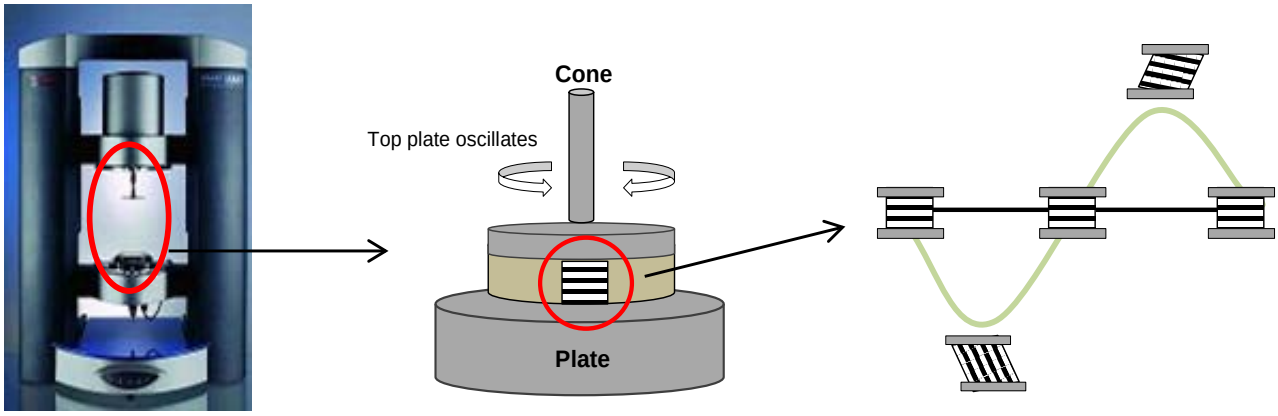

Figure 5.3: Schematic representation of the basic principles of oscillatory testing, displaying the back and forth movement of the cone and top plate and the sinusoidal stress or strain that is applied to the sample.

A preliminary oscillatory stress sweep at a frequency of 1Hz was performed to determine the EPBs Linear ViscoElastic Region (LVER) as shown in Figure 5.4. The oscillatory stress sweep provides information about the rigidity and yield stress of a material (Lippacher *et al.,* 2004). Initially, the stress applied to the sample is sufficiently low enough to preserve the structure of the material as indicated by the plateau shown in Figure 5.4. The internal breakdown of the material structure occurs as increasing amounts of stress are applied to the sample which results in a decrease in the elasticity (phase angle rises). Since the elastic modulus does not change within the LVER we know that this amount of stress is non-destructive to the material and thus, subsequent testing was kept within this LVER (Lippacher *et al.,* 2004).

An oscillatory temperature ramp was performed to determine the elastic and viscous modulus as well as the complex viscosity of the EPB as it changes from a solid at room temperature to a melt at 37°C. The inputted stress value for the temperature ramp needs to fall within the LVER and thus, several pre-tests were conducted to determine the optimum stress value. Figure 5.5a displays the typical rheological profile for the EPB obtained at a stress value of 1 Pa. It can be noted that at the beginning, the EPB is more solid-like and thus, has higher elastic properties than viscous properties as indicated by the higher storage modulus G' versus the loss modulus G" value (Hyun *et al.,* 2006). As the temperature increases, both material functions decrease and it might even be seen that the material becomes more viscous. In Figure 5.5a, at 37°C, a significant 30% drop in the G' value from 3610 Pa to 2508 Pa was noted. Proportionally a slight increase in the viscous modulus was noted at 37°C with both the G' and G" reaching equilibrium above 40°C.

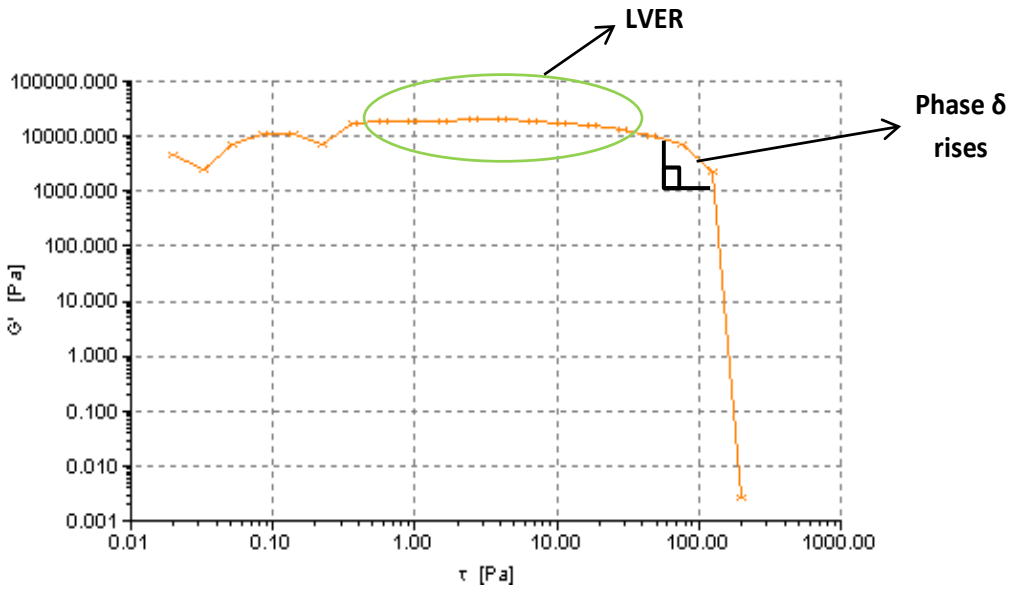

Figure 5.4: Oscillatory stress sweep curve indicating the Linear ViscoElastic Region (LVER) and the subsequent structural breakdown of the material indicated by the sharp decrease in G'.

The rheological profile in Figure 5.5b was obtained at a stress value of 4 Pa to facilitate a clearer indication of the pertinent rheological transitions occurring. The rheological behavior of the EPB in response to increasing temperatures was evaluated and the relevant regions were highlighted (Jones, 1999). Initially, within the glassy region, the G' value is greater than the G" and the EPB was thought to be primarily elastic in nature. Upon increases in temperature, the mobility of the molecules increase causing the EPB to become more viscous and subsequently transition into a rubbery state (Jones, 1999; Menard, 2008). At 37°C, a critical crossover was noted where G" > G'. This supports the intrinsic features of the EPB that remains solid at room temperature and softens at 37°C. Above 42°C, within the terminal region, the EPB becomes completely liquid-like and G" primarily dominates. In addition, the complex viscosity [η*] of both profiles decreased significantly with an increase in temperature as compared to the initial viscosities.

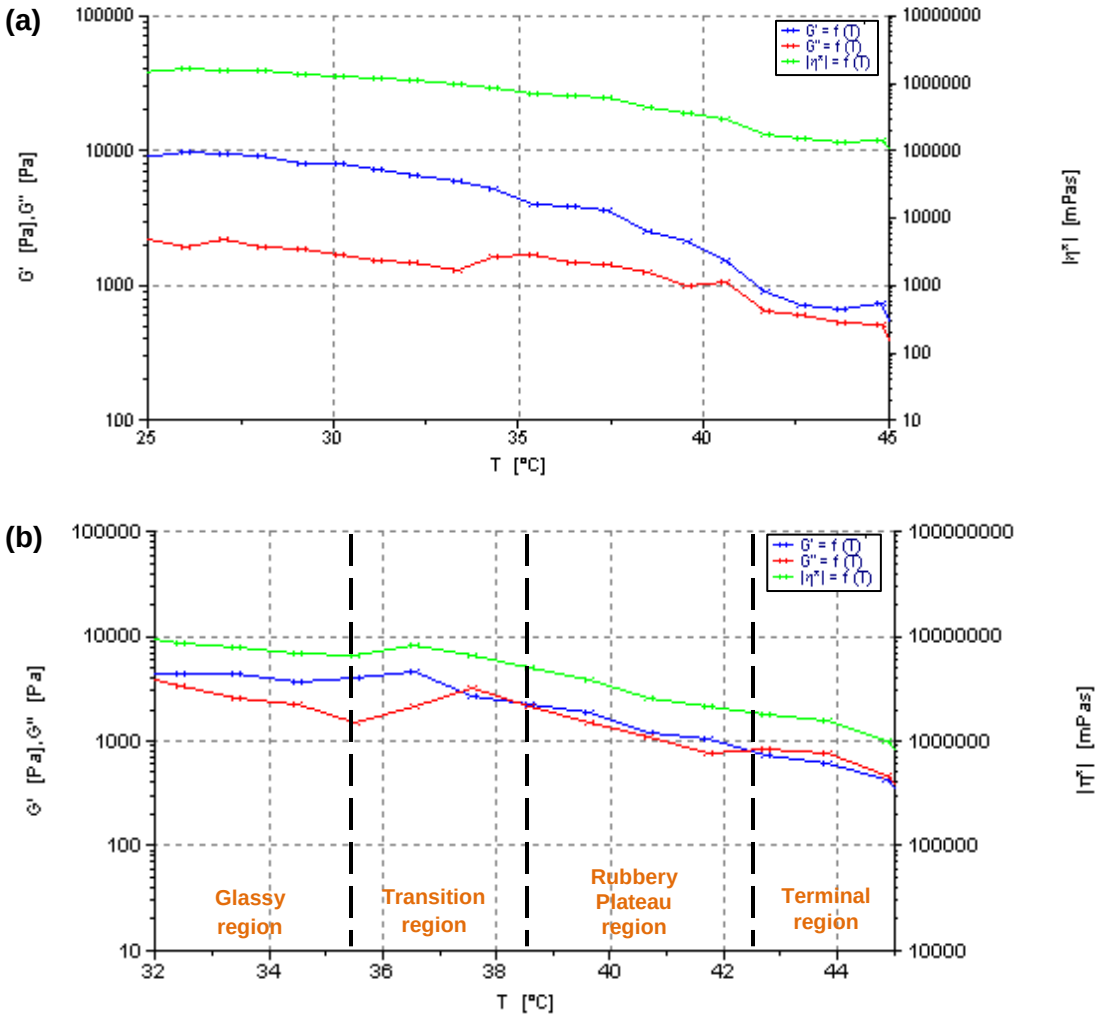

Figure 5.5: Oscillatory temperature sweep profiles of the EPB displaying pertinent rheological transitions in **a)** obtained at a stress value of 1 Pa and **b)** obtained at a stress value of 4 Pa.

The dynamic mechanical analysis of the EPB and its distinctive temperature-dependent effects on its viscoeleastic properties displayed typical amorphous material behavior (Jones, 1999). This was evidenced by the temperature-modulated change from a glassy state with restricted motion of molecules to a rubbery state with an enhanced molecular mobility, increased relaxation and decreased rigidity (Ward and Hardley, 1993; Jones, 1999). This resonates with the results previously emphasized in Choonara *et al*, (2016) where the EPB displayed characteristic changes in its thermal behavior, crystallinity and surface morphological structure.

5.3.3. Analysis of the vibrational molecular transitions of the optimized OCMT

FTIR studies confirmed the successful crosslinking between the outer polymer shell of the OCMT with the inner core eutectic region as evidenced by the ATR-FTIR spectra obtained. As

expected, the OCMT displayed bands characteristic to the molecular and vibrational transitions of all its components with a reduction and increase in intensity of certain bands as well as the appearance of new bands, accredited to the *in situ* crosslinking initiated by the presence of the chemical crosslinkers ($NaCO_3$ and K_2HPO_4). The ATR-FTIR split transmittance spectra of the native polymers and components are displayed in Figure 5.6.

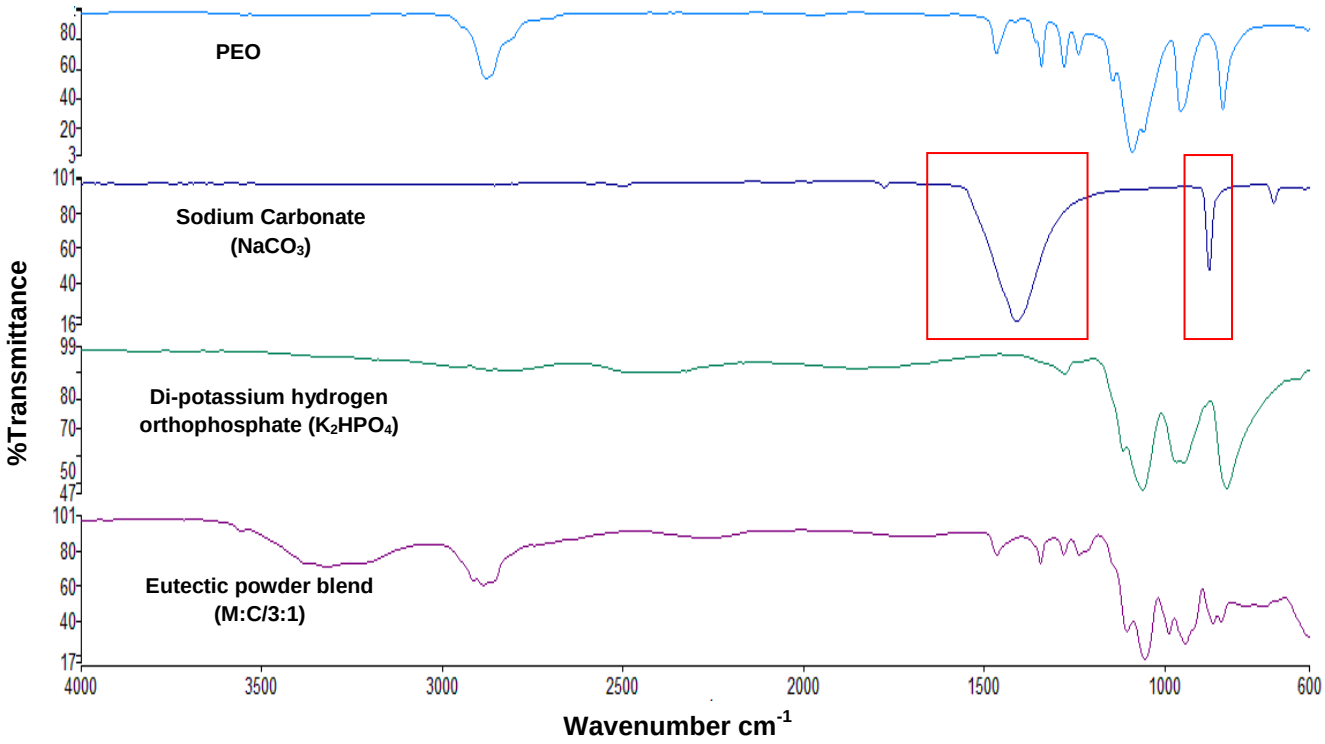

Figure 5.6: ATR-FTIR split transmittance spectra of the native compound PEO, crosslinkers ($NaCO_3$ and K_2HPO_4) and the eutectic powder blend. The two highlighted peaks are characteristic of carbonate ions.

In addition, the characterization of an *in vitro* physically crosslinked formulation provided a measurable standard by which the *in situ* cross-linked formulation could be compared. The *in vitro* crosslinked formulation displayed peaks identical to that of the OCMT as shown in Figure 5.7a, indicating the comparable crosslinking of PEO *in situ*. The process of *in situ* crosslinking is expected to create a crosslinked interface network between the core region of the OCMT and the outer polymer shell to primarily protect the incorporated protein or peptide and provide desirable controlled release behavior. The designated functional groups and fingerprint bond regions have been highlighted in Figure 5.7a.

Results from the ATR-FTIR spectra of the OCMT displayed a broad, low intensity peak at 3235cm^{-1}. This peak is characteristically indicative of a hydroxyl functional group and often indicates a high degree of association resulting from extensive inter and intra-molecular hydrogen bonding (Coates, 2000). The –OH group signified the presence of the menthol-containing EPB within the OCMT and was predictably absent from the *in vitro* crosslinked formulation spectrum. A high intensity methylene (>CH_2) symmetrical stretch at 2876cm^{-1} further alluded to the presence of organic material with at least one saturated aliphatic portion (Coates, 2000). The appearance of a new carbonyl band in the functional group region at 1599cm^{-1} as shown in Figure 5.7b is representative of a C=O stretching vibration, characteristic of carboxylic acid derivatives arising from crosslinks between PEO, $NaCO_3$ and K_2HPO_4 (Coates, 2000).

In the analysis of the fingerprint region of the OCMT, typical sodium carbonate-type peaks as shown in Figure 5.6 were identified at 1464cm^{-1} and 839cm^{-1}. Conventionally, carbonate ions (CO_3^{2-}) present themselves at two absorption bands indicative of in-plane and out-of-plane bending (Coates, 2000; Sreedhar *et al*., 2012). Macromolecular interactions corroborated the formation of the distinguishing sodium carbonate peak at 1464cm^{-1} by dwarfing the native PEO peak at 1359cm^{-1}. Several bond origins (>CH_2, >CH-, C-O, C-H) characteristic to PEO were noticeable in the transmittance spectra of the OCMT. Additionally, transformations originating from the influence of K_2HPO_4 in the crosslinking process was evidenced by the overlapping organic (P=O conjugation) and aliphatic (P-O-C conjugation) phosphate stretching vibrations (Coates, 2000). Overall bond designations and summations inferred from PEO interactions with $NaCO_3$ and K_2HPO_4 at a 23%$^{w}/_{w}$ concentration highlights the superior conjugation and crosslinking ability as observed in the FTIR spectra which were further corroborated by swellability and release kinetic results.

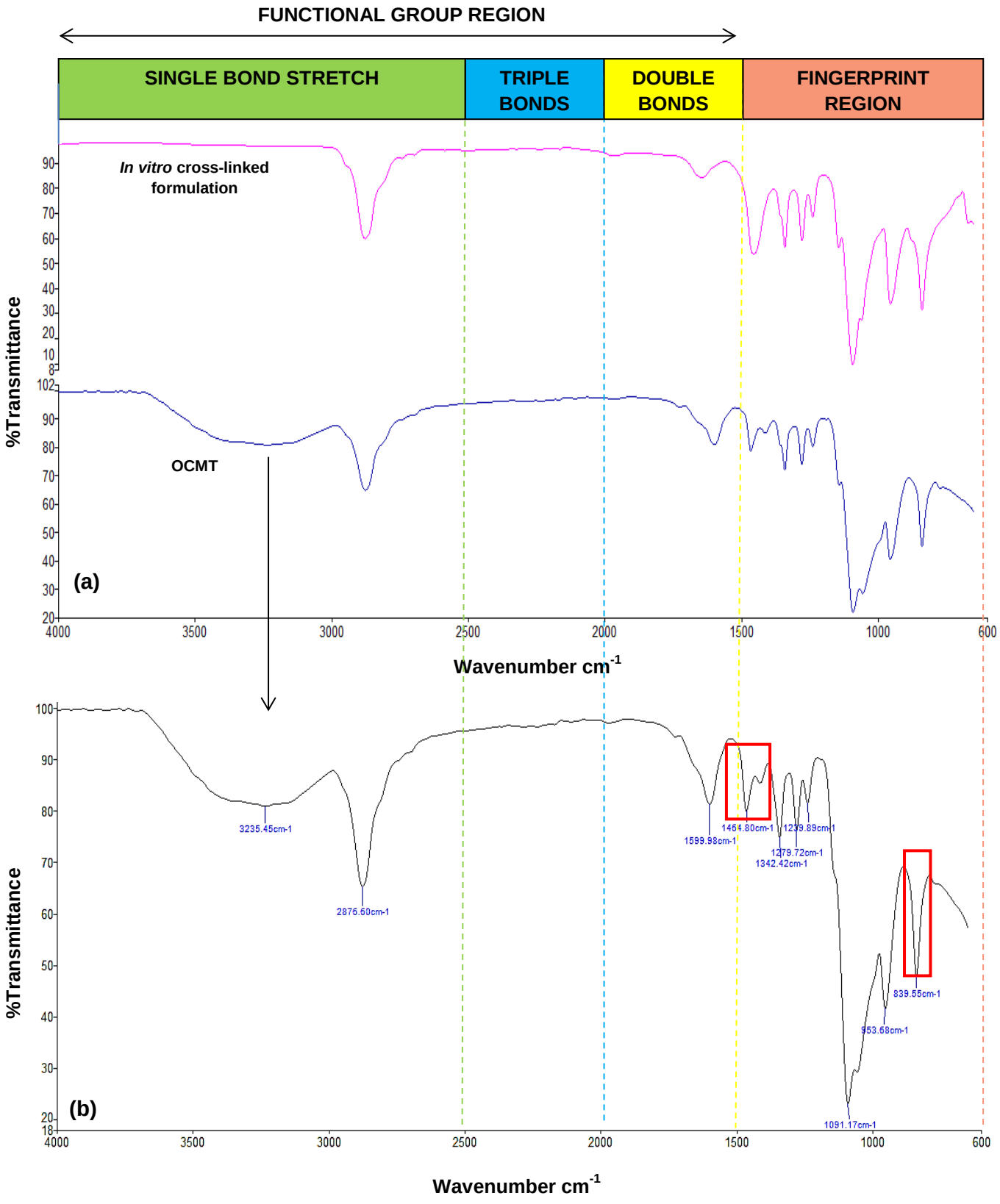

Figure 5.7: ATR-FTIR transmittance spectra: **a)** split transmittance spectra of the *in vitro* cross-linked formulation and the optimized OCMT and **b)** expansive spectra of the OCMT with labeled peaks and highlighted distinguishable sodium carbonate peaks.

5.3.4. Analysis of the swelling and erosion behavior of the optimized OCMT

The gravimetric swelling of the OCMT was analyzed by monitoring its change in weight over 24 hours. The increased swelling percentages of the intact OCMT at each measured time interval is illustrated in Figure 5.8a. A high swelling rate was recorded for the first hour, followed by a linear progress of fluid absorption within the next two hours. Following three hours, the rate of weight gain drops and only slight increases in the swelling percentage was recorded. After 4 hours, the weighty increase in the rate and extent of swelling was considerably noted and subsequently resulted in the gradual formation of a thick swollen front as shown in the digital images in Figure 5.8a.

The observed swelling results were primarily attributed to the porous configuration of the outer polymer shell which enabled fast and extensive swelling (Vlachou *et al.,* 2001). However, the slow progression of swelling between the time periods of 3hr and 4hr as well as 6hr and 8hr may be attributed to the formation of the crosslinked interface *in situ*. Swelling measurements are the simplest level of analysis in determining the effects of different concentrations of crosslinkers on the swelling behaviour as was demonstrated in Choonara *et al*, (2016). The extent of swelling is indirectly proportional to the degree of crosslinking and thus, the retardation of swelling reflects the intra and inter-molecular interactions between the outer polymer shell and the inner core melt region (Mahkam and Doostie, 2008; Carbinatto *et al*., 2014).

An equilibrium swelling was reached at 8 hours with the intact OCMT swelling up to ±750% of its original mass. After 8 hours, the effects of surface erosion became evident as the OCMT began to slowly lose its physical structure. The erosion percentage of the OCMT after 24 hours was just over half of its original mass at 53.94%. The erosion of the OCMT was recorded as a function of the dried weight of the tablet after 24 hours and thus is not reflected in the swelling profile results obtained. Pectin, contained within the outer polymer shell was responsible for the erosion characteristics of the OCMT by enabling controlled, surface erosion as was evident by the maintenance of a gelled mass of the tablet following 24 hours. Conclusive analysis of the swelling and erosion behavior generated results influenced by the porosity, crosslinking capabilities and surface erosion which may ultimately influence the dissolution and release kinetics in controlled release systems (Vlachou *et al.,* 2001; Sriamornsak *et al*., 2007).

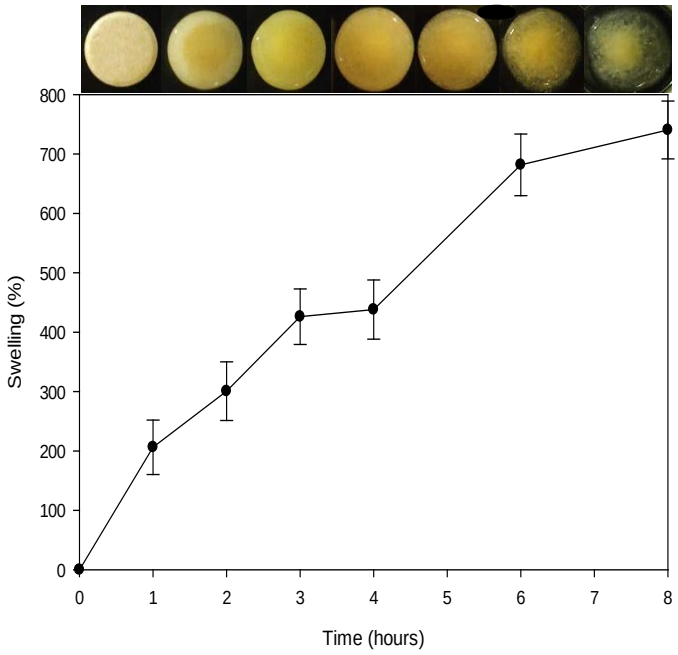

Figure 5.8: Swelling profile of the intact OCMT up to 8 hours in SHIF with insets displaying digital images of the swelled appearance, corresponding to each time point.

5.3.5. Analysis of the moisture content of the optimized OCMT

The determination of the moisture content is important as it has a significant effect on the chemical, physical and microbial properties of finished pharmaceutical products (Nokodchi, 2005; Gerhardt, 2009). The moisture in tablets originates from various sources, including the water of crystallization and surface adsorption of pure chemicals as well as the presence of inactive excipients (Crouter and Briens, 2014). Results from Karl Fischer analysis of the optimized OCMT revealed a water content of 6.822 ± 0.1%. Ideally, the value was a median of the moisture content of all the components contained within the outer polymer shell ranging from <1% for some components to 12% for other components (Bhaskar *et al.*, 1993; Rane *et al*., 2013; Crouter and Briens, 2014). This value was acceptable in terms of maintaining product stability and improving tablet compaction (Gerhardt, 2009). It is important to understand the capabilities of water and its effects on the pharmaceutical product as it provides valuable insight into combating these effects and ultimately improving the shelf life of the product.

5.3.6. Interpretation of the *in vitro* and *ex vivo* mucoadhesion of the optimized OCMT

Mucus covers several epithelial surfaces within the body, including the intestinal membrane. The ability of a molecule to attach to mucus-lined epithelial surfaces is termed mucoadhesion, a feature which enables the controlled delivery of drugs resulting from the close proximity of the system to the mucosal surface (Carreras *et al*., 2016). Mucin is the main component of mucus

and thus the interaction of the outer polymer shell of OCMT with mucin was investigated. Results from *in vitro* mucoadhesive studies revealed an average mucoadhesive percentage of 71.87%. The intrinsic nature of polymers is a key factor towards achieving effective mucoadhesion which was clearly evident by the results obtained. The molecular weight, flexibility and degree of ionization of the polymers were the main influences for the observed polymer-mucin interactions (Carreras *et al*., 2016).

The high molecular weight of PEO, flexibility and cationic nature of pectin and the anionic charge of CMC all contributed to the effective mucoadhesion percentage achieved. Typically, mucoadhesion increases with an increase in molecular weight with the chain flexibility being crucial in its ability to facilitate interpenetration (Lee *et al.,* 2000; Carvalho *et al.*, 2010). In addition, the ionic charge of the polymers significantly affects the mucoadhesive strength with anionic polymers showing the highest mucoadhesive strength followed by cationic and non-ionic polymers (Carreras *et al*., 2016; Mansuri *et al.*, 2016). The additive mucoadhesive nature of the outer polymer shell can be correlated to the *ex vivo* mucoadhesive strength determination.

The analysis of the *ex vivo* mucoadhesion generated the maximum detachment force and AUC which were computed into tensile stress ($N.cm^2$) and work of adhesion ($mJ.cm^2$). The tensile stress and work of adhesion were the maximum force and total amount of forces required for separation of the OCMT from the pig intestinal tissue, respectively (Manconi *et al*., 2010). A typical Force-Distance profile obtained from the mucoadhesive test is shown in Figure 5.9. The tensile stress result produced a value of 0.052 ± 0.002 $N.cm^2$, while calculations of the work of adhesion yielded a value 0.132 ± 0.012 $mJ.cm^2$. The results obtained not only corroborated the *in vitro* mucoadhesive strength determination, but also provided a reliable indicator of the enhanced mucoadhesion of the OCMT within a short contact time period (120s).

The *in vitro* and *ex vivo* mucoadhesion results can be summarized in three steps: the first involving the hydration and subsequent swelling of the OCMT to facilitate the tight contact with the pig intestinal tissue; the second involving ionic interactions and interpenetration of the OCMT with the mucin chains and; lastly the combination secondary chemical interactions and weak interfacial forces which all leads to enhanced adhesion of OCMT to the pig intestinal tissue (Carvalho *et al.,* 2010; Singh and Rana, 2012; Carreras *et al*., 2016). The ability of the OCMT to deliver on its mucoadhesive properties may significantly improve the tablets residence time *in vivo*, enhance its oral bioavailability and promote targeted delivery.

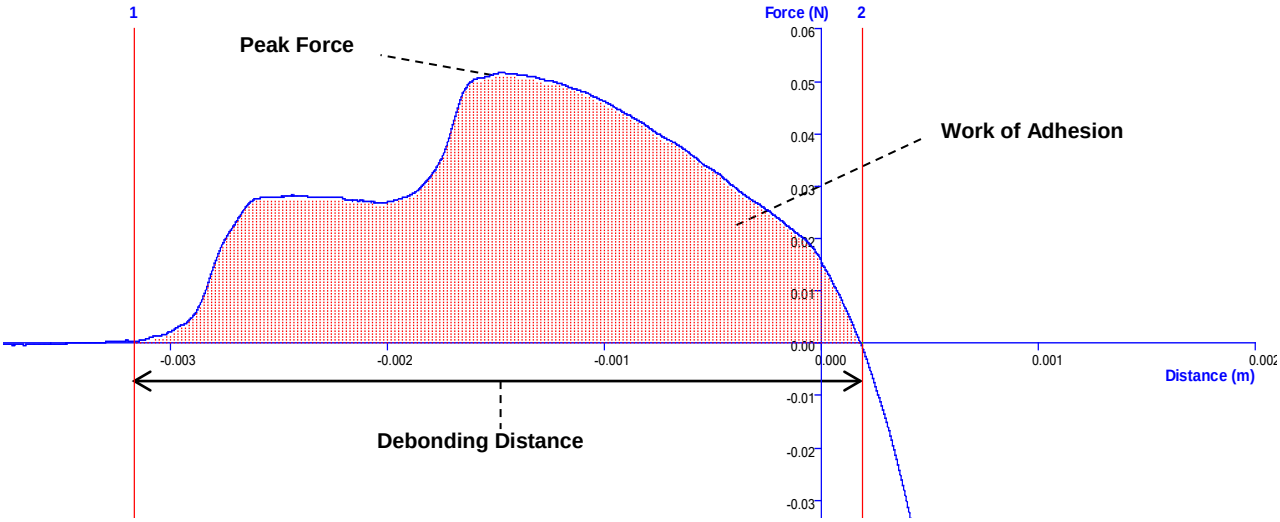

Figure 5.9: Typical Force-Distance profile obtained from *ex vivo* mucoadhesive analysis of the OCMT.

5.3.7. Evaluation of the physicomechanical properties of the optimized OCMT

Compressive and penetrative forces were applied to the optimized OCMT to determine the MH, MR, matrix rigidity and DE. Quantitative analysis of Force-Time and Force-Distance profiles yielded results for the surface and core textural profiling of the OCMT. The summary of the results obtained are provided in Table 5.7. The MH and rigidity are closely related as they both refer to the ability of the tablet to resist deformation when a force is applied. Both properties give an indication of the mechanical integrity of the tablet and its critical influence on other physical and chemical parameters (Tai *et al*., 2014). The surface matrix hardness of the OCMT was predictably greater than the core matrix hardness resulting from the inherent softening of the core at 37°C, as discussed previously (Choonara *et al*., 2016). The low matrix hardness of the core does not detract from the mechanical integrity of the OCMT but rather creates a platform for improved structural flexibility and hardness by facilitating the process of *in situ* crosslinking.

Analysis of the MR result obtained reflected positively on the tablet's ability to return to its original state after compression-related deformation. The deformation energy was considerably low, attributable to the softer core matrix. Furthermore, Figure 5.10 illustrates the multi-textural properties of the OCMT following penetration of the needle probe through the different layers of a cross-sectioned tablet and the corresponding responses observed in the Force-Time profile obtained. Initially, a rise to a high peak force was noted as the probe penetrates into the top layer of the outer polymer shell. Following further penetration into the softened core, a fracture

and subsequent decrease in the force is noted. The final penetration of the probe into the bottom layer of the outer polymer shell yields the additional increase in force observed. The overall results obtained from textural profiling, corroborated the structural mechanics of the OCMT in its achievement of desirable responses.

Table 5.7: Physicomechanical properties of the optimized OCMT

Textural Parameter	Value
Surface matrix hardness (N.mm^2)	205.91
Core matrix hardness (N.mm^2)	51.54
Matrix resilience (%)	74.66
Matrix rigidity (N.mm)	52.26
Deformation energy (J)	0.005

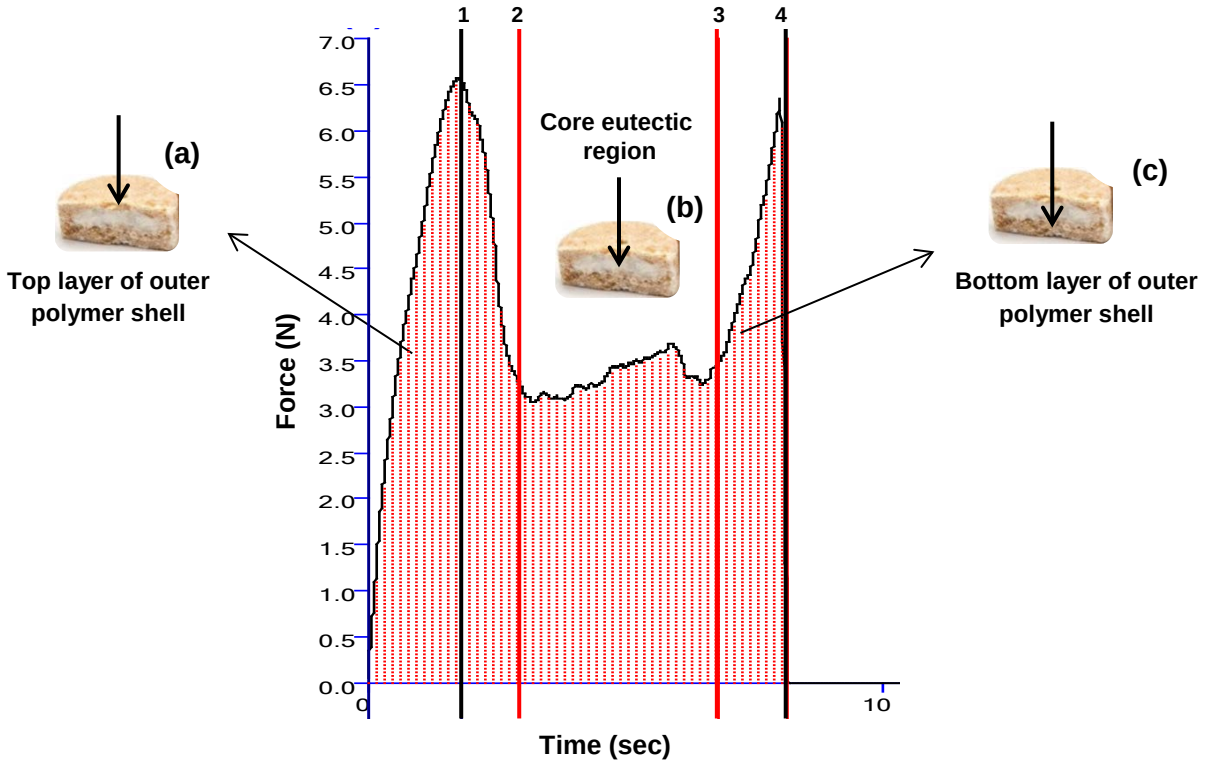

Figure 5.10: Annotated multi-textural profile indicating the penetration of the needle probe through the different layers of the OCMT and its corresponding response: **a)** the top layer of the outer polymer shell, **b)** the core eutectic region and **c)** the bottom layer of the outer polymer shell.

5.3.8. Dual analysis of the surface morphology and porosity of the optimized OCMT

The porositometric characterization of the OCMT was based on the phenomenon of physisorption, a macroscopic method that provides critical information about the porous

properties and structure of materials by evaluating the nitrogen adsorption as a function of relative pressure (P/Po). The BET and BJH methodologies were used to determine the specific surface area as well as the pore size and pore volume by adsorption and desorption techniques, respectively (Foo and Hameed, 2010). Adsorption isotherms are often generated from porositometric analysis and can be divided into different types depending on the degree and mechanism of adsorption, the nature of the adsorbent surface and the comparative strengths of the adsorbate-adsorbent interactions (Foo and Hameed, 2010).

According to the IUPAC classification system, the linear isotherm plot (Figure 5.11a) obtained for the optimized OCMT was typical of a Type II physisorption isotherm with a H3 hysteresis loop. This reversible physisorption isotherm is typically obtained for macroporous adsorbents, such as polyethylene oxide, and represents a clear monolayer-multilayer adsorption (Sing *et al.,* 1985; Sing and Williams, 2004; Sangwichien *et al*., 2002). The isotherm displayed an initial gradual curvature to the relative pressure axis which indicates strong interactions between adsorbate molecules and complete monolayer coverage followed by the linear middle region representative of the commencement of multilayer adsorption (Sing *et al.,* 1985). In addition, a hysteresis loop was noticeable between 0.9-1.0 P/Po. The characteristic shape of the hysteresis loop was attributed to the capillary condensation phenomenon that occurs in mesopores, wherein condensation of a gas to a liquid-like phase in a pore takes place at a pressure less than the saturation pressure of the bulk liquid (Sing *et al*, 1985; Sing and Williams, 2004).

Therefore, the OCMT was considered to be mesoporous with characteristic intermediate pore widths between 2nm and 50nm (Groen *et al*., 2003). This correlated with the results obtained for the average pore widths and diameters reported in Table 8. BET and BJH calculations yielded pore sizes for the OCMT ranging from 2.293nm-7.619nm. Furthermore, the hysteresis loop displayed a forced closure at a P/Po >0.45 which may be accredited to the process of *in situ* crosslinking (Figure 5.7) which creates an interpenetrating pore network in which larger pore sizes empty into smaller diameters (Sangwichien *et al*., 2002). Consequently, this causes a shift in the desorption branch to a lower pore size compared to the adsorption branch as shown in Figure 5.11b-c which was further corroborated by the BJH Desorption average pore diameter value presented in Table 5.8. The surface area and pore volume accounts for the observed swelling behavior of the OCMT by significantly impacting on the amount of water uptake (Figure 5.8).

SEM micrographs of the OCMT showed highly porous surface structures, supporting quantitative porositometric analysis. Surface area and porosity studies alluded to the OCMT's random size distribution and interconnected pore system. This was evidenced by the SEM micrographs for the OCMT shown in Figure 5.11a at different magnifications (i) and (ii). The honeycomb-type appearance of the micrographs represented the low-density pore domains that are interconnected. Comprehensive analysis of the porosity of the OCMT provides valuable information on its effect on other physicochemical and physicomechanical properties, specifically fluid uptake, *in situ* crosslinking and release kinetics.

Table 5.8: Summative analysis of the surface area, pore volume and pore size characteristics of the optimized OCMT

Surface Area	**OCMT**
Single point surface area at P/Po	0.199946691:6.9197 m^2/g
BET Surface Area	29.3120 m^2/g
t-Plot Micropore Area	5.8552 m^2/g
t-Plot External Surface Area	23.4568 m^2/g
BJH Adsorption cumulative surface area of pores between 17.000 Å and 3000.000 Å diameter	11.174 m^2/g
BJH Desorption cumulative surface area of pores between 17.000 Å and 3000.000 Å diameter	12.1105 m^2/g
Pore Volume	
Single point adsorption total pore volume of pores less than 788.870 Å diameter at P/Po	0.974834133:0.016800 cm^3/g
t-Plot micropore volume	-0.007212 cm^3/g
BJH Adsorption cumulative volume of pores between 17.000 Å and 3000.000 Å diameter	0.022861 cm^3/g
BJH Desorption cumulative volume of pores between 17.000 Å and 3000.000 Å diameter	0.023067 cm^3/g
Pore Size	
Adsorption average pore width (4V/A by BET)	22.9261 Å
BJH Adsorption average pore diameter (4V/A)	81.837 Å
BJH Desorption average pore diameter (4V/A)	76.189

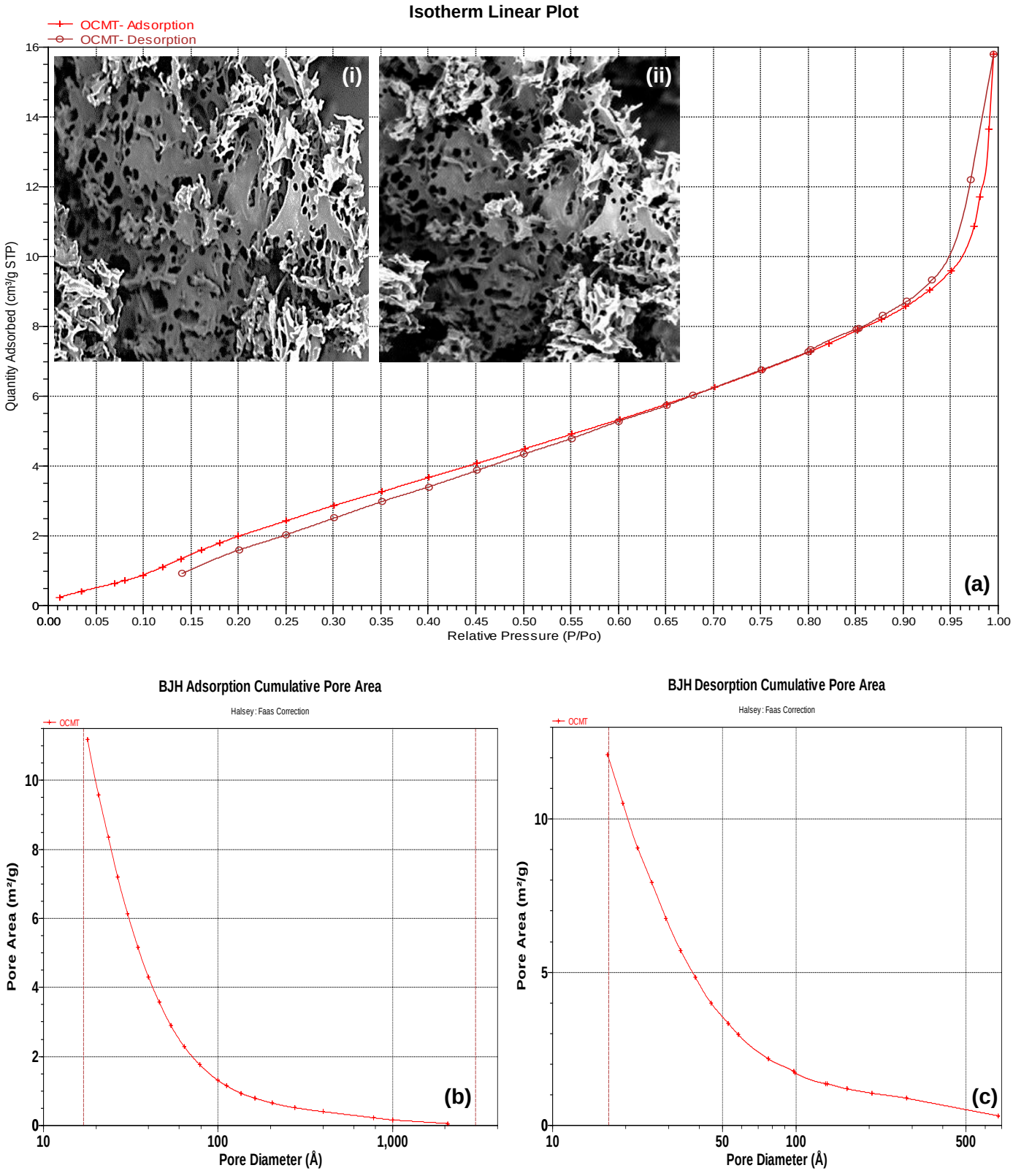

Figure 5.11: OCMT porosity plots: **a)** linear isothermic plot with insets of SEM micrograph images at magnifications of 3300x (i) and 4100x (ii) **b)** BJH Adsorption Cumulative Pore Area and **c)** BJH Desorption Cumulative Pore Area.

5.3.9. Analysis of the Pharma-Engineering and hydration characteristics of the optimized OCMT

The hydration characteristics of the OCMT are important for evaluating the performance of the device as highlighted previously in the analysis of the swelling and erosional behavior. Therefore, MRI was used to observe and measure the internal events underlying *in vitro* peptide release as a result of solvent penetration (Richardson *et al*., 2005; Dorozynski *et al*., 2012). The changes in hydration over 24 hours were noted in the MRI images presented in Figure 5.12. The intensity scale from black to white gives an indication of the degree of hydration of the OCMT. The darker, low intensity regions indicate minimal degrees of hydration, whereas the white, high intensity regions indicate extensive hydration and swelling. The characteristic Pharma-Engineering of the tablet was evident in the images obtained, highlighting the hydrated outer polymer shell and the un-hydrated core eutectic region.

The OCMT displayed a gradual increase in the swelling capacity of the outer polymer shell up to 3 hours as was apparent by the increase in the area and intensity of the white region. Following 30min, a clear infiltration of the SHIF into the core region was noticeable by the appearance of a grey area (50% hydration). The initial high swelling capacity of the outer polymer shell together with the slow infiltration of the core facilitated the release of the incorporated peptide. The border between the hydrated and non-hydrated region is known as the swelling front. Between 3-4hrs no significant increase in the hydration was noted, attributed to the formation of the crosslinked interface *in situ* which subsequently decreased the swelling capacity.

A slight collapsing of the OCMT after 4 hours was indicative of the relaxation and loose distribution of the polymer chains, promoting the surface erosion of the OCMT. The erosion front presented as a liquid layer of loosely distributed polymer chains between the simulated fluid and the gelled layer of the tablet. Complete hydration and continued surface erosion of the OMCT progressed up to 24 hours. MRI provided insight into the behavior of the OCMT's hydrating polymeric matrix both *in vitro* and *in vivo*. The resultant images not only provided structural confirmation of the layering of the tablet but also incidentally mirrored the swelling and erosional behavior observed in Figure 5.8. These hydrational transitions suggest that the release of the peptide from the core of the OCMT may be based on a complex interplay between swelling, *in situ* crosslinking and surface erosion.

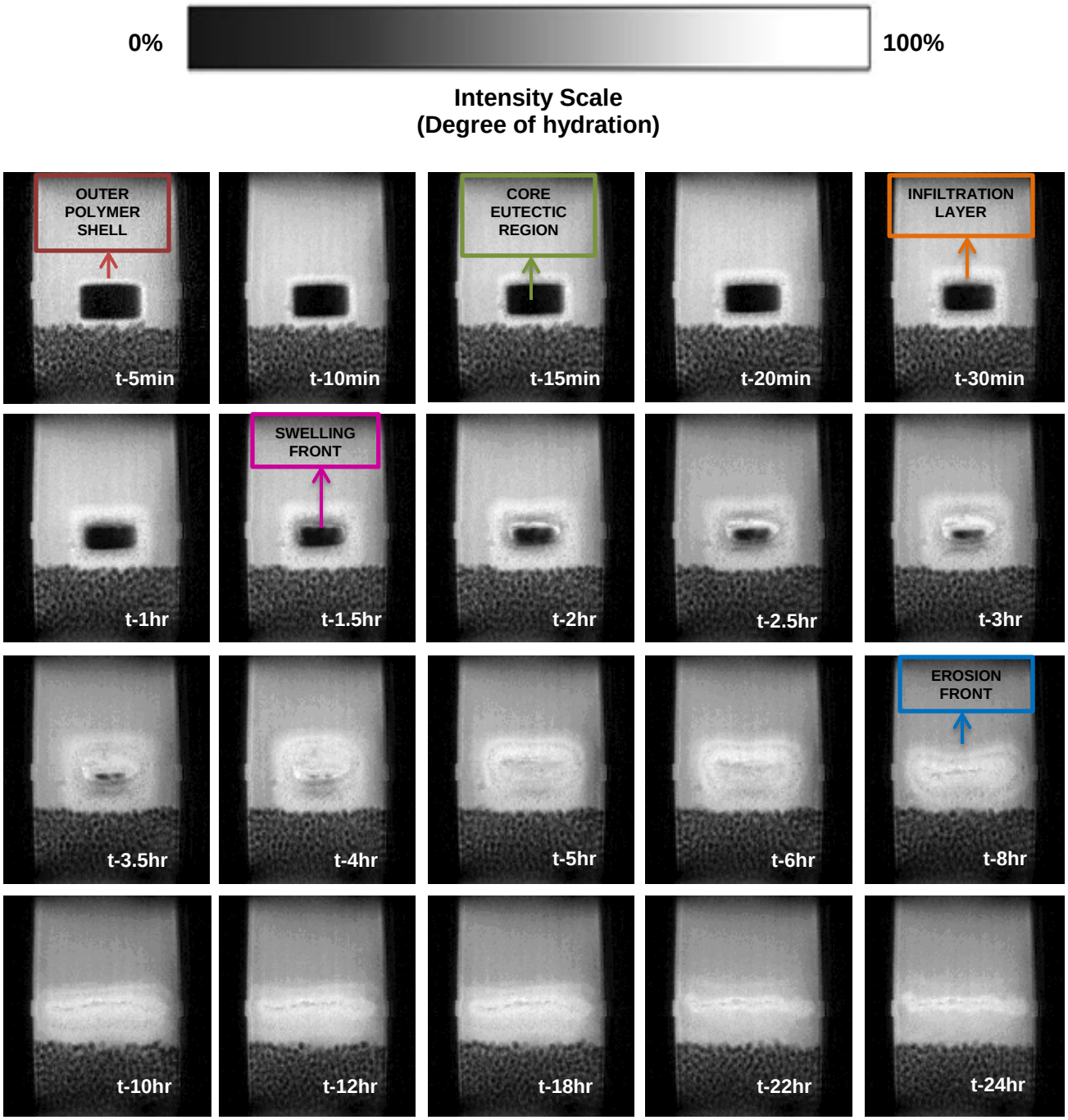

Figure 5.12: MRI of the OCMT over 24 hours with the intensity scale indicating the degree of hydration from 0% (non-hydrated) to 100% (hydrated).

5.3.10. *In vitro* peptide release analysis

The peptide release patterns of Octreotide from the optimized OCMT were obtained through evaluation of its experimental release in SHIF (pH 6.8). The concentration at each time point was evaluated utilizing an EIA according to the kits standard operating procedure. The standard

curve generated a 4-parameter logistic curve fit as a function of the OD (Optical Density) versus the log concentration. The parameters obtained from the 4-P fit were used to calculate the unknown concentrations of the experimental samples. Results were displayed as a function of fractional release against time as shown in Figure 5.13a. A sustained release of Octreotide over the 24-study period was noted.

The initial burst release within the first 3 hours was attributed to the OCMT's porous nature which facilitated the high swelling capacity observed in Figure 5.8a and the MRI images obtained. The release of the peptide slowed following 3 hours, corresponding to the decreased water uptake. This was attributed to the process of *in situ* crosslinking, assisted by the characteristic softening of the core eutectic region at 37°C as demonstrated by the rheological profiles in Figure 5.5. The peptide release pattern alternated between phases of slow and burst release for up to 8 hours, followed by a more stable release profile up to 24 hours. The characteristic peptide release profile obtained was attributed to the combined effects of swelling, surface erosion and *in situ* crosslinking.

Owing to the amorphous nature of the EPB as highlighted previously in Choonara *et al*, (2016), an enhanced dissolution and subsequent fractional release up to ±0.8 was noted. Furthermore, the mean dissolution time (MDT) of the OCMT provided information about the peptide release rate (Wadher *et al.,* 2011; Sathish and Syed, 2013). The MDT for the optimized formulation was 18.76 which ideally fell within the range of the desired targeted response (18.93) for the optimum formulation at the optimal concentrations of crosslinkers ($NaCO_3$ and K_2HPO_4), pectin and EPB as displayed in Figure 5.13b-c. The optimum amounts of EPB (60mg) and crosslinkers (115mg) represented in Figure 5.13b-c corresponds to the optimal concentrations of 12%$^{w}/_{w}$ and 23%$^{w}/_{w}$, respectively, as highlighted in Figure 5.1. The MDT further corroborated the role of the *in situ* crosslinking process in producing a slower release rate. The achievement of the optimum MDT confirms the appropriateness of the design in producing the desired responses from an optimum formulation. Summative assessment revealed that the combinatory effects of different physicochemical and physicomechanical processes ultimately influenced the peptide release behavior observed.

Moreover, the peptide release results were fitted into various kinetic models in order to determine the mechanism of release. The best-fit model for the peptide release data observed was based on the kinetic modelling of the regression coefficients and its proximity to the

numeral 1. A model depicting a value closest to 1 amongst the formulations would demonstrate the appropriateness of that model in explaining the peptide release mechanism. The release data was fitted into zero-order, first order, Higuchi and Korsmeyer–Peppas models. The best-fit model for the peptide release data was the Higuchi model (R^2=0.98) which describes the release of the peptide from a matrix as a function of the square-root of a time-dependent process based on Fickian diffusion. Interestingly, the release data was very close to zero-order release (R^2=0.95) and thus, the release kinetics may best be attributed to a combination of both models as a result of the complexity of the system.

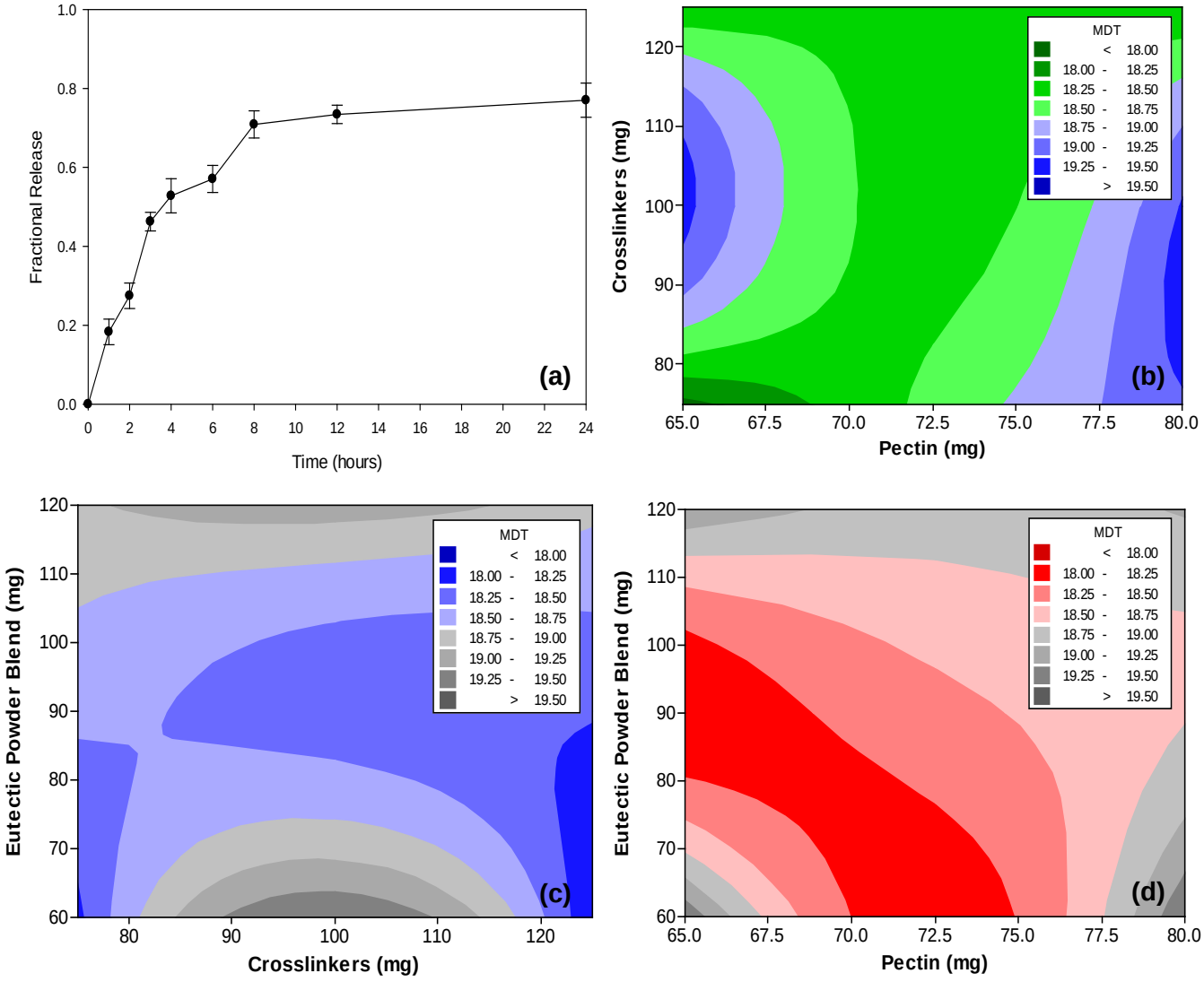

Figure 5.13: Profiles displaying: **a)** the fractional release of Octreotide from the optimized OCMT and **b-c)** contour plots depicting the effect of the crosslinkers ($NaCO_3$ and K_2HPO_4), EPB and pectin concentrations on the MDT response.

5.4. Concluding Remarks

The OCMT was optimized for the oral delivery of gastro-sensitive proteins and synthetic peptides. The in-depth physicochemical and physicomechanical characterization of the OCMT revealed the suitability of the design in producing an optimum formulation that delivers on its characteristic functions. Oscillatory studies highlighted the temperature-responsive rheological behavior of the EPB and its correlation to previously described thermal transitions. FTIR results highlighted the presence of *in situ* crosslinking due to intra and inter-molecular interactions, initiated by the chemical crosslinkers. Physicomechanical profiling provided an indication of the multi-textural properties of the OCMT. Comprehensive porositometric and morphological analysis provided information about the internal architecture of the OCMT, revealed its effect on fluid uptake and subsequently the peptide release characteristics. This was corroborated with MRI which highlighted the device hydration over 24 hours as a significant predictor of the *in vitro* peptide release profile. The *in vitro* release of Octreotide was influenced by the combined effects of swelling, surface erosion and *in situ* crosslinking, displaying a fractional release up to ±0.8. Owing to the complexity of the system, the mechanism of release was attributable to both the zero-order (R^2=0.95) and Higuchi models (R^2=0.98). Thus, physicochemical and physicomechanical characterization was necessary to confirm the suitability of the OCMT *in vitro* before proceeding to incorporation of components for Tri-functionalization, discussed in Chapter 6.

5.5. References

Bhaskar, G., Ford, J.L., Hollinsbee, D.A. (1998). Thermal analysis of the water uptake by hydrocolloids. *Thermochimica Acta,* 322, 153-165.

Carbinatto, F.M., Castro, A.D., Evangelista, R.C., Cury, B.S.F. (2014). Insights into the swelling process and drug release mechanisms from cross-linked pectin/high amylose starch matrices. *Asian Journal of Pharmaceutical Sciences,* 9, 27-34.

Carreras, J.J., Canales, P., Melero, A. (2016). Mucoadhesion of Polymeric Drug Delivery Systems: Polymeric Nanoparticles and its Interactions with the Intestinal Barrier. *JSM Nanotechnology and Nanomedicine,* 4, 1041.

Carvalho, F.C., Bruschi, M.L., Evangelista, R.C., Gremiao, M.P.D. (2010). Mucoadhesive drug delivery systems. *Brazilian Journal of Pharmaceutical Sciences*, 46, 1-17.

Cevher, E., Sensoy, D., Taha, M.A.M., Araman, A. (2008). Effect of Thiolated Polymers to Textural and Mucoadhesive Properties of Vaginal Gel Formulations Prepared with Polycarbophil and Chitosan. *AAPS PharmSciTech,* 9, 953-965.

Chen, T., Miller, T.F., Prasad, P., Lee, J., Krauss, J., Miscik, K., Kalafsky, G., McLeod, J.F. (2000). Pharmacokinetics, Pharmacodynamics, and safety of microencapsulated Octreotide Acetate in healthy subjects. *Journal of Clinical Pharmacology*, 40, 1-7.

Chin, J., Mahmud, K.A.F., Kim, S.E., Park, K., Byun, Y. (2012). Insight of current technologies for oral delivery of proteins and peptides. *Drug Discovery Today Technologies*, 9, 105–112.

Choonara, B.F., Choonara, Y.E., Kumar, P., du Toit, L.C., Pillay, V. (2016). Design of an *in situ* cross-linked eutectic tablet for enhanced delivery of gastro-sensitive proteins and peptides. *Journal of Pharmaceutical Sciences*, 105, 2086-2098.

Coates, J. (2000). *Interpretation of Infrared Spectra, A Practical Approach*. UK, Chichester: John Wiley and Sons Ltd. pp. 10815-10837.

Crouter, A., Briens, L. (2014). The Effect of Moisture on the Flowability of Pharmaceutical Excipients. *AAPS PharmSciTech,* 15, 65-74.

Dorozynski, P.P., Kulinowski, P., Mlynarczyk, A., Stanisz, G.J. (2012). Foundation review: MRI as a tool for evaluation of oral controlled release dosage forms. *Drug Discovery Today,* 17, 110-123.

Foo, K.Y., Hameed, B.H. (2010). Insights into the modeling of adsorption isotherm systems. *Chemical Engineering Journal,* 156, 2-10.

Gerhardt, A.H. (2009). Moisture Effects on Solid Dosage Forms—Formulation, Processing, and Stability. *Journal of GXP Compliance,* 13, 58-66.

Groen, J.C., Peffer, L.A.A., Pérez-Ramírez, J. (2003). Pore size determination in modified micro- and mesoporous materials. Pitfalls and limitations in gas adsorption data analysis. *Microporous and Mesoporous Materials,* 60, 1-17.

He, P., Davis, S.S., Illum, L. (1998). . *In vitro* evaluation of the mucoadhesive properties of chitosan microspheres. *International Journal of Pharmaceutics*, 166, 68-75.

Hyun, K., Nam J.G., Wilhellm, M., Ahn, K.H., Lee, S.J. (2006). Large amplitude oscillatory shear behavior of PEO-PPO-PEO triblock copolymer solutions. *Rheologica Acta,* 45, 239–249.

Jabarian, L.E., Rouini, M.R., Atyabi, F., Fouroumadi, A., Nassiri, S.M., Dinarvand, R. (2012). In vitro and in vivo evaluation of an in situ gel forming system for the delivery of PEGylated octreotide. *European Journal of Pharmaceutical Sciences*, 48, 87-96.

Jones, D.S. (1999). Dynamic mechanical analysis of polymeric systems of pharmaceutical and biomedical significance. *International Journal of Pharmaceutics,* 179, 167-178.

Lee, J.W., Park, J.H., Robinson, J.R. (2000). Bioadhesive-based dosage forms: The next generation. *Journal of Pharmaceutical Sciences,* 89, 850-866.

Lippacher, A., Müller, R.H., Mäder, K. (2002). Semisolid SLN™ dispersions for topical application: influence of formulation and production parameters on viscoelastic properties. *European Journal of Pharmaceutics and Biopharmaceutics,* 53, 155-160.

Lippacher, A., Müller, R.H., Mäder, K. (2004). Liquid and semisolid SLN™ dispersions for topical application: rheological characterization. *European Journal of Pharmaceutics and Biopharmaceutics,* 58, 561-567.

Mahkam, M., Doostie, L. (2008). The relationship between swelling properties and cross-linking of hydrogels designed for colon-specific delivery. *Drug Delivery*, 12, 343-347.

Manconia, M., Muraa, S., Manca, M.L., Fadda, A.M., Dolz, M., Hernandez, M.J.,Casanovas, A., Diez-Sales, O. (2010). Chitosomes as drug delivery systems for C-phycocyanin: Preparation and characterization. *International Journal of Pharmaceutics,* 392, 92–100*.*

Mansuri, S., Kesharwani, P., Jain, K., Tekade, R.K., Jain, N.K. (2016) Mucoadhesion: A promising approach in drug delivery system. *Reactive and Functional Polymers,* 100, 151–172.

Menard, K.P. (2008). *Dynamic Mechanical Analysis: A Practical Introduction. 2nd ed.* USA, Boca Raton: CRC Press. pp. 1-11.

Nokhodchi, A. (2005). An Overview of the Effect of Moisture on Compaction and Compression. *Tablets & Capsules*, 29, 46-66.

Park, K., Kwan, I.C., Park, K. (2011). Oral protein delivery: current status and future prospect. *Reactive Functional Polymer*, 71, 280–287.

Rane, M., Parma, J., Tiwari, S., Rajabi-Siahboomi, A. (2013). Application of Polyethylene Oxide in Hydrophilic Matrix Tablets. *Pharma Time,* 45, 41-48.

Richardson, J.C., Bowtell, R.W., Mäder, K., Melia, C.D. (2005). Pharmaceutical applications of magnetic resonance imaging (MRI). *Advanced Drug Delivery Reviews*, 57, 1191– 1209.

Sanwichien, C., Aranovich, G.L., Donuhue, M.D. (2002). Density functional theory predictions of adsorption isotherms with hysteresis loops. *Colloids and Surfaces A: Physicochemical and Engineering Aspect,* 206, 313-320.

Sathish, U., Syed, I.A. (2013). Formulation and characterization of matrix and triple layer matrix tablets for controlled delivery of tramadol hydrochloride. *International Journal of Pharmaceutical Sciences*, 5, 458-464.

Sathish, U., Syed, I.A. (2013). Formulation and characterization of matrix and triple layer matrix tablets for controlled delivery of tramadol hydrochloride*. International Journal of Pharmaceutical Sciences,* 5, 458-464.

Scholz, E. (1982). Karl-Fischer Reagentien ohne Pyridin. Zweikomponenten Reagentien mit Imidazol. *Fresenius Journal of Analytical Chemistry,* 312, 460-464.

Sing, K.S.W., Everett, D.H., Haul, R.A.W., Moscou, L., Pierotti, R.A., Rouquerol, J., Seimienewska, T. (1985). Reporting physisorption data for gas-solid systems. *Pure and Applied Chemistry*, 57, 603-619.

Sing, K.S.W., Everett, D.H., Haul, R.A.W., Moscou, L., Pierotti, R.A., Rouquerol, J., Siemieniewska, T. (1985). Reporting Physisorption Data for Gas/Solid Systems with Special Reference to the Determination of Surface Area and Porosity. *Pure and Applied Chemistry,* 57, 603-619.

Sing, K.S.W., Williams, R.T. (2004). Physisorption Hysteresis Loops and the Characterization of Nanoporous Materials. *Adsorption Science and Technology,* 22, 773-782.

Singh, I., Rana, V. (2012). Techniques for the Assessment of Mucoadhesion in Drug Delivery Systems: An Overview. *Journal of Adhesion Science and Technology*, 26, 2251-2267.

Sreedhar, B., Satya, V.C., Devi, K., Basaveswara, R.M.V., Rambabu, C. (2012). Shape Controlled Synthesis of Barium Carbonate Microclusters and Nanocrystallites using Natural Polysachharide – Gum Acacia. *American Journal of Materials Science*, 2, 5-13.

Sriamorsak, P., Thirawong, N., Weerapol, Y., Nunthanid, J., Sungthongjeen, S. (2007). Swelling and erosion of pectin matrix tablets and their impact on drug release behavior. *European Journal of Pharmaceutics and Biopharmaceutics,* 67, 211-219.

Tai, A., Bianchini, R., Jachowicz, J. (2014). Texture analysis of cosmetic/pharmaceutical raw materials and formulations. *International Journal of Cosmic Science,* 36, 291–304.

Tajiri, T., Morita, S., Sakamoto, R., Suzuki, M., Yamanashi, S., Ozaki, Y., Kitamura, S. (2010). Release mechanisms of acetaminophen from polyethylene oxide/polyethylene glycol matrix tablets utilizing magnetic resonance imaging*. International Journal of Pharmaceutics,* 395, 147-153.

Tuvia, S., Atsmon, J., Teichman, S.L., Katz, S., Salama, P., Pelled, P.D., et al. (2012) Oral octreotide absorption in human subjects: comparable pharmacokinetics to parenteral octreotide and effective growth hormone suppression. *Journal of Clinical Endocrinology and Metabolism*, 97, 1–8.

Vlachou, M., Naseef, H., Efentakis, M., Tarantili, A., Andreopoulos, G. (2001). Swelling Properties of Various Polymers Used in Controlled Release Systems. *Journal of Biomaterials Application,* 16, 125-38.

Wadher, K.J., Kakde, R.B., Umekhar, M.J. (2011). Study on sustained-release metformin hydrochloride from matrix tablet: Influence of hydrophilic polymers and *in vitro* evaluation. *International Journal of Pharmaceutical Investigation*, 1, 157-163.

Ward, I.M., Hadley, D.W. (1993). *An Introduction to the Mechanical Properties of Solid Polymer.* UK, Chichester: John Wiley and Sons. pp. 354.

White, J.L. (1990). *Principles of Polymer Engineering Rheology*. New York, USA: John Wiley & Sons, pp. 3-20.

CHAPTER 6

DESIGN OF THE CO-INHIBITORY 'SMART' POLYMERIC SHEET SURROUNDING A pH-MODIFIED OCMT FOR TRI-FUNCTIONALIZATION

To be submitted to Journal of Controlled Release

Bibi F. Choonara, Yahya E. Choonara, Pradeep Kumar, Lisa C. du Toit, Viness Pillay. Design of the Co-inhibitory 'Smart' Polymeric Sheet Surrounding a pH-Modified OCMT for Tri-Functionalization.

Abstract

An experimental design of the pH_M 'smart' polymeric sheet encapsulated-OCMT for tri-functionalization in the delivery of gastro-sensitive therapeutic proteins and synthetic peptides was investigated. Physicochemical and physicomechanical characterization techniques were undertaken to determine pertinent interactions of the incorporated co-inhibitor with CYP3A4 and P-glycoprotein (Pgp). In addition, the micro-environmental pH demonstrated the pH-lowering effects of citric acid and its potential in reducing the optimal environment for brush border enzyme activity. Comprehensive analysis of the 'smart' polymeric sheet via analysis of the rheological profile, mucoadhesion and physicomechanical strength and elasticity confirmed the favorable characteristics of prolamines in drug delivery applications. The *in vitro* release of Octreotide was influenced by the combined effects of swelling, surface erosion and *in situ* crosslinking, displaying fractional releases ranging from 0.79-0.89. Due to the complexity of the system, the release kinetics was attributed to both the Higuchi (R^2=0.98) and zero-order (R^2=0.97) models. Conclusive results from physicochemical and physicomechanical characterization of the design demonstrated the applicability of the pH_M 'smart' polymeric sheet encapsulated-OCMTs to provide tri-functionalization.

Keywords: oral peptide delivery; prolamines; CYP3A4; Pgp; pH modifier; physicochemical properties; physicomechanical properties

6.1. Introduction

Therapeutic protein and peptide drugs are currently administered by the less desirable parenteral routes of administration, resulting from the poor to limited oral bioavailability associated with their orally administered biotech-based pharmaceutical counterparts (Mahato *et al*., 2003). Technologies that have been used to improve the oral bioavailability of proteins and peptides are based on specific approaches as highlighted in Choonara *et al*, (2014). The approaches are primarily focused on preventing acid-based degradation and promoting epithelial permeability of proteins and peptides. Research in this field has intensified as pharmaceutical scientists vie for the opportunity to achieve the maximum oral absorption of proteins and peptides and consequently attain an optimum oral bioavailability (Arhewoh *et al.,* 2005).

The enzymatic degradation of proteins and peptides within the acidic environment of the stomach has been well documented. However, the role of the small intestine in the degradative process cannot be discounted, as the brush border membrane accounts for a significant amount of the protein and peptide degradation that occurs (Carino *et al*., 1999; Bruno *et al*., 2013). The brush border is a microvilli-covered surface of cells that express brush border enzymes such as exo- and endopeptidases (Mahato *et al.,* 2003). These enzymes contribute towards the cleavage of proteins and peptides into non-essential amino acids (Zhou 1994; Lee, 2002). This poses a significant enzymatic barrier and as a result is often a target for the successful development of oral protein and peptide technologies.

In addition, the inter-relationship and combined action of cytochrome P450 and the multidrug resistance transporter P-glycoprotein (Pgp) presents a formidable hindrance towards the achievement of an optimum oral bioavailability of proteins and peptides (Wacher *et al*., 1998; Bruno *et al*., 2013). The isoform CYP3A4 is predominantly expressed in the human intestine and is a member of the cytochrome P450 CYP3A family, accounting for the metabolism of ±50-70% of all administered drugs (Wacher *et al*., 1998; Mahato *et al*., 2003). Pgp is an ATP-dependent transporter, responsible for the efflux of drugs back into the intestinal lumen as they are being absorbed through the intestinal mucosa (Wacher *et al*., 1998). The shared location of CYP3A4 and Pgp within the small intestinal enterocytes promotes its synergistic action in reducing the oral bioavailability common to their substrate specificities (Mahato *et al*., 2003). Therefore, the inhibition of CYP3A4, Pgp or both may favorably improve the oral bioavailability of proteins and peptides.

The platform on which the OCMT is based, as highlighted previously in Choonara *et al,* (2016), enables the incorporation of a pH modifier into the outer polymer shell to facilitate the indirect inhibition of enzyme activity at the brush border by transiently lowering the micro-environmental pH and subsequently reducing the optimal environment for enzyme activity (Badawy and Hussain, 2006; Tatarvati and Hoag, 2006). Furthermore, a co-inhibitor containing prolamine-based 'smart' polymeric sheet encapsulates the OCMT. The co-inhibition of CYP3A4 and the Pgp efflux pump functions to reduce the metabolism and inhibit transmembrane efflux. In addition, the sheet possesses the inherent capabilities that enable it to interact well with hydrophilic molecules (i.e. proteins and peptides), allowing the passage of proteins and peptides through the GIT membrane and providing a protective function within the stomach.

This characteristic design imparts tri-functionalization capabilities that are expected to significantly improve the oral bioavailability. Thus, the determination of the physicochemical and physicomechanical properties of the advanced OCMT is a prerequisite in defining the performance of the device *in situ.* A Face-Centered Central Composite Design (FCCCD) generated a series of 13 formulations which were all synthesized and analyzed for their individual properties. Analysis of the advanced OCMT components included the determination of the optimum co-inhibitory potential, measurement of the changes to the micro-environmental pH, gastric acid resistance, mucoadhesion, rheological properties and in depth textural analysis. Ultimately, these investigations would determine the suitability of the advanced OCMT to deliver on its purported capabilities.

6.2. Materials and Methods

6.2.1. Materials

Menthol (2-isopropyl-5-methylcyclohexanol, 99% purity, M_W=156,27g/mol), cetomacrogol 1000, poly (ethylene oxide) (PEO) (Polyox™, WSR-303), polyoxyethylene (40) stearate (Myrj® 52), Zein (from maize) and excipients, sodium carboxymethylcellulose (CMC), magnesium stearate and sucrose were purchased from Sigma-Aldrich Corp. (St. Louis, MO, USA). The crosslinker sodium carbonate ($NaCO_3$) was purchased from Associated Chemical Enterprises (ACE) (Pty) Ltd. (Johannesburg, Gauteng, South Africa). Pectin citrous (poly-D-galacturonic acid methyl ester), the crosslinker di-potassium hydrogen orthophosphate anhydrous (K_2HPO_4; M_W=174.18g/mol), citric acid (≥99.5% purity, M_W=210.14g/mol), methyl paraben (methyl 4-hydrozybenzoate, M_W=152.15g/mol) and polypropylene glycol (1, 2–propanediol) were procured

from Merck Chemicals (Pty) Ltd. (Modderfontein, Gauteng, South Africa). Octreotide acetate ($C_{49}H_{66}N_{10}O_{10}S_2$; M_w=1019.247g/mol) was purchased from Bolon Pharmachem Co., Ltd. (Taizhou, Zheijang, China). Cytochrome P450 3A4 (CYP3A4) inhibitor screening kit (fluorometric) and MDR assay kit (fluorometric) were purchased from Peninsula Laboratories International , Inc. (San Carlos, CA, USA). Caco-2 cell line (ATCC® HTB-37™), Dulbecco's Modified Eagle's Medium (DMEM), Foetal bovine serum (FBS), Penicillin-streptomycin, Trypsin-EDTA (0.25mg/mL) and all other cell culture components were purchased from Separations (Pty) Ltd. (Randburg, Gauteng, South Africa). All other reagents were of analytical grade and were employed as received.

6.2.2. Formulation of the pH-modified (pH_M) OCMT

The OCMT was prepared according to the method prescribed in Choonara *et al*, (2016) comprising an outer polymer shell surrounding a core eutectic region. The core eutectic region of the tablet consisted of a compressed combination of; 12%$^w/_w$ Eutectic Powder Blend (EPB), 23%$^w/_w$ of crosslinking agents ($NaCO_3$ and K_2HPO_4) and 20mg Octreotide. The outer polymer shell consisted of a top and bottom layer each containing a polymeric blend of 100mg each of PEO, 65mg pectin, 12mg of CMC and 1mg of magnesium stearate. In addition, the pH modifier (citric acid) was incorporated into the outer polymer shell in concentrations ranging between the upper (10mg) and lower (5mg) limits generated from the FCCCD (Minitab®V15 statistical software, Minitab®Inc., PA, USA) as shown in Table 6.1.

The OCMT with incorporated pH modifier was assembled by directly compressing the polymeric powder blend of the bottom layer at 2 tons of pressure using a Carver Tableting Press (Wabash, Indiana, USA) loaded with punch and dies with a diameter of 10mm to produce a loosely compressed layer. The core eutectic tablet was subsequently placed above this layer and centered using the tip of a needle. The polymeric powder blend for the top layer of the tablet was added above the core eutectic tablet and levelled out. The punch was then inserted and the tablet was compressed at 5 tons of pressure using a Carver Tableting Press (Wabash, Indiana, USA) fitted with a flat-faced punch and die (diameter of 10mm) to produce the pH_M-OCMT. To minimize processing variables, all tablets were produced under identical conditions.

6.2.3. Synthesis of the prolamine-based 'smart' polymeric sheet

The 'smart' polymeric sheet was prepared by dissolving varying concentrations of Zein (%$^w/_v$), as shown in Table 6.1, in a 70%$^v/_v$ aqueous ethanol solution. The solution underwent constant

magnetic stirring at 300rpm for ±2 hours. Following ±2hours, propylene glycol (20%$^{v}/_{v}$) and a methyl paraben (0.2%$^{w}/_{v}$) solution was added to the formulation to function as a plasticizer and preservative, respectively. The resultant solution underwent further stirring at 300rpm for ±30minutes to ensure complete mixing and a homogenous distribution.

Table 6.1: Component concentrations generated from a Face-Centered Central Composite Design (FCCCD)

Formulation No.	Zein (%$^{w}/_{v}$)	Citric acid (mg)
1	20	10
2	20	5
3	17.5	5
4	17.5	7.5
5	15	5
6	17.5	10
7	15	7.5
8	15	10
9	20	7.5
10	17.5	7.5
11	17.5	7.5
12	17.5	7.5
13	17.5	7.5

6.2.4. Encapsulation of the pH_M-OCMT with the co-inhibitory 'smart' polymeric sheet

The encapsulation of the OCMT with the polymeric sheet was processed by a simple 'dip' and 'dry' method, typically used in the coating of tablets. The experimentally determined optimal concentration of the co-inhibitor (polyoxyethylene (40) stearate) was dissolved in 1mL of the 'smart' polymeric sheet solution. The resultant mixture was divided into equal amounts (0.5mL each) and placed in a 48-well microplate (well diameter-11.0mm) for dip encapsulation of both sides of the OCMT. The OCMT was dipped into the co-inhibitory polymeric sheet solution, placed on a petri dish and dried in a laboratory fumehood for ±15 minutes. This process was repeated several times for both sides of the OCMT until the solution was completely finished. Following the final coating, the OCMT was left to dry overnight to produce the thick, dried 'smart' polymeric sheet encapsulating the OCMT. A schematic of the advanced OCMT with the co-inhibitory 'smart' polymeric sheet is shown in Figure 6.1.

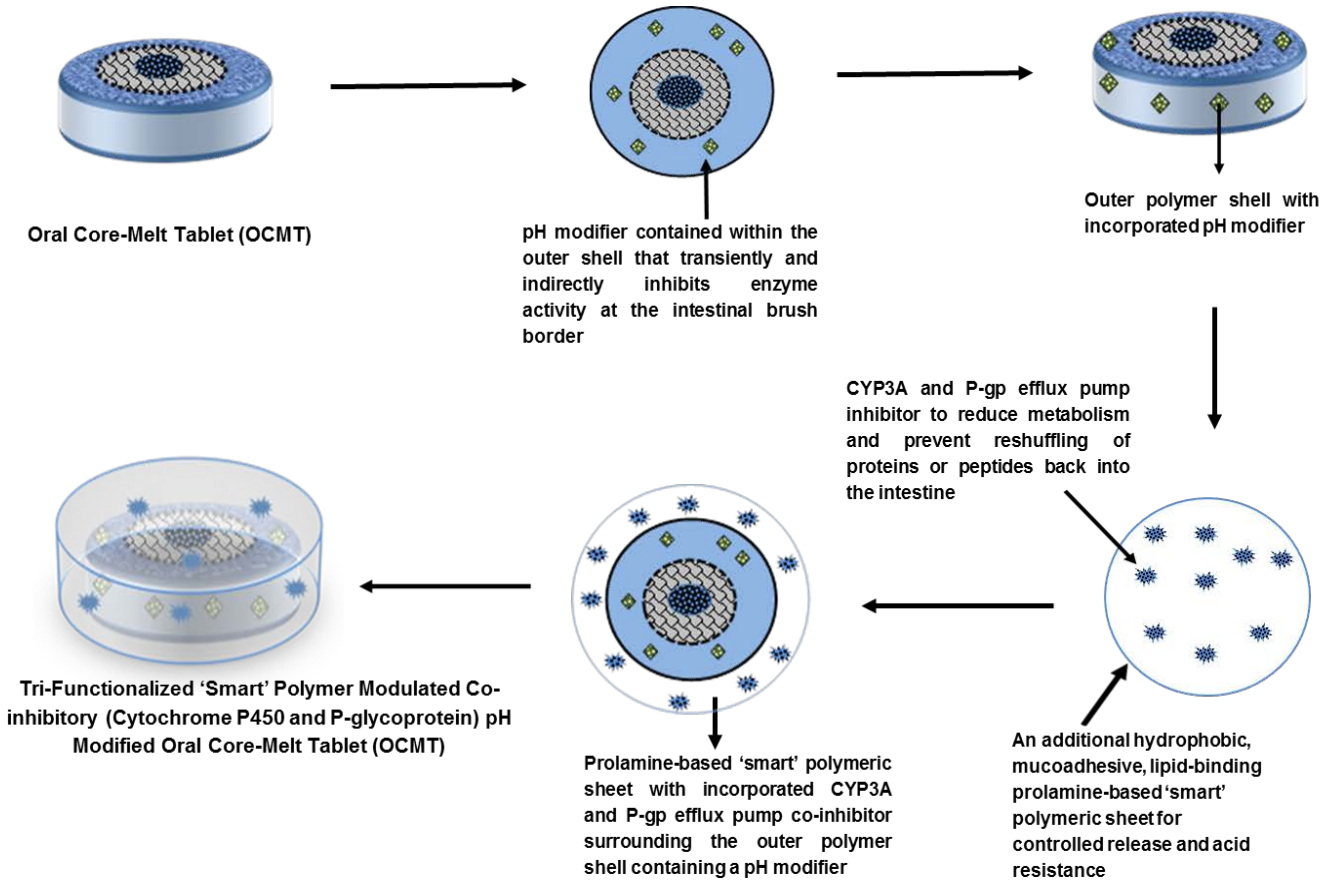

Figure 6.1: Annotated schematic of the characteristic features and functions of the advanced components of the OCMT.

6.2.5. Determination of the optimal Inhibitory Concentration (IC) of the co-inhibitor

6.2.5.1. Measurement of the polyoxyethylene (40) stearate-CYP3A4 interaction

A fluorometric Cytochrome P450 3A4 (CYP3A4) inhibitor screening kit (BioVision Incorporated, Milpitas, CA, USA) was used to quantitatively determine the optimal concentration required to inhibit CYP3A4. The assay utilized a non-fluorescent CYP3A4 substrate that was converted into a highly fluorescent metabolite detectable in the visible range (Ex/Em=535/587nm) as shown in Figure 6.2. The assay kit provided a rapid, high-throughput screening of the interaction between polyoxyethylene (40) stearate and CYP3A4 and was prepared according to the kits standard protocol which involved: a) the standard curve preparation, b) test compound and CYP3A4 enzyme preparation, c) reaction preparation, d) measurement and e) calculation.

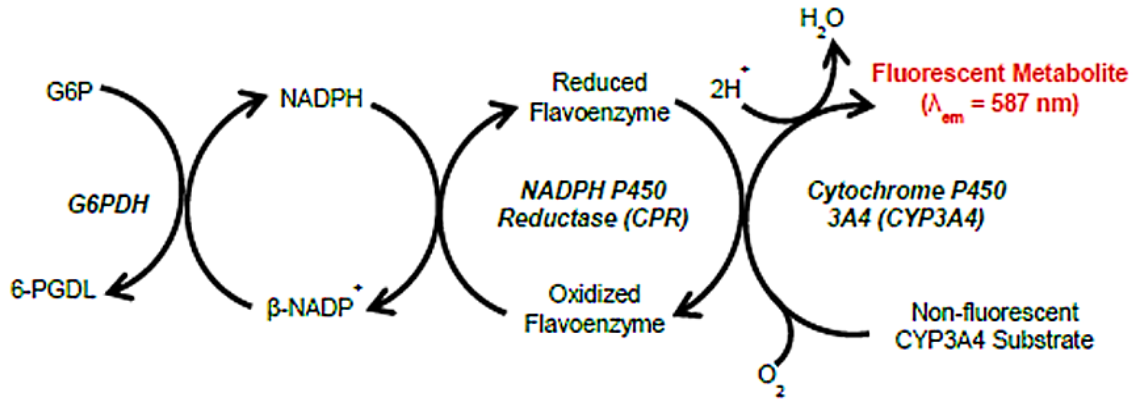

Figure 6.2: The mechanism of the enzyme catalyzed reaction utilized by the assay, depicting the conversion of the non-fluorescent substrate to the highly fluorescent metabolite in the presence of CYP3A4 (BioVision Incorporated CYP3A4 Inhibitor Screening Kit Protocol #K702-200).

a) Standard curve preparation: The Resorufin standard provided with the kit was dissolved in CYP3A4 Assay buffer to generate a final concentration of 1pmol/µL. This resorufin standard was added to a series of wells and adjusted to 100µL with CYP assay buffer to yield a standard curve of 0, 4, 8, 12, 16, 20, 30 and 40 pmole/well of resorufin. The fluorescence was measured at Ex/Em= 535/587nm and the plot of the background-subtracted values were used to calculate the slope of the standard curve.

b) Polyoxethylene (40) stearate and CYP3A4 Enzyme preparation: The polyoxyethylene (40) stearate was dissolved in a $1\%^{v}/_{v}$ acetonitrile: CYP3A4 assay buffer to produce a stock solution. The stock solution was used to prepare a 5X solution of a range of concentrations from 0.02mg/mL-10mg/mL (Table 6.2) in order to generate a multi-point dose-response curve. The CYP3A4 enzyme stock was prepared by reconstituting the Recombinant Human CYP3A4 stock (2X) with 1mL of CYP3A4 buffer which was mixed thoroughly until a homogenous solution was formed. The solution was transferred to a 15mL conical tube and was subsequently brought up to a volume of 4.9mL with CYP3A4 assay buffer. The addition of 100µL of the NADPH generating system (100X) yielded a final total volume of 5mL of CYP3A4 enzyme stock.

Table 6.2: Sample concentrations of polyoxyethylene (40) stearate prepared.

Sample No.	Concentration (mg/mL)
1	10
2	8.5
3	7.5
4	6.5
5	6
6	5.5
7	5
8	4.5
9	3.5
10	2.5
11	1
12	0.5
13	0.25
14	0.13
15	0.06
16	0.03
17	0.02

c) Reaction preparation: The reaction wells containing Test Compounds (TC), Solvent Control (SC), Background Control (BC) and Positive Inhibition Controls (PIC) were set up according to Table 6.3. Following preparation, the plate was incubated for 5-10min to allow the test compounds to permeate the microsomal membranes and interact with CYP3A4 in the absence of P450 catalytic turnover. During incubation, a CYP3A4 Substrate/ NADP+ mixture (3X) was prepared. The reaction was started by adding 30µl of the CYP3A4 Substrate/ NADP+ mixture (3X) to each well using a multichannel pipette to yield a final reaction volume of 100µL/well.

Table 6.3: Preparation of reactions wells for CYP3A4 assay

	BC	SC	PIC	TC
CYP3A4 Enzyme Stock (2X)	-	50µL	50µL	50µL
Polyoxyethylene 40 stearate solution (5X)	-	-	-	20uL
Ketoconazole 150Mm solution (5X)	-	-	20µL	-
Acetonitrile: CYP3A4 assay buffer (1%$^{v}/_{v}$)	-	20µL	-	-
CYP3A4 assay buffer (+5X solvent)	70µL	-	-	-

d) Measurement: The fluorescence was measured immediately (within 1 min) at Ex/Em=535/587nm in kinetic mode for 45min using a Synergy HT multiwell fluorescence microplate reader equipped with curve fitting software (BioTek® Instruments, Winooski, Vermont, USA).

e) Calculation: For each reaction, two time points (T_1 and T_2) in the linear phase of the reaction progress curve was selected and the corresponding fluorescence values at these time points (RFU_1 and RFU_2) were used to calculate the rate of change in fluorescence ($\Delta F/\Delta T$):

$$\frac{\Delta F}{\Delta T} = \frac{RFU_2 - RFU_1}{T_2 - T_1} \quad \textbf{(6.1)}$$

Subsequently, the rate of the BC wells was subtracted from the rates of each of the SC and TC wells to determine the background-corrected reaction rates for each well:

$$R_{SC} = \frac{\Delta F_{SC}}{\Delta T_{SC}} - \frac{\Delta F_{BC}}{\Delta T_{BC}} \quad \textbf{(6.2)}$$

Where, R_{SC} is the background-corrected reaction rate of the solvent control, $\frac{\Delta F_{SC}}{\Delta T_{SC}}$ is the rate of change in fluorescence of the solvent control and $\frac{\Delta F_{BC}}{\Delta T_{BC}}$ is the rate of change in fluorescence of the background control

$$R_{TC} = \frac{\Delta F_{TC}}{\Delta T_{TC}} - \frac{\Delta F_{BC}}{\Delta T_{BC}} \quad \textbf{(6.3)}$$

Where, R_{TC} is the background-corrected reaction rate of the test compound, $\frac{\Delta F_{TC}}{\Delta T_{TC}}$ is the rate of change in fluorescence of the test compound and $\frac{\Delta F_{BC}}{\Delta T_{BC}}$ is the rate of change in fluorescence of the background control

These values were used to calculate the relative percentage inhibition of the different concentrations of test compound according to Equation 6.4.

$$\%\ \text{Relative inhibition} = \frac{R_{SC} - R_{TC}}{R_{SC}} \times 100 \quad \textbf{(6.4)}$$

Where, R_{SC} is the background-corrected reaction rate of the solvent control and R_{TC} is the background-corrected reaction rate of the test compounds.

The reaction rate calculations can also be expressed in terms of pmole resorufin formed per unit time per unit amount of protein by interpolation from the standard curve.

6.2.5.2. Measurement of the polyoxyethylene (40) stearate-Pgp interaction

A fluorometric Multi-drug Resistant (MDR) assay kit (abcam®, USA) was used to determine the interaction between the co-inhibitor and Pgp. Pgp is an MDR1 transporter and thus, a fluorescent MDR indicator was used for assaying the MDR pump activity. The hydrophobic fluorescent dye molecule rapidly penetrates cell membranes and becomes trapped in cells, providing a high-throughput screening of MDR pump inhibitors. The assay was prepared according to the kits standard protocol and involved: a) the preparation of cells, b) preparation of dye-loading solution, c) running of the MDR assay and d) data analysis

a) Preparation of cells:

Cell Culture: A Caco-2 cell line (ATCC® HTB-37™) was used as it represented a reliable *in vitro* model of human small intestinal mucosa. Cells were grown on tissue culture treated 25cm^2 flasks at 37°C in a humidified 5% CO_2 incubator (RS Biotech Galaxy Standard, C&M Scientific, Livingston, West Lothian, UK). The growth medium was Dulbecco's Modified Eagle's Medium (DMEM) containing 4.0 mM L-Glutamine, 4500mg/L Glucose and sodium pyruvate, supplemented with 10% Foetal bovine serum (FBS) and a 0.1% penicillin-streptomycin solution. Cells were grown under standard conditions until 70-80% confluency was reached.

Cell Detachment: Following confluency, the cells were detached from the flask using Trypsin-EDTA (0.25mg/mL) and centrifuged at 2000rpm for ±10minutes. The supernatant was discarded and the cells were resuspended in growth medium to form a cell suspension.

Cell Counting: A sample of the cell suspension was removed and treated with Trypan Blue solution (0.4%) for hemocytometer counting. The Trypan blue-treated cell suspension was applied to a Bright-Line™ Hemocytometer (Hausser Scientific, Horsham, PA, USA). The hemocytometer was placed on a microscope stage (OLYMPUS CK2, Shibuya-ku, Tokyo, Japan) and counted using a 10x objective. The concentration of the cells were calculated by averaging all 1mm^2 areas counted and applying Equation 6.5.

$$C = \frac{n}{v} \qquad \textbf{(6.5)}$$

Where, C is the cell concentration in cells/mL, n is the average number of cells/mm^2 area and v is the volume counted (10^{-4}).

Cell seeding: Upon completion of counting, the appropriate dilutions were made and cells were seeded at 40,000 to 80,000 cells/well/90µL into a 96-well microplate for overnight incubation in growth medium.

b) Preparation of the dye-loading solution: An MDR sensor stock solution was prepared by mixing 200µL of DMSO into MDR sensor. Subsequently, 20µL of the MDR sensor stock solution was added into 10mL of assay buffer and mixed well to produce the MDR dye-loading solution.

c) Run MDR assay: Cells were treated with polyoxyethylene (40) stearate by adding 10µL of 10X solution of polyoxyethylene (40) stearate dissolved in phosphate buffer saline (PBS) at concentrations shown in Table 6.2. A corresponding amount of PBS was added to blank wells- containing medium without cells. The cell plate was then incubated in a 37°C, 5% CO_2 incubator for ±30minutes. Following incubation, 100µL/well of MDR dye-loading solution was added. The plate was further incubated overnight at room temperature, protected from light. Following complete incubation, the fluorescence intensity was monitored at Ex/Em=490/525nm using a Synergy HT multiwell fluorescence microplate reader equipped with curve fitting software (BioTek® Instruments, Winooski, Vermont, USA).

d) Data was analyzed by subtracting the fluorescence in the blank wells from the values of the wells with cells treated with the polyoxyethylene (40) stearate. The optimal concentration was obtained from the plot of the dose response curve.

6.2.6. Determination of the micro-environmental pH of the OCMT

The pH modulating effect of citric acid on the micro-environment was determined using a SevenMulti™ dual pH/conductivity meter (Mettler-Toledo International Inc., Im Langacher, Greifensee, Switzerland) (Badawy and Hussain, 2006; Tatarvati and Hoag, 2006). OCMT formulations F1-F13 containing varying concentrations of citric acid were prepared according to the specifications in Table 6.1. Samples were prepared by immersing the OCMT formulations (without the polymeric sheet) in 50mL of simulated human intestinal fluid (SHIF) pH 6.8 for a period of ±4 hours. The samples were hydrated for a short period of time in order to avoid the confounding factors that may result from complete leaching out of the pH modulator. Following hydration, the pH glass electrode tip was allowed to penetrate the swollen outer polymer shell of the tablet and held until a stable reading was obtained. The positioning of the electrode is important in the determination of the micro-environmental pH due to the presence of a pH gradient between the center and exterior of the OCMT (Tatarvati and Hoag, 2006). Thus, the electrode was positioned closer to the center of the swollen outer polymer shell to obtain an

accurate measurement of the micro-environmental pH. In addition, the influencing effects of the pH–modulator on the macro-environment was determined by measuring the pH of the SHIF immediately surrounding the OCMT formulations F1-F13.

6.2.7. Elucidation of the rheological properties of the prolamine-based 'smart' polymeric sheet solution

The flow characteristics of the zein aqueous-ethanol solutions, forming the basis of the 'smart' polymeric sheet, were evaluated by determining their intrinsic viscosities. The viscosity (η) was measured at a temperature of 25°C and a shear rate of $100s^{-1}$ for 360s using a Haake Modular Advanced Rheometer System (MARS) (ThermoFisher Scientific, Karlsruhe, Germany) fitted with a C35/1° titanium rotor sensor. Samples of the zein solutions (15%$^{w}/_{v}$, 17.5%$^{w}/_{v}$ and 20%$^{w}/_{v}$) as highlighted in Table 6.1 were placed on the sample stage and measured according to the parameters employed in Table 6.4. Determination of the viscosity was essential for informing on the suitability of the zein solutions to appropriately adhere to the surface of the OCMT in the formation of the 'smart' polymeric sheet.

Table 6.4: Rheological parameters employed for the analysis of the viscosity of the zein aqueous-ethanol solutions

Parameter	Value
Cone and plate gap	0.050mm
Driver version	1.29
Inertia	1.721×10^{-6} kg.m^2
A-factor	89051.00 Pa/Nm
M-factor	57.010 (1/s)/((rad/s)
Temperature	25°C
Damping	30.00

6.2.8. Mucoadhesive strength determination of the 'smart' polymeric sheet

Mucoadhesive studies were performed on all the FCCCD design formulations as per Table 6.1 to determine the influence of changes in variable concentration on the adhesiveness of the 'smart' polymeric sheet. The study involved the preparation of 0.1%$^{w}/_{v}$ solution of mucin in SHIF pH 6.8. Formulations F1-F13 were incubated in the prepared solution in an orbital shaker maintained at 37˚C and 50 rpm. The concentration of free mucin in the solution, after 6h duration, was determined by a UV spectrophotometer, at 201nm (IMPLEN NanophotometerTM, Implen GmbH, München Germany), using a 10 times dilution factor of path-length 0.1 mm. The difference in the concentration of the mucin solution before and after incubation was the

indication of the amount crosslinked with the 'smart' polymeric sheet as seen in Equation 6.6 (He *et al.,* 1998).

$$\text{Mucoadhesion}\% = \frac{[\text{Mucin before}]-[\text{Mucin after}]}{[\text{Mucin before}]} \times 100 \quad \textbf{(6.6)}$$

Where, [Mucin before] is the concentration of the mucin solution before incubation and [Mucin after] is the concentration of the mucin solution after incubation.

6.2.9. Qualitative and quantitative determination of the physicomechanical properties of the 'smart' polymeric sheet

The tensile characterization of the 'smart' polymeric sheet was determined through the use of a calibrated Texture Analyzer (TA.XT *plus*, Stable Microsystems, Surrey, UK) fitted with a 5kg load cell. Samples were prepared by casting the varying concentrations of zein solutions (as per Table 6.1) onto petri dishes and subsequently drying them in a laboratory fumehood until a thick film, mimicking the polymeric sheet surrounding the OCMT, was formed. Strips of the dried films were cut and measured for their width and thickness to an accuracy of 0.1µm at different places along the length of the film using a digital caliper (25 × 0.01mm capacity) (Taizhou hangyu tools gauge and blades Co., Ltd., Wenqiao, Zhejiang, China). The samples were subsequently fixed between miniature tensile grips (10mm apart) which were attached to the base plate and load cell carrier of the Texture Analyzer. The parameters employed for textural analysis are shown in Table 6.5.

Table 6.5: Textural profiling parameters used for tensile characterization of the 'smart' polymeric sheet

Parameters	Settings
Test mode	Tension
Pre-test speed	1 mm/s
Test speed	0.5 mm/s
Post-test speed	0.5 mm/s
Trigger type	Auto
Trigger force	0.05 N

Textural profiling of the 'smart' polymeric sheet was essential in determining its ability to adequately provide acid protection by maintaining a physicomechanically stable structure. This method yielded textural profiles that were used to generate the tensile stress and tensile strain (percent elongation) using Equations 6.7 and 6.8, respectively.

$$\sigma = \frac{F}{A_o} \quad \textbf{(6.7)}$$

Where, σ represents the tensile stress (N/mm^2), F is the breaking force (N) and A_o is the cross-sectional area of the sample (mm^2).

$$\varepsilon = \frac{l_i}{l_o} \times 100 \quad \textbf{(6.8)}$$

Where, ε represents the elongation at break (%), l_o is the original length of the sample and l_i is the increase in length of the sample at breaking point

The ratio of the tensile stress to the tensile strain was calculated using the Young's modulus (elasticity modulus) as represented in Equation 6.9.

$$\mathrm{E} = \frac{\sigma}{\varepsilon} = \frac{F.L_o}{A_o.\Delta L} \quad \textbf{(6.9)}$$

Where, E is the Young's modulus (MPa), F is the force at break, A_o is the cross-sectional area of the sample, ΔL is the change in the length of the sample and L_o is the original length of the sample.

In addition, a more realistic type of testing of the mechanical strength of the 'smart' polymeric sheet-encapsulated OCMT formulations were determined using a state-of-the-art biaxial tensile testing system (BioTester 5000, CellScale biomaterials testing, Waterloo, Ontario, Canada) fitted with a load cell of 5N. Randomly selected OCMT formulations, responding to varying concentrations of zein within the 'smart' polymeric sheet were selected for analysis. Typically, oral dosage forms are subjected to forces within the GIT, associated with the physiological phases of gastric digestion, motility and contractility (Laulict *et al*., 2010). Thus, reproducing physiological conditions during testing of the OCMTs mechanical strength provides information on its ability to withstand these forces and aids in predicting its clinical success. The BioTester brings together several high-precision components for the measurement and analysis of biomaterials by applying biaxial forces. It is fitted with a high resolution charge coupled device (CCD) camera (1280 x 960 pixels) to provide excellent image quality, video tracking and analysis. The OCMT formulations were hydrated in SHIF pH 6.8 to simulate the hydration of the tablet *in situ*. The OCMT was mounted and secured with tungsten rakes (tine diameter=305µm,

tine spacing=1.0mm, puncture depth=1.9mm) symmetrically attached 5mm apart on the X and Y axis of the sample as shown in Figure 6.3.

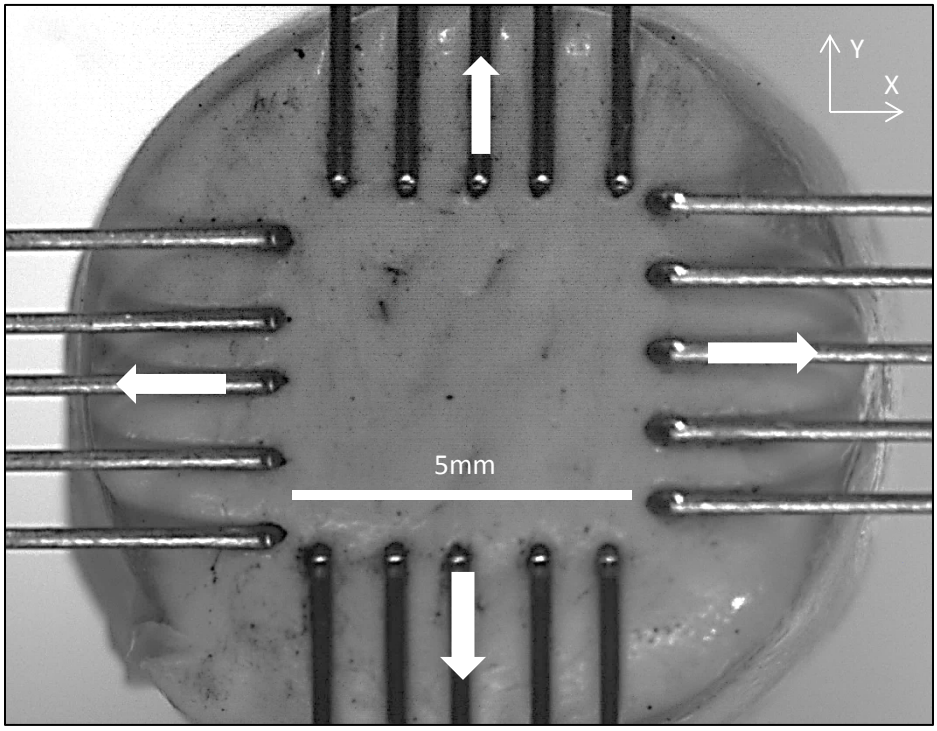

Figure 6.3: High resolution image of the OCMT sample mounted in the biaxial system. The tungsten rakes on each side secures the sample in place.

Once mounted in the testing system, the OCMT was simultaneously stretched in both the X and Y directions according to the parameters set out in Table 6.6. Biaxial force and displacement data were digitally sampled at 15Hz using the BioTester 5000 custom software (LabJoy 5.80, CellScale, Waterloo, Ontario, Canada).

Table 6.6: Biaxial tensile testing parameters employed for the 'smart' polymeric sheet encapsulated OCMT

Test Parameters	**X and Y Axis**
Control Mode	Displacement
Control Function	Ramp
Stretch Magnitude	40% strain
Preload	N/A
Stretch Duration	40s
Recovery Duration	40s
Repetitions	3
Data Output Frequency	15Hz
Image Output Frequency	15Hz

6.2.10. *In vitro* peptide release

The effect of the 'smart' polymeric sheet on the release behavior of the incorporated peptide was determined via *in vitro* analysis. *In vitro* peptide release studies were performed using a USP35 dissolution apparatus II (Caleva, Model 7ST, UK). The OCMT formulations F1-F13 were placed in 900mL SHIF at pH 6.8, beneath a ring mesh assembly within the dissolution vessel to prevent floatation. Dissolution was performed at a speed of 50rpm (37±0.5°C). Sampling of 3mL was undertaken at predetermined time intervals (0, 1, 2, 3, 6, 8, 10, 12, 24) and replaced with an equal quantity (3mL) of peptide-free dissolution medium to maintain sink conditions. Samples were analyzed using a Peptide Enzyme Immunoassay (Peninsula Laboratories International, Inc. San Carlos, CA, USA) which is a high sensitivity absorbance assay specific for the detection of Octreotide. Peptide release was calculated as a mean of three determinations as all studies were conducted in triplicate. In addition, the mean dissolution time (MDT) (Equation 6.10) was calculated from dissolution data to determine the peptide release rate (Sathish and Syed, 2013).

$$MDT = \frac{\sum_{i=1}^{i=n} t_{mid} \times \Delta M}{\sum_{i=1}^{i=n} \Delta M} \quad \textbf{(6.10)}$$

Where, *MDT* is Mean Dissolution Time; *i* is the dissolution sample number; *n* is the number of dissolution sample time; t_{mid} is time at mid-point between *i* and *i=1*; *ΔM* is the additional amount of protein dissolved between *i* and *i=1*.

6.2.11. Response surface analysis and constraint optimization

The response surface analysis of the variables for the FCCCD design formulations were computed using Minitab® statistical software (V15, Minitab Inc., PA, USA). Response surface and contour plots were derived for the measured responses (micro-environmental pH and degree of mucoadhesion) of the experimentally designed formulations and a statistical optimization was generated based on the responses obtained.

6.3. Results and Discussion

6.3.1. Analysis of the polyoxyethylene (40) stearate-CYP3A4 interaction

The efficacy of proteins and peptides is profoundly influenced by the limiting effects of the CYP 3A family and its major drug-metabolizing enzyme CYP3A4. Inhibition of CYP3A4 may

significantly improve the oral bioavailability of proteins and peptides. Thus, the influence of varying concentrations of the CYP3A4 inhibitor-polyoxyethylene (40) stearate (Table 6.2) on the catalytic activity of CYP3A4 was investigated. High-throughput fluorescence screening yielded the results shown in Figure 6.4. The reaction rates can be expressed in terms of pmole resorufin formed per unit time per unit amount of protein (50µg/well) by interpolation from the standard curve as presented in Figure 4a. The reaction kinetics of the recombinant human CYP3A4 enzyme in the presence of higher concentrations (4.5-10mg/mL) of polyoxyethylene (40) stearate displayed lower intensities of the emitted light as demonstrated by the lower RFU values obtained in Figure 6.4b-c, attributable to the successful inhibition of catalytic oxidation. In addition, the positive CYP3A4 inhibitor control-ketoconazole displayed a higher RFU then the test concentrations in Figure 4b-c, but a noticeably lower RFU then the solvent control. Since the solvent control contained no inhibitor, it readily permitted the catalytic oxidation of the non-fluorescent CYP3A4 substrate to its highly fluorescent metabolite (Figure 6.2), subsequently producing higher RFU values over the kinetic time period.

Polyoxyethylene (40) stearate concentrations within the lower end of the spectrum (0.02-3mg/mL) emitted more light and correspondingly displayed higher RFU values, compared to the higher concentrations, as depicted in Figure 6.4d-e. Noticeably, concentrations ≤0.5mg/mL demonstrated lower interactions with CYP3A4 then ketoconazole with the minimum concentrations (0.02-0.03mg/mL) approaching the RFU values of the solvent control as revealed by the reaction kinetics observed in Figure 6.4e. Owing to the observed interactions of polyoxyethylene (40) stearate with CYP3A4 at higher inhibitor concentrations, the results obtained were anticipated. Lower inhibitor concentrations did not significantly inhibit the catalytic oxidative process and predictably promoted the enzyme-substrate interaction. These results were further evaluated by interpreting the plot of the maximal velocity (V_{max}) as a function of the inhibitor concentration shown in Figure 6.4f. The results obtained follow the principles of the Michealis-Menten model which represents the best approach for explaining enzyme kinetics (Ainsworth, 1977; Ritchie and Prvan, 1996). The model takes the form of an equation (Equation 6.11) relating the reaction velocity to the substrate concentration (Ritchie and Prvan, 1996).

$$v = \frac{V_{max}\,[S]}{K_m + [S]} \qquad \textbf{(6.11)}$$

Where v is the velocity of the reaction, V_{max} is the maximal velocity achieved by the system at saturating substrate concentrations, K_m is the Michaelis constant and $[S]$ is the concentration of the substrate.

V_{max} is directly proportional to the enzyme concentration. Thus, it follows that at higher concentrations of polyoxyethylene (40) stearate, CYP3A4 does not convert much of the substrate to its fluorescent metabolite per unit of time despite the enzyme being saturated with substrate. This leads to a maximal velocity that is relatively small as observed in Figure 6.4f. Correspondingly, at lower concentrations of polyoxyethylene (40) stearate, an opposite effect is observed and lower maximal velocities are obtained. Essentially, the maximal velocity gives an indication of how fast the enzyme can catalyze the reaction.

Furthermore, the relative percent inhibition for the tested concentrations of polyoxyethylene (40) stearate were calculated by comparison to the activity of reactions containing no inhibitor and no enzyme. The dose-response curve obtained is presented in Figure 6.4g. The concentrations at 50% inhibition (IC_{50}) and maximal inhibition (IC_{100}) were calculated as 0.5mg/mL and 5mg/mL, respectively. The percentage inhibition of CYP3A4 increased exponentially with an increase in the polyoxyethylene (40) stearate concentration until a maximum saturated inhibitory potential was reached (5mg/mL). This was determined as the optimum inhibitor concentration that would successfully inhibit CYP3A4 enzyme activity and potentially produce the desired increased oral bioavailability of the incorporated peptide within the OCMT.

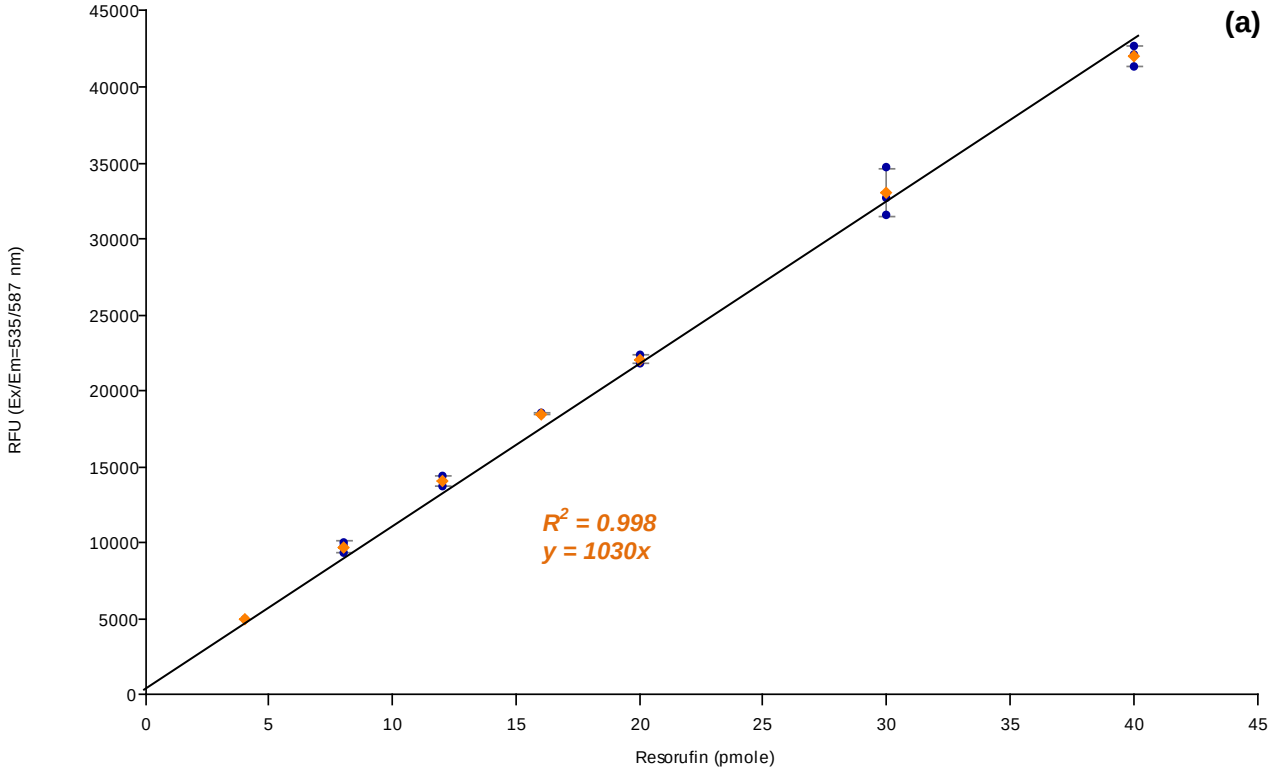
(a)
RFU (Ex/Em=535/587 nm)
Resorufin (pmole)
$R^2 = 0.998$
$y = 1030x$

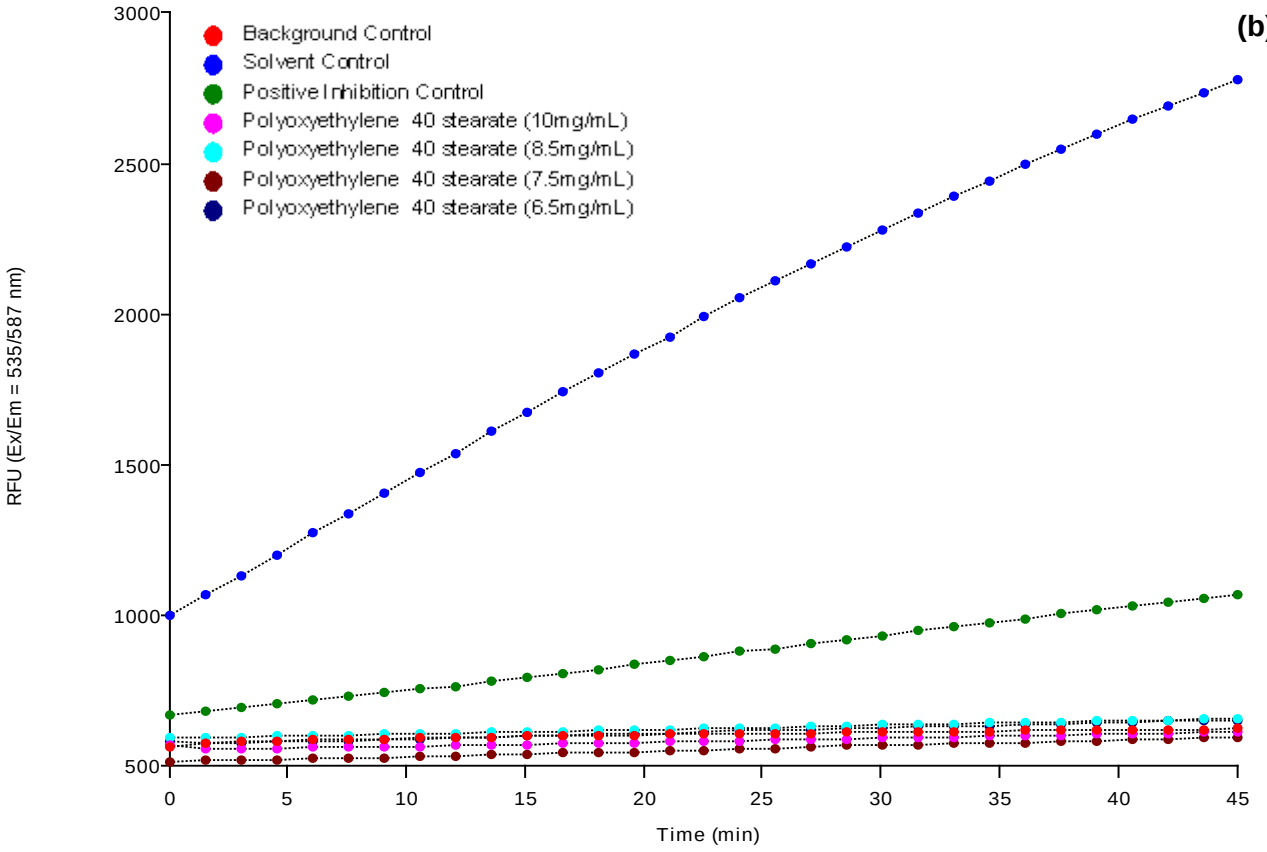
(b)
Background Control
Solvent Control
Positive Inhibition Control
Polyoxyethylene 40 stearate (10mg/mL)
Polyoxyethylene 40 stearate (8.5mg/mL)
Polyoxyethylene 40 stearate (7.5mg/mL)
Polyoxyethylene 40 stearate (6.5mg/mL)
RFU (Ex/Em = 535/587 nm)
Time (min)

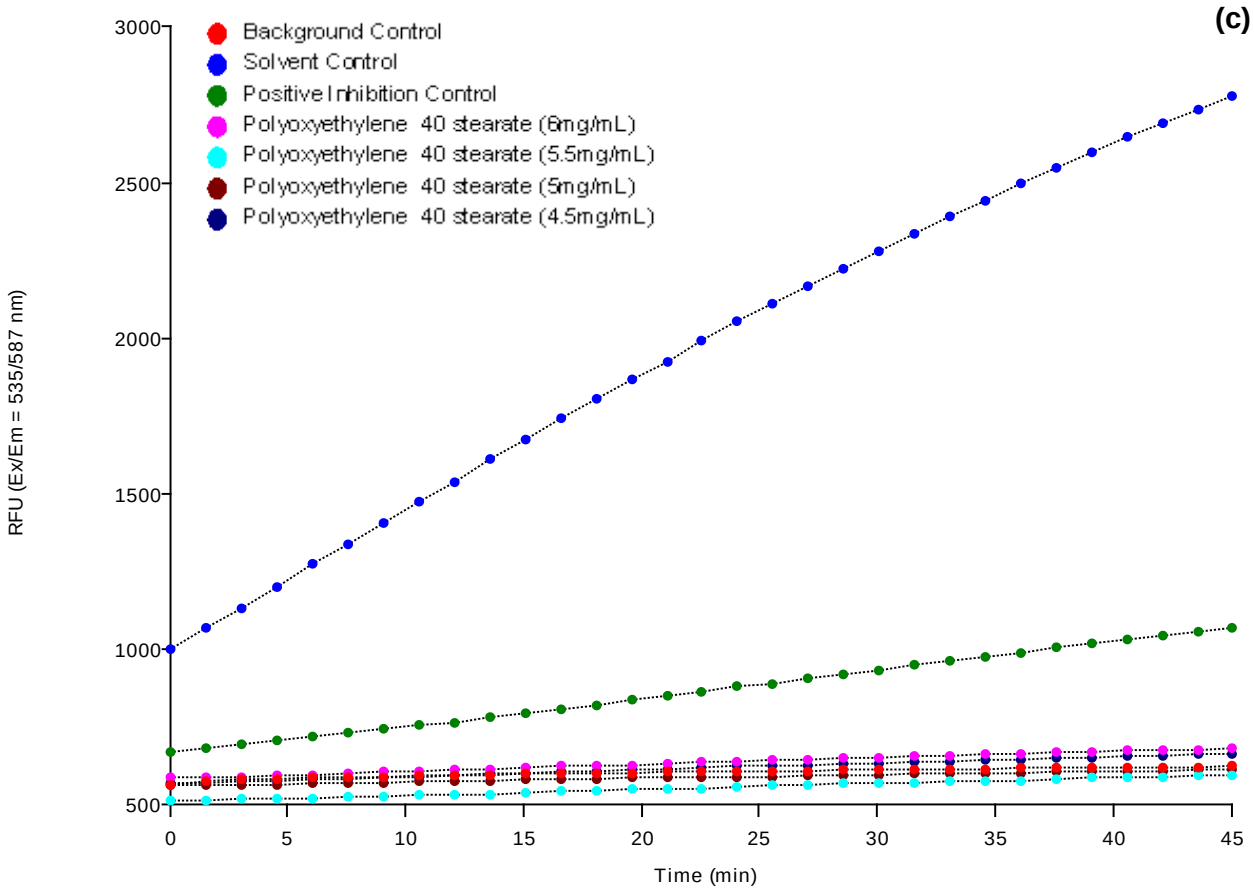
(c)
Background Control
Solvent Control
Positive Inhibition Control
Polyoxyethylene 40 stearate (6mg/mL)
Polyoxyethylene 40 stearate (5.5mg/mL)
Polyoxyethylene 40 stearate (5mg/mL)
Polyoxyethylene 40 stearate (4.5mg/mL)
RFU (Ex/Em = 535/587 nm)
Time (min)

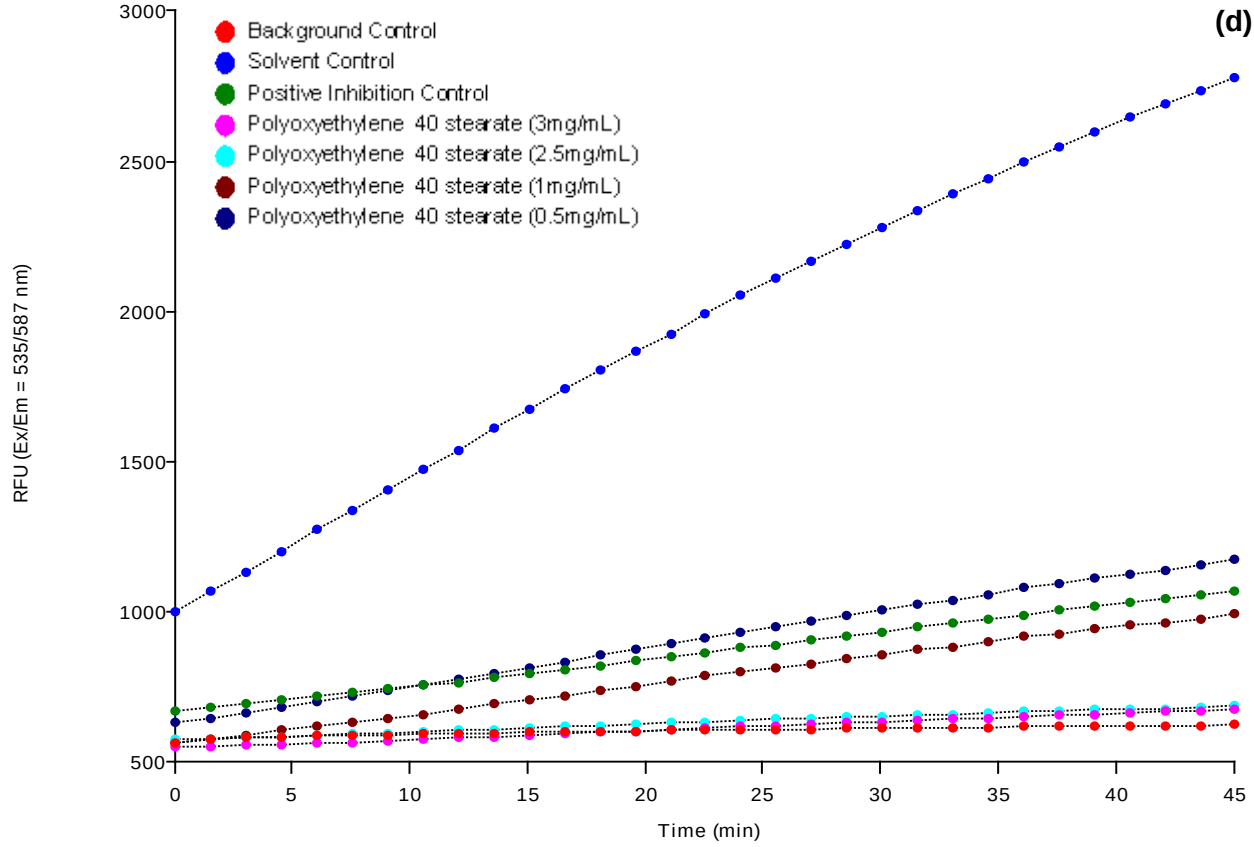
(d)
Background Control
Solvent Control
Positive Inhibition Control
Polyoxyethylene 40 stearate (3mg/mL)
Polyoxyethylene 40 stearate (2.5mg/mL)
Polyoxyethylene 40 stearate (1mg/mL)
Polyoxyethylene 40 stearate (0.5mg/mL)
RFU (Ex/Em = 535/587 nm)
Time (min)

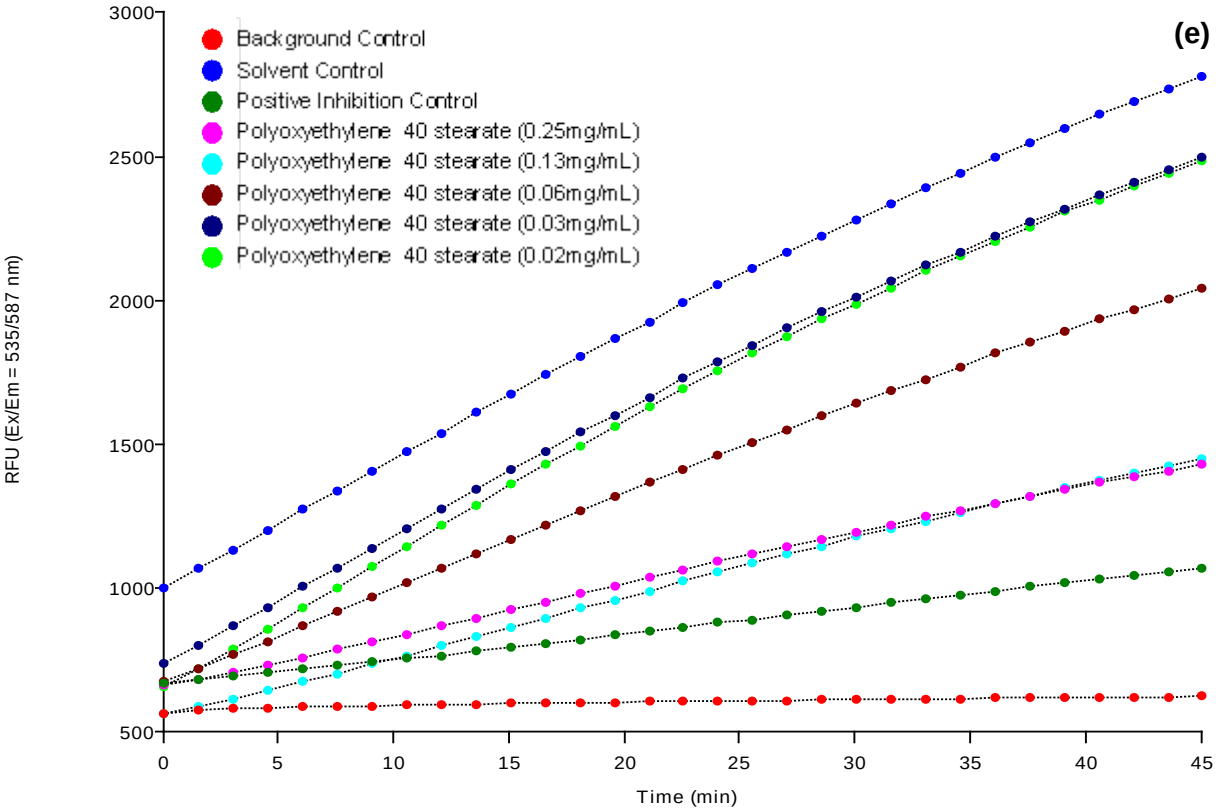
(e)
Background Control
Solvent Control
Positive Inhibition Control
Polyoxyethylene 40 stearate (0.25mg/mL)
Polyoxyethylene 40 stearate (0.13mg/mL)
Polyoxyethylene 40 stearate (0.06mg/mL)
Polyoxyethylene 40 stearate (0.03mg/mL)
Polyoxyethylene 40 stearate (0.02mg/mL)
RFU (Ex/Em = 535/587 nm)
Time (min)

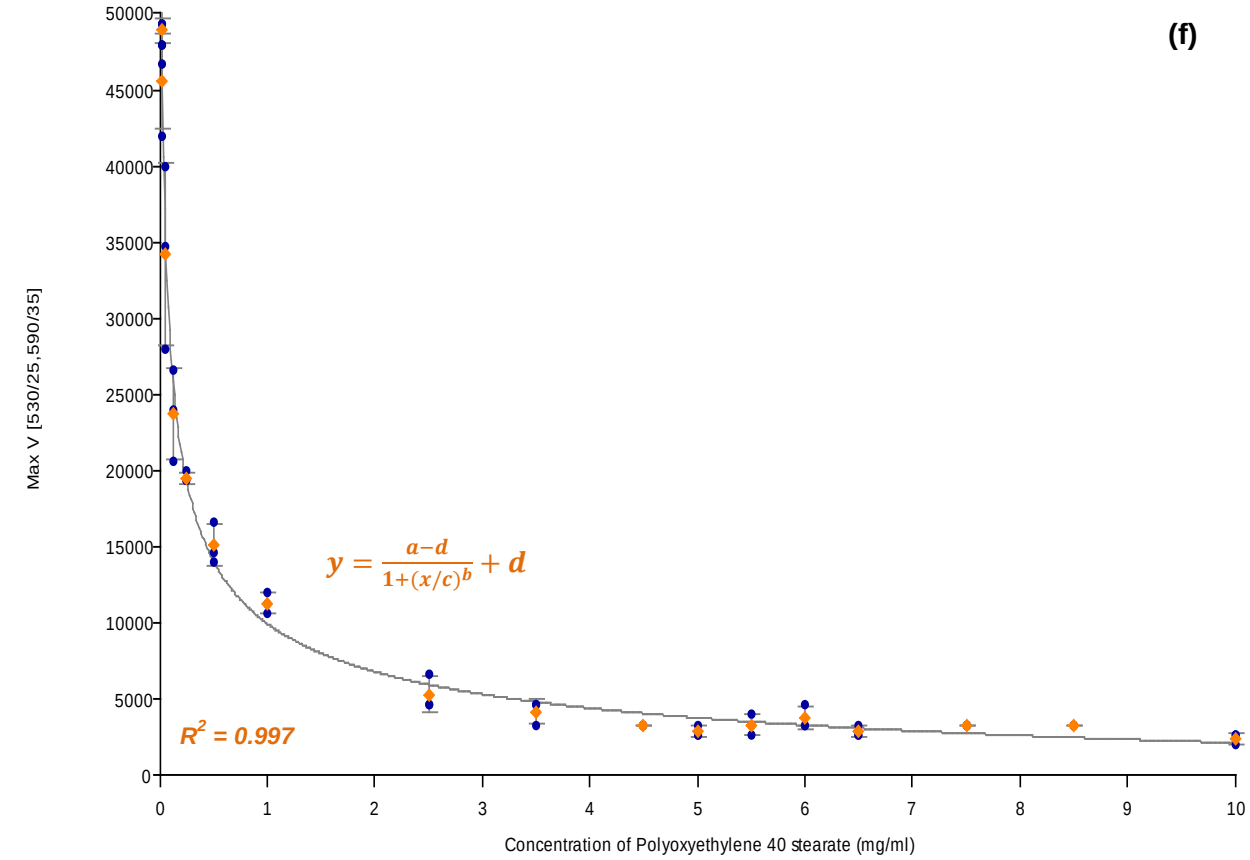
(f)
$y = \frac{a-d}{1+(x/c)^b} + d$
$R^2 = 0.997$
Max V [530/25,590/35]
Concentration of Polyoxyethylene 40 stearate (mg/ml)

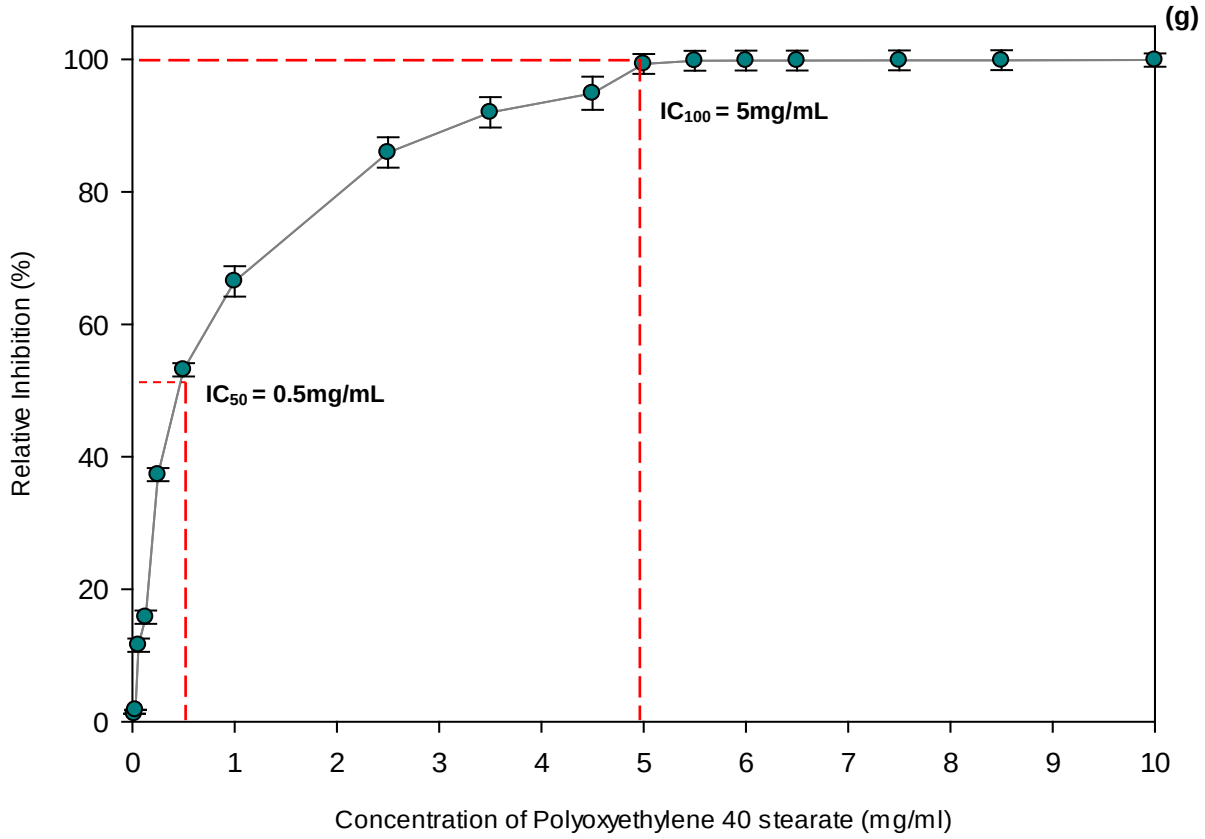

Figure 6.4: a) Resorufin standard curve. One mole of resorufin corresponds to the metabolism of one mole of CYP3A4 substrate. **b-e)** Reaction kinetics of recombinant human CYP3A4 enzyme at 25°C in the presence of the canonical competitive CYP3A4 inhibitor ketoconazole and the varying concentrations of Polyoxyethylene (40) stearate (the solvent control reaction contained a final concentration of 1% acetonitrile). **f)** Plot of maximal velocity (V_{max}) as a function of the inhibitor concentration (mg/mL) based on Michaelis-Menten kinetics. **g)** Dose-response curve of the calculated percent activity for each concentration of polyoxyethylene 40 stearate by comparison to the activity of reaction of the solvent and background controls. The IC_{50} (0.5mg/mL) and IC_{100} (5mg/mL) are highlighted and each value represents the mean of three replicate experiments.

6.3.2. Analysis of the polyoxyethylene (40) stearate-Pgp interaction

The transmembrane efflux of drugs, facilitated by the MDR1 transporter-Pgp influences the pharmacokinetics of oral formulations (Shugarts and Benet, 2009). Pgp in conjunction with CYP3A4 functions in a concomitant manner to reduce systemic oral bioavailability of drugs through their respective mechanisms (Kim *et al.,* 1999). Thus, it was essential to monitor the MDR1 pump activity in the presence of varying concentrations of polyoxyethylene (40) stearate (Table 6.2) in order to determine the optimum concentration of inhibitor that would potentially inhibit Pgp in addition to CYP3A4. Prior to running the assay, cells needed to be prepared to allow the penetration of the fluorescent MDR indicator into the cell membranes. Figure 6.5

displays live imaging of the cultured Caco-2 cells that were used for the screening of the MDR pump inhibitor.

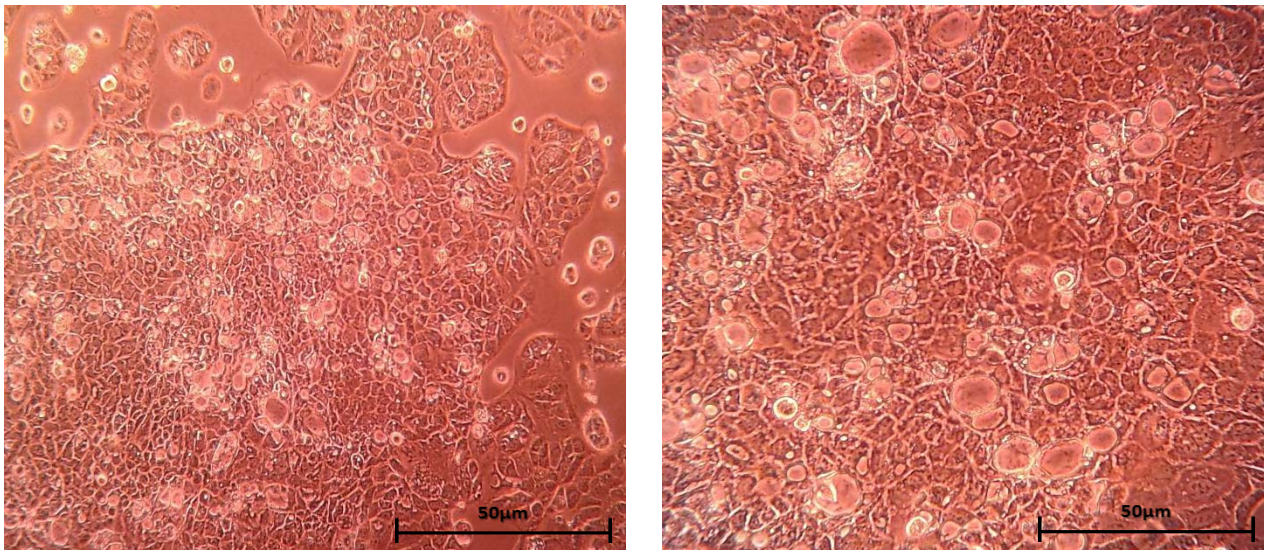

Figure 6.5: Still frame from live cell imaging of confluent Caco-2 cells in growth media (DMEM, 10% FBS), used for the preparation of the MDR assay.

The MDR assay measured the cellular fluorescent intensity in response to the varying concentrations of polyoxyethylene (40) stearate. The cellular fluorescent intensity is dependent on the intracellular free dye concentration which can increase significantly following a short incubation. This dye is extruded by the MDR transporters in cells that express MDR1, resulting in a decreased cellular fluorescence intensity. However, the presence of an agent/inhibitor that interferes with the MDR1 pump activity can block dye extrusion and cause a significant increase in cellular fluorescence intensity. The effect of polyoxyethylene (40) stearate on the inhibition of the Pgp pump in Caco-2 cells is shown in Figure 6.6. Results demonstrated that at increasing concentrations of polyoxyethylene (40) stearate, the fluorescence signal increased due to the inhibition of the Pgp pump which enhanced the intracellular accumulation of the MDR indicator dye.

The IC_{50} concentration of 0.13mg/mL was determined directly from the non-linear logistic curve fitting as shown in Figure 6.6. The cellular fluorescence intensity increased significantly up to an inhibitor concentration of 0.5mg/mL. Concentrations between 0.5mg/mL and 10mg/mL produced no significant increases in the cellular fluorescence intensity but rather fluctuated around a central RFU value of 32000. As a result, this concentration range was determined as the

maximum inhibitory potential of polyoxyethylene (40) stearate for inhibition of the Pgp pump in Caco-2 cells. Based on the analysis of the interaction of polyoxyethylene (40) stearate with both CYP3A4 and Pgp, it was determined that the final optimal concentration for use in the OCMT in the achievement of co-inhibition was 5mg/mL. This concentration fell within the range of the maximum inhibitory potential of the Pgp pump and was determined as the optimal inhibitory concentration for CYP3A4 activity, thus achieving the desirable co-inhibitory effect and potentially increasing the oral bioavailability of proteins and peptides.

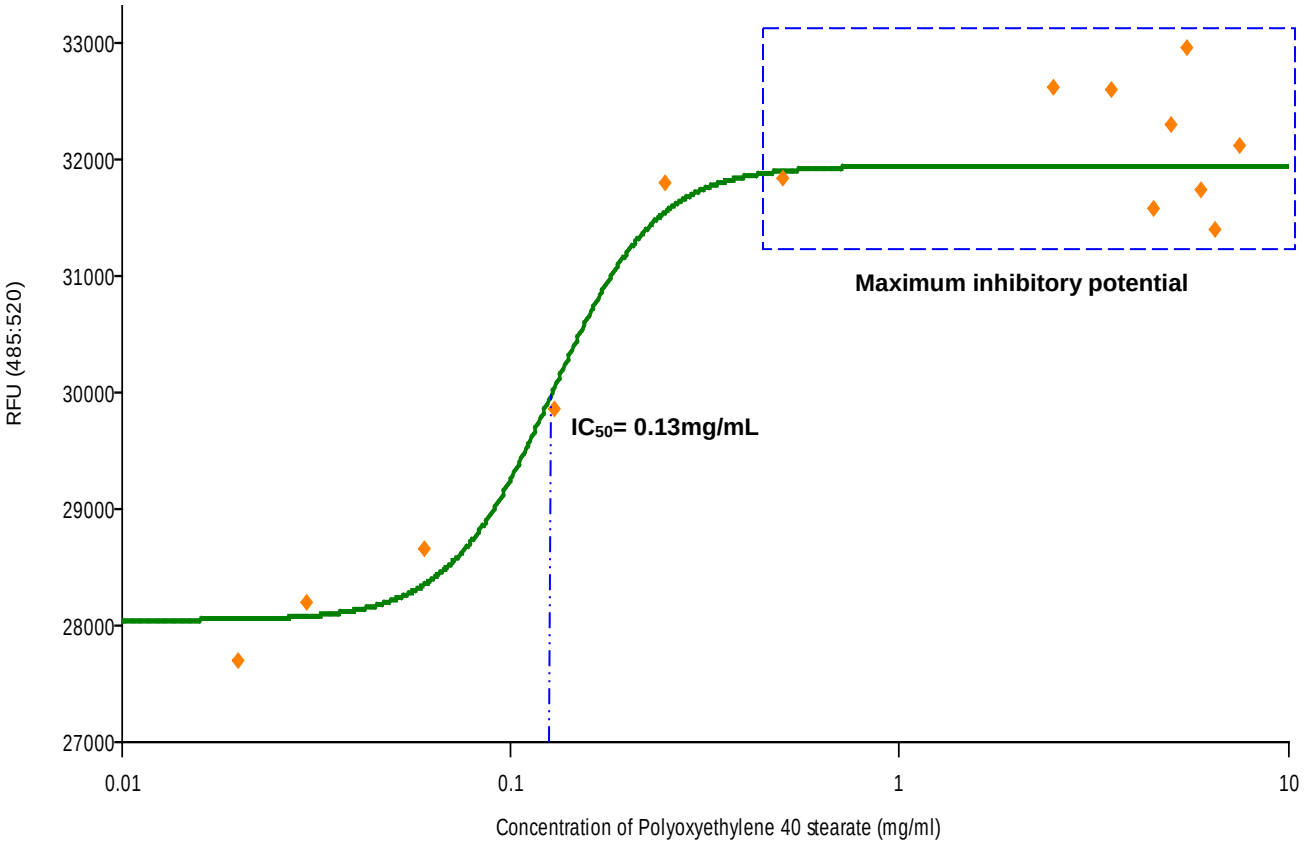

Figure 6.6: Effect of polyoxyethylene (40) stearate on the inhibition of the Pgp pump in Caco-2 cells. The IC_{50} (0.13mg/mL) was determined directly from logistic curve fitting results.

6.3.3. Evaluation of the micro-environmental pH modulation

The high enzyme activity at the intestinal brush border may significantly influence the degradation of proteins and peptides (Bruno *et al*., 2013). The enzymes predominantly found at the brush border membrane site include, disaccharidases and alkaline phosphatase (Holmes, 1971; Jiang and Yan, 2008). The point at which the enzyme is most active is known as the optimum pH and is typically in a range of neutral to alkaline pH (6.8-7.5) for the intestinal enzymes, as illustrated in Figure 6.7 (Jiang and Yan, 2008). Enzymes are notably affected by

changes in pH, with very high or very low pH values causing a loss in enzyme activity and overall stability.

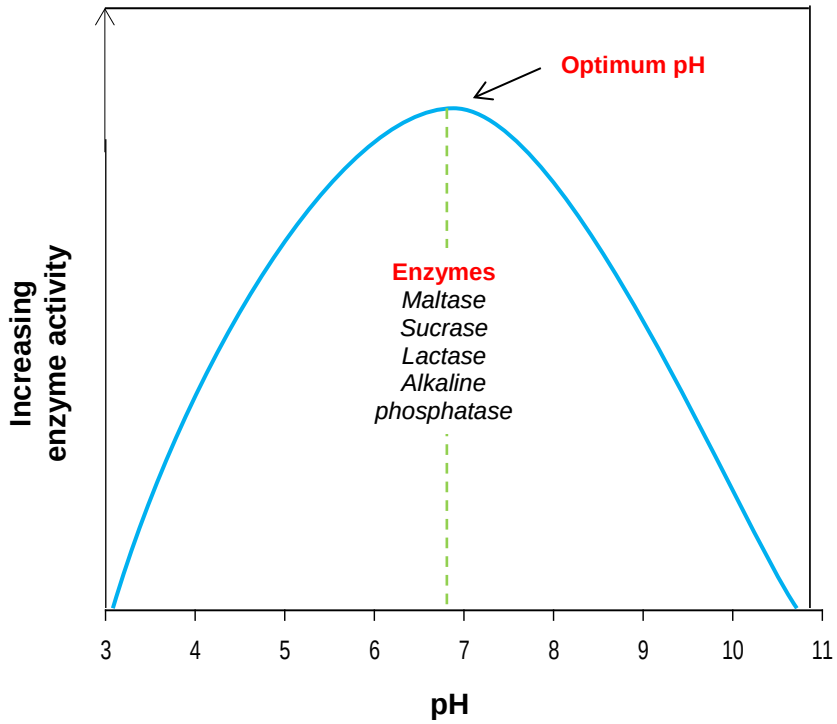

Figure 6.7: Graphical illustration of enzyme activity as a function of pH.

Thus, the incorporation of the nonpolymeric acid based pH modifier (citric acid) in the OCMT should function to reduce the optimal environment for enzyme activity by decreasing the micro-environmental pH. The effect of citric acid on the micro-environmental pH was monitored and results yielded the changes shown in Figure 6.8. The change in the pH over the 4-hour study period directly corresponded to the concentration of citric acid employed in the OCMT formulations F1-F13, presented in Table 6.1. F1, F6 and F8 contained a higher concentration (10mg) of citric acid, consequently producing a greater modulation in the micro-environmental pH ranging from 3.2-3.8. Correspondingly, lower concentrations (5mg/7.5mg) of citric acid produced a smaller, but nevertheless significant change in the micro-environmental pH (± 4.5). Furthermore, the macro-environmental pH of each formulation was determined at the start and end of the experiment to monitor the influence of citric acid on the surrounding environment. Ideally, the results shown in Figure 6.8 displayed no significant pH changes to the macro-environment. Overall, the results demonstrated the applicability of the pH modifier to successfully reduce the micro-environmental pH and indirectly inhibit enzyme activity at the brush border.

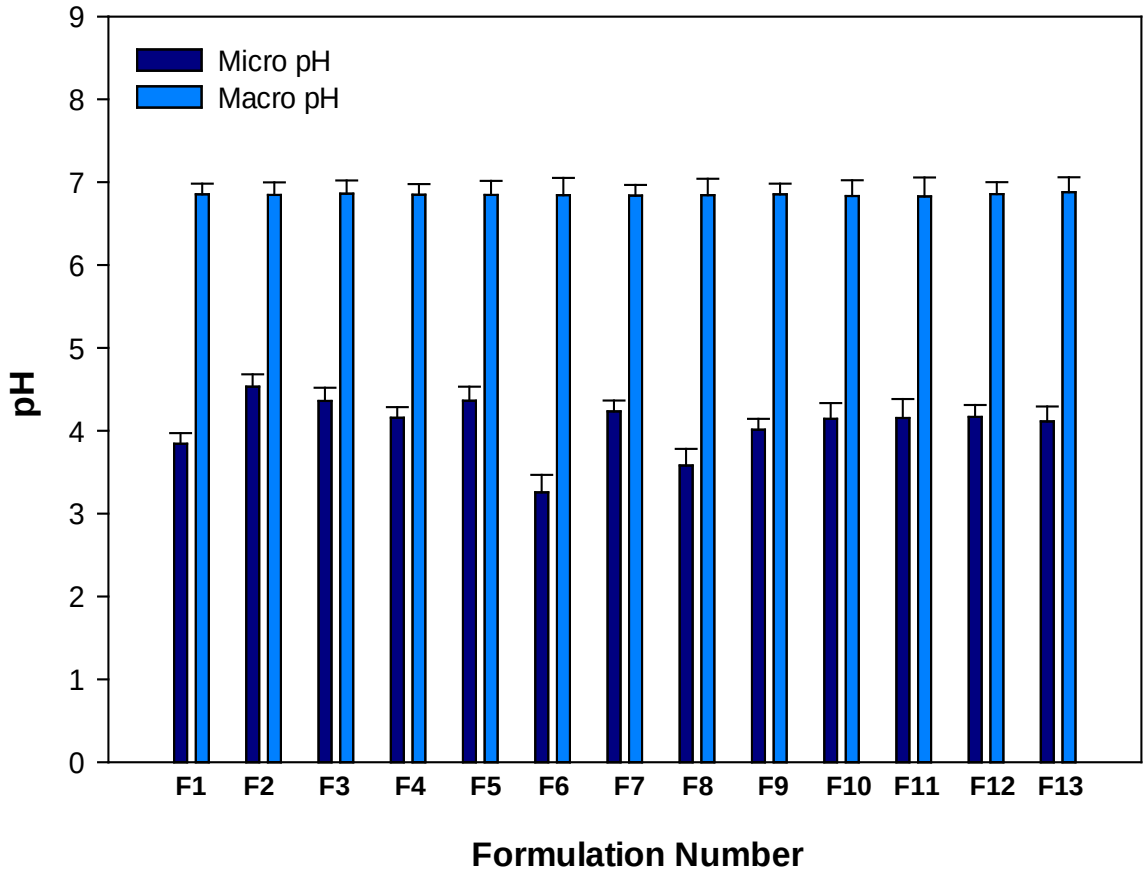

Figure 6.8: The changes in the micro and macro-environmental pH of the OCMT formulations F1-F13 in the presence of the pH-modulating agent-citric acid.

6.3.4. Assessment of the rheological characteristics of the prolamine-based 'smart' polymeric sheet solution

Viscosity is a physical property that describes a fluid's internal resistance to flow, influenced by various factors such as: concentration, temperature, pressure and shear rate (George and Qureshi, 2013). The measurement of the rheological behavior and more specifically, the viscosity of the polymeric sheet solution was necessary for determining its ability to adequately adhere to the surface of the OCMT during the 'dipping' process. Results of viscosity (η) and shear stress (τ) as a function of the shear strain rate (ẏ) of varying concentrations of zein (Table 6.1) are shown in Figure 6.9.

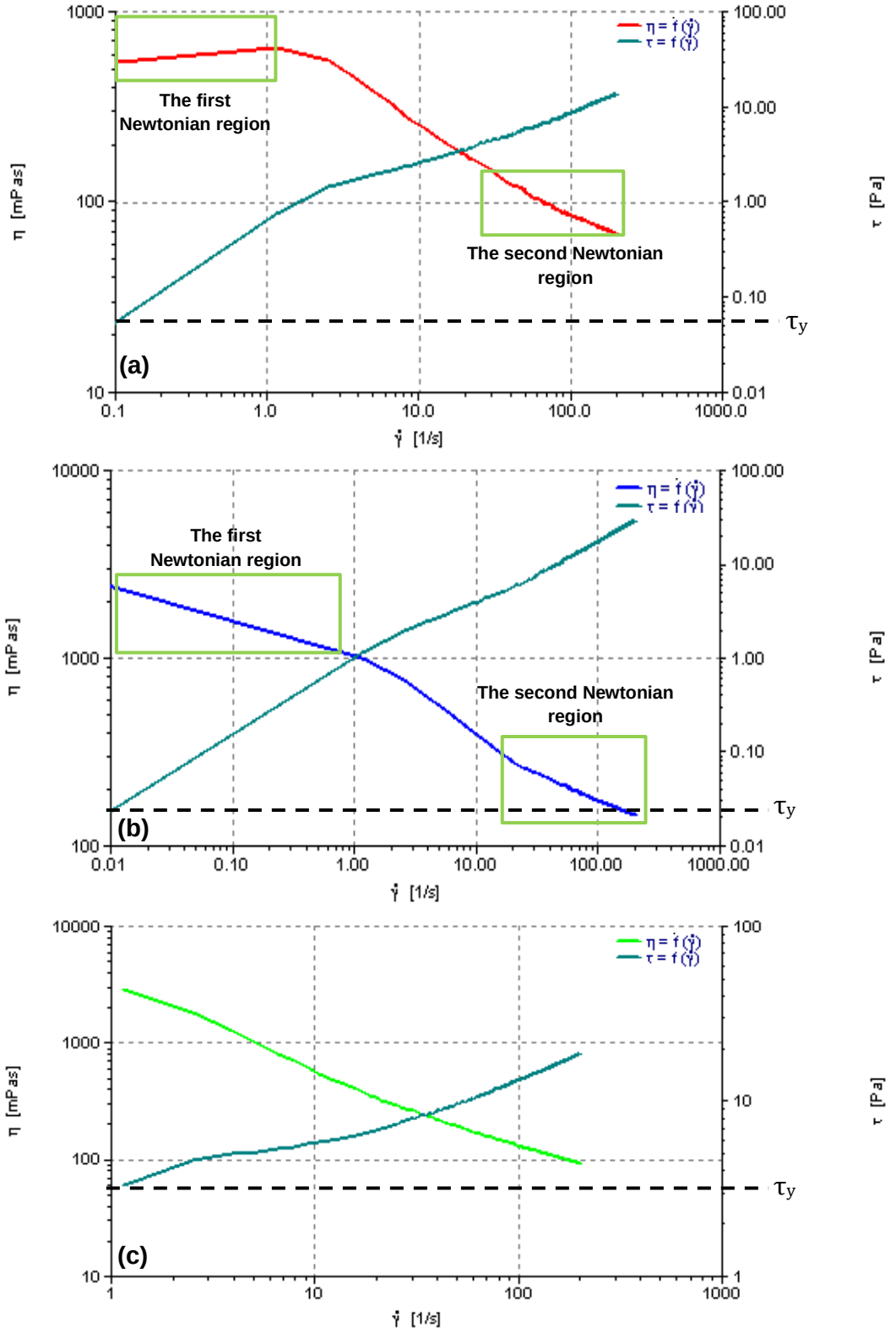

Figure 6.9: Rheological profiles depicting the flow curve and viscosity shear rate curve of **a)** 15%$^{w}/_{v}$ zein, **b)** 17.5%$^{w}/_{v}$ and **c)** 20%$^{w}/_{v}$ zein.

An interpretation of Newton's law of viscosity was used to characterize the flow properties of the polymeric solutions. Typically, Newtonian fluids display a constant viscosity at increasing shear rates as well as a linear relationship between the shear stress and shear rate (George and Qureshi, 2013; Irgens, 2014). However, the rheological profiles obtained for the zein solutions displayed a more complicated relationship between the viscosity, shear stress and shear rate and thus was characterized as a Non-Newtonian fluid. The shear viscosity decreased with an increase in the shear rates for all the zein solutions as shown in Figure 6.9a-c. This was characteristic of pseudoplastic (shear-thinning) fluids which are found for many polymer solutions.

Pseudoplastic fluids display Newtonian regions at very high and very low shear rates where the shear viscosity becomes almost constant (Irgenz, 2014). This was clearly evident in the rheograms obtained for the solutions in Figure 6.9a-b. Figure 6.9a characteristically displayed a zero shear viscosity observed within the first Newtonian region, attributable to the low concentration of zein (15%$^{w}/_{v}$) contained within the solution causing it to be more liquid-like when stationery. In addition, flow curves of the shear stress as a function of shear rate displayed interesting Bingham-plastic type behavior for all zein concentrations. Bingham fluids require a yield stress (τ_y) to initiate flow but follow a straight line after the yield stress is reached, as observed in Figure 6.9a-c. Although Bingham-plastic behavior is more characteristic of suspensions and emulsions, the rheograms obtained for the zein solutions suggest the applicability of attributing the rheology to a combination of pseudoplastic and bingham-plastic type behaviors.

Furthermore, since ethanol and plasticizer concentrations were kept constant, the major contributing factor to the observed viscosities was the zein concentrations. The viscosity increased with an increase in the zein concentrations as depicted in Table 6.7. Higher concentrations of zein (17.5%$^{w}/_{v}$ and 20%$^{w}/_{v}$) displayed higher average viscosities as compared to the lower concentration of zein (15%$^{w}/_{v}$). Correspondingly, a 15%$^{w}/_{v}$ concentration of the polymeric sheet solution displayed lower shear stress values compared to the 17.5%$^{w}/_{v}$ and 20%$^{w}/_{v}$ concentrations due to lower stresses being required to initiate the flow of low viscosity fluids. Ideally, the solution should be viscous enough to adhere to the OCMT and form a thick layer during the 'dip' and 'dry' method. The results obtained were further supported by the observations during preparation of the OCMT which demonstrated the improved adherence of the polymeric sheet solution to the OCMTs based on higher respective viscosities.

Table 6.7: Effects of varying concentrations of zein on the viscosity and shear stress of the polymeric sheet solution

Zein (%$^{w}/_{v}$)	Viscosity at a shear rate of 100s^{-1} (mPas)	Shear stress (Pa)
15	505.4	13.53
17.5	2426	18.68
20	2881	29.05

6.3.5. Elucidation of the mucoadhesive strength of the 'smart' polymeric sheet

Zein has been shown to possess mucoadhesive properties, making it desirable for multiple drug delivery applications (Patel *et al*., 2010; Wongasasulak *et al*., 2013; Paliwal and Palakurthi, 2014). Thus, the effect of zein on the mucoadhesive strength of the 'smart' polymeric sheet was analyzed for the OCMT formulations F1-F13. The mucoadhesion mechanism can be divided into three steps involving firstly, the intimate contact of the polymer with the tissue, secondly, the consolidation of the polymer with the mucin chains and thirdly, the formation of weak chemical bonds (Carvalho *et al*., 2010; Singh and Rana, 2012). The *in vitro* technique of measurement used for the determination of the mucoadhesive strength was centered around the adsorption theory, mechanistically based on surface forces that result in chemical bonding, by measuring the mucin remained after interaction (Singh and Rana, 2012).

The results obtained demonstrated the effect of the zein concentrations on the mucoadhesion percentages obtained for each formulation as displayed in Figure 6.10. Typically, OCMT formulations F5, F7 and F8 containing a 15%$^{w}/_{v}$ concentration of zein displayed lower mucoadhesion percentages (±22.49%). This was attributed to a lower degree of secondary chemical interactions between the polymer and the mucin. Comparatively, higher concentrations of zein (17.5%$^{w}/_{v}$ and 20%$^{w}/_{v}$) displayed a greater interaction and improved crosslinking with mucin, supported by the higher mucoadhesion percentages obtained. The mucoadhesion provided by zein creates an opportunity for the OCMT to have an increased residence time within the intestine, improved permeability and enhanced bioavailability of the incorporated peptide.

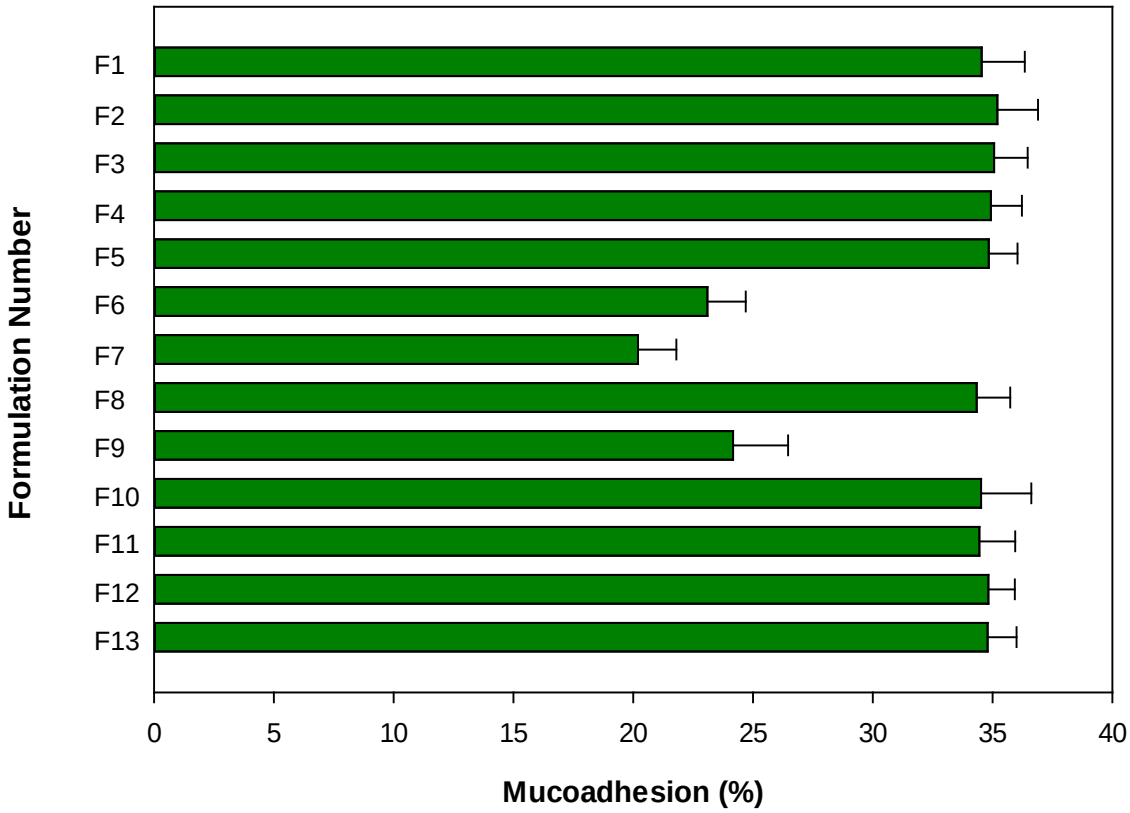

Figure 6.10: *In vitro* mucoadhesion percentages resulting from interactions with the varying concentrations of zein contained with the 'smart' polymeric sheet of the OCMT formulations F1-F13.

6.3.6. Comprehensive textural analysis of the 'smart' polymeric sheet and encapsulated OCMT

Comprehensive analysis of the film-casted zein solutions, mimicking the 'smart' polymeric sheet surrounding the OCMT, was analyzed with respect to their textural properties. The tensile strength, percentage elongation and elasticity of the varying concentrations of zein films were determined from quantitative analysis of the textural profiles obtained. The results are presented in Table 6.8, demonstrating the effects of increasing concentrations of zein on the tensile strength, percentage elongation and Young's modulus. The calculated tensile properties were directly proportional to the increasing concentrations of zein from 15%$^{w}/_{v}$ to 20%$^{w}/_{v}$. The highest concentration (20%$^{w}/_{v}$) of the film-casted zein solution was found to be the strongest, displaying the highest tensile strength (9.16 N/mm^2). Similarly, the percentage elongation at break (194.69%) was greater for higher concentrations of zein, attributable to an improved interaction with the incorporated plasticizer leading to greater molecular mobility and increased flexibility (Lim and Hoag, 2013). The Young's modulus for all concentrations of zein revealed no

significant differences, indicating the ability of all the concentrations to resist elastic deformation when a force is applied. The characterization of the mechanical properties of the film-casted zein solutions was essential for determining its ability to adequately form a strong polymeric sheet around the OCMT, functioning to withstand external stresses during processing or *in vivo* application. Furthermore, the intrinsic mechanical properties and the capability of the polymeric sheet to maintain its physical structure around the OCMT are important for providing necessary acid protection.

Table 6.8: Summary of the tensile strength, percent elongation at break and Young's elastic modulus at increasing concentrations of the film-casted zein solutions.

Zein ($\%^{w}/_{v}$)	Tensile strength (N/mm^2)	Percent Elongation at break (%)	Young's Modulus (MPa)
15	4.68	118.74	3.94
17.5	7.02	150.47	4.67
20	9.16	194.69	4.71

Additionally, a more realistic state testing of the complete OCMT with the surrounding 'smart' polymeric sheet was evaluated by measuring biaxial forces and displacements. The profiles obtained for the varying concentrations of zein as part of the 'smart' polymeric sheet is graphically depicted in Figure 6.11a-c. The force-time, displacement-time and force-displacement graphs obtained were proportional to the nominal stress, nominal strain and nominal stress-strain graphs, respectively (Gregory and Callaghan, 2012; Holmes *et al.,* 2012). The force-time graphs showed how the measured X and Y forces change over time. The superimposition noticed for the X and Y data indicated the uniformity of the 'smart' polymeric sheet, requiring equal forces to stretch on both axes. A 40% strain on all the samples produced a 1800um displacement of the 'smart' polymeric sheet from its original position. The application and release of load on the sample within each test cycle mimicked the propulsive contraction and relaxation movements within the GIT presenting as stretch and recovery phases within each cycle as shown in Figure 6.11a-c.

Oral dosage forms experience forces *in vivo*, resulting from muscular contractions experienced during gastric digestion and emptying. Laulicht and co-workers, (2010) investigated the gastric forces experienced *in vivo* by tablets via high resolution pill tracking. Results from the study revealed the average human gastric-emptying force in the fasted and fed state as being 414±194 dynes (±4.14 mN) and 657±84 dynes (±6.57mN), respectively. The average stresses that the 'smart' polymeric sheet of the OCMT could withstand was significantly high for all the

formulations with a 20%$^{w}/_{v}$ concentration displaying the highest breaking force as shown in the Force-time profiles obtained in Figure 6.11c. Although the breaking forces decreased with each test cycle, it still provided significant tensile strength which demonstrated the suitability of the 'smart' polymeric sheet to appropriately withstand gastric forces *in vivo*. These results favorably supported the independent testing of the film-casted 'smart' polymeric sheet solutions shown in Table 6.8.

In addition, the hysteresis loops noted in the force-displacement graphs of each of the samples provided a qualitative assessment of the elasticity of the sample and its ability to return back to its original position after a load has been removed (Jang *et al*., 2005). A purely elastic material will return along the same curve and no energy is lost. Due to the viscous properties of the zein solutions, as highlighted previously in Figure 6.9, the mechanical response of the 'smart' polymeric sheet experienced a time delay in returning back to its original shape indicated by the area between the load and unload curves. The area between the load and unload curves of the 20%$^{w}/_{v}$ concentration of zein was smaller than for the 15%$^{w}/_{v}$ and 17.5%$^{w}/_{v}$, respectively. This indicated that less energy was absorbed by the 20%$^{w}/_{v}$ polymeric sheet and a better recovery to its original shape.

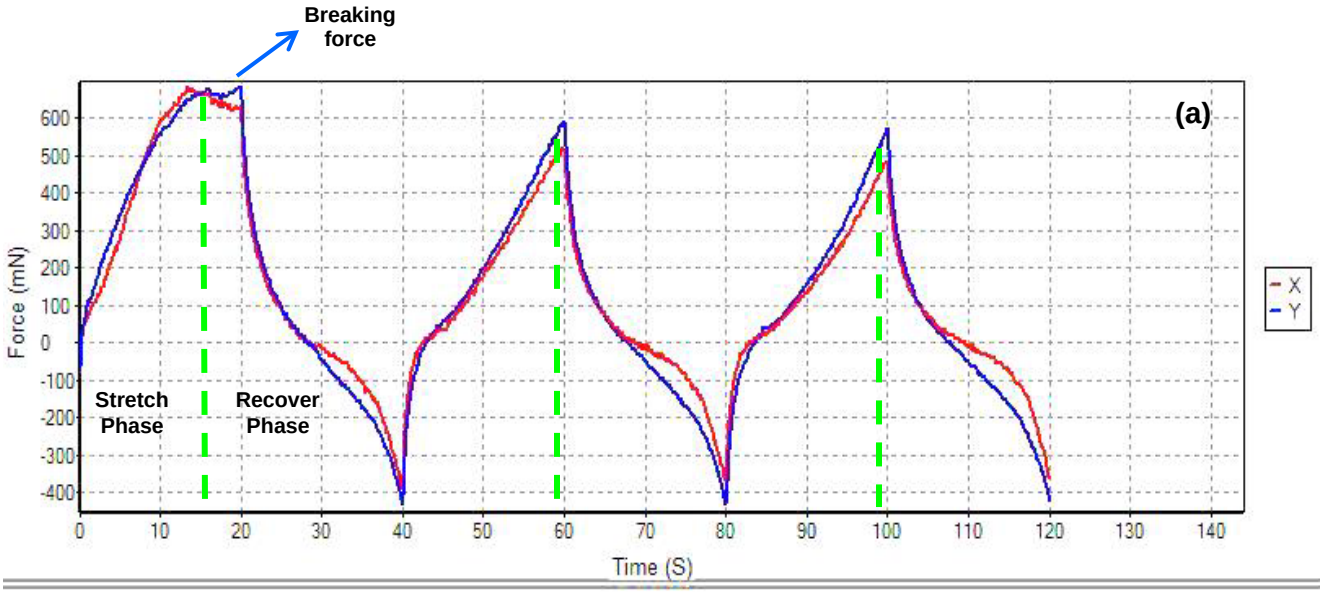
Breaking force
(a)
Force (mN)
Time (S)
Stretch Phase
Recover Phase
X
Y

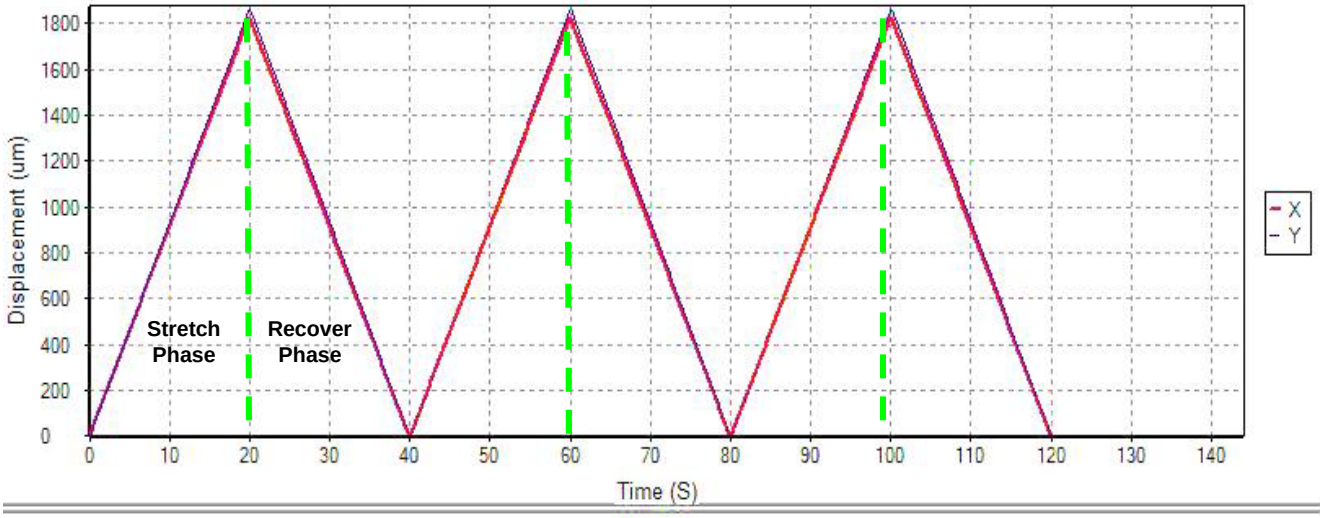
Displacement (um)
Time (S)
Stretch Phase
Recover Phase
X
Y

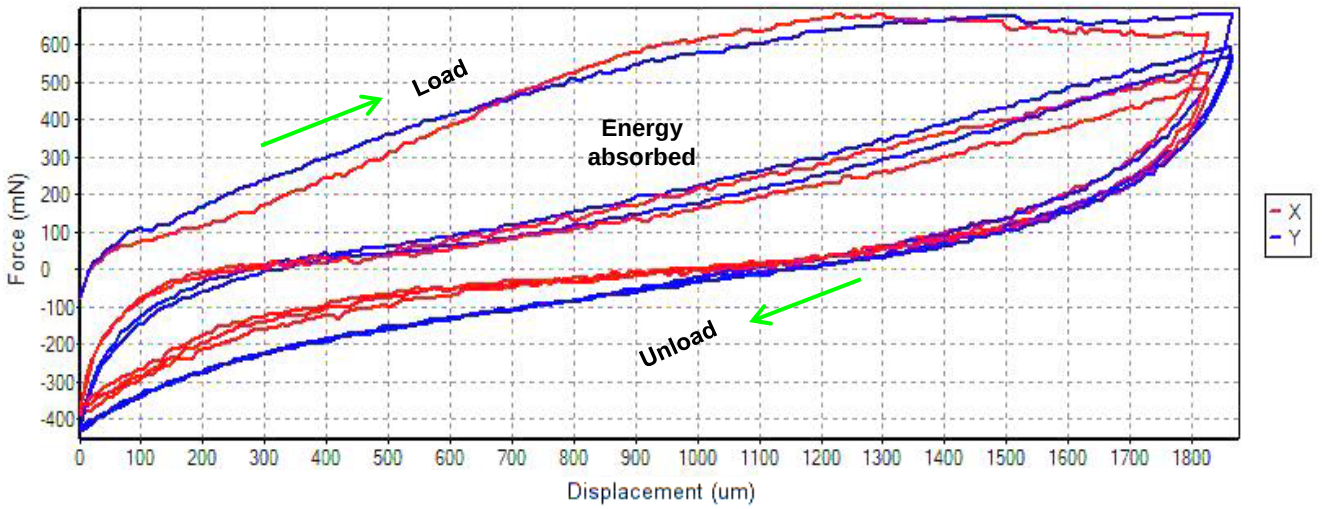
Load
Energy absorbed
Unload
Force (mN)
Displacement (um)
X
Y

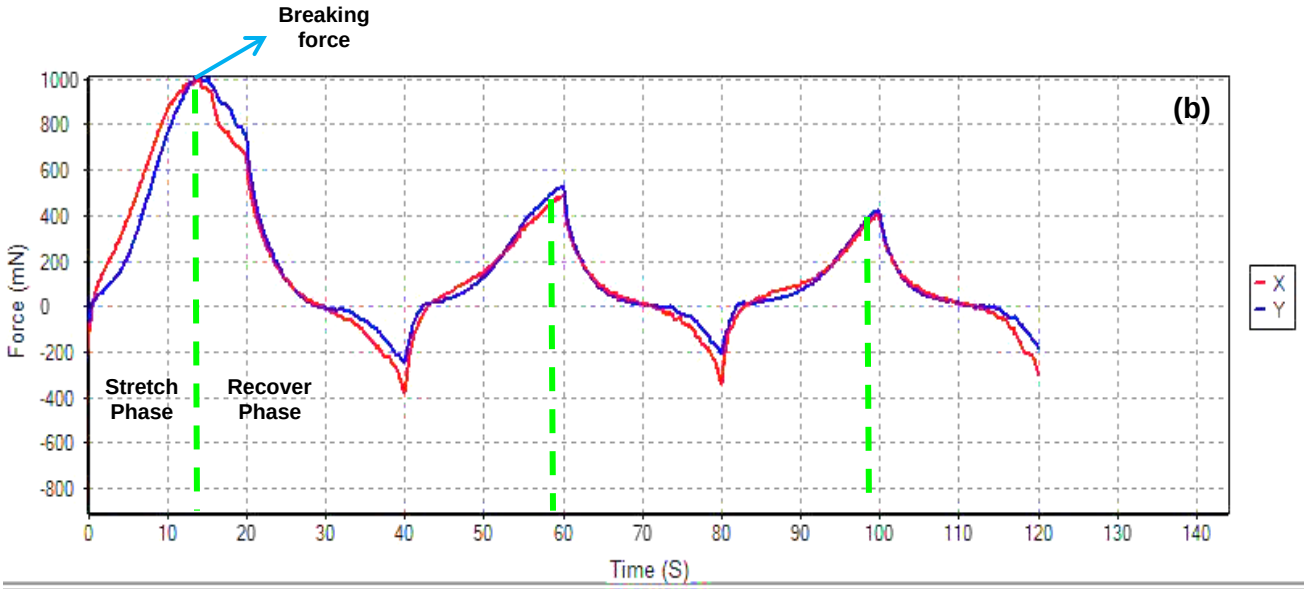
Breaking force
(b)
Force (mN)
Time (S)
Stretch Phase
Recover Phase
X
Y

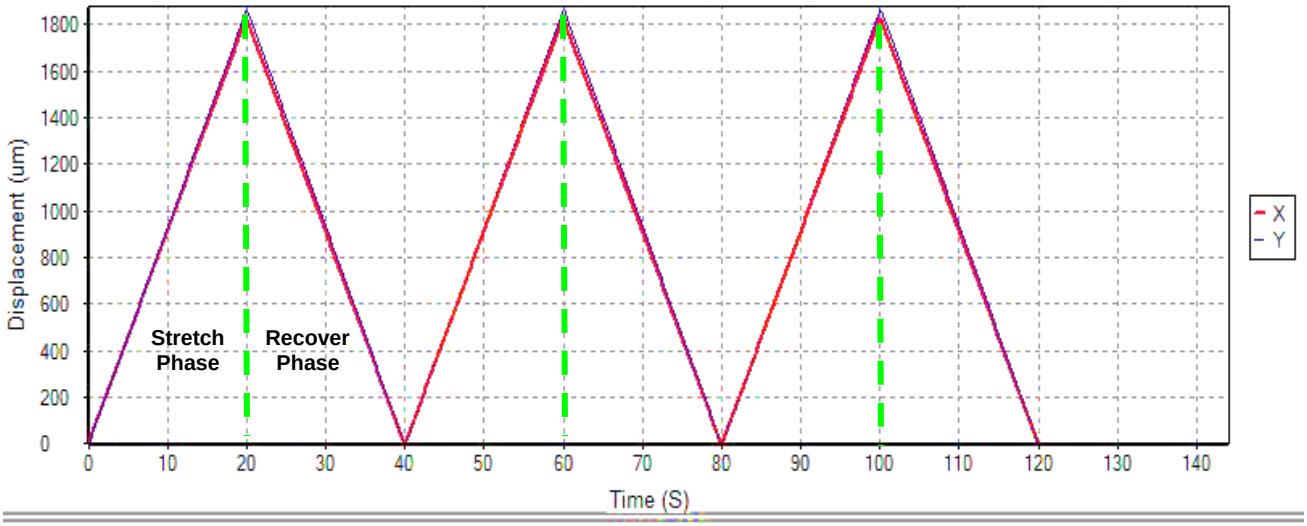
Displacement (um)
Time (S)
Stretch Phase
Recover Phase
X
Y

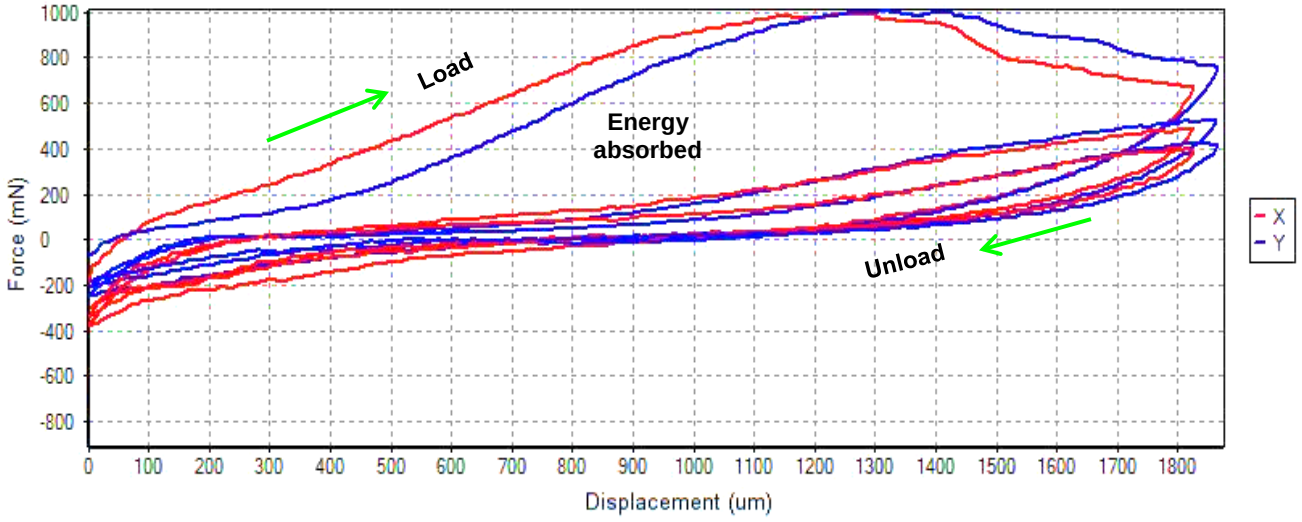
Load
Energy absorbed
Unload
Force (mN)
Displacement (um)
X
Y

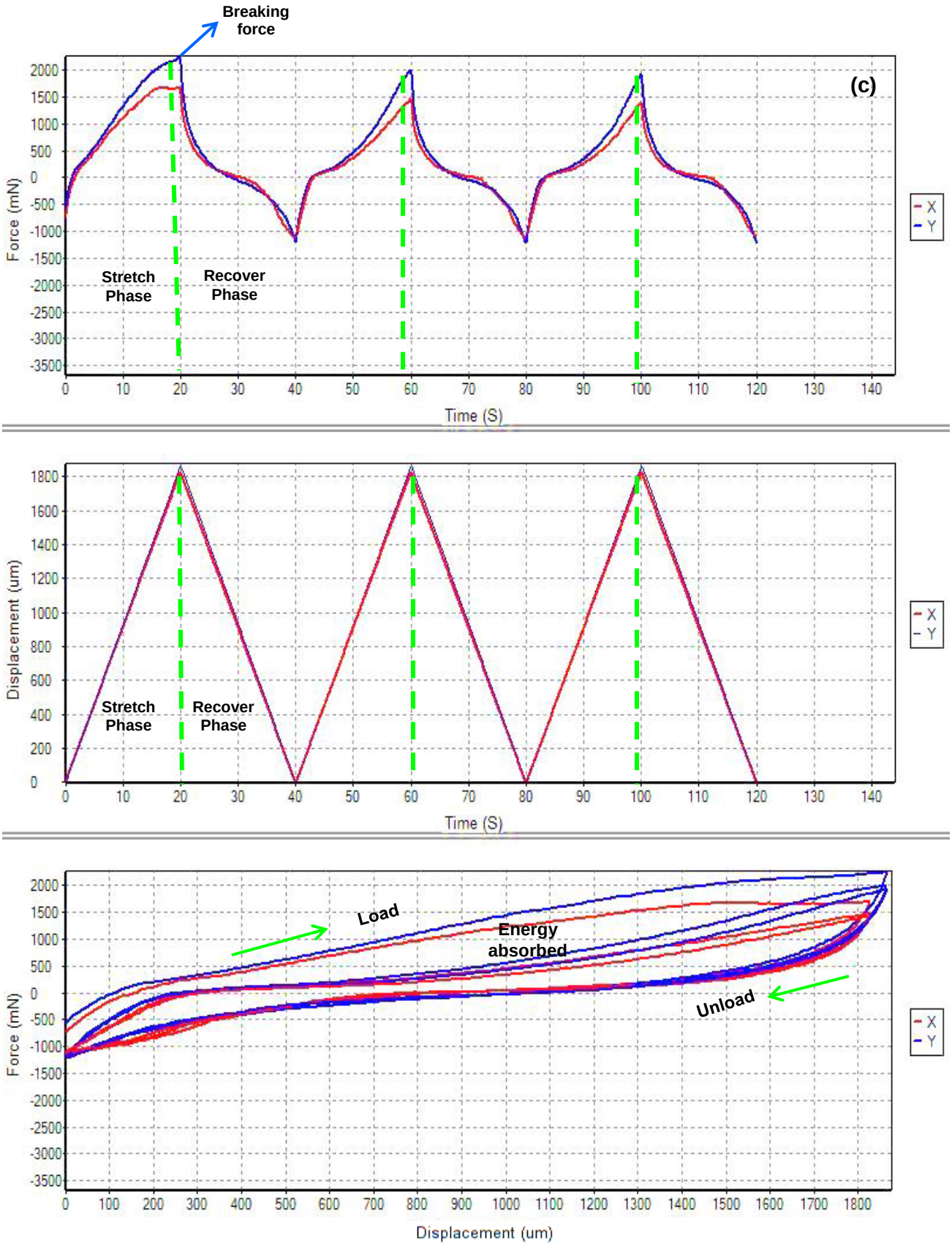

Figure 6.11: Biaxial tensile testing profiles of Force-Time, Displacement-Time and Force-Displacement in the X and Y direction for the 'smart' polymeric sheet-encapsulated OCMTs containing **a)** 15%$^{w}/_{v}$ zein, **b)** 17.5%$^{w}/_{v}$ zein and **c)** 20%$^{w}/_{v}$.

6.3.7. *In vitro* peptide release analysis

The experimental peptide release patterns of Octreotide from the pH_M 'smart' polymeric sheet encapsulated-OCMT formulations F1-F13 in SHIF (pH 6.8) was evaluated. A 4-parameter logistic curve generated from the peptide-specific ELISA kit was used to calculate the unknown concentrations of the experimental samples at each time point. Results were displayed as a function of fractional release against time as shown in Figure 6.12a-d. All formulations displayed similar release profiles to that of the optimized OCMT, containing no pH modifier or 'smart' polymeric sheet, as profiled previously (Choonara *et al*., 2016).

Similarly, the release profiles were attributed to the combined effects of swelling, surface erosion and *in situ* crosslinking with fractional releases ranging from 0.79-0.89. Ideally, the pH modifier did not significantly affect the release profiles obtained, however, the 'smart' polymeric sheet accounted for the improved control of release of Octreotide, specifically from 8hr to 24hr. This was further supported by the MDT values obtained which gave an indication of the peptide release rate (Wadher *et al.,* 2011; Sathish and Syed, 2013). The MDT values for the higher concentrations of zein (17.5%$^{w}/_{v}$ and 20%$^{w}/_{v}$) within the 'smart' polymeric sheet of the OCMT formulations were ±21.20, indicating a slower release rate as compared to the lower concentrations. These results indicated the ability of the polymeric sheet to further retard the release of the peptide from the OCMT formulations.

Moreover, the release data was fitted into zero-order, first order, Higuchi and Korsmeyer–Peppas models to determine the mechanism of release of the peptide. The best-fit model for the peptide release data observed was based on the kinetic modelling of the regression coefficients and its proximity to the numeral 1. A model depicting a value closest to 1 amongst the formulations would demonstrate the appropriateness of that model in explaining the peptide release mechanism. Based on this premise, all formulations were best-fit into the Higuchi (R^2=0.98) model which describes the release of the peptide from a matrix as a function of the square-root of a time-dependent process based on Fickian diffusion. Due to the complexity of the system, near zero-order (R^2=0.97) release was observed for many formulations. Thus, the release kinetics was attributed to both the Higuchi and zero-order models.

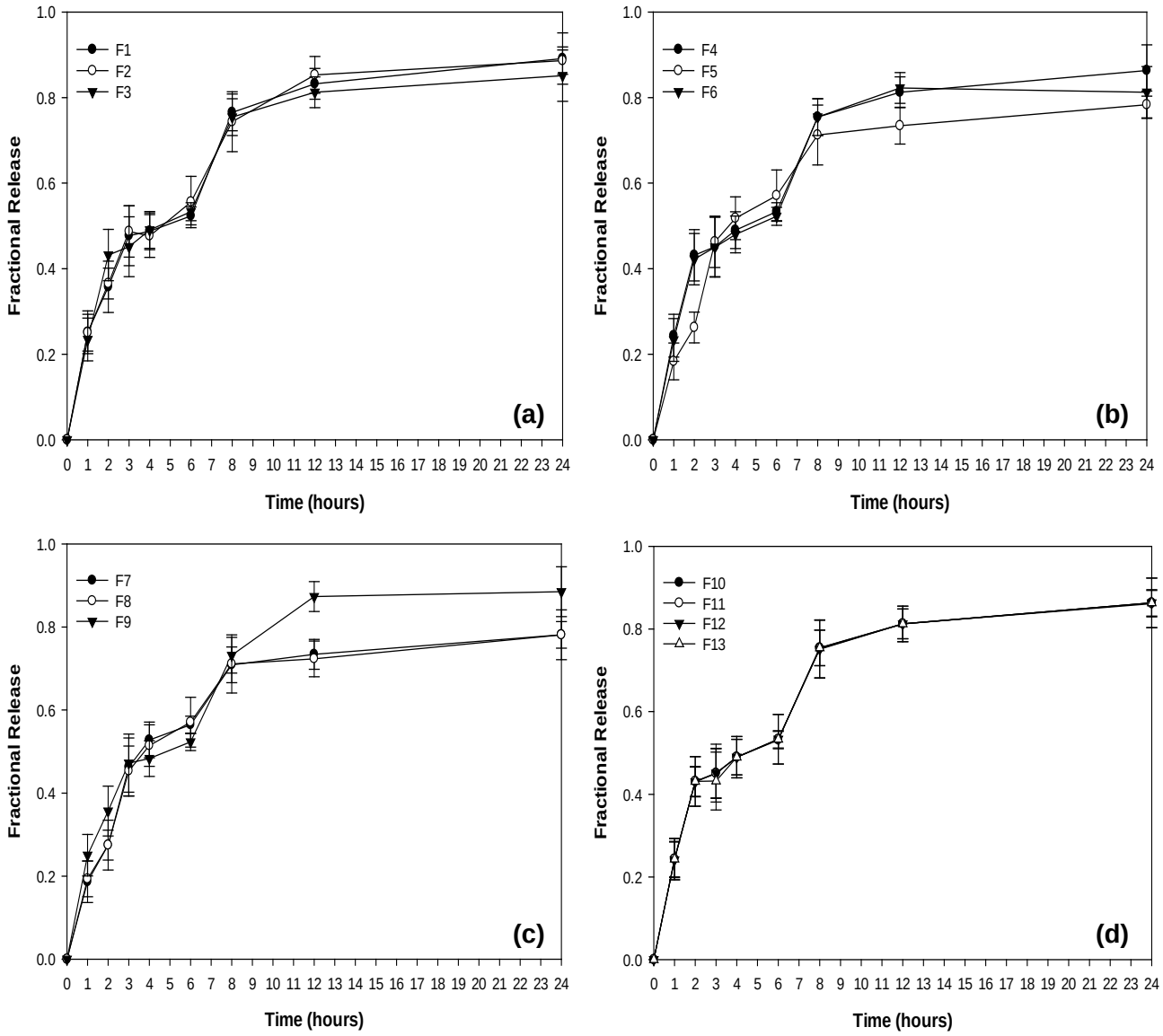

Figure 6.12: Fractional release of Octreotide from the pH_M 'smart' polymeric sheet encapsulated-OCMTs: **a)** formulations F1-F3, **b)** formulations F4-F6, **c)** formulations F7-F9 and **d)** formulations F10-F13.

6.3.8. Response surface analysis of the Face-Centered Central Composite Design (FCCCD)

Experimentally derived responses affecting the performance of the device were further evaluated to determine the distinct relationship between the variable components and the measured responses. The micro-environmental pH and degree of mucoadhesion were the measured responses that were fitted into the FCCCD design to ascertain the optimal OCMT formulation that would ultimately produce the desired outcome. Complete ANOVA analysis of the measured responses were undertaken to determine the adequacy of the model.

The residuals are part of the observation that is not explained by the fitted model, thus, comprehensive residual analysis of the measured responses was important for determining the accuracy of the model produced. The residual plots shown in Figure 6.13 depict the difference between the observed values and predicted or fitted values. This assists in determining whether the ordinary least square (OLS) assumptions are being met (Myers *et al*., 2015). The normal probability plots of the responses generally followed a straight line indicating that the data was normally distributed with only a few outliers and no unidentified variables.

This was further supported by the histogram of residuals showing a symmetrical distribution with slight clustering observed at the center for the micro-environmental pH response. The plots of residuals against their fitted values and in their observation orders appeared to be generally random (centered around zero) with a few outliers identified by the points far away from zero and from other points in the x-direction. These points were considered to be influential and were taken into account during statistical optimization. In addition, the same value was noted at certain points on the residual versus the order of data plots due to the similarity in the responses for the centre-points. Overall, the results demonstrated the suitability of the regression model and consistency of the residuals with stochastic error (Myers et al., 2015).

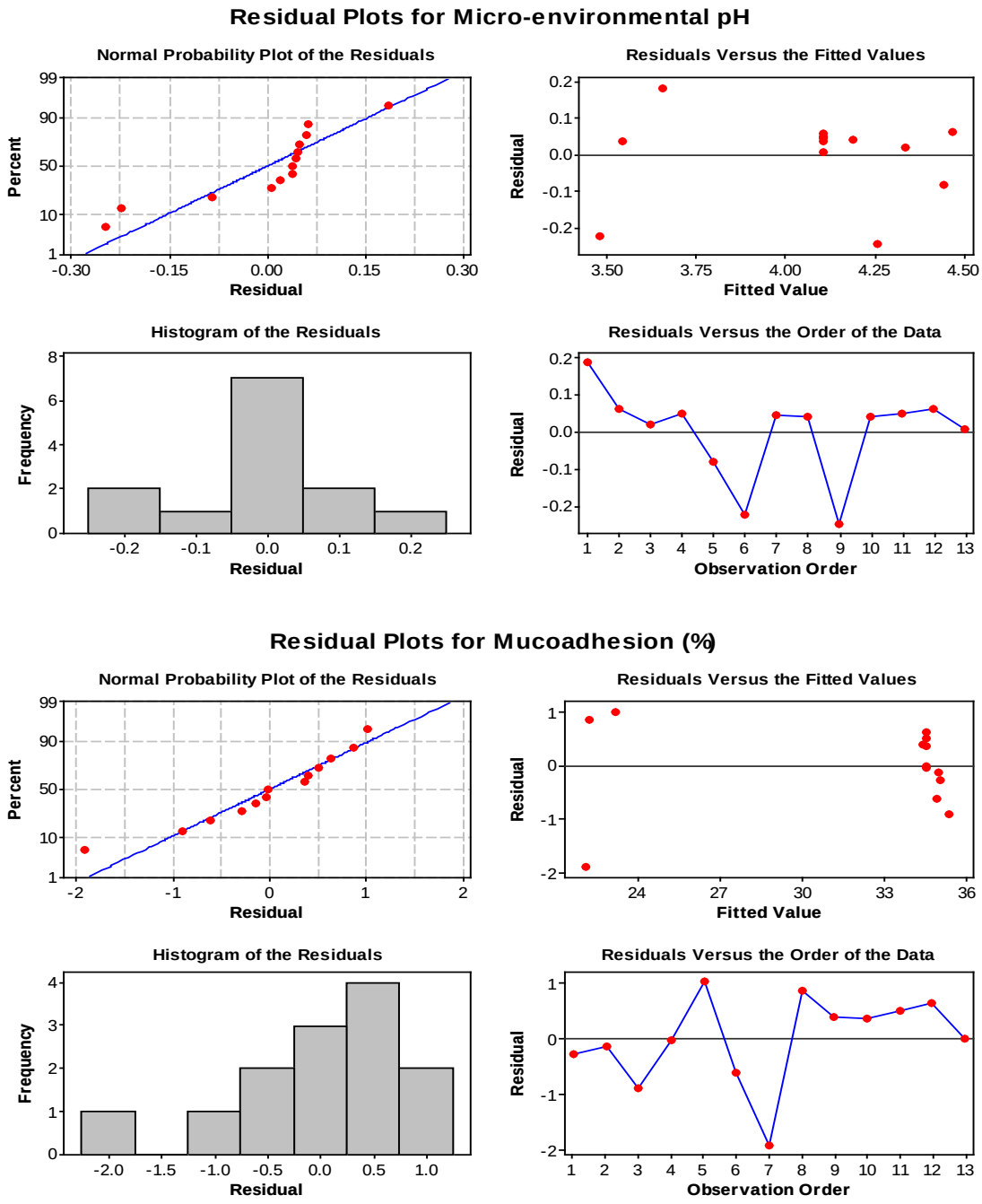

Figure 6.13: Residual plots of the responses; micro-environmental pH and mucoadhesion (%).

Furthermore, surface plots characterized the relationship between the experimental variables and responses achieved. The effects of citric acid on the micro-environmental pH is depicted in Figure 6.14a. High concentrations of citric acid (10mg) produced a greater decrease in the micro-environmental pH (3.2-3.8) potentially enabling the OCMT to reduce the optimal environment for enzyme activity to a greater degree *in vivo*. Contrastingly, lower concentrations of citric acid (5mg) produced smaller decreases in the micro-environmental pH (>4.5) and thus a

lessened effect on the enzyme activity. The concentration of zein did not display any significant effects on the pH values observed. However, the zein concentrations were a major contributing factor to the mucoadhesion percentages obtained as shown in Figure 6.14b. The mucoadhesion results demonstrated a directly proportional relationship to the concentration of zein contained within the 'smart' polymeric sheet. Predictably, citric acid did not affect display any significant effects on the mucoadhesion of the pH_M 'smart' polymeric sheet encapsulated-OCMT formulations F1-F13.

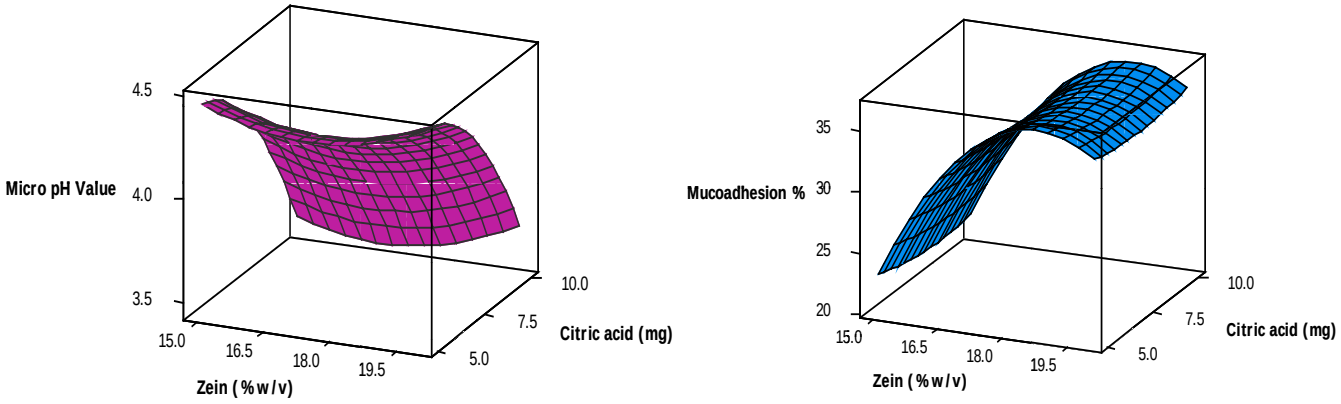

Figure 6.14: Response surface plots depicting the effects of citric acid (mg) and zein ($\%^{w}/_{v}$) on **a)** the micro-environmental pH and **b)** mucoadhesion percentage.

A full ANOVA analysis of response surface regressions was undertaken and results obtained are depicted in Table 6.9. The overall estimated analysis of variance for the regression coefficients for the micro-environmental pH and mucoadhesion percentages produced statistically significant effects for zein concentration levels on mucoadhesion, with p-values of 0.004 and <0.001, respectively. In addition, the R^2 and R^2-adjusted values for the pH (87.8% and 79.2%) and mucoadhesion percentages (97.8% and 96.3%) were satisfactory. Ultimately, statistical probability distributions confirmed the reliability of the statistical design in generating an optimal formulation (Myers *et al*., 2015).

Table 6.9: Estimated p-values for the measured responses.

	p-values	
Response variable	**Micro-pH**	**Mucoadhesion**
Zein ($\%^{w}/_{v}$)	0.244	<0.001
Citric acid (mg)	0.477	0.329
Zein ($\%^{w}/_{v}$)* Zein ($\%^{w}/_{v}$)	0.245	<0.001
Citric acid (mg)* Citric acid (mg)	0.074	0.383
Zein ($\%^{w}/_{v}$)* Citric acid (mg)	0.778	0.634

6.3.9. Response optimization of the pH_M 'smart' polymeric sheet encapsulated-OCMTs

A response optimization procedure (MINITAB®, V15, Minitab, USA) for the FCCCD design formulations was used to determine the optimum levels of the formulatory variables. An optimal formulation was developed following real-time constrained optimization of the micro-environmental pH and mucoadhesion percentages. The constrained settings that were utilized to determine the optimized levels of the independent variables that would generate the desired change in the micro-environmental pH and improved mucoadhesion are presented in Table 6.10. The optimized levels of the independent variables, the goal for the response, the predicted response, *y*, at the current factor settings, as well as the individual and composite desirability scores are shown in Figure 6.15. Based on the statistical desirability function, it was found that the composite desirabilities for the formulation was 1.0.

Table 6.10: Constrained settings for response optimization.

Response	Goal	Target
Micro-environmental pH	Minimize	3.8
Mucoadhesion	Maximize	34.0

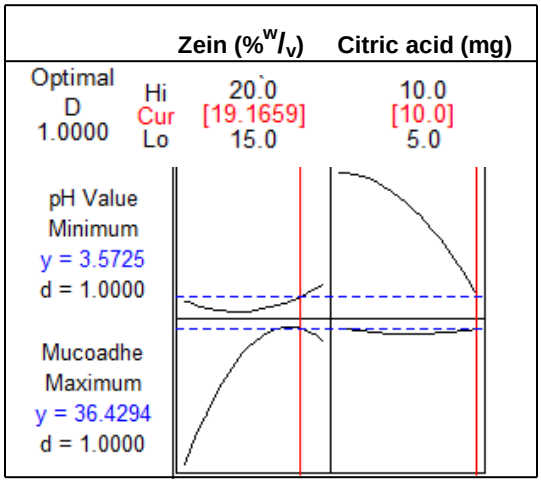

Figure 6.15: Optimization plots outlining factor settings and desirability values for the optimal formulation.

6.4. Concluding Remarks

Physicochemical and physicomechanical characterization of the FCCCD design formulations of the pH_M 'smart' polymeric sheet encapsulated-OCMTs was essential for determining the capability of the characteristic design to impart tri-functionalization. The co-inhibitory potential of polyoxyethylene (40) stearate was demonstrated by in-depth analysis of interactions between

CYP3A4 and Pgp which generated an optimum inhibitory concentration of 5mg/mL. The micro-environmental pH determination provided information about the change in the pH in the presence of the pH modifier. Analysis of the characteristic properties of the 'smart' polymeric sheet was undertaken by evaluation of the distinct rheological profiles and degree of mucoadhesion. In addition, critical physicomechanical characterization of the polymeric sheet favorably demonstrated its *in vivo* ability to withstand GIT forces. The *in vitro* release of Octreotide was influenced by the combined effects of swelling, surface erosion and *in situ* crosslinking, displaying fractional releases ranging from 0.79-0.89. The 'smart' polymeric sheet provided a slower release rate as evidenced by the higher MDT value (±21.20) obtained. Response surface analysis demonstrated the statistical significance ($p < 0.05$) of the regression model in producing single concentration variables for an optimized formulation. Conclusive results from physicochemical and physicomechanical characterization of the design demonstrated the applicability of the pH_M 'smart' polymeric sheet encapsulated-OCMTs to provide Tri-functionalization. The optimized Tri-functionalized OCMT was evaluated thoroughly in Chapter 7 to determine the suitability of the system to proceed with *in vivo* studies.

6.5. References

Ainsworth, S. (1977). *Steady-State Enzyme Kinetics*. *1st ed*. UK, London: Macmillan Education. pp. 43-73.

Arhewoh, I.M., Ahonkhai, E.I., Okhamafe, A.O. (2005). Optimising oral systems for the delivery of therapeutic proteins and peptides. *African Journal of Biotechnology*, 4, 1591-1597.

Badawy, S.I.F., Hussain, M.A. (2006). Microenvironmental pH Modulation in Solid Dosage Forms. *Journal of Pharmaceutical Sciences,* 96, 948-959.

Bruno, B.J., Miller, G.D., Lim, C.S. (2013). Basics and recent advances in peptide and protein drug delivery. *Therapeutic Delivery,* 4, 1443-1467.

Carino, G.P., Mathiowitz, E. (1999). Oral insulin delivery. *Advanced Drug Deliv*ery *Reviews,* 35, 249–257.

Carvalho, F.C., Bruschi, M.L., Evangelista, R.C., Gremiao, M.P.D. (2010). Mucoadhesive drug delivery systems. *Brazilian Journal of Pharmaceutical Sciences*, 46, 1-17.

Choonara, B.F., Choonara, Y.E., Kumar, P., Bijukumar, D., du Toit, L.C., Pillay, V. (2014). A review of advanced oral drug delivery technologies facilitating the protection and absorption of protein and peptide molecules. *Biotechnology Advances,* 32, 1269-1282.

Choonara, B.F., Choonara, Y.E., Kumar, P., du Toit, L.C., Pillay, V. (2016). Design of an *in situ* cross-linked eutectic tablet for enhanced delivery of gastro-sensitive proteins and peptides. *Journal of Pharmaceutical Sciences*, 105, 2086-2098.

George, H.F., Qureshi, F. (2013). *Newton's Law of Viscosity, Newtonian and Non-Newtonian Fluids: Encyclopedia of Tribology.* USA, New York: Springer. pp 2416-2420.

Gregory, D.E., Callagan, J.P. (2005). An examination of the mechanical properties of the annulus fibrosus: The effect of vibration on the intra-lamellar matrix strength. *Medical Engineering & Physics,* 34, 472-477.

He, P., Davis, S.S., Illum, L. (1998). . *In vitro* evaluation of the mucoadhesive properties of chitosan microspheres. *International Journal of Pharmaceutics*, 166, 68-75.

Holmes, M.W.R., Howarth, S.J., Callaghan, J.P., Keir, P.J. (2012). Biomechanical Properties of the Transverse Carpal Ligament under Biaxial Strain. *Journal of Orthopaedic Research,* 30, 757-763.

Holmes, R. (1971). The intestinal brush border. *Gut,* 12, 668-677.

Irgenz, F. (2014). *Rheology and Non-Newtonian Fluids.* USA, New York: Springer International. pp. 4-16.

Jang, J., Lance, M.J., Wen, S., Tsui, T.Y., Pharr, G.M. (2005). Indentation-induced phase transformations in silicon: influences of load, rate and indenter angle on the transformation behavior. *Acta Materialia,* 53, 1759-1770.

Jiang, Y., Yan, S. (2008). Effects of pH on the activities of digestive enzymes in *Panulirus stimpsoni*. *Acta Zoologica Sinica,* 54, 317-322.

Kim, R.B. Wandel, C., Leake, B., Cvetkovic, M., Fromm, M.F., Dempsey, P.J., Roden, M.M., Belas, F., Chaudhary, A.K., Roden, D.M., Wood, A.J.J, Wilkinson, G.R. (1999). Interrelationship between substrates and inhibitors of Human CYP3A and P-glycoprotein. *Pharmaceutical Research,* 16, 408-414.

Laulicht, B., Tripathi, A., Schlageter, V., Kucera, P., Mathiowitz, E. (2010). Understanding gastric forces calculated from high-resolution pill tracking. *Proceedings of the National Academy of Sciences,* 107, 8201-8206.

Lee, J.H. (2002). Protein drug oral delivery: the recent progress. *Archives of Pharmaceutical Research*, 25, 572–84.

Lim, H., Hoag, S.W. (2013). Plasticizer Effects on Physical–Mechanical Properties of Solvent Cast Soluplus® Films. *AAPS PharmSciTech,* 14, 903-910.

Mahato, R.I., Narang, A.S., Thoma, L., Miller, D.D. (2003). Emerging trends in oral delivery of peptide and protein drugs. *Critical Reviews™ in Therapeutic Drug Carrier System,* 20, 153-214.

Myers, R.H., Montgomery, D.H., Anderson-Cook, C.M. (2015). *Response Surface Methodology: Process and Product Optimization Using Designed Experiments.* Hoboken, New Jersey: John Wiley & Sons Inc. pp. 13-80.

Paliwal, R., Palakurthi, S. (2014). Zein in controlled drug delivery and tissue engineering. *Journal of Controlled Release,* 189, 108-122.

Patel, A., Hu, Y., Tiwari, J.K., Velikov, K.P. (2010). Synthesis and characterisation of zein-curcumin colloidal particles. *Soft Matter,* 6, 6192-6199.

Ritchie, R.J., Prvan T. (1996). Current Statistical Methods for Estimating the K_m and V_{max} of Michaelis-Menten Kinetics. *Biochemical Education,* 24, 196-206.

Sathish, U., Syed, I.A. (2013). Formulation and characterization of matrix and triple layer matrix tablets for controlled delivery of tramadol hydrochloride. *International Journal of Pharmaceutical Sciences*, 5, 458-464.

Sathish, U., Syed, I.A. (2013). Formulation and characterization of matrix and triple layer matrix tablets for controlled delivery of tramadol hydrochloride. *International Journal of Pharmaceutical Sciences*, 5, 458-464.

Shugarts, S., Benet, L.Z. (2009). The Role of Transporters in the Pharmacokinetics of Orally Administered Drugs. *Pharmaceutical Research,* 26, 2039-2054.

Singh, I., Rana, V. (2012). Techniques for the Assessment of Mucoadhesion in Drug Delivery Systems: An Overview. *Journal of Adhesion Science and Technology,* 26, 2251-2267.

Tatavarti, A.S., Hoag, S.W. (2006). Microenvironmental pH Modulation Based Release Enhancement of a Weakly Basic Drug from Hydrophilic Matrices. *Journal of Pharmaceutical Science,* 95, 1459-1468.

Wacher, V.J., Silverman, J.A., Zhang, Y., Benet, Z. (1998). Role of P-Glycoprotein and Cytochrome P450 3A in Limiting Oral Absorption of Peptides and Peptidomimetics. *Journal of Pharmaceutical Sciences,* 87, 1322-1330.

Wadher, K.J., Kakde, R.B., Umekhar, M.J. (2011). Study on sustained-release metformin hydrochloride from matrix tablet: Influence of hydrophilic polymers and *in vitro* evaluation. *International Journal of Pharmaceutical Investigation*, 1, 157-163.

Wongsasulak, S., Puttipaiboon, N., Yoovidhya, T. (2013). , Fabrication, gastromucoadhesivity, swelling, and degradation of zein–chitosan composite ultrafine fibers. *Journal of Food Science,* 78, 926-935.

Zhou, X.H. (1994). Overcoming enzymatic and absorption barriers to non-parenterally administered protein and peptide drugs. *Journal of Controlled Release,* 29, 239–52.

CHAPTER 7

COMPREHENSIVE CHARACTERIZATION OF THE STATISTICALLY OPTIMIZED TRI-FUNCTIONALIZED ORAL CORE-MELT TABLET (OCMT) FOR ENHANCED PROTEIN AND SYNTHETIC PEPTIDE DELIVERY

To be submitted to Nature Biotechnology

Bibi F. Choonara, Yahya E. Choonara, Pradeep Kumar, Lisa C. du Toit, Viness Pillay. Comprehensive In vitro and In vivo Characterization of the Statistically Optimized Tri-Functionalized Oral Core-Melt Tablet (OCMT) for Enhanced Protein and Synthetic Peptide Delivery.

Abstract

In-depth analysis of the statistically optimized Tri-functionalized OCMT for the delivery of gastro-sensitive proteins and synthetic peptides was undertaken. Physicochemical and physicomechanical characterization techniques demonstrated the optimum *in vitro* potential of the Tri-functionalized OCMT in the achievement of clinical efficacy. Analysis of the mucoadhesion and micro-environmental pH produced results that fell within the range of desired targeted responses. The gastro-resistant nature of the Tri-functionalized OCMT was demonstrated by achievement of <5% acid uptake. In addition, comprehensive mechanical analysis confirmed the multi-textural properties of the Tri-functionalized OCMT in the attainment of optimum mechanical strength. MRI imaging highlighted the hydrational transitions and unique pharma-engineering of the tablet. The release of Octreotide from the statistically optimized formulation demonstrated the effect of distinct formulatory components on the responsive potential of the Tri-functionalized OCMT. Fractional release reached a value of ±0.9 with the MDT (±21.58) indicating a slower peptide release rate. Lastly, critical cytotoxic analysis of the EPB showed a ±79.83% survival rate, indicating acceptable biocompatibility and safety for clinical use.

Keywords: OCMT; tri-fucntionalization; multi-textural; gastro-resistant; physicochemical properties; physicomechanical properties

7.1. Introduction

Therapeutic proteins and peptides have become the favored option in the treatment of multiple disease conditions (Park *et al*., 2011; Chin *et al*., 2012; Choonara *et al*., 2014). Due to their increased demand, pharmaceutical scientists have rallied in their efforts to produce a viable alternative to the conventional parenteral route of administration (Park *et al*., 2011). Widespread oral routes still remain the preeminent option for delivery of pharmaceuticals. However, the oral delivery of therapeutic proteins and peptides continue to face immense challenges due to the physical and chemical impediment of the gastrointestinal (GIT) barrier (Choonara *et al*., 2014). Despite active efforts, no clinically useful oral formulations have been developed and as a result, novel technologies attempting to breakthrough the field are of great interest.

The rational design of the OCMT promotes tri-functionalization through the novel incorporation of a core-melt archetype, a pH modifier and a 'smart' polymer modulated co-inhibitory component. This creates a platform for enhanced delivery of proteins and synthetic peptides by triple targeting of the major contributing factors hindering successful oral delivery of proteins and peptides. These factors include: 1) the exposure of proteins and peptides to unfavorable conditions within the stomach as a result of the fluid contents and acidic functioning environment; 2) poor absorption and low oral bioavailability of proteins and peptides resulting from their large molecular mass, hydrophilic properties, CYP3A4 metabolism and P-glycoprotein (Pgp) facilitated transmembrane efflux and lastly; 3) the enzymatic degradation at the intestinal brush border (Mahato *et al*., 2003; Arhewoh *et al.,* 2005; Park *et al*., 2011; Antunes *et al.,* 2013). The overall simplified *modus operandi* of the Tri-functionalized OCMT is presented in Figure 7.1.

The Tri-functionalized OCMT would possess the inherent capabilities that meet the following design criteria, which would form the basis of ultimate optimization of the device:

1. The characteristic design of the outer polymer shell with core-melt archetype and *in situ* crosslinking capabilities to provide structural protection and controlled release of the incorporated protein or synthetic peptide.
2. A prolamine-based 'smart' polymeric sheet providing acid resistance and mucoadhesion, interacting well with hydrophilic molecules (i.e. proteins and peptides) and functioning to enable passage of proteins and peptides through the GIT membrane. In addition, provision of sustained release capabilities in direct tablet compression.

3. A co-inhibitor within the 'smart' polymeric sheet to influence the activity of Cytochrome P450 3A4 (CYP3A4) and P-glycoprotein (Pgp) and improve oral bioavailability by reducing protein and peptide metabolism and inhibiting transmembrane efflux.
4. Incorporation of a pH modifier to facilitate indirect inhibition of enzyme activity at the brush border by transiently lowering the micro-environmental pH and subsequently reducing the optimal environment for enzyme activity.

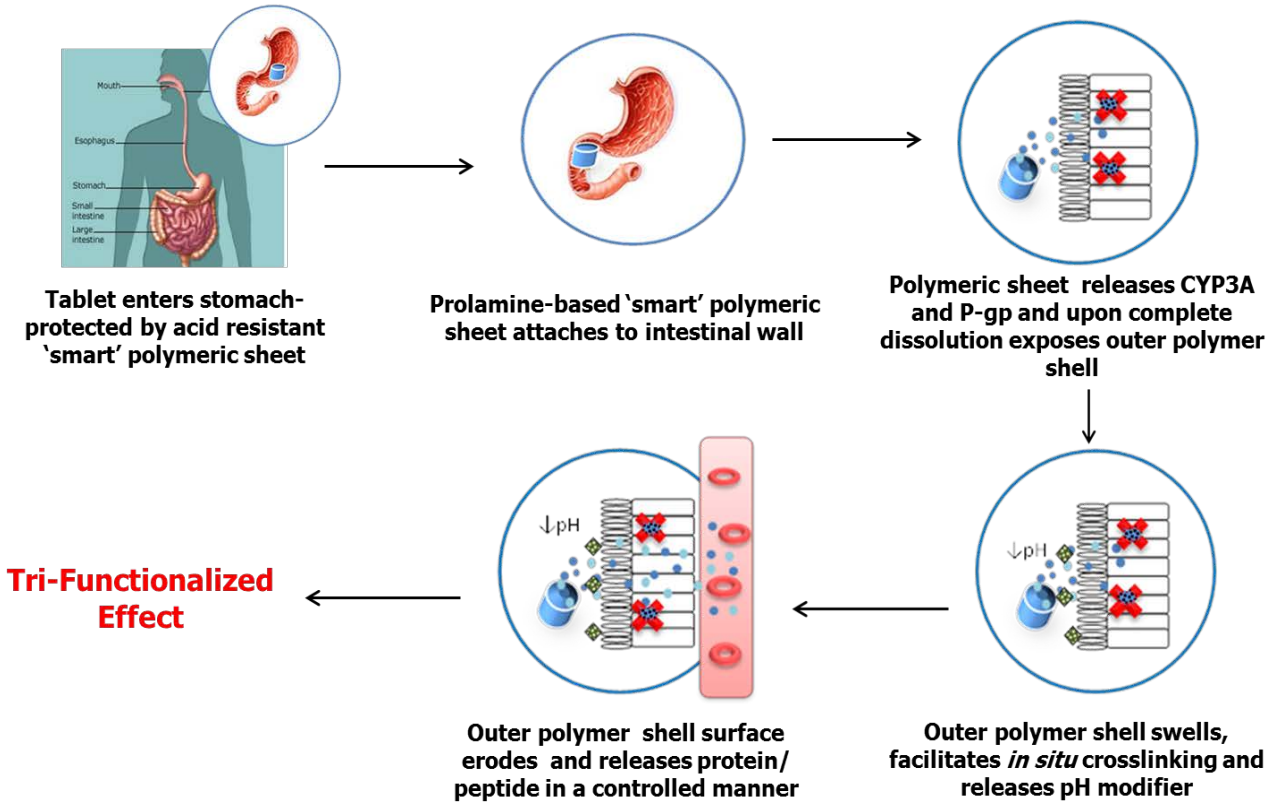

Figure 7.1: Diagrammatic representation of the proposed mechanism of action of the Tri-functionalized OCMT.

7.2. Materials and Methods

7.2.1. Materials

Menthol (2-isopropyl-5-methylcyclohexanol, 99% purity, M_W=156,27g/mol), cetomacrogol 1000, poly (ethylene oxide) (PEO) (Polyox™, WSR-303), polyoxyethylene (40) stearate (Myrj® 52), Zein (from maize) and excipients, sodium carboxymethylcellulose (CMC), magnesium stearate and sucrose were purchased from Sigma-Aldrich Corp. (St. Louis, MO, USA). The crosslinker

sodium carbonate ($NaCO_3$) was purchased from Associated Chemical Enterprises (ACE) (Pty) Ltd. (Johannesburg, Gauteng, South Africa). Pectin citrous (poly-D-galacturonic acid methyl ester), the crosslinker di-potassium hydrogen orthophosphate anhydrous (K_2HPO_4; M_W=174.18g/mol), citric acid (≥99.5% purity, M_W=210.14g/mol), methyl paraben (methyl 4-hydrozybenzoate, M_W=152.15g/mol) and polypropylene glycol (1, 2–propanediol) were procured from Merck Chemicals (Pty) Ltd. (Modderfontein, Gauteng, South Africa). Octreotide acetate ($C_{49}H_{66}N_{10}O_{10}S_2$; M_w=1019.247g/mol) was purchased from Bolon Pharmachem Co., Ltd. (Taizhou, Zheijang, China). *In vitro* Toxicology Assay kit, MTT based was purchased from Sigma-Aldrich Corp. (St. Louis, MO, USA). Caco-2 cell line (ATCC® HTB-37™), Dulbecco's Modified Eagle's Medium (DMEM), Foetal bovine serum (FBS), Penicillin-streptomycin, Trypsin-EDTA (0.25mg/mL) and all other cell culture components were purchased from Separations (Pty) Ltd. (Randburg, Gauteng, South Africa). All other reagents were of analytical grade and were employed as received.

7.2.2. Formulation of the statistically optimized Tri-functionalized OCMT

The Tri-functionalized OCMT was prepared in accordance with the detailed methods presented previously in Chapter 4, 5 and 6. The variables used in the preparation of the different components of the Tri-functionalized OCMT were statistically optimized through a combination of a Box-Behnken and Face-Centered Central Composite Design (FCCCD), as highlighted previously. The statistical optimization produced the variable concentrations shown in Table 7.1 which were subsequently used for preparation of the Tri-functionalized OCMT. All other components and excipients of the Tri-functionalized OCMT were used at concentrations originally specified in Choonara *et al*, (2016) or according to their experimentally determined optimal values.

Table 7.1: Formulation concentrations for the optimized Tri-functionalized OCMT

Variable	Optimized value
$NaCO_3$ and K_2HPO_4 ($\%^w/_w$)	23.093
Eutectic Powder Blend ($\%^w/_w$)	12
Pectin (mg)	65.314
Zein ($\%^w/_v$)	19.166
Citric acid (mg)	10

A summarized overview of the preparation method for the Tri-functionalized OCMT is presented in Figure 7.2. The EPB for the core eutectic region of the tablet was synthesized according to a co-melt method and served as a carrier for the crosslinking agents and therapeutically active

protein or peptide. The outer polymer shell was double layered and contained a pH modifier, assembling to form a pH-modified (pH_M) OCMT with inner core eutectic region. The prolamine-based 'smart' polymeric sheet was prepared by a simple solvation technique and successfully incorporated the co-inhibitor for CYP3A4 and P-glycoprotein. The complete Tri-functionalized OCMT was obtained by encapsulation of the pH_M-OCMT with the co-inhibitory 'smart' polymeric sheet via a 'dip' and 'dry' method.

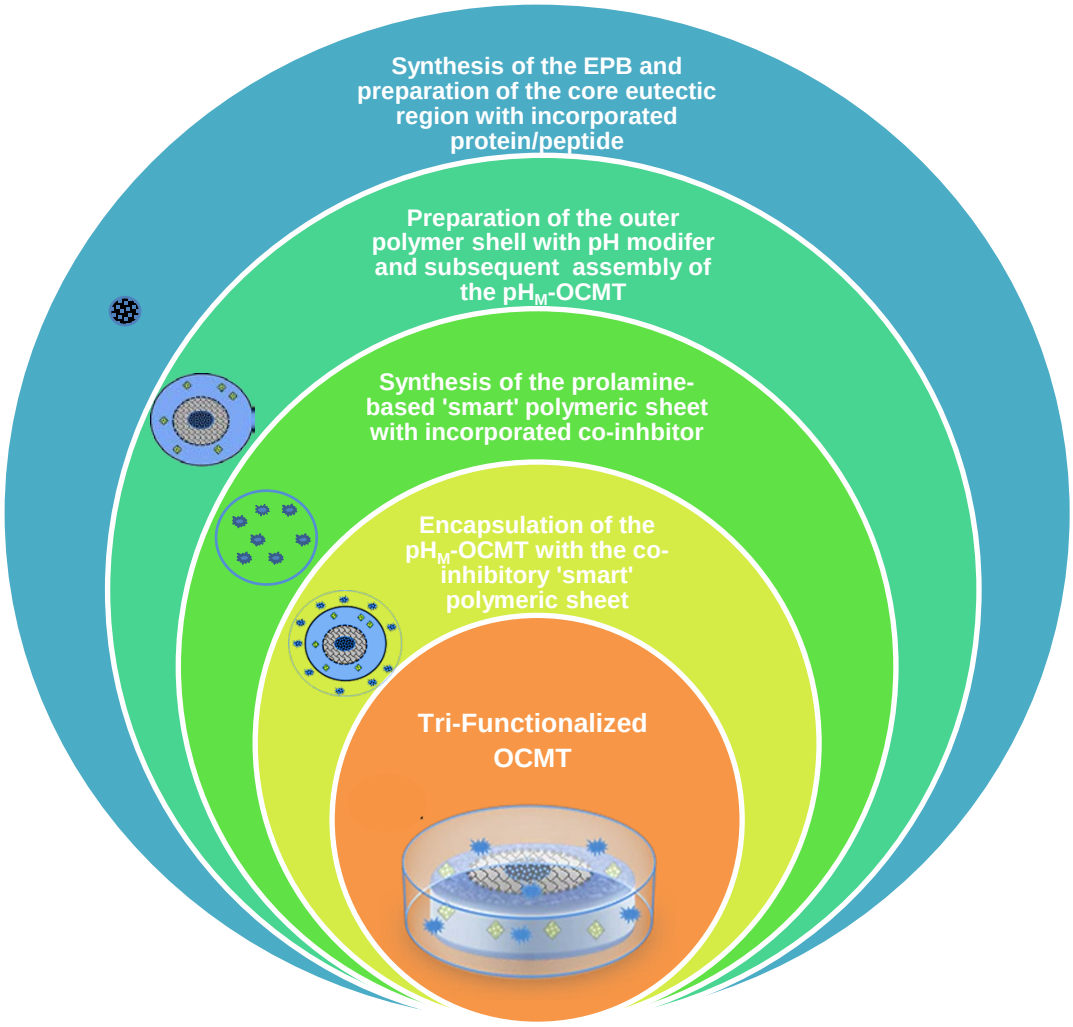

Figure 7.2: Overview of the preparation method for the statistically optimized Tri-functionalized OCMT.

7.2.3. In-process validation of the Tri-functionalized OCMT

Weight uniformity, thickness and friability analyses were performed on the statistically optimized Tri-functionalized OCMT. A sample of 5 units of the Tri-functionalized OCMT was analyzed to determine the standardization of the tablet-assembly and encapsulation process. The weight of

the OCMT was determined using an analytical digital balance (Mettler, Model AE 240, Griefensee, Switzerland) with readings recorded to 2 decimal places. The thickness of the Tri-functionalized OCMTs were determined using a digital caliper (25 × 0.01mm capacity) (Taizhou hangyu tools gauge and blades Co., Ltd., Wenqiao, Zhejiang, China). The friability was determined using a Friabilator (Erweka D-63150, Heusenstamm, Germany) set at 25 rpm for 4 minutes with 1% set as the upper limit of acceptability. The friability was calculated as percentage loss using Equation 7.1.

$$WL_t = \frac{(W_0 - W_t)}{W_0} \times 100 \quad \textbf{(7.1)}$$

Where, WL_t is the total weight loss; W_0 is the initial weight of the tablet and W_t is the final weight of the tablet.

7.2.4. Evaluation of the micro-environmental pH response of the statistically optimized Tri-functionalized OCMT

The micro-environmental pH response resulting from the pH modulating effects of the optimized concentration of citric acid, as shown in Table 7.1, was determined using a SevenMulti™ dual pH/conductivity meter (Mettler-Toledo International Inc., Im Langacher, Greifensee, Switzerland) (Badawy and Hussain, 2006; Tatarvati and Hoag, 2006). The optimized OCMT formulation containing 10mg of citric acid (without the polymeric sheet) was prepared (n=3) for evaluation by immersing in 50mL of simulated human intestinal fluid (SHIF) pH 6.8 for a period of ±4 hours. The optimized OCMT was hydrated for a short period of time in order to avoid the confounding factors that may result from complete leaching out of the pH modulator. Following hydration, the pH glass electrode tip was allowed to penetrate the swollen outer polymer shell of the tablet and held until a stable reading was obtained. In addition, the pH of the SHIF immediately surrounding the optimized OCMT was measured to confirm the observation of an unaltered macro-environmental pH.

7.2.5. Characterization of the molecular and vibrational transitions of the optimized co-inhibitory ‘smart’ polymeric sheet

The successful incorporation of polyoxyethylene (40) stearate with the optimized concentration of zein to form the co-inhibitory ‘smart’ polymeric sheet was evaluated by characterizing the vibrational and molecular transitions using Attenuated Total Reflectance-Fourier Transform Infrared Spectroscopy (ATR-FTIR). FTIR analysis was conducted on the native components

(polyoxyethylene (40) stearate and zein) as well as the blended combination to acquire critical microstructural information that would validate a successful incorporation process. Results were recorded on a PerkinElmer Spectrum 2000 FTIR spectrophotometer with a single-reflection diamond MIRTGS detector (PerkinElmer Spectrum 100, Llantrisant, Wales, UK) fitted with a universal ATR polarization accessory for the FTIR spectrum series at a resolution of $4cm^{-1}$. Samples were prepared by casting the optimized co-inhibitory 'smart' polymeric sheet solution into petri dishes and allowing them to dry in a laboratory fumehood overnight to form dried films (mimicking the dried polymeric sheet surrounding the OCMT). The films were subsequently placed on a diamond crystal for analysis between a scanning range of $4000\text{-}600cm^{-1}$ at a constant pressure of 120psi with 32 accumulations.

7.2.6. Determination of the pertinent rheological properties of the optimized 'smart' polymeric sheet solution

The flow characteristics of the optimized zein aqueous-ethanol solution, forming the basis of the 'smart' polymeric sheet was evaluated for its rheological properties via measurement of intrinsic viscosity. The viscosity (η) was measured at a temperature of 25°C and a shear rate of $100s^{-1}$ for 360s using a Haake Modular Advanced Rheometer System (MARS) (ThermoFisher Scientific, Karlsruhe, Germany) fitted with a C35/1° titanium rotor sensor. An optimized concentration of the zein solution ($19.166\%^{w}/_{v}$) was placed on the sample stage and measured according to the parameters employed in Table 7.2. Evaluation of the viscosity was important in validating the suitability of the zein solution to optimally adhere to the surface of OCMT during encapsulation.

Table 7.2: Parameters employed for analysis of the viscosity of the optimized 'smart' polymeric sheet solution

Parameter	Value
Cone and plate gap	0.050mm
Driver version	1.29
Inertia	1.721×10^{-6} kg.m^2
A-factor	89051.00 Pa/Nm
M-factor	57.010 (1/s)/((rad/s)
Temperature	25°C
Damping	30.00

7.2.7. Determination of the *in vitro* and *ex vivo* mucoadhesive response of the statistically optimized Tri-functionalized OCMT

The inherent mucoadhesivity imparted by the 'smart' polymeric sheet encapsulating the OCMT was evaluated both *in vitro* and *ex vivo*. The *in vitro* mucoadhesive strength determination involved the preparation of a $0.1\%^{w}/_{v}$ solution of mucin in SHIF pH 6.8. The optimized Tri-functionalized OCMT formulation was incubated in the prepared solution in an orbital shaker maintained at 37˚C and 50 rpm for 6 hours (n=3). Following incubation, the concentration of free mucin in the solution was determined by a UV spectrophotometer, at 201nm (IMPLEN NanophotometerTM, Implen GmbH, München Germany), using a 10 times dilution factor of path-length 0.1 mm. The difference in the concentration of the mucin solution before and after incubation was the indication of the amount crosslinked with the optimized 'smart' polymeric sheet as calculated using Equation 7.2 (He *et al.,* 1998).

$$\text{Mucoadhesion}\% = \frac{[\text{Mucin before}]-[\text{Mucin after}]}{[\text{Mucin before}]} \times 100 \quad \textbf{(7.2)}$$

Where, [Mucin before] is the concentration of the mucin solution before incubation and [Mucin after] is the concentration of the mucin solution after incubation.

In addition, pig intestinal tissue was used to determine the *ex vivo* bioadhesivity of the Tri-functionalized OCMT. A Texture Analyzer (TA.XT *plus*, Stable Microsystems, Surrey, UK) fitted with a mucoadhesion rig provided a vessel of a temperature-controlled (37°C) intestinal fluid and mucin environment for the pig intestinal tissue set-up. The Tri-functionalized OCMT was slightly hydrated in SHIF and attached to a cylindrical probe of the mucoadhesion rig using double-sided bioadhesive tape. The probe with attached OCMT was lowered at a constant speed of 0.1mm/s to bond with the mucin-coated tissue at a predetermined compression force (0.08N) for a period of 120s. After the contact time, the probe withdrew at a constant speed (0.1mm/s) from the intestinal tissue and the adhesive properties were measured. The work of adhesion was calculated from the Force-Distance profile obtained, using Equation 7.3 (Cevher *et al*., 2008).

$$\text{Work of adhesion } (\text{mJ}.\text{cm}^2) = \frac{\text{AUC}_{\text{F-D}}}{\pi \text{r}^2} \quad \textbf{(7.3)}$$

Where, AUC is the area under the curve of the Force-Distance profile and πr^2 is the surface area of the Tri-functionalized OCMT.

7.2.8. Determination of the gastric acid uptake of the optimized Tri-functionalized OCMT

Acid uptake tests in accordance with USP standards were performed to assess the gastric acid uptake and resistance of the gastro-resistant 'smart' polymeric sheet of the OCMT. The optimized 'smart' polymeric sheet encapsulated OCMTs were weighed prior to being subjected to dissolution conditions (n=6). The weighed OCMTs were placed in USP Simulated Gastric Fluid (SGF) pH 1.2 in a USP35 dissolution apparatus II (Caleva, Model 7ST, UK) at 37°C, 50rpm for 2 hours. Following 2 hours, the tablets were removed and excess SGF was drained and blotted dry with filter paper. The tablets were then reweighed and the SGF uptake was calculated according to Equation 7.4 (Liu *et al.*, 2011; Czarnocka and Alhnan, 2015).

$$\text{SGF uptake } (\%) = \frac{W_f - W_i}{W_i} \times 100 \quad \textbf{(7.4)}$$

Where, W_f is the final weight of the tablet and W_i is the initial weight of the tablet.

7.2.9. Evaluation of the surface and core matrix hardness, matrix resilience and deformation energy of the optimized Tri-functionalized OCMT

Textural profiling of the optimized Tri-functionalized OCMT was assessed using a calibrated Texture Analyzer (TA.XT *plus*, Stable Microsystems, Surrey, UK) fitted with a 5kg load cell (n=3). The Matrix Hardness (MH), Matrix Resilience (MR), Deformation Energy (DE) and rigidity of the Tri-functionalized OCMT were collectively determined. A flat-tipped steel probe (2mm diameter) was used for surface determination of MH and MR values of the OCMT. Further textural analyses of the OCMT were undertaken using a needle-tipped steel probe (2mm diameter) for determination of the MH and DE through penetration of the complete thickness of the Tri-functionalized OCMT. The samples were prepared and placed in a Temperature Controlled Peltier Cabinet (XT/PC) coupled to a Peltier Control Unit (PCU) (Stable Microsystems, Surrey, UK) for analysis by Texture Analyzer to mimic the internal body temperature environment. The Thermal Cabinet was equilibrated to 37°C (body temperature) to enable the melting of the core region of the Tri-functionalized OCMT before testing was performed within the cabinet. Data was captured at a rate of 200 points per second using Texture Exponent Software (V3.2). MR was computed as a percentage of the ratio between the Area under the Curve (AUC) of the peak to baseline (AUC_{2-3}) and the baseline to peak (AUC_{1-2}) from a Force-Time profile as shown in Equation 7.5.

$$\text{Resilience } \% = \left(\frac{\text{Area 2:3}}{\text{Area 1:2}}\right) \times 100 \quad \textbf{(7.5)}$$

The DE and matrix rigidity were both obtained from the AUC and gradient of the Force-Distance profiles, respectively. The MH was calculated using the Brinell Hardness Number (BHN) (Equation 7.6). Textural analysis on the OCMT was performed in triplicate. The parameters employed for the analysis are listed in Table 7.3.

$$\mathrm{BHN} = \frac{2\mathrm{F}}{\pi\mathrm{D}\left(\mathrm{D}-\sqrt{\mathrm{D}^2-\mathrm{d}^2}\right)} \quad \textbf{(7.6)}$$

Where, BHN is Brinell Hardness Number; D is diameter of indenter (mm); F is elucidated from the gradient of the initial force and the final force obtained and d is diameter of indentation (mm).

Table 7.3: Parameters employed for physicomechanical profiling of the optimized Tri-functionalized OCMT

Parameters	**Matrix Hardness, Deformation Energy & matrix rigidity**	**Matrix Resilience**
Pre-test speed	1 mm/s	1 mm/s
Test speed	0.5 mm/s	1mm/s
Post-test speed	1 mm/s	1mm/s
Trigger type	Auto	Auto
Trigger force	0.05 N	0.05 N
Compression strain	N/A	40%

*The distance for probe penetration into the tablet was set at 4mm for the needle-tipped steel probe

7.2.10. Biaxial tensile testing of the optimized Tri-functionalized OCMT

A realistic type of testing of the mechanical strength of the optimized Tri-functionalized OCMT was determined using a state-of-the-art biaxial tensile testing system (BioTester 5000, CellScale biomaterials testing, Waterloo, Ontario, Canada), fitted with a load cell of 5N. Typically, oral dosage forms are subjected to forces within the GIT, associated with the physiological phases of gastric digestion, motility and contractility (Laulict *et al*., 2010). Thus, reproducing physiological conditions during testing of the OCMTs mechanical strength provides information on its ability to withstand these forces and aids in predicting its clinical success. The BioTester brings together several high-precision components for the measurement and analysis of biomaterials. It measures biaxial forces to mirror the multidirectional tension experienced by materials *in vivo*. The system is fitted with a high resolution charge coupled device (CCD) camera (1280 x 960 pixels) to provide high quality images, video tracking and analysis. Samples were prepared by hydrating the Tri-functionalized OCMT in SHIF pH 6.8 for 30 minutes to simulate hydration of the tablet *in situ*. Following hydration, the OCMT was mounted

and secured with tungsten rakes (tine diameter=305μm, tine spacing=1.0mm, puncture depth=1.9mm) symmetrically attached 5mm apart on the X and Y axis of the sample as shown in Figure 7.3.

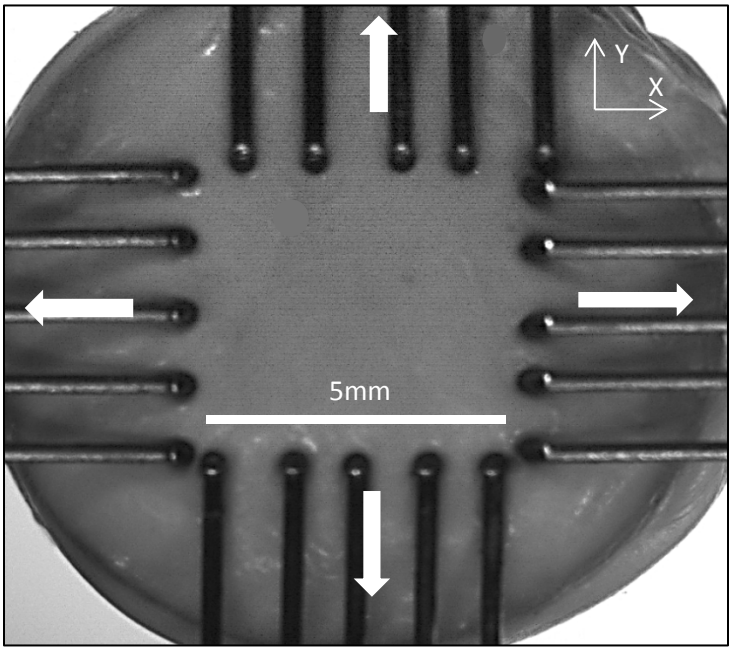

Figure 7.3: Image of the Tri-functionalized OCMT mounted in the biaxial system. Small rake one either side secure the sample in place. X and Y orientation is noted in the upper right hand corner.

Once mounted in the testing system, the OCMT was simultaneously stretched in both the X and Y directions according to the parameters set out in Table 7.4. The interior strains, resulting from the material stretching evenly in two directions, were tracked using image-tracking software (LabJoy 5.80, CellScale, Waterloo, Ontario, Canada). In addition, biaxial force and rake displacement data were digitally sampled at 15Hz using the BioTester 5000 custom software (LabJoy 5.80, CellScale, Waterloo, Ontario, Canada). Cross-sectional areas and rake displacement normalization values were used to calculate the stress and strain, respectively. Consequently, the ratio of the tensile stress to the tensile strain was calculated using the Young's modulus (elasticity modulus) as represented in Equation 7.7.

$$\mathrm{E} = \frac{\sigma}{\varepsilon} = \frac{F.L_o}{A_o.\Delta L} \qquad \textbf{(7.7)}$$

Where, E is the Young's modulus (MPa), F is the force at break, A_o is the cross-sectional area of the sample, ΔL is the change in the length of the sample and L_o is the original length of the sample.

Table 7.4: Biaxial tensile testing parameters employed for the Tri-functionalized OCMT

Test Parameters	X and Y Axis
Control Mode	Displacement
Control Function	Ramp
Stretch Magnitude	40% strain
Preload	N/A
Stretch Duration	40s
Recovery Duration	40s
Repetitions	3
Data Output Frequency	15Hz
Image Output Frequency	15Hz

7.2.11. Gravimetric evaluation of the swelling and erosion of the optimized Tri-functionalized OCMT

The mean percentage water uptake and erosion of the Tri-functionalized OCMT was determined by gravimetric analysis of the degree of swelling and erosion over a 24-hour period. The initial weight of the optimized Tri-functionalized OCMT was recorded prior to being placed in 50mL of SHIF pH 6.8 for 24 hours. At predetermined time intervals (0, 1, 2, 3, 6, 8, 12, 24 hours) the Tri-functionalized OCMTs were removed and blotted dry to remove surface water before being weighed on a calibrated electronic scale. The percentage increase in tablet weight, attributed to fluid uptake at each time point was determined using Equation 7.8. The erosion of the matrix, following its drying to a constant weight at each time interval was calculated using Equation 7.9.

$$\% \Delta \text{Swelling} = \frac{W_f - W_i}{W_i} \times 100 \quad \textbf{(7.8)}$$

Where, W_f is the weight of the swollen tablet at time *t* and W_i is the initial weight of the tablet. (n=3).

$$\% \text{Erosion} = \frac{W_i - W_f}{W_i} \times 100 \quad \textbf{(7.9)}$$

Where, W_i is the initial weight of the tablet and W_f is the final dried weight of the tablets after 24 hours. (n=3).

7.2.12. Magnetic Resonance Imaging (MRI) of the optimized Tri-functionalized OCMT

Magnetic Resonance Imaging (MRI) provides an opportunity for non-destructive and non-invasive monitoring of the fate of the dosage form *in vivo.* It extends the knowledge of the structural and physico-chemical properties of the sample and assists in correlating the *in vitro* behavior with *in vivo* performance. Live-acquisition of the pH- responsive transitions of the Tri-functionalized OCMT was determined using a digital MARAN-i System configured with a DRX2 HF Spectrometer console (Oxford Instruments Magnetic Resonance, Oxon, UK) equipped with a compact 0.5 Tesla permanent magnet and stabilized at 37°C in SHIF pH 6.8. The dynamics of fluid ingress into a drug delivery system is a contributing factor towards controlling drug release (Tajiri *et al*., 2010). The hydrational and erosional morphological transitions of the Tri-functionalized OCMT was captured every 10 min with MARAN-i version 1.0 software. MARAN-i software comprises image acquisition software and image analysis software. The image acquisition parameters are depicted in Table 7.5.

Table 7.5: MARAN-i image acquisition parameters employed for magnetic resonance imaging

S.No.	Parameter	Value
1.	Imaging protocol	FSHEF
2.	Requested gain (%)	4.17
3.	Signal strength	68.92
4.	Average	2
5.	Matrix size	128
6.	Repetition time (ms)	1000.00
7.	Spin Echo Tau (ms)	6.80
8.	Image acquired after	60min
9.	Total scans	64

T_1 weighted images were produced in the spin echo method and the signal intensity of the MRI images were defined according to Equation 7.10.

$$S = \mathrm{M_O} + \exp\frac{-\mathrm{TE}}{\mathrm{T_2}} \times \left(1 - \exp\frac{-\mathrm{TR}}{\mathrm{T_1}}\right) \quad \textbf{(7.10)}$$

Where, $\mathrm{M_O}$ is magnetization, T_1 and T_2 are relaxation times, TR is repetition time and TE is echo time.

7.2.13. *In vitro* peptide release

Determination of the *in vitro* release of the peptide from the Tri-functionalized OCMT is critical towards understanding the effects of the formulatory components on the mechanism of release

noted. *In vitro* peptide release studies were performed using a USP35 dissolution apparatus II (Caleva, Model 7ST, UK). The Tri-functionalized OCMT was placed in 900mL SHIF at pH 6.8, beneath a ring mesh assembly within the dissolution vessel to prevent floatation. Dissolution was performed at a speed of 50rpm (37±0.5°C). Sampling of 3mL was undertaken at predetermined time intervals (0, 1, 2, 3, 6, 8, 10, 12, 24) and replaced with an equal quantity (3mL) of peptide-free dissolution medium to maintain sink conditions. Samples were analyzed using a Peptide Enzyme Immunoassay Kit (Peninsula Laboratories International, Inc. San Carlos, CA, USA) which is a high sensitivity absorbance assay specific for the detection of Octreotide. Peptide release was calculated as a mean of three determinations as all studies were conducted in triplicate. The concentrations at each time point were calculated using results obtained from the standard curve. The resultant in vitro peptide release data were fitted into various mathematical modelling equations to determine the mechanism of peptide release from the Tri-functionalized OCMT. Furthermore, the mean dissolution time (MDT) (Equation 7.11) was calculated from dissolution data to determine the peptide release rate (Sathish and Syed, 2013).

$$\mathrm{MDT} = \frac{\sum_{i=1}^{i=n} t_{mid} \times \Delta M}{\sum_{i=1}^{i=n} \Delta M} \qquad \textbf{(7.11)}$$

Where, MDT is the Mean Dissolution Time; i is the dissolution sample number; n is the number of dissolution sample time; t_{mid} is time at mid-point between i and i=1; ΔM is the additional amount of protein dissolved between i and i=1.

7.2.14. Evaluation of the cytotoxicity of the Eutectic Powder Blend (EPB) in the core eutectic region of the Tri-functionalized OCMT

Due to the novel synthesis of the EPB, *in vitro* determination of its cytotoxic effects became necessary prior to the OCMT's evaluation *in vivo*. Traditionally, *in vitro* determination of toxic effects of compounds has been performed by counting viable cells after staining with a vital dye. Thus, a Caco-2 human intestinal cell line was selected as it represented the best *in vitro* model to assess the toxic effects of formulation components on the intestinal barrier. An MTT (3-[4,5-dimethylthiazol-2-yl]-2,5-diphenyl tetrazolium bromide)-based *in vitro* toxicology assay kit provided a simple, accurate and highly reproducible method for measuring the activity of living cells via mitochondrial dehydrogenases (Kowapradit *et al.,* 2010; Zhang *et al.,* 2013). The kit was carried out according to the standard protocol and involved the a) preparation of cells, b)

treatment with test compounds, c) running the MTT assay and d) calculation of the relative cell viability.

a) Preparation of cells:

Cell Culture: A Caco-2 cell line (ATCC® HTB-37™) was used as it represented a reliable *in vitro* model of human small intestinal mucosa. Cells were grown on tissue culture treated 25cm^2 flasks at 37°C in a humidified 5% CO_2 incubator (RS Biotech Galaxy Standard, C&M Scientific, Livingston, West Lothian, UK). The growth medium was Dulbecco's Modified Eagle's Medium (DMEM) containing 4.0 mM L-Glutamine, 4500mg/L Glucose and sodium pyruvate, supplemented with 10% Foetal bovine serum (FBS) and a 0.1% penicillin-streptomycin solution. Cells were grown under standard conditions until 70-80% confluency was reached.

Cell Detachment: Following confluency, the cells were detached from the flask using Trypsin-EDTA (0.25mg/mL) and centrifuged at 2000rpm for ±10minutes. The supernatant was discarded and the cells were resuspended in growth medium to form a cell suspension.

Cell Counting: A sample of the cell suspension was removed and treated with Trypan Blue solution (0.4%) for hemocytometer counting. The Trypan blue-treated cell suspension was applied to a Bright-Line™ Hemocytometer (Hausser Scientific, Horsham, PA, USA). The hemocytometer was placed on a microscope stage (OLYMPUS CK2, Shibuya-ku, Tokyo, Japan) and counted using a 10x objective. The concentration of cells was calculated by averaging all 1mm^2 areas counted and applying Equation 7.12.

$$C = \frac{n}{v} \qquad \textbf{(7.12)}$$

Where, C is the cell concentration in cells/mL, n is the average number of cells/mm^2 area and v is the volume counted (10^{-4}).

Cell seeding: Upon completion of counting, the appropriate dilutions were made and cells were seeded at 2 x 10^4 cells/well in a 96-well microplate for overnight incubation in growth medium.

b) Treatment with test compounds:

The optimized concentration of the EPB (12%$^w/_w$), as determined previously in Choonara *et al*, (2016), was dissolved in serum-free medium and sterilized overnight under UV radiation. The resultant solution (500uL) was added to the 96-well plate after removal of the growth

medium and incubated for a further 24 hours. After treatment, the solutions were removed and replaced with fresh growth medium for 1 hour to stabilize the cells.

c) Running the MTT assay:

Following stabilization, the media was removed and 100uL of MTT (0.1mg/mL MTT in serum-free medium) was added and incubated for 4 hours. After the incubation period, the resultant formazan crystals were dissolved by adding an amount of MTT Solubilization Solution equal to the original culture medium volume. Following complete dissolution of the MTT formazan crystals, the absorbance was spectrophotometrically measured at a wavelength of 570/690nm using a Synergy HT multiwell microplate reader (BioTek® Instruments, Winooski, Vermont, USA).

d) The relative cell viability was determined by comparing the mean Optical Density (OD) of the treated cells with the blank wells (medium with no cells) and non-treated control cells using Equation 7.13. The background absorbance at 690nm was subtracted from the 570nm measurement.

$$\text{Relative cell viability } (\%) = \frac{\text{OD}_{570\,(\text{sample})} - \text{OD}_{570\,(\text{blank})}}{\text{OD}_{570\,(\text{control})} - \text{OD}_{570\,(\text{blank})}} \times 100 \quad \textbf{(7.13)}$$

Where, $\text{OD}_{570\,(\text{sample})}$ is the optical density of the EPB sample, $\text{OD}_{570\,(\text{blank})}$ is the optical density of the blank wells (medium without cells) and $\text{OD}_{570\,(\text{control})}$ is the non-treated control cells.

7.3. Results and Discussion

7.3.1. Analysis of weight uniformity, thickness and friability of the optimized Tri-functionalized OCMT

The optimized Tri-functionalized OCMTs (n=5) displayed a uniformity in mass, each having an average weight of 585.52±0.25mg. Measurement of the thickness of the Tri-functionalized OCMTs yielded average readings of 4.5±0.03mg. In addition, evaluation of the friability revealed a result of 0.55±0.02%. The friability value desirably fell within the 1% limit of acceptability as defined in the USP and as a result reflected positively on the ability of the Tri-functionalized OCMT to withstand external stresses during storage. Overall, the results obtained for weight uniformity, thickness and friability validated the tablet assembly and encapsulation process and reliably demonstrated its reproducibility. Figure 7.4 displays the dimensions of the

optimized Tri-functionalized OCMT with in-process validation results as well as a digital image of the optimized tablet.

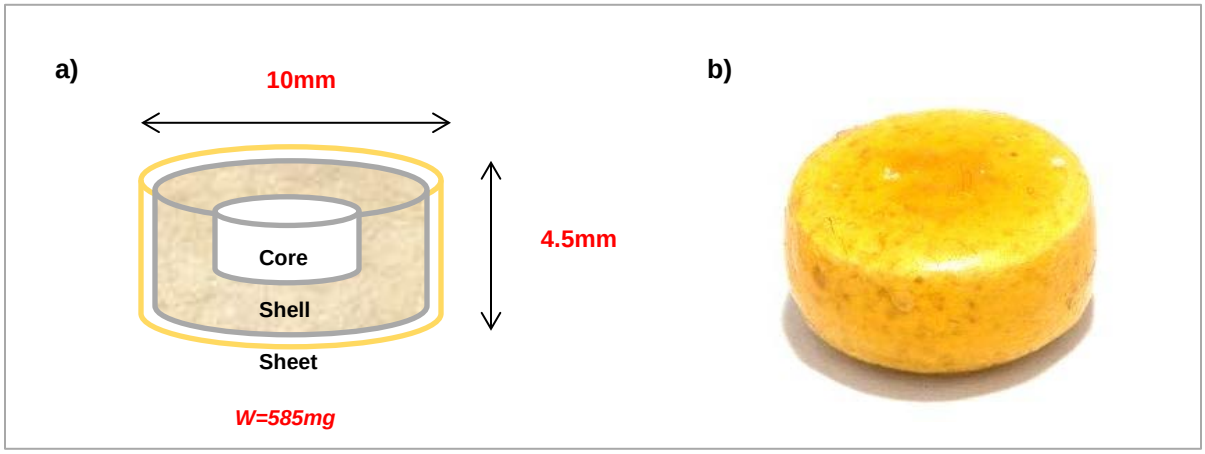

Figure 7.4: a) Schematic representation of the dimensions of the OCMT and **b)** a digital image of the optimized Tri-functionalized OCMT.

7.3.2. Influence of the pH modifier on the micro-environmental pH

The effect of the pH modifier-citric acid contained within the Tri-functionalized OCMT was evaluated. Enzymatic degradation at the intestinal brush border accounts for a significant amount of degradation of therapeutic proteins and peptides (Bruno *et al*., 2013). Typically, the brush border enzymes function optimally at a pH of 6.8-7.5 (Jiang and Yan, 2008). Thus, citric acid should preferably function to disrupt this optimal environment by decreasing the micro-environmental pH. Results from evaluation of the statistically optimized variable concentration of citric acid (10mg) contained within the Tri-functionalized OCMT, as shown in Table 7.1, yielded an approximate 3 point decrease in the micro-environmental pH from 6.8 to 3.4. This pH value ideally fell within the range of the desired targeted response, statistically generated for the optimized Tri-functionalized OCMT. At optimal concentrations of citric acid (10mg) and zein (19.166%$^{w}/_{v}$), the formulation should produce a pH of <3.6 as shown in Figure 7.5. Predictably no change in the macro-environmental pH (6.8) was noted, favorably supporting the ability of citric acid to influence the micro-environmental pH at the brush border via indirect enzyme inhibition and subsequent leading to improvement in the stability of therapeutic proteins and peptides.

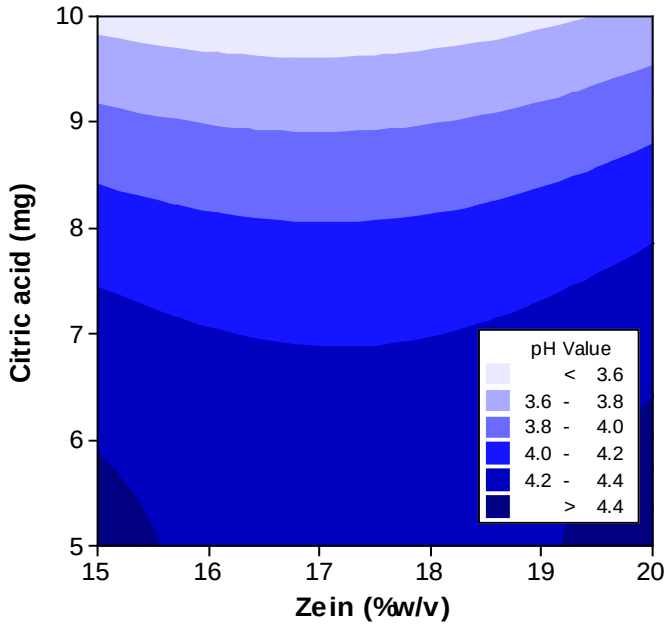

Figure 7.5: Contour plot depicting the effect of citric acid and zein concentrations on the micro-environmental pH response.

7.3.3. Analysis of the chemical structure transitions of the co-inhibitory 'smart' polymeric sheet

FTIR studies confirmed the appropriate blending of polyoxyethylene (40) stearate with the aqueous ethanol zein solution in the formation of the co-inhibitory 'smart' polymeric sheet, as evidenced by the spectra shown in Figure 7.6. As expected, transmittance bands characteristic to the native components (zein and polyoxyethylene (40) stearate) were apparent in the transmittance spectra obtained for the film-casted co-inhibitory 'smart' polymeric sheet solution. In the IR spectrum in Figure 7.6a, zein exhibited a broad band at 3312cm^{-1}, representative of parallel hydrogen-bonded O-H and N-H stretching frequencies (Coates, 2000; Müller *et al*., 2011). Furthermore, in the C-H stretch region of the spectrum, a high intensity peak at 2975cm^{-1} was assigned to symmetrical -CH_3 stretching vibrations. Zein also displayed intense spectral bands at 1650cm^{-1} and 1543cm^{-1}, assigned to amide I and amide II bands, respectively. The amide I band displayed a predominance of C=O vibrational stretching frequencies with N-H bending predominating the amide II band (Coates, 2000). These bands are characteristic to zein and allude to the presence of an alpha helix secondary protein structure (Hsu *et al.,* 2005). The sharp peak from 1043cm^{-1}-1083cm^{-1} signifies the presence of a primary amine group frequency (Coates, 2000).

Polyoxyethylene (40) stearate displayed a sharp, intense band at 2882cm^{-1}, as seen in Figure 7.6b, which was attributed to symmetrical -CH_3 stretching vibrations (Coates, 2000). Predictably, a C=O band at 1736cm^{-1} was observed in the transmittance spectra for polyoxyethylene (40) stearate, highlighting the ester carbonyl groups typical of stearates (Coates, 2000). Moreover, the characteristically related appearance of the first and second absorptions at 1464cm^{-1} and 840cm^{-1} suggests the presence of a carbonate ion functional group frequency. A sharp, narrow peak at 1341cm^{-1} was assigned to aliphatic bending vibrations with group frequencies between 1240cm^{-1} and 1270cm^{-1} within the fingerprint spectral region indicating C-O stretching vibrations. The high intensity peak at 1099cm^{-1} further supported the C-O stretching vibrations noted, resulting from intense hydrogen bonding causing a characteristically larger shift to lower frequencies (Coates, 2000).

The final film-casted solution of the co-inhibitory 'smart' polymeric sheet showed the presence of bands inherent to all its components, as shown in Figure 7.6c, with a shifting and change in intensity of certain bands indicating inter and intra-molecular interactions between the components. The shifting of the amide I and II bands of zein to lower frequencies at 1639cm^{-1} and 1536cm^{-1}, respectively, indicate a possible interaction between the individual components triggered by orthogonal dipolar interactions between amide carbonyl groups (Fischer *et al*., 2008). In addition, the first carbonate ion band characteristic of polyoxyethylene (40) stearate was dwarfed by the appearance of a spectral band at 1449cm^{-1}. This band was characteristic to the reactive nature of large quantities of glutamic acid (glutamine) making up the amino acid composition of zein (Hsu *et al.,* 2005; Gelder *et al*., 2007). Certain peaks within the fingerprint spectral region of the film-casted co-inhibitory 'smart' polymeric sheet spectrum confirmed the presence of polyoxyethylene (40) stearate. Furthermore, the distinct broadening of the transmittance band between the group frequencies of 1045cm^{-1}-1107cm^{-1} indicated the overlapping of amine groups and C-O stretching vibrations characteristic to the vibrational transitions of zein and polyoxyethylene (40) stearate, respectively. Summations inferred form the FTIR spectra ultimately corroborated the successful incorporation of polyoxyethylene (40) stearate with zein to form the co-inhibitory 'smart' polymeric sheet surrounding the Tri-functionalized OCMT.

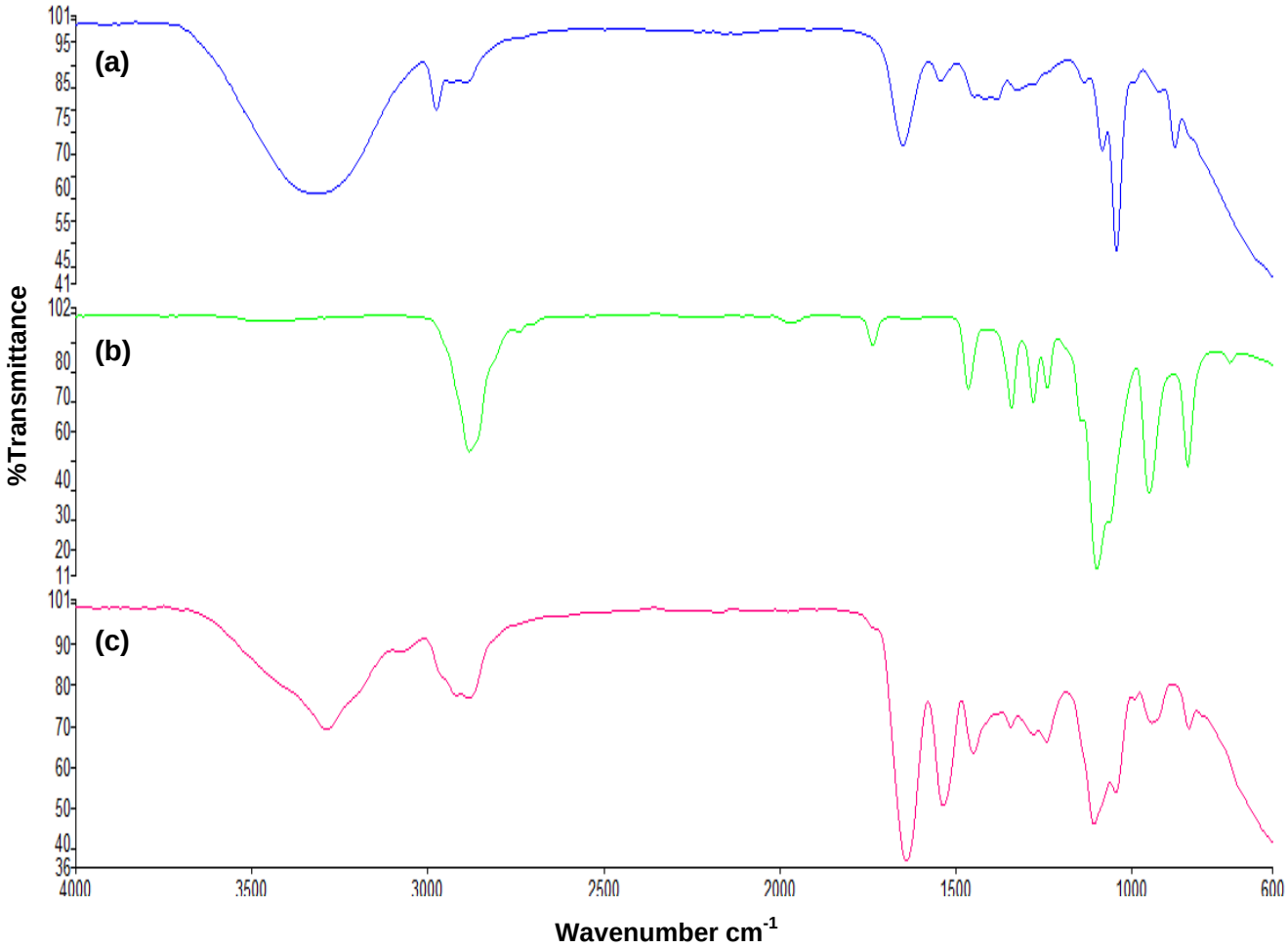

Figure 7.6: Comparative FTIR spectra of **a)** zein, **b)** polyoxyethylene (40) stearate and **c)** the film-casted blend forming the co-inhibitory 'smart' polymeric sheet.

7.3.4. Assessment of the rheological behavior of the optimized 'smart' polymeric sheet solution

Zein, forming the basis of the 'smart' polymeric sheet solution, has been used as a coating in pharmaceutical applications wherein the rheological characterization of the coating solution is a major physical property influencing the process design (Foo and Weller, 1999; Selling *et al.,* 2005). Although the 'smart' polymeric sheet provides numerous functionalities, it structurally resembles a much thicker conventional tablet coating. Thus, it follows that characterization of its viscosity and overall rheological profile would be crucial in determining its ability to adequately adhere to the surface of the OCMT. Rheological characterization of the statistically optimized concentration of zein (19.166%$^{w}/_{v}$) produced the rheogram shown in Figure 7.7. The viscosity (η) and shear stress (τ) were represented as a function of the shear strain rate ($\dot{y}$). Due to the

complexity of the system, the rheological profile differed from Newton's viscous laws and was considered to exhibit non-Newtonian behavior.

Further characterization of the non-Newtonian behavior of the optimized polymeric sheet solution demonstrated both pseudoplastic and bingham-plastic type fluidity, as shown in Figure 7.7. The assignment of pseudoplastic and bingham-plastic behavior was based on the apparent observation of an exponential decrease in the viscosity with increasing shear rates and the presence of a yield stress in the flow curve required to initiate flow, respectively (Irgenz, 2014). The viscosity of the polymeric sheet at zero shear rate was 2761mPas. The high viscosity obtained reliably supports optimum adherence of the polymeric sheet solution to the OCMT during formulation processing.

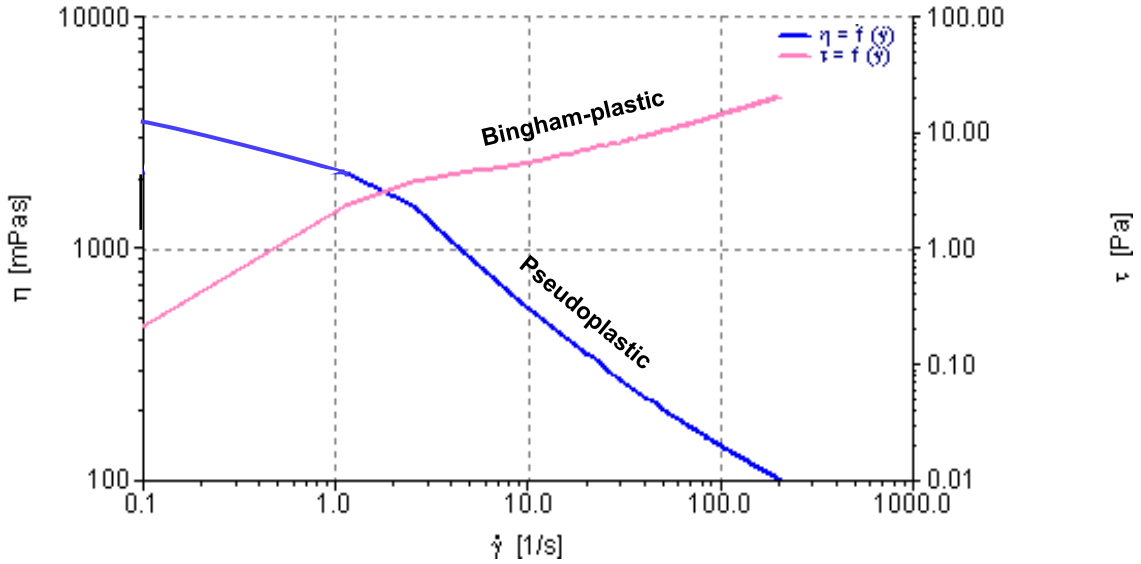

Figure 7.7: Graphical representation of the flow curve and viscosity shear rate curve of the optimized 'smart' polymeric sheet solution.

7.3.5. Comprehensive analysis of the mucoadhesive strength of the Tri-functionalized OCMT

The mucoadhesivity imparted by the 'smart' polymeric sheet surrounding the Tri-functionalized OCMT was evaluated by *in vitro* and *ex vivo* mucoadhesion methodologies. The phenomenon of mucoadhesion has been extensively exploited in oral drug delivery technologies and remains the preferred technique for prolonging the residence time at the site of absorption, facilitating improved contact and interaction with the mucus-lined epithelial barrier (Carvalho *et al*., 2010; Singh and Rana, 2012; Carreras *et al*., 2016). The *in vitro* mucoadhesive potential of zein in the

design of the 'smart' polymeric sheet of the Tri-functionalized OCMT has been previously evaluated in Chapter 6. Optimization of the design variables and subsequent *in vitro* testing of the amount of mucin crosslinked yielded a 37.34% mucoadhesion for the optimized Tri-functionalized OCMT, ideally falling within the range of the desired targeted response at statistically optimized concentrations of zein (19.166%$^{w}/_{v}$) and citric acid (10mg), as shown in Figure 7.8.

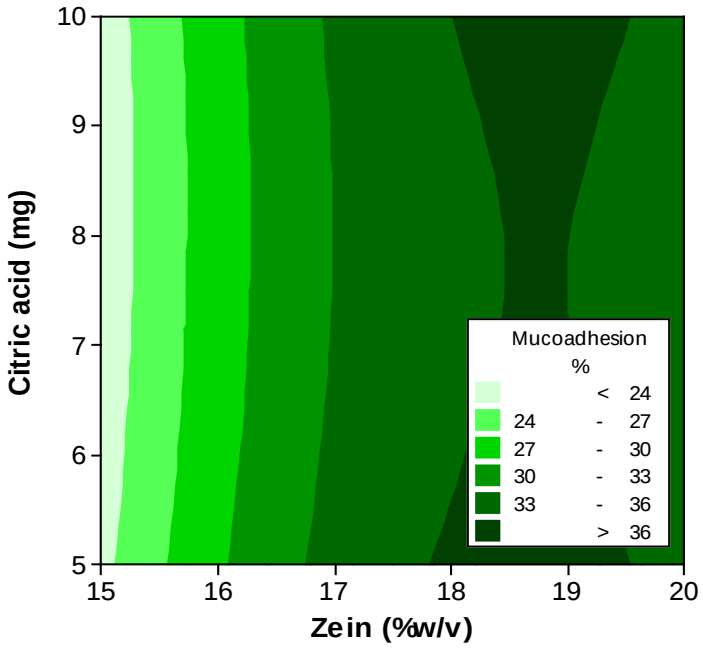

Figure 7.8: Contour plot depicting the effect of zein and citric acid on the mucoadhesive response of the Tri-functionalized OCMT.

Furthermore, the consolidation of the Tri-functionalized OCMT with the intestinal tissue was evaluated by determining the force as well as the work required to detach the tablet from the tissue surface. Results revealed a maximum detachment force (F_{max}) and work of adhesion of 0.02±0.005N and 0.09±0.008mJ.cm^2, respectively. These results supported the *in vitro* mucoadhesive percentage obtained and demonstrated the ability of the 'smart' polymeric sheet to impart notable bioadhesive properties. The dual mucoadhesion provided by the 'smart' polymeric sheet and outer polymer shell (demonstrated in Chapter 5) makes the Tri-functionalized OCMT the optimum formulation to deliver on its bioadhesive potential and site-specific delivery *in vivo*.

7.3.6. Evaluation of the gastro-resistant Tri-functionalized OCMT

Protein and peptide degradation is highest in the stomach, as a result of the acidic gastric environment and high enzyme activity, causing the irreversible cleavage of proteins and peptides into non-essential amino acids and small, absorbable oligopeptides (Fei *et al.,* 1994; Choonara *et al*., 2014). Consequently, protection from this harsh environment is critical towards achieving a clinically viable system for the oral delivery of proteins and peptides. Zein, forming the basis of the 'smart' polymeric sheet, possesses gastro-resistant properties and thus has gained increased attention due to its attractiveness in providing a protective coating for pharmaceuticals (Shukla and Cheryan, 2001; Hussan et al., 2012; Paliwal and Palakurthi, 2014). Therefore, acid uptake tests were undertaken for the Tri-functionalized OCMT to expound the capabilities of the prolamine-based 'smart' polymeric sheet. Results displayed low acid uptake values of 4.23±0.12%. This showed acceptable acid protection as it displayed a value less than 5%, indicating that the incorporated protein and peptide could be protected from degradation in the gastric environment (Kumar *et al*., 2011; Liu *et a*l., 2011; Czarnocka and Alhnan, 2015). In addition, the Tri-functionalized OCMT remained intact and displayed no physical changes after being exposed to the SGF.

7.3.7. Multi-textural analysis of the Tri-functionalized OCMT

The complete MH, MR, DE and matrix rigidity of the Tri-functionalized OCMT was determined through the comprehensive analysis of the textural response to compressive and penetrative forces. The surface and core textural profiling of the Tri-functionalized OCMT was obtained by quantitative analysis of the Force-Time and Force-Distance profiles. A summary of the results obtained are presented in Table 7.6. The high values for the MH and rigidity indicated the ability of the Tri-functionalized OCMT to resist deformation when a force is applied, alluding to the overall mechanical integrity of the tablet. The 'smart' polymeric sheet imparted an improved hardness to the tablet, attributable to the high tensile strength of zein (forming the basis of the sheet) as highlighted previously in Chapter 6. Unsurprisingly, the surface matrix hardness was much greater than the core matrix hardness due to the softening of the core at 37°C. The low matrix hardness of the core does not detract from the mechanical integrity of the OCMT but rather creates a platform for improved structural flexibility and hardness by facilitating the process of *in situ* crosslinking. Further analysis and calculation of the MR revealed the ability of the tablet to recover almost completely to its original structure after being exposed to external forces. This property aptly reflects the ability of the Tri-functionalized OCMT to withstand external stresses during handling, processing and storage.

Qualitative analysis of a Force-Time profile, produced from the penetration of a needle probe through the complete thickness of the Tri-functionalized OCMT, revealed the multi-textural profile observed in Figure 7.9. The initial increase in the gradient is due to the penetration into the 'smart' polymeric sheet, followed by a further increase in the force resulting from further penetration of the probe into the top layer of the outer polymer shell. At approximately 2N, a fracture is observed in the profile causing a notable decrease in the gradient and appearance of a noisy pattern. This was attributed to the penetration of the needle probe into the softened core eutectic region of the tablet. Following further penetration into the relatively hard bottom layer of the outer polymer shell, the force increased substantially. This supports the theory that greater forces are required to penetrate harder surfaces as opposed to their softer counterparts. The withdrawal of the probe yielded the decrease in the force and the recovery of the tablet with a slight negative peak at the end representing the adhesiveness of the 'smart' polymeric sheet. Summations inferred from overall textural profiling demonstrated the desired multi-textural properties of the Tri-functionalized OCMT for attaining optimal functionality.

Table 7.6: Quantitative textural profiling results of the Tri-functionalized OCMT

Textural Parameter	Value
Surface matrix hardness ($N.mm^2$)	242.32
Core matrix hardness ($N.mm^2$)	53.12
Matrix resilience (%)	71.61
Matrix rigidity (N.mm)	49.07
Deformation energy (J)	0.003

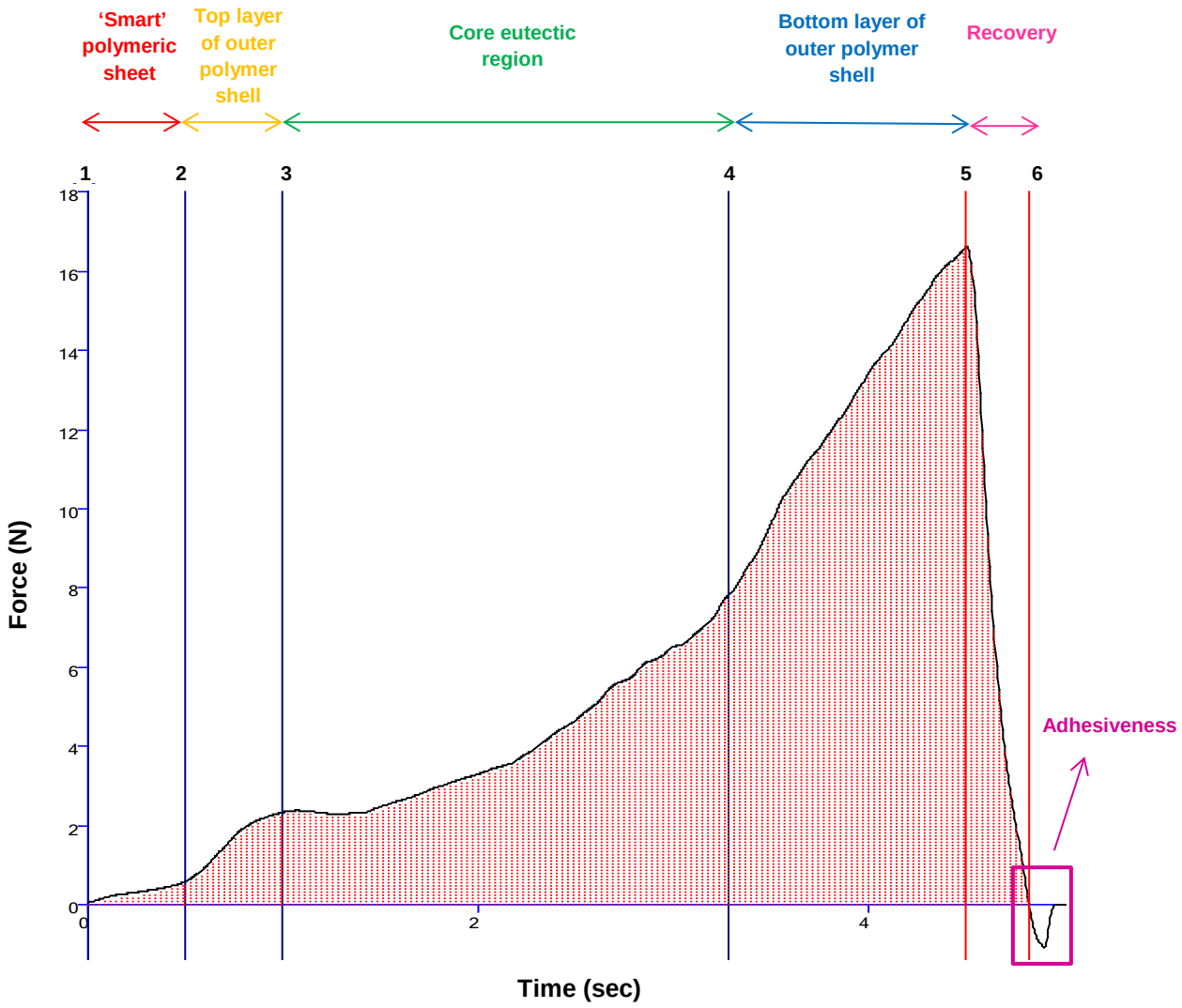

Figure 7.9: Multi-textural profile indicating needle probe penetration into the different layers of the Tri-functionalized OCMT.

7.3.8. Qualitative and quantitative analysis of the biaxial tensile strength of the Tri-functionalized OCMT

Critical analysis of the tensile strength of the Tri-functionalized OCMT was undertaken to determine the ability of the tablet to withstand maximum GIT forces *in vivo.* Biaxial tensile testing permitted the tracking of the response of the Tri-functionalized OCMT by measuring the force and displacement at 40% strain. Image tracking of the displacement and strain is shown in Figure 7.10. The displacement tracking images indicated the movement of the 'smart' polymeric sheet of the Tri-functionalized OCMT from its original position after the first stretch cycle occurred in both directions, as shown in Figure 7.10a-b. The displacement of the 'smart' polymeric sheet was quite irregular in both directions, revealing only slight changes in the

shifting modalities which was further supported by the average displacement value obtained (1600um).

Image tracking analysis of the strain during cyclic stretching produced the results shown in Figure 7.10c-d. The increase in intensity from the original yellow color signifies the weak points in the sample. As stretching increases from the original position, a predictable increase in the strain on the sample is noted. This manifests as the high intensity, weaker boundary areas shown in Figure 7.10c-d. Regardless, the 'smart' polymeric sheet displayed uniform interior strains in both directions, attractively demonstrating its resistance to failure. The complete response of strain and displacement with data overlays, following cyclic stretch and recovery, are presented in Video 7.1 and Video 7.2, respectively (See Video CD in the back cover of this Thesis).

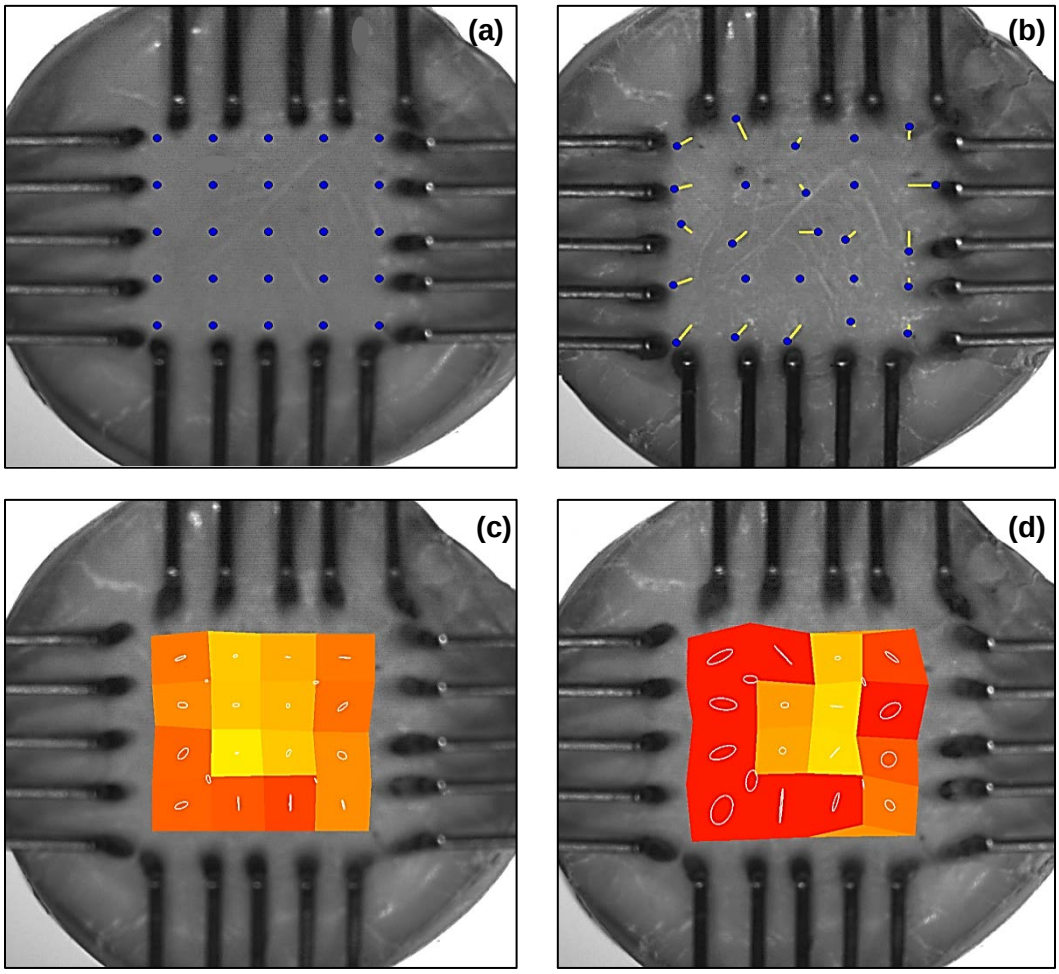

Figure 7.10: Image tracking analysis of **a)** displacement before cyclic stretch, **b)** displacement after cyclic stretch **c)** strain at mid-cyclic stretch and **d)** strain after complete cyclic stretch.

Furthermore, the force and rake displacement data obtained was used to calculate the ratio of the tensile stress to tensile strain. Results generated elastic moduli of 0.38MPa for the X and Y directions, indicating suitable stiffness and resistance to deformation of the 'smart' polymeric sheet. The Force-Time profile, displayed in Figure 7.11, further confirmed the ability of the Tri-functionalized OCMT to resist gastric forces. Laulicht and co-workers, (2010) determined the average human gastric-emptying forces in the fasted and fed state as being 414±194 dynes (±4.14 mN) and 657±84 dynes (±6.57mN), respectively. The Force-Time profile obtained showed a much higher withstanding force (2500-4000mN) before breaks in the 'smart' polymeric sheet occurred, following repeated stretch and recovery cycles in both directions. Ultimately, the results obtained demonstrated the rational design of the Tri-functionalized OCMT in providing remarkable mechanical strength for optimal *in vivo* delivery.

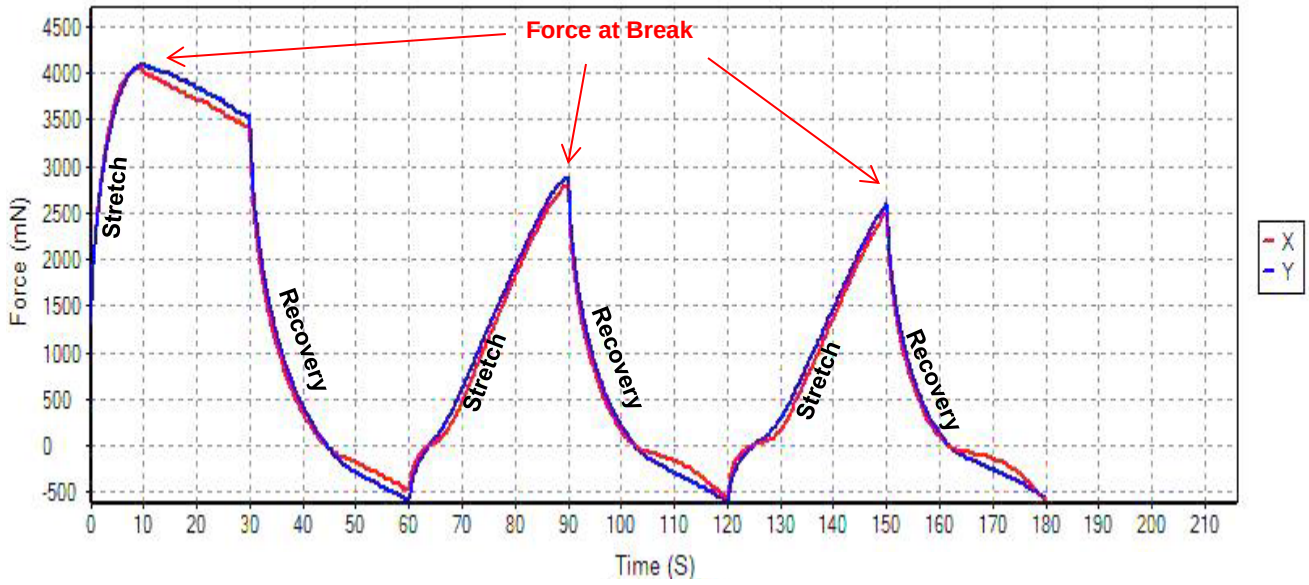

Figure 7.11: Biaxial tensile testing profile of the Force-Time in the X and Y directions for the Tri-functionalized OCMT.

7.3.9. Analysis of the fluid uptake and erosional behavior of the Tri-functionalized OCMT

The analysis of the fluid uptake and erosional behavior of the optimized Tri-functionalized OCMT was evaluated by monitoring the change in weight of the tablet over a 24-hour period. The water uptake of the tablet was calculated as a percentage in reference to the original weight, as shown in Figure 7.12. The tablet displayed a 40-80% increase in fluid uptake within the first 2 hours, notably lower than the fluid uptake percentages presented in Chapter 5 for the optimized OCMT without the 'smart' polymeric sheet. This was attributed to the characteristically different properties of zein and PEO contained within the 'smart' polymeric sheet and outer

polymer shell, respectively. The hydrophobic nature of zein retards the fluid uptake and thus smaller percentages are noted.

Further analysis of the fluid uptake behavior revealed the indirectly proportionate effects of *in situ* crosslinking between 2-4 hours. Following 4 hours, slow dissolution of the 'smart' polymeric sheet and greater exposure of the outer polymer shell resulted in the sharp increase in fluid uptake between 6-8 hours. The uptake increased steadily up to 12 hours after which slow surface erosion dominated, evident by observations of a loss in the physical structure. The pectin-controlled surface erosion produced a result of 38.32% after 24 hours as the 'smart' polymeric sheet still remained partially intact. The fluid uptake and erosional behavior noted is a critical determinant that influences numerous functional characteristics of the Tri-functionalized OCMT such as mucoadhesion, *in situ* crosslinking and *in vitro* peptide release behavior.

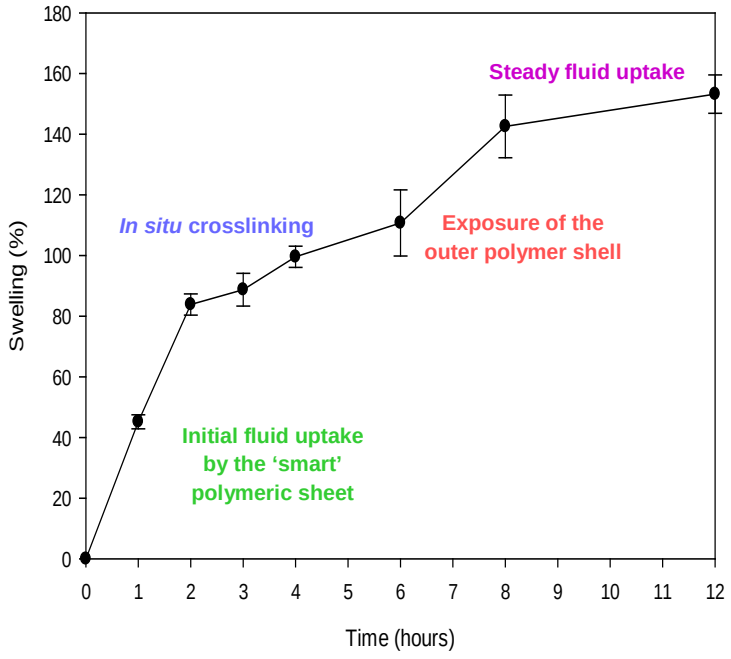

Figure 7.12: Fluid uptake profile of the Tri-functionalized OCMT in response to different processes occurring within the tablet.

7.3.10. Imaging analysis of the Pharma-Engineering and hydration characteristics of the Tri-functionalized OCMT

Qualitative evaluation of the changes in hydration, underpinning the performance of the Tri-functionalized OCMT was evaluated using MRI. The images obtained, shown in Figure 7.13, represents the internal events unfolding as a consequence of solvent penetration into the tablet.

In each image, a lower degree of hydration or gelling of the Tri-functionalized OCMT is visualized as lower intensity, darker areas and more extensive hydration or gelling presents a whiter appearance falling towards the higher intensity region of the scale. Due to its hydrophobic nature, a slow increase in the fluid uptake by the 'smart' polymeric sheet was noticed up to 2 hours. Following 2 hours, further solvent penetration into the tablet proposedly facilitated the process of *in situ* crosslinking which further retarded the hydration of the tablet. The slow dissolution and exposure of the outer polymer shell to SHIF promoted increased hydration of the tablet up to 12 hours. The imagery after 12 hours shows complete hydration and loss in the physical structure suggesting the prevalence of surface erosion. The results supported the fluid uptake behavior shown in Figure 7.12, essentially demonstrating the importance of MRI in studying the internal mechanisms of the Tri-functionalized OCMT *in vitro* and predicting its performance *in vivo.* In addition, the MRI images impeccably elucidated the internal structure and pharma-engineering of the Tri-functionalized OCMT.

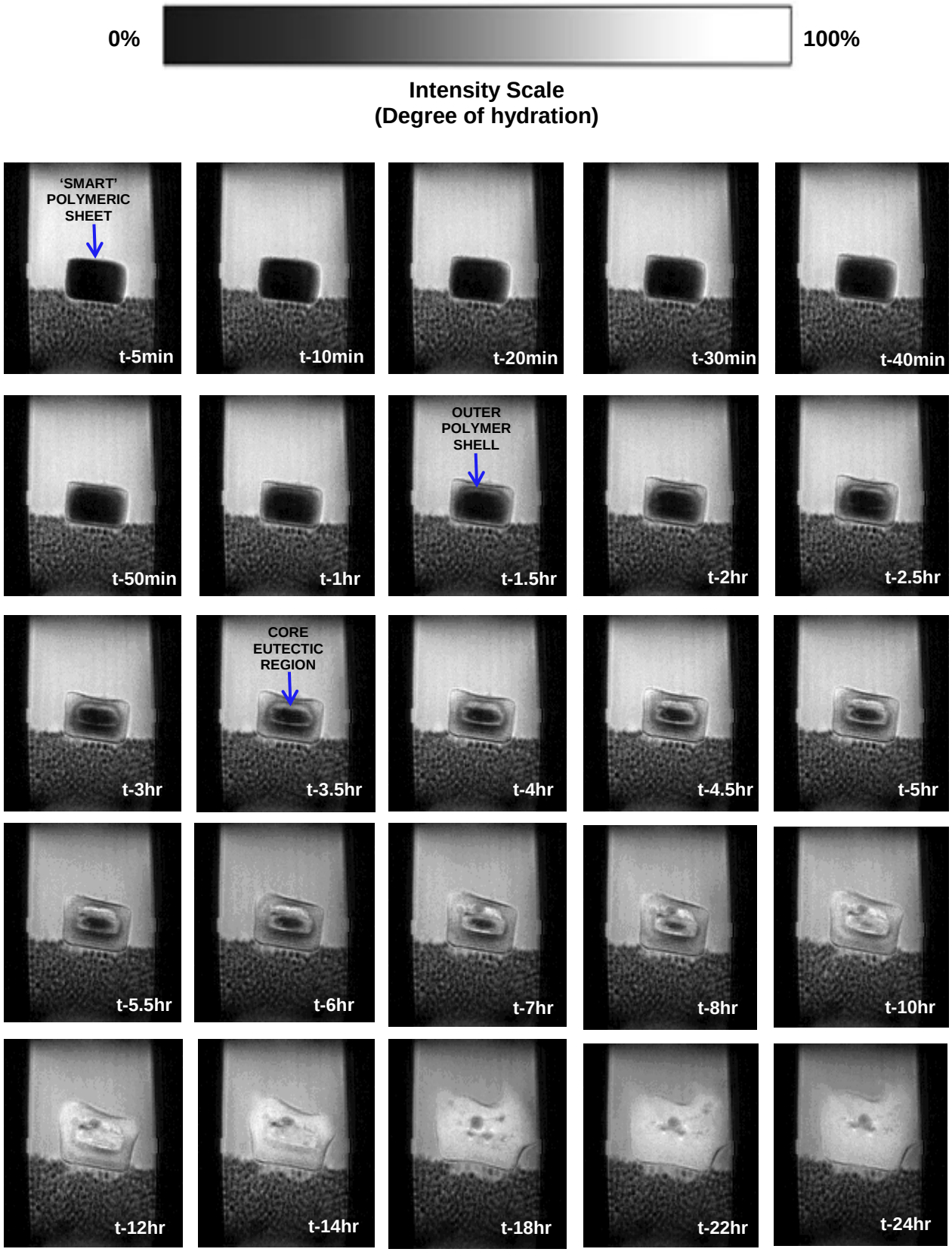

Figure 7.13: MRI of the Tri-functionalized OCMT over 24 hours with the intensity scale indicating the degree of hydration from 0% (non-hydrated) to 100% (hydrated).

7.3.11. *In vitro* peptide release analysis of the Tri-functionalized OCMT

The peptide release profile obtained for the statistically optimized formulation demonstrates the culmination of distinct formulatory components on the responsive potential of the Tri-functionalized OCMT. A 4-parameter logistic curve generated from the peptide-specific ELISA kit was used to calculate the unknown concentrations of the optimized formulation at each time point. The plot of the fractional release against time is represented in Figure 7.14. Sustained release of octreotide was noted over the 24 hour study period with an overall fractional release of ±0.9. Upon further evaluation of the release profile, patterns of burst and slow release were noted. This was attributed to the combined effects of swelling, surface and *in situ* crosslinking, as previously demonstrated. Interestingly, the outline of the release profile obtained was identical to the swelling behavior observed in Figure 7.12. This reinforced the effect of swelling on the release patterns generated. Although the pH modifier did not significantly affect the release behavior, the 'smart' polymeric sheet functioned to further sustain the peptide release from 8-24 hours. These results were corroborated by the MDT value of ±21.58 obtained, which gave an indication of a slow peptide release rate (Wadher *et al.,* 2011; Sathish and Syed, 2013). These results highlight the potential of the system to adequately release the incorporated peptide. The successful translation of the *in vitro* profile to *in vivo* performance will be ascertained in Chapter 8.

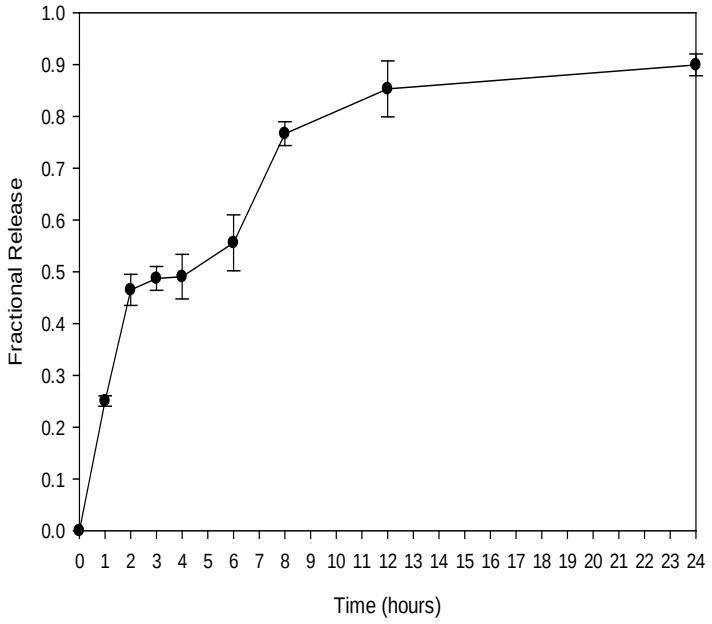

Figure 7.14: Profile displaying the fractional release of Octreotide from the Tri-functionalized OCMT.

Furthermore, the release data was fitted into various kinetic models to determine the mechanism of peptide release. The regression coefficients (R^2) obtained for the optimized formulation is presented in Table 7.7. A model depicting a value closest to 1 would demonstrate the appropriateness of that model in explaining the peptide release mechanism. Thus, the release kinetics of the Tri-functionalized OCMT was best exemplified by the Higuchi model, signifying release of the peptide from the matrix as a function of the square-root of a time-dependent process based on Fickian diffusion. Since near zero-order release was observed, the kinetics was attributed to a combination of both the Higuchi models and zero-order models, ultimately attesting to the complexity of the system.

Table 7.7: Kinetic modelling of the Tri-functionalized OCMT.

	Zero-order	**First order**	**Higuchi**	**Korsmeyer–Peppas**	
	Regression Coefficient (R^2)	Regression Coefficient (R^2)	Regression Coefficient (R^2)	Regression Coefficient (R^2)	Best-fit Model
Tri-functionalized OCMT	0.9714	0.8832	0.9832	0.924	Higuchi

7.3.12. Cytotoxic analysis of the EPB in the Tri-functionalized OCMT

The EPB of the Tri-functionalized OCMT was evaluated for its potential cytotoxicity by using an MTT cell culture assay. This cytotoxic test provides a quantitative evaluation of the *in vitro* toxicity and irritancy potential of the EPB prior to *in vivo* testing in animals. The mechanistic action of the assay is based on the cleavage of the tetrazolium ring of MTT by mitochondrial dehydrogenases of viable cells, yielding the purple formazan crystals shown in Figure 7.15. An increase or decrease in the cell number results in a concomitant change in the amount of formazan formed. Results from screening of the cytotoxic potential of the EPB, at the optimized concentration of 12%$^{w}/_{w}$, yielded a relative cell viability of ±79.83%. Consequently, the EPB was considered to be safe as there was ~80% cell survival following exposure to the EPB. These results essentially demonstrated the biocompatibility of the system and its clinical potential for safe administration *in vivo*.

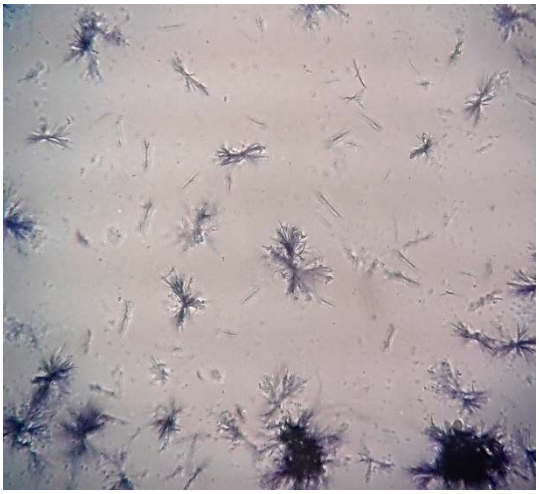

Figure 7.15: Still frame from live cell imaging of the purple formazan crystals formed following tetrazolium ring cleavage.

7.4. Concluding Remarks

Deductions from in-depth physicochemical and physicomechanical characterization of the Tri-functionalized OCMT demonstrated its optimal *in vitro* potential for achievement of clinical efficacy. Micro-environmental pH studies favorably supported the ability of the Tri-functionalized OCMT to influence the micro-environmental pH at the brush border via indirect enzyme inhibition leading to improvement in the stability of therapeutic proteins and peptides. FTIR analysis highlighted the successful incorporation of the co-inhibitor into the 'smart' polymeric sheet for achievement of its characteristic co-inhibitory function. *In vitro* and *ex vivo* mucoadhesive studies demonstrated the potential of the entire system to provide increased residence time at the absorption site via prolonged contact and increased interaction with mucin. Textural profiling and acid uptake tests revealed the enhanced mechanical strength and gastro-resistant nature provided by the 'smart' polymeric sheet of the Tri-functionalized OCMT, respectively. MRI highlighted the hydrational transitions within the Tri-functionalized OCMT and together with gravimetric swelling profiles can be considered a significant predictor of *in vitro* peptide release and *in vivo* performance of the device. The release of octreotide from the statistically optimized formulation demonstrated the effect of distinct formulatory components on the responsive potential of the Tri-functionalized OCMT. Fractional release reached a value of ±0.9 with the MDT (±21.58) indicating a slow peptide release rate. Finally, critical cytotoxic analysis of the EPB showed a ±79.83% survival rate, indicating acceptable biocompatibility and safety for clinical use. Comprehensive physicochemical and physicomechanical characterization was therefore an essential determinant for evaluating the *in vitro* potential of the system and predicting its *in vivo* performance prior to testing in the animal model.

7.5. References

Antunes, F., Andrade, F., Ferreira, D., Nielson, H.M., Sarmento, B (2013). Models to predict intestinal absorption of therapeutic peptides and proteins. *Current Drug Metabolism*, 14, 4–20.

Arhewoh, I.M., Ahonkhai, E.I., Okhamafe, A.O. (2005). Optimising oral systems for the delivery of therapeutic proteins and peptides. *African Journal of Biotechnology*, 4, 1591-1597.

Badawy, S.I.F., Hussain, M.A. (2006). Microenvironmental pH Modulation in Solid Dosage Forms. *Journal of Pharmaceutical Sciences,* 96, 948-959.

Bruno, B.J., Miller, G.D., Lim, C.S. (2013). Basics and recent advances in peptide and protein drug delivery. *Therapeutic Delivery,* 4, 1443-1467.

Carreras, J.J., Canales, P., Melero, A. (2016). Mucoadhesion of Polymeric Drug Delivery Systems: Polymeric Nanoparticles and its Interactions with the Intestinal Barrier. *JSM Nanotechnology and Nanomedicine,* 4, 1041.

Carvalho, F.C., Bruschi, M.L., Evangelista, R.C., Gremiao, M.P.D. (2010). Mucoadhesive drug delivery systems. *Brazilian Journal of Pharmaceutical Sciences*, 46, 1-17.

Cevher, E., Sensoy, D., Taha, M.A.M., Araman, A. (2008). Effect of Thiolated Polymers to Textural and Mucoadhesive Properties of Vaginal Gel Formulations Prepared with Polycarbophil and Chitosan. *AAPS PharmSciTech,* 9, 953-965.

Chin, J., Mahmud, K.A.F., Kim, S.E., Park, K., Byun, Y. (2012). Insight of current technologies for oral delivery of proteins and peptides. *Drug Discovery Today Technologies*, 9, 105–12.

Choonara, B.F., Choonara, Y.E., Kumar, P., Bijukumar, D., du Toit, L.C., Pillay, V. (2014). A review of advanced oral drug delivery technologies facilitating the protection and absorption of protein and peptide molecules. *Biotechnology Advances,* 32, 1269-1282.

Choonara, B.F., Choonara, Y.E., Kumar, P., du Toit, L.C., Pillay, V. (2016). Design of an *in situ* cross-linked eutectic tablet for enhanced delivery of gastro-sensitive proteins and peptides. *Journal of Pharmaceutical Sciences*, 105, 2086-2098.

Coates, J. (2000). *Interpretation of Infrared Spectra, A Practical Approach*. UK, Chichester: John Wiley and Sons Ltd. pp. 10815-10837.

Czarnocka, J.K., Alhnan, M.A. (2015). Gastro-resistant characteristics of GRAS-grade enteric coatings for pharmaceutical and nutraceutical products. *International Journal of Pharmaceutics,* 486, 167-174.

Fei, Y.J., Kanai, Y., Nussberger, S., Ganapathy, V., Leibach, F.H., Romero, M.F. (1994). Expression cloning of a mammalian proton-coupled oligopeptide transporter. *Nature,* 368, 563-566.

Fischer, F.R., Wood, P.A., Allen, F.H., Diederich, F. (2008). Orthogonal dipolar interactions between amide carbonyl groups. *Proceedings of the National Academy of Sciences,* 105, 17290-17294.

Fu, D., Weller, C.L. (1999). Rheology of Zein Solutions in Aqueous Ethanol. *Journal of Agricultural and Food Chemistry,* 47, 2103-2108.

Gelder, J.D., Gussem, K.D., Vandenabeele, P., Moens, L. (2007). Reference database of Raman spectra of biological molecules. *Journal of Raman Spectroscopy,* 38, 1133-1147.

He, P., Davis, S.S., Illum, L. (1998). . In vitro evaluation of the mucoadhesive properties of chitosan microspheres. *International Journal of Pharmaceutics*, 166, 68-75.

Hsu, B., Weng, Y., Liao, Y., Chen, W. (2005). Structural Investigation of Edible Zein Films/Coatings and Directly Determining Their Thickness by FT-Raman Spectroscopy. *Journal of Agricultural and Food Chemistry,* 53, 5089-5095.

Hussan, S.D., Santunu, R., Verma, P., Bhandari, V. (2012). A review on recent advances of enteric coating. *IOSR Journal of Pharmacy,* 2, 2250-3013.

Irgenz, F. (2014). *Rheology and Non-Newtonian Fluids.* USA, New York: Springer International. pp. 4-16.

Jiang, Y., Yan, S. (2008). Effects of pH on the activities of digestive enzymes in *Panulirus stimpsoni*. *Acta Zoologica Sinica,* 54, 317-322.

Kowapradit, J., Opanasopit, P., NNgawhirunpat, T., Apirakaramwong, A., Rojanarata, T., Ruktanonchai, U., Sajomsang, W. (2010). In vitro Permeability Enhancement in Intestinal Epithelial Cells (Caco-2) Monolayer of Water Soluble Quaternary Ammonium Chitosan Derivatives. *AAPSPharmSciTech,* 11, 497-508.

Kumar, P.R., Doddayya, H., Reddy, S.R. (2011). Enteric coated tablets of novel proton pump inhibitor with super disintegrants design, *in-vitro* evaluation and stability studies. *Journal of Applied Pharmaceutical Science,* 1, 106-111.

Laulicht, B., Tripathi, A., Schlageter, V., Kucera, P., Mathiowitz, E. (2010). Understanding gastric forces calculated from high-resolution pill tracking. *Proceedings of the National Academy of Sciences,* 107, 8201-8206.

Liu, F., Merchant, H.A., Kulkarni, R.P., Alkademi, M., Basit, A.W. (2011). Evolution of a physiological pH 6.8 bicarbonate buffer system: Application to the dissolution testing of enteric coated products. *European Journal of Pharmaceutics and Biopharmaceutics,* 78, 151-157.

Mahato, R.I., Narang, A.S., Thoma, L., Miller, D.D. (2003). Emerging trends in oral delivery of peptide and protein drugs. *Critical Reviews™ in Therapeutic Drug Carrier System,* 20, 153-214.

Müller, V., Piai, J.F., Fajardo, A.R., Fávaro, S.L., Rubira, A.F., Muniz, E.C. (2011). Preparation and Characterization of Zein and Zein-Chitosan Microspheres with Great Prospective of Application in Controlled Drug Release. *Journal of Nanomaterials,* 11, 1-6.

Paliwal, R., Palakurthi, S. (2014). Zein in controlled drug delivery and tissue engineering. *Journal of Controlled Release,* 189, 108-122.

Park, K., Kwan, I.C., Park, K. (2011). Oral protein delivery: current status and future prospect. *Reactive and Functional Polymers*, 71, 280–7.

Sathish, U., Syed, I.A. (2013). Formulation and characterization of matrix and triple layer matrix tablets for controlled delivery of tramadol hydrochloride. *International Journal of Pharmaceutical Sciences*, 5, 458-464.

Selling, G.W., Lawton, J., Bean, S., Dunlap, C., Sessa, D.J., Willett, J.L., Byars, J. (2005). Rheological studies utilizing various lots of zein in N, N-dimethylformamide solutions. *Journal of Agricultural and Food Chemistry,* 16, 9050-9055.

Shukla, R., Cheryan, M. (2001). Zein: the industrial protein from corn. *Industrial Crops and Products,* 13, 171-192.

Singh, I., Rana, V. (2012). Techniques for the Assessment of Mucoadhesion in Drug Delivery Systems: An Overview. *Journal of Adhesion Science and Technology*, 26, 2251-2267.

Tajiri, T., Morita, S., Sakamoto, R., Suzuki, M., Yamanashi, S., Ozaki, Y., Kitamura, S. (2010). Release mechanisms of acetaminophen from polyethylene oxide/polyethylene glycol matrix tablets utilizing magnetic resonance imaging*. International Journal of Pharmaceutics,* 395, 147-153.

Tatavarti, A.S., Hoag, S.W. (2006). Microenvironmental pH Modulation Based Release Enhancement of a Weakly Basic Drug from Hydrophilic Matrices. *Journal of Pharmaceutical Science,* 95, 1459-1468.

Wadher, K.J., Kakde, R.B., Umekhar, M.J. (2011). Study on sustained-release metformin hydrochloride from matrix tablet: Influence of hydrophilic polymers and *in vitro* evaluation. *International Journal of Pharmaceutical Investigation*, 1, 157-163.

Zhang C., Chanteux, H., Zuo, Z., Kwan, P., Baum, L. (2013). Potential role for human P-glycoprotein in the transport of lacosamide. *Epilepsia,* 54, 1154-1160.

CHAPTER 8

IN VIVO EVALUATION OF OCTREOTIDE AND EXENATIDE RELEASE FROM THE TRI-FUNCTIONALIZED OCMT IN THE LARGE WHITE PIG MODEL

To be submitted in conjunction with Chapter 5 and Chapter 7 to International Journal of Pharmaceutics and Nature Biotechnology, respectively

Bibi F. Choonara, Yahya E. Choonara, Pradeep Kumar, Lisa C. du Toit, Viness Pillay. In Vitro and In Vivo Evaluation of a Novel Oral Core-Melt Tablet (OCMT).

Bibi F. Choonara, Yahya E. Choonara, Pradeep Kumar, Lisa C. du Toit, Viness Pillay. Comprehensive In vitro and In vivo Characterization of the Statistically Optimized Tri-Functionalized Oral Core-Melt Tablet (OCMT) for Enhanced Protein and Synthetic Peptide Delivery.

Abstract

In vivo analysis of the Tri-functionalized OCMT in the Large White pig model was undertaken to determine the effectiveness of the device in delivering proteins and peptides via the oral route. Octreotide and exenatide release from the Tri-functionalized OCMT was compared to their conventional subcutaneous counterparts, respectively. Comprehensive pharmacokinetic analysis of release profiles revealed an enhanced oral bioavailability represented by a three-fold and five-fold increase in $AUC_{0-\infty}$ of octreotide and exenatide as compared to their conventional subcutaneous systems, respectively. In addition, the peak plasma concentrations for the conventional systems were much higher than those obtained for release from the Tri-functionalized OCMT, possibly reaching toxic levels and increasing the side effect profile. Analysis of *in vivo* profiles demonstrated sustained therapeutic levels of octreotide (>0.5ng/mL) and exenatide (>0.05ng/mL) over the 24 hour study period. Moreover, the Level A IVIVC analysis that was undertaken for both octreotide and exenatide showed a good correlation between *in vitro* dissolution and *in vivo* performance with an overall predictability error of <15%.

Keywords: octreotide; exenatide; large white pig model; bioavailability; minimum effective concentration; IVIVC

Animal ethics clearance for this in vivo investigation was obtained from the Animal Ethics Screening Committee (AESC) of the University of the Witwatersrand.
Ethics Clearance Number: 2014/38/C (Appendix 10.3)

8.1. Introduction

Performance of *in vivo* studies is crucial towards determining the clinical efficacy of a system. While *in vitro* and *ex vivo* testing provides important insights into the fundamental mechanisms and release of therapeutic actives from drug delivery systems, it cannot completely simulate *in vivo* conditions. Thus, *in vivo* release of therapeutic actives from the Tri-functionalized OCMT was undertaken to foster an *in vitro-in vivo* correlation (IVIVC) and define critical pharmacokinetic parameters. The selection of an appropriate animal model for evaluation of the system was based on its accuracy in providing a suitable correlation of data with respect to humans. Typically, larger animals such as monkeys, dogs and pigs are used for evaluation of oral drug delivery systems on account of the size of the dosage form excluding the use of smaller animals. The pig has been established as a good animal model for research as they are easier to handle and more socially acceptable than other animal models. More importantly, pigs share anatomical and physiological characteristics with humans which make them a viable model for biomedical research (Swindle and Smith, 1998; Kobayashi *et al*., 2012; Bassols *et al*., 2014). The widespread use of the pig model in multiple studies further validated the appropriateness of the model in providing a reliable *in vivo* evaluation of oral dosage forms (Dorkoosh *et al*., 2002; Brunet *et al*., 2006; Persson *et al*., 2008; Bergman *et al*., 2009). Thus, the Large White Pig was selected as the appropriate model for evaluation of the Tri-functionalized OCMT.

The characteristic design of the Tri-functionalized OCMT should enable enhanced oral delivery of gastro-sensitive proteins and peptides. The individual release and analysis of the synthetic peptides, octreotide and exenatide, from the Tri-functionalized OCMT was investigated. Octreotide is a synthetic octapeptide responsible for inhibiting growth hormone and other chemical messengers such as gastrin and vasoactive intestinal peptide that cause disease symptoms. Exenatide is a glucagon-like peptide-1 agonist (GLP-1 agonist) that is used in the treatment of type 2 diabetes by reducing the blood glucose levels. Both these peptides are currently administered via the parenteral routes as no clinically useful oral formulations are available. They often require multiple and frequent dosing to maintain therapeutic levels. The Tri-functionalized OCMT attempts to breakthrough this market by providing a clinically useful

oral formulation that delivers sustained therapeutic levels of these peptides following a single daily dose. *In vivo* analysis of novel delivery systems cannot be complete without comparison to their therapeutic gold standards. Thus, thorough analysis of the release profiles of the conventional systems of octreotide and exenatide were examined to provide notable comparisons for the Tri-functionalized OCMT.

This chapter essentially emphasizes the preclinical efficacy as a culmination of the unique features and functions of the Tri-functionalized OCMT by providing an in-depth *in vivo* evaluation of peptide concentrations and pharmacokinetic analysis with establishment of an IVIVC. Ultimately, *in vivo* studies are central to demonstrating the performance, safety, tolerability, efficacy and clinical potential of the Tri-functionalized OCMT in the oral delivery of therapeutic proteins and peptides.

8.2. Materials and Methods

8.2.1. Materials

The materials used for the preparation of the optimized Tri-functionalized OCMT have been highlighted previously as per the requirements found in Chapter 7, Section 7.2.1. The bioactive peptides; Octreotide acetate ($C_{49}H_{66}N_{10}O_{10}S_2$; M_w=1019.247g/mol) was purchased from Bolon Pharmachem Co., Ltd. (Taizhou, Zheijang, China) and Exenatide Acetate ($C_{184}H_{282}N_{50}O_{60}S$; M_w=4246.62g/mol) was purchased from BCN peptides (Sant Quintí de Mediona, Barcelona, Spain). The conventional subcutaneous delivery systems for Octreotide and Exenatide were purchased from Netcare Park Lane Pharmacy (Johannesburg, Gauteng, South Africa) and GenScipt® (Piscataway, New Jersey, USA), respectively. The peptide-specific Enzyme-linked Immunosorbent Assay (ELISA) kits for analysis of octreotide and exenatide were purchased from Peninsula Laboratories International, Inc. (San Carlos, CA, USA) and AB Biolabs (Ballwin, MO, USA), respectively. The peptide plasma extraction kit was purchased from Peninsula Laboratories International, Inc. (San Carlos, CA, USA). All other reagents were of analytical grade and were employed as received.

A total of 6 female Large White Pigs with an average weight of ±35kg were utilized in this study and were obtained as per the standard procurement protocols of the Central Animal Services (CAS) of the University of the Witwatersrand (Johannesburg, Gauteng, South Africa). Anesthetics, painkillers and antibiotics for administration to the pigs pre and post-operatively

were supplied and managed by the chief veterinarian of the Central Animal Services (CAS) of the University of the Witwatersrand (Johannesburg, Gauteng, South Africa).

8.2.2. Preparation of the optimized Tri-functionalized OCMT for *in vivo* analysis

The Tri-functionalized OCMT components were prepared according to the detailed methodologies and statistically optimized concentrations presented in Chapter 4 (Section 4.2.2., 4.2.3., 4.2.4., 4.2.5.) and Chapter 7 (Section 7.2.2) involving:

a. Synthesis of the lyophilized Eutectic Powder Blend (EPB) for the core eutectic region of the tablet
b. Formulation of the of the core eutectic region of the tablet.
c. Manufacture of the outer polymer shell of the tablet.
d. Incorporation of a pH modifier into the outer polymer shell.
e. Assembly of the pH_M-OCMT.
f. Synthesis of a prolamine-based smart' polymeric sheet.
g. Incorporation of a co-inhibitor into the 'smart' polymeric sheet.
h. Encapsulation of the pH_M-OCMT with the co-inhibitory 'smart' polymeric sheet to form the Tri-functionalized OCMT.

The concentrations of octreotide and exenatide used in the preparation of the Tri-functionalized OCMT were 20mg and 5mg, respectively.

8.2.3. Animal husbandry and habituation of pigs prior to commencement of the study

The pigs were housed in the farm unit in large, single, straw-bedded pens that allowed access to water *ad libitum* (Figure 8.1a-b). Since pigs are very social animals, they were housed in pens adjacent to each other that provided them visual access to the other animals. The farm unit was maintained under a 12/12 light/dark cycle and all pens were fitted with UV heat lamps to provide radiant heat and minimize stress to the animals. The pigs were fed twice a day according to the specific diets set out by the CAS staff. The habituation of animals prior to dosage form administration was critical towards improving interaction with the pigs and essentially easing the handling of the pigs during dose administration and multiple blood samplings. Habituation occurred for 7 days and involved visits with the pigs twice a day. Distributing of treats and brushing down of the pigs were some of the activities carried out during habituation as shown in Figure 8.1c. In addition, pigs were given play items as part of their environmental enrichment.

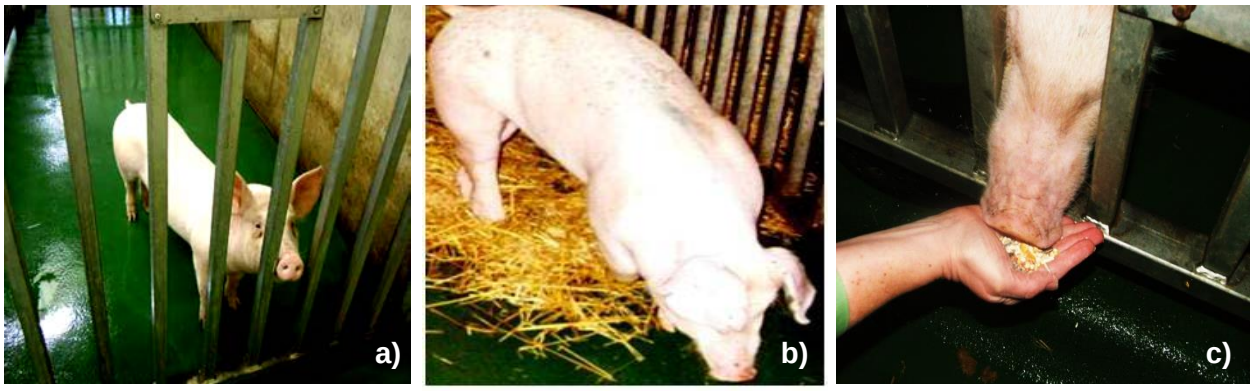

Figure 8.1: Digital images of **a-b)** farm unit housing of pigs in single, straw-bedded pens and **c)** daily feeding of treats as part of the habituation process.

8.2.4. Surgical implantation of an intra-jugular catheter into the Large White Pig

8.2.4.1. Pre-operative procedure

Insertion of a catheter into the left jugular vein of the pig was considered the most efficient portal for blood sampling. The pre-operative preparation procedure involved the anesthetization of the Large White Pig prior to catheterization using Ketamine HCL (11mg/kg) and Midazolam (0.3mg/kg). The pigs were subsequently intubated and anaesthesia was maintained with 100% medical oxygen and 2% isoflurane gas for the remainder of the procedure (Figure 8.2a). The pigs were prepared for surgery by shaving and sterilizing the surgical sites and inserting a Jelco® peripheral catheter into a vein of the right ear for rapid delivery of drugs during surgery, as shown in Figure 8.2b-c. Buprenorphine 0.05mg/kg intramuscularly and Carpofen 4mg/kg intramuscularly was administered prior to surgery to manage pain and inflammation. Following completion of the pre-operative procedure, the pigs were wheeled into the sterile theatre room for surgical catheter implantation. All surgical procedures were performed by the chief veterinarian, veterinary nurse and support staff of the Central Animal Services (CAS) at the University of the Witwatersrand.

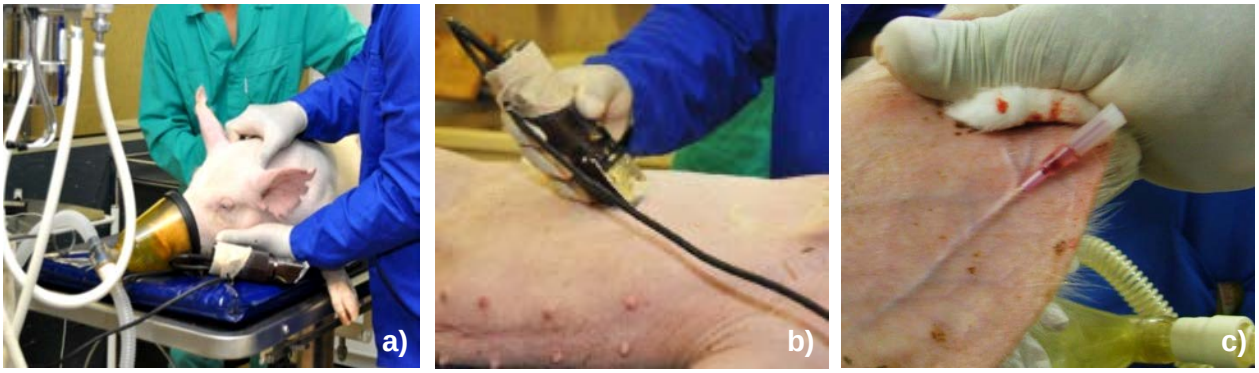

Figure 8.2: Digital images of **a)** intubation and maintenance of anaesthesia with medical oxygen and isoflurane gas, **b)** shaving and sterilization of the surgical site and **c)** insertion of catheter into the right ear vein.

8.2.4.2. Surgical procedure

Under aseptic conditions, a 7 gauge double lumen 35cm catheter (CS- 28702, Arrow Deutchland GmdH, and Erding, Germany) was surgically inserted into the left jugular vein. The detailed surgical procedure involved the exposure of the jugular vein by an incision made dorsal to the jugular groove on the left lateral aspect of the neck. The jugular vein was then isolated by blunt dissection and insertion of 10cm of the catheter into the lumen of the vein. The inserted catheter was fastened to the wall of the vein using a purse suture technique. Following this, the remaining 25cm of the catheter was tunneled subcutaneously to an exit point cranial at the dorsal aspect of the scapula with the use of a trocar. The external injection ports of the catheter were sutured to the skin to prevent excess bending and detachment. The functionality of the catheter was determined by blood sampling and subsequent flushing with heparinised saline (5000IU heparin in 1L of 0.9% saline). Vital signs such as heart rate, blood pressure, respiratory rate and body temperature of the pigs were monitored throughout the surgery. Upon completion of the surgery, the pigs were sutured up and returned to their pens to recover under observation. Digital images of the surgical procedure are presented in Figure 8.3a-i.

8.2.4.3. Post-operative procedure

The pigs were monitored closely after surgery for any signs of infection or inflammatory reactions. The pigs were given a 10 day recovery period after surgery. During this time, blood sampling and flushing of ports with heparinized saline was done twice a day to prevent blockage of ports. In addition, the surgical entry and exit points were monitored daily for signs of infection.

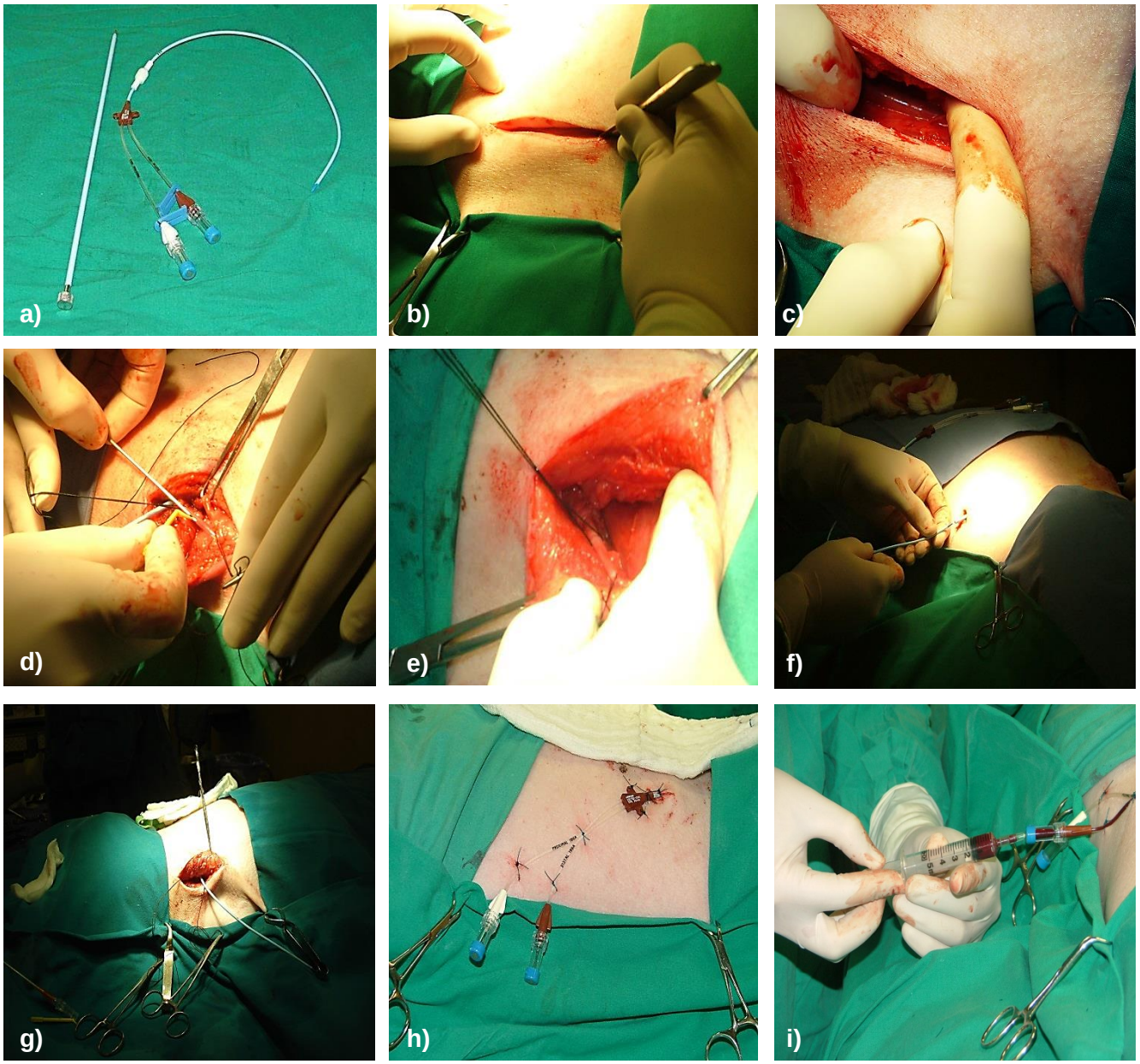

Figure 8.3: Photographic representation of the intra-jugular surgery procedure done on the anaesthetized pigs in **a)** the 7 gauge double lumen 35cm catheter, **b)** the incision made dorsal to the jugular groove on the left lateral aspect of the neck, **c)** exposure of the jugular vein, **d)** blunt dissection of the jugular vein and insertion of 10cm of the catheter into the lumen of the vein, e) fastening of the catheter using a purse suture technique, **f-g)** the remaining 25cm of the catheter subcutaneously tunneled to an exit point cranial at the dorsal aspect of the scapula with the use of a trocar, **h)** the sutured external ports of the catheter to the dorsal aspect of the neck and **i)** functional evaluation of the catheter via blood sampling and heparin flushing.

8.2.5. Administration of the conventional delivery systems and the optimized formulations to the Large White Pig

The animal studies were conducted in a total of 6 pigs which were dosed as per the experimental design highlighted in Figure 8.4, following wash-out periods between each dosing corresponding to the half-life of the drug. Dosage administration was divided into three groups namely; the experimental, the conventional and the placebo group. Within each group, 5 pigs were dosed and 1 pig served as a control. In addition, the experimental groups for both octreotide and exenatide included formulation controls which were identified as the optimized OCMTs containing no polymeric sheet or pH modifier. The conventional systems are only available as parenteral formulations, thus, octreotide and exenatide were injected subcutaneously into the dorsal aspect of the Large White Pig. Anaesthetization was not necessary for the conventional system as pigs were administered the SC injection whilst in their respective pens.

The dosing procedure for the experimental and placebo groups involved the use of an intra-gastric tube. This enabled consistent administration of the dosage form to the pigs and prevented damage to the OCMTs characteristic structural features that may be caused by chewing. The oral dosing procedure involved initial anaesthetization of pigs with Ketamine HCL (11mg/kg) and Midazolam (0.3mg/kg) followed by maintenance of anaesthesia using medical oxygen (100%) and isoflurane gas (2%). All pigs were weighed prior to each dosing procedure to monitor changes in weights. Following weight monitoring, the intra-gastric tube was lubricated with KY jelly and inserted into the stomach of the pig (Figure 8.5a). The pig was then held upright and the dosage form was placed into the tube and washed down with 10-50mL of water (Figure 8.5b-c). After the intra-gastric tube was removed, the pig was returned to its housing unit for recovery under observation.

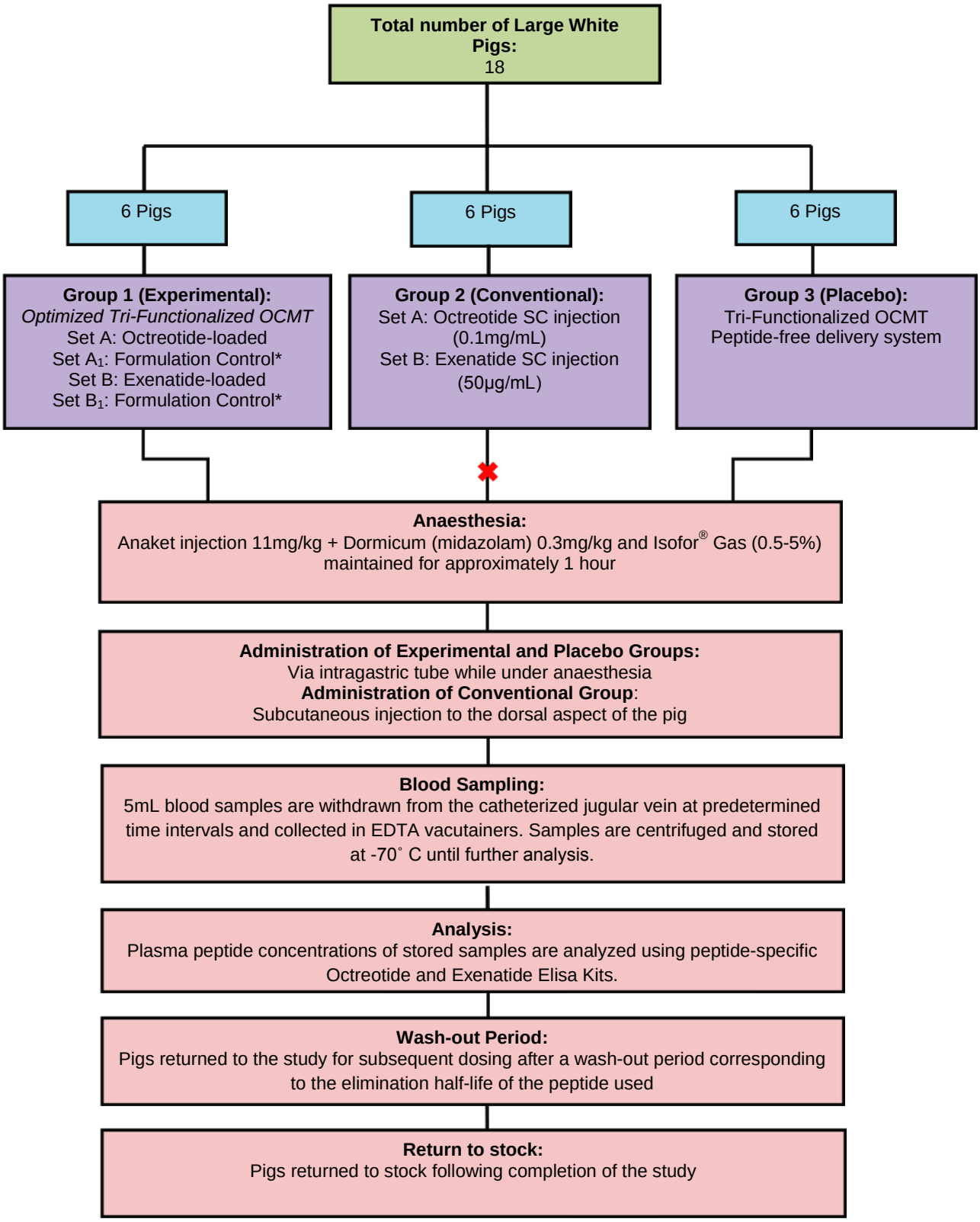

Figure 8.4: Schematic of the experimental design of the *in vivo* study indicating the distinctive groups and procedural steps involved.

***Formulation controls for the experimental groups can be identified as the optimized OCMT formulation containing no polymeric sheet or pH modifier**

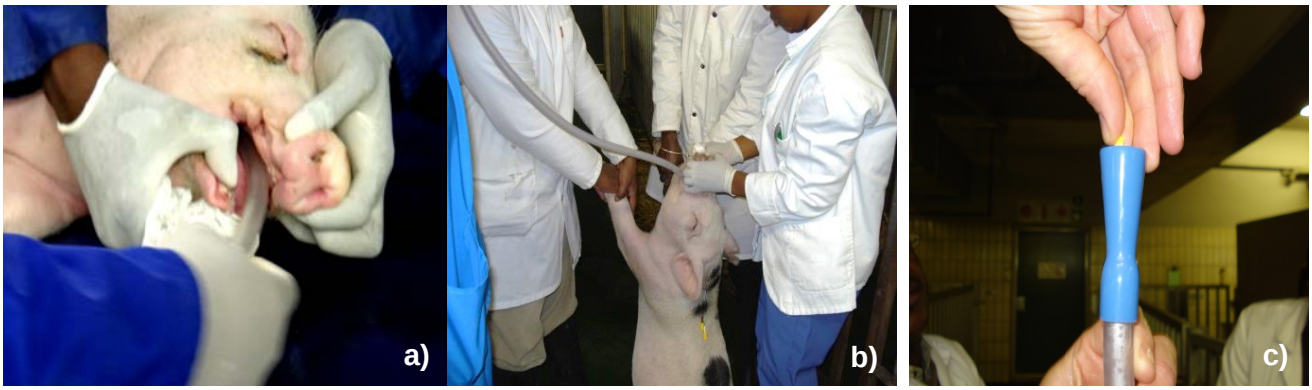

Figure 8.5: Digital images of the oral dosing procedure for the experimental and placebo groups in **a)** insertion of the gastric tube, **b)** holding the pig upright and **c)** placing the dosage form into the intra-gastric tube.

8.2.6. Blood sampling procedure from the surgically implanted intra-jugular catheter

Following dose administration to the pigs and reversal of anaesthesia, blood sampling was undertaken at pre-determined time intervals over a 24 hour study period. The blood sampling time periods for the experimental and placebo groups were 0, 0.5, 1, 2, 3, 4, 6, 8, 10, 12, 18, 22 and 24 hours. Blood sampling for the conventional systems were undertaken at shorter time intervals within the first hour after dosing due to the predictably faster reaching of peak levels following subcutaneous administration. The habituation process greatly facilitated easier handling and blood sampling of pigs. Prevention of infection at the catheter external port entry sites was critical to maintaining a healthy pig throughout the entire study, thus, hands were washed and disinfected thoroughly before blood sampling was undertaken. The blood sampling procedure involved the disinfection of the intra-jugular catheter external ports using a veterinary disinfectant spray (Figure 8.6a). The ports were than flushed with heparinized saline and the first blood withdrawn was discarded (Figure 8.6b-c). Further withdrawal of 5ml of blood was placed in EDTA vacutainers®. Following withdrawal, the ports were again flushed with heparin and disinfected. The collected blood samples were centrifuged at 5000rpm for 15 minutes and the plasma supernatant was extracted and stored at -70°C until further analysis.

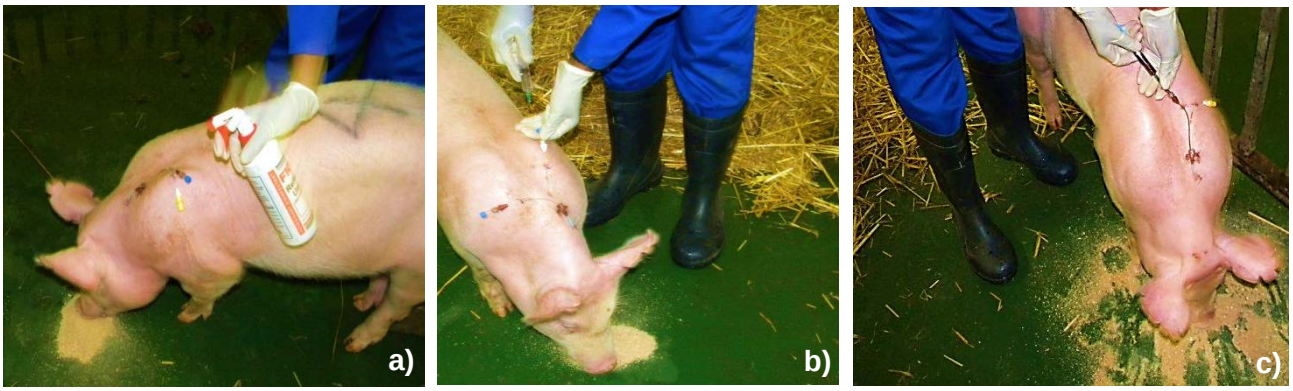

Figure 8.6: Digital images of the blood sampling procedure in **a)** disinfection of the external ports, **b)** flushing of the ports with heparinized saline and **c)** blood withdrawal.

8.2.7. Quantification of the *in vivo* release of the experimental groups and conventional systems using peptide specific Enzyme-linked Immunosorbent Assays (ELISA)

Competitive immunoassay-based ELISA kits were used for the quantification of plasma concentrations of octreotide and exenatide. Competitive enzyme immunoassays kits are based on the principle of competition between the peptide and its tracer (biotinylated peptide) for a limited number of antiserum binding sites. Typically, the antiserum is captured by antibodies coated on a 96-well plate. The addition of a constant concentration of Bt-tracer (biotinylated tracer) and varying concentrations of unlabeled standard or sample peptide compete for binding specifically to the antiserum. Captured Bt-tracer is subsequently bound by SA-HRP (streptavidin-conjugated horseradish peroxidase), producing a soluble colored product after substrate addition as illustrated in Figure 8.7.

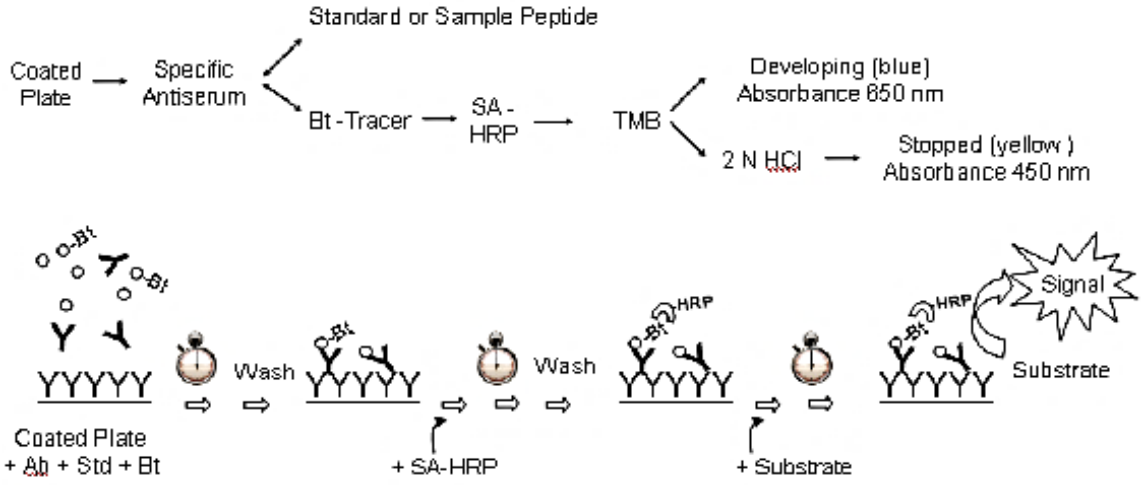

Figure 8.7: Schematic representation of the mechanistic principle of the competitive ELISA kit used for quantification of plasma concentrations (Peninsula Laborotories International, Peptide Enzyme Immunoassay Datasheet).

8.2.8. Summarized technical procedure for ELISA kit evaluation of plasma peptide sample concentrations

The ELISA kits for individual evaluation of octreotide and exenatide plasma samples were prepared according to the kits standard operating protocol and involved; a) preparation of peptide standards, b) sample extraction and c) preparation of immunoplate and running of the assay. All materials used were provided with the kit.

a) Preparation of peptide standards:

   The peptide standards provided were reconstituted and serially diluted to the standard concentrations suggested by the kit. Octreotide standards were prepared at concentrations of 1000ng/mL, 10ng/mL, 2.5ng/mL, 0.63ng/mL, 0.16ng/mL, 0.04ng/mL, 0.01ng/mL and 0ng/mL. Exenatide standards were prepared at concentrations of 1000ng/mL, 100ng/mL, 10ng/mL, 1ng/mL, 0.1ng/mL and 0.01ng/mL.

b) Sample extraction:

   The extraction of peptides from plasma samples is important for eliminating potentially interfering substances, such as albumin. A solid phase extraction (SPE) kit was used for extraction of the peptides. *In vivo* octreotide and exenatide plasma samples were thawed to room temperature (±25°C). Two buffers, Buffer A (1% trifluoroacetic acid) and Buffer B (60% acetonitrile with 1% trifluroacetic acid) were provided with the kit. The extraction involved adding an equal amount of Buffer A to the plasma samples and centrifuging at 6000xg for 20 minutes at 4°C. Thereafter, a SEP-COLUMN containing 200mg of C18 was equilibrated with Buffer B (1mL, once) followed by Buffer A (3mL, three times). The plasma solution was loaded onto the pre-treated C-18 SEP-COLUMN and a light vacuum was applied. Subsequently, the column was slowly washed with Buffer A (3mL, twice) and the resultant wash was discarded. Following this step, the peptide was slowly eluted with Buffer B (3mL, once) and the eluent was collected in a polypropylene tube. Finally, the eluent was evaporated to dryness and the residue was dissolved in EIA buffer.

c) Preparation of immunoplate and running of the assays:

   The immunoplate was prepared by adding 50µL of standard or sample (in diluent), 25µL of antiserum in EIA buffer and 25µL of Bt-tracer in EIA buffer into each well. All samples and standards were assayed in duplicate. Blank wells were prepared by adding 75µL of diluent and 25µL of Bt-tracer. The plate was covered and incubated at room temperature for 2 hours. Orbital shaking (300-400rpm) during incubation was recommended for the exenatide kit and was carried out using a ThermoStar microplate incubator (BMG

LABTECH, Ortenburg, Bavaria, Germany). Following incubation, the immunoplate was washed using a ELx50 microplate washer (BioTek® Instruments, Winooski, Vermont, USA), 3/5 times with 350µL/well and 300µL/well of EIA buffer for the exenatide and octreotide assay kits, respectively. On completion of washing, 100µL of SA-HRP solution was added to each well. The plate was subsequently covered and incubated for 1 hour at room temperature with orbital shaking (300-400rpm) recommended for the exenatide kit. The plate was washed again after incubation as per the washing procedure mentioned previously. The TMB substrate solution (100µL) was added to each well and further incubated at room temperature for 30-60 minutes for optimum development of the blue color. Lastly, the reaction was terminated by adding 100µL 2N HCL to each well, causing a color change from blue to yellow. The absorbance was read at 450nm within ten minutes using a Synergy HT multiwell microplate reader equipped with curve fitting software (BioTek® Instruments, Winooski, Vermont, USA).

8.2.9. Pharmacokinetic modelling of peptide release data using compartmental and non-compartmental algorithms

The *in vivo* release of octreotide and exenatide was subjected to extensive pharmacokinetic data analysis by fitting the concentration-time data obtained into PKSolver, a menu-driven add-in program for Microsoft Excel written in Visual Basic for Applications (VBA), facilitating compartmental and non-compartmental analysis of the *in vivo* release data (Zhang *et al*., 2010).

Non-compartmental analysis is the simplest and most commonly used pharmacokinetic analysis that does not assume compartments. Calculation of the area under the zero and area under the first moment curves from 0 to last time t, ($AUC_{0\text{-}t}$, $AUMC_{0\text{-}t}$) as well as from the last sampling time to infinity ($AUC_{t\text{-}\infty}$; $AUMC_{t\text{-}\infty}$) were determined via the trapezoidal method and calculations based on the last or predicted concentrations; respectively (Equation 8.1 and 8.2).

$$\mathrm{AUC} = \mathrm{AUC}_{0-\mathrm{t}} + \frac{\mathrm{C}_{\mathrm{last}}}{\lambda_z} \quad \textbf{(8.1)}$$

Where, $\mathrm{C}_{\mathrm{last}}$ is the last observed or predicted concentration and λ_z is the terminal elimination slope.

$$\mathrm{AUMC} = \mathrm{AUMC}_{0-\mathrm{t}} + \frac{\mathrm{C}_{\mathrm{last}} \times \mathrm{t}_{\mathrm{last}}}{\lambda_z} + \frac{\mathrm{C}_{\mathrm{last}}}{{\lambda_z}^2} \quad \textbf{(8.2)}$$

Where, C_{last} is the last observed or predicted concentration, t_{last} is the time at last observed or predicted concentration and λ_z is the terminal elimination slope.

The terminal elimination slope, λ_z, can be calculated using user-specified terminal data points or automatically estimated using the regression with the largest R^2, as shown in Equation 8.3.

$$\text{Adjusted } R^2 = 1 - \frac{(1-R^2)\times(n-1)}{n-2} \quad \textbf{(8.3)}$$

Where, n is the number of data points in the regression and R^2 is the square of the correlation coefficient.

Additional parameters calculated included the half-life ($t_{1/2}$), mean residence time (MRT), clearance (Cl) and volume of distribution based on the terminal slope.

Furthermore, compartmental analysis was used to quantitatively determine the *in vivo* fate of the peptide by fitting the concentration-time data obtained into an appropriate pharmacokinetic compartmental model (Zhang *et al*., 2010). Administration of the Tri-functionalized OCMT was considered as a single extravascular dose and thus, the system was inputted into three distinct pharmacokinetic algorithms:

1. Non-compartmental Model (Extravascular)
2. One-compartmental Model (Extravascular)
3. Two-compartmental Model (Extravascular)

The model diagnostics such as correlation coefficient, sum of squares of residuals (SS), standard error of weighted residuals (SE), Akaike's information criterion (AIC) and Schwarz criterion (SC) are generated from the pharmacokinetic models and are essential towards selecting the appropriate model for the fitted concentration-time data. The quantitative evaluation provides valuable information about the drug transport processes in the body (Zhang *et al.,* 2010). AIC and SC are considered the most important diagnostics for enabling the selection of a model with small bias and good precision, and were calculated according to Equation 8.4 and 8.5, respectively (Ludden *et al*., 1994; Zhang *et al*., 2010).

$$\text{AIC} = N \cdot \ln(\text{WSS}) + 2p \quad \textbf{(8.4)}$$

$$SC = N \cdot \ln(WSS) + p \cdot \ln(N) \quad \textbf{(8.5)}$$

Where, N is the number of observations, WSS is the weighted sum of squared residuals and p is the number of estimated parameters.

8.2.10. Establishment of an *in vitro-in vivo* correlation (IVIVC)

Establishing a mathematical relationship between *in vitro* release data and *in vivo* performance is essential towards further optimization and development of the device. Four levels of IVIVC for extended release dosage forms have been identified by the Food and Drug Administration (FDA) and include; Level A, B, C and Multi-level C as defined in Table 8.1 (Ostrowski and Baczek, 2010; Chakraborty *et al.*, 2014). Level D is considered as a rank order correlation, providing qualitative analysis and thus is not considered useful for regulatory purposes. The levels of correlation are based on the ability of the correlation to reproduce the complete plasma concentration-time profiles resulting from administration of a dosage form.

Table 8.1: Levels of IVIVC as identified by the Food and Drug Administration (FDA)

Levels of IVIVC	
Level A	IVIVC that predicts the entire *in vivo* time course from the *in vitro* data. It is generally a linear correlation that represents a point-to-point relationship between *in vitro* dissolution data and *in vivo* input rate. Non-linear relationships may also be appropriate.
Level B	Based on the principles of statistical moment analysis in which the mean in vitro dissolution time ($MDT_{in\ vitro}$) is compared to either the mean *in vivo* residence time (MRT) or the mean in vivo dissolution time ($MDT_{in\ vivo}$). This correlation does not reflect the actual *in vivo* plasma curves as different *in vivo* curves produce similar MRT values.
Level C	IVIVC that establishes a single-point relationship between a dissolution parameter (e.g. $t_{50\%}$,$t_{90\%}$) and a pharmacokinetic parameter (e.g. AUC, C_{max}). Considered a weak correlation as it does reflect complete shape of a plasma drug concentration time curve.
Multiple Level C	Establishes a relationship between one or more pharmacokinetic parameters of interest and amount of drug dissolved at several time points of the dissolution profile.

Based on the distinct properties of each level, a Level A IVIVC was identified as the highest category of correlation as it is considered the most informative for predicting the *in vivo* performance of a drug product from its *in vitro* dissolution. Thus, WinNonLin® software (V5.3 with IVIVC Toolkit Build 20091211139, Pharsight Software, Statistical Consultants Inc., Apex,

NC, USA) was used to establish a Level A IVIVC. The inputted data included; *in vitro* octreotide and exenatide release data and *in vivo* plasma concentration data. Establishment of an IVIVC model involves development and validation processes. Accordingly, the Level A IVIVC was developed using a two-stage process (Chakraborty *et al*., 2014).

1. Deconvolution: This technique requires the comparison of *in vivo* dissolution profiles with *in vitro* dissolution profiles. The observed fraction of the drug absorbed is estimated based on the Wagner-Nelson method. Once the pharmacokinetic parameters were estimated using a non-linear regression tool, the predicted fraction of the drug absorbed was calculated from the observed fraction of the drug dissolved.
2. Convolution: the prediction fraction of the drug absorbed is then convolved to the predicted plasma concentrations instituting the convolution method.

Following development of the IVIVC model, the validity of the correlation was determined by evaluating the magnitude of the predictive performance. The percentage prediction error (P.E.) was calculated for C_{max} and AUC using Equation 8.6 and 8.7, respectively (Chakraborty *et al*., 2014).

$$\%\,\mathrm{P.E.} = \frac{C_{max}observed - C_{max}predicted}{C_{max}observed} \times 100 \quad \textbf{(8.6)}$$

$$\%\,\mathrm{P.E.} = \frac{AUCobserved - AUCpredicted}{AUCobserved} \times 100 \quad \textbf{(8.7)}$$

Where, P.E. is the prediction error, C_{max} is the maximum plasma concentration and AUC is the Area under the curve.

8.3. Results and Discussion

8.3.1. Clinical and behavioral assessment of the pig model following surgical implantation of the intra-jugular catheter and dosage form administration

The pigs were monitored closely for any signs of infection, pain and inflammation following post-surgical implantation. All pigs displayed a quick recovery, despite being initially drowsy, returning fully to their normal levels of activity and appetite relative to their observed behaviors before surgery. Ideally, the pigs displayed no signs of infection or inflammation during recovery and throughout the study. Furthermore, the pigs showed no side effects following the

administration of the octreotide and exenatide experimental systems. This confirmed the biocompatibility of the optimized Tri-functionalized OCMT. The pigs experienced the common side effects of lethargy and a loss of appetite within the first 2 hours following administration of the exenatide conventional system. This was attributed to the reaching of possibly high plasma concentrations of exenatide following SC injection. Generally, the pigs were monitored twice a day throughout the entire study and any clinical or behavioral changes observed were recorded on a monitoring chart.

8.3.2. A calibration curve for the quantification of plasma octreotide and exenatide concentrations

Evaluation of the octreotide and exenatide standards generated 4-parameter logistic curve fits as shown in Figure 8.8a-b, respectively. The calibration curves were deemed satisfactory for the determination of the unknown plasma sample concentrations as they displayed excellent fits, indicated by the R^2 values obtained of 0.99.

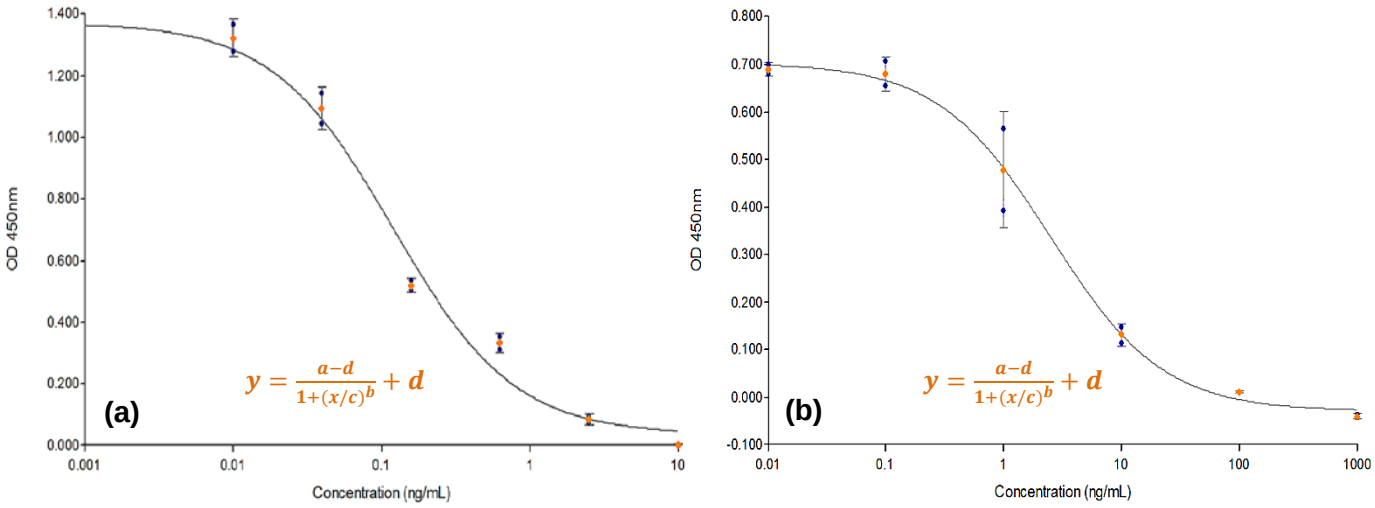

Figure 8.8: Calibration curves of **a)** octreotide measured at 450nm and **b)** exenatide measured at 450nm.

8.3.3. *In vivo* release profile analysis of octreotide from the Tri-functionalized OCMT and the conventional system

The comparative *in vivo* concentration profiles of octreotide from the Tri-functionalized OCMT, formulation control (optimized OCMT containing no co-inhibitory 'smart' polymeric sheet or pH modifier) and conventional system are presented in Figure 8.9a-b. Results revealed the effectiveness of the Tri-functionalized OCMT in delivering therapeutic levels of octreotide

following oral administration. Profiling analysis demonstrated an initial similar concentration-time pattern for the formulation control and Tri-functionalized OCMT (Figure 8.9a). However, noticeable changes were observed between 2-3 hours wherein, the formulation control displayed higher peak plasma levels (±2.2ng/mL) as compared to the Tri-functionalized OCMT (±1.5ng/mL). This was followed by a rapid decrease in the plasma concentrations after 3 hours, in sharp contrast to the concentrations quantified for the Tri-functionalized OCMT. This was attributed to the absence of the co-inhibitory 'smart' polymeric sheet and pH modifier. These components ideally function to directly or indirectly control the release of the incorporated peptide by virtue of its characteristic properties that have been extensively highlighted in previous Chapters. However, despite the absence of these functional components, the formulation control still displayed an acceptable controlled release profile possibly resulting from the effects of *in situ* crosslinking.

The *in vivo* concentration profile obtained for the Tri-functionalized OCMT supported the functional effects of the co-inhibitory 'smart' polymeric sheet and pH modifier as well as other functional components by attractively displaying a slower sustained release of octreotide between biphasic peak concentrations for up to 12 hours. This was followed by achievement of steady state plasma concentrations. In addition, therapeutic levels were maintained up to 22 hours for both the Tri-functionalized OCMT and the formulation control. Furthermore, comparison of the Tri-functionalized OCMT to the conventionally administered subcutaneous injection emphasized the inability of the latter to provide sustained release capabilities, as evidenced by results obtained in Figure 8.9b.

Although the conventional system displayed much higher peak plasma concentrations (±5.8ng/mL), it failed to achieve steady-state plasma concentrations and reached sub-therapeutic levels after only 4 hours. This indicates the need for frequent and multiple doses to achieve consistent therapeutic levels. The attainment of consistent and sustained therapeutic levels over a 24 hour period, as observed for the Tri-functionalized OCMT, promotes once-daily dosing and greatly minimizes the side effect profile associated with higher plasma concentrations. Summations inferred from overall octreotide *in vivo* plasma profile analysis for the experimental and conventional groups revealed the exemplary performance of the Tri-functionalized OCMT in providing sustained, therapeutic levels of octreotide following oral administration. Overall, the *in vivo* results alluded to the potential of the optimized Tri-

functionalized OCMT to provide a viable alternative to the parenteral route of administration for gastro-sensitive proteins and peptides.

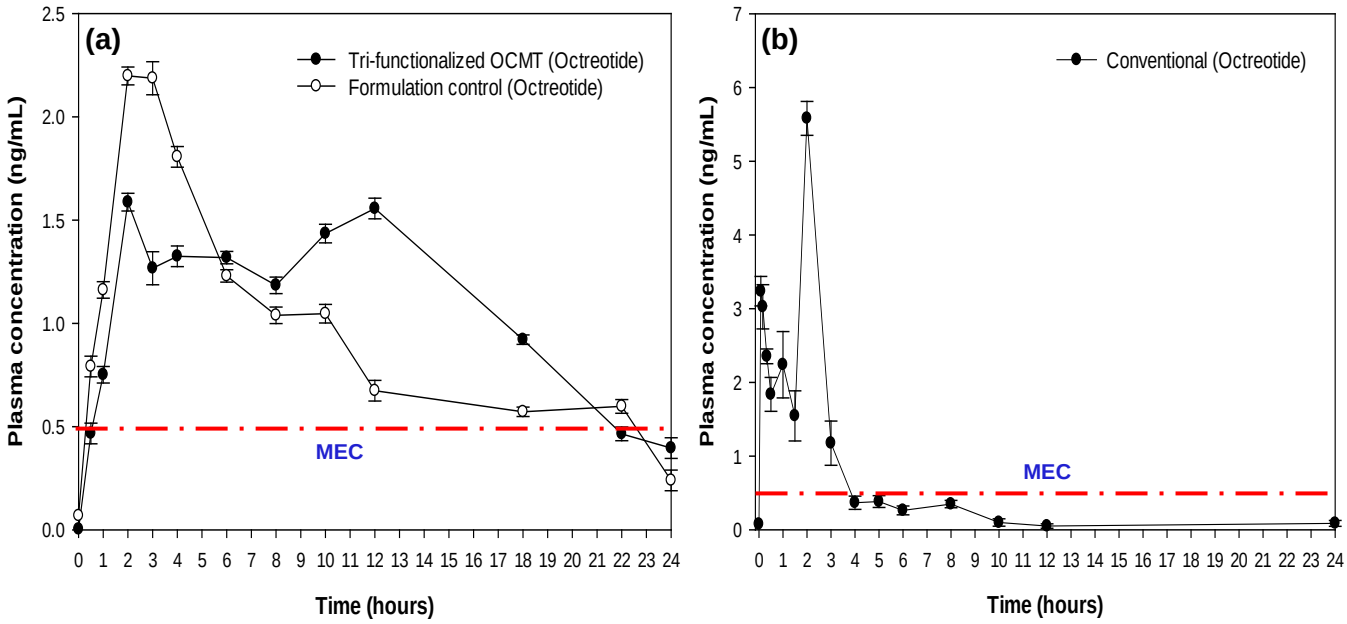

Figure 8.9: *In vivo* plasma octreotide concentration-time profiles for **a)** the orally administered Tri-functionalized OCMT and formulation control (optimized OCMT with no polymeric sheet or pH modifier) and **b)** the subcutaneously administered conventional system indicating the minimum effective concentration (MEC) for octreotide (0.5ng/mL).

8.3.4. *In vivo* release profile analysis of exenatide from the Tri-functionalized OCMT and the conventional system

The comparative *in vivo* concentration profiles of exenatide from the Tri-functionalized OCMT, formulation control (optimized OCMT containing no co-inhibitory 'smart' polymeric sheet or pH modifier) and conventional system are presented in Figure 8.10a-b. Results revealed the achievement of therapeutic levels of exenatide from the Tri-functionalized OCMT and formulation control, as evidenced by the observation of peak and sustained plasma concentrations levels above the minimum effective concentration (MEC) of 50pg/mL (0.05ng/mL). The concentration-time profile for the formulation control of exenatide followed the same profiling pattern as that of the Tri-functionalized OCMT with peak plasma levels reaching ±1.55ng/mL and ±1.6ng/mL for the Tri-functionalized OCMT and formation control, respectively (Figure 8.10a). However, the Tri-functionalized OCMT displayed higher consistent levels of exenatide up to 24 hours as compared to the formulation control, attributable to the mechanistic action of the co-inhibitor, contained within the 'smart' polymeric sheet, which functions to inhibit drug metabolism and prevent transmembrane efflux. Interestingly, an apparent tri-phasic

release of exenatide was noticeable for the Tri-functionalized OCMT as evidenced by the increased concentrations following phases of sustained release.

Comparison of the Tri-functionalized OCMT to the conventional system, as shown in Figure 8.10b, demonstrated a significantly high dose-related peak plasma concentration following subcutaneous administration. Typically, the conventional system provides higher concentrations of exenatide for a short period of time followed by diminished levels, compared to the continuous but lower, yet effective, concentration of exenatide observed over the entire 24-hour period for the Tri-functionalized OCMT. The high concentrations achieved for the conventional system increased the likelihood of observed side effects, as evident by the behavioral observation of lethargy and loss of appetite in the pigs following subcutaneous administration. Conversely, the lower concentrations of the Tri-functionalized OCMT translates into a reduced side effect profile. In addition, sub-therapeutic levels of exenatide from the conventional system were observed after 8 hours, indicating the need for multiple dosing to achieve steady-state plasma concentrations. Generally, the sustained release capabilities and plasma concentration levels of exenatide from the Tri-functionalized OCMT was attributed to the functional effects of distinct formulatory components that have been highlighted extensively in previous Chapters. The results obtained further supported the potential of the Tri-functionalized OCMT to successfully deliver therapeutic proteins and peptides via the oral route, consequently increasing patient compliance and acceptability.

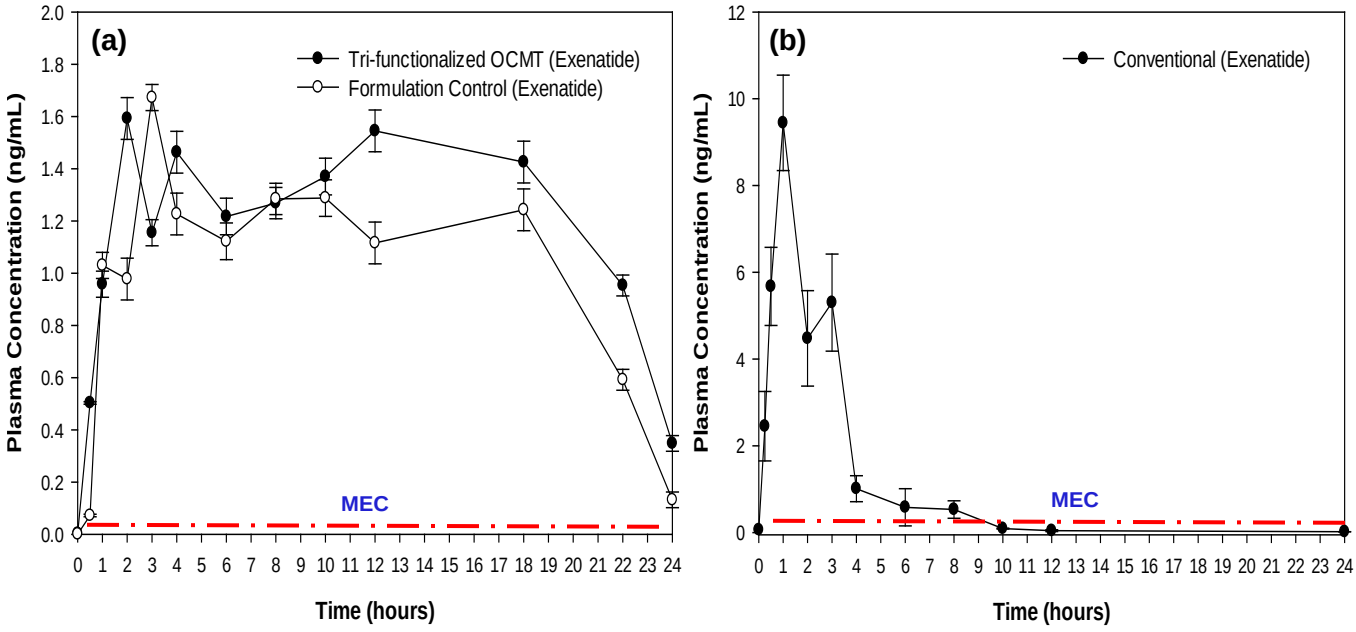

Figure 8.10: *In vivo* plasma exenatide concentration-time profiles for **a)** the orally administered Tri-functionalized OCMT and formulation control (optimized OCMT with no polymeric sheet or pH modifier) and **b)** the subcutaneously administered conventional system indicating the minimum effective concentration (MEC) for exenatide (0.05ng/mL).

8.3.5. Pharmacokinetic analysis

8.3.5.1. Octreotide non-compartmental and compartmental analysis

The results of the extravascular non-compartmental and compartmental analysis for octreotide are presented in Figure 8.11a-b, respectively. The one compartmental and two compartmental pharmacokinetic analysis of octreotide release indicated favorably small AIC and SC values. Further evaluation of the R^2 values indicated a higher value for the two compartmental model as compared to the non-compartmental model and one compartment model. Evaluation of the combined diagnostics of AIC, SC and R^2 values obtained indicated that the octreotide release from the Tri-functionalized OCMT was best described by the two compartment model shown in Table 8.2.

Moreover, pharmacokinetic analysis of the subcutaneously administered conventional system revealed that octreotide release was best described by the non-compartmental model, as it displayed a higher R^2 value and enabled identification of dual C_{max} and T_{max} peaks, as shown in Table 8.3. The maximum plasma concentration (C_{max}) and corresponding time (T_{max}) were obtained from the fitted plasma concentration-time data shown in Figure 8.9a-b. Following

administration of the subcutaneous injection, higher plasma concentrations were reached more rapidly as indicated by C_{max}^{1} (3.238ng/mL) and C_{max}^{2} (5.5810ng/mL) which were reached at T_{max} of 15min and 2 hours, respectively. In contrast, the C_{max} of octreotide from the Tri-functionalized OCMT was 1.5062ng/mL at a corresponding T_{max} of 4.5669 hours. The higher T_{max} obtained in comparison to the conventional system indicates a slower release of octreotide from the Tri-functionalized OCMT. In addition, the first order absorption rate (K_a) for octreotide in the intestine was 0.5761/h and the elimination rate constant (K_{el}) was 0.0528/h. The pharmacokinetic parameters generated for the Tri-functionalized OCMT thus all point to the prolonged release of octreotide.

Furthermore, the *MRT* for octreotide following oral administration of the Tri-functionalized OCMT was predictably higher at 20.6761 hours as compared to the conventional system at 5.9454 hours. This supported the observed prolonged release of octreotide and was further attributed to the inhibition of CYP3A4 causing a reduced metabolism and a subsequent decreased elimination of the peptide. Lastly, the achievement of a good oral bioavailability is a critical determinant in evaluating the possible therapeutic potential of an oral system for the delivery of gastro-sensitive therapeutic proteins and peptides. Thus, the relative bioavailability was determined by measuring the area under the curve (*AUC*) for both the oral and subcutaneous systems (Musther *et al.*, 2014). This value represented the total extent of octreotide absorption/uptake into the systemic circulation following their respective administrations. Results revealed an $AUC_{0\text{-}inf}$ of octreotide following SC administration of the conventional system at 11.9485ng/mL*h as compared to the oral administration of the Tri-functionalized OCMT which generated an $AUC_{0\text{-}inf}$ value of 36.3075ng/mL*h, indicating a three-fold increase in the oral bioavailability of octreotide compared to the SC injection. The overall results obtained from pharmacokinetic analysis demonstrated the feasibility of the Tri-functionalized OCMT in delivering sustained, therapeutic levels of octreotide with an enhanced oral bioavailability.

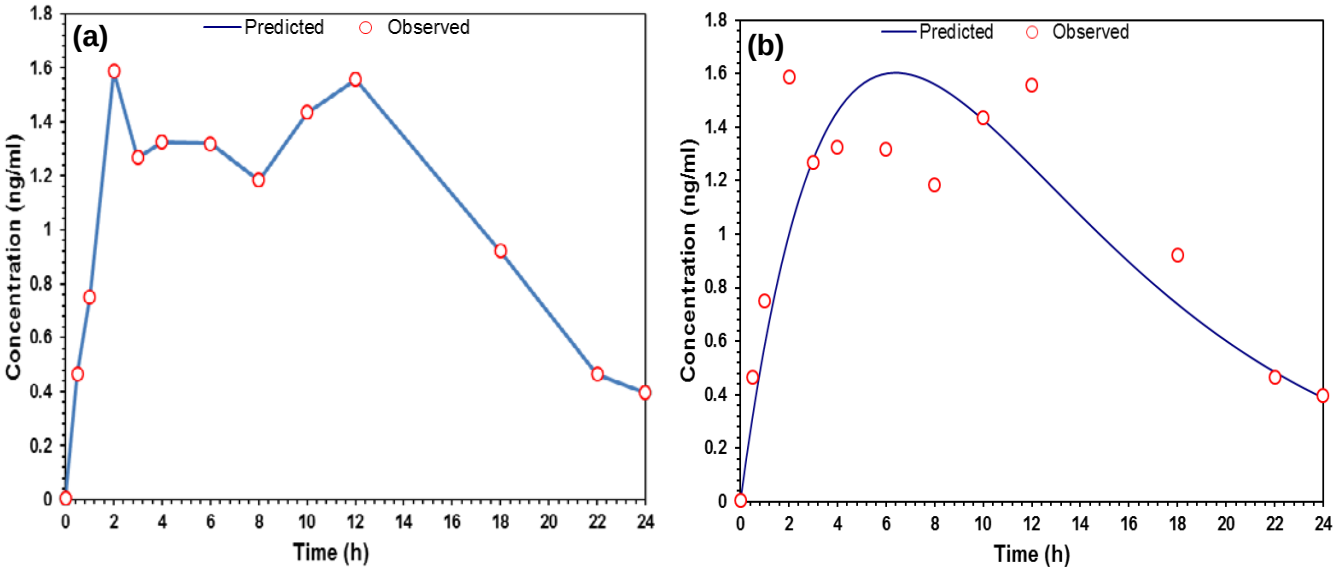

Figure 8.11: Graphical results showing the observed and predicted values for **a)** non-compartmental and **b)** compartmental pharmacokinetic analysis of octreotide release from the Tri-functionalized OCMT.

Table 8.2: Results of two compartmental analysis of octreotide release from the orally administered Tri-functionalized OCMT

Parameter	Unit	Value	Diagnostics	Value
A	ng/ml	0.000001	r obs-pre	0.9066
Alpha	1/h	0.2694	SS	0.5600
B	ng/ml	2.1104	WSS	0.5600
Beta	1/h	0.0528	R^2	0.9639
K_a	1/h	0.5761	WR^2	0.9639
k_{10}	1/h	0.0528	SE	0.2646
k_{12}	1/h	0.00000005	AIC	2.4631
k_{21}	1/h	0.2694	SC	5.2879
$t_{1/2Alpha}$	H	2.5732		
$t_{1/2Beta}$	H	13.1283		
$t_{1/2ka}$	H	1.2032		
V/F	(mg)/(ng/ml)	10.4332		
CL/F	(mg)/(ng/ml)/h	0.5508		
V_2/F	(mg)/(ng/ml)	0.00000187		
CL_2/F	(mg)/(ng/ml)/h	0.00000050		
T_{max}	H	4.5669		
C_{max}	ng/ml	1.5062		
AUC $_{0-t}$	ng/ml*h	25.0504		
AUC $_{0-inf}$	ng/ml*h	36.3075		
AUMC	ng/ml*h^2	750.6979		
MRT	H	20.6761		

Table 8.3: Results of non-compartmental analysis of octreotide release from the subcutaneously administered conventional system

Parameter	Unit	Value
λ_z	1/h	0.1079
$t_{1/2}$	h	6.4227
T_{max}	h	2
C_{max}	ng/mL	5.5810
T_{lag}	h	0
C_{last_obs}/C_{max}		0.0158
AUC $_{0\text{-}t}$	ng/mL*h	11.1331
AUC $_{0\text{-}inf\_obs}$	ng/mL*h	11.9485
AUC $_{0\text{-}t/0\text{-}inf\_obs}$		0.9318
AUMC $_{0\text{-}inf\_obs}$	ng/mL*h^2	71.0385
MRT $_{0\text{-}inf\_obs}$	h	5.9454
$Cl/F_{\_obs}$	(mg)/(ng/ml)/h	0.0775
$Tmax^1$	h	0.08
$Cmax^1$	ng/ml	3.238
$Tmax^2$	h	2
$Cmax^2$	ng/ml	5.581
TmaxH	h	2
CmaxH	ng/ml	5.581
CmaxL/CmaxH		0.580182763
CmaxH-L	ng/ml	2.343
NumBtwPeaks		5
DuraBtwPeaks	h	1.92

8.3.5.2. Exenatide non-compartmental and compartmental analysis

The results of the extravascular non-compartmental and compartmental analysis for exenatide are presented in Figure 8.12a-b, respectively. Evaluation of analysis revealed that exenatide release was similarly best described by a two compartmental model with the most favorable AIC and SC values determined with this algorithm (Table 8.4). In addition, the diagnostic evaluation of the regression coefficients (R^2) indicated a significantly greater fit for the two compartmental model as compared to the non-compartmental model and one compartmental model. Further diagnostic of the sum of squares (SS) and standard error (SE) with compartmental analysis revealed SS=13.5370; SE=1.1635 and SS=1.2097; SE=0.3889 for the one compartment and two compartment analysis, respectively. This indicated the variance in the modelled values, further supporting the two compartmental model fit. Furthermore, the pharmacokinetic analysis of the subcutaneously administered conventional system revealed that exenatide release was best described by a one compartmental model with the most favorable AIC and SC values obtained, as shown in Table 8.5.

The pharmacokinetic parameters determined by the one compartmental model for the conventional system indicated a first order absorption rate constant (K_a) of 0.9806/h and an elimination rate constant (K_{el}) of 0.8333/h. This confirmed the rapid absorption and equally rapid elimination of exenatide following SC administration of the conventional system. As a result of the rapid absorption, a peak plasma concentration (C_{max}=7.6783ng/mL) was reached at 1.1050 hours (T_{max}). In contrast, the two compartmental analysis of octreotide release from the Tri-functionalized OCMT indicated a lower C_{max} (1.1981ng/mL) at a corresponding T_{max} of 2.2597 hours. Consideration of the large comparative differences between the peak plasma concentrations of the conventional system and the Tri-functionalized OCMT, retrospectively accounts for the side effects observed in the pig following SC injection. Higher peak plasma concentrations may enter the toxic range and significantly increase the side effect profile. Thus, the lower C_{max} values observed for exenatide following oral administration of the Tri-functionalized OCMT may greatly reduce the side effect profile while still maintaining therapeutic levels of exenatide over a sustained period of time as indicated by the higher *MRT* (99.37h) value obtained.

The *MRT* further supported the prolonged release and slow elimination rate (K_{el} =0.0126/h) of exenatide which may be attributed to the inhibition of CYP3A4 which causes a reduction in exenatide metabolism, consequently affecting its ADME profile. A final critical parameter in pharmacokinetic evaluations, following oral and SC administration, is the *AUC* as it is used as a measure of oral bioavailability (Musther *et al*., 2014). Understanding the bioavailability is a key consideration in the evaluation of the feasibility of a dosage form, specifically oral formulations, as its availability can be affected by additional elements along the GIT pathway. Thus, parametric evaluation revealed an $AUC_{0\text{-}inf}$ of exenatide following SC administration of the conventional system at 23.1396ng/mL*h as compared to the oral administration of the Tri-functionalized OCMT which generated an $AUC_{0\text{-}inf}$ value of 117.3464ng/mL*h. Comparative analysis indicated a five-fold increase in the oral bioavailability of exenatide compared to the SC injection. The improved oral bioavailability, sustained release and comprehensive pharmacokinetic profiling analysis demonstrated the feasibility of the Tri-functionalized OCMT to provide an alternative therapeutic tool for exenatide delivery, potentially substituting the conventional SC administration.

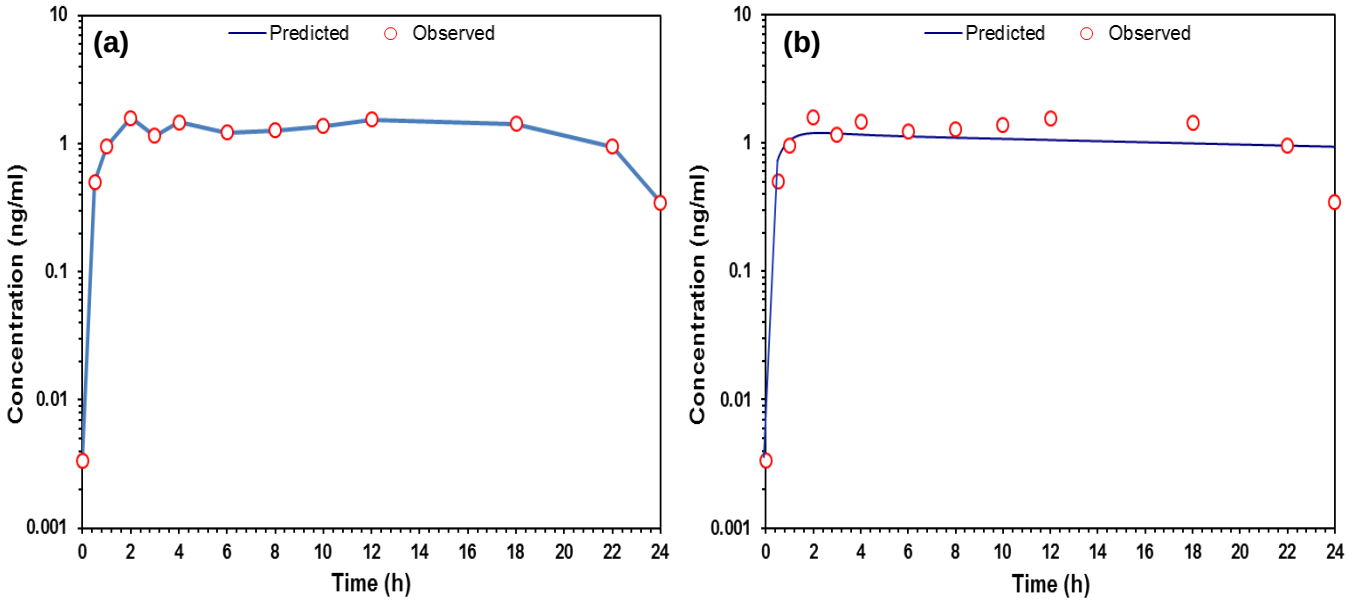

Figure 8.12: Logarithmic graph results showing the observed and predicted values for **a)** non-compartmental and **b)** compartmental pharmacokinetic analysis of exenatide release from the Tri-functionalized OCMT.

Table 8.4: Results of two compartmental analysis of exenatide release from the orally administered Tri-functionalized OCMT

Parameter	Unit	Value	Diagnostics	Value
A	ng/ml	0.7127	r obs-pre	0.8125
Alpha	1/h	0.8599	SS	1.2097
B	ng/ml	1.1901	WSS	1.2097
Beta	1/h	0.0101	R^2	0.9313
K_a	1/h	1.4788	WR^2	0.9313
k_{10}	1/h	0.0126	SE	0.3889
k_{12}	1/h	0.1687	AIC	12.4745
k_{21}	1/h	0.6886	SC	15.2992
$t_{1/2Alpha}$	H	0.8061		
$t_{1/2Beta}$	H	68.6098		
$t_{1/2ka}$	H	0.4687		
V/F	(mg)/(ng/mL)	3.3777		
CL/F	(mg)/(ng/mL)/h	0.0426		
V_2/F	(mg)/(ng/mL)	0.8276		
CL_2/F	(mg)/(ng/mL)/h	0.5699		
T_{max}	h	2.2597		
C_{max}	ng/ml	1.1981		
AUC $_{0-t}$	ng/ml*h	24.9065		
AUC $_{0-inf}$	ng/ml*h	117.3464		
AUMC	ng/ml*h^2	11660.7134		
MRT	h	99.3700		

Table 8.5: Results of one compartmental analysis of exenatide release from the subcutaneously administered conventional system

Parameter	Unit	Value	Diagnostics	Value
A	ng/mL	128.4042	r obs-pre	0.9424
K_a	1/h	0.9806	SS	11.6327
k_{10}	1/h	0.8333	WSS	11.6327
$t_{1/2ka}$	h	0.7069	R^2	0.9344
$t_{1/2k10}$	h	0.8318	WR^2	0.9344
V/F	(mg)/(ng/mL)	0.0041	SE	1.1369
CL/F	(mg)/(ng/mL)/h	0.0035	AIC	35.4458
T_{max}	h	1.1050	SC	36.9006
C_{max}	ng/mL	7.6783		
AUC $_{0-t}$	ng/mL*h	23.1396		
AUC $_{0-inf}$	ng/mL*h	23.1396		
AUMC	ng/mL*h^2	51.3642		
MRT	h	2.2198		

8.3.6. Establishment of an IVIVC for peptide release from the Tri-functionalized OCMT

8.3.6.1. Establishment of *in vitro-in vivo* correlation for octreotide

A Level A IVIVC was established for evaluation of octreotide release using all the information of the *in vitro* dissolution and *in vivo* absorption curves, generating a one-to-one relationship based directly on each of the assayed time points (Emami, 2006). The amount of peptide absorbed following oral administration of the Tri-functionalized OCMT, which is important in terms of its further pharmaceutical development, was calculated by the Wagner-Nelson deconvolution technique using the linear trapezoidal rule. For the analysis of a Level A IVIVC, the percentage of peptide absorbed up to time *t* was plotted versus the amount of peptide released *in vitro*. The pharmacokinetic conditions derived from this investigation conforms to the requirements of the two-stage developmental process of deconvolution through convolution since the octreotide release from the Tri-functionalized OCMT was best described by a two compartmental pharmacokinetic model. Deconvolution of observed plasma octreotide concentration-time data against the *in vitro* release profile (Figure 8.13a) provided the predicted *in vitro* and *in vivo* release profiles, shown in Figure 8.13b.

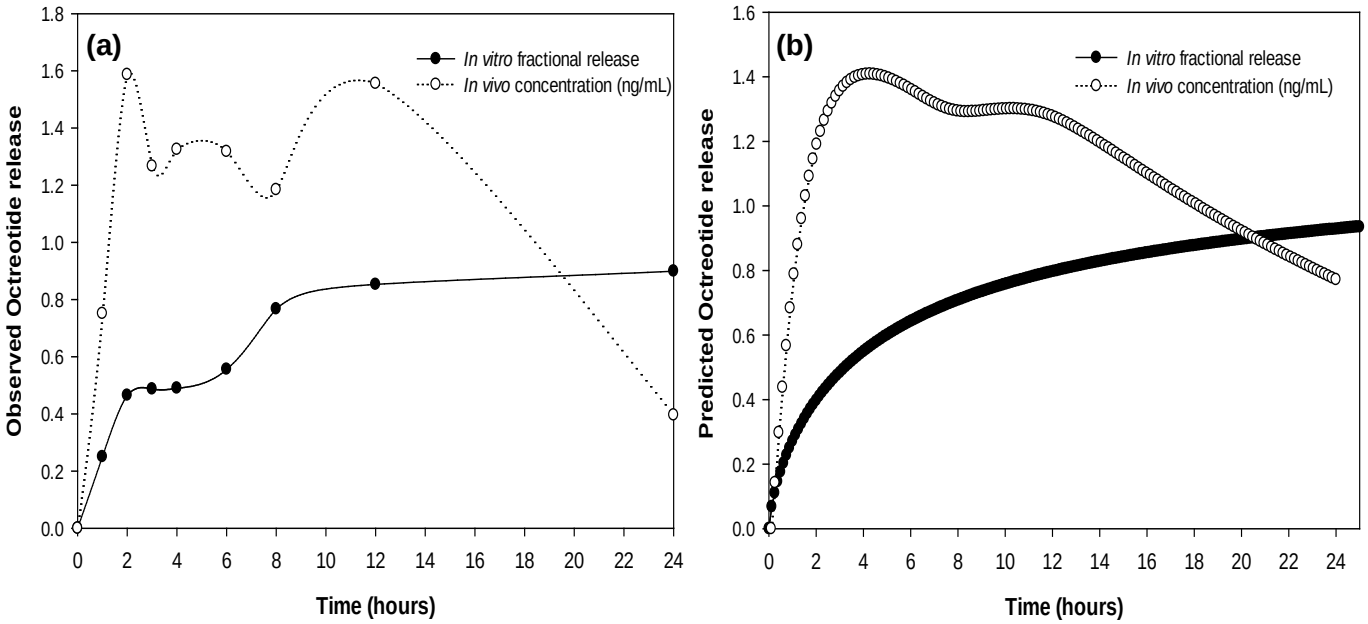

Figure 8.13: *In vitro* and *in vivo* release profiles in **a)** observed octreotide release from the Tri-functionalized OCMT and **b)** predicted octreotide release extracted using deconvolution analysis.

Level A IVIVC analysis for octreotide yielded a levy plot with an R^2 value of 0.9366 and a slope of 0.026, as shown in Figure 8.14. Thus, *in vitro* data was predictive of *in vivo* data with 93.66% accuracy. However, the slope of the curve was lower than 1, indicating that the *in vivo* absorption rate was underestimated which may be attributed to the hepatic first pass effect (Sirisuth and Eddington, 2002). Central to development of an IVIVC is the validation of the model and thus, the prediction errors (PE) for C_{max} and $AUC_{0-\infty}$ were calculated in order to determine the validity of the correlation. According to the FDA guidelines, the mean absolute %PE should be ≤10% and the absolute prediction error should be ≤15%. The calculated PE for C_{max} and $AUC_{0-\infty}$ were 12.70% and 0%, respectively. These results indicated a good validation of the IVIVC model with a 0% PE indicating no error between the observed and predicted $AUC_{0-\infty}$ value. Based on qualitative parameters, a Level A correlation was approached despite the plots not being perfectly superimposable. The complexity of the Tri-functionalized OCMT accounts for the slight variations between the *in vitro* and *in vivo* data. Generally, the *in vitro* data seems to run ahead of *in vivo* data as *in vivo* conditions cannot be completely simulated *in vitro*, specifically with respect to the co-inhibition of CYP3A4 and Pgp by the Tri-functionalized OCMT. Nevertheless, the *in vitro* data did display a good predictability of the *in vivo* data, reliably demonstrating that the IVIVC model can possibly be used a surrogate for bioequivalence studies.

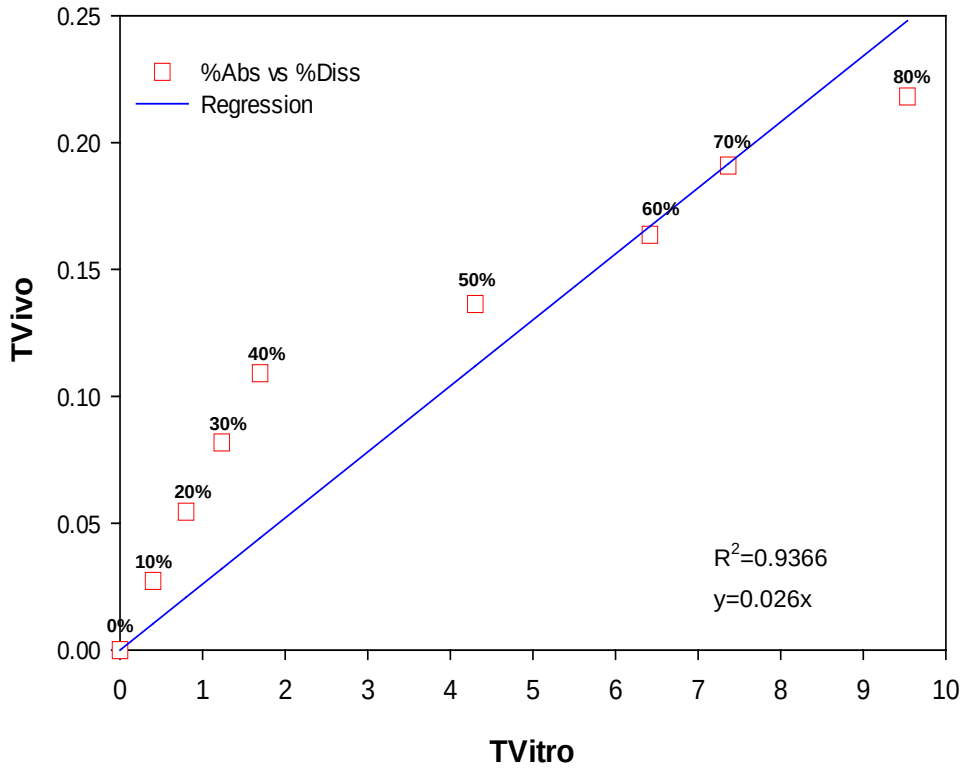

Figure 8.14: A levy plot depicting the relationship between the percentage of octreotide release *in vitro* and the percentage of octreotide absorbed *in vivo.*

8.3.6.2. Establishment of *in vitro-in vivo* correlation for exenatide

A Level A IVIVC was established for exenatide release via a two-stage process of deconvolution through convolution (Chakraborty *et al*., 2014). Deconvolution of all the observed data of the *in vitro* dissolution and *in vivo* absorption curves (Figure 8.15a) at each assayed time point was used to calculate the predicted *in vitro* and *in vivo* release profiles (Figure 8.15b) using the Wagner-Nelson method.

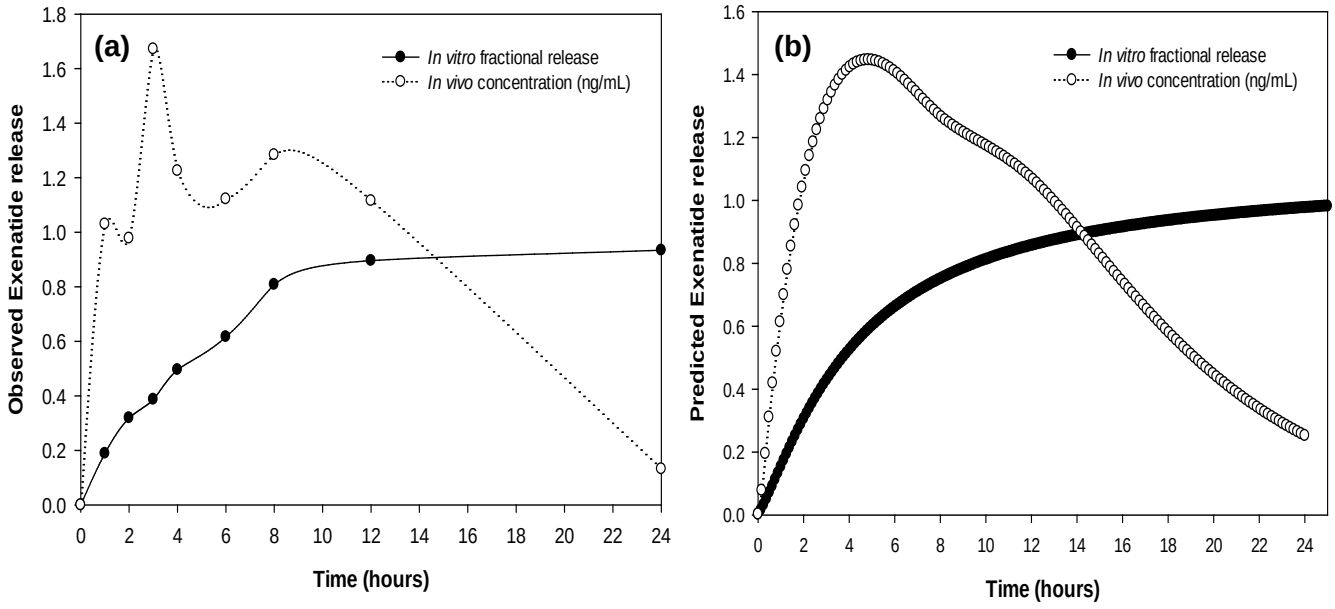

Figure 8.15: *In vitro* and *in vivo* release profiles of **a)** observed exenatide release from the Tri-functionalized OCMT and **b)** predicted exenatide release extracted using deconvolution analysis.

The established Level A IVIVC analysis for exenatide release yielded a levy plot with an R^2 value of 0.9407 and a slope of 0.022, as shown in Figure 8.16. Thus, *in vitro* data was predictive of *in vivo* data with 94.07% accuracy. However, the slope of the curve was lower than 1, indicating an underestimation of the *in vivo* absorption rate which may be attributed to the hepatic first pass effect (Sirisuth and Eddington, 2002). Central to development of an IVIVC is the validation of the model and thus, the prediction errors (PE) for C_{max} and $AUC_{0-\infty}$ were calculated in order to determine the validity of the correlation. According to the FDA guidelines, the mean absolute %PE should be ≤10% and the absolute prediction error should be ≤15%. The calculated PE for C_{max} and $AUC_{0-\infty}$ were 10.81% and 0%, respectively. These results indicated a good validation of the IVIVC model with a 0% PE indicating no error between the observed and predicted $AUC_{0-\infty}$ value. The plots were not directly superimposable; however, based on the qualitative patterns of this fit, a Level A correlation was approached. The complexity of the Tri-functionalized OCMT accounts for the slight variations between the *in vitro* and *in vivo* data. Generally, the *in vitro* data seems to run ahead of *in vivo* data as *in vivo* conditions cannot be completely simulated *in vitro*, specifically with respect to the co-inhibition of CYP3A4 and Pgp by the Tri-functionalized OCMT. Nevertheless, the *in vitro* data did display a good predictability, matching the *in vivo* data more closely than octreotide and reliably demonstrating that the IVIVC model can possibly be used a surrogate for bioequivalence studies.

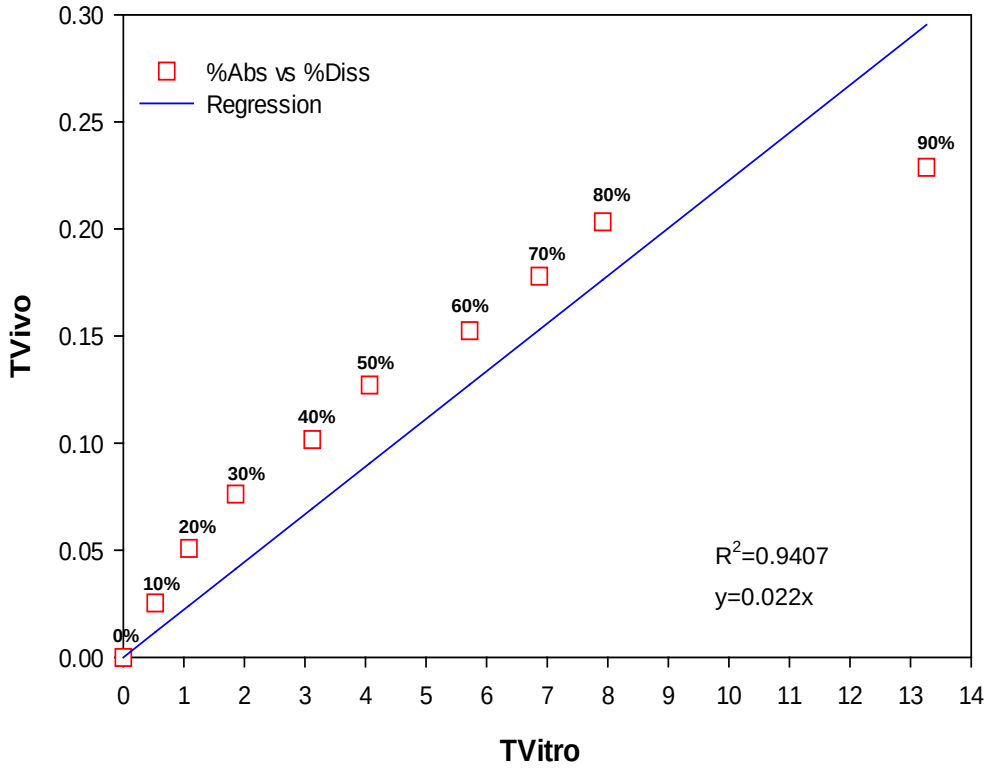

Figure 8.16: A levy plot depicting the relationship between the percentage of exenatide release *in vitro* and the percentage of exenatide absorbed *in vivo.*

8.4. Concluding Remarks

In vivo analysis of the Tri-functionalized OCMT in the Large White pig model has demonstrated the potential of the device to successfully delivery therapeutic peptides orally. The novel features of the Tri-functionalized OCMT function synergistically to provide an optimal therapeutic profile. The oral bioavailability of both octreotide and exenatide was enhanced as evidenced by the three-fold and five-fold increase in $AUC_{0-\infty}$ as compared to their conventional subcutaneous systems, respectively. Octreotide displayed a C_{max} of 1.5062ng/mL at a corresponding T_{max} of 4.5669 hours and exenatide displayed a C_{max} of 1.1981ng/mL at a corresponding T_{max} of 2.2597 hours. Both of the C_{max} values obtained were significantly lower than the conventional systems but still higher than the minimum effective concentration (MEC). Generally, the *in vivo* profiles of both octreotide and exenatide displayed sustained therapeutic levels over the 24 hour period with phases of peak concentrations attributed to a combination of the distinct functionalities of formulatory components, producing *in situ* crosslinking and co-inhibition of CYP3A4 and Pgp, causing further sustained release. In addition, the evaluation of the IVIVC undertaken for both octreotide and exenatide attained a Level A correlation with a good predictability, providing further evidence of the feasibility of the Tri-functionalized OCMT,

and advancing the development for clinical application. Conclusive *in vivo* analysis of both octreotide and exenatide demonstrated the capability of the Tri-functionalized OCMT to serve as prototypical device for incorporation and delivery of a multitude of gastro-sensitive proteins and peptides, potentially replacing the conventional parenteral routes of administration.

8.5. References

Bassols, A., Costa, C., Eckersall, P.D., Osada J., Sabria, J., Tibau, J. (2014). The pig as an animal model for human pathologies: A proteomics perspective. *Proteomics Clinical Application,* 8, 715-731.

Bergman, E., Lundahl, A., Fidblom, P., Hedeland, M., Bondesson, U., Knutson, L., Lennernäs, H. (2009). Enterohepatic disposition of rosuvastatin in pigs and the impact of concomitant dosing with cyclosporine and genfibrozil. *Drug Metabolism and Disposition*, 37, 2349-2358.

Brunet, B., Doucet, C., Venisse, N., Hauet, T., Hebrand, W., Papet, Y., Mauco, G., Mura, P. (2006). Validation of Large White Pig as an animal model for the study of cannabinoids metabolism: Application to the study of THC distribution in tissues. *Forensic Science International,* 161, 169-174.

Chakraborty, S., Pandya, K., Aggarwal, D. (2014). Establishing Prospective IVIVC for Generic Pharmaceuticals: Methodologies Assessment. *The Open Drug Delivery Journal,* 5, 1-7.

Dorkoosh, F.A., Verhoef, J.C., Borchard, G., Rafiee-Tehrani, M., Verheijden, J.H.M., Junginger, H.E. (2002). Intestinal absorption of human insulin in pigs using delivery systems based on superporous hydrogel polymers. *International Journal of Pharmaceutics,* 247, 47-55.

Emami, J. (2006). *In vitro - In vivo* Correlation: From Theory to Applications. *Journal of Pharmacy and Pharmaceutical Sciences,* 9, 31-51.

Kobayashi, E., Hishikawa, S., Teratani, T., Lefor, A.T. (2012). The pig as a model for translational research: overview of porcine animal models at Jichi Medical University. *Translational Research,* 8, 1-9.

Ludden, T.M., Beal, S.L., Sheiner, L.B. (1994). Comparison of the Akaike Information Criterion, the Schwarz criterion and the *F* test as guides to model selection. *Journal of Pharmacokinetics and Biopharmaceutics,* 22, 431-445.

Musther, H., Olivares-Morales, A., Hatley, O.J.D., Liu, B., Hodjegan, A.M. (2014). Animal versus human oral drug bioavailability: Do they correlate? *European Journal of Pharmaceutical Sciences*, 57, 280–291.

Ostrowski, M., Baczek, T. (2010). The Progress on the *In Vivo-In Vitro* Correlation (IVIVC) for Immediate Release Dosage Form as an Alternative to Bioavailability Studies. *Current Pharmaceutical Analysis,* 6, 289-298.

Persson, E.M., Nordgren, A., Forsell, P., Knutson, L., Ohgren, C., Forssen, S., Lennernäs, H., Abrahamsson, B. (2008). Improved understanding of the effect of food on drug absorption and bioavailability for lipophilic compounds using an intestinal pig perfusion model. *European Journal of Pharmaceutical Sciences*, 34, 22-29.

Sirisuth, N., Eddington, N.D. (2002). The influence of first pass metabolism on the development and validation of an IVIVC for metoprolol extended release tablets. *European Journal of Pharmaceutics and Biopharmaceutics,* 53, 301-309.

Swindle, M.M., Smith, A.C. (1998). Comparative anatomy and physiology of the pig. *Scandinavian Journal of Laboratory Science,* 25, 11-21.

Zhang, Y., Huo, M., Zhou, J., Xie, S. (2010). PKSolver: An add-in program for pharmacokinetic and pharmacodynamic data analysis in Microsoft Excel. *Computer Methods and Programs in Biomedicine,* 99, 306-314.

CHAPTER 9

CONCLUSIONS, RECOMMENDATIONS AND FUTURE OUTLOOK

9.1. Conclusion

The global pharmaceutical biotechnology industry is continually growing and increased amounts of protein and peptide-based therapeutics are entering into the market. The interest in this field stems from the high specificity and activity of these molecules which make them the preferred choice for multiple disease conditions. However, the conventional delivery systems available for these therapeutic proteins and peptides limit patient acceptability and convenience.

Thus, pharmaceutical companies and research-based institutions are progressively focusing their efforts towards developing simple and effective delivery alternatives. Oral dosage forms still remain the simplest and most preferred delivery route, however it poses numerous physical and chemical challenges with regards to the successful delivery of therapeutic proteins and peptides. Therefore, any developments in this field need to successfully overcome these challenges in order to provide a clinically useful oral formulation.

The Tri-functionalized OCMT device that was formulated in this study was designed with the intention of overcoming the challenges relating to the oral administration of therapeutic proteins and peptides by triple targeting three major issues, namely; 1) the exposure of proteins and peptides to unfavorable conditions within the gastrointestinal tract (GIT), 2) poor absorption through the GIT membrane and 3) enzymatic degradation within the GIT.

This was achieved by incorporating the bioactive into a core-melt archetype within the tablet and facilitating the process of *in situ* crosslinking which significantly affects the way the bioactive is protected within the compressed tablet matrix as well providing desirable bioactive release kinetics. In addition, the incorporation of a co-inhibitory ‘smart’ polymeric sheet provided added protection and enabled an improved absorption by virtue of its intrinsic properties and co-inhibition of the major determinants, CYP3A4 and Pgp, of poor absorption and low oral bioavailability. Lastly, targeting of enzymatic degradation was achieved by incorporation of a pH modifier that functions to transiently lower the micro-environmental pH and reduce the optimal environment for enzyme activity.

The combination of the distinct formulatory components contained within the Tri-functionalized OCMT was extensively evaluated through in-depth *in vitro* physicochemical and physicomechanical characterization, *ex vivo* analyses and *in vivo* performance. *In vitro* and *ex vivo* characterization enabled the optimization of design variables and promoted the achievement of desirable functionalities for attainment of optimum *in vivo* performance. *In vivo* analyses of the Tri-functionalized OCMT in the Large White pig model revealed an enhanced oral bioavailability of the incorporated peptides, octreotide and exenatide, following oral administration, as compared to their conventionally administered subcutaneous counterparts. In addition, pharmacokinetic analysis of the Tri-functionalized OCMT confirmed the maintenance of sustained, therapeutic levels of both octreotide and exenatide over the 24 hour period, supporting a convenient once-daily dosing.

The advanced research presented in this thesis has brought the Tri-functionalized OCMT from the stage of conceptual design to the completion of preclinical studies. Essentially, it has been successfully demonstrated that the Tri-functionalized OCMT enhances the oral delivery of therapeutic proteins and peptides, potentially serving as a viable alternative to the conventional parenteral route of administration for multiple disease conditions.

9.2. Recommendations

In vivo studies that were undertaken successfully demonstrated the achievement of peptide levels above the minimum effective concentration. However, the C_{max} for both octreotide and exenatide was much lower than the parenterally administered conventional systems. This can be overcome by increasing the concentration of peptide incorporation into the Tri-functionalized OCMT, however, care must be taken that plasma concentrations do not reach toxic levels as this could result in unwanted side effects that are commonly associated with the high peak plasma concentrations reached with parenteral formulations.

Although animal studies provided valuable information regarding the *in vivo* fate of the Tri-functionalized OCMT, alternative methods for modeling intestinal absorption may eliminate the need for animal testing. The *ex vivo* permeation studies that were undertaken provide an approximate correlation to the permeation-enhancing effects of certain components, however, advanced cellular transport studies may prove to be more useful in determining the exact mechanism facilitating the permeation process across the intestinal membrane, in addition to providing a reliable estimate of oral absorption.

Whilst the Tri-functionalized OCMT has been refined to a stage of formulation optimization and preclinical investigation, implications for further considerations becomes paramount in advancing the system to clinical stage development. An important consideration is the scaling-up of the manufacturing process. The Tri-functionalized OCMT is relatively cost-effective to produce. However, due to the incorporation of different components and the formation of a core-melt archetype, specialized machinery may be required to provide a reproducible tablet assembly process.

9.3. Future Outlook

The novel Tri-functionalized OCMT certainly opens up clinical advancement opportunities with respect to the development of innovator devices for oral protein and peptide delivery. The Tri-functionalized OCMT was evaluated for its clinical potential using octreotide and exenatide, however the versatility of the formulation renders the Tri-functionalized OCMT applicable for incorporation of a multitude of therapeutic proteins and peptides. Moreover, the device can aid in the delivery of Biopharmaceutics Classification System (BCS) Class drugs which possess varying degrees of solubility and permeability. This ultimately increases the disease targeting database of the device and enhances its clinical potential. The intellectual property of the Tri-functionalized OCMT device has been by protected its provisional patent. In addition, the licensing of the technology to a suitable pharmaceutical company has been instigated and potential positive outcomes may promote economic growth within South Africa. The development of this technology in South Africa will not only enable the country to compete on an international level against the importation of innovator and generic products but also, enable the recognition of the country as being capable of achieving research excellence on par with international standards.

10. Appendices

10.1. Publications

10.1.1. Review Paper

Biotechnology Advances 32 (2014) 1269–1282

Contents lists available at ScienceDirect

Biotechnology Advances

journal homepage: www.elsevier.com/locate/biotechadv

Research review paper

A review of advanced oral drug delivery technologies facilitating the protection and absorption of protein and peptide molecules

Bibi F. Choonara, Yahya E. Choonara, Pradeep Kumar, Divya Bijukumar, Lisa C. du Toit, Viness Pillay *

Wits Advanced Drug Delivery Platform Research Unit, Department of Pharmacy and Pharmacology, School of Therapeutic Sciences, Faculty of Health Sciences, University of the Witwatersrand, Johannesburg, 7 York Road, Parktown 2193, South Africa

ARTICLE INFO

Article history:
Received 21 May 2014
Received in revised form 21 July 2014
Accepted 28 July 2014
Available online 3 August 2014

Keywords:
Oral drug delivery
Therapeutic proteins and peptides
Bioavailability
Gastrointestinal barrier
Advanced oral biotechnology

ABSTRACT

The oral delivery of proteins and peptides is a dynamic research field despite the numerous challenges limiting their effective delivery. Successful oral delivery of proteins and peptides requires the accomplishment of three key tasks: protection of the macromolecules from degradation in the gastrointestinal tract (GIT), permeation through the intestinal barrier and absorption of molecules into the systemic circulation. Currently, no clinically useful oral formulations have been developed but several attempts have been made to overcome the challenges of low oral bioavailability resulting from poor absorption, poor permeation and enzymatic degradation of the proteins and peptides in the GIT. Present strategies attempt to provide structural protection of the proteins and peptides and improved absorption through the use of enzyme inhibitors, absorption enhancers, novel polymeric delivery systems and chemical modification. However, each of these technologies has their limitations despite showing positive results. This review attempts to discuss the physical and chemical barriers of the GIT with particular emphasis on the current approaches employed to overcome these barriers, including the evaluation of other non-parenteral routes of protein and peptide delivery. In addition, this review assimilates oral formulation strategies under development and within the clinical trial stage in relation to their benefits and drawbacks with regard to facilitating optimal protection and absorption of proteins and peptides, as well as pertinent future challenges and opportunities governing oral drug delivery.

10.1.2. Research Paper 1

AAPS PharmSciTech, Vol. 16, No. 4, August 2015 (© 2014)
DOI: 10.1208/s12249-014-0271-z

Research Article

A Menthol-Based Solid Dispersion Technique for Enhanced Solubility and Dissolution of Sulfamethoxazole from an Oral Tablet Matrix

Bibi F. Choonara,[1] Yahya E. Choonara,[1] Pradeep Kumar,[1] Lisa C. du Toit,[1] Lomas K. Tomar,[1] Charu Tyagi,[1] and Viness Pillay[1,2]

Received 11 November 2014; accepted 10 December 2014; published online 31 December 2014

Abstract. A menthol-based solid dispersion was designed to improve the intrinsic solubility of the poorly soluble sulfamethoxazole- a class II drug molecule of Biopharmaceutics Classification System (BCS) displaying widespread antibacterial activity. Solid dispersions of menthol and sulfamethoxazole were compressed with hydroxypropyl methylcellulose (HPMC) into suitable sulfamethoxazole-loaded matrix tablets for oral drug delivery. The sulfamethoxazole-loaded solid dispersions and compressed tablets were characterized for their physicochemical and physicomechanical properties such as changes in crystallinity, melting point, molecular transitions, and textural analysis for critical analysis of their effects on the solubility and dissolution of sulfamethoxazole. The formulations were further evaluated for swelling, degradation, solubility, and *in vitro* drug release behavior. *In vitro* drug release from the sulfamethoxazole-loaded matrix tablets displayed a minimum and maximum fractional release of 0.714 and 0.970, respectively. The tablets further displayed different release rate profiles over the study periods of 12, 16, 48, and 56 h which were attributed to the varying concentrations of menthol within each formulation. Menthol was determined as a suitable hydrophilic carrier for sulfamethoxazole since it functioned as a solubilizing and release-retarding agent for improving the solubility and dissolution of sulfamethoxazole as well as controlling the rate at which it was released.

KEY WORDS: crystallinity; menthol; oral solubility and dissolution; solid dispersion; sulfamethoxazole.

10.1.3. Research Paper 2

Journal of Pharmaceutical Sciences 105 (2016) 2086-2098

Contents lists available at ScienceDirect

Journal of Pharmaceutical Sciences

journal homepage: www.jpharmsci.org

Pharmaceutics, Drug Delivery and Pharmaceutical Technology

Design of an *In Situ* Cross-Linked Eutectic Tablet for Enhanced Delivery of Gastro-Sensitive Proteins and Peptides

Bibi F. Choonara, Yahya E. Choonara, Pradeep Kumar, Lisa C. du Toit, Viness Pillay*

Wits Advanced Drug Delivery Platform Research Unit, Department of Pharmacy and Pharmacology, School of Therapeutic Sciences, Faculty of Health Sciences, University of the Witwatersrand, Johannesburg, 7 York Road, Parktown, 2193, South Africa

ARTICLE INFO

Article history:
Received 8 December 2015
Revised 11 March 2016
Accepted 5 April 2016
Available online 1 June 2016

Keywords:
oral protein delivery
bovine serum albumin
controlled release
solid dispersion
intestinal absorption
eutectic mixture

ABSTRACT

In the present study, a eutectic platform was designed as an *in situ* cross-linked eutectic tablet for structural protection, enhanced intestinal permeation, and controlled release of proteins after oral administration. Physicochemical and physicomechanical analyses of the eutectic tablets were undertaken to elucidate the *in situ* cross-linking mechanism, thermal transitions, crystallinity, *ex vivo* permeation, and *in vitro* release of the protein. Following thermal characterization, results revealed successful eutectic formation with a melting point to 37°C. Protein release from the formulation was controlled over 24 h with a maximum fractional release of ±0.8 for all formulations. The release pattern alternated between phases of burst and slow release which was attributed to the combined effects of swelling, surface erosion, and *in situ* cross-linking. Mathematical modeling of the protein release kinetics corresponded best with the Higuichi model with near zero-order ($R^2 \approx 0.9787$) release. The permeation-enhancing effect of menthol contained within the eutectic powder blend was investigated and results showed an enhanced protein flux (0.0576-0.0720 $mg \cdot cm^{-2}\ h^{-1}$) across the intestinal tissue model compared with a control formulation. Extensive *in vitro* characterization highlighted the successful design of the eutectic tablets as a potential oral delivery system for proteins with structural protection, enhanced intestinal permeation, and controlled release.

10.1.4. Research Paper 3

(To be submitted to *International Journal of Pharmaceutics*)

IN VITRO AND *IN VIVO* EVALUATION OF A NOVEL ORAL CORE-MELT TABLET (OCMT)

Bibi F. Choonara, Yahya E. Choonara, Pradeep Kumar, Lisa C. du Toit, Viness Pillay*

Wits Advanced Drug Delivery Platform Research Unit, Department of Pharmacy and Pharmacology, School of Therapeutic Sciences, Faculty of Health Sciences, University of the Witwatersrand, Johannesburg, 7 York Road, Parktown, 2193, South Africa

***Corresponding Author:**
Professor Viness Pillay
Tel: +27-11-717-2274
Fax: +27-11-642-4355
Fax2Email: +27-86-553-4733
Email: viness.pillay@wits.ac.za

ABSTRACT
A complex polymer-eutectic platform was optimized as an Oral Core-Melt Tablet (OCMT), producing a novel oral controlled release system for the delivery of gastro-sensitive therapeutic proteins and synthetic peptides. Physicochemical and physicomechanical characterization techniques were undertaken to determine the rheological properties, *in-situ* crosslinking mechanisms, porositometric evaluations, imagery and *in vitro* peptide release from the OCMT. The inherent transitions observed in the Fourier Transform Infrared Spectroscopy spectrums confirmed the presence of *in situ* crosslinking, facilitated by the porous structure promoting the ingress of fluid into the OCMT. This was corroborated with MRI which highlighted the device hydration over 24 hours as a significant predictor of the *in vitro* peptide release profile. The *in vitro* release of the peptide was influenced by the combined effects of swelling, surface erosion and *in situ* crosslinking, displaying a fractional release up to ±0.8. Owing to the complexity of the system, the mechanism of release was attributable to both the zero-order (R^2=0.95) and Higuichi models (R^2=0.98). Conclusive results from extensive *in vitro* characterization emphasized the applicability of the optimized OCMT in providing a controlled release alternative system capable of delivering peptides orally.

KEYWORDS: Oral peptide delivery; octreotide; controlled release; eutectic powder blend; physicochemical properties; physicomechanical properties

10.1.5. Research Paper 4

(To be submitted to the *Journal of Controlled Release*)

DESIGN OF THE CO-INHIBITORY 'SMART' POLYMERIC SHEET SURROUNDING A pH-MODIFIED OCMT FOR TRI-FUNCTIONALIZATION

Bibi F. Choonara, Yahya E. Choonara, Pradeep Kumar, Lisa C. du Toit, Viness Pillay*

Wits Advanced Drug Delivery Platform Research Unit, Department of Pharmacy and Pharmacology, School of Therapeutic Sciences, Faculty of Health Sciences, University of the Witwatersrand, Johannesburg, 7 York Road, Parktown, 2193, South Africa

***Corresponding Author:**
Professor Viness Pillay
Tel: +27-11-717-2274
Fax: +27-11-642-4355
Fax2Email: +27-86-553-4733
Email: viness.pillay@wits.ac.za

ABSTRACT
An experimental design of the pH_M 'smart' polymeric sheet encapsulated-OCMT for tri-functionalization in the delivery of gastro-sensitive therapeutic proteins and synthetic peptides was investigated. Physicochemical and physicomechanical characterization techniques were undertaken to determine pertinent interactions of the incorporated co-inhibitor with CYP3A4 and P-glycoprotein (Pgp). In addition, the micro-environmental pH demonstrated the pH lowering effects of citric acid and its potential in reducing the optimal environment for brush border enzyme activity. Comprehensive analysis of the 'smart' polymeric sheet via analysis of the rheological profile, mucoadhesion and physicomechanical strength and elasticity confirmed the favorable characteristics of prolamines in drug delivery applications. The *in vitro* release of Octreotide was influenced by the combined effects of swelling, surface erosion and *in situ* crosslinking, displaying fractional releases ranging from 0.79-0.89. Due to the complexity of the system, the release kinetics was attributed to both the Higuichi (R^2=0.98) and zero-order (R^2=0.97) models. Conclusive results from physicochemical and physicomechanical characterization of the design demonstrated the applicability of the pH_M 'smart' polymeric sheet encapsulated-OCMTs to provide tri-functionalization.

KEYWORDS: Oral peptide delivery; prolamines; CYP3A4; Pgp; physicochemical properties; physicomechanical properties

10.1.6. Research Paper 5

(To be submitted to *Nature Biotechnology*)

IN VITRO AND *IN VIVO* CHARACTERIZATION OF THE STATISTICALLY OPTIMIZED TRI-FUNCTIONALIZED ORAL CORE-MELT TABLET (OCMT) FOR ENHANCED PROTEIN AND SYNTHETIC PEPTIDE DELIVERY

Bibi F. Choonara, Yahya E. Choonara, Pradeep Kumar, Lisa C. du Toit, Viness Pillay*

Wits Advanced Drug Delivery Platform Research Unit, Department of Pharmacy and Pharmacology, School of Therapeutic Sciences, Faculty of Health Sciences, University of the Witwatersrand, Johannesburg, 7 York Road, Parktown, 2193, South Africa

***Corresponding Author:**
Professor Viness Pillay
Tel: +27-11-717-2274
Fax: +27-11-642-4355
Fax2Email: +27-86-553-4733
Email: viness.pillay@wits.ac.za

ABSTRACT
In-depth analysis of the statistically optimized Tri-functionalized OCMT for the delivery of gastro-sensitive proteins and synthetic peptides was undertaken. Physicochemical and physicomechanical characterization techniques demonstrated the optimum *in vitro* potential of the Tri-functionalized OCMT in the achievement of clinical efficacy. Analysis of the mucoadhesion and micro-environmental pH produced results that fell within the range of desired targeted responses. The gastro-resistant nature of the Tri-functionalized OCMT was demonstrated by achievement of <5% acid uptake. In addition, comprehensive mechanical analysis confirmed the multi-textural properties of the Tri-functionalized OCMT in the attainment of optimum mechanical strength. MRI imaging highlighted the hydrational transitions and unique pharma-engineering of the tablet. The release of Octreotide from the statistically optimized formulation demonstrated the effect of distinct formulatory components on the responsive potential of the Tri-functionalized OCMT. Fractional release reached a value of ±0.9 with the MDT (±21.58) indicating a slower peptide release rate. Lastly, critical cytotoxic analysis of the EPB showed a ±79.83% survival rate, indicating acceptable biocompatibility and safety for clinical use.

KEYWORDS: OCMT; Tri-functionalization; pH modifier; gastro-resistant; physicochemical properties; physicomechanical properties

10.2. Research Presentations

2015 School of Therapeutic Sciences Research Day, University of the Witwatersrand, South Africa

Design of a Novel Oral Core-Melt Tablet (OCMT) for Enhanced Delivery of Gastro-Sensitive Biotech Drug Molecules

Bibi F. Choonara, Yahya E. Choonara, Lisa C. du Toit, Pradeep Kumar, Viness Pillay*

University of the Witwatersrand, Faculty of Health Sciences, Department of Pharmacy and Pharmacology, 7 York Road, Parktown, Johannesburg 2193, South Africa
*** Corresponding Author: viness.pillay@wits.ac.za**

PURPOSE:
The oral delivery of proteins and peptides is limited by the gastrointestinal (GIT) barrier which acts a physical and chemical impediment towards achieving successful oral delivery. Advancements towards achieving successful oral delivery of proteins and peptides remains an active area of research and thus, this technology aims to collectively target the major challenges by significantly improving permeation, increasing structural protection and enabling controlled release of the incorporated protein/peptide.

METHODS:
The premise of the design is the formulation of an innovative matrix-type tablet technology by utilizing a mixture of salts and temperature-responsive polymer composites capable of creating prefabricated core-melt archetypes within tablets. The tablet provides structural protection and ensures controlled release of the biotech drug molecule due to *in situ* crosslinking within the tablet core, facilitated by the proposed melting of the temperature-responsive polymer composite at body temperature (37°C). An experimental design of 15 formulations for the OCMTs was generated and each formulation was characterized with respect to *in vitro* protein/peptide release, *ex vivo* permeation capabilities (Franz diffusion), swelling and erosion, in situ crosslinking abilities (Fourier Transform Infrared Spectroscopy-FTIR), Magnetic Resonance Imaging (MRI) and textural analysis. In addition, advanced thermal (Differential Scanning Calorimetry and Thermogravimetric Analysis) and crystallinity analysis (Scanning Electron Microscopy (SEM) and X-ray Diffraction) was performed on the temperature-responsive polymer composite.

RESULTS:
Physicochemical and physicomechanical characterization tests confirmed successful formation of the temperature-responsive polymer composite. Protein/peptide release from the OCMTs was calculated as a function of fractional release versus time with all formulations displaying similar controlled release patterns over the 24hour study period with a maximum fractional release of ±0.8 for all formulations. Mathematical modelling of the protein release kinetics corresponded best with the Higuchi model with near zero order ($R^2 \approx 0.9787$) release obtained. The permeation enhancing effect of the temperature-responsive polymer composite was investigated and results displayed an enhanced drug flux (0.0576-0.0720mg.cm^{-2}h^{-1}) across the porcine intestinal tissue model. FTIR results indicated successful in situ crosslinking. Textural analysis of the OCMTs revealed the softening of the polymer composite at 37°C, which mirrored the MRI image and thermal analysis results obtained. Essentially, this novel technology demonstrates the applicability of the design in improving the oral delivery of a multitude of proteins and peptides and may potentially serve as a viable alternative to the parenteral route of administration for sensitive proteins and peptides.

Design of a Novel *In Situ* Cross-linked Eutectic Tablet for Enhanced Delivery of Gastro-Sensitive Biotech Drug Molecules

Bibi F. Choonara[1], Yahya E. Choonara[1], Lisa C. du Toit[1], Pradeep Kumar[1], Viness Pillay[1]

[1]Department of Pharmacy and Pharmacology, Faculty of Health Sciences, University of the Witwatersrand, 7 York Road, Parktown, 2193, Johannesburg, South Africa

PURPOSE: Polymer eutectics was used in the design of an innovative *In Situ* Cross-linked Eutectic Tablet- utilizing a suite of salts and eutectic polymer composites capable of creating prefabricated core-melt archetypes within a tablet, producing a controlled release system that provides structural protection, increased permeation and enhanced the oral delivery of proteins and peptides. This study assessed the *in vitro* potential of the *In Situ* Cross-linked Eutectic Tablet and the applicability of the design in improving the oral delivery of proteins and peptides.

METHODS: An experimental design of 15 formulations for the *In Situ* Cross-linked Eutectic Tablets was generated and each formulation was characterized with respect to *in vitro* protein/peptide release; *ex vivo* permeation capabilities through the pig intestinal tissue model; swelling and erosion; *in situ* crosslinking abilities; and physicomechanical profiling. In addition, advanced thermal analysis was significant for characterizing and comparing pertinent transitions such as melting, glass transitions, phase changes and heat of fusion of the eutectic composite and its reagents. Qualitative and quantitative crystallinity analysis was performed on the eutectic composite to determine fingerprint changes in crystallinity.

RESULTS: Characterization tests confirmed eutectic composite formation as was evidenced by the lowering of the melting point to 37°C, the decreased crystallinity percentage for the eutectic powder melt (9.6%) as compared to the eutectic reagents menthol (30%) and cetomacrogol (16%), as well as the shift in the SEM images to an amorphous structure which is typically characteristic of eutectic mixtures. Protein/peptide release from the tablets displayed similar controlled release patterns over the 24hour study period with a maximum fractional release of ±0.8 for all formulations. The release pattern alternated between phases of burst and slow release which was attributed to the combined effects of swelling, surface erosion and *in situ* crosslinking. Mathematical modelling of the protein release kinetics corresponded best with the Higuchi model with near zero order (R^2≈0.9787) release obtained. The permeation enhancing effect of menthol contained within the eutectic powder melt (EPM) was investigated and results displayed an enhanced drug flux (0.0576-0.0720mg.cm^{-2}h^{-1}) across the intestinal tissue model as compared to the control (EPM-free) formulation which displayed a drug flux of 0.0289mg.cm^{-2} h^{-1}. FTIR results highlighted the shifting and changing of band intensities as well as the appearance of new bands and the disappearance of bands indicating successful *in situ* crosslinking within the core eutectic region with higher concentrations of crosslinkers displaying superior crosslinking abilities. Textural analysis of the tablets revealed the softening of the core region at 37°C, which mirrored the MRI and thermal analysis results obtained.

CONCLUSION: Physicochemical and physicomechanical characterization that was undertaken was essential for delineating the *in vitro* attributes, predicting the *in vivo* performance of the device and demonstrating the applicability of the design in improving the oral delivery of a multitude of proteins and peptides. Essentially, this novel technology may potentially serve as a viable alternative to the parenteral route of administration for sensitive proteins and peptides.

TITLE: Design of a Novel Oral Core-Melt Tablet (OCMT) for Enhanced Delivery of Gastro-Sensitive Biotech Drug Molecules

AUTHORS: Bibi F. Choonara, Yahya E. Choonara, Lisa C. du Toit, Pradeep Kumar, Viness Pillay

PURPOSE: The oral delivery of proteins and peptides is limited by the gastrointestinal (GIT) barrier which acts a physical and chemical impediment towards achieving successful oral delivery. Pharmaceutical technologies and approaches targeting the complications in the oral delivery of proteins and peptides although useful in some instances, nevertheless hold limitations that enable optimal delivery. Consequently, advancements towards achieving successful delivery of proteins and peptides remains an active area of research and thus, this technology aims to collectively target the major challenges by significantly improving permeation, increasing structural protection and enabling controlled release of the incorporated protein/peptide

METHODS: The premise of the design is the formulation of a tablet with an outer polymer shell surrounding a core eutectic region that contains the incorporated protein or peptide and suitable crosslinking agents which provides structural protection and ensures controlled release of the biotech drug molecule due to *in situ* crosslinking within the tablet core which is facilitated by the ingress of fluid into the outer polymer shell and the proposed melting of the core eutectic region at body temperature (37°C). This was achieved through the utilization of a suite of salts and eutectic polymer composites capable of creating prefabricated core-melt archetypes within tablets. An experimental design of 15 formulations for the OCMTs was generated and each formulation was characterized with respect to *in vitro* protein/peptide release, *ex vivo* permeation capabilities (Franz diffusion), swelling and erosion, *in situ* crosslinking abilities (Fourier Transform Infrared Spectroscopy-FTIR), Magnetic Resonance Imaging (MRI) and textural analysis. In addition, advanced thermal (Differential Scanning Calorimetry and Thermogravimetric Analysis) and crystallinity analysis (Scanning Electron Microscopy (SEM) and X-ray Diffraction) was performed on the eutectic powder melt.

RESULTS: Physicochemical and physicomechanical characterization tests confirmed eutectic formation as was evidenced by the lowering of the melting point to 37°C (Figure 1a), the decreased crystallinity percentage for the eutectic powder melt (9.6%) as compared to the eutectic reagents menthol (30%) and cetomacrogol (16%), as well as the shift in the SEM images to an amorphous structure which is typically characteristic of eutectic mixtures. Protein/peptide release from the OCMTs was calculated as a function of fractional release *versus* time with all formulations displaying similar controlled release patterns over the 24hour study period with a maximum fractional release of ±0.8 for all formulations. The release pattern alternated between phases of burst and slow release which was attributed to the combined effects of swelling, surface erosion and *in situ* crosslinking. Mathematical modelling of the protein release kinetics corresponded best with the Higuchi model with near zero order ($R^2 \approx 0.9787$) release obtained. The permeation enhancing effect of menthol contained within the eutectic powder melt (EPM) was investigated and results displayed an enhanced drug flux (0.0576-0.0720mg.cm^{-2}h^{-1}) across the intestinal tissue model as compared to the control (EPM-free) formulation which displayed a drug flux of 0.0289mg.cm^{-2} h^{-1}. FTIR results highlighted the shifting and changing of band intensities as well as the appearance of new bands and the disappearance of bands indicating successful *in situ* crosslinking within the core eutectic region with higher concentrations of crosslinkers displaying superior crosslinking abilities. Textural analysis of the OCMTs revealed the softening of the core region at 37°C, which mirrored the MRI image (Figure 1b) and thermal analysis results obtained.

CONCLUSION: Physicochemical and physicomechanical characterization that was undertaken was essential for delineating the *in vitro* attributes, predicting the *in vivo* performance of the device and demonstrating the applicability of the design in improving the oral delivery of a multitude of proteins and peptides. Essentially, this novel technology may potentially serve as a viable alternative to the parenteral route of administration for sensitive proteins and peptides.

Design of a Novel *In Situ* Crosslinked Oral Core Melt Tablet (OCMT) for Enhanced Delivery of Gastro-sensitive Proteins and Peptides

Bibi F. Choonara[1], Yahya E. Choonara[1], Lisa C. duToit[1], Pradeep Kumar[1], Viness Pillay[1]

[1]Department of Pharmacy and Pharmacology, Faculty of Health Sciences, University of the Witwatersrand, 7 York Road, Parktown, 2193, Johannesburg, South Africa

INTRODUCTION

Polymer eutectics was used in the design of an innovative *In Situ* Crosslinked OCMT- utilizing a suite of salts and eutectic polymer composites capable of creating prefabricated core-melt archetypes within a tablet, producing a controlled release system that provides structural protection, increased permeation and enhanced the oral delivery of proteins and peptides. This study assessed the *in vitro* potential of the *In Situ* Cross-linked Eutectic Tablet and the applicability of the design in improving the oral delivery of proteins and peptides

MATERIALS AND METHODS

An experimental design of 15 formulations was generated and each formulation was characterized with respect to *in vitro* protein/peptide release; *ex vivo* permeation capabilities through the pig intestinal tissue model; swelling and erosion; *in situ* crosslinking abilities; and physicomechanical profiling. In addition, advanced thermal analysis was significant for characterizing and comparing pertinent transitions such as melting, glass transitions, phase changes and heat of fusion of the eutectic composite and its reagents. Qualitative and quantitative crystallinity analysis was performed on the eutectic composite to determine fingerprint changes in crystallinity.

RESULTS AND DISCUSSION

Physicochemical and physicomechanical characterization tests confirmed eutectic formation as was evidenced by the lowering of the melting point to 37°C (Figure 1a), the decreased crystallinity for the eutectic powder blend (EPB) as compared to the eutectic reagents menthol and cetomacrogol and the shift in the SEM images to an amorphous structure which is typically characteristic of eutectic mixtures. Protein/peptide release from the OCMTs was calculated as a function of fractional release *versus* time with all formulations displaying similar controlled release patterns over the 24hour study period with a maximum fractional release of ±0.8 for all formulations. The release pattern alternated between phases of burst and slow release which was attributed to the combined effects of swelling, surface erosion and *in situ* crosslinking. Mathematical modelling of the protein release kinetics corresponded best with the Higuichi model with near zero order ($R^2 \approx 0.9787$) release obtained. The permeation enhancing effect of menthol contained within the EPB was investigated and results displayed an enhanced protein flux ($0.0576\text{-}0.0720 mg.cm^{-2}h^{-1}$) across the intestinal tissue model as compared to the control (EPB-free) formulation which displayed a protein flux of $0.0289 mg.cm^{-2} h^{-1}$. FTIR results highlighted the shifting and changing of band intensities as well as the appearance of new bands and the disappearance of bands indicating successful *in situ* crosslinking within the core eutectic region with higher concentrations of crosslinkers displaying superior crosslinking abilities. Textural analysis of the OCMTs revealed the softening of the core region at 37°C, which mirrored the MRI image (Figure 1b) and thermal analysis results obtained.

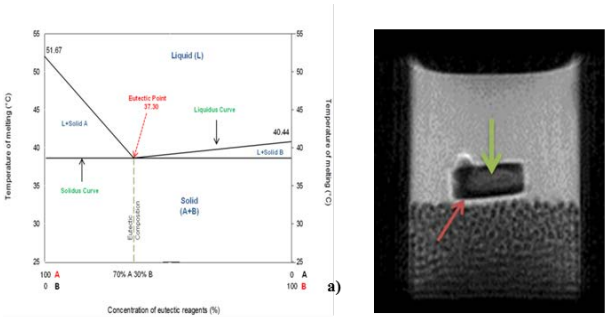

Fig. 1. **a)** Binary phase diagram constructed for the EPB using thermal analysis results and **b)** Magnetic Resonance Imaging (MRI) of the OCMT with the red arrow indicating the outer polymer shell and the green arrow indicating the softened core at 37°C.

CONCLUSIONS

Physicochemical and physicomechanical characterization that was undertaken was essential for delineating the *in vitro* attributes, predicting the *in vivo* performance of the device and demonstrating the applicability of the design in improving the oral delivery of a multitude of proteins and peptides. Essentially, this novel technology may potentially serve as a viable alternative to the parenteral route of administration for sensitive proteins and peptides.

ACKNOWLEDGMENTS

National Research Foundation (NRF)

REFERENCES

[1] B.F. Choonara, Y.E. Choonara, L.C. duToit, P. Kumar and V. Pillay, "Design of an *In Situ* Crosslinked Eutectic Tablet for Enhanced Delivery of Gastro-sensitive Proteins and Peptides", *J. Pharm. Sci*, in press.

10.3. Animal Ethics Clearance Certificate

STRICTLY CONFIDENTIAL

ANIMAL ETHICS SCREENING COMMITTEE (AESC)

CLEARANCE CERTIFICATE NO. 2014/38/C

INVESTIGATORS: Prof V Pillay

CO-INVESTIGATORS (For postgraduate degree purposes): Ms B Choonara
Ms M Siyawamwaya
Mr M Sithole

SCHOOL: Pharmacy & Pharmacology

LOCATION: Faculty of Health Sciences

PROJECT TITLE: *In vivo assessment of innovative polymeric oral drug delivery systems in large White Pigs*

Number and Species

18 Large White Pigs

Approval was given for to the use of animals for the project described above at an AESC meeting held on 24 June 2014 . This approval remains valid until 23 June 2016.

The use of these animals is subject to AESC guidelines for the use and care of animals, is limited to the procedures described in the application form and is subject to any additional conditions listed below:

None.

Signed: _____ (Chairperson, AESC) Date: 1/7/2014

I am satisfied that the persons listed in this application are competent to perform the procedures therein, in terms of Section 23 (1) (c) of the Veterinary and Para-Veterinary Professions Act (19 of 1982)

Signed: _____ (Registered Veterinarian) Date: 27 June 2014

cc: Supervisor: N/A
Director: CAS

Works 2000/lain0015/AESCCert.wps